

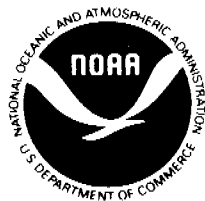
BLM - ALASKA RESOURCES LIBRARY
3 0455 00000467 1



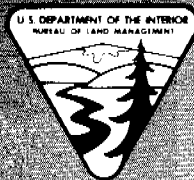
Environmental Assessment of the Alaskan Continental Shelf

**Annual Reports of Principal Investigators
for the year ending March 1980**

Volume V: Hazards



**U.S. DEPARTMENT OF COMMERCE
National Oceanic & Atmospheric Administration
Office of Marine Pollution Assessment**



**U.S. DEPARTMENT OF INTERIOR
Bureau of Land Management**

February 1981

APR 24 1981
Merged With
ARLIS
ANCHORAGE, ALASKA
Est. 1997

GC
85.2
.A4
E57
1980
V.5

Environmental Assessment of the Alaskan Continental Shelf

**Annual Reports of Principal Investigators
for the year ending March 1980
Volume V: Hazards**



**U.S. DEPARTMENT OF COMMERCE
National Oceanic & Atmospheric Administration
Office of Marine Pollution Assessment**



**U.S. DEPARTMENT OF INTERIOR
Bureau of Land Management**

February 1981

ARLIS
Alaska Resources
Library & Information Services
Anchorage, Alaska

The facts, conclusions and issues appearing in these reports are based on interim results of an Alaskan environmental studies program managed by the Outer Continental Shelf Environmental Assessment Program (OCSEAP) of the National Oceanic and Atmospheric Administration (NOAA), U.S. Department of Commerce, and primarily funded by the Bureau of Land Management (BLM), U.S. Department of Interior, through interagency agreement.

DISCLAIMER

Mention of a commercial company or product does not constitute an endorsement by National Oceanic and Atmospheric Administration. Use for publicity or advertising purposes of information from this publication concerning proprietary products or the tests of such products is not authorized.

TABLE OF CONTENTS
VOLUME V: HAZARDS

<u>RU #</u>	<u>PI - Agency</u>	<u>Title</u>	<u>Page</u>
271	Rogers, J.C. Morak, J.L. - Geophysical Institute Fairbanks, AK	Beaufort Seacoast Permafrost Studies	1
327	Hampton, M.A. - USGS, Menlo Park, CA	Shallow Faulting, Bottom Instability and Movement of Sediment in Lower Cook Inlet and Western Gulf of Alaska	45
429	Nelson, C.H. - USGS, Menlo Park, CA	Faulting, Sediment Instability, Erosion & Deposition Hazards of the Norton Basin Area	181
483	Biswas, N.N. Sackinger, W.M. Gedney, L. - Geophysical Institute Fairbanks, AK	Seismotectonic Studies of Western Alaska and Sea Ice Studies in Beaufort Sea	515
530	Cannon, J.P. Rawlinson, S.E. - University of Alaska Fairbanks, AK	The Environmental Geology and Geomorphology of the Berrier Island - Lagoon System Along the Beaufort Sea Coastal Plain from Prudhoe Bay to the Colville River	619
579	Latham, G.V. Dorman, H.J. Ibrahim, A.K. - University of Texas Marine Science Institute Galveston, TX	Coordinated Ocean Bottom Seismograph Measurements in the Kodiak Shelf Area	635

ANNUAL REPORT

Contract # 03-5-022-55
Research Unit # 271
Reporting Annual Report
Period: Period Ending
April 1, 1980
Number of Pages: 42

BEAUFORT SEACOAST PERMAFROST STUDIES

J.C. Rogers and J.L. Morack
Geophysical Institute
University of Alaska
Fairbanks, Alaska 99701
(907)263-1859

April 1, 1980

TABLE OF CONTENTS

	<u>Page</u>
I. Summary	3
II. Introduction	4
III. Current State of Knowledge	6
IV. Study Area	7
V. Sources and Methods of Data Collection	7
VI. Results	9
VII. Discussion	26
VIII. Conclusions	31
IX. Needs for Further Study	33
X. Summary of Last Quarter	34
References for Annual Report	43

I. SUMMARY

A primary objective of this study is to develop an understanding of the distribution and nature of permafrost beneath the ocean and barrier islands along the Alaskan Sea Coast. Marine seismic refraction equipment, the primary tool used in this study, has shown submarine permafrost to be present at relatively shallow depths to distances of at least 20 km from shore. To put these observations into perspective, the reader is referred to three principal points discussed at the Barrow Synthesis Meeting in January, 1978. Those points provide bounds on the distribution of offshore permafrost and founded on bathymetry and sea level history.

(1) Shallow (water depth 2 m or less) inshore areas where ice rests directly on the sea bottom are underlain at depths of a few meters by ice-bonded equilibrium permafrost.

(2) Ice-bonded permafrost was once present beneath all parts of the continental shelf exposed during the last low sea level interval, and consequently relict ice-bonded permafrost may persist beneath any part of the shelf inshore from the 90 m isobath.

(3) Ice-bonded permafrost is probably absent from parts of the Beaufort Sea shelf seaward from the 90 m isobath, although subsea temperatures are probably below 0 C.

Some specific conclusions resulting from the current studies can be listed in addition to these general guidelines.

a. Seismic studies outside of the barrier islands have shown that the depths of ice-bonded permafrost are not simply related to their distance from shore. In the Prudhoe Bay area shallow ice-bonded materials (within

10 m of the ocean bottom) have been mapped offshore of the islands while nearer to shore these materials are considerably deeper (up to 140 m beneath the bottom). Permafrost 80 m thick (limited by drill depth) has been observed.

b. The barrier islands are not uniformly underlain by ice-bonded permafrost. Areas with no ice-bonding have been observed and areas with continuous ice-bonding have been observed.

c. The presence of salt brine complicates the distribution of offshore permafrost, it appears that relatively impermeable materials such as clays are a dominant factor in determining the depth to subsea permafrost.

d. Former thaw lakes and old river valley which contribute to the variability of the upper permafrost surface can be found in subsea permafrost of land origin.

e. The seismic indications of permafrost correlate well with drilling evidence.

II. INTRODUCTION

A. General Nature and Scope

A particular concern to the project are the areas offshore and along the barrier islands in the Alaskan Beaufort Sea where subsea permafrost has been shown to exist. Mapping the distribution of offshore permafrost and determining the depth to the top of the permafrost have been given a high priority.

Seismic refraction techniques are used in the study to probe the ocean bottom along the Alaskan Beaufort Sea coast. Because of the nature of the geophysical tool the primary data gathered are depths to the upper surface of the subsea permafrost. Permafrost is interpreted to be present where seismic velocities above a predetermined threshold are observed. The study will provide information relevant to task D-8 in NOAA's proposal to BLM.

B. Specific Objectives and Relevance to Problems of Petroleum Development.

Data are being gathered, using the equipment purchased by the program, which enable determination of the distribution and nature of offshore permafrost. The most important parameters to be determined in this study are the distribution and the depth of offshore permafrost. Another objective is compilation of the above parameters for use by other principal investigators and appropriate agencies and industries.

The Prudhoe Bay area and adjacent offshore islands is the primary focus of this study. (Seismic studies to date have extended along approximately 100 km of coast around Prudhoe Bay.) The truncation of permafrost beneath the ocean is of interest, particularly the shape of the frozen-nonfrozen boundary. Thus, the second major objective is the determination of the shape of the boundary.

A third major objective is determining the nature and extent of permafrost beneath the barrier islands. These results will provide valuable information for refinement and testing of thermal models as well as for determining operational methods for offshore oil and gas development.

The fourth major objective is to provide information to support reconnaissance drilling programs. These include programs of the University of Alaska, CRREL, and the USGS. It is possible, using the seismic technique, to extend site specific drilling information to areas remote from the drill site, by correlating seismic data at the drill site and at the remote locations. Finally, areas for future drilling investigations can be suggested on the basis of seismic information.

Detailed and specific relevance to problems of offshore petroleum development have been addressed in the synthesis documents developed by the Earth Science Study Group. The reader is referred to these documents.

III. CURRENT STATE OF KNOWLEDGE

The sea floor along the Arctic Coast is known to be underlain by permafrost. Definite progress is being made toward understanding its distribution and the dynamics of its formation and destruction. Several of the problem areas needing investigation have been listed in the introduction of this report.

Extensive permafrost has been reported beneath the Canadian Beaufort Sea (Hunter, et al, 1978) and beneath the water of Prudhoe Bay, Alaska (Osterkamp and Harrison, 1976, 1977). Some of the physical processes involved in the degradation of relict permafrost are beginning to be understood and in addition to temperature, the porosity of the sediments and the salinity of the interstitial liquids have been shown to be important. Current data are available in the 1979 annual reports of research units 253, 255, 256, by Harrison and Osterkamp. Some details of the processes involved are also found in Harrison and Osterkamp (1976). The results reported here are in agreement with the drilling results obtained by the Joint USACRREL/USGS drilling program (R.U. 105) as reported by Sellman et al. (1976) (see also Chamberlain et al, 1978 and Sellmann et al, 1979). In last years annual report a close correlation between their drilling and our geophysical results were shown. Also, the geophysical results are in general agreement with those of Osterkamp and Harrison. The depth of the permafrost upper surface is currently known along several transects made both inside and outside of the barrier islands. Widespread aerial distribution and depth information remain to be determined although it is possible to make some general statements regarding offshore permafrost, (see the summary section of this report), and

to sketch regions of known shallow permafrost (see area map later in this report). Presently our geophysical investigations cover approximately 100 km of coastline around Prudhoe Bay.

IV. STUDY AREA

Figure 1 shows the area investigated during the study. All of the vessel tracks taken over the past several summer field seasons are shown in the figure. Past reports by this research unit have shown some of the lines in the area covered by Figure 1. However, this is the most complete compilation of the data to date.

V. SOURCES AND METHODS

The application of shallow refraction techniques, documented by Grant and West (1965), to the detection of subsea permafrost has been described previously (Hunter, 1974; Hunter and Hobson, 1974). The seismic refraction data taken in and near Prudhoe Bay were collected using a 40 cubic inch air gun as an acoustic source and the refracted signal was detected along a hydrophone line towed behind a 21' vessel. All the data taken during the last field season were recorded using an enhancement seismograph which allowed field evaluation of the data at the time of acquisition. These data were gathered at several points along the ship transects, scaled and reduced to time-distance plots. Over 350 of these plots were made last season along 140 km of vessel track.

Seismic velocities are determined in the sub-bottom material and depths to various layers are calculated from the time-distance plots. The velocities are then used to determine whether the bottom materials are frozen. Permafrost

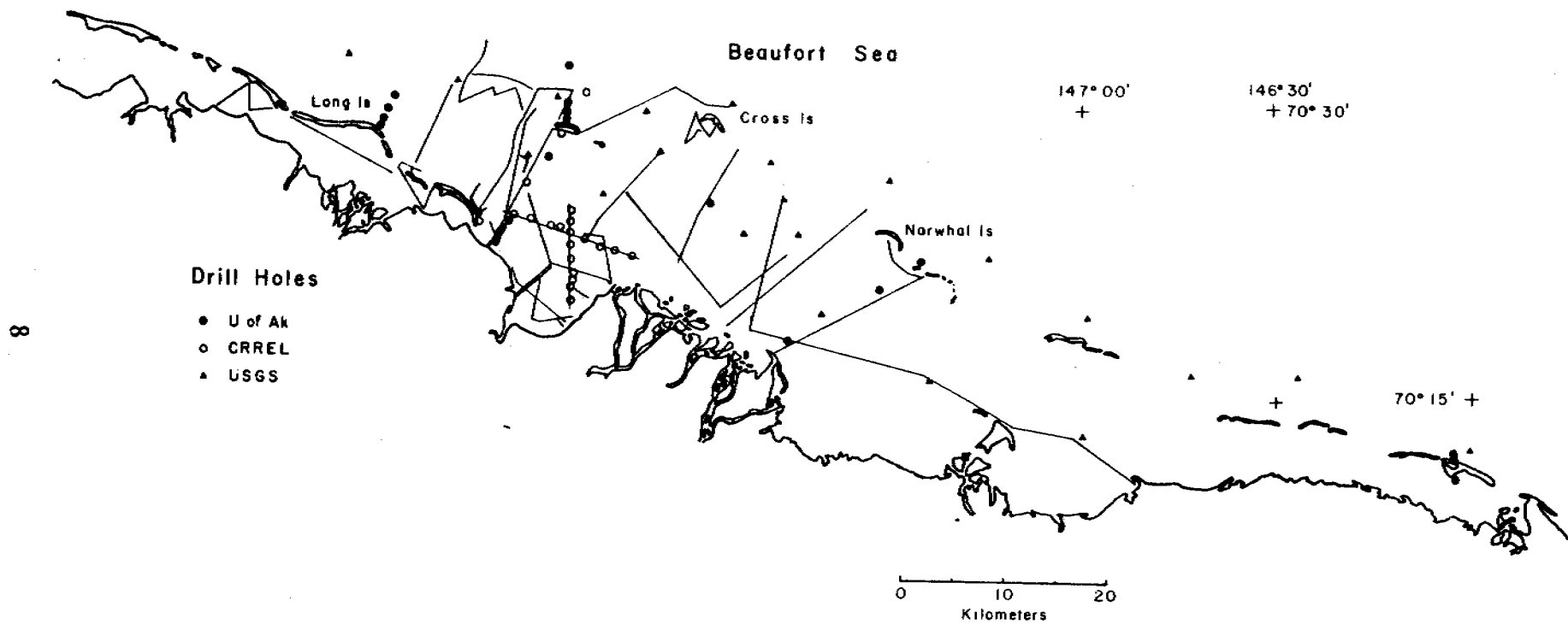


Figure 1. Area of subsea permafrost study showing all seismic lines run to date and the location of drill holes in the area.

velocities in the materials near Prudhoe Bay are typically between 2500 m/s and 3000 m/s while similar materials in the nonfrozen state typically have velocities ranging from 1600 m/s to 2000 m/s (Rogers et al., 1975). Significant velocity contrasts such as these, which are typical of coarse sandy materials, allow easy classification of materials into the frozen or unfrozen state.

Various errors exist in the data acquisition and reduction procedures. Several of these are indicated in Appendix A1 and an estimate of the possible variations in the depth calculation is made. The cumulative errors in the calculated depth to permafrost are estimated to be -5% due to cable slack and -5% due to cable curvature. The random errors are estimated to be $\pm 8\%$ and are judged to be additive with respect to the cable slack and curvature errors.

VI. RESULTS

Marine Refraction:

Additional seismic lines were run during the 1979 summer field season. A primary emphasis was correlation of our data with core holes drilled by Harding-Lawson for the U.S. Geological Survey Conservation Division in Spring 1979. Twelve of the twenty core hole sites were visited and seismic lines were run in the immediate vicinity. (See report by Harding-Lawson to USGS.)

Figure two indicates several of the refraction lines run in the Prudhoe Bay vicinity last field season. Three of these lines, V-V', W-W' and X-X' have been plotted in vertical sections showing the location of ice-bonded materials identified by refraction techniques. (Note that all depths to bonded materials in this report are referenced to the ocean surface.) Line V-V' which runs from Dinkum Sands to "Duck Island" (man made island near Duck

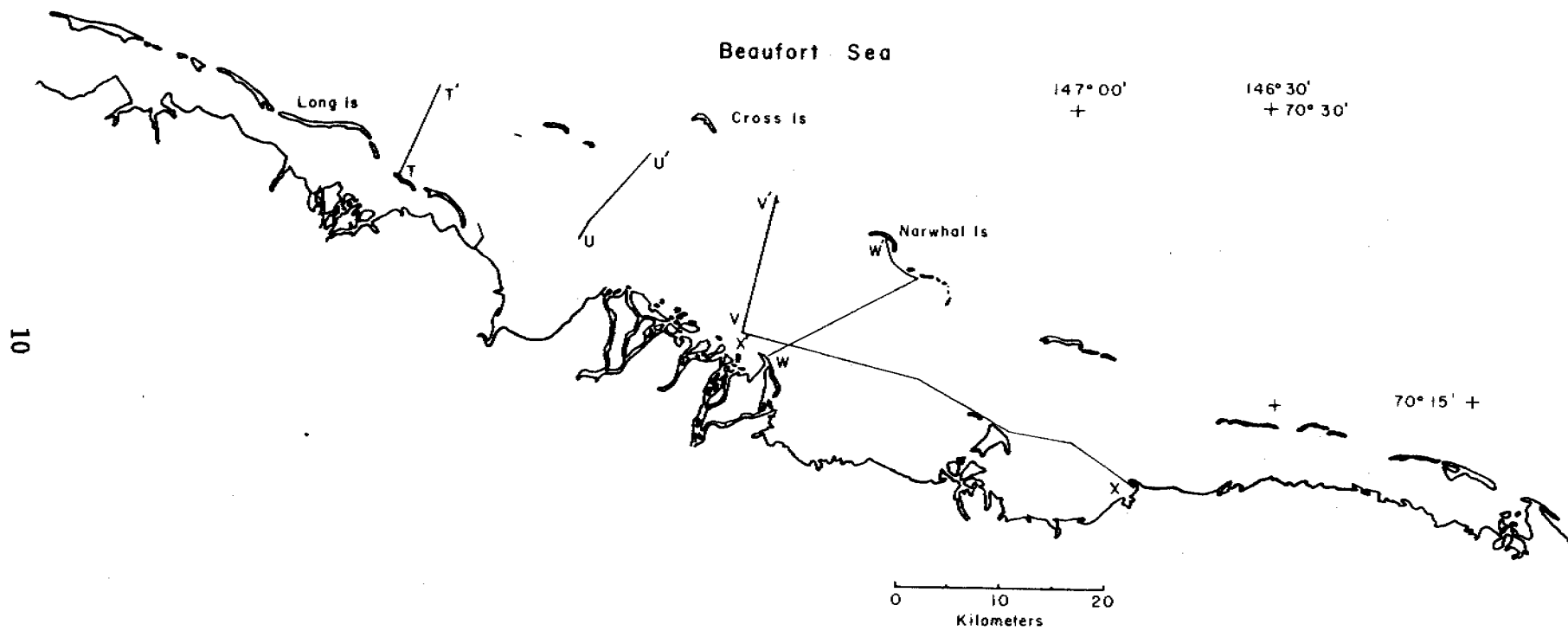


Figure 2. Seismic lines taken during August 1979.

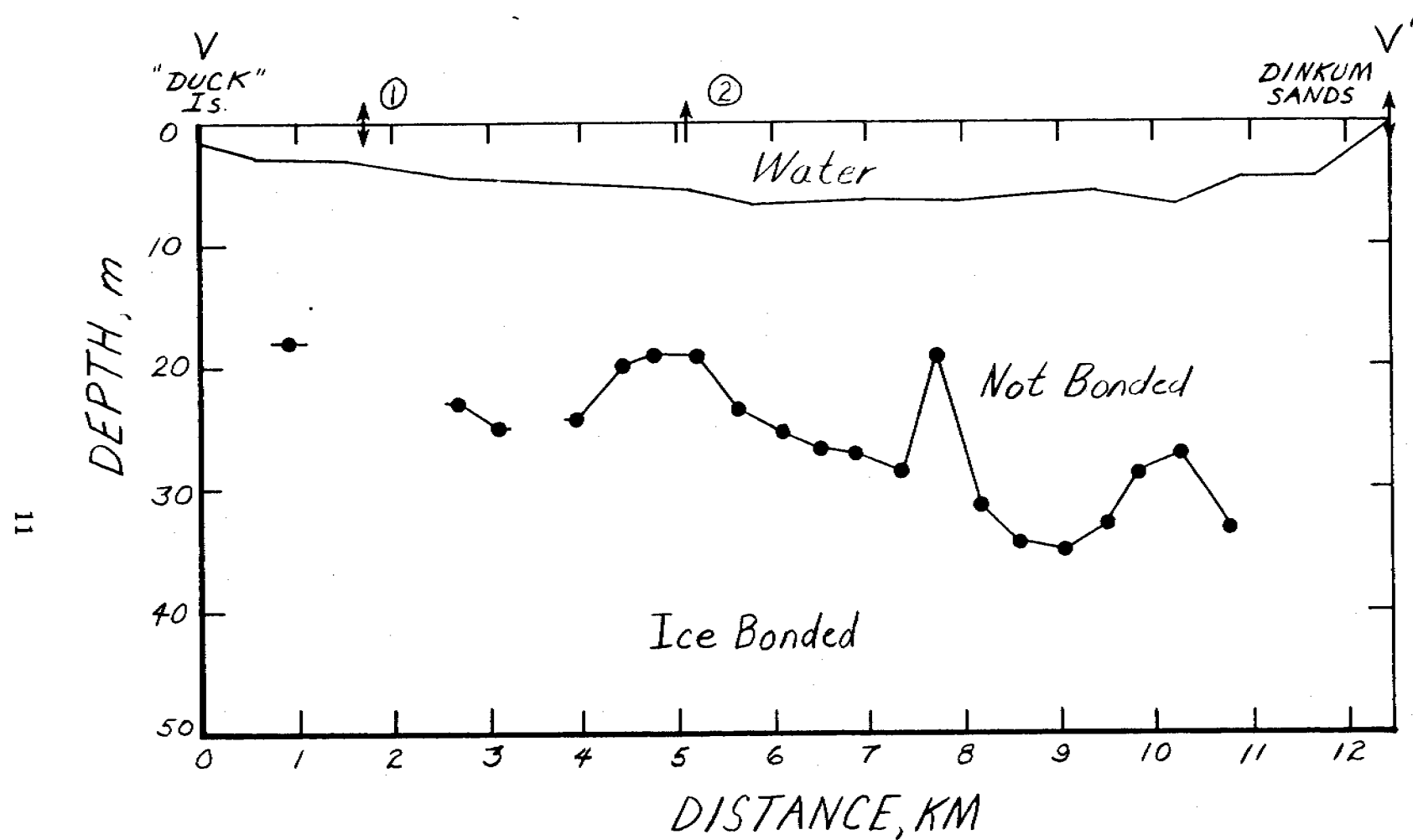


Figure 3. Vertical section along seismic line V-V'

- ① Intersection with line N-N'-N'' at 14 km. No bonded material observed on either line
- ② Intersection with line 0-0' at 5.1 km. Bonded material observed at 24 m depth on line 0-0'.

Island) is shown in Figure 3. There is discontinuous shallow permafrost near "Duck Island" with a continuous surface present at greater distances from the island. The data tend to show a relatively smooth surface with the exception of the point 7.5 km along the line which appears to be relatively shallow. The refraction data for this point have been reexamined and we conclude that the shallow permafrost interpretation is correct.

Figures 4a and 4b indicate permafrost conditions along line W-W'. Similar to line V-V' there are some discontinuities in the shallow permafrost near the mouth of the Sag River delta. There appears to be a general trend in the data toward deeper permafrost in the second half of the line. It may be that the upper permafrost surface is below 50 m at distances of 19 to 22 km along the line.

One of the longest lines run to date, shown in Figures 5a through 5d, runs from Bullen Point to "Duck Island". Only sporadic bonded materials were observed along the first 26 km of line. Approximately one-half of the fast refractors observed were in close proximity to Tigvariak Island. The last 12 km of line showed a more continuous permafrost surface.

Table 1, a comparison of geophysical and drilling data on offshore permafrost, lists 15 core holes drilled by Harding-Lawson for the USGS and three holes drilled by Harrison and Osterkamp of the University of Alaska. Past reports (see our 1979 annual report) have used drilling information obtained by CRREL and the USGS for correlation with geophysical data.

There is general agreement between the drilling data and the geophysical data shown in Table 1. One of the major concerns in correlation of drilling and geophysical evidence for permafrost is the geographical proximity of the data. Figure 6 displays the seismic data and drilling data compared in Table I so the reader can access their correlation.

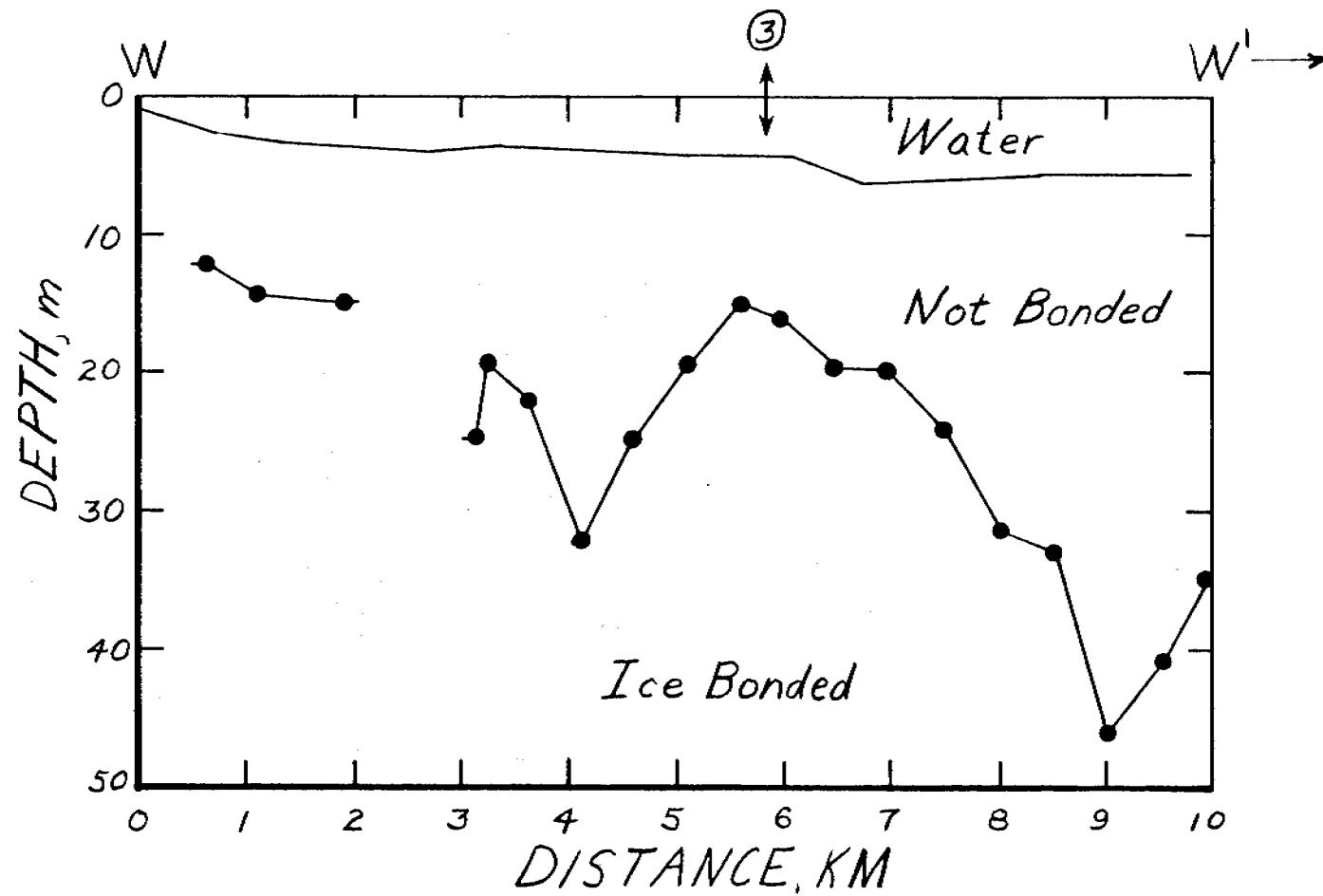


Figure 4a. Vertical section along a portion of seismic line W-W'.

③ Closest approach to drill hole #13, USGS (approximately 1.2 km).

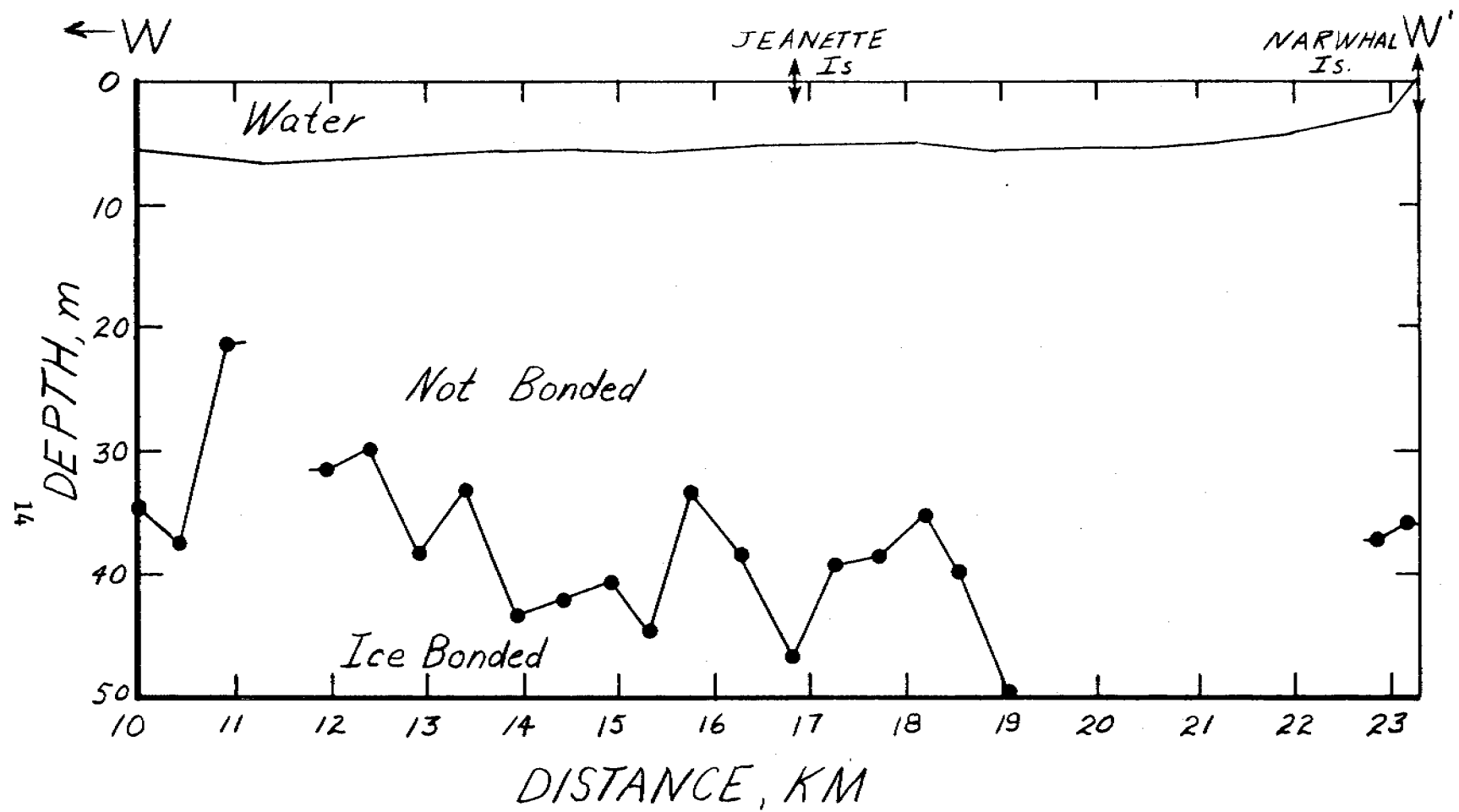
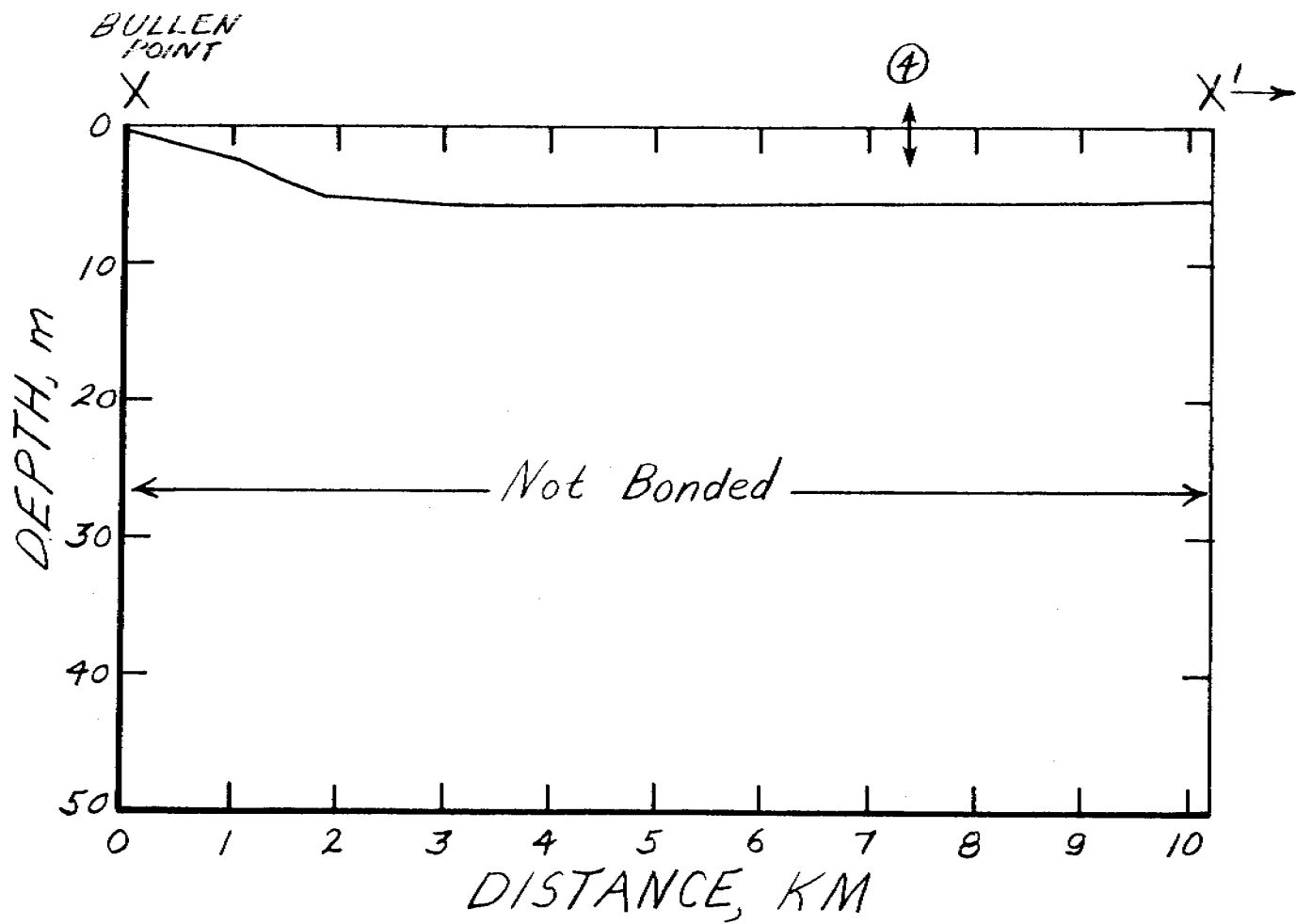


Figure 4b. Vertical section along a portion of seismic line W-W'.



15

Figure 5a. Vertical section along a portion of seismic line X-X'.

④ Closest approach to drill hole #15, USGS (approximately 0.5 km)

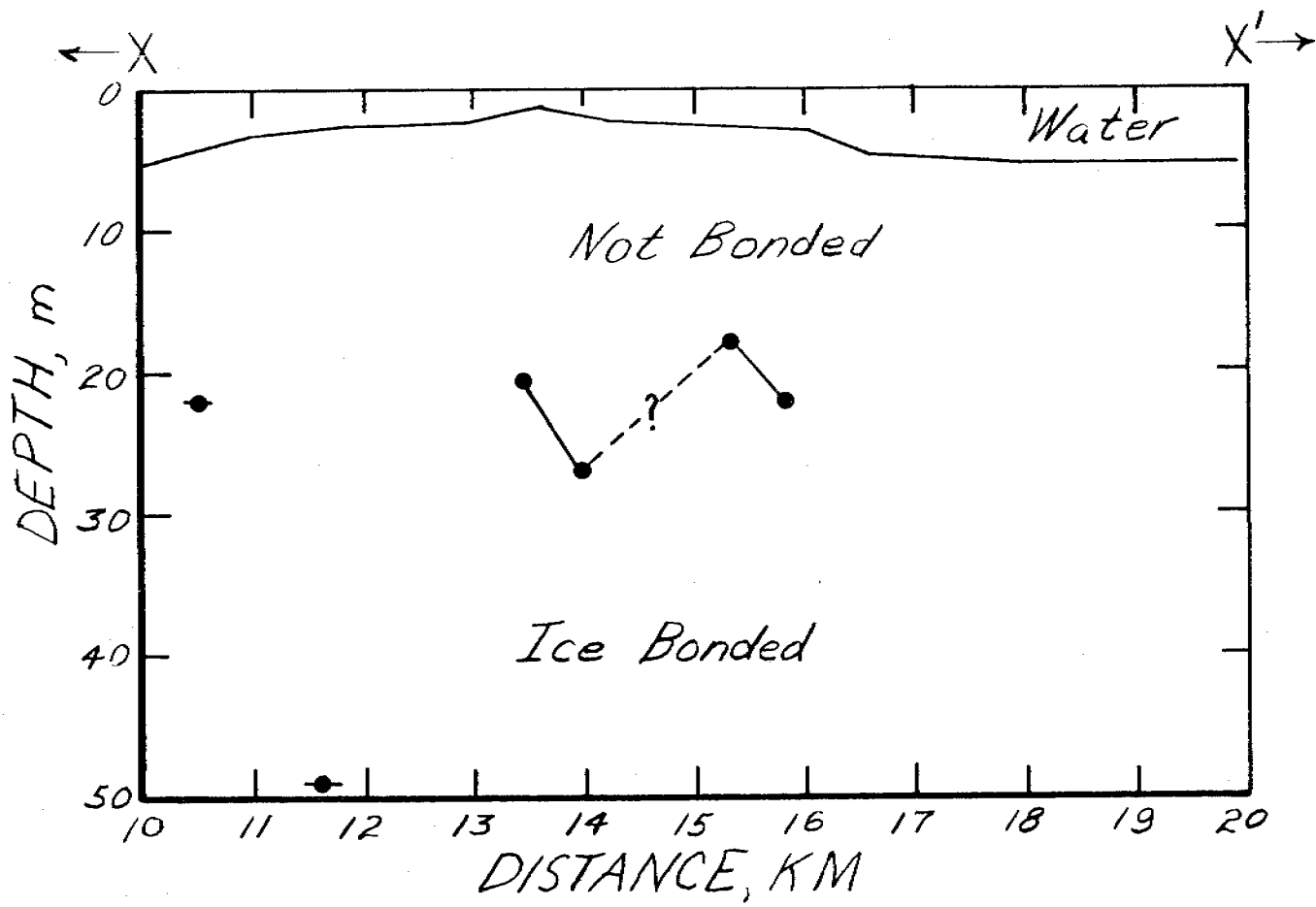


Figure 5b. Line X-X' continued

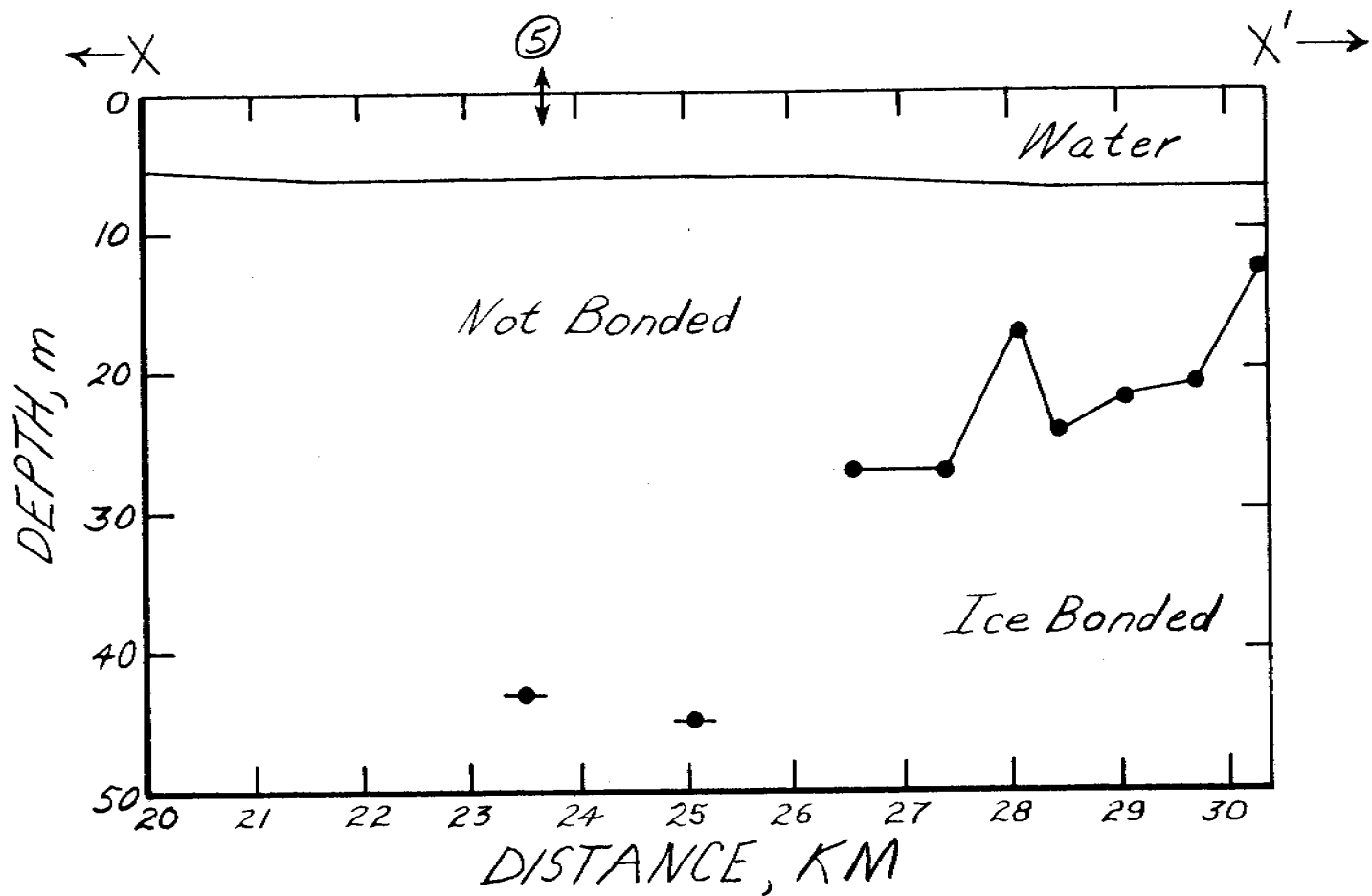


Figure 5c. Line X-X' continued

⑤ Closest approach to drill hole #14, USGS (approximately 0.5 km)

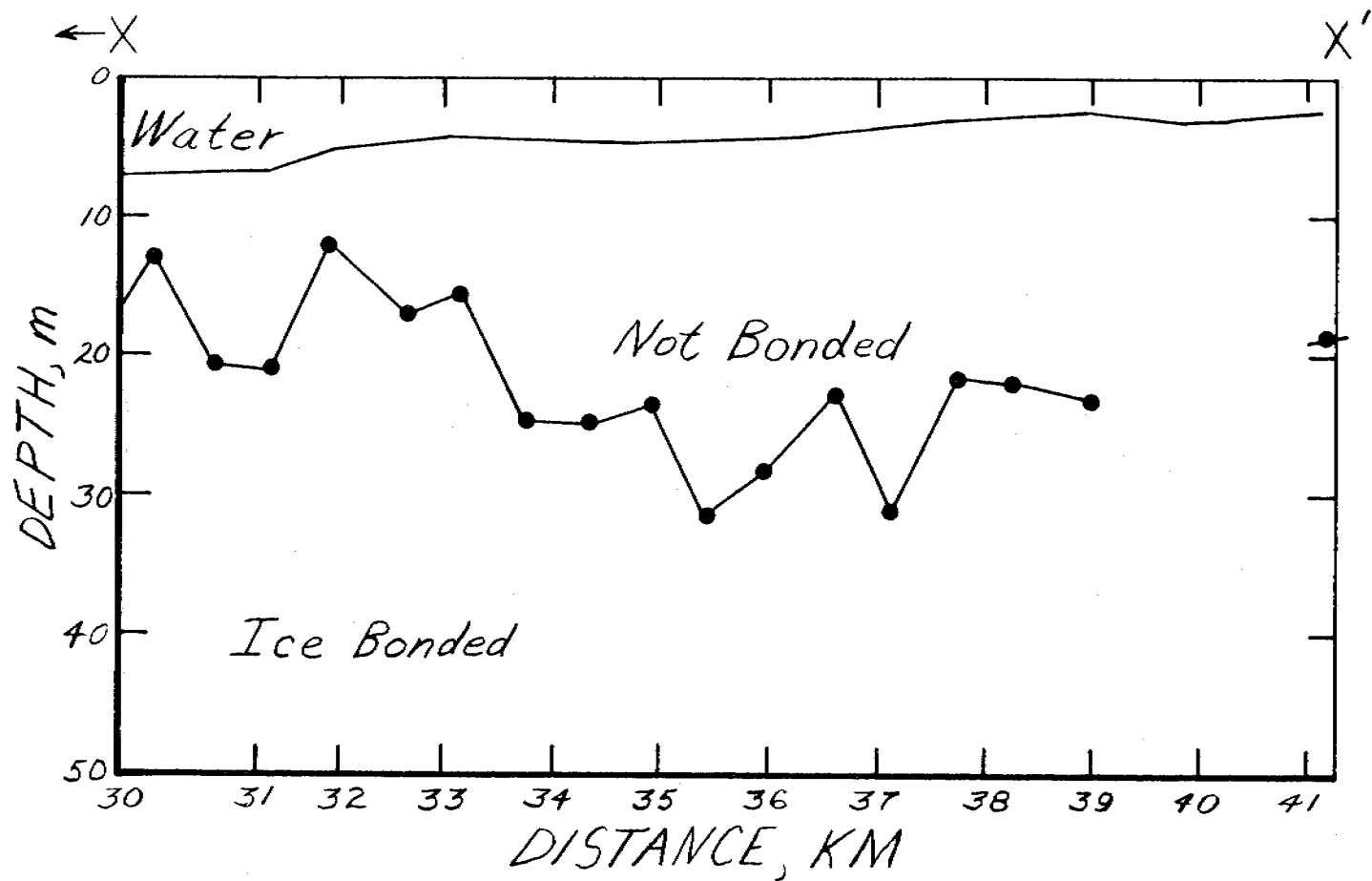


Figure 5d. The end of Line X-X'.

TABLE 1

Drilling, Identification	Location (Latitude) (Longitude)	Depth (below water surface)		Seismic identification	Adjacent Geophysical Lines		Depth to Permafrost (below water surface)		Notes
		Water	Core Hole		Dist. along seismic line	Closest dist. to core hole	Drilling	Geophysics	
HL-1 (HL=Harding Lawson)	70° 24' 47.61"N 148° 13' 16.50"W	5.03 m	29.9 m	U-U'	4 km	1.5 km	none	none	Confirms interpretations made previously.
HL-2	70° 27' 7.48" 148° 26' 45.1"	6.94	37.6	14-1 through 14-9	0.5	0.5	none	none	Confirms interpretations made previously lines run using radar position on Boston Whaler.
HL-3	70° 31' 54.5" 148° 53' 53.5"	13.5	42.8	T-T'	9.0	10.5	none	none	No seismic lines in immediate vicinity of the core hole.
HL-4	70° 30' 16.3" 148° 22' 42.9"	8.5	39.4	H-H' 14-27	14	0.7	20.7 m (thin)	26 m	Core hole data indicated a thin ice bonded layer (0.12 m thick). Core hole within one km of interpreted shallow permafrost boundary.
HL-5	70° 30' 41" 148° 37' 49.5"	12.8	104.2	T-T'	9.0	0.5	none	none	Confirms interpretations made previously.
HL-6	70° 29' 25.4" 148° 07' 42.5"	11.1	42.3	F-F'	9.2	0.6	none	28	Core hole within 0.5 km of interpreted shallow permafrost boundary.
HL-7	70° 27' 12.1" 148° 05' 16.7"	7.7	38.2	11-34 through 11-67	10.5	0.1	none	none	Lines were run over core hole in tow of USGS vessel "Karluk", typical high velocity perhaps 2000 m/s or less.
HL-8	70° 30' 1.8" 147° 53' 21.4"	14.0	44.5	F-F'	18.5 (at F') 18.0	0.5 1.0	33.4	36 28	The nearest seismic line correlates well. Local variability in permafrost depth is evident from adjacent record.
HL-9	70° 22' 48.3" 147° 42' 42.3"	5.3	44.9	11-1 through 11-33		0.1	13.8 m	average=23.8 std dev=2.9	Lines were run over core hole area using USGS vessel "Karluk" for navigation. Average permafrost depth is for 10 lines in immediate vicinity, i.e. within 1 km of drill site

Drilling, Identification	Location (Latitude) (Longitude)	Depth (below water surface)		Seismic Identification	Adjacent Geophysical Lines		Depth to Permafrost (below water surface)		Notes		
		Water	Core Hole		Dist. along seismic line	Closest dist. to core hole	Drilling	Geophysics			
HL-10	70° 27' 7.6" 147° 48' 28.1"	6.5 m	39.4 m	M-M' V-V'	at M' at V'	3.3 km 3.7	29.6 m	27 m none observed. (shallow water problem?)	Although neither line well suited for core hole correlation, the water depth at m' (7 m) is more representative than the water depth of v' (less than 1 m, at Dinkum Sands).		
HL-11	70° 23' 0.4" 147° 41' 0.1"	7.5	36.5	V-V'		9.7 km	2.2	31.6	30	No lines run directly over the core hole.	
HL-12	70° 23' 0.4" 147° 30' 26"	15.2	107	N-N'	at N'		3.5	23.7	28	Bonded material in core hole from 23.7 m through 107 m with the exception of a non-frozen band 0.9 m thick at 85 m depth.	
HL-13	70° 18' 56.7" 147° 38' 48.5"	5.6	36.4	17-1 through 17-22 W-W'			0.1	15.1	avg = 29.6 std dev = 4.6	16	Lines were run over core hole area with "Karluk". Of 23 lines only 6 produced fast refractors. Possible seismic source problems, deemed an unusual area by USGS Karluk.
HL-14	70° 16' 36" 147° 23' 42.4"	6.55	37.2	X-X'		23.5	0.5	none	43	Only one seismic record of those within 1 km of core hole indicated frozen material - near penetration limit of refraction equipment.	
HL -15	70° 13' 18.4" 147° 00' 20.1"	5.5	96.9	X-X'		7.5	0.5	18.2 (thin)	none		Core hole permafrost thickness; 3.5 m no layer observed on seismic records in vicinity. A local feature observed in core hole?
O-H - α 9.5 km north of Prudhoe Bay (O-H = Osterkamp, Harrison)	70° 25.90 148° 22.69	6.9	2.5	A-A' E-E'		10 9	2.5 .7	estimated 110	110-140 not seen		Determined from reflection data. No reflection data available.
O-H - β 5.9 km north of Reindeer Island (2 holes)	70° 32.29 148° 19.64	17	10-12	G-G'		3	2.4	24-25	30		Hard clay above permafrost layer.
O-H - γ Sag Delta	70° 25.46 147° 57.90	7.6	18.3	M-M'		5.5	<.2	25	20-30		Material type in drill hole identified as hard clay or ice-bonded clay.

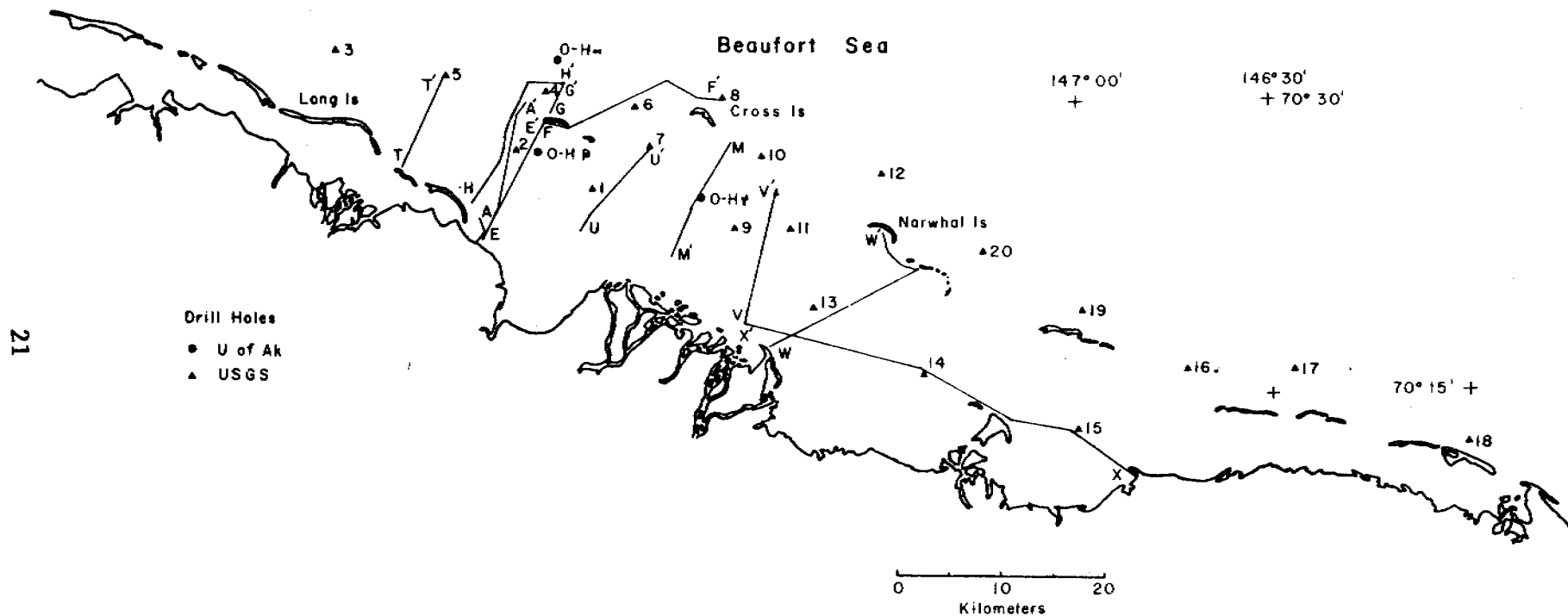


Figure 6. Map showing seismic lines and drill holes discussed in Table I.

Eleven of the drilling sites are within one kilometer of the geophysical lines with which they are compared. These data are expected to correlate the best of all the data. The following six of these eleven holes correlate well with the geophysical data: (Harding-Lawson) HL-2, 5, 7, 8, 14 and (Osterkamp-Harrison) OH- α . Two of the eleven holes, HL-4 and HL-15, showed thin frozen materials (0.12 and 3.5 m thick respectively) present but the geophysical data did not indicate any fast materials present. This is to be expected in that thin layers of frozen material will not support refracted energy and therefore they will be invisible to the refraction technique. Thus the drilling and geophysical data at these two holes are judged not to be in disagreement. Of the 18 correlations made only two holes demonstrated thin frozen materials present. In general the permafrost was continuous in the vertical direction and did not consist of a series of layers or even one thin layer.

Two of the eleven holes (HL-9 and HL-13) were similar in that the drilling data indicated relatively shallow frozen material (13.8 m and 15.1 m respectively) while the seismic data indicated a deeper frozen layer in each case (23.8 m and 29.6 m respectively). Both of these sites were visited by us with our boat in tow of the USGS vessel "Karluk" in order to take advantage of their high precision location equipment. Thus the drilling and geophysical data were gathered within a few hundred meters of each other. Ten refraction measurements were averaged for comparison with the data at HL-9 and 6 refraction measurements were averaged for comparison with the data at HL-13. The depths indicated by the geophysical data are self-consistent and we believe represent a continuous bonded material. The records taken while in tow of the Karluk were generally noisier than our normal records due to tow noise and the noise caused by the "Karluk" but this is not believed to be the cause for the discrepancy. One possible explanation is that there may be isolated frozen

material that is 10 to 15 meters above the continuous bonded materials observed by the refraction method. Such isolated patches of bonded material would probably not be observed by the refraction system.

The final drill site of the eleven that are in close proximity to seismic lines is HL-6. No bonded materials were indicated by the drilling investigations while the geophysical data indicated permafrost at 28 m depth. It will be seen in a later figure that this core hole is approximately at the site of the shallow permafrost boundary and that it is more southerly positioned than the seismic data with which it is correlated. We therefore believe the discrepancy between the geophysical data and the drilling data can be accounted for by the presence of the shallow permafrost boundary.

Seven of the drill sites listed in Table I are located at distances greater than 1 km from the seismic data with which they were compared. The depth to bonded materials determined by drilling and by seismic methods compares quite well for five of these seven sites. These favorable comparisons were obtained at sites HL-1, 10, 11 and O-H α , β . The depth data from site HL-12 which is approximately 3.5 km from the seismic data taken at seismic line N-N" do not correspond. It is concluded that permafrost conditions at these two sites are different. The final comparison, at HL-3, is made with data that were taken 10.5 km from the drill site. These data do not conflict. That is, our previous interpretation of an area free of shallow permafrost at HL-5 and to the west of that location is supported by HL-3. Additional lines adjacent to HL-3 are anticipated next field season.

Offshore Island Studies:

Seismic refraction studies were conducted during the summer of 1979 on Jeanette Island, Karluk Island, and Narwhal Island which are located along the Beaufort Sea coast near Prudhoe Bay. The experimental techniques

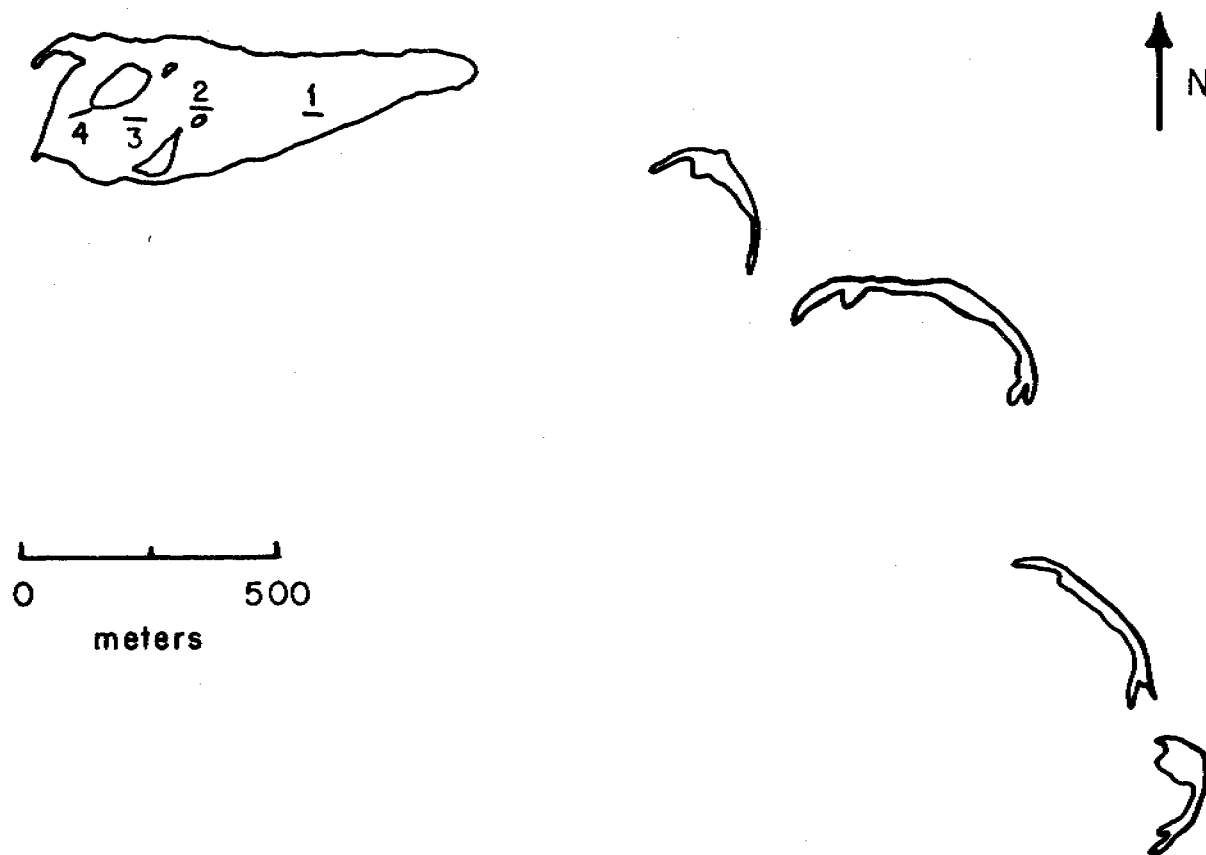


Figure 7. Location of Narwhal Island refraction work. Drawn from NASA U2 photograph of Narwhal Island and associated constructional features taken 15 July 1979. (Courtesy of Dr. Jan Cannon)

and equipment used were similar to those used in earlier work (Rogers *et al.*, 1975; Rogers and Morack, 1978). Areas underlain by both frozen and unfrozen material were located on the islands.

Narwhal Island

Figure 7, showing Narwhal Island, indicates the site of refraction studies during August 1979. Approximate locations of seismic lines are shown on the figure. Their orientations, which were established with a compass, are approximate.

Karluk and Jeanette Islands

Two seismic lines were taken near the eastern end of Karluk Island and two lines were taken on the eastern end of Jeanette Island. None of these lines gave any indication of a fast refractor.

A summary of the maximum velocities measured on these island is presented in Table II along with calculated values of the depths observed to the high velocity layer. The errors indicated are the standard deviations of the straight line fits to the time-distance plots of the seismic data.

Table II

Island	Line #	Maximum Velocity m sec ⁻¹	Depth to Maximum Velocity Layer m
Narwhal	1	3115 ± 214	1.9 errors .1
	2	3261 ± 100	2.0
	3	2055 ± 54	2.0
	4	1646 ± 29	1.0
Karluk	1	1515 ± 69	1.2
	2	1471 ± 71	4.1
Jeanette	1	1828 ± 261	5.6
	2	1429 ± 19	1.8

None of the lines taken on Jeanette Island or Karluk indicates a fast refractor. These islands are constructional features, are probably migrating rapidly landward, and are probably not underlain by bonded permafrost. It

U.S. GEOLOGICAL SURVEY
 WASHINGTON, D.C. 20548

is noteworthy that the Line 2 on Jeanette indicated a refracting layer at 5.6 meters in depth. This line can be used as an indication of the minimum penetration for the hammer seismograph system. We estimate the penetration depth to be 5 to 8 meters for a 30 meter seismic line.

Lines 1 and 2, taken on the eastern half of Narwhal Island, indicate bonded permafrost at a depth of 2 meters. From Figure 7 one can see that the island has eroded into several smaller islands to the east. These remnants are migrating rapidly landward, much like Karluk and Jeanette Islands and are probably not underlain by bonded permafrost. The eastern end of the largest remnant is probably the most stable part of the whole island system and is underlain by ice-bonded materials. The western end of this remnant has several large bodies of water, covered with very coarse gravel and is not underlain by ice-bonded material.

VII. DISCUSSION

A. Marine Investigations.

Figure 8, a Prudhoe Bay area map, indicates our interpretation of the marine refraction taken to date. The shaded areas on the map indicate the location of shallow submarine permafrost. In all cases the observed permafrost is 50 meters or less beneath the water surface and in most cases it is 40 meters or less beneath the water surface. Areas where refraction lines have consistently shown high velocity refractors (velocities greater than 2500 m/s) have been connected together to indicated probable regions of continuous bonded permafrost. The area north of Cross Island is an example of such a region. Where refraction lines have only sporadically shown bonded materials, local

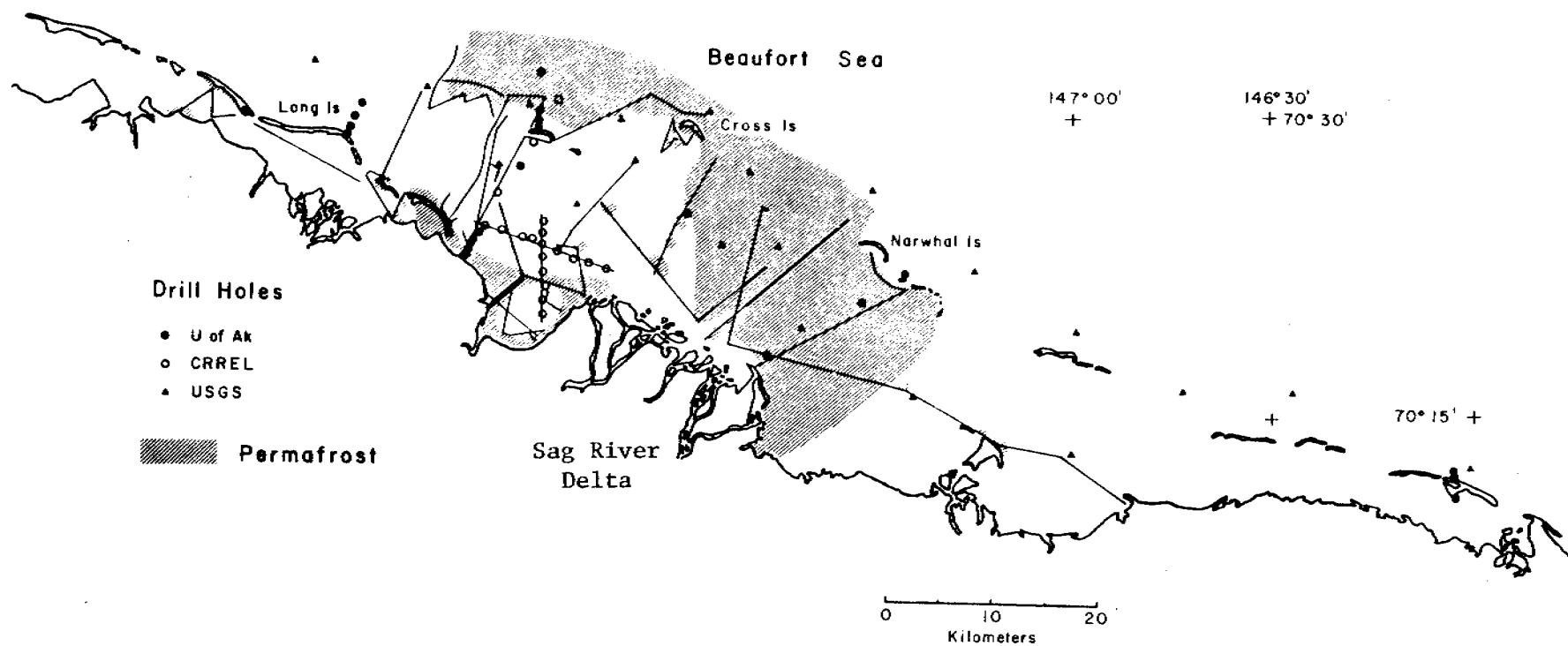


Figure 8. Shallow offshore permafrost in the Prudhoe Bay area as determined from geophysical data.

shading has been used to indicate the sporadic nature of the observation. The shaded patches between Cross Island and the Sagavanirktok River delta are examples of this interpretation.

Correlation has been made with geological information supplied by the recent shallow offshore drilling program of the conservation division, U.S. Geological Survey. This correlation is generally supportive of the seismic interpretation as is seen in Table I.

The area south of Cross Island is particularly interesting as it is an area that is free of continuous shallow permafrost. The area seems to originate at the mouth of the Sagavanirktok River and to proceed eastward. It remains south of the outer Barrier Islands and has been mapped as far east as Long Island. It is possible that this may be the site of the Sagavanirktok River channel in previous times when the ocean shoreline was considerably to the north of its present location. Smith and Hopkins (1979) suggested that paleo valleys excavated by major rivers may be the present sites of deeply thawed materials offshore. In earlier reports we discussed the possibility that former river valleys, which are presently submerged offshore, might provide regions free from shallow permafrost. These regions might be selected for permafrost free burial of offshore facilities such as pipelines. No other possible river valley, as delineated by the absence of shallow permafrost, appears to exist near the present delta of the Sagavanirktok River. We believe this fact lends support to the interpretation that the river once flowed to the east toward Long Island on its way to the ocean.

Regions where bonded materials occur at depths greater than 50 meters have not been included because we have little information at these depths.

(The present refraction system is depth limited due to energy limitations.)
However, deeper permafrost is known to occur in the area between the West Dock and Reindeer Island (see our April 1, 1978 Annual Report).

B. Island Investigations.

The fact that ice-bonded permafrost exists beneath several islands in the Beaufort Sea has been determined from seismic data taken during the past three summers and confirmed by shallow probing and drill holes. The presence of permafrost beneath these islands will be an important consideration in their anticipated uses for offshore resource development.

It is possible that specific information on the distribution and depth of permafrost beneath the offshore islands will help in understanding the complicated physical processes which are causing the islands to slowly migrate. A more detailed understanding of these processes coupled with the permafrost information will also be needed before the complete geological history of the area can be determined.

The area between the Coville River in the west and the Canning River to the east contains several chains of barrier islands, and it is this area where most of the data has been taken. Some additional data has been taken near Point Barrow.

The research of Shackleton and Updyke (1973) suggests that the world sea level fell to a minimum level during the late Wisconsin period about 18,000 years ago. During this period of low sea level, permafrost was formed under much of the present continental shelf in the Beaufort Sea.

As the sea level rose due to glacial melting, a set of distinctively Arctic processes began to erode the coastline along the Beaufort Sea. Ice-rich Pleistocene sediments subject to localizing thawing were effected by thermokarst collapse. As the excessive ground ice was melted, it led to

a collapse of the material and thaw lakes were formed. These thaw lakes grew and were overrun by the receding coastline, forming a highly crenulated shoreline. Along the coast, where the bluffs were composed of ice-rich sediments, a combination of thermal and wave erosion led to a slow disintegration of the coastline. These processes continue today and are eroding the coastline an average of approximately 1.5 meters a year in the Beaufort Sea (Hopkins and Hartz, 1978).

As the coastline receded, areas which were higher were left as islands. These high tundra remnants are formed of Pleistocene sediments having frozen cores. In some cases, areas of thick peat accumulations have slowed the erosion processes since these materials are resistant to wave attack. Examples of this kind of island are Flaxman, Tigvariak, Pingok, and Cottle Islands. These islands are still covered by tundra vegetation and are underlain by relict permafrost. Thermal and wave action are even today eroding away the shoreline of these islands.

Many of the islands, which were initially high tundra remnants, have been eroded by the processes discussed earlier over a long enough period that the fine sediments have been washed away, leaving only accumulations of sand and gravel. These erosional remnants are not static, but are migrating generally westward and landward due to a complicated process involving wave motion, currents, winds and ice rafting. Examples of such constructional islands where seismic data has been taken are Cross (1977, 1978), Narwhal (1980), Jeanette (1980), Karluk (1980), Stump (1978), and Reindeer Islands (1977). These islands are the most interesting from a scientific standpoint since the processes involved are not completely understood. The details of the data collected on these islands can be found in past annual reports as indicated above.

The seismic reconnaissance on the several barrier islands listed above indicates that they are no longer all completely underlain by bonded permafrost. Indeed, Jeanette and Karluk Islands appear to be rapidly migrating and are free of bonded permafrost. Cross, Narwhal and Reindeer Islands are partially underlain by bonded permafrost and Stump Island, which is very near shore, is entirely underlain by bonded permafrost. Additional permafrost data coupled with a better understanding of coastal recession and island migration may complete our understanding of the dynamics of these barrier islands.

VIII. CONCLUSIONS

We summarize below a series of conclusions from past reports with appropriate modifications resulting from more recent data. The somewhat limited geographical coverage to date means that the conclusions are perhaps regionally limited. However, the conclusions are certainly appropriate to the very important offshore area adjacent to existing Prudhoe Bay oil fields.

- A. The depths to permafrost reported here and in past reports are supported by drilling evidence. No data have been compiled on the permafrost thickness but the shallow drill data compiled by Harding-Lawson indicate the bottom of bonded materials to be deeper than their drill penetration (maximum 90 meters) in all cases. Also, almost all bonded materials were found to be monolithic in the vertical direction, only one case of a thick non-frozen layer in the bonded materials was reported.
- B. At least two occurrences of relative shallow submarine permafrost (7 m and 8 m beneath the ocean bottom in water depths of 10 m and 6 m

respectively) have been observed at distances up to 18 km from shore. We have also detected permafrost at depths of 140 m at distances of 8 km from shore. Thus the surface of the bonded materials is seen to be highly irregular and local studies of permafrost conditions will be necessary for sub-bottom engineering designs.

- C. The existence of paleo vales which may present large depressions in the permafrost surface or the absence of permafrost in these areas has been suggested previously (Hopkins, 1978). It appears such a valley exists just offshore of Prudhoe Bay between the present mouth of the Sagavanirktok River and the area north of Long Island.
- D. Prudhoe Bay appears to be an old thaw lake (see our 1978, 1977 annual reports) and therefore presents a large dip or possibly a window in the surrounding bonded permafrost surface. Both thermal and seismic data support this conclusion. It seems likely that there are other old thaw lakes offshore along the Beaufort Seacoast.
- E. Seismic reconnaissance on six barrier islands indicates that they are not all underlain by continuous bonded permafrost, but that some are free of ice-bonded permafrost. This fact is dependent upon the history of the islands, the size of any particular island, its migration rate and soil types. We have observed continuous bonded materials beneath Stump Island along its entire length. In contrast, no high velocity refractors have been observed on Reindeer Island. Jet drilling on the island indicates a highly variable material beneath this island some frozen and some not frozen (conversation with Will Harrison). We have observed high velocity refractors on portions of Cross Island and Narwhal Island but none on Jeanette or Karluk Island. Thus, the islands seen to be highly variable with regard to their permafrost conditions.

It is clear that islands which are former land remnants, Cottle and Flaxman for example, are underlain by continuous bonded materials.

F. Several island sites have been studied where seismic velocity data and drilling data seem not to agree; drilling evidence indicated frozen material, but refraction velocities were not high. Our conclusion is that ice-bearing materials should be distinguished from ice-bonded materials. The distinctions between ice bearing and ice-bonded is important from the standpoint of material properties. For example, an ice-bonded material may have a high resistance to shear stress, but the same material when not ice-bonded may have little shear resistance. An important parameter affecting offshore permafrost is temperature; in contrast to permafrost on land it is relatively warm and consequently more thermally fragile. This fact coupled with the presence of salt water accounts for some of its local variability.

IX. NEEDS FOR FURTHER STUDY

The extensive drilling program conducted by the U.S. Geological Survey, provided 20 core holes for correlation with the seismic data. Refraction lines will be run in the locations not yet visited, principally to the east of past work areas. This will extend the geographical coverage of our work.

Another feature requiring further investigation is the possible existence of a paleo valley at the mouth of the Sagavanirktok River. Additional lines need to be run in the vicinity of and to the west of Long Island.

Erk Reimnitz (personal communication) has indicated the possibility of shallow gas in the vicinity of Harding-Lawson core hole #11. Our records will need to be examined for possible confirmation of this interpretation.

X. SUMMARY OF LAST QUARTER

FIELD WORK:

None

DATA COLLECTED:

None

ANALYSIS:

Reduction and interpretation of the data taken during the last field season have been completed and estimates of regional permafrost distributions have been prepared. Correlation of seismic refraction, down hole seismic records and drilling data at core hole #9 has yet to be accomplished.

APPENDIX AI

SOURCES OF ERROR IN REFRACTION RESULTS

Several possible sources of error can be identified that affect the determination of permafrost depth. The effects of these errors can best be described in terms of the time distance plots. Many of the errors are random; these probably affect each data point on the time distance plot differently. However, some of the possible errors are systematic. The sources of error are discussed below. The magnitude of the possible systematic errors on the permafrost depth calculation is estimated in each case. The effects of the random errors on the depth estimate are more difficult to determine. An estimate of the aggregate of these effects is made by considering a particular time distance plot and by determining the standard deviation in depth.

A. Equipment, Geometry:

1. Slack hydrophone cable, reduced cable length. Distributed slack in the hydrophone cable systematically increases the error in the distance to each hydrophone as one proceeds away from the boat. The data in Figure AI indicate permafrost at a depth of 26 m. We can estimate the effect of cable slack upon the interpretation by systematically moving each data point in Figure AI to the left by 10% of its distance from the ordinate axis. The velocities are again calculated and a new permafrost depth is determined. The result is a permafrost layer velocity that is 10.9% lower than actual and an upper material velocity that is 10.5% lower than actual. The new permafrost

depth is 23.3 m; a figure 10.5% smaller than before. Thus the percent error in the depth calculations is approximately equal to the percent shortening in the cable length.

2. Streamer curvature in the horizontal plane. Hunter et. al., (1976) determined the effect of streamer curvature on apparent velocity. A streamer positioned in water to lie along a circular arc with radius equal to one hydrophone cable length was considered. Using their time-distance curve to determine an apparent water velocity, a value of 1650 ms^{-1} is determined which is 10.2% higher than the actual velocity. The curvature presumed for this case is very noticeable to the boat operator as the streamer tail buoy will be seen almost 29° off a line through the length of the boat. After considering our field operations we estimate that curvature effects may amount to perhaps a 5% error in our velocity determination. Curvature and cable slack will have the same effect on the depth estimates. We therefore estimate our depth determinations may be too small by perhaps 5% as the result of cable curvature.
3. Streamer-source separation not maintained. Errors of this type will affect the time distance plot in a predictable manner: a straight line fit to the data from the top layer will not project through the origin of the time distance plot. Thus, the effect is observable and has been eliminated.
4. Wave effects and random variation in boat direction. The random displacement of the hydrophones from their presumed position will cause a random variation in the data point location. Although the effects of this error are difficult to estimate it is believed that they are not significant compared to A1 and A2 discussed above.

It should be noted that the aggregate effect of wave and boat direction perturbation is to shorten the effective cable. Thus this error would be expected to contribute slightly to a permafrost depth calculation that is too shallow.

B. Equipment, Timing:

1. Shot time in error. The time distance plot will be affected in a manner similar to A3 above.
2. Random error in seismograph timing. Data points on the time distance curve can be expected to vary in a random manner about their true position due to random timing error and no systematic error in depth determination will result.
3. Scaler error in timing. The timing of the seismographs used was accurate within at least 1%. A 1% scaler error in timing will affect the velocity determinations by 1% and the relationship is inverse: a 1% smaller time scale will result in a 1% larger velocity. As the result of such an error, the data points on the time distance curve will be shifted systematically in a manner similar to that discussed in A1. Consequently, the percent error in permafrost depth determination is approximately equal to the percent error in the time scale, except that a larger time scale results in a smaller depth estimate.

C. Operator Scaling First Breaks:

1. Random scaling errors. Given the presence of noise on the seismograph records and the fact that a data scaler can't always pick a first break exactly some random scatter is expected in the time distance plot. No systematic error in depth determination will result from these errors.

2. Fixed scaling error. Such errors are the result of the data scaler consistently picking the first break early or late. The result is the same as A3 above.
3. Diminishing signal strength effects. The signal received at the hydrophones farthest from the source are weakest. The effect of the attenuation is that the data points farthest from the source will be subject to more uncertainty due to background noise. No systematic effect on the depth determination is expected to result from this fact. However, it is possible that the data scaler might miss the first break due to weak signal strength and pick the second cycle of the first arrival. Such an error should be plainly visible in the time distance curve as a vertical offset and that part of the data would not be used to determine permafrost depth. In our experience this is not a common error.

D. Reduction of Time-Distance Plot:

1. Analytical technique. All time distance plots which are prepared by scaling the seismic records are fitted with straight lines by a computer operator. The judgement of the operator is required to arrive at the final interpretation of the data and no quantitative rules will alone suffice. Since the straight line fits are not graphical this part of the analysis is exact.
2. Variability of velocity data obtained from time-distance plot.

In order to provide some estimate of the possible variation in velocity that might be calculated from a time distance plot the data shown in Figure AI were analyzed in the following manner. Two data points, points a and b in Figure AI, were used to determine the permafrost velocity and this velocity (2333 ms^{-1}) was plotted on Figure AII-a. Points a, b and c were used to determine another velocity (3336 ms^{-1}) which is also plotted in Figure AII-a. In this manner

Line 14-81, Tape 2540
1977, Segment #2

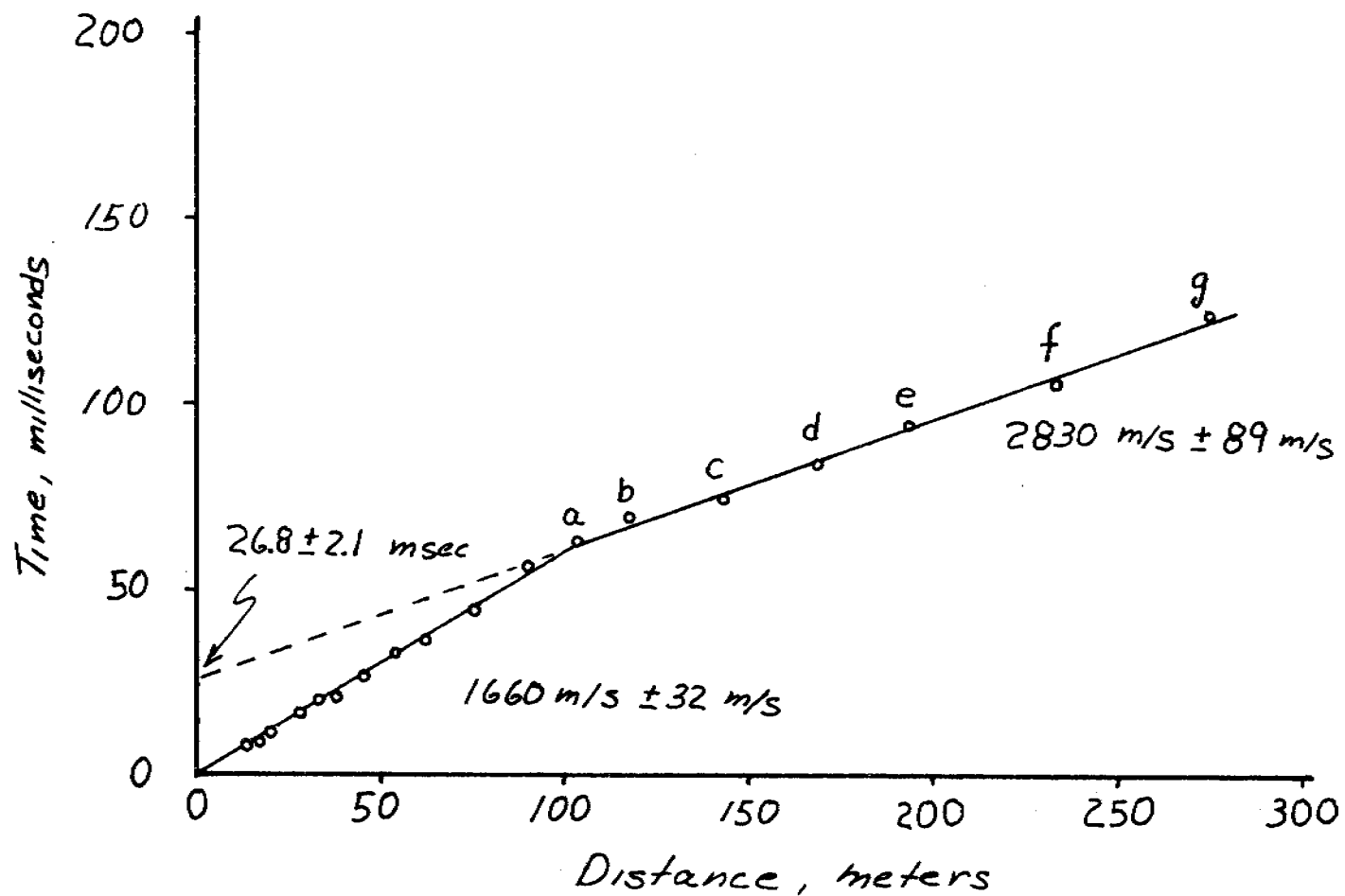
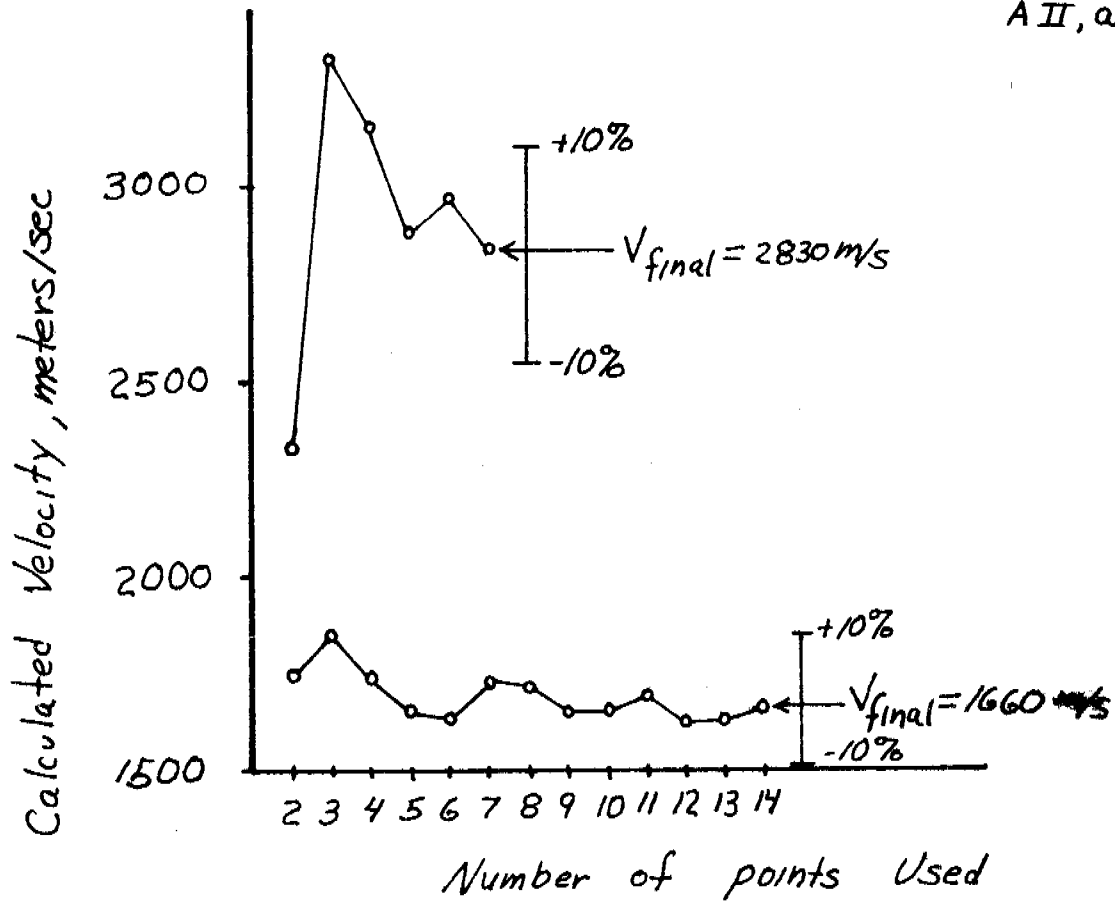


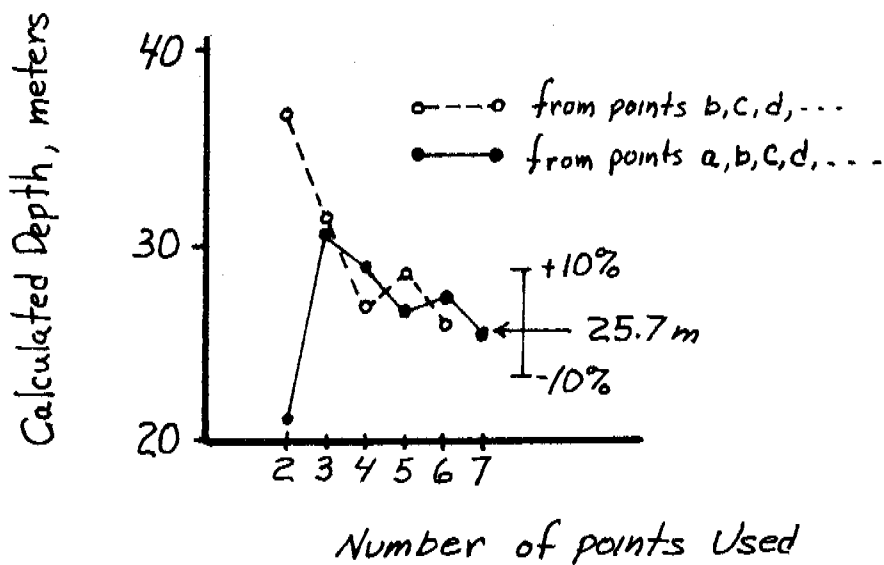
Figure AI. Time distance plot used to demonstrate possible range of uncertainty in permafrost depth determination. Individual data points a through g are marked for use with Figure AII, b.

A II, a



a. Dependence of the velocity calculated from time-distance plot upon the number of data points used in the calculation.

A II, b



b. Variability of depth calculated to permafrost, seismic data taken from Line 14-81.

FIGURE A II, a and b

6 velocities were plotted. Scatter in the data points about a straight line results in the first two velocities being considerably different from the final velocity obtained from points a through g (2830 ms^{-1}). The third velocity is 11.8% from the final value while the fourth and fifth points are well within 10% of the final value. A similar approach was used to calculate the velocity for the low velocity portion of the time distance curve shown in Figure AI. The results of these calculations are plotted as the lower curve in Figure AII-a.

3. Variability of permafrost depth determination. Figure AII-b indicates the dependence of the calculated permafrost depth upon the number of data points used in the calculation. The analysis was performed in a manner similar to that described in section D2 above. In this case two different initial points, a and b, were used for calculation. The last seven values calculated for permafrost depth are seen to be within 10% of 25.7 m, the value judged to be most reliable since it utilizes the most data points.

The aggregate sum of the errors discussed above can be estimated if we combine the cumulative errors with the random errors by simple addition. We approximate the cumulative effect of the random errors with a $\pm 10\%$ uncertainty in the depth determination. The rationale for this approach is that the time distance plot of Figure AI is judged to be typical of most records indicating permafrost and all such records will contain the effects of the random errors discussed above. The cumulative errors are: -5% due to cable slack, -5% due to cable curvature and $\pm 1\%$ due to timing errors. The effect of the cumulative errors is $-11\% \pm 1\%$ and the total error estimate is $-21\% \pm 11\%$.

No separate estimate of the effects of random variations in material properties has been made. No doubt some of these effects are embodied in the above random error estimate but it is not clear how to separate these effects from other random effects discussed above.

SOURCES OF ERROR IN REFRACTION RESULTS, METHOD # 2

In order to obtain another estimate of the random errors, the standard deviations of the intercept and inverse slope of the lines shown in Figure AI were calculated. These errors were then used to obtain the standard deviation in the calculated depth. This technique gave a value of 26.4 ± 2.0 m which is an uncertainty of $\pm 8\%$. The data shown in the figure are typical of the many records indicating permafrost, and this uncertainty is judged to be typical of the random error associated with the data.

The cumulative errors in the depth to the permafrost are thus estimated as -5% due to cable slack, -5% due to cable curvature, and $\pm 8\%$ due to random errors. This method gives a range of uncertainty from -18% to $+8\%$ and is believed to provide a reliable estimate of the uncertainty in the depth calculation. The first method of analysis discussed above provides a physical understanding of the uncertainties in the depth estimate and supplies bounds on the depth estimate that include the results obtained by the second method. We use the results of the second method to indicate uncertainty in our depth determination.

REFERENCES

- Barnes, P.W., and Hopkins, D.M., eds., 1978, Geological Sciences, in Environmental Assessment of the Alaskan Continental Shelf, Interim Synthesis; Beaufort/Chukchi: National Oceanic and Atmospheric Administration and U.S. Bureau of Land Management, Boulder, Co. p. 101-133.
- Chamberlain, E.J., Sellmann, P.V., Blouin, S.E., Hopkins, D.M., and Lewellen, R.T., "Engineering Properties of Subsea Permafrost in the Prudhoe Bay Region of the Beaufort Sea", 3rd International Conference on Permafrost, Vol. 1, Edmonton, Alberta, Canada, 1978.
- Grant, West, "Interpretation Theory in Applied Geophysics", McGraw-Hill, 1965.
- Harding-Lawson Geotechnical Investigation, Beaufort Sea, Alaska, 1979. Report to US Geological Survey, Conservation Division, Anchorage office, July 1979, Volume I, II, III.
- Harrison, W.D., and Osterkamp, T.E., 1979, "Subsea Permafrost: Probing, Thermal Regime and Data Analysis vs. National Oceanographic and Atmospheric Administration", Environmental Assessment of Alaskan Continental Shelf, Principal Investigators. Reports for year ending March 1979.
- Harrison, W.D., Osterkamp, T.E., "Coupled Heat and Salt Transport Model for Subsea Permafrost", University of Alaska, Geophysical Report UAF 247, U of A Seagrant Report 76-15.
- Harrison, W.D., and Osterkamp, T.E., 1978, "Heat and Mass Transport Processes in Subsea Permafrost I: An analysis of Molecular Diffusion and its Consequences", Journal of Geophysical Research, Vol. 83, No. C9, p. 4707-4712.
- Hopkins, D.M., Hartz, R.W., Smith, D.A., and Nelson, R.E., "Offshore Permafrost Studies and Shoreline History of Chukchi and Beaufort Seas as an Aid to Predicting Offshore Permafrost Conditions". Quarterly Report OCSEP, Dec. 1978.
- Hunter, J.A.M., Hobson, G.D., "A Seismic Refraction Method to Detect Subsea Bottom Permafrost", Beaufort Sea Symposium Proceedings, Arctic Institute of North America, San Francisco, J.D. Reed, J.E. Sater, Eds., 1974.
- Hunter, J.A.M., "The Application of Shallow Seismic Methods to Mapping of Frozen Surficial Materials, Permafrost," Second International Conference, 1974.
- Hunter, J.A.M., Neave, K.G., MacAulay, H.A., Holson, G.D., "Interpretation of Sub-bottom Permafrost in the Beaufort Sea by Seismic Methods, Part I." 3rd International Conference on Permafrost, Vol. 1, Edmonton, Alberta, Canada, 1978.

- Lewellen, R.I., "Offshore Permafrost of Beaufort Sea, Alaska". The coast and shelf of the Beaufort Sea, Arctic Institute of North America, J.D. Reed and J.E. Sater, Eds., 1974.
- Osterkamp, T.E., Harrison, W.D., 1976. "Subsea Permafrost at Prudhoe Bay, Alaska: Drilling Report", University of Alaska, Geophysical Institute, Scientific Report, UAGR 245.
- Rogers, J.C., Harrison, W.D., Shapiro, L.H., Osterkamp, T.E., Gedney, L.D., Van Wormer, J.D., 1975. "Near Shore Permafrost Studies in the Vicinity of Point Barrow, Alaska." University of Alaska, Geophysical Institute Scientific Report, UAGR 237.
- Rogers, J.C., Morack, J.L., 1978. "Geophysical Investigation of Offshore Permafrost, Prudhoe Bay, Alaska." Permafrost, Third International Conference, 1978.
- Sellmann, P.V., Chamberlain, E., Arcone, S., Blouin, S., Delaney, A., Kneave, K.G., "Delineation and Engineering Characteristics of Permafrost Beneath the Beaufort Sea" OCSEAP Annual Report, RV 105, April, 1979.
- Sellmann, P.V., Lewellen, R.I., Ueda, H.T., Chamberlain, E., Blouin, S.E., 1976. "Operational Report 1976 USACREEL-USGS Subsea Permafrost Program Beaufort Sea, Alaska," U.S. Army Cold Regions Research and Engineering Laboratory, Hanover, New Hampshire, SR 76-12.
- Shackleton, M.J., and Updyke, N.D., Quaternary Research, V. 3, pp. 39-55, 1973.
- Smith, P.A., Hopkins, D.M., 1979, "Offshore Permafrost Studies and Shoreline History of Chukchi and Beaufort Seas as an aid to Predicting Offshore Permafrost Conditions", U.S. National Oceanic and Atmospheric Administration, Environmental Assessment of the Alaskan Continental Shelf, Annual Report of Principal Investigators for the year ending April 1979.

Annual Report
1979-1980
Research Unit #327

Shallow faulting, bottom instability, and movement of
sediment in lower Cook Inlet and western Gulf of Alaska

Monty A. Hampton
U.S. Geological Survey
Menlo Park, California

April 15, 1980

I. Summary of Objectives, Conclusions, and Implication with Respect to OCS Oil and Gas Development.

Kodiak Shelf: A synthesis of geologic data collected over the past four years shows several environmental conditions of concern to resource development. This area of tectonism poses problems of fault movement, strong seismic ground shaking, and seafloor deformation. The shelf-break area shows evidence of tectonic segmentation (areal concentration of epicenters and structural deformation), implying areal variation in the severity of tectonic hazards.

Inferred sediment dispersal patterns indicate that pollutants incorporated into bottom sediment could be concentrated in troughs that trend transversely across the shelf. Fields of large sand waves have been identified, indicating potential erosion and loading problems for seafloor installations.

Most shelf sediment appears to be strong and stable under existing environmental forces. Gas-charged sediment has been found at several locations, but it shows no evidence of instability. Large sediment slides have been identified just beyond the shelf break.

Lower Cook Inlet: Sedimentological studies conducted since 1976 within lower Cook Inlet, Alaska, a large tidally dominated embayment, have delineated six major depositional environments. The environments are: high-energy shoreface, trough-edge platform, trough slope, trough floor, trough-mouth plateau, and seaward progradational ramp. Common to these environments are sandy sediments concentrated in sand patches, sand ribbons and sand-wave fields as well as coarser sediments found as mixed cobble-sand "hard bottom" and sand-shell-gravel complexes. The distribution of the modern surficial sediments is controlled primarily by the strength of the tidal current regime.

Sea level rise since the last major glacial advance has led to the modern high-energy tidal environment of lower Cook Inlet. Sand and gravel are being deposited while older glacial sediments are being winnowed. High-resolution seismic-reflection evidence indicates that Holocene sediments are deposited upon a strongly glaciated topography. Numerous buried or partly buried channels are present on the platform areas.

Four primary sedimentologic units are recognized in the shallow stratigraphy on the basis of high-resolution geophysical data. Unit D represents unsorted glacial sediments that overlie the glaciated basement and locally exceeds 75 meters in thickness. On high-resolution seismic records, Unit D is characterized by irregular discontinuous reflectors. Overlying Unit D is a thin unit, Unit C, which has a high acoustic reflectivity and is thought to be a layer of glacial outwash sediments. Unit B locally overlies Unit C and is composed of large-scale sand-wave complexes. Unit B appears to be limited to trough floor, trough-mouth plateau and seaward progradational ramp environments. The uppermost unit, Unit A, overlies Unit B or Unit C. It is acoustically identified by its pattern of flat-lying multiple reflectors and is considered to consist of intercalated layers of sand and silt. Unit A is present only where hydrodynamic energies are low.

II. Introduction

A. General Nature and Scope of Study: Assessment of the environmental geologic hazards, sediment types and sediment distribution in lower Cook Inlet and on the Kodiak shelf, western Gulf of Alaska.

B. Specific Objectives: The identification of active surface faults, and areas of sediment instability, the relation of sediment types to bottom morphology and circulation patterns, and study of types and movement of bedforms.

C. Relevance to Problems of Petroleum Development: Active faulting and sediment instability are potential dangers to offshore structures. The relation between morphology and sediment characteristics will identify the presence of areas where erosion is more active than deposition and areas that are sediment traps and consequently may act as sinks for pollutants as well as nutrients. Transport of sand over bedforms likely will increase once the sediments are stirred up by anchoring and trenching activities thereby removing fine clay and organic matter that presently decreases the natural erodibility.

III. Current State of Knowledge: See attachments A and B.

IV. Study Area:

1) Lower Cook Inlet between Shelikof Strait at latitude $58^{\circ}40'N$ and Cape Ninilchik at latitude $60^{\circ}00'N$, mainly encompassing OCS lease-sale area 60.

2) Kodiak Shelf between Amatuli Trough at latitude $59^{\circ}00'N$ and southern Albatross Bank at latitude $56^{\circ}40'N$, mainly encompassing OCS lease-sale area 46.

V. Sources, Methods, and Rationale of Data Collection

Data were collected during cruises in 1976-1979, aboard the R/V SEA SOUNDER. Some additional data came from copies of a 1976 Petty-Ray Geophysical, Inc. survey made under contract to the U.S. Geological Survey, Conservation Division in Anchorage. Additional high-resolution seismic records were collected by R. von Huene aboard R/V S.P. LEE during his 1976 survey off Kodiak.

Seismic and sampling methods have been discussed by Bouma and Hampton (1976) and Hampton and Bouma (1976). The rationale for collecting data with the instruments and equipment described in the above-mentioned U.S. Geological Survey Open-File Reports is that such procedures are the only ones generally recognized to achieve the proposed objectives.

VI, VII, VIII, Results, Discussion, and Conclusions: See attachments A and B.

IX. Needs for Further Study

Lower Cook Inlet: The field work conducted to date provides enough

information about geo-environmental hazards within lower Cook Inlet proper. Shelikof Strait, also included in OCS sale 60, has received only minimal study and needs further general environmental analysis.

Kodiak Shelf: The area of Tugidak Basin, between and northwest of Chirikof Island and Trinity Islands is a potential petroleum source and needs environmental work. The rest of the shelf has received adequate study.

X. Summary of January-March Quarter:

Synthesis of all available environmental data for both lower Cook Inlet and Kodiak Shelf was conducted.

ATTACHMENT A

SYNTHESIS REPORT: ENVIRONMENTAL GEOLOGY OF KODIAK SHELF

By Monty A. Hampton

INTRODUCTION

Environmental geologic studies of Kodiak Shelf, western Gulf of Alaska, have been conducted in support of the federal government's outer continental shelf petroleum leasing program (Fig. 1). Geological and geophysical data were gathered aboard the R/V SEA SOUNDER on four cruises in 1976-1979. Seismic reflection surveys were run along 8200 km of trackline, using combinations of 30-to 160-kilojoule sparker, 800-joule boomer, and 3.5- and 12-kilohertz high resolution systems (Fig. 2), and limited side-scanning sonar and underwater photography and television work was done. Sediment samples were gathered at 158 stations (Fig. 3). High resolution records contracted in 1976 and 1977 by the U.S. Geological Survey Conservation Division over about 10,000 km of trackline were also used.

The approach to this environmental analysis was through examination of the surficial and shallow sub-surficial geology. Initial field work was a reconnaissance to characterize the regional geology, and to identify the types of problems existing on Kodiak Shelf and to generally delineate areas of their occurrence. Succeeding efforts were more topically oriented, with attention focused on specific problem areas.

INSTRUMENTATION AND PROCEDURES

Navigation

The principal navigation system was a Magnavox integrated satellite-Loran C unit. Dead-reckoning positions were computed every two seconds, based on Loran C, the ship's single-axis speed log, and the gyro. The dead-reckoning positions were updated with satellite fixes.

Data were automatically recorded on magnetic tape, displayed on a CRT, and typed out on a keyboard printer. Every 15-minutes the positions were plotted on a 1:500,000-scale chart. For easy reference, a "shot-point" number was given to each 15-minute position. In addition to routine plots, satellite fixes and course changes were plotted. Post-cruise corrections to navigation were made, making use of satellite-update information.

Seismic Profiling and Visual Format Systems

Sparker: Sparker data were recorded on the Kodiak shelf and slope using a Teledyne system, typically at a power of 40 to 80 kilojoules. Seismic signals were received on a Teledyne 100-element, single-channel hydrophone, and the record was printed on a Raytheon model 1900 Precision Recorder. Usually, sweep firing rates were at 2 to 3 seconds. Several different settings were used, but filters generally were adjusted to receive signals between 50 and 200 hertz. Records were annotated at 15-minute intervals with shot-point

number, time (Greenwich Mean Time, GMT), and water depth.

Uniboom: The Uniboom system used four EG&G model 234 power sources of 200 joules, each driving hull-mounted plates. The hydrophone was an EG&G model 265. Data were recorded on an EPC 4100 recorder. Sweep and firing rates were typically at one-half second, and filter settings at about 500 to 1600 hertz. Annotations were made in the same manner as those on the sparker system.

High-resolution: A Raytheon TR-109 3.5-kilohertz seismic system, with a Raytheon 105 PTR transceiver and a CESP-II correlator, was used to gather high-resolution shallow-penetration seismic data, as well as bathymetry. The system operated with 12 hull-mounted transducers, and the data were recorded on an EPC 4100 recorder. Sweep and firing rates were at one-half second. Annotations were made in the same manner as those on the uniboom system.

Bathymetry: A Raytheon TR-73A transducer and a Raytheon 105 PTR transceiver 12-kilohertz system was used to gather bathymetric data, which were displayed on a digital readout and recorded on magnetic tape. Sweep and firing rates typically were at $\frac{1}{2}$ second, and annotations were made the same as for the other acoustic systems.

Record quality: Four factors that significantly affected quality of the seismic records were 1) the typically coarse-grained and hard nature of the unconsolidated surficial sediment, 2) the shallow water depth throughout most of the area, 3) acoustic vibrations from the vessel, and 4) rough seas.

Coarse-grained and hard sediment most severely effected the Uniboom and 3.5-kHz records, causing much of the outgoing energy from these high-frequency systems to be reflected directly from the sea bottom with only a minor amount penetrating through to subbottom reflectors. Some Uniboom records show subtle, irregular traces of subbottom reflectors, which can be traced and correlated only with difficulty. Many 3.5-kHz records show no sign of subbottom reflectors and can be used only as indicators of water depth.

The shallow water depth caused multiples to appear at small distances below the initial sea-bottom reflection, partially or totally obscuring signals from deeper reflectors.

Although these four factors each have a deleterious effect on record quality, it was found by varying ship speeds and filter settings that the nature of the bottom sediments was the main reason for the seismic systems to display "poor" subbottom acoustic reflections on the records. Depth of penetration and details in the record consequently varied with type of bottom and water depth. Except for certain parts, the records allow adequate subbottom interpretation of geology.

Side-scanning sonar: The side-scanning sonar units used were an EG&G analog and digital models, normally operated at a 125-m scale and towed above the bottom at 10% of the scale employed. High quality records were generally obtained. Although most side-scan sonar surveys were run at a ship speed of 4 to $4\frac{1}{2}$ knots, currents could be responsible for a different speed over the bottom.

Normally the Uniboom and 3.5-kHz units were run simultaneously with side-scanning sonar for depth control and possible subbottom information.

Bottom television and bottom camera: A Hydro Products bottom television unit, underwater mercury lights, and a 70-mm camera were mounted in a large frame. Photographic exposures could be made by remote control by the TV-screen observer. A multiconductor cable, leading to the camera and light, was taped at 5-m intervals to the winch cable.

Sampling Devices

Grab samplers: The normal Van Veen grab sampler proved to be too light for adequate sampling of the typically sandy-gravelly bottoms. Generally, successful attempts were obtained with a heavy modified grab sampler designed by Andy Soutar of Scripps Institution of Oceanography.

A four-legged frame housed two vertical rails along which the actual grab could move. The top covers could be opened completely for full access. The addition of weight up to 400 pounds on top of the grab provided sufficient force for the half-round sides to dig into coarse material during the closing operation. When rock fragments got caught between the jaws of the grab, incomplete closure resulted and part or all of the sample was lost. In general the results were good, and this instrument retrieved samples where other devices failed.

Gravity corer: The gravity corer consisted of a 1500-pound weight to which one to three 3-m, 7.6-cm ID steel core barrels were attached. A clear polybutyrate liner was inserted in the barrels, and the sediment was retained by a brass-fingered core catcher.

The cores were cut into 1.5-m sections, and 10-cm long pieces were cut from the ends of some sections for hydrocarbon gas analysis. The remaining core was x-rayed and then split lengthwise into working and archive halves. From the working half, samples were taken for grain size and physical properties. The archive half was described and photographed. Both sections were put into storage tubes that were capped, taped, labelled, and stored under refrigeration.

Sediment Analysis

Subsamples were taken from the upper few centimeters of each grab sample or core, and grain size and compositional measurements were made. Subsamples were wet-sieved into coarse (> 2 mm), sand (2 mm-0.062 mm), and fine (< 0.062 m) fractions. The fine fraction was divided into silt (0.062 mm-0.004 mm) and clay (< 0.004 mm) fractions by the pipette method. Weight percentages of each fraction were calculated.

Splits of each size fraction were examined visually for compositional estimates. Six compositional classes were used: terrigenous minerals and rock fragments (excluding clay minerals), volcanic ash, megafaunal carbonate shells (mostly molluscs), microfaunal carbonate shells (foraminifera), and microfaunal silica (diatoms and sponge spicules). The coarse and sand fractions were examined directly by eye and with a binocular microscope. The

fine fraction was analyzed by mounting grains on a microscope slide, using a mixture of water, glycerin, and malachite green as the mounting medium. Malachite green preferentially stained the clay minerals, facilitating compositional analysis of the fine fraction. The fine fraction was analyzed as a unit; the silt and clay fractions were not separated. The compositional data were tabulated as visual (volume percentages) for individual size classes, but recomputed to weight percents in calculating whole-sediment compositions. Raw data for each size fraction are given in Appendix A, and whole-sediment data are given in Table 1.

Hydrocarbon Gas Analysis

Samples for gas analyses were recovered by means of gravity core, piston core, vibracore, and surface grab sampler. Each sediment sample (0.5L in volume) was placed in an 0.95L can that had two septa-covered entry ports for removal of gas. The can was filled with distilled water that had been purged with helium to remove any dissolved gases. From the can 100 mL of water was removed, and the can was sealed with a double-friction seal top. The 100 mL headspace was purged with helium through the septa. The can was shaken for ten minutes to extract into the headspace gases mainly dissolved in the interstitial water of the sediment. The amount of interstitial water was estimated from the moisture content that was determined later by measuring the weight loss on drying of a sample taken near the sample used for gas analysis. From the can about 5 mL of gas mixture was removed in a gas-tight syringe. Exactly 1 mL of this mixture was injected into a gas chromatograph equipped with both flame ionization and thermal conductivity detectors. The instrument was calibrated by means of standard mixtures of hydrocarbon gases and CO₂. Calculations of gas concentrations were made from peak height measurements on the resulting chromatograms. Partition coefficients were used to correct for differences in gas solubilities, and concentrations are reported as $\mu\text{L/L}$ or nL/L of interstitial water.

TECTONIC, STRUCTURAL, AND STRATIGRAPHIC FRAMEWORK

Kodiak shelf is located on the North America lithospheric plate near its boundary with the Pacific plate. The general tectonic setting is that of a normally convergent margin, as indicated by the presence of a Benioff zone, deep ocean trench, and volcanic arc. The environmental geology of Kodiak shelf is strongly influenced by this setting.

The convergent margin extends westward to the end of the Aleutian islands. But, adjacent to Kodiak Shelf to the northeast, from about Middleton Island to Cross Sound, the margin is obliquely convergent, and then to the east and southeast it becomes a transform margin (Fig. 4; see von Huene et al, 1979).

Kodiak Shelf is the outer portion of a forearc area, comprising two major structural basins separated by an intervening structural high (Fig. 5; see Fisher and von Huene, 1980). The basins and the high are defined by depth to a regional unconformity, 1 to 7 km beneath the seafloor. Strata above the unconformity are younger than middle or late Miocene age. A series of uplifts, commonly truncated by erosion, trends along the shelf break and forms the seaward boundaries of the basins and the high.

Major transverse tectonic boundaries cross the shelf, extending from the northeast and southwest ends of the Kodiak islands (Fig. 5; see Fisher, et al., 1980). Several lines of evidence suggest that the crustal block between the two boundaries stands higher than the blocks on either side. The boundaries appear to involve mostly vertical displacement but there is no indication of fault control. The ultimate geologic nature of the boundaries is unknown.

SEISMICITY

The seismicity of Kodiak Shelf is being studied in detail by Kienle and Pulpan in RU251, and only a summary is given here. The aspects of seismicity that are important for geo-environmental assessment include spatial distribution of hypocenters, recurrence intervals of seismic events, and ground motion characteristics. These are imprecisely understood at the present time, but some general patterns are emerging from the historic record.

The Gulf of Alaska - Aleutian area is one of the most seismically active on earth, accounting for about 7 percent of the annual worldwide release of seismic energy. Most of this energy release is associated with great earthquakes (larger than magnitude 7.8). Since recording of large earthquakes began in 1902, at least 95 potentially destructive events ($M > 6$) have occurred in the vicinity of Kodiak Shelf. These earthquakes are a consequence of interaction between the North America and Pacific plates; in particular along the shallow portion of the Benioff zone that extends from the Aleutian trench to beneath the Kodiak islands (Pulpan and Kienle, 1979).

Great earthquakes in the Gulf of Alaska - Aleutian area occur in a spatial-temporal series. Aftershock zones are non-overlapping and define segments of lithosphere that experience separate episodes of major seismic activity (Sykes, 1971). Certain segments that have recently been inactive are identified as seismic gaps, judged most likely for the next great earthquakes. Estimates of recurrence intervals within segments range from 800 years based on long-term geological evidence (Plafker and Rubin, 1967) to 30 years based on the historic record (Sykes, 1971). The Shumagin seismic gap, as proposed by Pulpan and Kienle (1979), may extend to within a few kilometers of the southwest boundary of sale area 46 on Kodiak Shelf.

The last great earthquake to affect Kodiak Shelf was the 1964 event of magnitude 8.5. The epicenter was in Prince William Sound, a few hundred kilometers to the northeast, but aftershocks covered the entire shelf. Seafloor uplift of 15 m occurred in the central Gulf of Alaska (Malloy and Merrill, 1972) and 7 m on Kodiak Shelf (von Huene et al., 1972).

The historic record shows a cluster of seismic events near the mouth of Kiliuda Trough and nearby on southern and middle Albatross Banks (Fig. 6). The southwestern boundary of this zone is about at the same location as one of the transverse tectonic segments described by Fisher et al. (1980, see Fig. 5) and also near the southwestern extent of aftershocks from the 1964 Alaska earthquake. Other shallow seismicity on the shelf is diffuse and shows no linear trends or alignment along known faults (Pulpan and Kienle, 1979).

SHALLOW STRUCTURES

Shallow folds and faults on Kodiak Shelf trend approximately N45° E, parallel to the Aleutian Trench, except for a few local divergences (Fig. 7). Structures occur in zones, indicating areal variation in the intensity of related environmental concerns on the shelf.

Faults are discerned in high-resolution seismic profiles by offset of the seafloor, discontinuity of reflectors, non-stratigraphic divergences in dip, and occurrence of diffractions. Some faults merge with folds along strike.

A major fault zone extends along the southeast coast of Kodiak Island, both on and offshore (Capps, 1937; Moore, 1967; von Huene et al., 1972), and continues some 600 km to Montague Island in the eastern Gulf. Fault lengths range up to at least 60 km on Kodiak Shelf (Fig. 7), and perhaps up to 140 km (Thrasher, 1979). Faults in this zone are steep and have both landward and seaward dips.

A less extensive zone of faults, with associated large folds, occurs near the shelf break along southern and middle Albatross Banks. A similar structural style exists near the shelf break on Portlock Bank, close to the boundary of our areal coverage, but faults die out and folds become broad and subdued on the intervening area of northern Albatross Bank.

A transverse zone of folds trends across Portlock Bank. These folds are part of a series of structures that may form one of the transverse tectonic boundaries described by Fisher et al. (1980).

Several lines of evidence suggest that the major zones of shallow structures are actively forming and related to modern tectonism. Von Huene et al. (1972) compared bathymetric records before and after the 1964 Alaska earthquake and determined that up to 7 m of uplift occurred on middle Albatross Bank. Fault offset in 1964 was documented on and adjacent to Montague Island (Malloy and Merrill, 1972) at the northeast extent of the zone that trends along the coast of Kodiak Island. Only indirect evidence, such as sharp bathymetric expression of fault scarps and occurrence of aftershocks, suggests offset on Kodiak Shelf itself.

Folds along the shelf break commonly deform the seafloor, indicating recent deformation. They have been breached by erosion in several places, exposing semilithified to lithified Pleistocene and older rocks (McClellan et al., 1980).

PHYSIOGRAPHY

The physiography of Kodiak Shelf consists of a series of flat banks, generally 50 to 100 m deep, cut by transverse troughs, up to 200 m deep (Fig. 8). The main elements of the physiography have structural and/or erosional origin.

The banks have many low hills and shallow depressions (Fig. 9). Closed depressions also exist in the troughs.

A significant second-order physiographic feature is a discontinuous series of arches along the shelf break. These arches are the seafloor expression of anticlines described previously and have a relief of up to 60 m. They extend along the banks and across the troughs, forming a discontinuous sill along the edge of the shelf. The arches are best developed from southern to middle Albatross Bank, including Kiliuda and Chiniak Troughs, but are poorly developed to absent on northern Albatross Bank. The arch across the mouth of Stevenson Trough is breached by two erosional channels. Arches are well developed on Portlock Bank and across the middle of Amatuli Trough, far from the shelf edge. Low areas cut transversely across the middle of middle Albatross and Portlock Banks, interrupting the arch.

No arch exists in Sitkinak Trough, which also differs from other troughs in that it is deep and only indents the shelf edge, rather than extending across the shelf. The walls of this trough are relatively steep.

The position of the shelf break along Kodiak Shelf is fundamentally controlled by structure and is highly variable in form and depth (Fig. 8). The change in seafloor gradient that defines the shelf break typically occurs on the seaward flank of a shelf-edge anticline. The precise location of the break commonly is at the edge of a prograding body of sediment building seaward from the fold, with strata conformable to the seafloor (Fig. 10). In some places strata are truncated at the shelf break and uppermost continental slope, suggesting an erosional origin. The shape of the shelf break varies from sharp to broad.

Young anticlines growing seaward of the main shelf break are forming a new break off Kiliuda Trough and southwest middle Albatross Bank, and off Portlock Bank (Fig. 11). The shelf break is therefore a discontinuous, en echelon feature in these areas, as depicted in Fig. 8.

Other second-order physiographic features that have environmental significance are bedrock ridges, fault scarps, and sand waves. Ridges occur where steeply inclined bedrock crops out at the seafloor and has experienced differential erosion (Fig. 12). Maximum relief of these features is about 5 m.

Fields of large sand waves appear at three locations, in Stevenson Trough, on northern Albatross Bank, and between Chirikof and Trinity Islands (Fig. 13). Wave heights reach 15 meters, and wave lengths reach 300 meters. Smaller sandwaves, on the order of a meter high, have been noted on side-scanning sonar records but are not considered in this report.

Abrupt scarps are abundant in the zones of faults described previously, and occur locally in other places over the shelf. Maximum offset is about 10 m but varies significantly along the length of a fault.

The slope of the seafloor is low over much of Kodiak Shelf, being nearly flat on most parts of the banks, and rarely exceeding 5% on the flanks of troughs (Fig. 14). A notable exception is Sitkinak Trough, where gradients reach 20%. The upper continental slope is also relatively steep, with gradients of 10-40% being typical.

STRATIGRAPHY, FACIES, AND SURFICIAL SEDIMENT

Surficial unconsolidated sediment on Kodiak Shelf consists of various proportions of terrigenous, volcanic, and biogenic debris (Gershanovich, 1968; Bouma and Hampton, 1976, 1978, 1979). A thickness map of unconsolidated sediment is shown in Figure 15. The map is of generalized nature because of wide trackline spacing and because the quality of seismic reflection records does not allow precise measurement of thickness in all places. (See Hampton and Bouma, 1978, for a discussion of methods used in constructing the map). But, it is apparent that unconsolidated sediment forms a thin veneer over much of the shelf, typically less than 100 ms of acoustic penetration measured as two-way travel time. (Note that 1 ms two-way travel time = 1 m thickness for acoustic velocity of 2000 m/sec.) Local closed basins have up to 200 ms of fill, and sediment thickness in Sitkinak Trough exceeds 400 ms.

Sedimentary bedrock crops out over broad areas of the shelf. It is well stratified and folded. Where covered with unconsolidated material, a marked structural discordance typically occurs, and it is the depth to this unconformity surface that is given in Figure 15.

A variety of sediment types exists on the shelf (Figs. 16 and 17; Table 1, Appendix A). Distribution of sediment types is related to physiography and also to stratigraphic units that have been defined on the basis of seismic-reflection signature (Fig. 18 and Table 2; see Thrasher, 1979). On the banks, typical unconsolidated sediment is coarse grained (gravelly to bouldery sand), with the main compositional components being terrigenous debris and megafaunal shells. Silt- and clay-size material are present in minor amounts, and the composition of this fraction is volcanic ash, with siliceous microfossils, clay minerals, and other terrigenous material present in small amounts. This sediment type correlates with Thrasher's (1979) stratigraphic unit Qgf, which is the most widespread unconsolidated facies on the shelf and is interpreted to be of glacial-fluvial and glacial-marine origin. It also correlates with stratigraphic unit Qgm, which occurs along the margins of the banks adjacent to the trans-shelf troughs and atop the sills at the mouths of the troughs. These deposits are speculated to be lateral and terminal moraines. Typical Qgm sediment is somewhat muddier and lower in megafaunal shells than typical Qgf, although a sharp distinction cannot be made.

Typical sediment flooring the troughs, corresponding to Thrasher's stratigraphic unit Qs, is finer grained and of different composition than typical sediment on the banks. Moreover, sediment type varies from trough to trough. Sitkinak Trough contains muddy sand, with some coarse debris, that is composed of terrigenous material and moderate amounts of volcanic ash. Amatuli Trough apparently contains similar sediment although only two samples have been collected. Kiliuda Trough has mud and sandy mud composed of terrigenous minerals volcanic ash and with large amounts of siliceous microfossils in the sand fraction. Chiniak Trough contains sandy muds composed mostly of volcanic ash. Stevenson Trough contains terrigenous sands, with moderate amounts of mud and volcanic ash.

Two distinctive sediment types occur on the banks that show no obvious correlation with facies or physiographic detail. One type consists dominantly of finely broken carbonate shell material (reflected by high percentages of

carbonate megafaunal shell material in the sand fraction, Table 1; e.g. samples 63, 64, 65, 66, 70, 75, 80, 90, 127, 245). The other contains many foraminifera in the sand fraction (e.g., samples 61, 128, 141, 246).

Another distinctive sediment type - clean terrigenous sand - was sampled from stratigraphic unit Qb in Stevenson Trough and between the Trinity and Chirikof Islands. This unit contains large sand waves and apparently represents areas of strong reworking and sorting.

Volcanic ash, derived from the 1912 eruption of Katmai volcano on the Alaska Peninsula, is an important constituent of surficial sediment (Hampton et al., 1979). The abundances of volcanic ash, relative to the total sand size and finer terrigenous material, are shown in Figure 19. In general, the ash distribution on the seafloor of Kodiak Shelf shows high concentrations in Chiniak Trough and in shallow depressions on the banks. Low concentrations exist on flat parts of the banks.

Clay minerals are present in small to moderate quantities in all surficial sediment types. Composition of the clays was analyzed by Hein et al. (1979), and two major sources were identified: the Copper River about 400 km away in the eastern Gulf of Alaska and local bedrock outcrops on Kodiak Shelf itself. Clay-mineral suites from these two sources are mixed over most of the shelf, but the Copper River suite appears to collect on flat parts of the banks. Bedrock-derived clays collect around outcrops and in nearby shallow depressions on the banks. Mixtures from the two sources are found in the trans-shelf troughs. Microscopic analysis shows that some Katmai ash has been altered to clay, but most is surprisingly fresh.

Bedrock samples, taken as dart cores from areas of seafloor outcrop, are composed of semilithified to lithified siltstone and fine-grained sandstone. Outcrops occur in the crestal regions of large anticlines, and microfauanal age determinations are as old as middle or late Miocene (McClellan et al., 1980). Grab samples of poorly sorted mixtures of terrigenous and megafaunal shell debris were obtained at some areas designated as bedrock outcrop on Figure 18. This implies a thin cover of unconsolidated material, especially in valleys between bedrock ridges.

The sedimentary processes and history of Kodiak Shelf can be deduced from available data. The sedimentary bedrock probably was eroded during Pleistocene time. The coarse-grained unconsolidated sediment that covers bedrock, to judge from sediment texture and the inferred regional history, was deposited by Pleistocene glacial processes (Karlstrom, 1964; University of Alaska, 1974). Thrasher (1979) has delineated glacial ground, lateral, and end moraine deposits.

The glacial deposits were reworked during the Holocene transgression. As evidence, some seismic records show probable glacial deposits, with an irregular upper surface that has been partially planed off at the present seafloor, to have low areas filled with acoustically more transparent material that is horizontally stratified. Along trough margins the strata are inclined toward the trough axes (Fig. 20). This unit could reflect planation of glacial deposits during a marine transgression, with infilling of low areas and construction of progradational sedimentary wedges laterally into

troughs. Also, the bank sediment containing large amounts of finely broken shell material, which now exists far from shore in water depths of 70-100 m, probably was produced by nearshore wave action during the transgression.

The influx of modern sediment is low, because no large rivers drain onto Kodiak Shelf. The Copper River and local submarine outcrops provide minor epiclastic material. Occasional strong volcanic eruptions such as the Katmai event in 1912 are a relatively major source of sediment (volcanic ash), although the absolute amount is minor. Biogenic sources provide some siliceous and carbonate shell debris.

The present-day sedimentary setting is therefore one of reworking of predominantly pre-Holocene deposits. Currents impinge on the seafloor from the southwestward-flowing Alaska current and from large storm waves. Fine sediment is winnowed from the surficial deposits on the banks, and its fate is determined by the pattern of ocean currents and by physiography. A minor amount is redeposited on the banks in broad, shallow depressions where thin, surficial layers of ash- and clay-rich material have been sampled (e.g., samples 91 and 115; see also Hampton et al., 1979). A much greater amount is deposited in troughs. Kiliuda and Chiniak Troughs in particular are floored by fine-grained, ash-rich sediment. The negative relief of the troughs and the sills across their mouths have created quiet depositional settings. Sitkinak Trough contains thick accumulations of terrigenous muddy sediment that may be derived mainly as first-cycle input from Shelikof Strait, plus some reworked Kodiak Shelf debris.

The sedimentary environment in Stevenson Trough is distinct from the others. The presence of clean sand that has been molded into large, predominantly seaward-facing sand waves suggests strong bottom currents. The sill across the trough has been breached. Sediment on the sill is similar to that on the adjacent banks (i.e., modified glacial), whereas within a breach and on the adjacent continental slope it is more similar to sediment within the trough. Transport appears to have occurred out of the trough and onto the continental slope. But, it is uncertain whether this occurs significantly at present or if it took place mainly during the Holocene transgression.

SAND WAVES

Three major sand wave fields exist on Kodiak Shelf; in Stevenson Trough, on northern Albatross Bank, and on southern Albatross Bank between Chirikof and the Trinity Islands (Fig. 13). In Stevenson Trough, the waves have heights up to 8 m and lengths up to 300 m (Fig. 21a). They face seaward for the most part, except for the waves in the northern part of the field, which face landward. Wave crests are straight to slightly sinuous on side-scan sonographs. On middle Albatross Bank, the waves are a maximum of 5 m high and face seaward.

The sand waves between Chirikof and the Trinity Islands are up to 15 m high and 300 m long (Fig. 21b). Most are sharp-crested, symmetrical features, but landward and seaward-facing waves are present. These waves occur within an acoustically distinct sediment body, overlying bedrock and glacial deposits, that reaches a maximum thickness of about 40 m and pinches out abruptly landward and seaward of the sand waves.

Hydrocarbon gases in sediments from Kodiak Shelf
(by Keith A. Kvenvolden)

Hydrocarbon gases, methane (C_1), ethane (C_2), ethene ($C_{2:1}$), propane (C_3) and propene ($C_{3:1}$) are common in near-surface sediment of Kodiak Shelf. Of these gases, C_1 is the only one of quantitative importance. Concentrations of C_1 range from about 5×10^{-1} to 1.2×10^5 $\mu\text{L/L}$ of interstitial water, whereas concentrations of the other hydrocarbons rarely exceed 1 $\mu\text{L/L}$. In this study, hydrocarbon gases and CO_2 were extracted from 101 samples taken at 32 stations during three field seasons from four general areas: (1) Kiliuda Trough, (2) Chiniak Trough, (3) Sitkinak Trough, and (4) the continental slope including the Aleutain Trench (Fig.22). The first area was examined in greatest detail. The objectives of the work were to determine how the concentrations and compositions of hydrocarbon gases and CO_2 vary in each of these areas and to relate gas concentrations to near-surface acoustic anomalies observed at some sampling stations by geophysical profiling.

At each of the 32 stations one to six samples were taken at various intervals down a core for gas analyses. In order to simplify the presentation of these data, gas concentrations at each station are reported for a sediment depth of one meter (Table 3). These numbers were obtained by interpolation or extrapolation of the concentrations observed in each core and represent the best estimate of the gas concentrations at a one-meter subbottom datum. C_1 , C_2 , $C_{2:1}$, C_3 , and $C_{3:1}$ and CO_2 are present in almost all samples. Higher molecular weight hydrocarbon gases, isobutane ($i\text{-C}_4$) and n -butane ($n\text{-C}_4$) were detected in some samples. C_1 and CO_2 are the most abundant gases present: the other hydrocarbon gases are present in abundances orders of magnitude lower. From a quantitative viewpoint the hydrocarbon gases larger than C_1 , that is the C_{2+} hydrocarbons, are not particularly important; however, the distribution of the gases relative to methane is important in assessing possible sources for the mixtures of hydrocarbon gases present. In all cases here, the abundances of C_{2+} relative to C_1 are small and in the range of values generally expected for gases associated with C_1 that has been derived through dominantly biological processes. If the hydrocarbon gases observed in these sediments had been derived mainly through thermogenic processes, the abundances of C_{2+} relative to C_1 would be expected to be much larger. Even at stations 224G1, 225P1, and 356G1 where the concentrations of C_{2+} hydrocarbons are anomalously large, the ratio of C_{2+} to C_1 are not sufficiently great to indicate the presence of thermogenically derived hydrocarbons. The CO_2 concentrations are in the range of those expected to accompany biogenically derived hydrocarbons.

Further evidence indicating that biological processes are likely responsible for the C_1 and CO_2 , at least at stations 439G2 and 440G1 in the Kiliuda Trough, comes from carbon isotopic abundance measurements (Table 4). $^{13}\text{C}_1$ values range from -76.9 to -85.5%. These carbon isotopic compositions are clearly in the range for C_1 derived from biological processes and unfractionated by thermal processes. Likewise the ^{13}C of CO_2 ranges from -14.3 to -23.4%, and indicates that this CO_2 is likely generated by biological

processes operating on organic matter in the sediments.

Because C_1 is quantitatively the most important hydrocarbon gas observed here, further discussion will focus on this compound. In this work, as in previous studies in the eastern Gulf, southern Bering Sea, Norton Sound and the Aleutian Basin, concentrations of C_1 generally increase with depth in the sediment; in contrast, the other hydrocarbon gases show no definite trends with depth. The increasing gradient in C_1 concentrations with sediment depth is illustrated in Figure 23 for stations having the highest C_1 concentrations. At stations 344G1, 348G1, 439G2, 440G1, 441G1, 356G1, 329G1, and 225P1, concentrations of C_1 increase abruptly with depth and at the one meter datum level exceed 5×10^2 uL/L. C_1 concentrations increase three or more orders of magnitude within the sampled interval and approach or reach concentrations that exceed the solubility limit of C_1 at ambient conditions of about 40×10^3 uL/L. Gas-expansion voids are present in some of these cores. In each of the four areas sampled, the core from at least one station has high abundances of C_1 ; cores at five stations in the Kiliuda Trough contain high C_1 concentrations (Fig. 22).

Lowest concentrations of C_1 are generally found associated with sediment from the continental slope and Aleutian Trench. With the exception of station 225P1, on the slope south of middle Albatross Bank, all other stations show methane concentrations lower than 90 uL/L and usually less than 20 uL/L (Table 3).

Highest concentrations of C_1 , as well as C_2 and C_3 , are generally found in sediment in the Kiliuda Trough (Table 3). Shallow acoustic anomalies are present at or near eight of the sampling stations. At stations 441G1, 440G1, 344G1, 439G2, and 348G1 acoustic anomalies correlate with high C_1 concentrations and steep C_1 concentration gradients with depth. This correlation suggests that the hydrocarbon gases may be present in bubble phase at shallow depths in the sediment and that the sediment is gas-charged, thus producing anomalous acoustic returns during geophysical profiling. Acoustic anomalies were also noted at stations 343G1, 442V1, 347G1, and 349G1, but at these stations, the C_1 concentrations measured were average or low. At stations 358G1 and 359G2, located near faults which at one time were leaking gas, no unusual gas concentrations were observed.

In the Chiniak Trough acoustic anomalies at stations 432G1/V1 and 433V1 do not correlate with high C_1 concentrations, and high C_1 concentrations at station 329G1 at the head of the trough are not associated with acoustic anomalies. In Sitkinak Trough at station 356G1, high concentrations of hydrocarbons are not associated with an acoustic anomaly. Where high C_1 concentrations are not accompanied by acoustic anomalies, it suggests that although C_1 concentrations are large, they are not sufficient to permit free gas to exist in the sediment and cause the sediment to have anomalous acoustic properties.

Acoustic anomalies

Seismic reflection records from uniboom and minisparker systems show acoustic anomalies at several places on Kodiak Shelf. A variety of anomaly types is present, but they are all defined on the basis of an abrupt departure

from normal in strength, continuity, or geometry of acoustic reflectors along a profile. Six anomaly types have been observed and mapped on Kodiak Shelf (Figs. 24-31):

1. Acoustic turbidity or inpenetrability below a certain subbottom level (Fig. 25). Reflectors terminate abruptly and a non-layered gray to white return is seen on the records within the anomalous zone. On Kodiak Shelf, this type of anomaly occurs exclusively within soft sediment (unit Qs of Thrasher, 1979) of Kiliuda and Chiniak Troughs.

2. Jumpy reflectors, wherein the acoustic signal is discontinuous along certain horizons (Fig. 26). Commonly, where reflections are received from a certain level, lower reflections are attenuated or not recorded at all. Where reflections are not received from the upper level, lower reflections are strong. This alternation over short distances gives a "jumpy" appearance to the seismic signature. Jumpy reflectors occur both on the banks and in the troughs.

3. Stratigraphic intervals that are variably transparent to weakly reflective along their extent (Fig. 27). The interval is wavy and may be discordant with underlying or overlying stratigraphy. Top and bottom boundaries are approximately parallel. This anomaly type has been seen only in Kiliuda Trough.

4. Discontinuous sets of reflectors that are variable in the strength of their return (Fig. 28a,b). Typically, the return alternates between sharp, distinct reflectors (normal signature) to murky or transparent intervals.

5. A basal reflector of undulatory to highly irregular morphology, overlain by a stratigraphic interval with discontinuous reflectors (Fig. 29). The upper surface of the discontinuously reflective interval may cut across higher reflectors, and some reflectors in this interval may cut across hills in the basal reflector. The basal reflector and the upper boundary to the discontinuous interval appear to be acoustic artifacts rather than real stratigraphy or a buried topographic surface. This anomaly type occurs only on the margin of southern Albatross Bank and Kiliuda Trough.

6. Steeply inclined secondary reflectors in otherwise horizontally stratified material, giving a fractured appearance to the stratigraphy (Fig. 30). This anomaly type also only occurs on the margin of southern Albatross Bank and Kiliuda Trough.

The various acoustic anomaly types, with the exception of type 6, are somewhat gradational and cannot always be classified uniquely with certainty. Moreover, subtle deviations from normal, undisturbed seismic signature occur commonly in the records, and it is a matter of judgement what to identify as a true acoustic anomaly. Only definite examples of acoustic anomalies are mapped in Figure 24.

Acoustic anomalies occur in three primary areas on Kodiak Shelf: 1) along the length of Chiniak Trough and nearby on northern Albatross Bank, 2) on middle Albatross Bank near Kiliuda Trough, and 3) within the recurved area of Kiliuda Trough and nearby on southern Albatross Bank. In Chiniak Trough the

anomalies are mostly local occurrences of jumpy and discontinuous reflectors, with one zone of acoustic turbidity near the mouth of the trough. On middle Albatross Bank is a broad area of jumpy and discontinuous reflectors. The recurved area of Kiliuda Trough and nearby southern Albatross Bank shows a variety of anomaly types. The typical sequence is fractured appearance (type 6) on southern Albatross Bank, with undulatory reflector-discontinuous interval (type 5) on the sloping margin of Kiliuda Trough and extending some distance under the soft sediment fill, followed by an acoustically turbid zone (type 1) within the soft sediment fill in the deepest part of the trough, and followed by a transparent zone (type 3) on the northern slope of the trough.

Acoustic anomalies have been correlated with the presence of bubble-phase gas in sediment, especially for acoustically turbid zones (type 1) (Schubel, 1974; Whelan et al., 1977). Indeed, as was stated in the previous section, gas-charged cores have been collected at locations of acoustic anomalies on Kodiak Shelf, although correspondence between gas-charged cores and acoustic anomalies is not one-to-one.

In a series of cores collected at close spacing, such as in Kiliuda Trough, some show gas-charging but others do not. The distribution of gas appears to be patchy at depths from which samples can be obtained. A detailed sampling program, using deep in situ or pressurized sampling and testing equipment is necessary to understand the distribution of bubble-phase gas and its relation to acoustic anomalies.

Some anomaly types (4, 5, and 6) occur in stiff, coarse-grained sediment that we have not been able to core, so they have not been confirmed to represent gas charging. Their common association with other anomaly types makes them suspect, however. In particular, the region of middle Albatross Bank showing jumpy and discontinuous reflectors has not yielded cores. However, an apparent gas seep from the seafloor was noted at 57°01.1'N, 152°10.3'W, along the extension of a fault mapped in the area, strengthening the suspicion that these anomalies indicate gas charging.

SEDIMENT SLIDES

Sediment slides in the area of Kodiak Shelf have been identified in seismic reflection profiles, and the distribution of slides is shown in Figure 31. The presence of slides is inferred with various degrees of confidence from several diagnostic features including abrupt scarps, acoustic indications of a subbottom slide surface, offset and rotated bodies of sediment, discontinuous or distorted bedding, and hummocky seafloor topography. These features appear in many combinations. In Figure 31, those occurrences showing convincing morphologic features of slides are designated by solid lines. Slide surfaces and headwall scarps are typically visible, as are slide masses delineated by offset and rotated bedding (e.g., Fig. 32). Occurrences identified by dashed lines in Figure 31 are areas of hummocky seafloor, commonly with distorted subbottom reflectors but no other features of slides (Fig. 33). Heights of the hummocks range from a few meters to several tens of meters. These occurrences are less certain indicators of slides, and some may be depositional or tectonic structures.

Indications of slides are rare on Kodiak Shelf whereas they are abundant

on the adjacent continental slope. The two possible slides identified on the shelf are in Stevenson Trough and appear as small hummocks on the seafloor. Self and Mahmood (1977) report slides on the flanks of unidentified troughs southwest of Kodiak Island and south of Sitkinak Island, but exact locations are not given. Steep slopes occur in this area (Fig. 14), but our records do not reveal slides.

Two kinds of slides have been described on the upper continental slope (Hampton and Bouma, 1977). Large slides cover areas exceeding 100 km^2 in some places and involve thicknesses of slumped material of a few hundred meters. Slide surfaces are curved, and these slides have the general appearance of large rotational slumps according to the classification scheme of Varnes (1978) (Fig. 32). Smaller slides cover small areas and typically appear on single profile lines. Thicknesses are on the order of a few tens of meters, and slide surfaces appear to be planar. These slides fit the general description of translational slides according to Varnes' terminology (Fig. 34).

The distribution of large slides is uneven along the upper continental slope. They are abundant off southern and middle Albatross Bank and off Portlock Bank but have not been found off northern Albatross Bank. (The slides identified off northern Albatross Bank in Figure 31 are small. Small slides occur in other areas, also). The occurrence of large slides shows a relation to structural and tectonic elements of the region. Near-surface folds and faults are actively growing, with consequent slope steepening, and the shelf-break arch is well developed (Fig. 35a,b). Recent epicenters are concentrated near the large slides adjacent to southern and middle Albatross Banks (Fig. 6). In contrast, gentle folding, low seafloor inclinations, and a subdued shelf-break arch characterize the area where large slides are absent (Fig. 36). Recent epicenters are sparse.

The large slumps are controlled by tectonic processes; i.e., active growth of structures along the shelf break. A quantitative evaluation by Hampton et al. (1978) of two specific large slumps indicates that steep slopes, removal of lateral ground support by faulting, and earthquake accelerations are the most likely environmental forces to activate these slumps. Magnitudes of these forces are probably less in the area off northern Albatross Bank, implying a variation of the intensity of tectonism along the shelf break. Future generation of large slumps can be expected on the upper continental slope in the areas of intense tectonism.

Small slides on the continental slope occur both in tectonically active and inactive areas. The slides noted off northern Albatross Bank are of that variety (Fig. 34). The planar slide surface and wide areal distribution suggests stratigraphic control (weak sediment layers). But, earthquakes may trigger these slides.

The scarcity of slides on Kodiak Shelf probably is accounted for by the presence of relatively strong sediment on sloping portions of the seafloor and the low seafloor slopes in general. This is in strong contrast to the nearby northeastern Gulf of Alaska where large slumps occur on slopes less than 1° in fine-grained, underconsolidated sediment derived from coastal glaciers and the Copper River (Carlson and Molnia, 1977; Molnia et al., 1977). Analysis shows

that low strength due to rapid sedimentation rates and consequent underconsolidation, earthquake acceleration, wave loading, and perhaps bubble-phase gas are the important environmental driving forces (Hampton et al., 1978). The weakest sediment on Kodiak Shelf (sediment type Qs, Fig. 18), which commonly shows evidence of gas-charging and is exposed to strong earthquake forces, is not prone to sliding. This sediment is present mainly on nearly flat seafloor, but is also stable in most relatively steep areas such as Sitkinak Trough. Other forms of sediment instability such as liquefaction and consolidation subsidence are possible in the soft sediment, but indications of these phenomena could be subtle and have not been detected.

ENVIRONMENTAL ASSESSMENT

Geologic processes pose several environmental conditions of concern to resource development on Kodiak Shelf. Some processes may affect the operation and safety of offshore engineering activities. For example, seismic events may severely disrupt petroleum exploration and production operations on drilling platforms. Other geologic processes in turn may be affected by resource development, with deleterious environmental consequences. For example, incorporation of spilled contaminants into bottom sediment may affect benthic life.

Environmental geologic concerns on Kodiak Shelf are broadly related to tectonic and sedimentary processes. Most processes affect broad areas, and their origin or occurrence at a specific location can have both local and widespread consequences. The following analysis is on a regional, rather than tract-by-tract basis.

Seismic-Tectonic Effects

The tectonic setting of Kodiak Shelf creates many potential environmental hazards. Convergence of the Pacific and North America plates generates large-magnitude earthquakes that make the entire shelf subject to seismic shaking. But, seismicity and structural deformation are spatially variable across the region posing different sets of concerns from place-to-place. Zonation of seismicity has been postulated, with identification of a seismic gap near Kodiak Shelf where the potential for a major earthquake is great. Folding and faulting are more severe along sections of the shelf break and near Kodiak Island than other places, and postulated transverse tectonic boundaries may indicate other areas of concentrated deformation.

The minimum recurrence interval of 30 years for a major earthquake could be exceeded by the lifetime of an oil-producing province, because the last major event to affect Kodiak Shelf was in 1964. So, although earthquakes cannot be predicted with confidence, seismic hazards are a valid concern for offshore development. Strong ground shaking, fault rupture, sediment displacement, and tectonic deformation of the seafloor have all occurred on or adjacent to Kodiak Shelf and can be expected in the future.

Kodiak Shelf might be affected seismically from major events in either of two regional zones; that involved with the 1964 Alaska earthquake or that identified as the Shumagin seismic gap. The 1964 earthquake had aftershocks across the entire Kodiak Shelf, and seafloor deformation or ground shaking of

the magnitude associated with this event could affect operation of bottom-founded installations such as drilling platforms. A major event in the Shumagin seismic gap may not have epicenters located on Kodiak Shelf, if present theory is correct (e.g., Sykes, 1971; Pulpan and Kienle, 1979), but significant ground shaking could be generated at least in the southwest part of the area.

Another area of seismic concern is near the mouth of Kiliuda Trough and adjacent sections of southern and middle Albatross Banks, where several moderate earthquakes have occurred (Fig. 6). This area displays a much higher rate of strain release than elsewhere on Kodiak Shelf, and seismic reflection records show evidence of folding, faulting, seafloor deformation, and sediment sliding (Pulpan and Kienle, 1979; Hampton et al., 1979). The shelf-break area of Portlock bank shows similar structural features (Fig. 35), suggesting similar tectonic behavior, but the historic record shows no concentration of seismic activity there (Fig. 6).

The area along the shelf break on northern Albatross Bank appears from structural and seismic evidence to be less active and therefore less prone to local tectonic hazards than the two adjacent zones of strong deformation described above (Fig. 36). Regional seismicity could still produce significant ground shaking there, of course.

Displacement of the seafloor can result from movement along shallow faults, causing damage to installations that span them. Present-day seismicity does not indicate any clear linear seismic trends that define active faults (Pulpan and Kienle, 1979). But, offset in 1964 along faults within the zone extending along and offshore of Kodiak Island has been documented in places and inferred in others (Malloy and Merrill, 1972; von Huene, 1972), raising special concern for proper routing of pipeline corridors across the zone. Another significant fault zone exists along the shelf break of southern and middle Albatross Bank, and other individual examples have been noted across the shelf (Fig. 7). Faulting and tectonic deformation of the seafloor can generate tsunamis, which can devastate coastal areas as happened on Kodiak Island in 1964 (Kachadoorian and Plafker, 1967).

Large volcanic eruptions have spread blankets of ash across Kodiak Shelf from time-to-time; the Katmai event in 1912 being an example (Wilcox, 1959). The most severe volcanic hazards are local and would not have an affect on Kodiak Shelf, because the nearest volcanoes are about 200 km away on the Alaska Peninsula. But, the abraisive action of ash particles and acid rains associated with eruptions can be a nuisance to offshore operations.

Sediment

The sedimentary environment of Kodiak Shelf has many unusual features of practical significance. Semilithified to lithified bedrock is exposed over large areas, and a diverse suite of unconsolidated sediment is present including coarse-grained material nearly lacking in mud, volcanic ash, clean sand, and normal terrigenous muds. Furthermore, input of modern sediment is small, and ocean currents impinging on the seafloor can be strong in places but are insignificant in others. Broad areas are being reworked whereas others serve as quiet repositories for winnowed debris.

Sedimentary bedrock appears to provide strong foundation material at the seafloor over broad expanses of Kodiak Shelf, although geotechnical data are lacking. Resistance to trenching and pile driving might be significant, and problems with emplacement of engineering structures might be encountered on bedrock ridges, due to rough topography.

Accumulations of unconsolidated sediment on Kodiak Shelf are generally thin, and in many places firm bedrock is within reach of subbottom structural foundations. The banks appear overall to be composed of strong, stable material, and foundation problems should be minimal. Boulders in unconsolidated debris might interfere with drilling and setting of casings, however.

The localized concentrations of fine sediment in some of the troughs might have engineering importance, although the deposits typically are only a few tens of meters thick. Accumulations in Chiniak, Kiliuda, and perhaps Amatuli Troughs might be composed of volcanic ash grains and siliceous microfossils throughout much of their thickness. The ash particles are plate- to rod-shaped and some are highly vesicular. Siliceous shells are hollow and fragile. Individual grains are therefore weak, and the deposits have high void ratios. Grain crushing and rearrangement during loading might result in substantial consolidation. Also, liquefaction, with associated strength loss and subsidence, is a possibility during earthquakes. Similar problems might be encountered with the fine-grained sediment in Sitkinak Trough, but the higher percentage of terrigenous material suggests greater stability. The large thickness of unconsolidated sediment in Sitkinak Trough might necessitate different foundation design than in areas of less fine sediment accumulation. The sandy material in Stevenson Trough appears to be a type of material that would be stable under loading, but its engineering properties have not been studied in detail.

The volcanic ash recovered in sediment samples is relatively fresh, as has also been reported for buried ash deposits in the Gulf of Alaska (Scheidegger and Kulm, 1975). So, the sediment stability problems commonly encountered in terrestrial ash deposits that have been altered to clay are unlikely to be met on Kodiak Shelf.

The surficial deposits of volcanic ash that were sampled on the banks are only a few centimeters thick and of no engineering importance.

Strong currents are indicated where large bedforms occur (Fig. 13), although the degree of modern activity compared to times of lower sea level is uncertain. Scour of sediment can cause loss of support and differential settlement at the base of seafloor installations (Posey, 1971; Wilson and Abel, 1973; Palmer, 1976). Also, fluttering due to resonance set up by vortex shedding can occur where pipelines have become suspended as a result of scour. This has been documented in nearby Cook Inlet (Goepfert, 1969). Unsuspected loads can be applied to structures as bedforms migrate past them.

Slope instability does not appear to be a major problem on the shelf, having been reported only from a few areas (Fig. 31; see also Self and Mahmood, 1977). The high degree of stability is related to the restricted occurrence of soft sediment mainly on flat areas of seafloor, whereas slopes

are underlain by coarse-grained material. Sitkinak Trough is a notable exception, but no large slides have been specifically located there. Because there is low influx of modern sediment onto the shelf, large accumulations of unstable, underconsolidated sediment like those in the nearby northeastern Gulf of Alaska do not occur (see Carlson and Molnia, 1977).

Sediment slides are abundant on the upper continental slope and will become of prime concern only as development moves beyond the shelf break. However, the distribution of these slides does have important implication regarding tectonic hazards on the shelf.

Locations of gas-charged sediment have been identified on Kodiak Shelf, and environmental problems are possible. Most gas appears to be generated by shallow microbial decay, although the gas seep on middle Albatross Bank may indicate a deeper thermogenic source there.

Slope instability, low strength, and overpressuring have been found associated with gas-charged sediment (Whelan et al., 1976; Nelson et al., 1978). Direct evidence that similar problems exist on Kodiak Shelf is sparse; the gas seep on middle Albatross Bank suggests overpressuring. Gas-related craters, subsidence, or slope instability have not been noticed (see, for example, Nelson et al., 1979). But, although large blowouts and failures may not have been initiated by natural environmental forces, engineering activities may serve to trigger them, and special attention is warranted in the specified areas.

Man-induced pollution of Kodiak Shelf waters can have magnified effects at certain places on the seafloor. Sediment particles can serve as carriers of contaminants, and localized concentration and storage are determined by the current patterns and hydraulic sorting processes that control sediment dispersal pathways and the locations of depositional sites. The distribution of benthic fauna should vary spatially with sediment type (although supporting biological data are lacking), so specific faunal populations might be affected more than others by a contamination event. For example, the localized occurrence of Katmai ash in some troughs and in bank depressions implies that these sites are presently repositories for fine-grained sediment. Pollutants that become incorporated into bottom sediment should be swept from other areas into them, and local fauna would be affected. Also, it is likely that sediment transport across the shelf break is localized where physiographic barriers are absent or have been breached, which could cause disturbance of local populations after a pollution event.

REFERENCES

- Bouma, A.H., and Hampton M.A., 1976, Preliminary report on the surface and shallow subsurface geology of lower Cook Inlet and Kodiak Shelf, Alaska: U.S. Geol. Survey Open-File Report 76-695.
- Bouma, A.H., and Hampton, M.A., 1978, Notes on the acquisition of high resolution seismic profiles, side scan records, and sampling locations from lower Cook Inlet and Kodiak Shelf, R/V SEA SOUNDER cruise 57-77-WG, September - October 1977: U.S. Geol. Survey Open-File Report 78-727.
- Capps, S.R., 1937, Kodiak and adjacent islands: U.S. Geol. Survey Bull., no. 880-c, 73 p.
- Carlson, P.R., and Molnia, B.F., 1977, Submarine faults and slides on the continental shelf, northern Gulf of Alaska: Marine Geotechnology, V. 2, p.275-290.
- Fisher, M.A., Bruns, T.R., and von Huene, R., 1980, Transverse tectonic boundaries near Kodiak Island, Alaska: Geol. Soc. America Bull. (pt. 1), in press.
- Fisher, M.A., and von Huene, R., 1980, Structure of upper Cenozoic strata beneath Kodiak Shelf, Alaska: Amer. Assoc. Petroleum Geologists Bull., in press.
- Gershanovich, D.E., 1968, New data on the geomorphology and recent sediments of the Bering Sea and the Gulf of Alaska: Marine Geology, V.6, p.281-296
- Goepfert, B.L., 1969, An engineering challenge - Cook Inlet, Alaska: Preprints 1st Offshore Technology Conference, p. 511-524.
- Hampton, M.A., and Bouma, A.H., 1977, Slope instability near the shelf break, Western Gulf of Alaska: Marine Geotechnology, v.2, p.309-331.
- Hampton, M.A., and Bouma, A.H., 1978, Generalized thickness map of unconsolidated surficial sedimentary units, Kodiak Shelf, western Gulf of Alaska: U.S. Geol. Survey Open-File Report 78-729.
- Hampton, M.A., and Bouma, A.H., 1979, Notes on the acquisition of high-resolution seismic reflection profiles, side-scanning sonar records, and sediment samples from lower Cook Inlet and Kodiak Shelf, R/V SEA SOUNDER cruise S8-78-WG, August 1978: U.S. Geol. Survey Open-File Report 79-1311.
- Hampton, M.A., Bouma, A.H., Frost, T.P., and Colburn, I.P., 1979, Volcanic ash in surficial sediments of the Kodiak Shelf - An indicator of sediment dispersal patterns: Marine Geology, v.29, p.347-356.
- Hampton, M.A., Bouma, A.H., Pulpan, H., and von Huene, K., 1979, Geo-environmental assesment of the kodiak shelf, western Gulf of Alaska: Preprints 11th Offshore Technology Conference, p.365-376.

- Hampton, M.A., Bouma, A.H., Sangrey, D.A., Carlson, P.R., Molnia, B.F., and Clukey, E.C., 1978, Quantitative study of slope instability in the Gulf of Alaska: Preprints 10th Offshore Technology Conference, p. 2308-2318.
- Hein, J.R., Bouma, A.H., Hampton, M.H., and Ross, C.R., 1979, Clay mineralogy, fine-grained sediment dispersal, and inferred current patterns, lower Cook Inlet and Kodiak Shelf, Alaska: *Sedimentary Geology*, v.24, p. 291-306.
- Kachadoorian, R., and Plafker, G., 1967, Effects of the earthquake of March 27, 1964 on the communities of Kodiak and nearby islands: U.S. Geol. Survey Prof. Paper 542-F.
- Karlstrom, T.N.V., 1964, Quaternary geology of the Kenai Lowland and glacial history of the Cook Inlet Region, Alaska: U.S. Geol. Survey Professional Paper 443.
- Malloy, R.J., and Merrill, G.F., 1972, Vertical crustal movements on the seafloor: in The Great Alaska Earthquake of 1964, Oceanography and Coastal Engineering: Washington, D.C., National Research Council, National Academy of Sciences, p. 252-265.
- McClellan, P.H., Arnal, R.E., Barron, J.A., von Huene, R., Fisher, M.A., and Moore, G.W., 1980, Biostratigraphic results of dart-coring in the western Gulf of Alaska, and their tectonic implications: U.S. Geol. Survey Open-File Report 80-63.
- Molnia, B.F., Carlson, P.R., and Bruns, T.R., 1977, Large submarine slide in Kayak Trough, Gulf of Alaska: *Reviews in Engineering Geology*, v. III, Geol. Soc. America, p.137-148.
- Moore, G.W., 1967, Preliminary geologic map of Kodiak Island and vicinity, Alaska: U.S. Geol. Survey Open-File Report 67-271.
- Nelson, C.H., Kvenvolden, K.A., and Clukey, E.C., 1978, Thermogenic gases in near-surface sediments in Norton Sound, Alaska: Preprints 10th Offshore Technology Conference, p.,2623-2633.
- Nelson, C.H., Thor, D.R., Sandstrom, M.W., and Kvenvolden, K.A., 1979, Modern biogenic gas-generated craters (sea-floor "pockmarks") on the Bering Shelf, Alaska: *Geol. Soc. America Bull.*, v. 90, p.1144-1152.
- Palmer, H.D., 1976, Sedimentation and ocean engineering structures: in D.J. Stanley and D.J. P. Swift (eds.), *Marine Sediment Transport and Environmental Management*: New York John Wiley and Sons, p.519-534.
- Plafker, G., and Rubin, M., 1967, Vertical tectonic displacements in south-central Alaska during and prior to the great 1964 Earthquake: *Jour. Geosci. Osaka City Univ.*, p.53-72.
- Posey, C.J., 1971, Protection of offshore structures against underscour: *Jour. Hydraulics Division, Amer. Soc. Civil Engineers*, No. Hy7, Proc. Paper 8230, p.1011-1016

- Pulpan, H. and Kienle, J., 1979, Western Gulf of Alaska seismic risk: Preprints 11th Offshore Technology Conference, p.2209-2218.
- Scheidegger, K.F., and Kulm, L.D., 1975, Late Cenozoic volcanism in the Aleutian arc: information from ash layers in the northeastern Gulf of Alaska: Geol. Soc. America, v.86, p.1407-1412.
- Schubel, J.R., 1974, Gas bubbles and the acoustically impenetrable, or turbid, character of some marine sediments: in I.R. Kaplan (ed.), Natural Gases in Marine Sediments, New York, Plenum Press, p.275-298.
- Self, G.W., and Mahmood, A., 1977, Assessment of relative slope stability of Kodiak Shelf, Alaska, using high-resolution acoustic profiling data: Marine Geotechnology, v.2, p.333-347.
- Sykes, L.R., 1971 Aftershock zones of great earthquakes, seismicity gaps, and earthquake prediction for Alaska and the Aleutians: Jour. Geophysical Research, v.75, p.8021-8041.
- Thrasher, G.P., 1979, Geologic map of the Kodiak outer continental shelf, western Gulf of Alaska: U.S. Geol. Survey Open-File Report 79-1267.
- University of Alaska, 1974, The Western Gulf of Alaska - A summary of available knowledge: Anchorage, Arctic Environmental Information and Data Center, 599 p.
- Whelan, T., Coleman, J.M., Roberts, H.A., and Suhayda, J.N., 1976, The occurrence of methane in recent deltaic sediments and its effect on soil stability: International Assoc. Engineering Geologists Bull., no. 14, p. 55-64.
- Wilcox, R.E., 1959, Some effects of recent volcanic ash falls with special reference to Alaska: U.S. Geol. Survey Bull., no. 1028-N, p.409-476.
- Wilson, N.D., and Abel, W., 1973, Seafloor scour protection for a semi-submarine drilling rig on the Nova Scotian shelf: Preprints 5th Offshore Technology Conference, p.631-646.
- Varnes, D.J., 1978, Slope movement types and processes: in R.L. Schuster and R.J. Krizek (eds.), Landslides-Analysis and Control, Washington, D.C., National Academy of Sciences, p.12-33
- von Huene, R., 1972, Structure of the continental margin and tectonism of the eastern Aleutian Trench: Geol. Soc. America Bull., v. 83, p.3613-3636
- von Huene, R., Fisher, M.A., and Bruns, T.R., 1979, Continental margins of the Gulf of Alaska and late Cenozoic tectonic plate boundaries: in A. Sisson (ed.), Proceedings of the Sixth Alaska Geological Society Symposium, Anchorage, Alaska Geological Society, p.J-1 - J-33.
- von Huene, K., Shore, G.G., and Malloy, R.J., 1972, Offshore tectonic features in the affected region: in The Great Alaska Earthquake of 1964,

Oceanography and Coastal Engineering, Washington, D.C., National
Research Council, National Academy of Sciences, p.266-289.

FIGURE CAPTIONS

- FIG. 1 - Location map of Kodiak Shelf, western Gulf of Alaska.
- FIG. 2 - Tracklines of seismic reflection profiles run by R/V SEA SOUNDER and R/V S.P. LEE, 1976-1979.
- FIG. 3 - Sample locations.
- FIG. 4 - Lithospheric plate boundaries, Gulf of Alaska. (From von Huene et al., 1979).
- FIG. 5 - Locations of deep structural basins and transverse tectonic boundaries. (After Fisher et al., 1980).
- FIG. 6 - Epicenters in the vicinity of Kodiak Shelf. a) magnitudes $M_B > 4$ from 1954-1963, b) magnitudes $M_B > 5$ in the 1964 Alaska earthquake, c) magnitudes $M_B > 5$ from 1965-1975, d) January-June 1978. Letter code represents hypocentral depth range (A: 0-25 km, B: 25-50 km, etc.) Data compiled by H. Pulpan, University of Alaska.
- FIG. 7 - Shallow folds and faults. Compiled by R. von Huene and D. Varchal (U.S. Geological Survey Open-File Report, in press). No coverage southwest of Sitkalidak Island.
- FIG. 8 - Major physiographic features.
- FIG. 9 - Bathymetry of Kodiak Shelf and the adjacent continental slope. Contours in meters. Compiled by R. von Huene and J. Dunlavey (U.S. Geological Survey Open-File Report, in press).
- FIG. 10- Sparker seismic reflection profile showing typical geologic nature of the shelf break. Dashed line separates bedrock anticline (below) from prograding unconsolidated sediment (above).
- FIG. 11- Sparker seismic reflection profile showing double shelf breaks.
- Fig. 12- Uniboom seismic reflection profile showing inclined strata and bedrock ridges on the seafloor.
- FIG. 13- Locations of large sand waves and major sand wave fields.
- FIG. 14- Seafloor slopes. Coverage extends from 3-mile limit to 1000 m contour.
- FIG. 15- Generalized thickness map of surficial unconsolidated sedimentary units.
- FIG. 16- Grain sizes of unconsolidated surficial sediment samples. Size fractions present in amounts less than 3% not shown.
- FIG. 17- Major compositional components of unconsolidated surficial sediment samples. Components present in amounts less than 3% not shown.

- FIG. 18- Surficial sedimentary units (from Thrasher, 1979). See Table 2 for description.
- FIG. 19- Weight percents of volcanic ash in surficial sediment samples, relative to total terrigenous material (including clay minerals) finer than 2 mm. (Revised from Hampton et al., 1979).
- FIG. 20- Uniboom seismic reflection profile showing glacial deposit with rough, partially truncated upper surface, infilled and overlain by probable reworked material.
- FIG. 21- Uniboom seismic reflection profiles showing large sand waves.
a) seaward-facing sand waves, Stevenson Trough, b) symmetrical and asymmetrical waves, southern Albatross Bank
- FIG. 22- Locations of stations where sediment samples were analyzed for hydrocarbon gases and CO₂. Numbered stations are those where C₁ concentrations exceed 500 mL/L at a sediment depth of one meter. Compiled by K.A. Kvenvolden.
- FIG. 23- Gradients with depth of C₁ concentrations at eight stations having the highest C₁ concentrations. Compiled by K.A. Kvenvolden.
- FIG. 24- Locations of acoustic anomalies. See text for description of anomaly types.
- FIG. 25- Uniboom seismic reflection profile showing acoustic anomaly type 1 (see text) in center of record, flanked by type 5 on left and type 3 on right.
- FIG. 26- Uniboom seismic reflection profile showing acoustic anomaly type 2 (see text).
- FIG. 27- Uniboom seismic reflection profile showing acoustic anomaly type 3 (see text).
- FIG. 28- Uniboom seismic reflection profile showing acoustic anomaly type 4 (see text). a) sharply discontinuous reflectors with more-or-less transparent intervals, b) discontinuous reflectors with murky intervals.
- FIG. 29- Uniboom seismic reflection profile showing acoustic anomaly type 5 (see text).
- FIG. 30- Uniboom seismic reflection profile showing acoustic anomaly type 6 (see text).
- FIG. 31- Locations of sediment slides.
- FIG. 32- Sparker seismic reflection profile showing features indicating sediment slides.

- FIG. 33- Sparker seismic reflection profile showing hummocky seafloor; an indicator of possible sediment slides.
- FIG. 34- Uniboom seismic reflection profile showing small, shallow sediment slides.
- FIG. 35- Sparker seismic reflection profiles showing similar structural styles near the shelf break of a) southern Albatross Bank and b) Portlock Bank, indicating severe tectonic deformation.
- FIG. 36- Sparker seismic reflection profile near the shelf break of northern Albatross Bank showing structural style indicating relatively minor tectonic deformation.

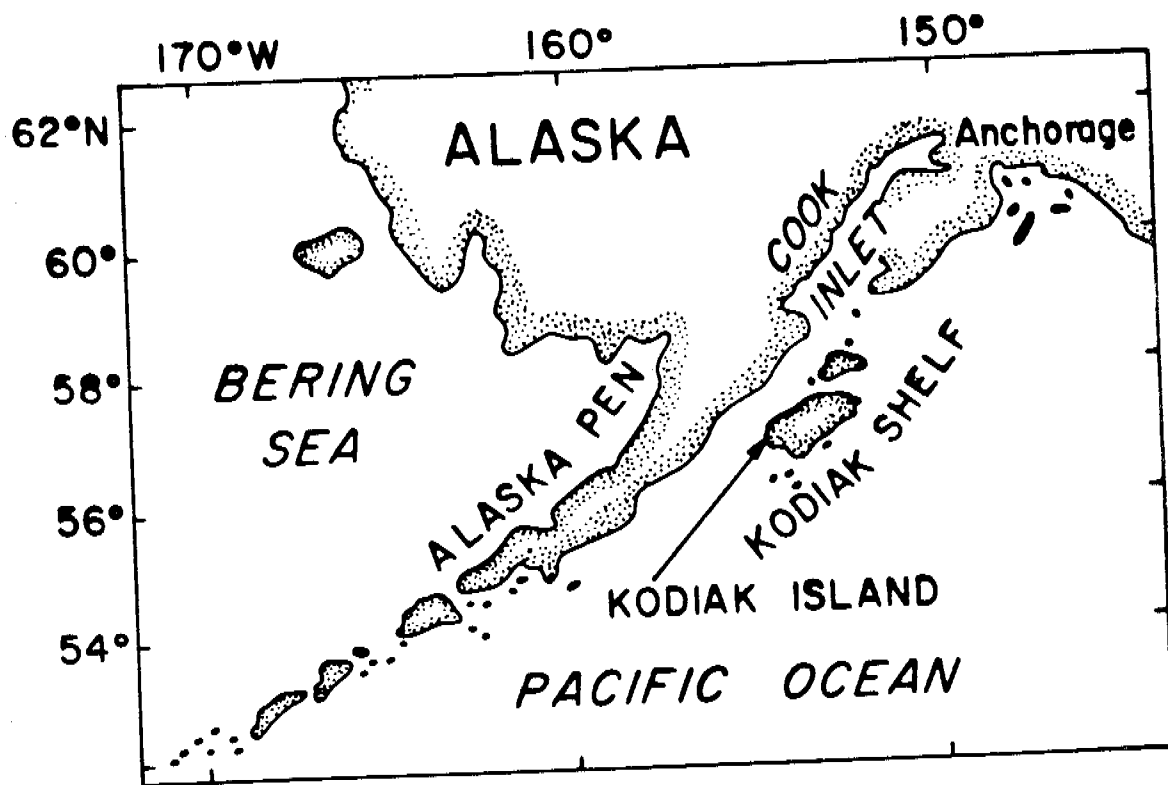


Fig. 1

76

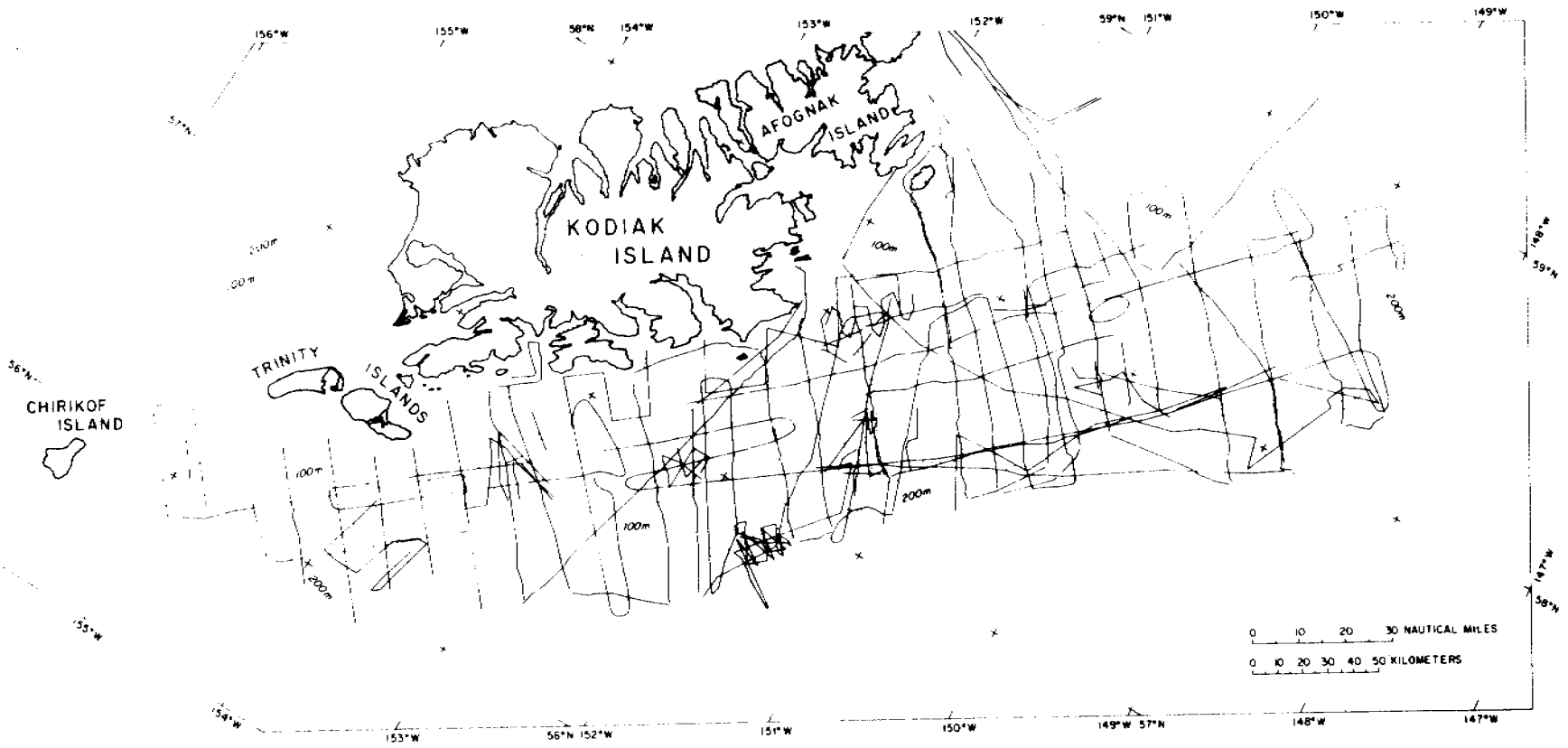
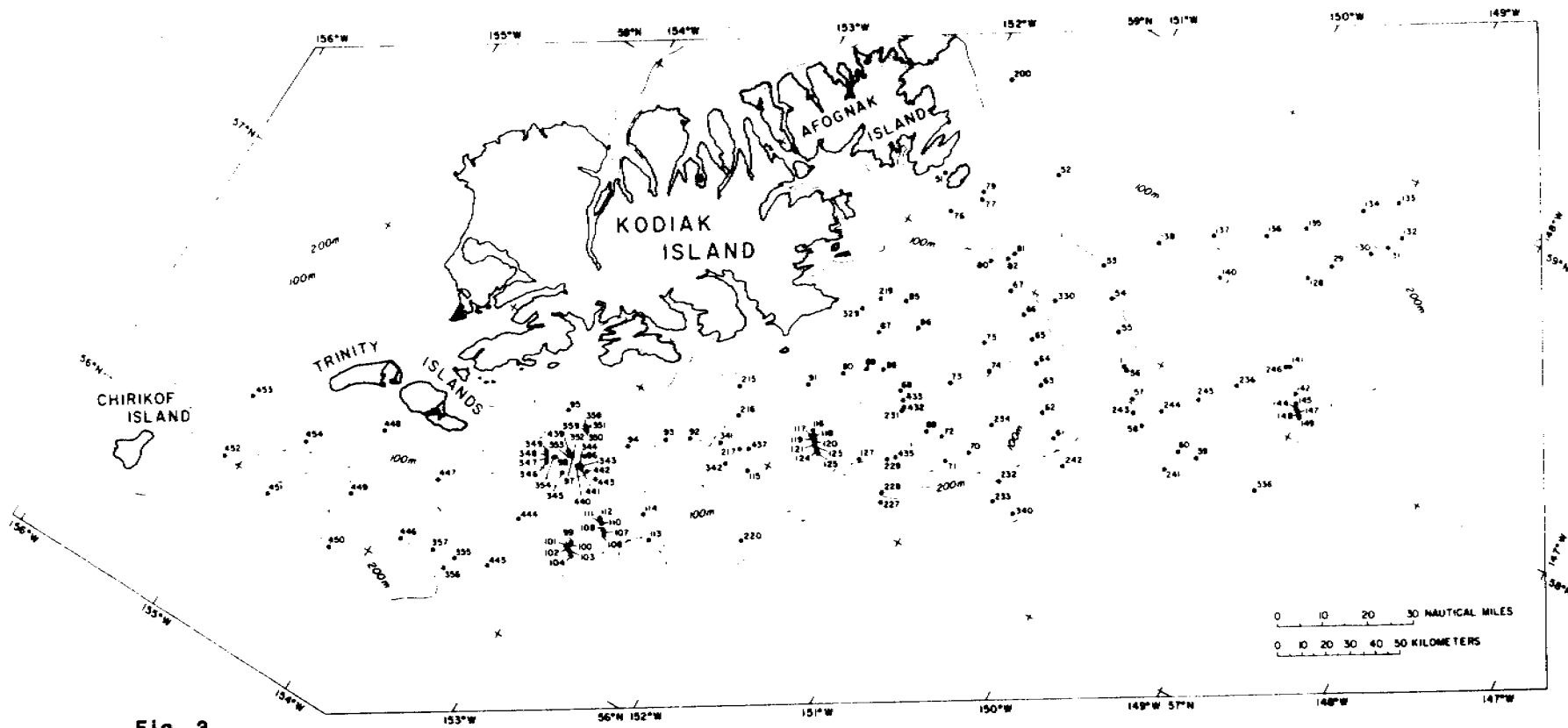


Fig. 2



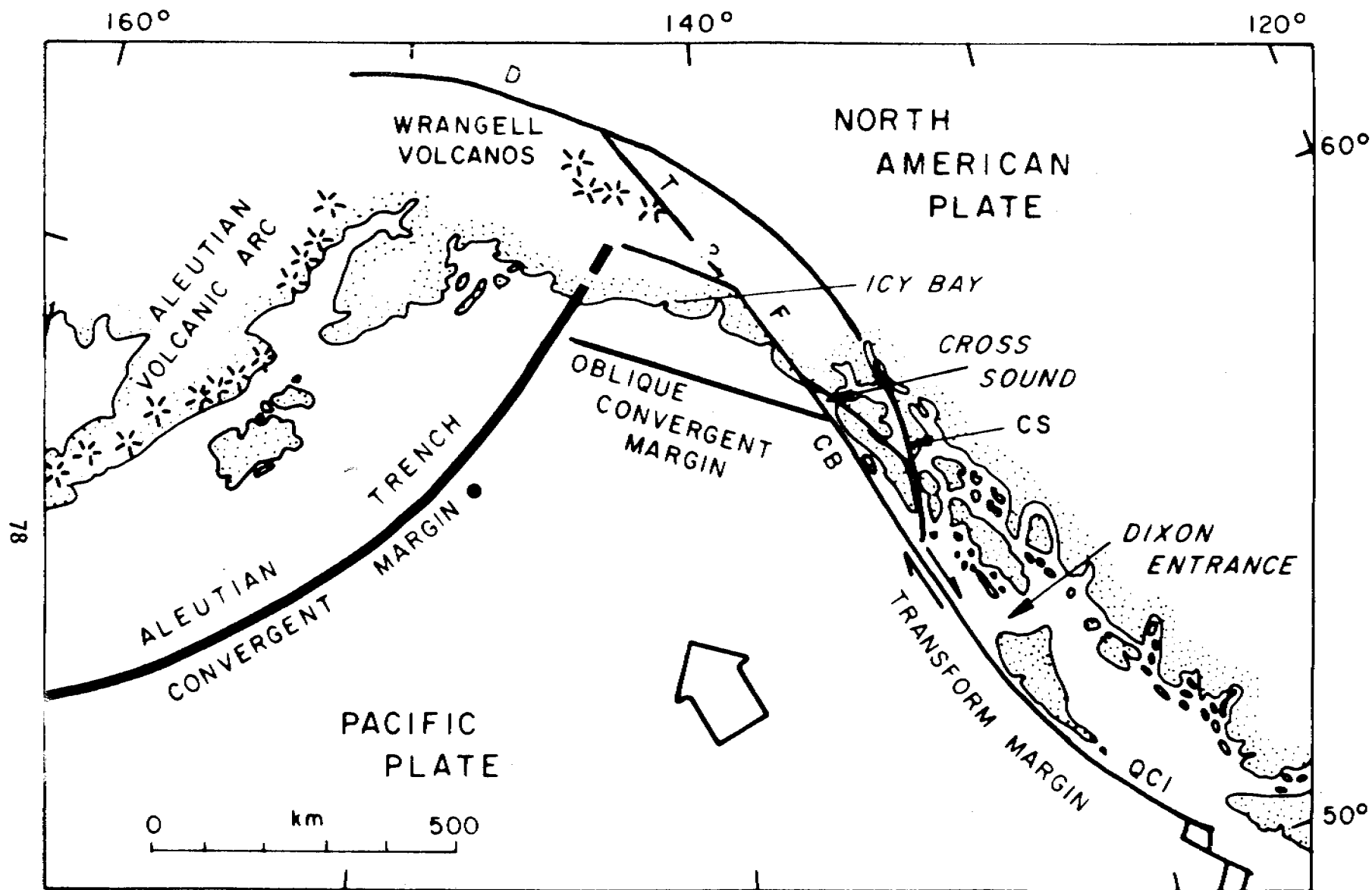


Fig. 4

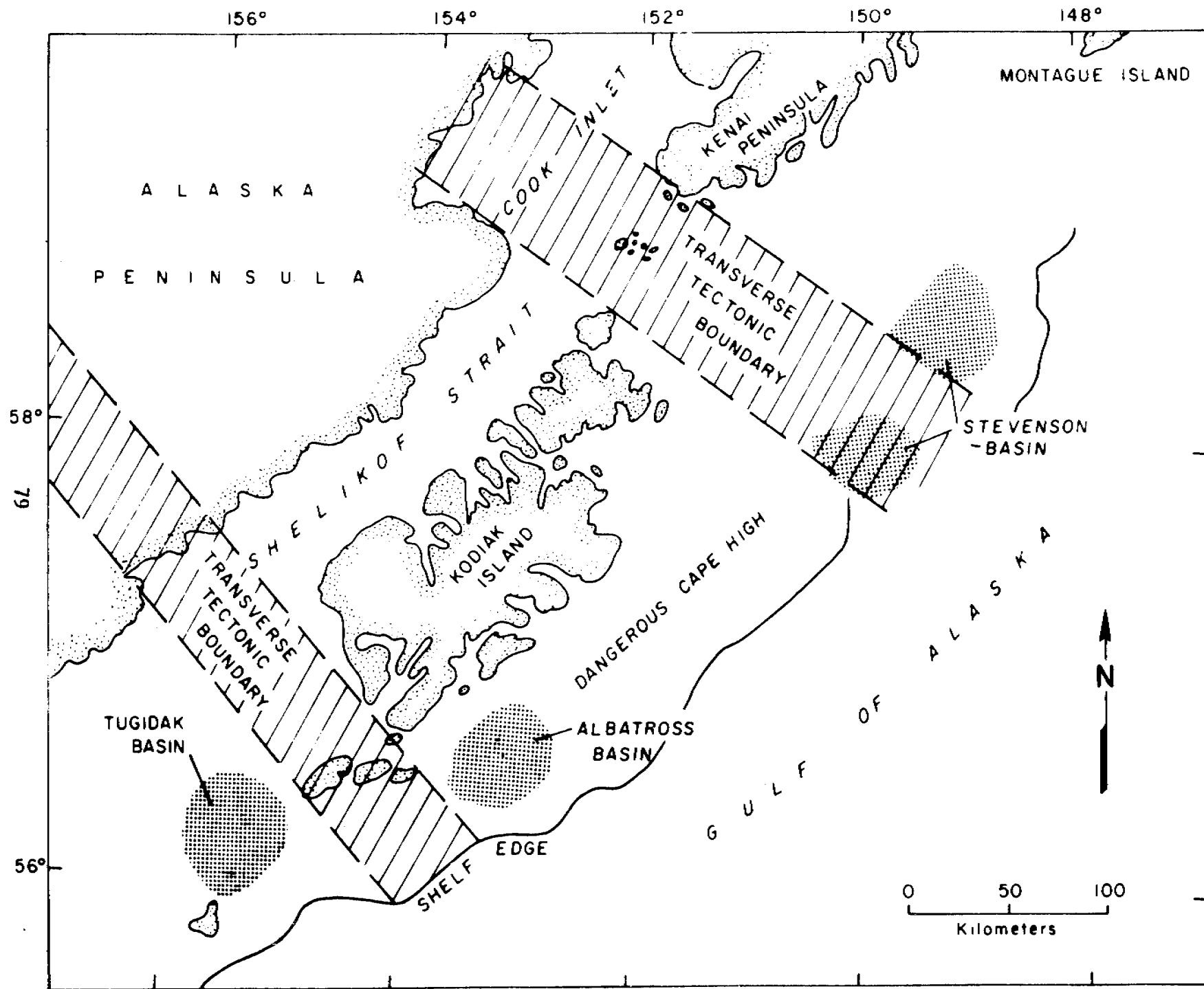


Fig. 5

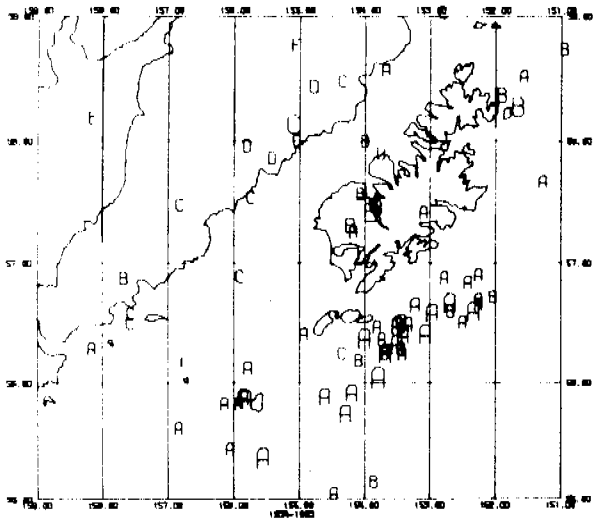


Fig. 6a

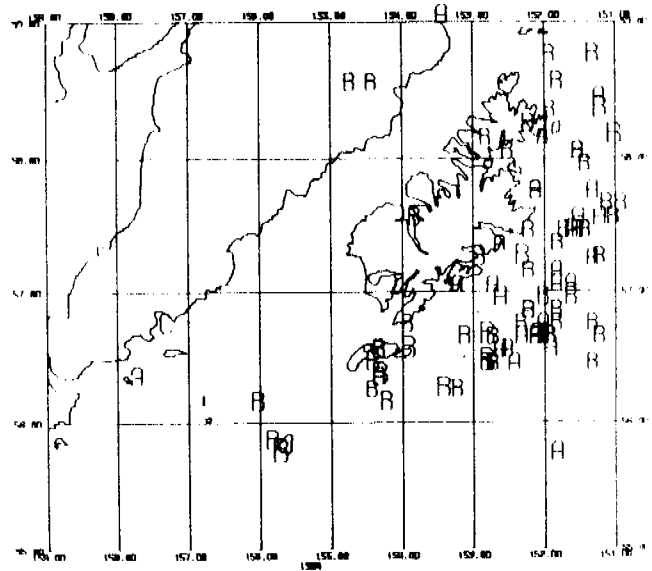


Fig. 6b

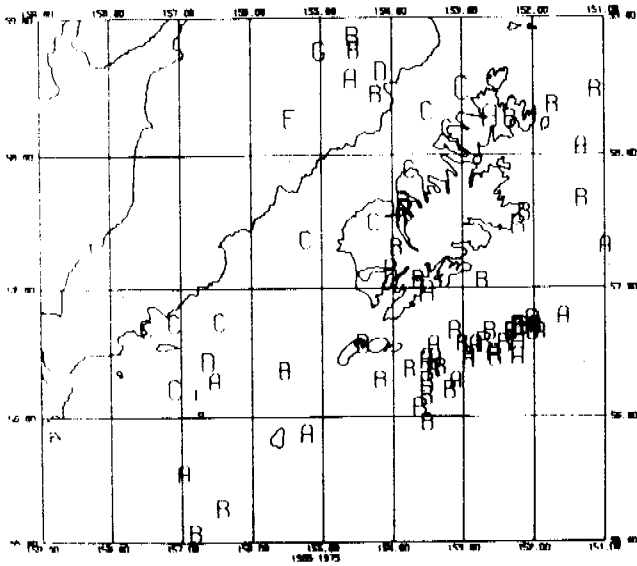


Fig. 6c

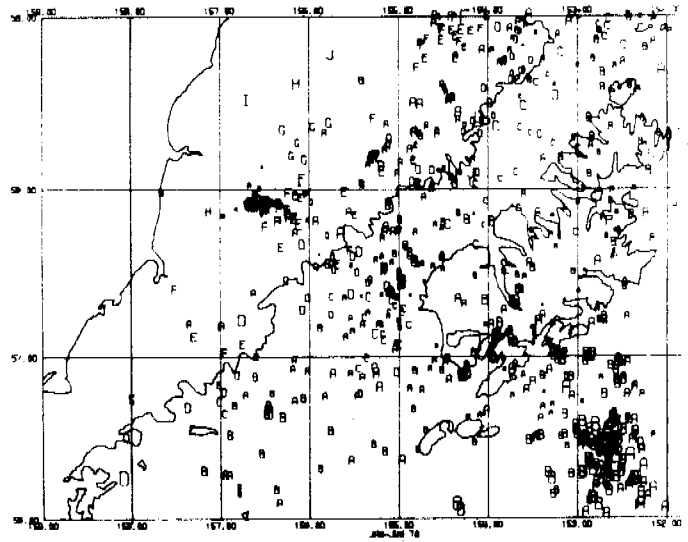
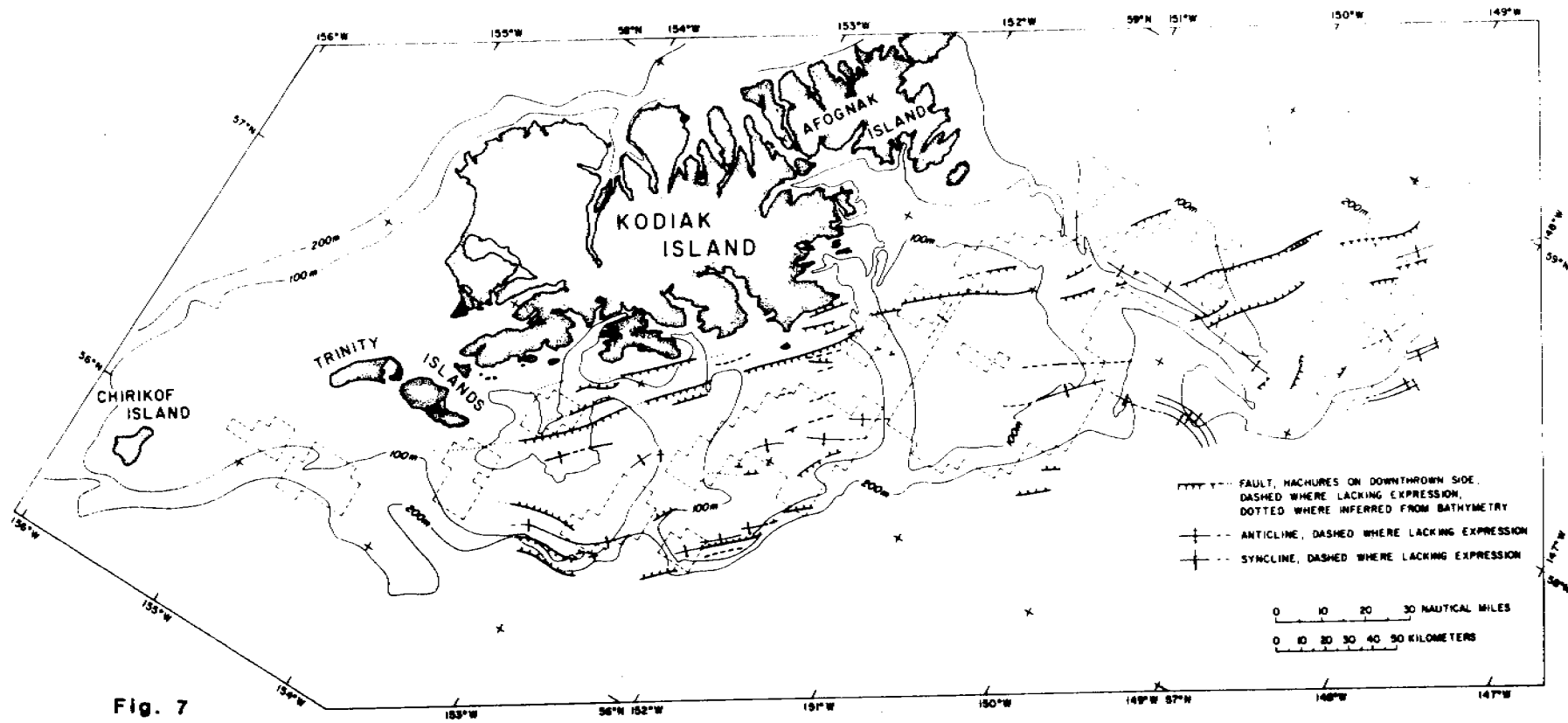


Fig. 6d



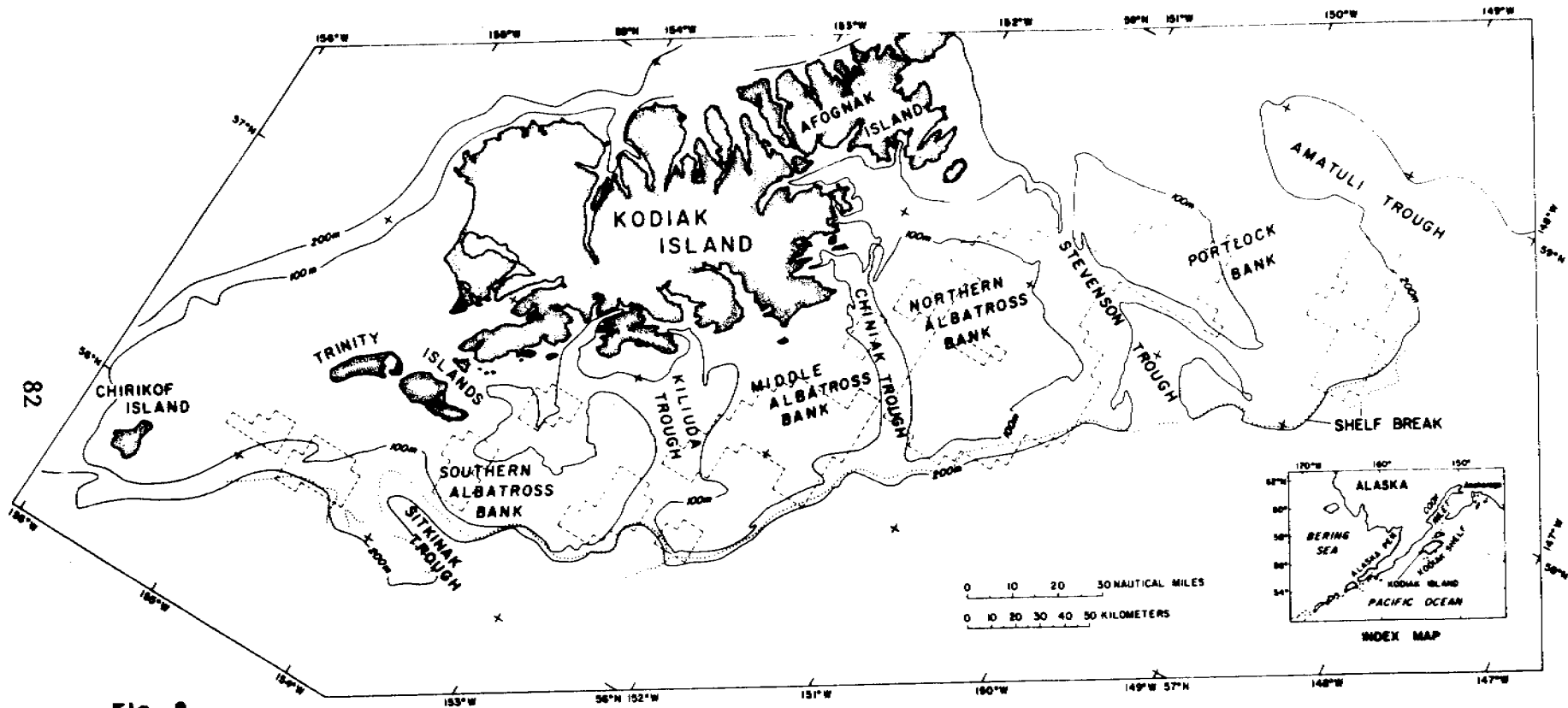


Fig. 8

82

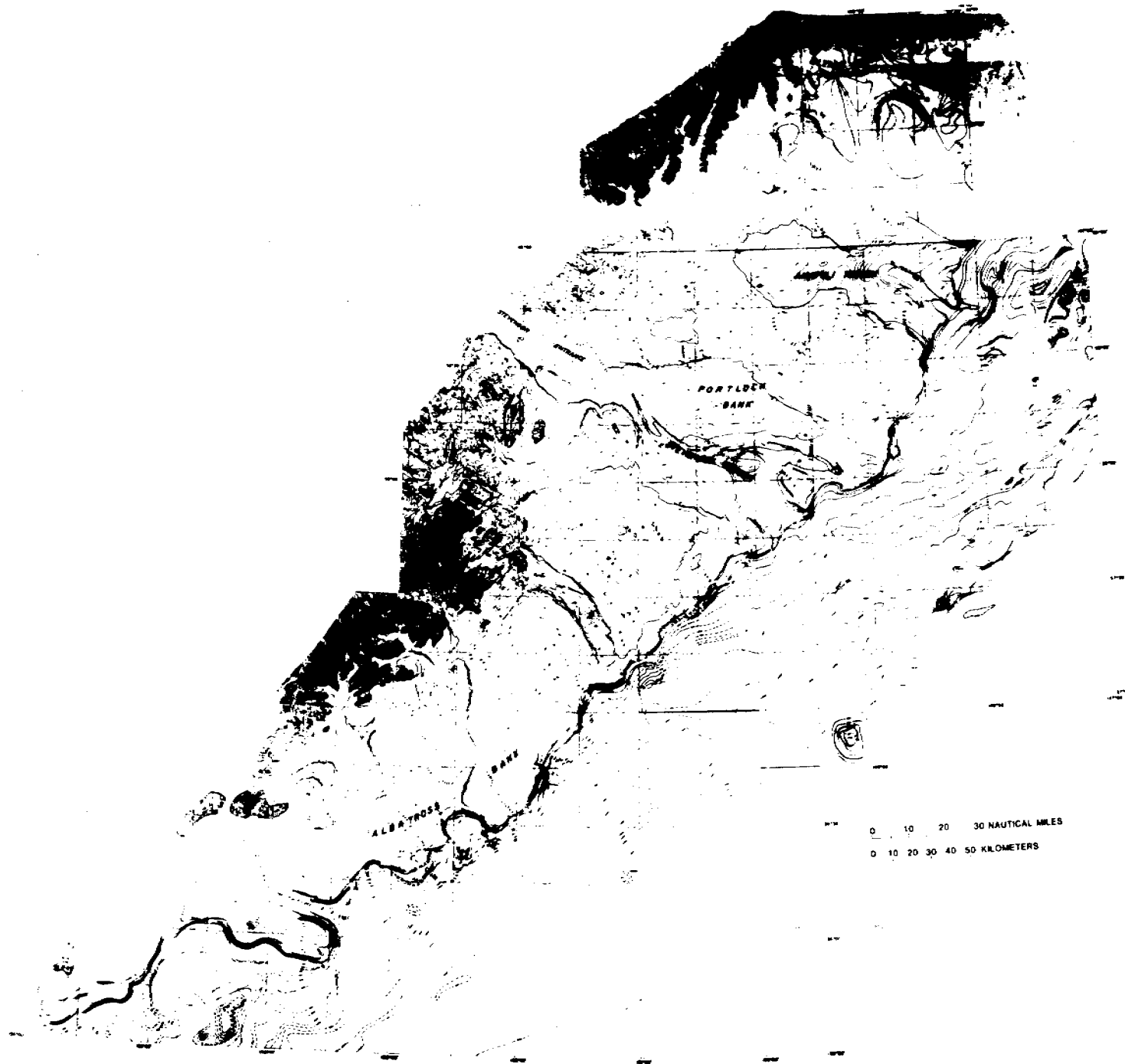


Fig. 9

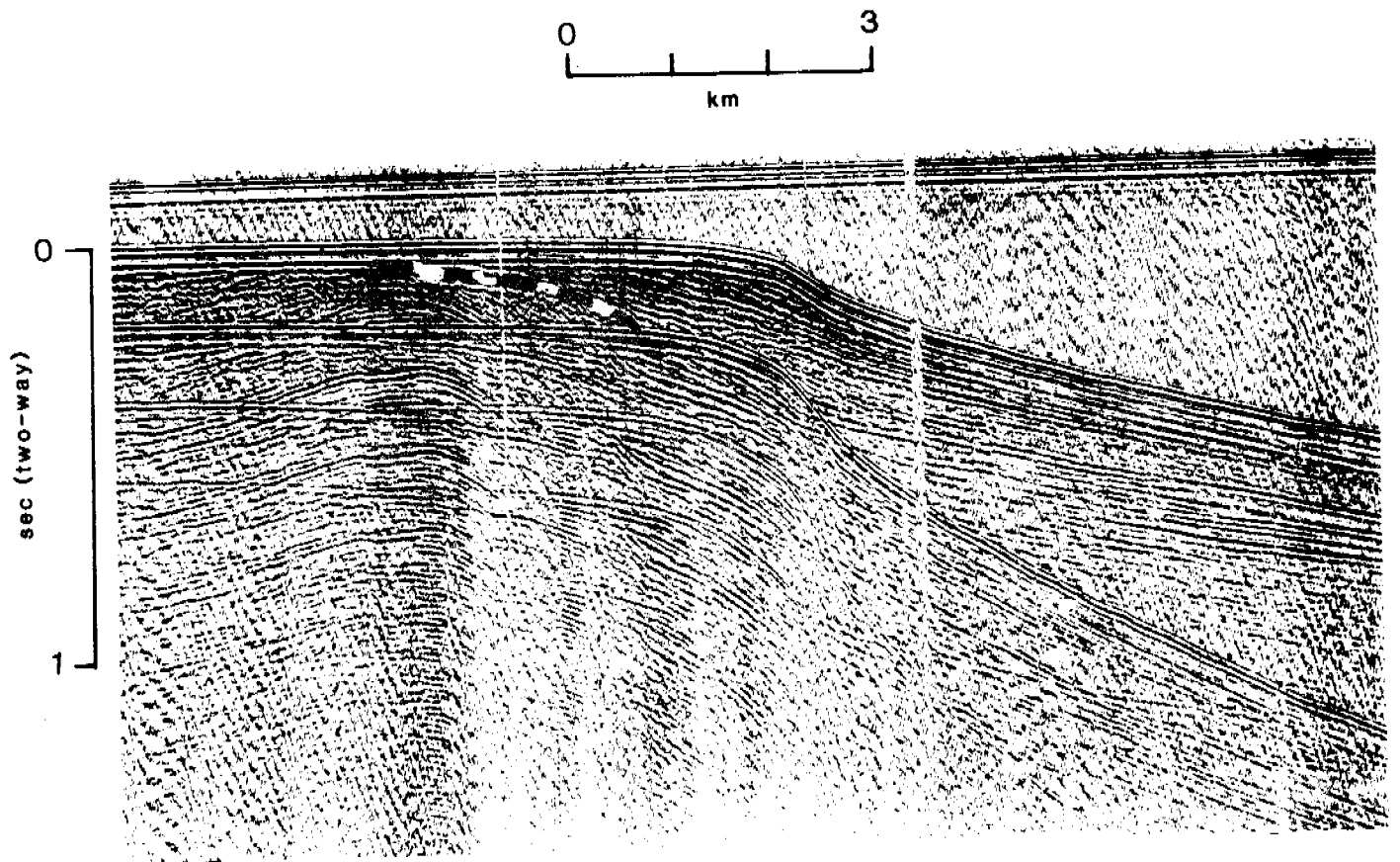


Fig. 10

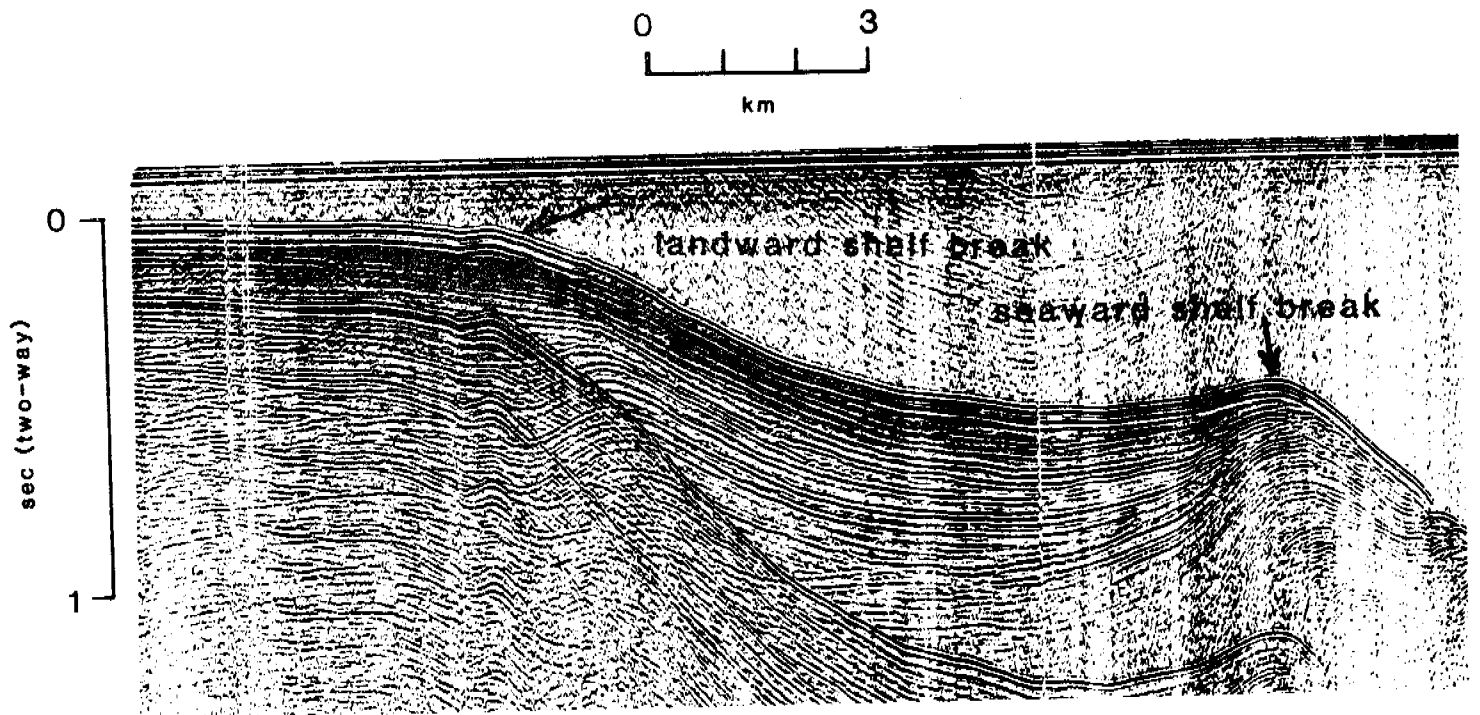


Fig. 11

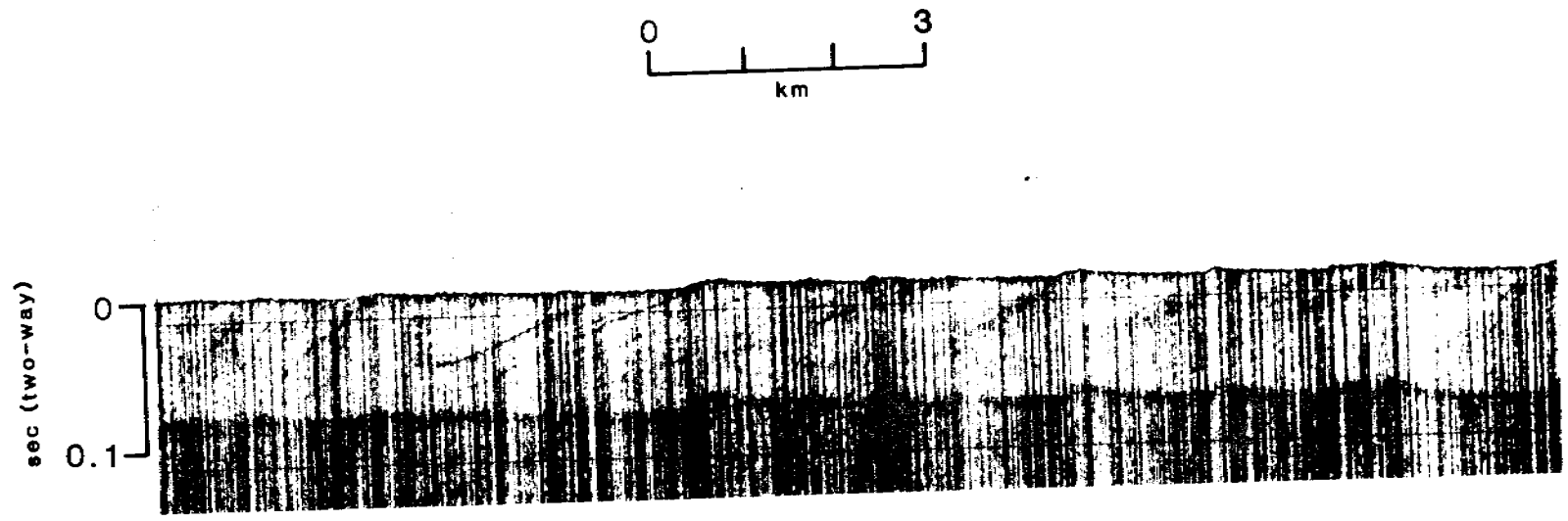


Fig. 12

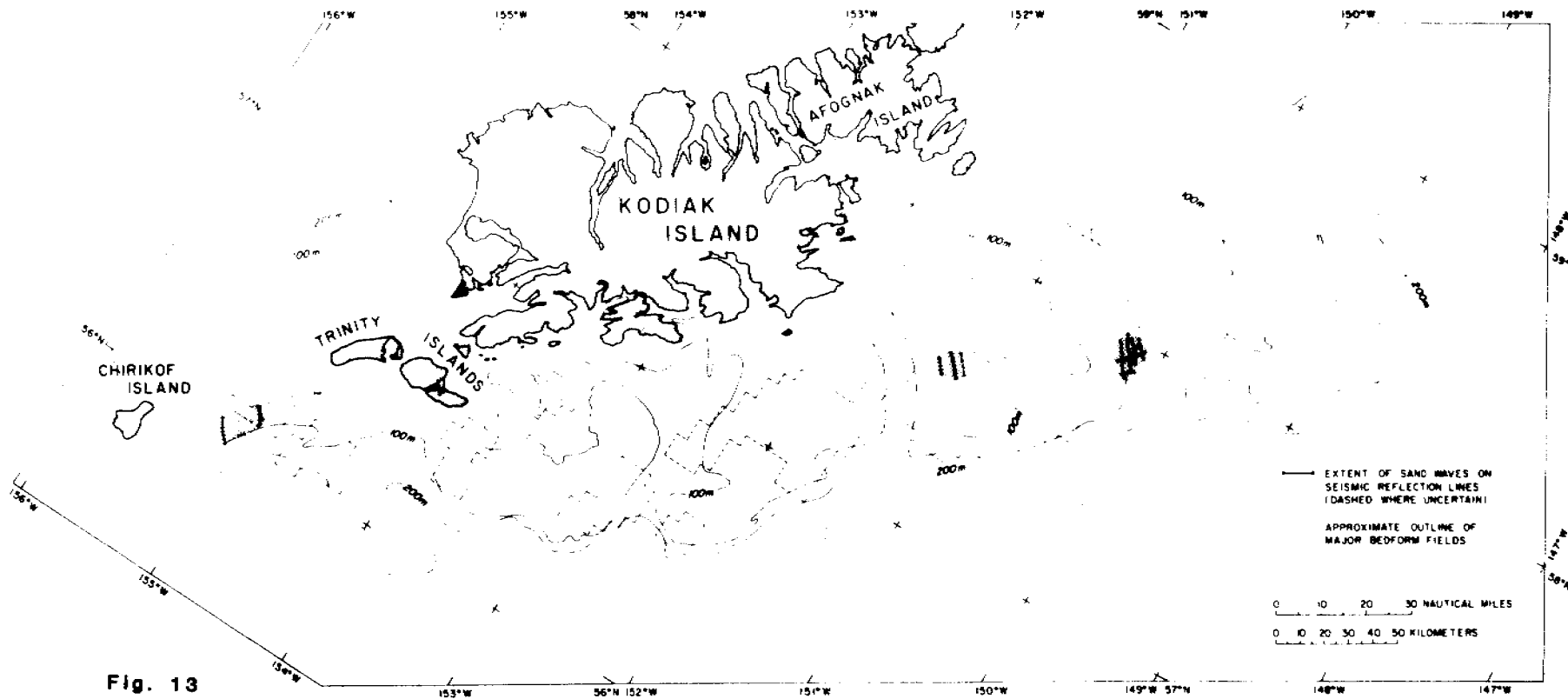


Fig. 13

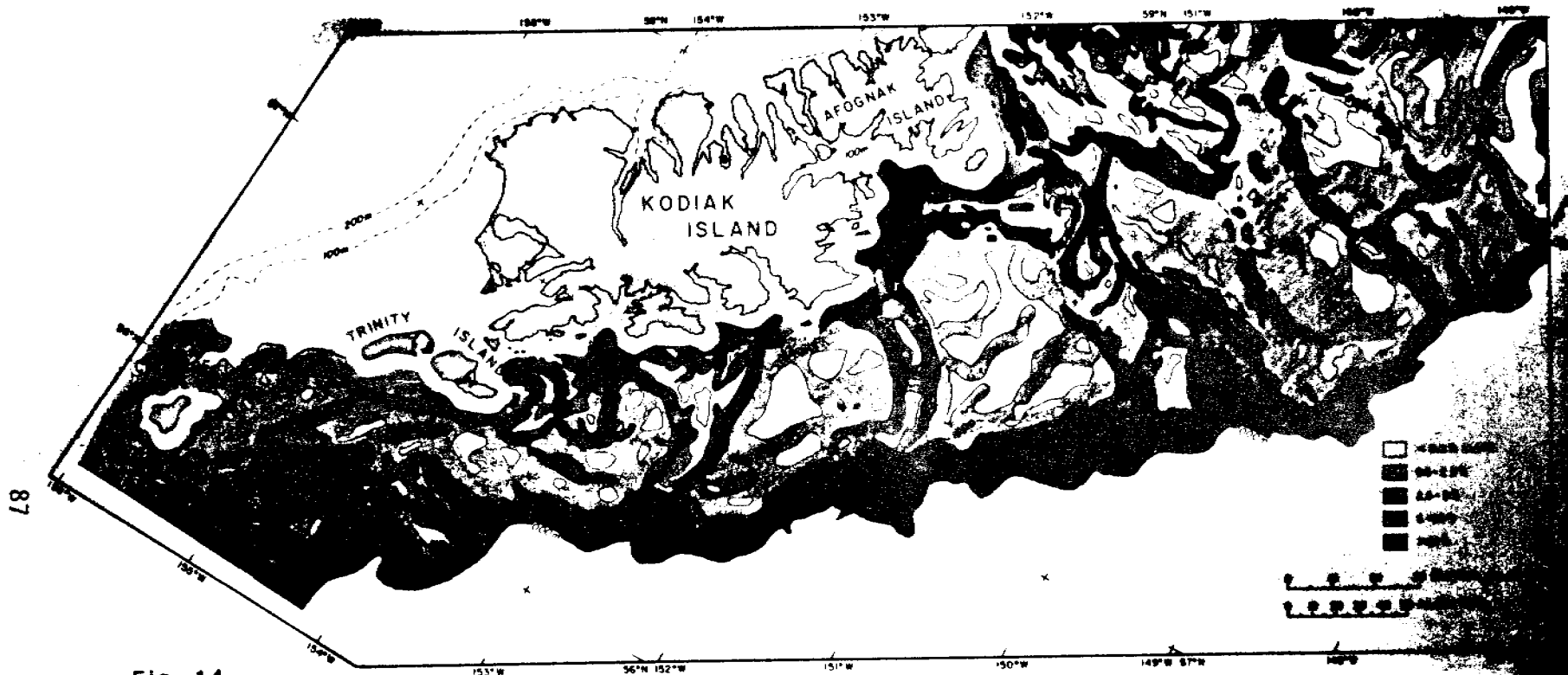


Fig. 14

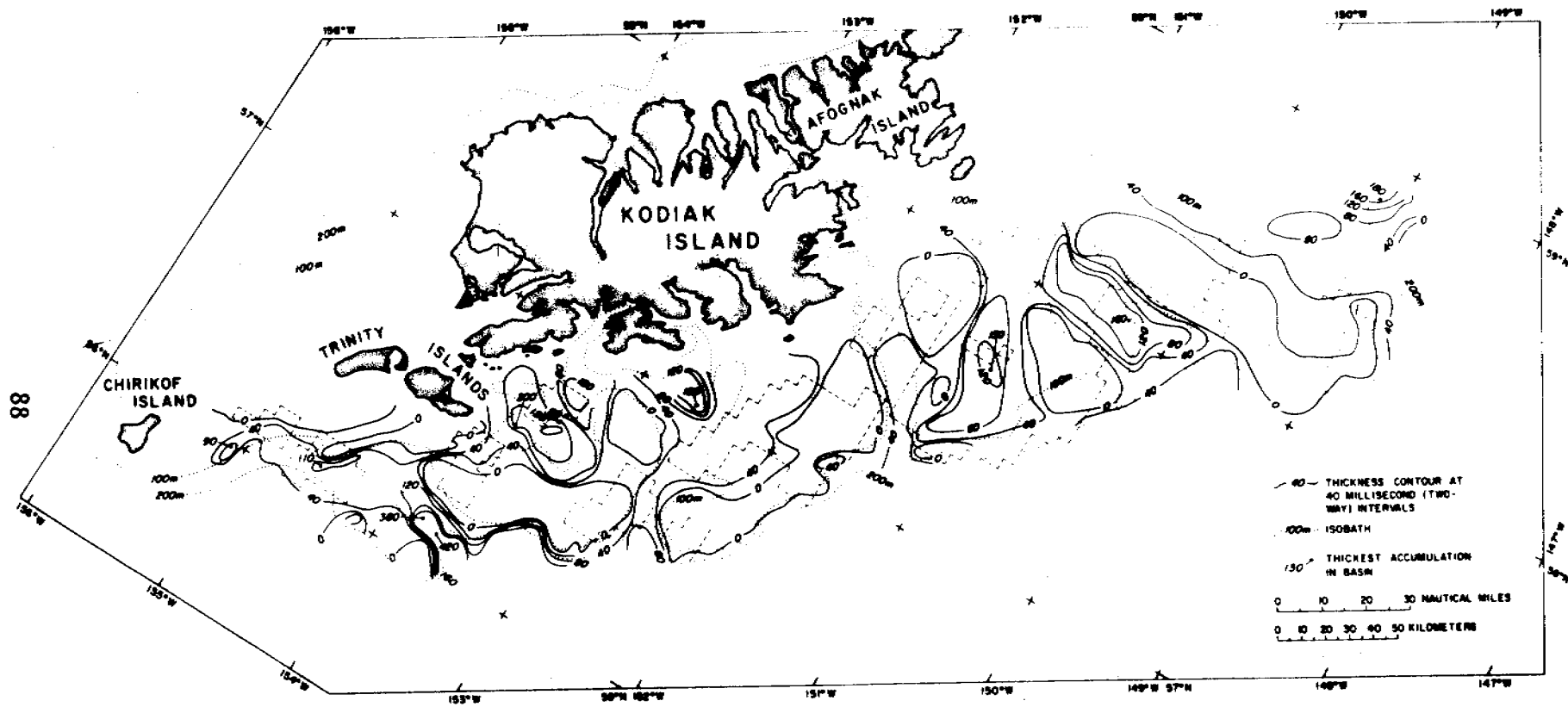


Fig. 18

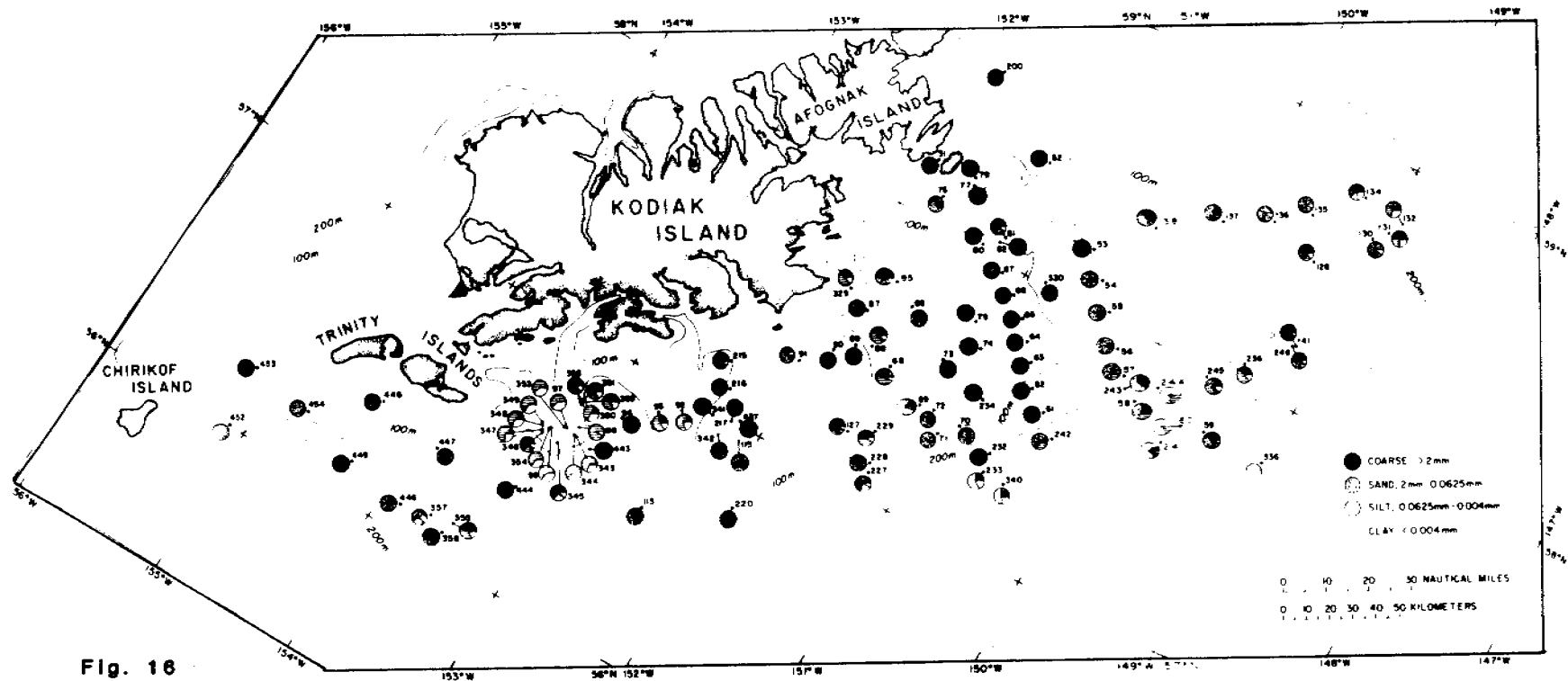


Fig. 16

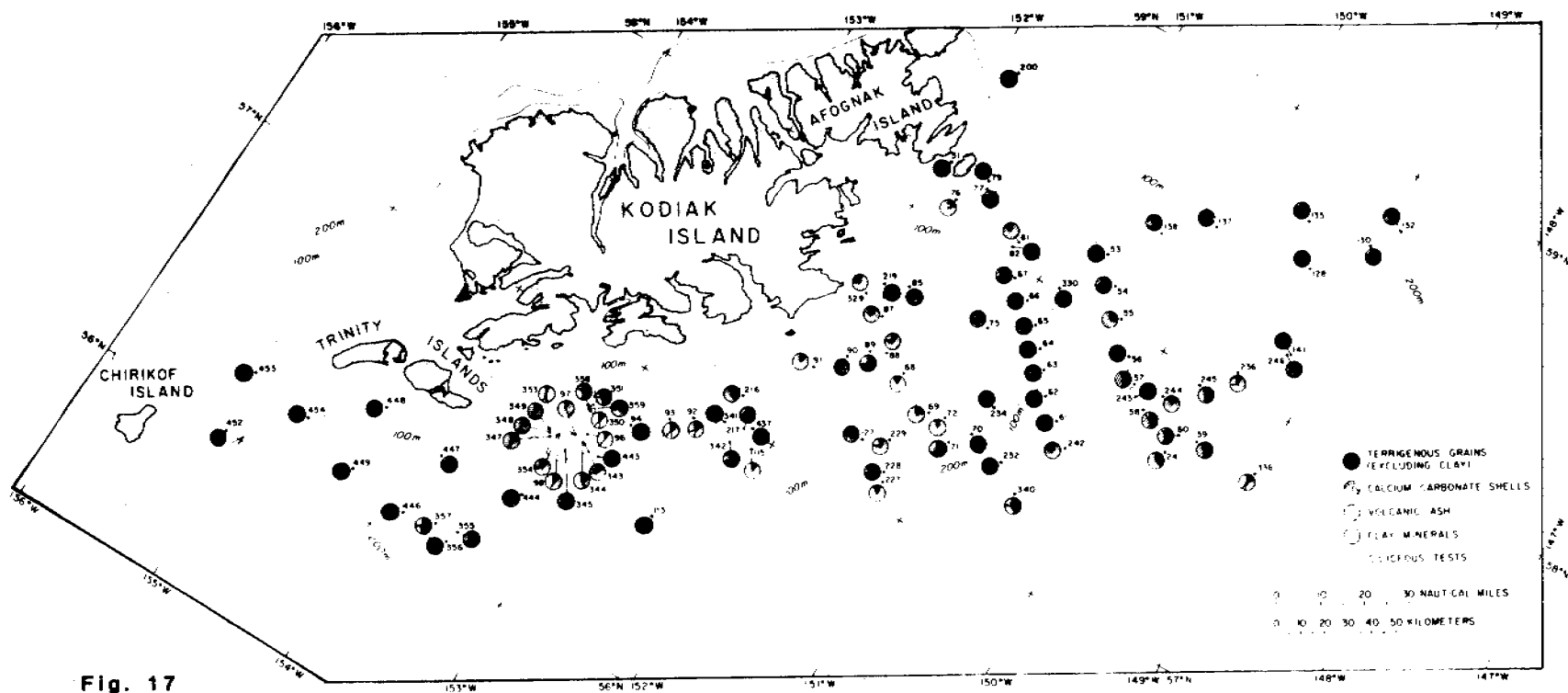


Fig. 17

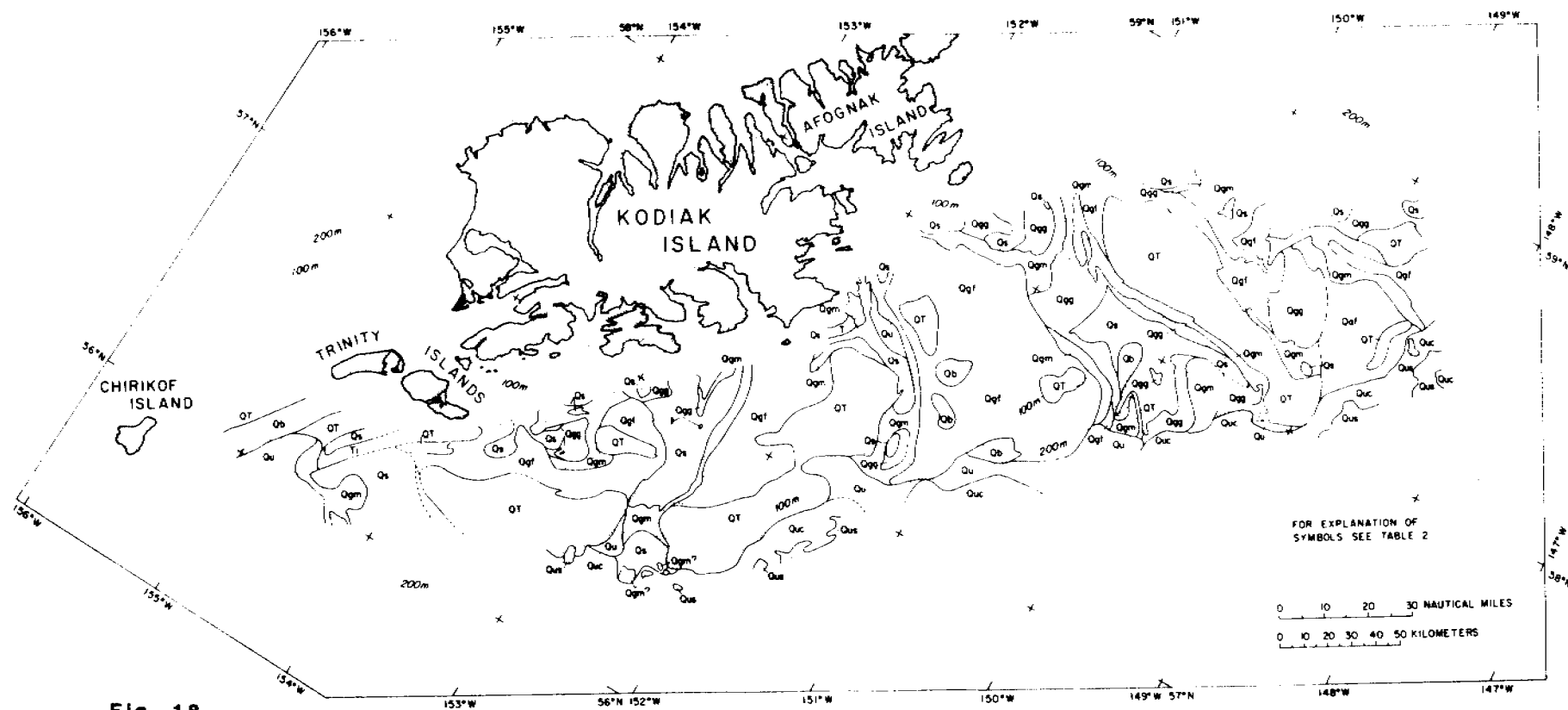


Fig. 18

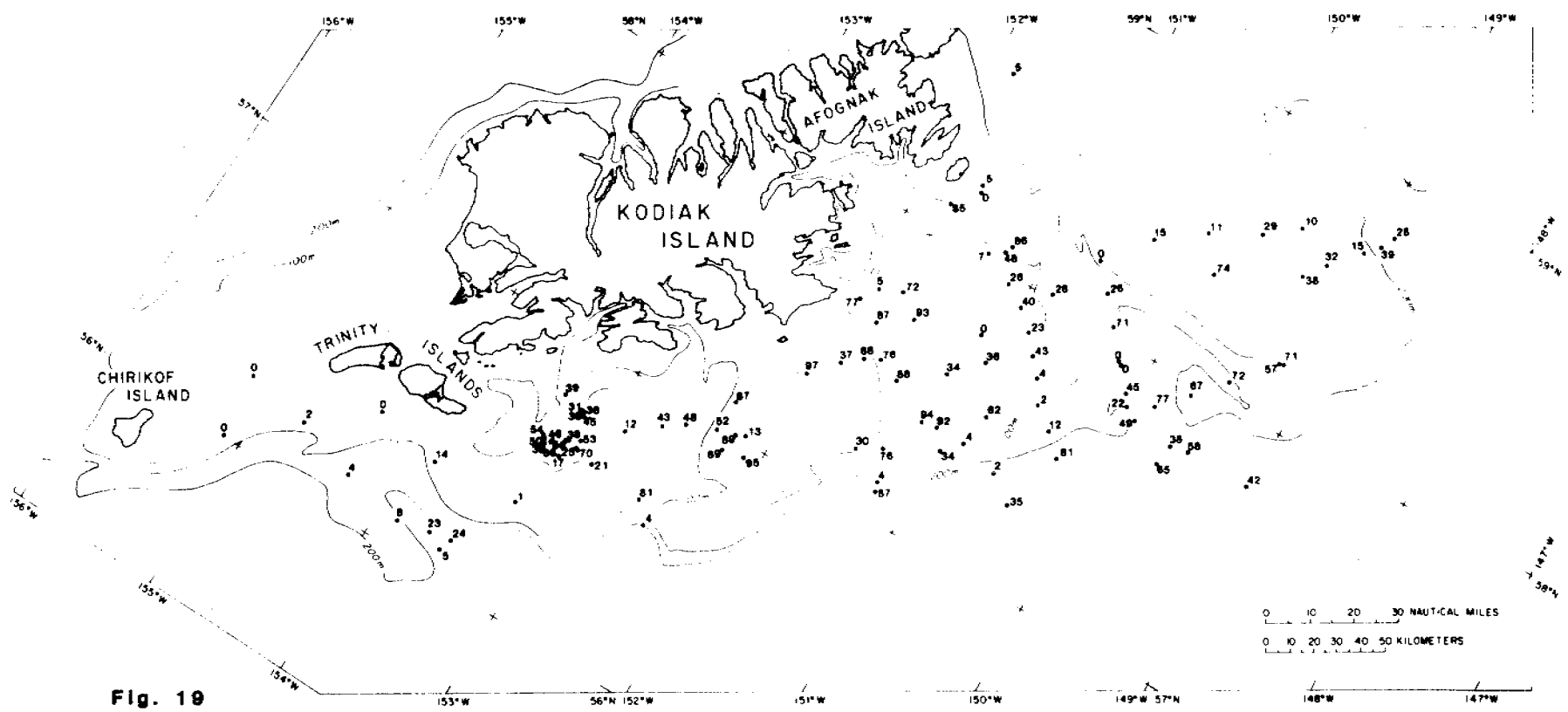
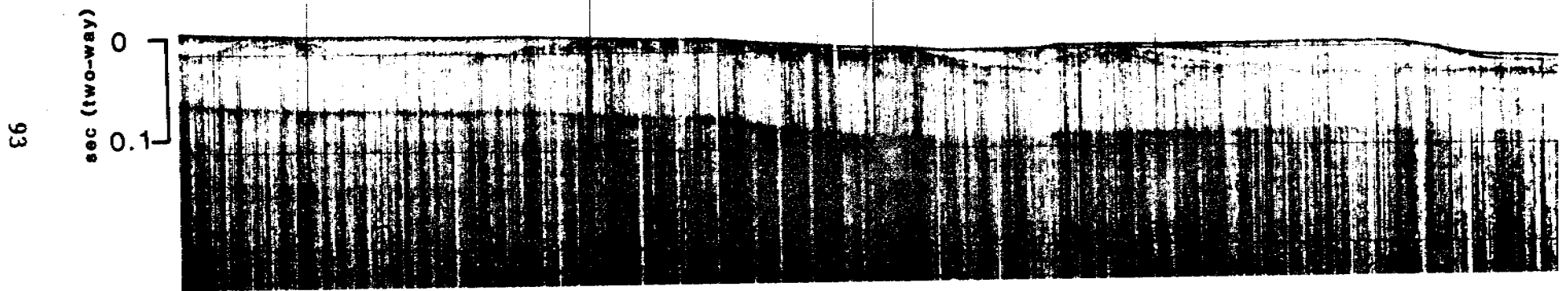
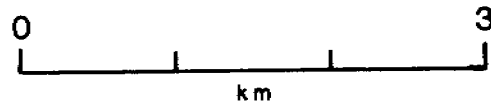


Fig. 19



93

sec (two-way)
0
0.1

Fig. 20

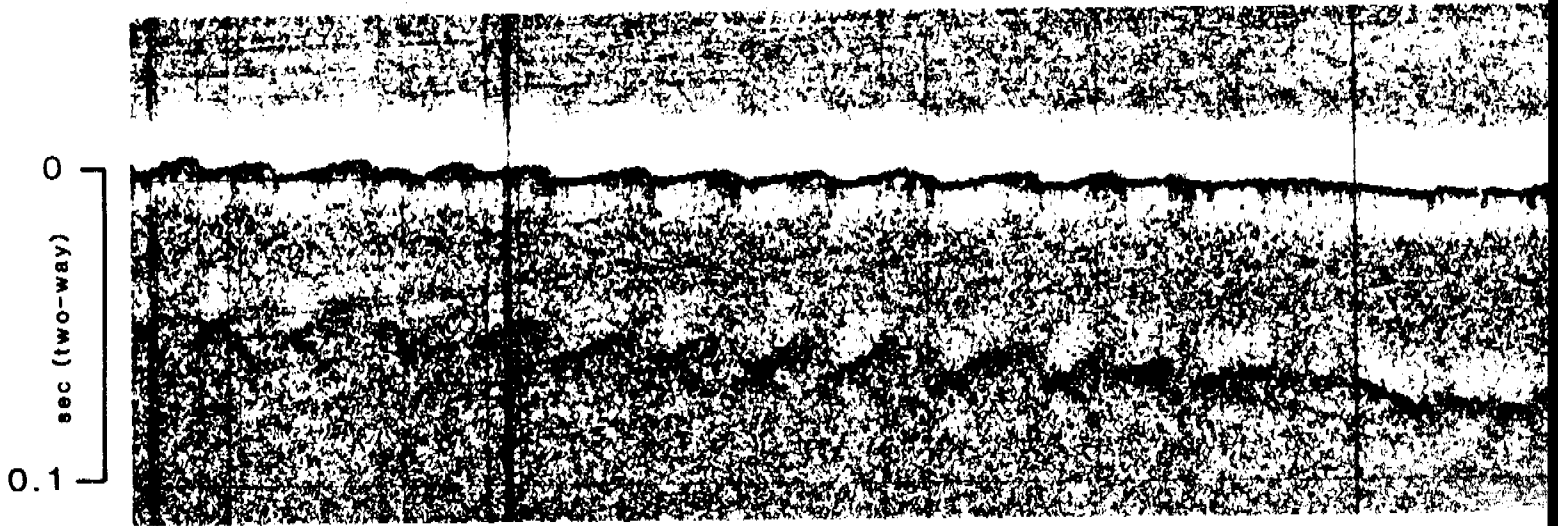
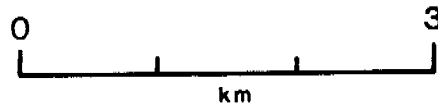


Fig. 21a

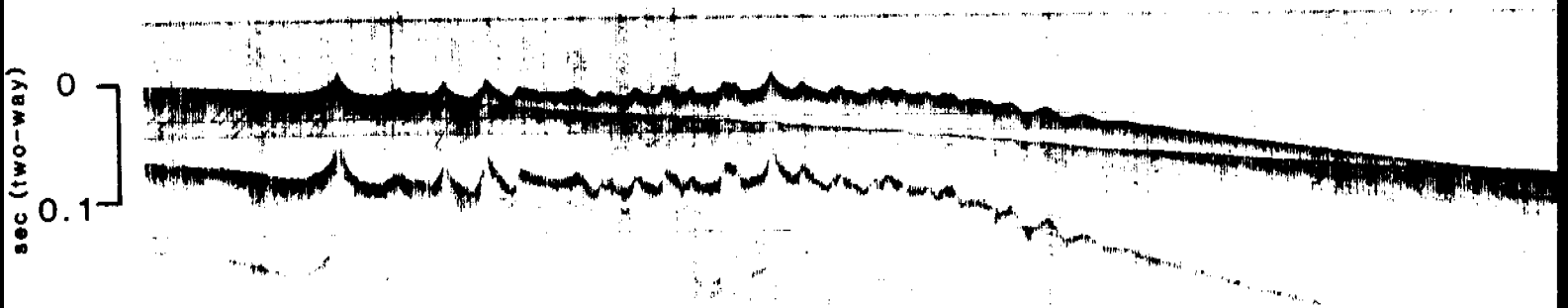
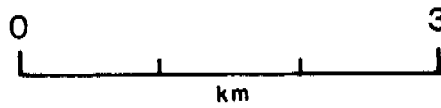


Fig. 21b

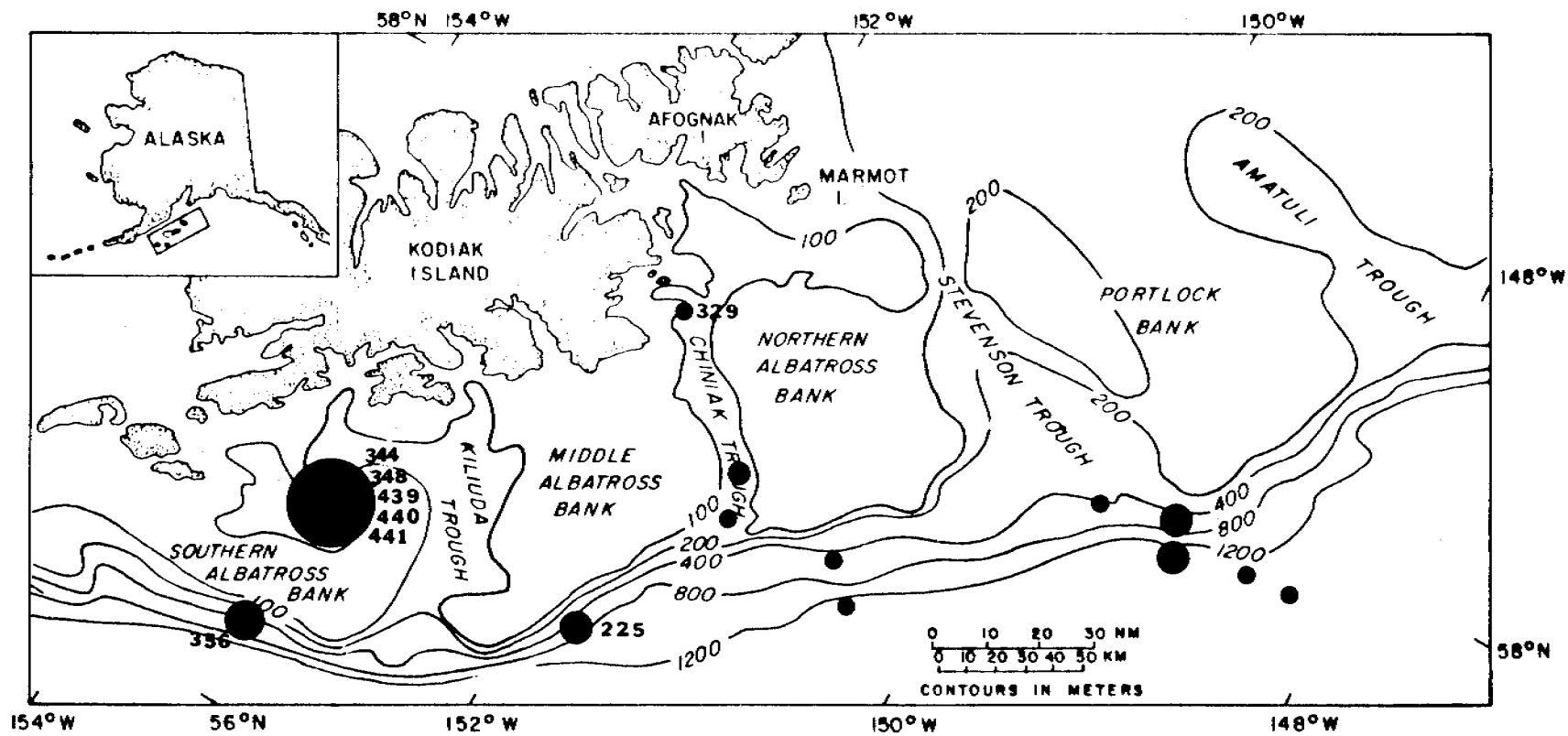


Fig. 22

Concentrations of C_1 ($10^x \mu\text{L/L}$ interstitial water)

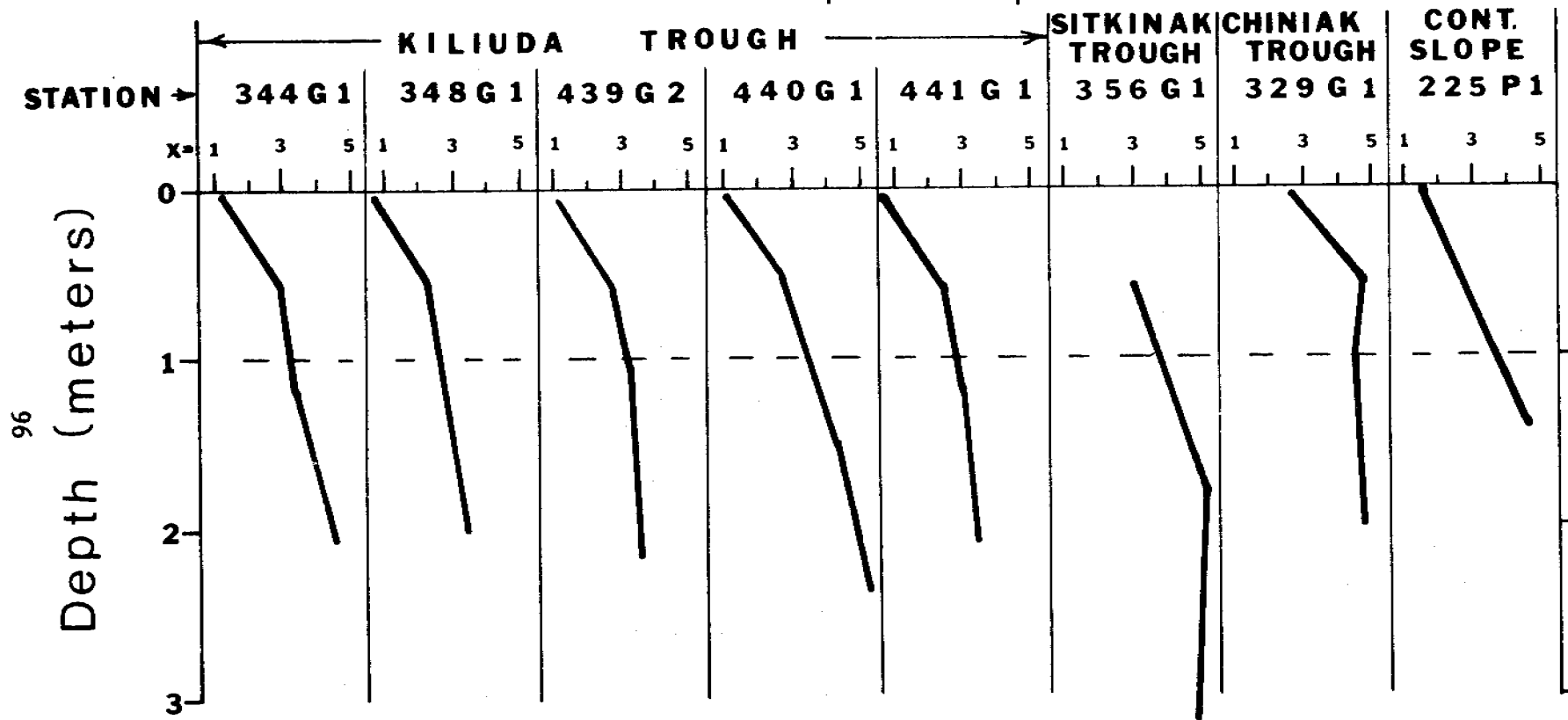


Fig. 23

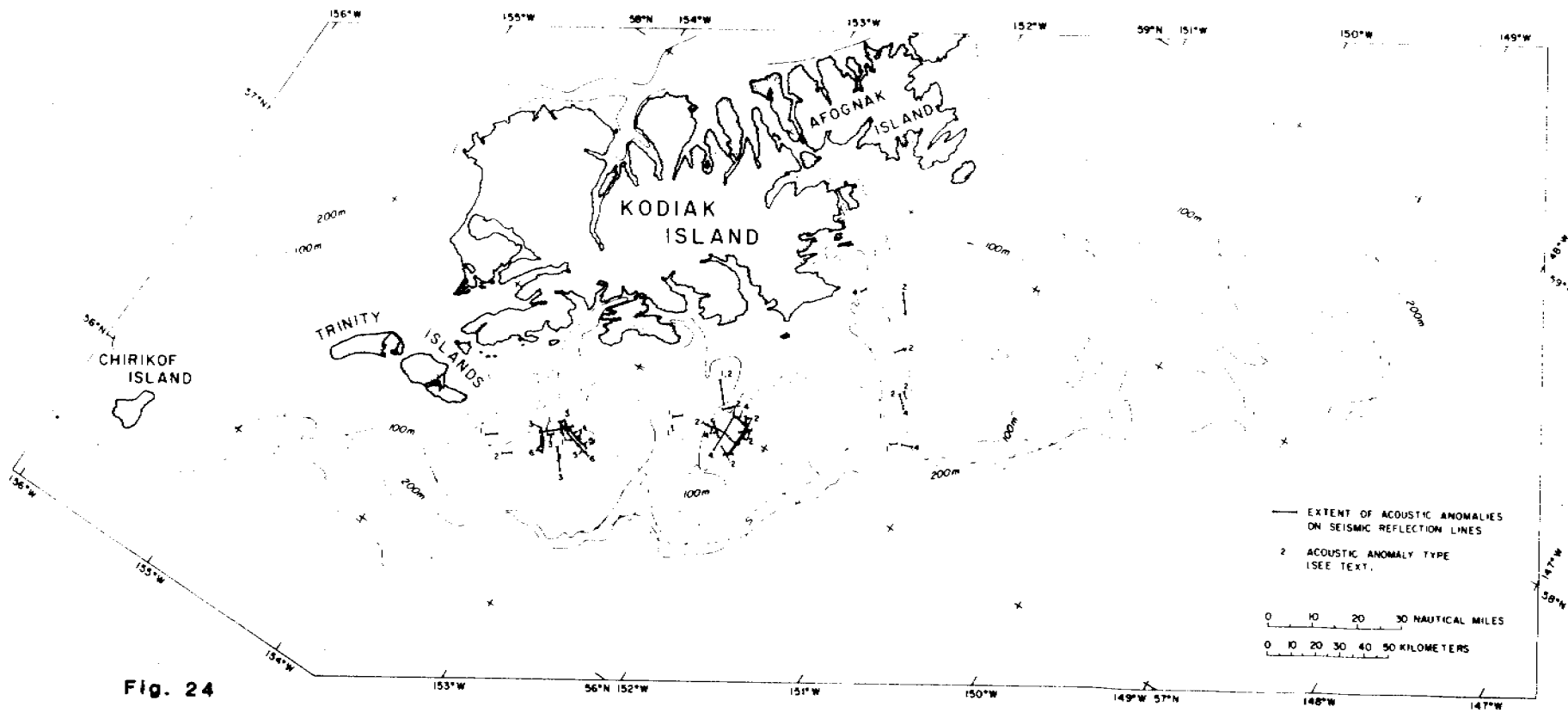


Fig. 24

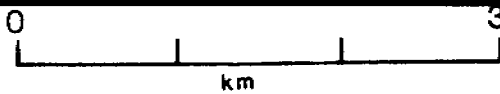


Fig. 25

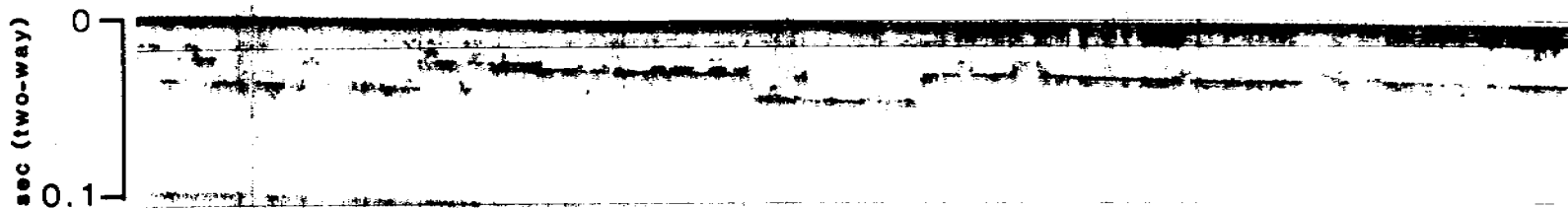
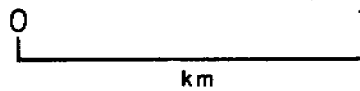


Fig. 26

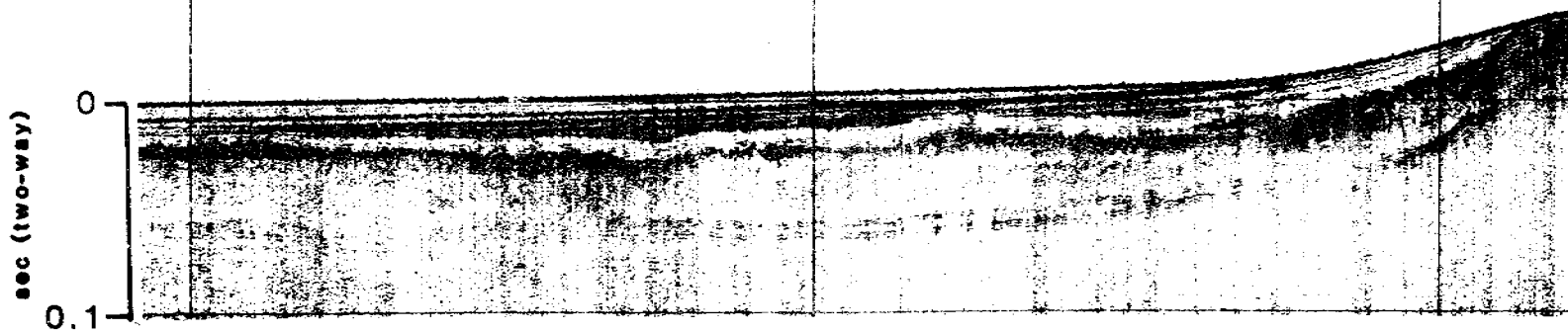


Fig. 27

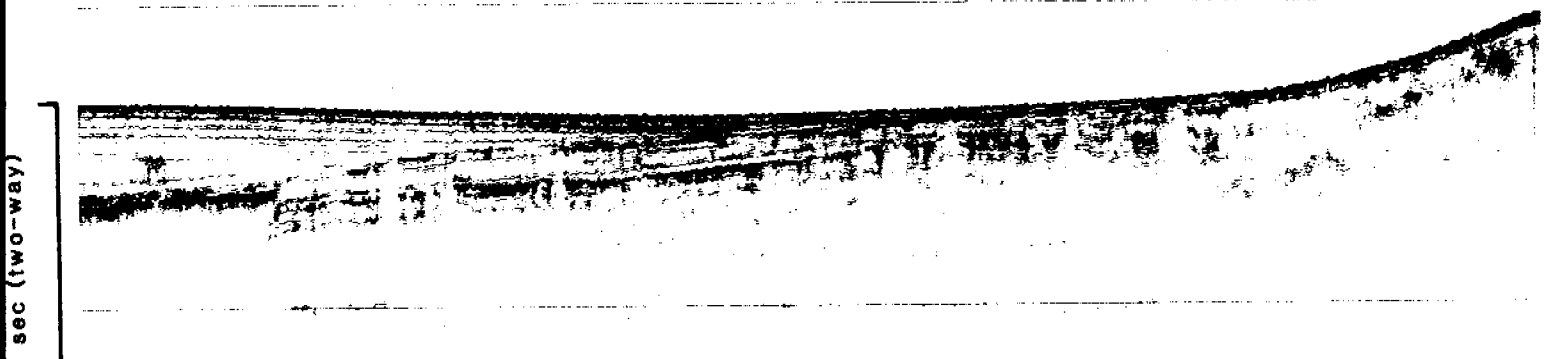
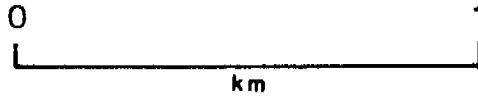


Fig. 28a

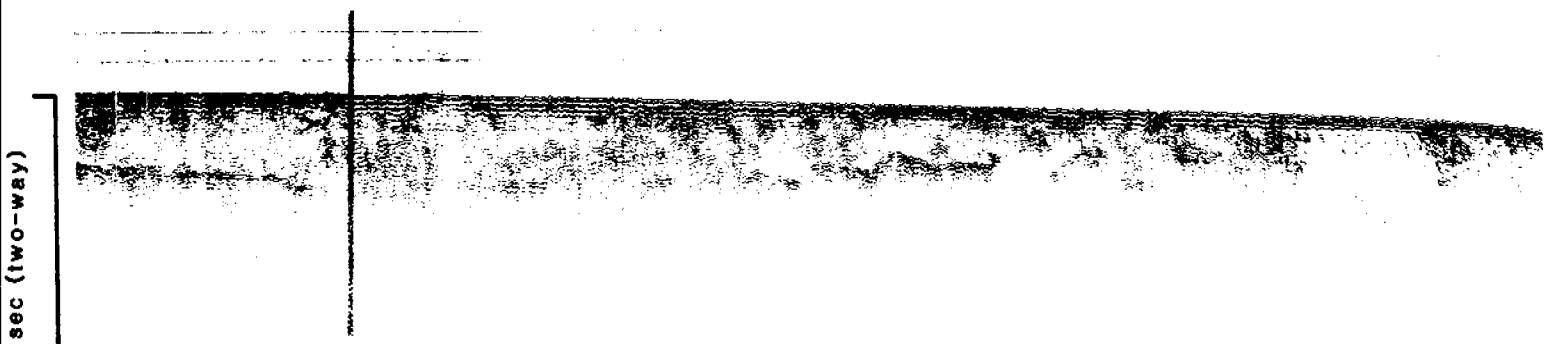
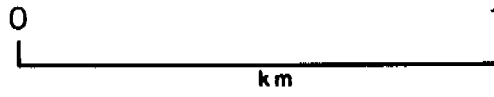


Fig. 28b

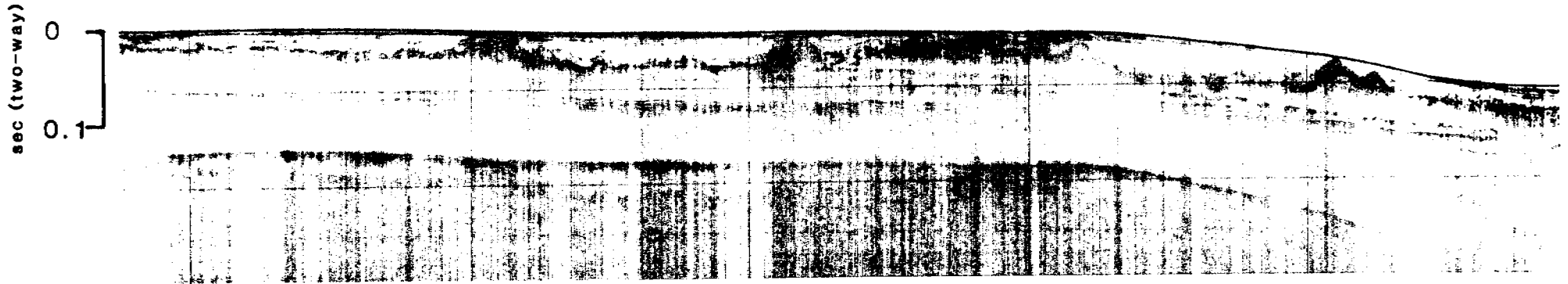
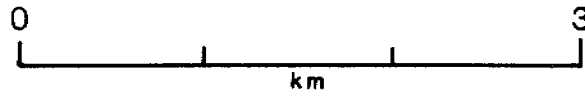


Fig. 29

100

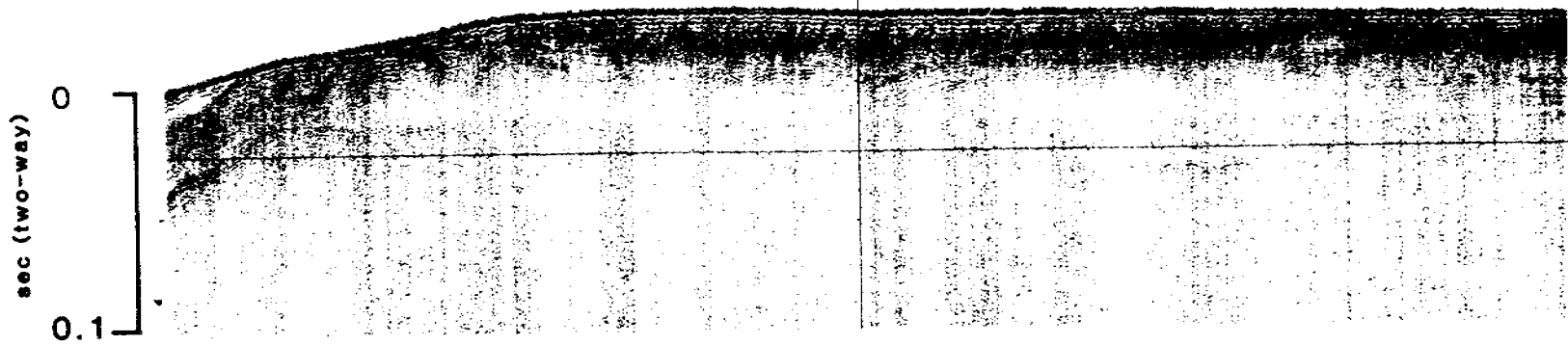
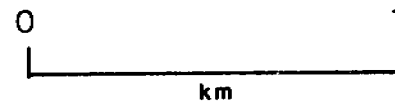


Fig. 30

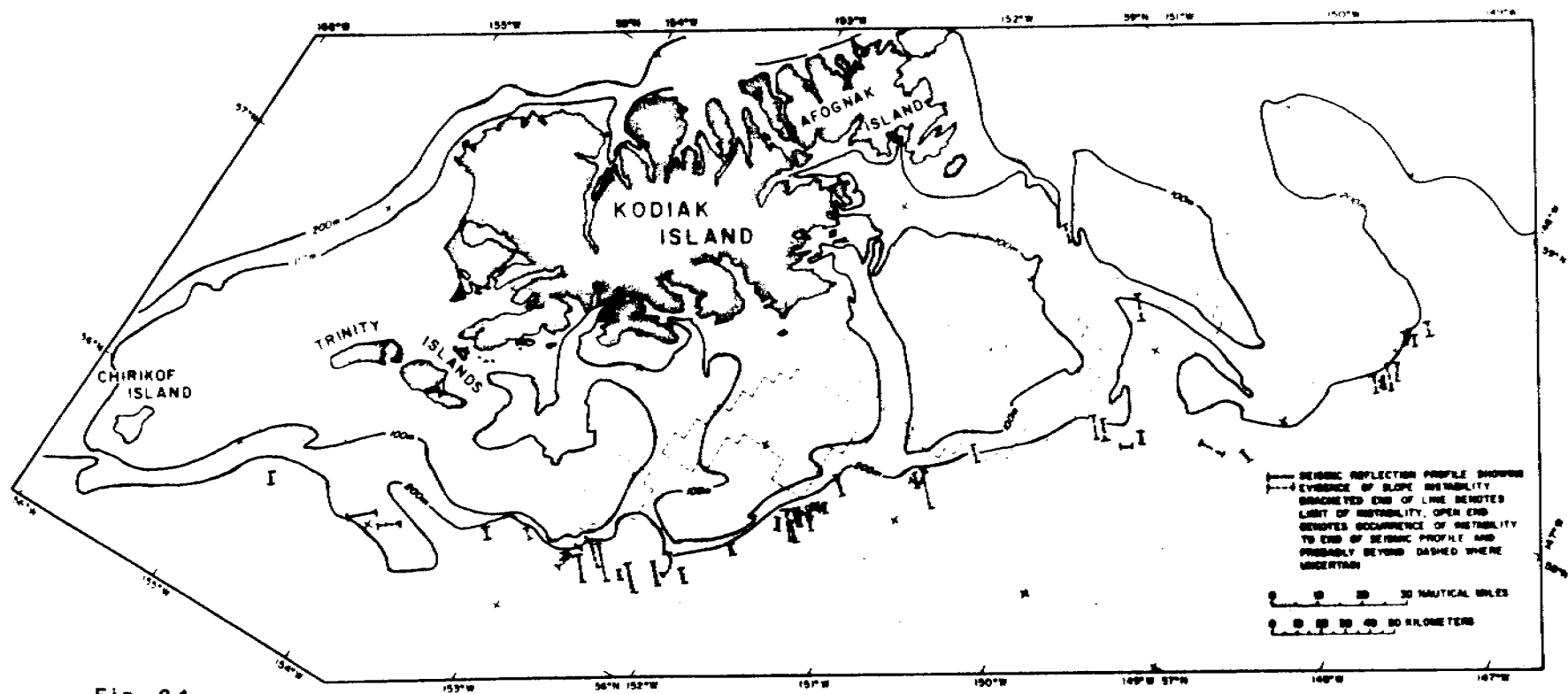


Fig. 31

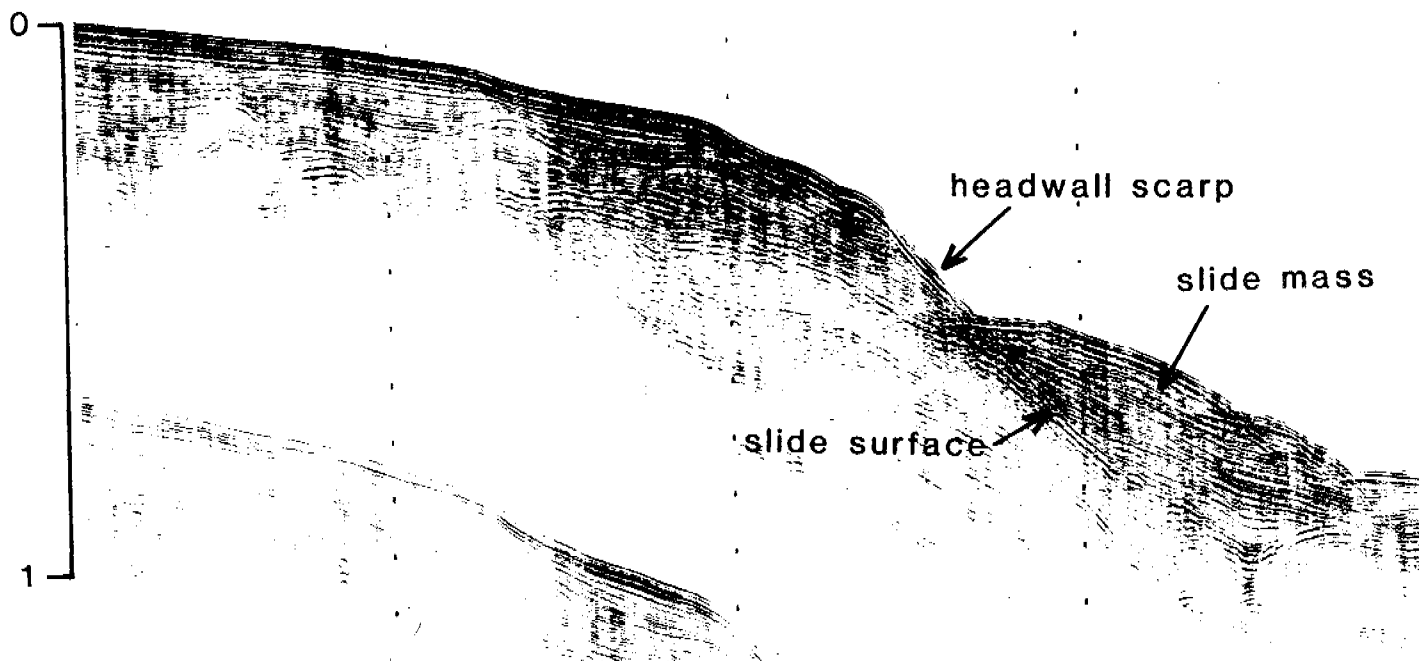
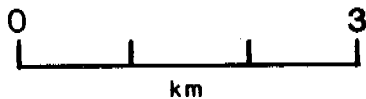


Fig. 32

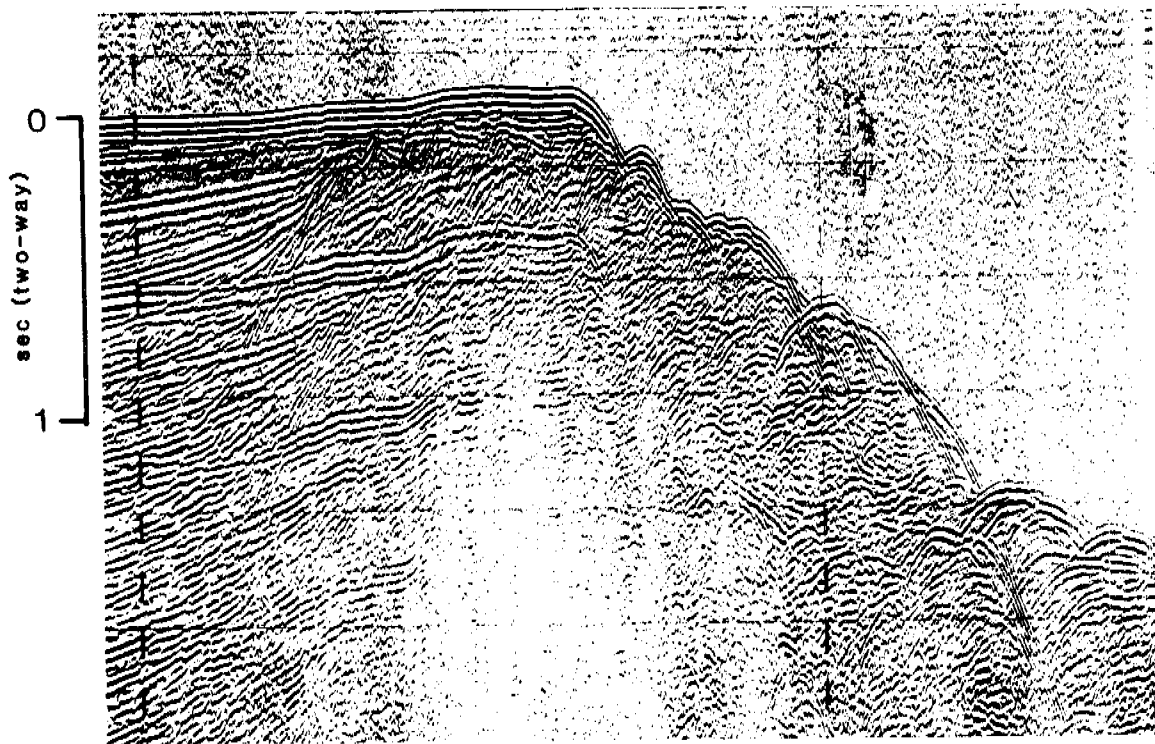
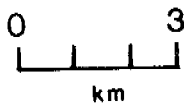


Fig. 33

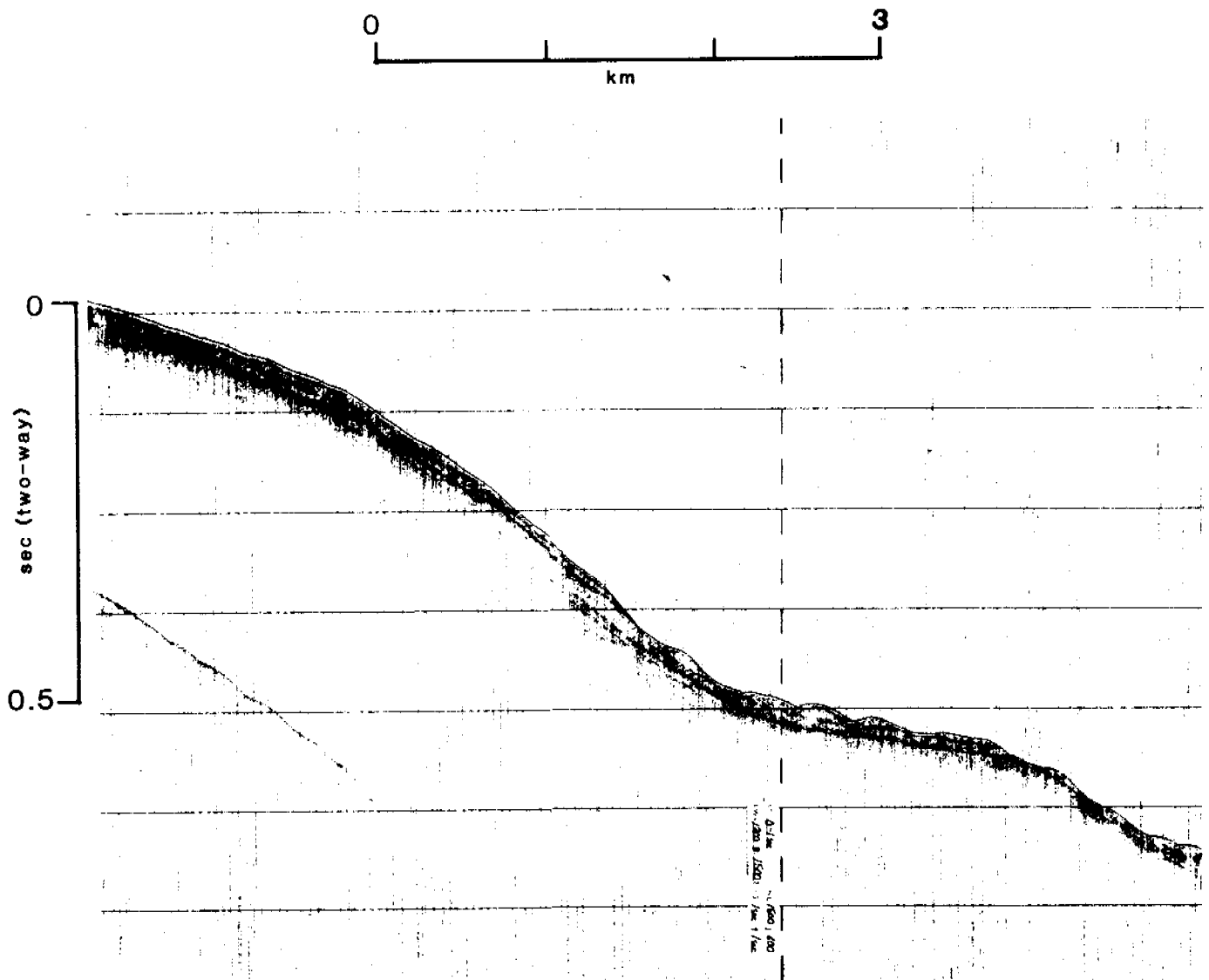


Fig. 34

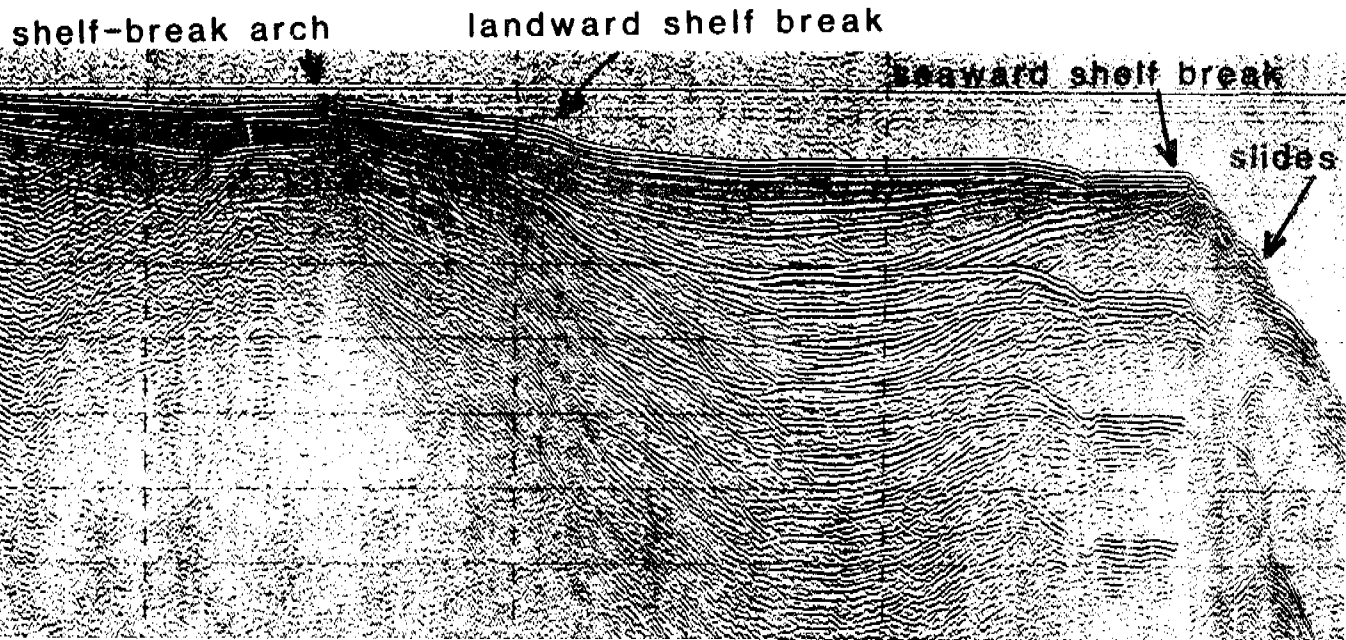
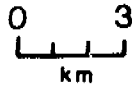


Fig. 35a

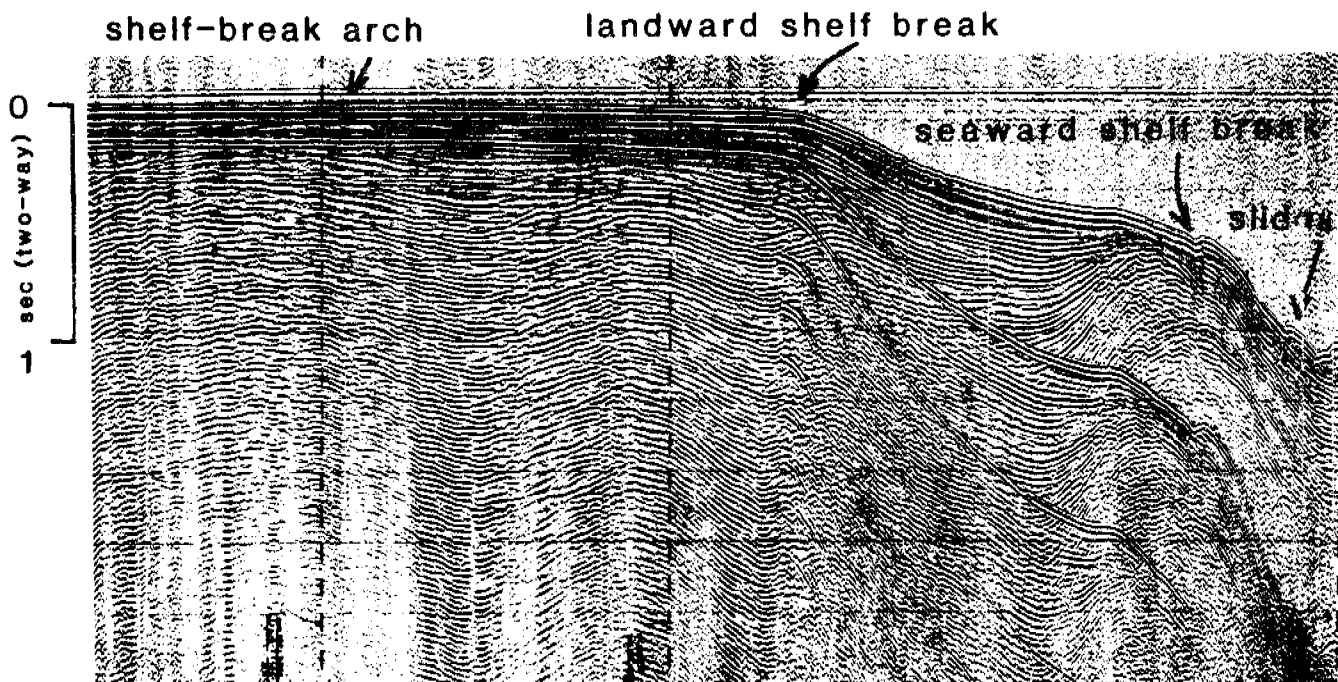
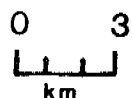


Fig. 35b

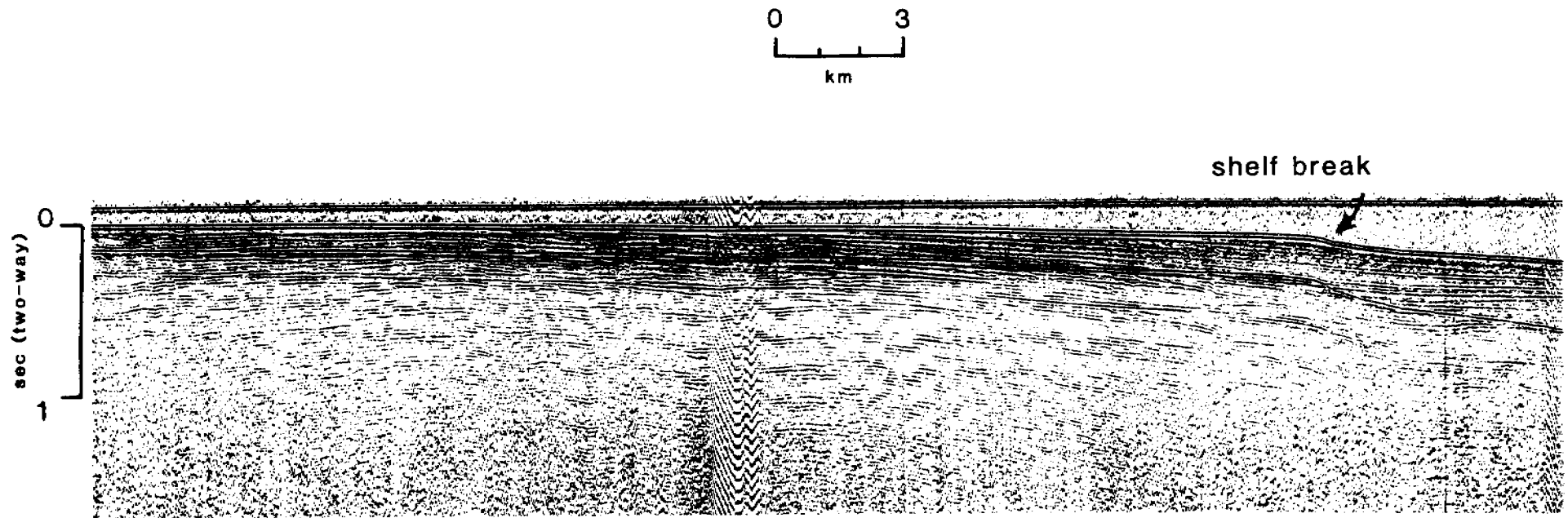


Fig. 36

Table 1a. Locations, textures, and compositions of sediment samples.

Sample	North Latitude	West Longitude	Water Depth (m)	Location*	Sed. Unit**	Texture (weight percents)				Compositions (weight percents)				
						Coarse	Sand	Silt	Clay	Terrig.	Carb.	Ash	Clay	Silic.
1	57°56.54'	150°13.56'	192	StT	Qb		98	1	1	100	tr	tr	tr	
50	59°52.50'	151°54.50'	32			58	42	tr	tr	94	6			tr
51	58°12.54'	151°55.74'	60			100				95	5			
52	58°24.42'	151°13.80'	107	StT		70	25	3	2					
53	58°12.56'	150°39.79'	86	PB	Qgm	100				88	12			
54	58°73.62'	150°30.26'	175	StT	Qs	2	78	14	6	61	14	22	3	tr
55	58°01.86'	150°21.64'	184	StT	Qs		83	12	5	27	1	70	2	tr
56	57°55.56'	150°11.34'	190	StT	Qb		99	tr	1	99	tr		1	
57	57°50.94'	150°03.74'	194	StT	QT	2	76	17	5	48	4	43	4	1
58	57°46.99'	149°55.40'	232	StT	Qs	15	56	22	7	49	tr	41	9	1
59	57°46.60'	149°29.66'	495	CS		28	56	10	6	52	1	41	6	
60	57°45.96'	149°37.41'	444	CS		2	81	10	7	56	tr	36	7	1
61	57°35.61'	150°24.46'	112	NAB	Qgf	38	54	5	3	73	17	5	4	1
62	57°39.15'	150°33.49'	102	NAB	Qgf	12	85	2	1	68	29	2	1	tr
63	57°43.96'	150°39.25'	90	NAB	QT	17	79	3	1	40	58	1	1	tr
64	57°47.50'	150°45.00'	83	NAB	Qgf	34	62	2	2	51	34	14	1	tr
65	57°51.50'	150°51.50'	77	NAB	Qgf	32	62	3	3	47	46	5	2	tr
66	57°55.10'	150°59.30'	81	NAB	Qgf	13	75	8	4	20	64	12	3	1
67	57°59.70'	151°06.40'	82	NAB	Qgf	21	53	18	8	53	18	17	10	2
68	57°28.15'	151°28.35'	154	CT	Qs	1	43	46	10	5	2	86	7	tr
69	57°23.43'	151°11.44'	80	NAB	Qgf	13	82	2	3	14	5	79	2	tr
70	57°24.08'	150°52.25'	96	NAB	Qgf	1	97	1	1	94	1	4	1	tr
71	57°20.01'	150°59.08'	95	NAB	Qgf		96	3	1	61	1	34	1	tr
72	57°24.20'	151°05.10'	92	NAB	Qgf	tr	94	3	3	6	1	91	2	tr
75	57°45.80'	151°08.05'	70	NAB	Qgf	10	90			13	87			
76	58°06.20'	151°46.10'	95			tr	96	1	3	12	6	80	2	tr
77	58°11.60'	151°37.00'	38			95	5			94	6			
79	58°13.23'	151°38.07'	68			36	62	tr	2	41	58	1	tr	tr
80	58°01.50'	151°21.63'	181	NAB	Qgm	32	62	4	2					
81	58°05.21'	151°14.55'	143	NAB/StT	Qgm		60	30	10	2	1	85	11	1

82	58°03.60'	151°15.90'	103	NAB	Qgm	64	16	15	5	58	18	14	8	2
85	57°45.00'	151°44.00'	55	NAB	Qgf	28	70	1	1	5	85	10		tr
86	57°41.40'	151°34.70'	61	NAB	QT	36	61	1	2					
87	57°36.45'	151°47.60'	132	CT	Qu	4	58	31	7	3	4	80	10	3
88	57°30.00'	151°38.80'	167	CT	Qs		22	69	9	6	tr	75	17	2
89	57°28.50'	151°44.50'	70	MAB	QT	68	24	6	2	63	11	25	1	tr
90	57°25.10'	151°51.90'	67	MAB	QT	6	91	1	2	3	93	3	1	tr
91	57°19.29'	152°01.82'	73	MAB	Qgf	5	91	2	2	3	14	84	1	tr
92	56°56.40'	152°32.90'	167	KT	Qs		6	74	20	15	tr	41	29	15
93	56°53.50'	152°41.00'	128	KT	Qs		24	62	14	12	1	38	37	12
94	56°48.15'	152°52.75'	63	SAB	Qgf	87	10	2	1	83	14	1	2	tr
96	56°41.40'	153°05.90'	146	KT	Qs		3	61	36	11	tr	52	36	1
97	56°40.10'	153°10.20'	150	KT	Qs		1	60	39	5	tr	38	56	1
98	56°38.00'	153°16.00'	145	KT	Qs		1	62	37	13	tr	46	41	tr
112														
113	56°33.50'	152°27.20'	197	KT	Qgm	25	70	3	2	94	2	3	1	tr
115	56°57.02'	152°06.28'	76	MAB	Qgf		92	5	3	2	9	87	2	tr
127	57°11.24'	151°29.59'	69	MAB	QT	17	25	11	7	31	54	10	5	tr
128	58°31.47'	149°21.90'	121	PB	Qgg	25	45	15	15	37	36	15	11	1
130	58°42.23'	149°03.38'	145	PB	Qgm		79	11	10	81		15	3	1
131	58°44.99'	148°58.18'	214	AT	QT	3	45	25	27					
132	58°48.16'	148°54.71'	236	AT	QT	5	33	32	30	56	tr	26	15	3
134	58°49.42'	149°14.22'	206	AT		20	41	17	22					
135	58°40.39'	149°31.82'	136	PB	Qgg		77	15	8	78		10	11	1
136	58°34.90'	149°45.19'	125	PB	Qgg		73	17	10					
137	58°29.46'	150°05.25'	93	PB	Qgm	10	72	13	5	53	42	6	9	tr
138	58°22.30'	150°24.07'	60	PB	QT	24	70	3	3	41	51	7	1	tr
141	58°13.12'	149°11.85'	120	PB	Qgm	56	26	11	7	60	13	22	5	tr
200	58°36.79'	151°50.26'	159			48	46	2	4	92	3	2	2	1
201	58°42.24'	152°17.77'	126			54	43	1	2	67	31	tr	2	tr
202	58°46.12'	152°42.85'	190			3	65	13	19	72	3	12	10	3
204	58°51.37'	152°54.13'	164			36	32	19	13	52	tr	34	12	2
205	58°58.89'	153°13.38'	118			35	47	11	7	80	2	12	5	1
215	57°11.38'	152°25.89'	115	MAB/KT	Qs	15	63	14	8					
216	57°06.00'	152°20.60'	96	MAB	Qgm	1	88	7	4	6	35	56	3	tr

217	57°00.00'	152°13.50'	76	MAB	Qgf	52	44	3	1	49	27	23	1	tr
219	57°42.65'	151°53.60'	79	CT	Qgm	73	25	1	1	89	10	1		tr
227	57°05.60'	151°14.00'	358	CS	Qu		72	19	9	7	tr	87	6	tr
228	57°07.50'	151°15.40'	185	CT	Qu	33	59	5	3	67	28	2	3	tr
229	57°14.20'	151°19.90'	172	CT	Qs		55	36	9	6	1	74	17	2
232	57°22.01'	150°35.92'	262	CS	Qu	29	69	1	1	98	tr	1	1	tr
233	57°17.60'	150°34.50'	630	CS	Quc		23	55	22					
234	57°31.54'	150°49.42'	93	NAB	Qgf	50	47	2	1	52	28	19	1	tr
236	58°04.20'	149°28.20'	230	StT	Qs		38	48	14	5	tr	71	23	1
241	57°41.29'	149°39.16'	606	CS		5	86	4	5	37		62	1	tr
242	57°31.40'	150°16.00'	300	CS	Qu		64	30	6	7	tr	80	12	1
243	57°48.50'	150°01.10'	190	StT	Qgm	24	66	7	3	77	2	16	5	tr
244	57°51.70'	149°50.90'	257	StT	Qs	1	80	15	4	17	tr	75	7	1
245	57°57.60'	149°39.70'	135	StT	Qgm	9	72	6	13	21	33	41	4	1
246	58°12.80'	149°13.40'	134	PB	Qgm	32	47	13	8	35	29	23	13	tr
329	57°38.95'	151°58.03'	218	CT	Qs		36	50	14	3	tr	76	20	1
330	58°00.96'	150°50.59'	135	StT	Qgg	10	78	7	5	50	28	17	5	tr
336	57°46.60'	149°02.08'	1700	CS			1	50	49	16		40	39	5
340	57°17.48'	150°24.92'	762	CS		2	23	51	24	43	2	34	21	tr
341	56°59.00'	152°21.47'	80	MAB	Qgm	50	43	4	3	50	41	6	3	tr
342	56°55.77'	152°15.17'	79	MAB	Qgf	59	34	4	3	66	5	26	3	tr
343	56°39.37'	153°04.72'	155	KT	Qs		5	64	31	14	1	66	15	4
344	56°39.47'	153°05.63'	160	KT	Qs		1	60	39	16	2	23	56	3
345	56°36.11'	153°10.00'	119	KT	Qgm		65	23	12	69	1	17	12	1
346	56°36.22'	153°12.51'	120	KT	Qgg		67	22	11					
347	56°36.76'	153°17.92'	130	KT	Qs		4	67	29	16	tr	36	44	3
348	56°37.66'	153°18.89'	143	KT	Qs		3	63	34	12		48	36	4
349	56°38.24'	153°19.80'	148	KT	Qs		1	61	38	3		53	42	2
350	56°46.20'	153°10.00'	154	KT	Qgm		13	53	34	11		40	37	12
351	56°46.86'	153°11.02'	125	KT	Qgm	22	32	29	17	52	tr	26	16	6
353	56°39.90'	153°11.08'	148	KT	Qs		1	61	38	6	tr	43	45	6
354	56°37.85'	153°16.05'	143	KT	Qs		1	61	38	11	3	60	21	5
355	56°08.53'	153°29.41'	314	StT		10	45	26	19	67	2	21	10	tr
356	56°05.55'	153°31.28'	370	StT		43	49	5	3	93	tr	3	4	tr
357	56°07.56'	153°38.46'	240	StT			56	30	14	53	1	22	21	3

358	56°47.03'	153°11.70'	122	KT	Qgm	2	69	16	13	54	tr	30	15	1
359	56°46.47'	153°10.59'	152	KT	Qgm		49	32	19	37	tr	37	22	4
437	57°01.14'	152°10.31'	72	MAB	Qgf	80	18	1	1	90	7	2	1	tr
443	56°38.56'	152°57.42'	82	SAB	Qgm	71	18	7	4	89	2	5	3	1
444	56°22.91'	153°15.75'	35	SAB	QT	39	59	1	1	96	2	1	1	
446	56°05.88'	153°51.49'	213	StT		10	76	10	4	86		7	6	1
447	56°20.68'	153°50.84'	94	StT		9	75	10	6	55	31	8	4	2
448	56°23.19'	154°18.80'	42	SAB			99	tr	1	100		tr	tr	tr
449	56°08.13'	154°17.33'	97	SAB	Qgm	63	30	4	3	93	1	1	4	1
452	55°59.97'	155°07.08'	67	SAB	Qb	1	99			100	tr			
453	56°13.90'	155°09.84'	32	SAB		91	9	tr	tr	96	4	tr	tr	tr
454	56°12.08'	154°42.77'	89	SAB	QT		97	1	2	97	tr	2	1	tr

*Refer to Fig. 8. At=Amatuli Trough, PB=Portlock Bank, StT=Stevenson Trough, NAB=northern Albatross Bank, CT=Chiniak Trough, MAB=middle Albatross Bank, CT=Chiniak Trough, SAB=southern Albatross Bank, StT=Sitkinak Trough, CS=continental slope.

**According to map by Thrasher (1979). Refer to Table 2 and Fig. 18.

Table 1b. Descriptions of samples for which detailed analyses were not made

Sample	North Latitude	West Longitude	Water Depth (M)	Location	Sed. Unit	Visual Description
50	59° 52.50'	151° 54.50'	32			Sandy gravel
95	56° 48.10'	153° 21.40'	170	KT	Qs	Pebbly sand
99	56° 24.50'	152° 53.70'	50	SAB	QT	Bedrock (siltstone)
100	56° 24.00'	152° 53.50'	50	SAB	QT	Bedrock (siltstone)
101	56° 23.20'	152° 54.10'	49	SAB	QT	Bedrock (silty, fine-grained sandstone)
102	56° 23.10'	152° 53.90'	45	SAB	QT	Bedrock (siltstone)
103	56° 22.70'	152° 52.00'	50	SAB	QT	Bedrock (silty, fine-grained sandstone)
104	56° 22.00'	152° 50.90'	75	SAB	QT	Bedrock (silty, fine-grained sandstone)
106	56° 29.60'	152° 43.70'	60	SAB	QT	Bedrock (siltstone)
107	56° 30.15'	152° 44.10'	56	SAB	QT	Bedrock (siltstone)
108	56° 30.30'	152° 44.90'	56	SAB	QT	Bedrock (siltstone)
110	56° 31.40'	152° 46.70'	64	SAB	QT	Bedrock (siltstone)
111	56° 31.70'	152° 47.50'	65	SAB	QT	Bedrock (sandy siltstone)
112	56° 32.00'	152° 48.50'	70	SAB	QT	Coarse sand with broken shells
114	56° 37.60'	152° 34.00'	160	KT	Qs	Slightly muddy sand
116	57° 12.00'	151° 51.10'	75	MAB	QT	Bedrock (pebbly, sandy siltstone)
117	57° 10.90'	151° 50.70'	54	MAB	QT	Bedrock (pebbly, sandy siltstone)
118	57° 11.00'	151° 50.00'	54	MAB	QT	Bedrock (sandy siltstone)
119	57° 10.60'	151° 49.10'	56	MAB	QT	Pebbly sand with broken shells
120	57° 10.00'	151° 48.40'	60	MAB	QT	Bedrock (sandy siltstone)
121	57° 09.25'	151° 47.50'	70	MAB	QT	Bedrock (sandy siltstone)
123	57° 08.75'	151° 46.30'	76	MAB	QT	Bedrock (sandy siltstone)
124	57° 08.50'	151° 45.60'	78	MAB	QT	Bedrock (fine sandstone)
125	57° 08.00'	151° 45.00'	80	MAB	QT	Sandy silt
129	58° 35.85'	149° 14.91'	95	PB	Qgm	Pebbly muddy sand
133	58° 54.41'	149° 01.95'	250	AT	Qgg	Muddy sand
140	58° 22.25'	149° 54.26'	83	PB	Qgf	Pebbly sand
142	58° 08.66'	149° 04.71'	114	PB	QT	Bedrock (muddy sand)
144	58° 05.92'	149° 01.38'	88	PB	QT	Bedrock (sandy siltstone)
145	58° 06.59'	149° 02.46'	90	PB	QT	Bedrock (sandy siltstone)

147	58°05.55'	149°00.97'	88	PB	QT	Bedrock (fine-grained sandstone)
148	58°04.96'	148°59.95'	90	PB	QT	Bedrock (sandy siltstone)
149	58°04.64'	148°59.49'	98	PB	QT	Bedrock (sandy siltstone)
220	56°43.80'	151°55.90'	62	MAB	QT	Boulder
231	57°24.90'	151°23.60'	187	CT	Qs	Ash-rich mud
352	56°40.19'	153°10.88'	150	KT	Qs	Ash-rich mud
432	57°25.40'	151°23.50'	175	CT	Qs	Ash-rich mud
433	57°26.71'	151°25.26'	174	CT	Qs	Ash-rich mud
435	57°15.04'	151°17.10'	158	CT	Qgg	Ash-rich mud
439	56°40.51'	153°12.30'	159	KT	Qs	Ash-rich mud
440	56°39.15'	153°06.36'	156	KT	Qs	Ash-rich mud
441	56°39.50'	153°04.62'	164	KT	Qs	Ash-rich mud
442	56°39.15'	153°02.11'	135	KT	Qgm	Ash-rich mud
445	56°11.17'	153°17.28'	1003	SiT		Mud
450	55°56.06'	154°14.13'	390	CS		Mud, with sand layers
451	55°58.50'	154°45.80'	371	CS		

Table 2. Description of sedimentary units (From Thrasher, 1979. Refer to Fig. 18).

Qs: Holocene Soft Sediments. Shallow basins of Holocene sediments that exhibit well-defined, continuous, horizontal reflectors.

Qb: Holocene Bedforms and Sand-Fields. Mapable regions of bedforms and, where possible, the massive sand unit with which they correlate.

Qu: Holocene and Pleistocene Undifferentiated Deposits. Exhibit well-developed, non-horizontal, parallel layering, with occasional indications of internal layering.

Qgm: Pleistocene Glacial Lateral and Terminal Moraines. Fairly linear deposits generally located along the sides and across the mouths of sea valleys. Very little or no acoustic internal structure.

Qgg: Pleistocene Glacial Ground Moraine. Hummocky upper surface; no internal structure.

Qgf: Pleistocene Glacial-Fluvial and Glacial-Marine Deposits. Thick deposits exhibiting some discontinuous, non-parallel, non-horizontal reflectors.

QT: Plio-Pleistocene Sedimentary Rocks. Gently depping, truncated sedimentary rocks that exhibit well-developed parallel internal reflectors.

T: Tertiary Sedimentary Rocks. No seismically determinable internal structure. Observed only in small outcrops along the landward edge of the mapped area.

Quc: Quaternary Undifferentiated Continental slope Deposits. Large seismic vertical exaggeration and steep slopes seaward of the continental shelf edge preclude accurate mapping on the continental slope.

Qus: Quaternary Undifferentiated Sediment Basins on the Upper Continental Slope. Exhibit well-defined, near-horizontal, continuous reflectors.

APPENDIX A. Textural and compositional data for sediment samples.

Measurements are given for weight percentages of four grain-size classes, and visual (volume) percents of compositional elements within each size class. Size grades of terrigenous rock fragments present in the coarse fraction are noted: granules (2-4 mm), pebbles (4-64 mm), cobbles (64-256 mm), and boulders (>256 mm). TR indicates presence in trace amounts (<1%).

SAMPLE NUMBER 1

Coarse fraction (>2 mm)

Weight percent of total sample _____

Composition:

Terrigenous rock fragments _____

_____ granules _____ pebbles
_____ cobbles _____ boulders

Carbonate shells _____

Sand fraction (2 mm - 0.062 mm)

Weight percent of total sample 98

Composition:

Terrigenous rock fragments and mineral grains 100

Carbonate megafaunal shell fragments TR

Foraminifera _____

Volcanic ash _____

Siliceous spicules and shells _____

Fine fraction (<0.062 mm)

Weight percent silt (0.062 mm - 0.0039 mm) in total sample 1

Weight percent clay (<0.0039 mm) in total sample 1

Composition:

Clay minerals _____

Volcanic ash _____

Terrigenous mineral grains _____

Siliceous shells and spicules _____

Carbonate shells _____

SAMPLE NUMBER 50

Coarse fraction (>2 mm)

Weight percent of total sample 58

Composition:

Terrigenous rock fragments 97

granules pebbles
_____ cobbles _____ boulders

Carbonate shells 3

Sand fraction (2 mm - 0.062 mm)

Weight percent of total sample 42

Composition:

Terrigenous rock fragments and mineral grains 90

Carbonate megafaunal shell fragments 9

Foraminifera 1

Volcanic ash _____

Siliceous spicules and shells _____

Fine fraction (<0.062 mm)

Weight percent silt (0.062 mm - 0.0039 mm) in total sample TR

Weight percent clay (<0.0039 mm) in total sample TR

Composition:

Clay minerals 10

Volcanic ash 35

Terrigenous mineral grains 55

Siliceous shells and spicules TR

Carbonate shells _____

SAMPLE NUMBER 51

Coarse fraction (>2 mm)

Weight percent of total sample 100

Composition:

Terrigenous rock fragments 95
Carbonate shells 5

granules pebbles
 cobbles boulders

Sand fraction (2 mm - 0.062 mm)

Weight percent of total sample _____

Composition:

Terrigenous rock fragments and mineral grains _____
Carbonate megafaunal shell fragments _____
Foraminifera _____
Volcanic ash _____
Siliceous spicules and shells _____

Fine fraction (<0.062 mm)

Weight percent silt (0.062 mm - 0.0039 mm) in total sample _____
Weight percent clay (<0.0039 mm) in total sample _____

Composition:

Clay minerals _____
Volcanic ash _____
Terrigenous mineral grains _____
Siliceous shells and spicules _____
Carbonate shells _____

SAMPLE NUMBER 52

Coarse fraction (>2 mm)

Weight percent of total sample 70

Composition:

Terrigenous rock fragments 95
Carbonate shells 5

granules pebbles
 cobbles boulders

Sand fraction (2 mm - 0.062 mm)

Weight percent of total sample 25

Composition:

Terrigenous rock fragments and mineral grains _____
Carbonate megafaunal shell fragments _____
Foraminifera _____
Volcanic ash _____
Siliceous spicules and shells _____

Fine fraction (<0.062 mm)

Weight percent silt (0.062 mm - 0.0039 mm) in total sample 3
Weight percent clay (<0.0039 mm) in total sample 2

Composition:

Clay minerals _____
Volcanic ash _____
Terrigenous mineral grains _____
Siliceous shells and spicules _____
Carbonate shells _____

SAMPLE NUMBER 53

Coarse fraction (>2 mm)

Weight percent of total sample 100

Composition:

Terrigenous rock fragments 89

granules

pebbles

Carbonate shells 11

cobbles

boulders

Sand fraction (2 mm - 0.062 mm)

Weight percent of total sample _____

Composition:

Terrigenous rock fragments and mineral grains _____

Carbonate megafaunal shell fragments _____

Foraminifera _____

Volcanic ash _____

Siliceous spicules and shells _____

Fine fraction (<0.062 mm)

Weight percent silt (0.062 mm - 0.0039 mm) in total sample _____

Weight percent clay (<0.0039 mm) in total sample _____

Composition:

Clay minerals _____

Volcanic ash _____

Terrigenous mineral grains _____

Siliceous shells and spicules _____

Carbonate shells _____

SAMPLE NUMBER 54

Coarse fraction (>2 mm)

Weight percent of total sample 2

Composition:

Terrigenous rock fragments 50

granules

pebbles

Carbonate shells 50

cobbles

boulders

Sand fraction (2 mm - 0.062 mm)

Weight percent of total sample 78

Composition:

Terrigenous rock fragments and mineral grains 70

Carbonate megafaunal shell fragments 15

Foraminifera _____

Volcanic ash 10

Siliceous spicules and shells TR

Fine fraction (<0.062 mm)

Weight percent silt (0.062 mm - 0.0039 mm) in total sample 14

Weight percent clay (<0.0039 mm) in total sample 6

Composition:

Clay minerals 15

Volcanic ash 75

Terrigenous mineral grains 10

Siliceous shells and spicules TR

Carbonate shells _____

SAMPLE NUMBER 55

Coarse fraction (>2 mm)

Weight percent of total sample _____

Composition:

Terrigenous rock fragments _____ granules _____ pebbles
Carbonate shells _____ cobbles _____ boulders

Sand fraction (2 mm - 0.062 mm)

Weight percent of total sample 83

Composition:

Terrigenous rock fragments and mineral grains 26
Carbonate megafaunal shell fragments _____
Foraminifera 1
Volcanic ash 73
Siliceous spicules and shells _____

Fine fraction (<0.062 mm)

Weight percent silt (0.062 mm - 0.0039 mm) in total sample 12

Weight percent clay (<0.0039 mm) in total sample 5

Composition:

Clay minerals 12
Volcanic ash 63
Terrigenous mineral grains 20
Siliceous shells and spicules Tr
Carbonate shells _____

SAMPLE NUMBER 56

Coarse fraction (>2 mm)

Weight percent of total sample _____

Composition:

Terrigenous rock fragments _____ granules _____ pebbles
Carbonate shells _____ cobbles _____ boulders

Sand fraction (2 mm - 0.062 mm)

Weight percent of total sample 99

Composition:

Terrigenous rock fragments and mineral grains 100
Carbonate megafaunal shell fragments TR
Foraminifera _____
Volcanic ash _____
Siliceous spicules and shells _____

Fine fraction (<0.062 mm)

Weight percent silt (0.062 mm - 0.0039 mm) in total sample TR

Weight percent clay (<0.0039 mm) in total sample 1

Composition:

Clay minerals 57
Volcanic ash 35
Terrigenous mineral grains 3
Siliceous shells and spicules 5
Carbonate shells Tr

SAMPLE NUMBER 57

Coarse fraction (>2 mm)

Weight percent of total sample 2

Composition:

Terrigenous rock fragments 60
Carbonate shells 40

granules pebbles
 cobbles boulders

Sand fraction (2 mm - 0.062 mm)

Weight percent of total sample 76

Composition:

Terrigenous rock fragments and mineral grains 56
Carbonate megafaunal shell fragments 2
Foraminifera 2
Volcanic ash 40
Siliceous spicules and shells TR

Fine fraction (<0.062 mm)

Weight percent silt (0.062 mm - 0.0039 mm) in total sample 17
Weight percent clay (<0.0039 mm) in total sample 5

Composition:

Clay minerals 15
Volcanic ash 65
Terrigenous mineral grains 15
Siliceous shells and spicules 5
Carbonate shells _____

SAMPLE NUMBER 58

Coarse fraction (>2 mm)

Weight percent of total sample 15

Composition:

Terrigenous rock fragments 100
Carbonate shells TR

granules pebbles
 cobbles boulders

Sand fraction (2 mm - 0.062 mm)

Weight percent of total sample 56

Composition:

Terrigenous rock fragments and mineral grains 50
Carbonate megafaunal shell fragments _____
Foraminifera TR
Volcanic ash 50
Siliceous spicules and shells TR

Fine fraction (<0.062 mm)

Weight percent silt (0.062 mm - 0.0039 mm) in total sample 22
Weight percent clay (<0.0039 mm) in total sample 7

Composition:

Clay minerals 30
Volcanic ash 50
Terrigenous mineral grains 15
Siliceous shells and spicules 5
Carbonate shells _____

SAMPLE NUMBER 59

Coarse fraction (>2 mm)

Weight percent of total sample 28

Composition:

Terrigenous rock fragments 100

Carbonate shells _____

granules
_____ cobbles

pebbles
_____ boulders

Sand fraction (2 mm - 0.062 mm)

Weight percent of total sample 56

Composition:

Terrigenous rock fragments and mineral grains 34

Carbonate megafaunal shell fragments _____

Foraminifera 1

Volcanic ash 65

Siliceous spicules and shells _____

Fine fraction (<0.062 mm)

Weight percent silt (0.062 mm - 0.0039 mm) in total sample 10

Weight percent clay (<0.0039 mm) in total sample 6

Composition:

Clay minerals 35

Volcanic ash 40

Terrigenous mineral grains 20

Siliceous shells and spicules 3

Carbonate shells 2

SAMPLE NUMBER 60

Coarse fraction (>2 mm)

Weight percent of total sample 2

Composition:

Terrigenous rock fragments 100

Carbonate shells _____

granules
_____ cobbles

_____ pebbles
_____ boulders

Sand fraction (2 mm - 0.062 mm)

Weight percent of total sample 81

Composition:

Terrigenous rock fragments and mineral grains 60

Carbonate megafaunal shell fragments _____

Foraminifera TR

Volcanic ash 40

Siliceous spicules and shells TR

Fine fraction (<0.062 mm)

Weight percent silt (0.062 mm - 0.0039 mm) in total sample 10

Weight percent clay (<0.0039 mm) in total sample 7

Composition:

Clay minerals 45

Volcanic ash 40

Terrigenous mineral grains 15

Siliceous shells and spicules 10

Carbonate shells _____

SAMPLE NUMBER 61

Coarse fraction (>2 mm)

Weight percent of total sample 39

Composition:

Terrigenous rock fragments 100
Carbonate shells TR

granules pebbles
 cobbles boulders

Sand fraction (2 mm - 0.062 mm)

Weight percent of total sample 54

Composition:

Terrigenous rock fragments and mineral grains 64
Carbonate megafaunal shell fragments 3
Foraminifera 27
Volcanic ash 5
Siliceous spicules and shells 1

Fine fraction (<0.062 mm)

Weight percent silt (0.062 mm - 0.0039 mm) in total sample 5
Weight percent clay (<0.0039 mm) in total sample 3

Composition:

Clay minerals 45
Volcanic ash 35
Terrigenous mineral grains 8
Siliceous shells and spicules 12
Carbonate shells _____

SAMPLE NUMBER 62

Coarse fraction (>2 mm)

Weight percent of total sample 12

Composition:

Terrigenous rock fragments 16
Carbonate shells 74

granules _____ pebbles
 cobbles boulders

Sand fraction (2 mm - 0.062 mm)

Weight percent of total sample 85

Composition:

Terrigenous rock fragments and mineral grains 78
Carbonate megafaunal shell fragments 20
Foraminifera 1
Volcanic ash 1
Siliceous spicules and shells TR

Fine fraction (<0.062 mm)

Weight percent silt (0.062 mm - 0.0039 mm) in total sample 2
Weight percent clay (<0.0039 mm) in total sample 1

Composition:

Clay minerals 30
Volcanic ash 28
Terrigenous mineral grains 30
Siliceous shells and spicules 9
Carbonate shells 3

SAMPLE NUMBER 63

Coarse fraction (>2 mm)

Weight percent of total sample 17

Composition:

Terrigenous rock fragments 75
Carbonate shells 25

granules pebbles
 cobbles boulders

Sand fraction (2 mm - 0.062 mm)

Weight percent of total sample 79

Composition:

Terrigenous rock fragments and mineral grains 35
Carbonate megafaunal shell fragments 63
Foraminifera 2
Volcanic ash TR
Siliceous spicules and shells TR

Fine fraction (<0.062 mm)

Weight percent silt (0.062 mm - 0.0039 mm) in total sample 3
Weight percent clay (<0.0039 mm) in total sample 1

Composition:

Clay minerals 15
Volcanic ash 35
Terrigenous mineral grains 45
Siliceous shells and spicules TR
Carbonate shells 5

SAMPLE NUMBER 64

Coarse fraction (>2 mm)

Weight percent of total sample 34

Composition:

Terrigenous rock fragments 99
Carbonate shells 1

granules pebbles
 cobbles boulders

Sand fraction (2 mm - 0.062 mm)

Weight percent of total sample 62

Composition:

Terrigenous rock fragments and mineral grains 28
Carbonate megafaunal shell fragments 50
Foraminifera 1
Volcanic ash 21
Siliceous spicules and shells TR

Fine fraction (<0.062 mm)

Weight percent silt (0.062 mm - 0.0039 mm) in total sample 2
Weight percent clay (<0.0039 mm) in total sample 2

Composition:

Clay minerals 30
Volcanic ash 60
Terrigenous mineral grains 5
Siliceous shells and spicules 4
Carbonate shells 1

SAMPLE NUMBER 65

Coarse fraction (>2 mm)

Weight percent of total sample 32

Composition:

Terrigenous rock fragments 95
Carbonate shells 5

granules pebbles
 cobbles boulders

Sand fraction (2 mm - 0.062 mm)

Weight percent of total sample 62

Composition:

Terrigenous rock fragments and mineral grains 26
Carbonate megafaunal shell fragments 63
Foraminifera 5
Volcanic ash 5
Siliceous spicules and shells Tr

Fine fraction (<0.062 mm)

Weight percent silt (0.062 mm - 0.0039 mm) in total sample 3

Weight percent clay (<0.0039 mm) in total sample 3

Composition:

Clay minerals 37
Volcanic ash 48
Terrigenous mineral grains 15
Siliceous shells and spicules Tr
Carbonate shells Tr

SAMPLE NUMBER 66

Coarse fraction (>2 mm)

Weight percent of total sample 13

Composition:

Terrigenous rock fragments 33
Carbonate shells 67

granules pebbles
 cobbles boulders

Sand fraction (2 mm - 0.062 mm)

Weight percent of total sample 75

Composition:

Terrigenous rock fragments and mineral grains 20
Carbonate megafaunal shell fragments 68
Foraminifera 3
Volcanic ash 8
Siliceous spicules and shells 1

Fine fraction (<0.062 mm)

Weight percent silt (0.062 mm - 0.0039 mm) in total sample 8

Weight percent clay (<0.0039 mm) in total sample 4

Composition:

Clay minerals 25
Volcanic ash 60
Terrigenous mineral grains 6
Siliceous shells and spicules 6
Carbonate shells 3

SAMPLE NUMBER 67

Coarse fraction (>2 mm)

Weight percent of total sample 21

Composition:

Terrigenous rock fragments 70

Carbonate shells 30

granules pebbles
 cobbles boulders

Sand fraction (2 mm - 0.062 mm)

Weight percent of total sample 53

Composition:

Terrigenous rock fragments and mineral grains 70

Carbonate megafaunal shell fragments 15

Foraminifera 5

Volcanic ash 10

Siliceous spicules and shells TR

Fine fraction (<0.062 mm)

Weight percent silt (0.062 mm - 0.0039 mm) in total sample 18

Weight percent clay (<0.0039 mm) in total sample 8

Composition:

Clay minerals 35

Volcanic ash 50

Terrigenous mineral grains 7

Siliceous shells and spicules 8

Carbonate shells _____

SAMPLE NUMBER 68

Coarse fraction (>2 mm)

Weight percent of total sample 1

Composition:

Terrigenous rock fragments _____

Carbonate shells 100

granules pebbles
 cobbles boulders

Sand fraction (2 mm - 0.062 mm)

Weight percent of total sample 43

Composition:

Terrigenous rock fragments and mineral grains TR

Carbonate megafaunal shell fragments TR

Foraminifera 1

Volcanic ash 98

Siliceous spicules and shells 1

Fine fraction (<0.062 mm)

Weight percent silt (0.062 mm - 0.0039 mm) in total sample 46

Weight percent clay (<0.0039 mm) in total sample 10

Composition:

Clay minerals 12

Volcanic ash 80

Terrigenous mineral grains 8

Siliceous shells and spicules Tr

Carbonate shells Tr

SAMPLE NUMBER 69

Coarse fraction (>2 mm)

Weight percent of total sample 13

Composition:

Terrigenous rock fragments 89

granules pebbles

Carbonate shells 11

cobbles boulders

Sand fraction (2 mm - 0.062 mm)

Weight percent of total sample 82

Composition:

Terrigenous rock fragments and mineral grains 3

Carbonate megafaunal shell fragments 2

Foraminifera 1

Volcanic ash 94

Siliceous spicules and shells TR

Fine fraction (<0.062 mm)

Weight percent silt (0.062 mm - 0.0039 mm) in total sample 2

Weight percent clay (<0.0039 mm) in total sample 3

Composition:

Clay minerals 31

Volcanic ash 54

Terrigenous mineral grains 8

Siliceous shells and spicules 6

Carbonate shells 1

SAMPLE NUMBER 70

Coarse fraction (>2 mm)

Weight percent of total sample 1

Composition:

Terrigenous rock fragments _____

granules pebbles

Carbonate shells 100

cobbles boulders

Sand fraction (2 mm - 0.062 mm)

Weight percent of total sample 97

Composition:

Terrigenous rock fragments and mineral grains 97

Carbonate megafaunal shell fragments _____

Foraminifera _____

Volcanic ash 3

Siliceous spicules and shells _____

Fine fraction (<0.062 mm)

Weight percent silt (0.062 mm - 0.0039 mm) in total sample 1

Weight percent clay (<0.0039 mm) in total sample 1

Composition:

Clay minerals 26

Volcanic ash 62

Terrigenous mineral grains 5

Siliceous shells and spicules 7

Carbonate shells _____

SAMPLE NUMBER 71

Coarse fraction (>2 mm)

Weight percent of total sample _____

Composition:

Terrigenous rock fragments _____ granules _____ pebbles _____
Carbonate shells _____ cobbles _____ boulders _____

Sand fraction (2 mm - 0.062 mm)

Weight percent of total sample 96

Composition:

Terrigenous rock fragments and mineral grains 64
Carbonate megafaunal shell fragments TR
Foraminifera 1
Volcanic ash 35
Siliceous spicules and shells _____

Fine fraction (<0.062 mm)

Weight percent silt (0.062 mm - 0.0039 mm) in total sample 3

Weight percent clay (<0.0039 mm) in total sample 1

Composition:

Clay minerals 31
Volcanic ash 60
Terrigenous mineral grains 7
Siliceous shells and spicules 2
Carbonate shells _____

SAMPLE NUMBER 72

Coarse fraction (>2 mm)

Weight percent of total sample TR

Composition:

Terrigenous rock fragments _____ granules _____ pebbles _____
Carbonate shells 100 cobbles _____ boulders _____

Sand fraction (2 mm - 0.062 mm)

Weight percent of total sample 94

Composition:

Terrigenous rock fragments and mineral grains 5
Carbonate megafaunal shell fragments TR
Foraminifera 1
Volcanic ash 94
Siliceous spicules and shells _____

Fine fraction (<0.062 mm)

Weight percent silt (0.062 mm - 0.0039 mm) in total sample 3

Weight percent clay (<0.0039 mm) in total sample 3

Composition:

Clay minerals 35
Volcanic ash 60
Terrigenous mineral grains 5
Siliceous shells and spicules TR
Carbonate shells _____

SAMPLE NUMBER 75

Coarse fraction (>2 mm)

Weight percent of total sample 10

Composition:

Terrigenous rock fragments 46 granules pebbles
Carbonate shells 54 cobbles boulders

Sand fraction (2 mm - 0.062 mm)

Weight percent of total sample 90

Composition:

Terrigenous rock fragments and mineral grains 10
Carbonate megafaunal shell fragments 90
Foraminifera
Volcanic ash
Siliceous spicules and shells

Fine fraction (<0.062 mm)

Weight percent silt (0.062 mm - 0.0039 mm) in total sample

Weight percent clay (<0.0039 mm) in total sample

Composition:

Clay minerals
Volcanic ash
Terrigenous mineral grains
Siliceous shells and spicules
Carbonate shells

SAMPLE NUMBER 76

Coarse fraction (>2 mm)

Weight percent of total sample TR

Composition:

Terrigenous rock fragments granules pebbles
Carbonate shells 100 cobbles boulders

Sand fraction (2 mm - 0.062 mm)

Weight percent of total sample 96

Composition:

Terrigenous rock fragments and mineral grains 12
Carbonate megafaunal shell fragments 4
Foraminifera 1
Volcanic ash 83
Siliceous spicules and shells TR

Fine fraction (<0.062 mm)

Weight percent silt (0.062 mm - 0.0039 mm) in total sample 1

Weight percent clay (<0.0039 mm) in total sample 3

Composition:

Clay minerals 36
Volcanic ash 47
Terrigenous mineral grains 5
Siliceous shells and spicules 11
Carbonate shells 1

SAMPLE NUMBER 77

Coarse fraction (>2 mm)

Weight percent of total sample 95

Composition:

Terrigenous rock fragments 95
Carbonate shells 5

granules pebbles
 cobbles boulders

Sand fraction (2 mm - 0.062 mm)

Weight percent of total sample 5

Composition:

Terrigenous rock fragments and mineral grains 80
Carbonate megafaunal shell fragments 19
Foraminifera 1
Volcanic ash _____
Siliceous spicules and shells _____

Fine fraction (<0.062 mm)

Weight percent silt (0.062 mm - 0.0039 mm) in total sample _____
Weight percent clay (<0.0039 mm) in total sample _____

Composition:

Clay minerals _____
Volcanic ash _____
Terrigenous mineral grains _____
Siliceous shells and spicules _____
Carbonate shells _____

SAMPLE NUMBER 79

Coarse fraction (>2 mm)

Weight percent of total sample 96

Composition:

Terrigenous rock fragments 68
Carbonate shells 32

granules pebbles
 cobbles boulders

Sand fraction (2 mm - 0.062 mm)

Weight percent of total sample 62

Composition:

Terrigenous rock fragments and mineral grains 28
Carbonate megafaunal shell fragments 70
Foraminifera 2
Volcanic ash TR
Siliceous spicules and shells _____

Fine fraction (<0.062 mm)

Weight percent silt (0.062 mm - 0.0039 mm) in total sample TR
Weight percent clay (<0.0039 mm) in total sample 2

Composition:

Clay minerals 20
Volcanic ash 50
Terrigenous mineral grains 30
Siliceous shells and spicules TR
Carbonate shells _____

SAMPLE NUMBER 80

Coarse fraction (>2 mm)

Weight percent of total sample 32

Composition:

Terrigenous rock fragments 65 granules pebbles
Carbonate shells 35 cobbles boulders

Sand fraction (2 mm - 0.062 mm)

Weight percent of total sample 62

Composition:

Terrigenous rock fragments and mineral grains 85
Carbonate megafaunal shell fragments 3
Foraminifera TR
Volcanic ash 7
Siliceous spicules and shells _____

Fine fraction (<0.062 mm)

Weight percent silt (0.062 mm - 0.0039 mm) in total sample 4

Weight percent clay (<0.0039 mm) in total sample 2

Composition:

Clay minerals _____
Volcanic ash _____
Terrigenous mineral grains _____
Siliceous shells and spicules _____
Carbonate shells _____

SAMPLE NUMBER 81

Coarse fraction (>2 mm)

Weight percent of total sample _____

Composition:

Terrigenous rock fragments _____ granules pebbles
Carbonate shells _____ cobbles boulders

Sand fraction (2 mm - 0.062 mm)

Weight percent of total sample 60

Composition:

Terrigenous rock fragments and mineral grains 1
Carbonate megafaunal shell fragments _____
Foraminifera TR
Volcanic ash 99
Siliceous spicules and shells TR

Fine fraction (<0.062 mm)

Weight percent silt (0.062 mm - 0.0039 mm) in total sample 30

Weight percent clay (<0.0039 mm) in total sample 10

Composition:

Clay minerals 25
Volcanic ash 65
Terrigenous mineral grains 5
Siliceous shells and spicules 3
Carbonate shells 2

SAMPLE NUMBER 82

Coarse fraction (>2 mm)

Weight percent of total sample 64

Composition:

Terrigenous rock fragments 83

Carbonate shells 17

granules pebbles
 cobbles boulders

Sand fraction (2 mm - 0.062 mm)

Weight percent of total sample 16

Composition:

Terrigenous rock fragments and mineral grains 30

Carbonate megafaunal shell fragments 25

Foraminifera 7

Volcanic ash 38

Siliceous spicules and shells TR

Fine fraction (<0.062 mm)

Weight percent silt (0.062 mm - 0.0039 mm) in total sample 15

Weight percent clay (<0.0039 mm) in total sample 5

Composition:

Clay minerals 40

Volcanic ash 42

Terrigenous mineral grains 7

Siliceous shells and spicules 10

Carbonate shells 1

SAMPLE NUMBER 85

Coarse fraction (>2 mm)

Weight percent of total sample 28

Composition:

Terrigenous rock fragments 1

Carbonate shells 99

granules pebbles
 cobbles boulders

Sand fraction (2 mm - 0.062 mm)

Weight percent of total sample 70

Composition:

Terrigenous rock fragments and mineral grains 5

Carbonate megafaunal shell fragments 80

Foraminifera _____

Volcanic ash 15

Siliceous spicules and shells _____

Fine fraction (<0.062 mm)

Weight percent silt (0.062 mm - 0.0039 mm) in total sample 1

Weight percent clay (<0.0039 mm) in total sample 1

Composition:

Clay minerals 23

Volcanic ash 65

Terrigenous mineral grains 5

Siliceous shells and spicules 7

Carbonate shells Tr

SAMPLE NUMBER 86

Coarse fraction (>2 mm)

Weight percent of total sample 36

Composition:

Terrigenous rock fragments 4 granules pebbles
Carbonate shells 96 cobbles boulders

Sand fraction (2 mm - 0.062 mm)

Weight percent of total sample 61

Composition:

Terrigenous rock fragments and mineral grains 6
Carbonate megafaunal shell fragments 12
Foraminifera TR
Volcanic ash 82
Siliceous spicules and shells _____

Fine fraction (<0.062 mm)

Weight percent silt (0.062 mm - 0.0039 mm) in total sample 1

Weight percent clay (<0.0039 mm) in total sample 2

Composition:

Clay minerals _____
Volcanic ash _____
Terrigenous mineral grains _____
Siliceous shells and spicules _____
Carbonate shells _____

SAMPLE NUMBER 87

Coarse fraction (>2 mm)

Weight percent of total sample 4

Composition:

Terrigenous rock fragments _____ granules pebbles
Carbonate shells 100 cobbles boulders

Sand fraction (2 mm - 0.062 mm)

Weight percent of total sample 58

Composition:

Terrigenous rock fragments and mineral grains _____
Carbonate megafaunal shell fragments TR
Foraminifera _____
Volcanic ash 100
Siliceous spicules and shells TR

Fine fraction (<0.062 mm)

Weight percent silt (0.062 mm - 0.0039 mm) in total sample 31

Weight percent clay (<0.0039 mm) in total sample 7

Composition:

Clay minerals 25
Volcanic ash 60
Terrigenous mineral grains 5
Siliceous shells and spicules 10
Carbonate shells _____

SAMPLE NUMBER 88

Coarse fraction (>2 mm)

Weight percent of total sample _____

Composition:

Terrigenous rock fragments _____ granules _____ pebbles _____
Carbonate shells _____ cobbles _____ boulders _____

Sand fraction (2 mm - 0.062 mm)

Weight percent of total sample 22

Composition:

Terrigenous rock fragments and mineral grains _____
Carbonate megafaunal shell fragments 1
Foraminifera _____
Volcanic ash 97
Siliceous spicules and shells 2

Fine fraction (<0.062 mm)

Weight percent silt (0.062 mm - 0.0039 mm) in total sample 69

Weight percent clay (<0.0039 mm) in total sample 9

Composition:

Clay minerals 20
Volcanic ash 70
Terrigenous mineral grains 8
Siliceous shells and spicules 2
Carbonate shells _____

SAMPLE NUMBER 89

Coarse fraction (>2 mm)

Weight percent of total sample 68

Composition:

Terrigenous rock fragments 90 X granules _____ pebbles _____
Carbonate shells 10 _____ cobbles _____ boulders _____

Sand fraction (2 mm - 0.062 mm)

Weight percent of total sample 24

Composition:

Terrigenous rock fragments and mineral grains 3
Carbonate megafaunal shell fragments 12
Foraminifera Tr
Volcanic ash 85
Siliceous spicules and shells _____

Fine fraction (<0.062 mm)

Weight percent silt (0.062 mm - 0.0039 mm) in total sample 6

Weight percent clay (<0.0039 mm) in total sample 2

Composition:

Clay minerals 12
Volcanic ash 70
Terrigenous mineral grains 18
Siliceous shells and spicules Tr
Carbonate shells _____

SAMPLE NUMBER 90

Coarse fraction (>2 mm)

Weight percent of total sample 6

Composition:

Terrigenous rock fragments _____ granules pebbles
Carbonate shells 100 _____ cobbles _____ boulders

Sand fraction (2 mm - 0.062 mm)

Weight percent of total sample 91

Composition:

Terrigenous rock fragments and mineral grains 4
Carbonate megafaunal shell fragments 95
Foraminifera Tr
Volcanic ash 1
Siliceous spicules and shells _____

Fine fraction (<0.062 mm)

Weight percent silt (0.062 mm - 0.0039 mm) in total sample 1

Weight percent clay (<0.0039 mm) in total sample 2

Composition:

Clay minerals 26
Volcanic ash 60
Terrigenous mineral grains 5
Siliceous shells and spicules 8
Carbonate shells 1

SAMPLE NUMBER 91

Coarse fraction (>2 mm)

Weight percent of total sample 5

Composition:

Terrigenous rock fragments _____ granules pebbles
Carbonate shells 100 _____ cobbles _____ boulders

Sand fraction (2 mm - 0.062 mm)

Weight percent of total sample 91

Composition:

Terrigenous rock fragments and mineral grains 1
Carbonate megafaunal shell fragments 7
Foraminifera 1
Volcanic ash 91
Siliceous spicules and shells _____

Fine fraction (<0.062 mm)

Weight percent silt (0.062 mm - 0.0039 mm) in total sample 2

Weight percent clay (<0.0039 mm) in total sample 2

Composition:

Clay minerals 23
Volcanic ash 60
Terrigenous mineral grains 17
Siliceous shells and spicules Tr
Carbonate shells _____

SAMPLE NUMBER 92

Coarse fraction (>2 mm)

Weight percent of total sample _____

Composition:

Terrigenous rock fragments _____

___ granules

___ pebbles

Carbonate shells _____

___ cobbles

___ boulders

Sand fraction (2 mm - 0.062 mm)

Weight percent of total sample 6

Composition:

Terrigenous rock fragments and mineral grains 1

Carbonate megafaunal shell fragments _____

Foraminifera 1

Volcanic ash 15

Siliceous spicules and shells 83

Fine fraction (<0.062 mm)

Weight percent silt (0.062 mm - 0.0039 mm) in total sample 74

Weight percent clay (<0.0039 mm) in total sample 20

Composition:

Clay minerals 30

Volcanic ash 45

Terrigenous mineral grains 15

Siliceous shells and spicules 12

Carbonate shells Tr

SAMPLE NUMBER 93

Coarse fraction (>2 mm)

Weight percent of total sample _____

Composition:

Terrigenous rock fragments _____

___ granules

___ pebbles

Carbonate shells _____

___ cobbles

___ boulders

Sand fraction (2 mm - 0.062 mm)

Weight percent of total sample 24

Composition:

Terrigenous rock fragments and mineral grains 10

Carbonate megafaunal shell fragments _____

Foraminifera 4

Volcanic ash 66

Siliceous spicules and shells 20

Fine fraction (<0.062 mm)

Weight percent silt (0.062 mm - 0.0039 mm) in total sample 62

Weight percent clay (<0.0039 mm) in total sample 14

Composition:

Clay minerals 46

Volcanic ash 30

Terrigenous mineral grains 12

Siliceous shells and spicules 12

Carbonate shells Tr

SAMPLE NUMBER 94

Coarse fraction (>2 mm)

Weight percent of total sample 87

Composition:

Terrigenous rock fragments 90
Carbonate shells 10

granules pebbles
 cobbles boulders

Sand fraction (2 mm - 0.062 mm)

Weight percent of total sample 10

Composition:

Terrigenous rock fragments and mineral grains 53
Carbonate megafaunal shell fragments 45
Foraminifera 1
Volcanic ash 1
Siliceous spicules and shells _____

Fine fraction (<0.062 mm)

Weight percent silt (0.062 mm - 0.0039 mm) in total sample 2
Weight percent clay (<0.0039 mm) in total sample 1

Composition:

Clay minerals 55
Volcanic ash 33
Terrigenous mineral grains 12
Siliceous shells and spicules Tr
Carbonate shells Tr

SAMPLE NUMBER 96

Coarse fraction (>2 mm)

Weight percent of total sample _____

Composition:

Terrigenous rock fragments _____
Carbonate shells _____

____ granules ____ pebbles
____ cobbles ____ boulders

Sand fraction (2 mm - 0.062 mm)

Weight percent of total sample 3

Composition:

Terrigenous rock fragments and mineral grains 29
Carbonate megafaunal shell fragments 10
Foraminifera _____
Volcanic ash 30
Siliceous spicules and shells 31

Fine fraction (<0.062 mm)

Weight percent silt (0.062 mm - 0.0039 mm) in total sample 61
Weight percent clay (<0.0039 mm) in total sample 36

Composition:

Clay minerals 35
Volcanic ash 55
Terrigenous mineral grains 10
Siliceous shells and spicules Tr
Carbonate shells _____

SAMPLE NUMBER 97

Coarse fraction (>2 mm)

Weight percent of total sample _____

Composition:

Terrigenous rock fragments _____
Carbonate shells _____

_____ granules _____ pebbles
_____ cobbles _____ boulders

Sand fraction (2 mm - 0.062 mm)

Weight percent of total sample 1

Composition:

Terrigenous rock fragments and mineral grains 1
Carbonate megafaunal shell fragments _____
Foraminifera 3
Volcanic ash 31
Siliceous spicules and shells 65

Fine fraction (<0.062 mm)

Weight percent silt (0.062 mm - 0.0039 mm) in total sample 60
Weight percent clay (<0.0039 mm) in total sample 39

Composition:

Clay minerals 55
Volcanic ash 40
Terrigenous mineral grains 5
Siliceous shells and spicules Tr
Carbonate shells Tr

SAMPLE NUMBER 98

Coarse fraction (>2 mm)

Weight percent of total sample _____

Composition:

Terrigenous rock fragments _____
Carbonate shells _____

_____ granules _____ pebbles
_____ cobbles _____ boulders

Sand fraction (2 mm - 0.062 mm)

Weight percent of total sample 1

Composition:

Terrigenous rock fragments and mineral grains 1
Carbonate megafaunal shell fragments 3
Foraminifera _____
Volcanic ash 46
Siliceous spicules and shells 50

Fine fraction (<0.062 mm)

Weight percent silt (0.062 mm - 0.0039 mm) in total sample 62
Weight percent clay (<0.0039 mm) in total sample 37

Composition:

Clay minerals 40
Volcanic ash 48
Terrigenous mineral grains 12
Siliceous shells and spicules Tr
Carbonate shells _____

SAMPLE NUMBER 113

Coarse fraction (>2 mm)

Weight percent of total sample 25

Composition:

Terrigenous rock fragments 100

granules pebbles
 cobbles boulders

Carbonate shells _____

Sand fraction (2 mm - 0.062 mm)

Weight percent of total sample 70

Composition:

Terrigenous rock fragments and mineral grains 98

Carbonate megafaunal shell fragments Tr

Foraminifera 2

Volcanic ash Tr

Siliceous spicules and shells _____

Fine fraction (<0.062 mm)

Weight percent silt (0.062 mm - 0.0039 mm) in total sample 3

Weight percent clay (<0.0039 mm) in total sample 2

Composition:

Clay minerals 25

Volcanic ash 60

Terrigenous mineral grains 15

Siliceous shells and spicules Tr

Carbonate shells _____

SAMPLE NUMBER 115

Coarse fraction (>2 mm)

Weight percent of total sample _____

Composition:

Terrigenous rock fragments _____

granules pebbles
 cobbles boulders

Carbonate shells _____

Sand fraction (2 mm - 0.062 mm)

Weight percent of total sample 92

Composition:

Terrigenous rock fragments and mineral grains 2

Carbonate megafaunal shell fragments 6

Foraminifera 2

Volcanic ash 90

Siliceous spicules and shells Tr

Fine fraction (<0.062 mm)

Weight percent silt (0.062 mm - 0.0039 mm) in total sample 5

Weight percent clay (<0.0039 mm) in total sample 3

Composition:

Clay minerals 19

Volcanic ash 73

Terrigenous mineral grains 6

Siliceous shells and spicules 2

Carbonate shells Tr

SAMPLE NUMBER 127

Coarse fraction (>2 mm)

Weight percent of total sample 17

Composition:

Terrigenous rock fragments 74
Carbonate shells 26

granules pebbles
 cobbles boulders

Sand fraction (2 mm - 0.062 mm)

Weight percent of total sample 65

Composition:

Terrigenous rock fragments and mineral grains 25
Carbonate megafaunal shell fragments 73
Foraminifera 1
Volcanic ash 1
Siliceous spicules and shells Tr

Fine fraction (<0.062 mm)

Weight percent silt (0.062 mm - 0.0039 mm) in total sample 11

Weight percent clay (<0.0039 mm) in total sample 7

Composition:

Clay minerals 25
Volcanic ash 55
Terrigenous mineral grains 20
Siliceous shells and spicules Tr
Carbonate shells _____

SAMPLE NUMBER 128

Coarse fraction (>2 mm)

Weight percent of total sample 25

Composition:

Terrigenous rock fragments 98
Carbonate shells 2

granules pebbles
 cobbles boulders

Sand fraction (2 mm - 0.062 mm)

Weight percent of total sample 45

Composition:

Terrigenous rock fragments and mineral grains 5
Carbonate megafaunal shell fragments 25
Foraminifera 50
Volcanic ash 20
Siliceous spicules and shells Tr

Fine fraction (<0.062 mm)

Weight percent silt (0.062 mm - 0.0039 mm) in total sample 15

Weight percent clay (<0.0039 mm) in total sample 15

Composition:

Clay minerals 35
Volcanic ash 24
Terrigenous mineral grains 35
Siliceous shells and spicules 5
Carbonate shells 1

SAMPLE NUMBER 130

Coarse fraction (>2 mm)

Weight percent of total sample _____

Composition:

Terrigenous rock fragments _____

_____ granules

_____ pebbles

Carbonate shells _____

_____ cobbles

_____ boulders

Sand fraction (2 mm - 0.062 mm)

Weight percent of total sample 79

Composition:

Terrigenous rock fragments and mineral grains 99

Carbonate megafaunal shell fragments _____

Foraminifera Tr

Volcanic ash Tr

Siliceous spicules and shells 1

Fine fraction (<0.062 mm)

Weight percent silt (0.062 mm - 0.0039 mm) in total sample 11

Weight percent clay (<0.0039 mm) in total sample 10

Composition:

Clay minerals 15

Volcanic ash 75

Terrigenous mineral grains 10

Siliceous shells and spicules Tr

Carbonate shells _____

SAMPLE NUMBER 131

Coarse fraction (>2 mm)

Weight percent of total sample 3

Composition:

Terrigenous rock fragments 100

granules

pebbles

Carbonate shells _____

_____ cobbles

_____ boulders

Sand fraction (2 mm - 0.062 mm)

Weight percent of total sample 45

Composition:

Terrigenous rock fragments and mineral grains 99

Carbonate megafaunal shell fragments _____

Foraminifera 1

Volcanic ash Tr

Siliceous spicules and shells Tr

Fine fraction (<0.062 mm)

Weight percent silt (0.062 mm - 0.0039 mm) in total sample 25

Weight percent clay (<0.0039 mm) in total sample 27

Composition:

Clay minerals _____

Volcanic ash _____

Terrigenous mineral grains _____

Siliceous shells and spicules _____

Carbonate shells _____

SAMPLE NUMBER 132

Coarse fraction (>2 mm)

Weight percent of total sample 5

Composition:

Terrigenous rock fragments 100

granules pebbles
 cobbles boulders

Carbonate shells _____

Sand fraction (2 mm - 0.062 mm)

Weight percent of total sample 33

Composition:

Terrigenous rock fragments and mineral grains 88

Carbonate megafaunal shell fragments _____

Foraminifera 1

Volcanic ash 10

Siliceous spicules and shells 1

Fine fraction (<0.062 mm)

Weight percent silt (0.062 mm - 0.0039 mm) in total sample 32

Weight percent clay (<0.0039 mm) in total sample 30

Composition:

Clay minerals 23

Volcanic ash 39

Terrigenous mineral grains 34

Siliceous shells and spicules 5

Carbonate shells Tr

SAMPLE NUMBER 134

Coarse fraction (>2 mm)

Weight percent of total sample 20

Composition:

Terrigenous rock fragments 100

granules pebbles
 cobbles boulders

Carbonate shells _____

Sand fraction (2 mm - 0.062 mm)

Weight percent of total sample 41

Composition:

Terrigenous rock fragments and mineral grains 94

Carbonate megafaunal shell fragments _____

Foraminifera Tr

Volcanic ash 5

Siliceous spicules and shells 1

Fine fraction (<0.062 mm)

Weight percent silt (0.062 mm - 0.0039 mm) in total sample 17

Weight percent clay (<0.0039 mm) in total sample 22

Composition:

Clay minerals _____

Volcanic ash _____

Terrigenous mineral grains _____

Siliceous shells and spicules _____

Carbonate shells _____

SAMPLE NUMBER 135

Coarse fraction (>2 mm)

Weight percent of total sample _____

Composition:

Terrigenous rock fragments _____

_____ granules

_____ pebbles

Carbonate shells _____

_____ cobbles

_____ boulders

Sand fraction (2 mm - 0.062 mm)

Weight percent of total sample 77

Composition:

Terrigenous rock fragments and mineral grains 100

Carbonate megafaunal shell fragments _____

Foraminifera Tr

Volcanic ash Tr

Siliceous spicules and shells Tr

Fine fraction (<0.062 mm)

Weight percent silt (0.062 mm - 0.0039 mm) in total sample 15

Weight percent clay (<0.0039 mm) in total sample 8

Composition:

Clay minerals 44

Volcanic ash 46

Terrigenous mineral grains 4

Siliceous shells and spicules 6

Carbonate shells _____

SAMPLE NUMBER 136

Coarse fraction (>2 mm)

Weight percent of total sample _____

Composition:

Terrigenous rock fragments _____

_____ granules

_____ pebbles

Carbonate shells _____

_____ cobbles

_____ boulders

Sand fraction (2 mm - 0.062 mm)

Weight percent of total sample 73

Composition:

Terrigenous rock fragments and mineral grains 97

Carbonate megafaunal shell fragments _____

Foraminifera _____

Volcanic ash 3

Siliceous spicules and shells Tr

Fine fraction (<0.062 mm)

Weight percent silt (0.062 mm - 0.0039 mm) in total sample 17

Weight percent clay (<0.0039 mm) in total sample 10

Composition:

Clay minerals _____

Volcanic ash _____

Terrigenous mineral grains _____

Siliceous shells and spicules _____

Carbonate shells _____

SAMPLE NUMBER 137

Coarse fraction (>2 mm)

Weight percent of total sample 10

Composition:

Terrigenous rock fragments 62
Carbonate shells 38

granules pebbles
 cobbles boulders

Sand fraction (2 mm - 0.062 mm)

Weight percent of total sample 72

Composition:

Terrigenous rock fragments and mineral grains 45
Carbonate megafaunal shell fragments 43
Foraminifera 8
Volcanic ash 4
Siliceous spicules and shells Tr

Fine fraction (<0.062 mm)

Weight percent silt (0.062 mm - 0.0039 mm) in total sample 13

Weight percent clay (<0.0039 mm) in total sample 5

Composition:

Clay minerals 50
Volcanic ash 20
Terrigenous mineral grains 30
Siliceous shells and spicules Tr
Carbonate shells Tr

SAMPLE NUMBER 138

Coarse fraction (>2 mm)

Weight percent of total sample 24

Composition:

Terrigenous rock fragments 3
Carbonate shells 97

granules pebbles
 cobbles boulders

Sand fraction (2 mm - 0.062 mm)

Weight percent of total sample 70

Composition:

Terrigenous rock fragments and mineral grains 57
Carbonate megafaunal shell fragments 35
Foraminifera 2
Volcanic ash 6
Siliceous spicules and shells _____

Fine fraction (<0.062 mm)

Weight percent silt (0.062 mm - 0.0039 mm) in total sample 3

Weight percent clay (<0.0039 mm) in total sample 3

Composition:

Clay minerals 10
Volcanic ash 60
Terrigenous mineral grains 30
Siliceous shells and spicules Tr
Carbonate shells _____

SAMPLE NUMBER 141

Coarse fraction (>2 mm)

Weight percent of total sample 56

Composition:

Terrigenous rock fragments 99

granules pebbles
 cobbles boulders

Carbonate shells 1

Sand fraction (2 mm - 0.062 mm)

Weight percent of total sample 26

Composition:

Terrigenous rock fragments and mineral grains 6

Carbonate megafaunal shell fragments 3

Foraminifera 41

Volcanic ash 50

Siliceous spicules and shells Tr

Fine fraction (<0.062 mm)

Weight percent silt (0.062 mm - 0.0039 mm) in total sample 11

Weight percent clay (<0.0039 mm) in total sample 7

Composition:

Clay minerals 25

Volcanic ash 60

Terrigenous mineral grains 15

Siliceous shells and spicules Tr

Carbonate shells _____

SAMPLE NUMBER _____

Coarse fraction (>2 mm)

Weight percent of total sample _____

Composition:

Terrigenous rock fragments _____

____ granules ____ pebbles
____ cobbles ____ boulders

Carbonate shells _____

Sand fraction (2 mm - 0.062 mm)

Weight percent of total sample _____

Composition:

Terrigenous rock fragments and mineral grains _____

Carbonate megafaunal shell fragments _____

Foraminifera _____

Volcanic ash _____

Siliceous spicules and shells _____

Fine fraction (<0.062 mm)

Weight percent silt (0.062 mm - 0.0039 mm) in total sample _____

Weight percent clay (<0.0039 mm) in total sample _____

Composition:

Clay minerals _____

Volcanic ash _____

Terrigenous mineral grains _____

Siliceous shells and spicules _____

Carbonate shells _____

SAMPLE NUMBER 200

Coarse fraction (>2 mm)

Weight percent of total sample 48

Composition:

Terrigenous rock fragments 98

Carbonate shells 2

granules pebbles
 cobbles boulders

Sand fraction (2 mm - 0.062 mm)

Weight percent of total sample 46

Composition:

Terrigenous rock fragments and mineral grains 97

Carbonate megafaunal shell fragments _____

Foraminifera 3

Volcanic ash Tr

Siliceous spicules and shells Tr

Fine fraction (<0.062 mm)

Weight percent silt (0.062 mm - 0.0039 mm) in total sample 2

Weight percent clay (<0.0039 mm) in total sample 4

Composition:

Clay minerals 28

Volcanic ash 42

Terrigenous mineral grains 18

Siliceous shells and spicules 10

Carbonate shells 2

SAMPLE NUMBER 201

Coarse fraction (>2 mm)

Weight percent of total sample 54

Composition:

Terrigenous rock fragments 90

Carbonate shells 10

granules pebbles
 cobbles boulders

Sand fraction (2 mm - 0.062 mm)

Weight percent of total sample 43

Composition:

Terrigenous rock fragments and mineral grains 43

Carbonate megafaunal shell fragments 54

Foraminifera 3

Volcanic ash Tr

Siliceous spicules and shells _____

Fine fraction (<0.062 mm)

Weight percent silt (0.062 mm - 0.0039 mm) in total sample 1

Weight percent clay (<0.0039 mm) in total sample 2

Composition:

Clay minerals 50

Volcanic ash 15

Terrigenous mineral grains 30

Siliceous shells and spicules 5

Carbonate shells _____

SAMPLE NUMBER 202

Coarse fraction (>2 mm)

Weight percent of total sample 3

Composition:

Terrigenous rock fragments 65
Carbonate shells 35

granules pebbles
 cobbles boulders

Sand fraction (2 mm - 0.062 mm)

Weight percent of total sample 65

Composition:

Terrigenous rock fragments and mineral grains 97
Carbonate megafaunal shell fragments 1
Foraminifera 1
Volcanic ash 1
Siliceous spicules and shells TR

Fine fraction (<0.062 mm)

Weight percent silt (0.062 mm - 0.0039 mm) in total sample 13
Weight percent clay (<0.0039 mm) in total sample 19

Composition:

Clay minerals 30
Volcanic ash 38
Terrigenous mineral grains 22
Siliceous shells and spicules 9
Carbonate shells 1

SAMPLE NUMBER 204

Coarse fraction (>2 mm)

Weight percent of total sample 36

Composition:

Terrigenous rock fragments 100
Carbonate shells _____

granules pebbles
 cobbles boulders

Sand fraction (2 mm - 0.062 mm)

Weight percent of total sample 32

Composition:

Terrigenous rock fragments and mineral grains 40
Carbonate megafaunal shell fragments _____
Foraminifera 1
Volcanic ash 58
Siliceous spicules and shells 1

Fine fraction (<0.062 mm)

Weight percent silt (0.062 mm - 0.0039 mm) in total sample 19
Weight percent clay (<0.0039 mm) in total sample 13

Composition:

Clay minerals 34
Volcanic ash 52
Terrigenous mineral grains 9
Siliceous shells and spicules 5
Carbonate shells TR

SAMPLE NUMBER 205

Coarse fraction (>2 mm)

Weight percent of total sample 35

Composition:

Terrigenous rock fragments 95
Carbonate shells 5

granules pebbles
 cobbles boulders

Sand fraction (2 mm - 0.062 mm)

Weight percent of total sample 47

Composition:

Terrigenous rock fragments and mineral grains 98
Carbonate megafaunal shell fragments Tr
Foraminifera 1
Volcanic ash 1
Siliceous spicules and shells _____

Fine fraction (<0.062 mm)

Weight percent silt (0.062 mm - 0.0039 mm) in total sample 11

Weight percent clay (<0.0039 mm) in total sample 7

Composition:

Clay minerals 25
Volcanic ash 67
Terrigenous mineral grains 3
Siliceous shells and spicules 5
Carbonate shells Tr

SAMPLE NUMBER 216

Coarse fraction (>2 mm)

Weight percent of total sample 1

Composition:

Terrigenous rock fragments _____
Carbonate shells 100

granules pebbles
 cobbles boulders

Sand fraction (2 mm - 0.062 mm)

Weight percent of total sample 88

Composition:

Terrigenous rock fragments and mineral grains 4
Carbonate megafaunal shell fragments 19
Foraminifera 15
Volcanic ash 62
Siliceous spicules and shells _____

Fine fraction (<0.062 mm)

Weight percent silt (0.062 mm - 0.0039 mm) in total sample 7

Weight percent clay (<0.0039 mm) in total sample 4

Composition:

Clay minerals 30
Volcanic ash 50
Terrigenous mineral grains 12
Siliceous shells and spicules 5
Carbonate shells 3

SAMPLE NUMBER 217

Coarse fraction (>2 mm)

Weight percent of total sample 52

Composition:

Terrigenous rock fragments 91
Carbonate shells 9

granules pebbles
 cobbles boulders

Sand fraction (2 mm - 0.062 mm)

Weight percent of total sample 44

Composition:

Terrigenous rock fragments and mineral grains 3
Carbonate megafaunal shell fragments 30
Foraminifera 14
Volcanic ash 53
Siliceous spicules and shells _____

Fine fraction (<0.062 mm)

Weight percent silt (0.062 mm - 0.0039 mm) in total sample 3
Weight percent clay (<0.0039 mm) in total sample 1

Composition:

Clay minerals 25
Volcanic ash 50
Terrigenous mineral grains 10
Siliceous shells and spicules 7
Carbonate shells 8

SAMPLE NUMBER 219

Coarse fraction (>2 mm)

Weight percent of total sample 73

Composition:

Terrigenous rock fragments 100
Carbonate shells Tr

granules pebbles
 cobbles boulders

Sand fraction (2 mm - 0.062 mm)

Weight percent of total sample 25

Composition:

Terrigenous rock fragments and mineral grains 60
Carbonate megafaunal shell fragments 25
Foraminifera 14
Volcanic ash 1
Siliceous spicules and shells Tr

Fine fraction (<0.062 mm)

Weight percent silt (0.062 mm - 0.0039 mm) in total sample 1
Weight percent clay (<0.0039 mm) in total sample 1

Composition:

Clay minerals 20
Volcanic ash 35
Terrigenous mineral grains 35
Siliceous shells and spicules 4
Carbonate shells 6

SAMPLE NUMBER 227

Coarse fraction (>2 mm)

Weight percent of total sample _____

Composition:

Terrigenous rock fragments _____ granules _____ pebbles _____
Carbonate shells _____ cobbles _____ boulders _____

Sand fraction (2 mm - 0.062 mm)

Weight percent of total sample 72

Composition:

Terrigenous rock fragments and mineral grains 1
Carbonate megafaunal shell fragments _____
Foraminifera Tr
Volcanic ash 99
Siliceous spicules and shells _____

Fine fraction (<0.062 mm)

Weight percent silt (0.062 mm - 0.0039 mm) in total sample 19
Weight percent clay (<0.0039 mm) in total sample 9

Composition:

Clay minerals 20
Volcanic ash 60
Terrigenous mineral grains 20
Siliceous shells and spicules Tr
Carbonate shells Tr

SAMPLE NUMBER 228

Coarse fraction (>2 mm)

Weight percent of total sample 33

Composition:

Terrigenous rock fragments 86 granules pebbles
Carbonate shells 14 cobbles boulders

Sand fraction (2 mm - 0.062 mm)

Weight percent of total sample 59

Composition:

Terrigenous rock fragments and mineral grains 63
Carbonate megafaunal shell fragments 27
Foraminifera 10
Volcanic ash Tr
Siliceous spicules and shells Tr

Fine fraction (<0.062 mm)

Weight percent silt (0.062 mm - 0.0039 mm) in total sample 5
Weight percent clay (<0.0039 mm) in total sample 3

Composition:

Clay minerals 40
Volcanic ash 25
Terrigenous mineral grains 30
Siliceous shells and spicules 5
Carbonate shells _____

SAMPLE NUMBER 229

Coarse fraction (>2 mm)

Weight percent of total sample _____

Composition:

Terrigenous rock fragments _____
Carbonate shells _____

_____ granules _____ pebbles
_____ cobbles _____ boulders

Sand fraction (2 mm - 0.062 mm)

Weight percent of total sample 55

Composition:

Terrigenous rock fragments and mineral grains _____
Carbonate megafaunal shell fragments Tr
Foraminifera _____
Volcanic ash 99
Siliceous spicules and shells _____

Fine fraction (<0.062 mm)

Weight percent silt (0.062 mm - 0.0039 mm) in total sample 36
Weight percent clay (<0.0039 mm) in total sample 9

Composition:

Clay minerals 35
Volcanic ash 45
Terrigenous mineral grains 15
Siliceous shells and spicules 5
Carbonate shells _____

SAMPLE NUMBER 232

Coarse fraction (>2 mm)

Weight percent of total sample 29

Composition:

Terrigenous rock fragments 100
Carbonate shells _____

granules pebbles
 cobbles boulders

Sand fraction (2 mm - 0.062 mm)

Weight percent of total sample 69

Composition:

Terrigenous rock fragments and mineral grains 99
Carbonate megafaunal shell fragments _____
Foraminifera Tr
Volcanic ash 1
Siliceous spicules and shells Tr

Fine fraction (<0.062 mm)

Weight percent silt (0.062 mm - 0.0039 mm) in total sample 1
Weight percent clay (<0.0039 mm) in total sample 1

Composition:

Clay minerals 55
Volcanic ash 35
Terrigenous mineral grains 7
Siliceous shells and spicules 3
Carbonate shells _____

SAMPLE NUMBER 234

Coarse fraction (>2 mm)

Weight percent of total sample 50

Composition:

Terrigenous rock fragments 85
Carbonate shells 15

granules pebbles
 cobbles boulders

Sand fraction (2 mm - 0.062 mm)

Weight percent of total sample 47

Composition:

Terrigenous rock fragments and mineral grains 20
Carbonate megafaunal shell fragments 3
Foraminifera 35
Volcanic ash 42
Siliceous spicules and shells TR

Fine fraction (<0.062 mm)

Weight percent silt (0.062 mm - 0.0039 mm) in total sample 2
Weight percent clay (<0.0039 mm) in total sample 1

Composition:

Clay minerals 24
Volcanic ash 30
Terrigenous mineral grains 40
Siliceous shells and spicules 3
Carbonate shells 3

SAMPLE NUMBER 236

Coarse fraction (>2 mm)

Weight percent of total sample _____

Composition:

Terrigenous rock fragments _____
Carbonate shells _____

granules pebbles
 cobbles boulders

Sand fraction (2 mm - 0.062 mm)

Weight percent of total sample 38

Composition:

Terrigenous rock fragments and mineral grains TR
Carbonate megafaunal shell fragments _____
Foraminifera TR
Volcanic ash 100
Siliceous spicules and shells _____

Fine fraction (<0.062 mm)

Weight percent silt (0.062 mm - 0.0039 mm) in total sample 48
Weight percent clay (<0.0039 mm) in total sample 14

Composition:

Clay minerals 35
Volcanic ash 55
Terrigenous mineral grains 8
Siliceous shells and spicules 2
Carbonate shells _____

SAMPLE NUMBER 241

Coarse fraction (>2 mm)

Weight percent of total sample 5

Composition:

Terrigenous rock fragments 97
Carbonate shells 3

granules pebbles
 cobbles boulders

Sand fraction (2 mm - 0.062 mm)

Weight percent of total sample 86

Composition:

Terrigenous rock fragments and mineral grains 30
Carbonate megafaunal shell fragments _____
Foraminifera _____
Volcanic ash 70
Siliceous spicules and shells Tr

Fine fraction (<0.062 mm)

Weight percent silt (0.062 mm - 0.0039 mm) in total sample 4
Weight percent clay (<0.0039 mm) in total sample 5

Composition:

Clay minerals 14
Volcanic ash 37
Terrigenous mineral grains 47
Siliceous shells and spicules 2
Carbonate shells _____

SAMPLE NUMBER 242

Coarse fraction (>2 mm)

Weight percent of total sample _____

Composition:

Terrigenous rock fragments _____
Carbonate shells _____

____ granules ____ pebbles
____ cobbles ____ boulders

Sand fraction (2 mm - 0.062 mm)

Weight percent of total sample 64

Composition:

Terrigenous rock fragments and mineral grains 2
Carbonate megafaunal shell fragments _____
Foraminifera Tr
Volcanic ash 98
Siliceous spicules and shells Tr

Fine fraction (<0.062 mm)

Weight percent silt (0.062 mm - 0.0039 mm) in total sample 30
Weight percent clay (<0.0039 mm) in total sample 6

Composition:

Clay minerals 32
Volcanic ash 51
Terrigenous mineral grains 13
Siliceous shells and spicules 4
Carbonate shells Tr

SAMPLE NUMBER 243

Coarse fraction (>2 mm)

Weight percent of total sample 24

Composition:

Terrigenous rock fragments 99
Carbonate shells 1

granules pebbles
 cobbles boulders

Sand fraction (2 mm - 0.062 mm)

Weight percent of total sample 66

Composition:

Terrigenous rock fragments and mineral grains 77
Carbonate megafaunal shell fragments 3
Foraminifera _____
Volcanic ash 20
Siliceous spicules and shells Tr

Fine fraction (<0.062 mm)

Weight percent silt (0.062 mm - 0.0039 mm) in total sample 7
Weight percent clay (<0.0039 mm) in total sample 3

Composition:

Clay minerals 45
Volcanic ash 40
Terrigenous mineral grains 10
Siliceous shells and spicules 5
Carbonate shells Tr

SAMPLE NUMBER 244

Coarse fraction (>2 mm)

Weight percent of total sample 1

Composition:

Terrigenous rock fragments 100
Carbonate shells _____

granules pebbles
 cobbles boulders

Sand fraction (2 mm - 0.062 mm)

Weight percent of total sample 80

Composition:

Terrigenous rock fragments and mineral grains 15
Carbonate megafaunal shell fragments Tr
Foraminifera _____
Volcanic ash 85
Siliceous spicules and shells _____

Fine fraction (<0.062 mm)

Weight percent silt (0.062 mm - 0.0039 mm) in total sample 15
Weight percent clay (<0.0039 mm) in total sample 4

Composition:

Clay minerals 35
Volcanic ash 45
Terrigenous mineral grains 15
Siliceous shells and spicules 5
Carbonate shells Tr

SAMPLE NUMBER 245

Coarse fraction (>2 mm)

Weight percent of total sample 9

Composition:

Terrigenous rock fragments 60

Carbonate shells 40

granules
 cobbles

pebbles
 boulders

Sand fraction (2 mm - 0.062 mm)

Weight percent of total sample 72

Composition:

Terrigenous rock fragments and mineral grains 20

Carbonate megafaunal shell fragments 30

Foraminifera 7

Volcanic ash 43

Siliceous spicules and shells _____

Fine fraction (<0.062 mm)

Weight percent silt (0.062 mm - 0.0039 mm) in total sample 6

Weight percent clay (<0.0039 mm) in total sample 13

Composition:

Clay minerals 21

Volcanic ash 66

Terrigenous mineral grains 7

Siliceous shells and spicules 4

Carbonate shells 2

SAMPLE NUMBER 246

Coarse fraction (>2 mm)

Weight percent of total sample 32

Composition:

Terrigenous rock fragments 96

Carbonate shells 4

granules
 cobbles

pebbles
 boulders

Sand fraction (2 mm - 0.062 mm)

Weight percent of total sample 47

Composition:

Terrigenous rock fragments and mineral grains 5

Carbonate megafaunal shell fragments 15

Foraminifera 40

Volcanic ash 40

Siliceous spicules and shells Tr

Fine fraction (<0.062 mm)

Weight percent silt (0.062 mm - 0.0039 mm) in total sample 13

Weight percent clay (<0.0039 mm) in total sample 8

Composition:

Clay minerals 60

Volcanic ash 30

Terrigenous mineral grains 10

Siliceous shells and spicules Tr

Carbonate shells Tr

SAMPLE NUMBER 329

Coarse fraction (>2 mm)

Weight percent of total sample _____

Composition:

Terrigenous rock fragments _____

_____ granules _____ pebbles
_____ cobbles _____ boulders

Carbonate shells _____

Sand fraction (2 mm - 0.062 mm)

Weight percent of total sample 36

Composition:

Terrigenous rock fragments and mineral grains _____

Carbonate megafaunal shell fragments _____

Foraminifera Tr

Volcanic ash 100

Siliceous spicules and shells Tr

Fine fraction (<0.062 mm)

Weight percent silt (0.062 mm - 0.0039 mm) in total sample 50

Weight percent clay (<0.0039 mm) in total sample 14

Composition:

Clay minerals 30

Volcanic ash 65

Terrigenous mineral grains 4

Siliceous shells and spicules 1

Carbonate shells _____

SAMPLE NUMBER 330

Coarse fraction (>2 mm)

Weight percent of total sample 10

Composition:

Terrigenous rock fragments 99

granules _____ pebbles
_____ cobbles _____ boulders

Carbonate shells 1

Sand fraction (2 mm - 0.062 mm)

Weight percent of total sample 78

Composition:

Terrigenous rock fragments and mineral grains 47

Carbonate megafaunal shell fragments 20

Foraminifera 13

Volcanic ash 20

Siliceous spicules and shells Tr

Fine fraction (<0.062 mm)

Weight percent silt (0.062 mm - 0.0039 mm) in total sample 7

Weight percent clay (<0.0039 mm) in total sample 5

Composition:

Clay minerals 40

Volcanic ash 30

Terrigenous mineral grains 30

Siliceous shells and spicules Tr

Carbonate shells _____

SAMPLE NUMBER 336

Coarse fraction (>2 mm)

Weight percent of total sample _____

Composition:

Terrigenous rock fragments _____
Carbonate shells _____

____ granules ____ pebbles
____ cobbles ____ boulders

Sand fraction (2 mm - 0.062 mm)

Weight percent of total sample 1

Composition:

Terrigenous rock fragments and mineral grains _____
Carbonate megafaunal shell fragments _____
Foraminifera _____
Volcanic ash 2
Siliceous spicules and shells 98

Fine fraction (<0.062 mm)

Weight percent silt (0.062 mm - 0.0039 mm) in total sample 50
Weight percent clay (<0.0039 mm) in total sample 49

Composition:

Clay minerals 38
Volcanic ash 42
Terrigenous mineral grains 15
Siliceous shells and spicules 5
Carbonate shells _____

SAMPLE NUMBER 340

Coarse fraction (>2 mm)

Weight percent of total sample 2

Composition:

Terrigenous rock fragments 100
Carbonate shells _____

granules pebbles
 cobbles boulders

Sand fraction (2 mm - 0.062 mm)

Weight percent of total sample 23

Composition:

Terrigenous rock fragments and mineral grains 10
Carbonate megafaunal shell fragments _____
Foraminifera 2
Volcanic ash 87
Siliceous spicules and shells 1

Fine fraction (<0.062 mm)

Weight percent silt (0.062 mm - 0.0039 mm) in total sample 51
Weight percent clay (<0.0039 mm) in total sample 24

Composition:

Clay minerals 28
Volcanic ash 20
Terrigenous mineral grains 50
Siliceous shells and spicules Tr
Carbonate shells 2

SAMPLE NUMBER 341

Coarse fraction (>2 mm)

Weight percent of total sample 50

Composition:

Terrigenous rock fragments 94 granules pebbles
Carbonate shells 6 cobbles boulders

Sand fraction (2 mm - 0.062 mm)

Weight percent of total sample 43

Composition:

Terrigenous rock fragments and mineral grains 5
Carbonate megafaunal shell fragments 73
Foraminifera 12
Volcanic ash 10
Siliceous spicules and shells _____

Fine fraction (<0.062 mm)

Weight percent silt (0.062 mm - 0.0039 mm) in total sample 4

Weight percent clay (<0.0039 mm) in total sample 3

Composition:

Clay minerals 40
Volcanic ash 42
Terrigenous mineral grains 15
Siliceous shells and spicules Tr
Carbonate shells 3

SAMPLE NUMBER 342

Coarse fraction (>2 mm)

Weight percent of total sample 59

Composition:

Terrigenous rock fragments 98 granules pebbles
Carbonate shells 2 cobbles boulders

Sand fraction (2 mm - 0.062 mm)

Weight percent of total sample 34

Composition:

Terrigenous rock fragments and mineral grains 20
Carbonate megafaunal shell fragments 5
Foraminifera 5
Volcanic ash 70
Siliceous spicules and shells _____

Fine fraction (<0.062 mm)

Weight percent silt (0.062 mm - 0.0039 mm) in total sample 4

Weight percent clay (<0.0039 mm) in total sample 3

Composition:

Clay minerals 45
Volcanic ash 40
Terrigenous mineral grains 10
Siliceous shells and spicules 5
Carbonate shells _____

SAMPLE NUMBER 343

Coarse fraction (>2 mm)

Weight percent of total sample _____

Composition:

Terrigenous rock fragments _____

_____ granules _____ pebbles
_____ cobbles _____ boulders

Carbonate shells _____

Sand fraction (2 mm - 0.062 mm)

Weight percent of total sample 5

Composition:

Terrigenous rock fragments and mineral grains 50

Carbonate megafaunal shell fragments _____

Foraminifera 5

Volcanic ash 25

Siliceous spicules and shells 20

Fine fraction (<0.062 mm)

Weight percent silt (0.062 mm - 0.0039 mm) in total sample 64

Weight percent clay (<0.0039 mm) in total sample 31

Composition:

Clay minerals 15

Volcanic ash 70

Terrigenous mineral grains 10

Siliceous shells and spicules 4

Carbonate shells 1

SAMPLE NUMBER 344

Coarse fraction (>2 mm)

Weight percent of total sample _____

Composition:

Terrigenous rock fragments _____

_____ granules _____ pebbles
_____ cobbles _____ boulders

Carbonate shells _____

Sand fraction (2 mm - 0.062 mm)

Weight percent of total sample 1

Composition:

Terrigenous rock fragments and mineral grains 42

Carbonate megafaunal shell fragments _____

Foraminifera 3

Volcanic ash 35

Siliceous spicules and shells 20

Fine fraction (<0.062 mm)

Weight percent silt (0.062 mm - 0.0039 mm) in total sample 60

Weight percent clay (<0.0039 mm) in total sample 39

Composition:

Clay minerals 55

Volcanic ash 25

Terrigenous mineral grains 15

Siliceous shells and spicules 3

Carbonate shells 2

SAMPLE NUMBER 345

Coarse fraction (>2 mm)

Weight percent of total sample _____

Composition:

Terrigenous rock fragments _____
Carbonate shells _____

___ granules ___ pebbles
___ cobbles ___ boulders

Sand fraction (2 mm - 0.062 mm)

Weight percent of total sample 65

Composition:

Terrigenous rock fragments and mineral grains 99
Carbonate megafaunal shell fragments _____
Foraminifera 1
Volcanic ash Tr
Siliceous spicules and shells Tr

Fine fraction (<0.062 mm)

Weight percent silt (0.062 mm - 0.0039 mm) in total sample 23
Weight percent clay (<0.0039 mm) in total sample 12

Composition:

Clay minerals 32
Volcanic ash 50
Terrigenous mineral grains 15
Siliceous shells and spicules 2
Carbonate shells 1

SAMPLE NUMBER 346

Coarse fraction (>2 mm)

Weight percent of total sample _____

Composition:

Terrigenous rock fragments _____
Carbonate shells _____

___ granules ___ pebbles
___ cobbles ___ boulders

Sand fraction (2 mm - 0.062 mm)

Weight percent of total sample 67

Composition:

Terrigenous rock fragments and mineral grains 99
Carbonate megafaunal shell fragments _____
Foraminifera Tr
Volcanic ash 1
Siliceous spicules and shells Tr

Fine fraction (<0.062 mm)

Weight percent silt (0.062 mm - 0.0039 mm) in total sample 22
Weight percent clay (<0.0039 mm) in total sample 11

Composition:

Clay minerals _____
Volcanic ash _____
Terrigenous mineral grains _____
Siliceous shells and spicules _____
Carbonate shells _____

SAMPLE NUMBER 347

Coarse fraction (>2 mm)

Weight percent of total sample _____

Composition:

Terrigenous rock fragments _____

___ granules

___ pebbles

Carbonate shells _____

___ cobbles

___ boulders

Sand fraction (2 mm - 0.062 mm)

Weight percent of total sample 4

Composition:

Terrigenous rock fragments and mineral grains 54

Carbonate megafaunal shell fragments 4

Foraminifera _____

Volcanic ash 24

Siliceous spicules and shells 18

Fine fraction (<0.062 mm)

Weight percent silt (0.062 mm - 0.0039 mm) in total sample 67

Weight percent clay (<0.0039 mm) in total sample 29

Composition:

Clay minerals 40

Volcanic ash 35

Terrigenous mineral grains 12

Siliceous shells and spicules 3

Carbonate shells _____

SAMPLE NUMBER 348

Coarse fraction (>2 mm)

Weight percent of total sample _____

Composition:

Terrigenous rock fragments _____

___ granules

___ pebbles

Carbonate shells _____

___ cobbles

___ boulders

Sand fraction (2 mm - 0.062 mm)

Weight percent of total sample 3

Composition:

Terrigenous rock fragments and mineral grains 57

Carbonate megafaunal shell fragments _____

Foraminifera 3

Volcanic ash 40

Siliceous spicules and shells _____

Fine fraction (<0.062 mm)

Weight percent silt (0.062 mm - 0.0039 mm) in total sample 63

Weight percent clay (<0.0039 mm) in total sample 34

Composition:

Clay minerals 35

Volcanic ash 50

Terrigenous mineral grains 10

Siliceous shells and spicules 5

Carbonate shells _____

SAMPLE NUMBER 349

Coarse fraction (>2 mm)

Weight percent of total sample _____

Composition:

Terrigenous rock fragments _____
Carbonate shells _____

_____ granules _____ pebbles
_____ cobbles _____ boulders

Sand fraction (2 mm - 0.062 mm)

Weight percent of total sample 1

Composition:

Terrigenous rock fragments and mineral grains 2
Carbonate megafaunal shell fragments _____
Foraminifera 3
Volcanic ash 41
Siliceous spicules and shells 54

Fine fraction (<0.062 mm)

Weight percent silt (0.062 mm - 0.0039 mm) in total sample 61
Weight percent clay (<0.0039 mm) in total sample 38

Composition:

Clay minerals 40
Volcanic ash 55
Terrigenous mineral grains 3
Siliceous shells and spicules 2
Carbonate shells _____

SAMPLE NUMBER 350

Coarse fraction (>2 mm)

Weight percent of total sample _____

Composition:

Terrigenous rock fragments _____
Carbonate shells _____

_____ granules _____ pebbles
_____ cobbles _____ boulders

Sand fraction (2 mm - 0.062 mm)

Weight percent of total sample 13

Composition:

Terrigenous rock fragments and mineral grains 30
Carbonate megafaunal shell fragments _____
Foraminifera 3
Volcanic ash 47
Siliceous spicules and shells 20

Fine fraction (<0.062 mm)

Weight percent silt (0.062 mm - 0.0039 mm) in total sample 53
Weight percent clay (<0.0039 mm) in total sample 34

Composition:

Clay minerals 40
Volcanic ash 40
Terrigenous mineral grains 8
Siliceous shells and spicules 12
Carbonate shells _____

SAMPLE NUMBER 351

Coarse fraction (>2 mm)

Weight percent of total sample 22

Composition:

Terrigenous rock fragments 100
Carbonate shells _____

___ granules X pebbles
___ cobbles ___ boulders

Sand fraction (2 mm - 0.062 mm)

Weight percent of total sample 32

Composition:

Terrigenous rock fragments and mineral grains 80
Carbonate megafaunal shell fragments _____
Foraminifera Tr
Volcanic ash 20
Siliceous spicules and shells Tr

Fine fraction (<0.062 mm)

Weight percent silt (0.062 mm - 0.0039 mm) in total sample 29

Weight percent clay (<0.0039 mm) in total sample 17

Composition:

Clay minerals 32
Volcanic ash 45
Terrigenous mineral grains 8
Siliceous shells and spicules 15
Carbonate shells _____

SAMPLE NUMBER 353

Coarse fraction (>2 mm)

Weight percent of total sample _____

Composition:

Terrigenous rock fragments _____
Carbonate shells _____

___ granules ___ pebbles
___ cobbles ___ boulders

Sand fraction (2 mm - 0.062 mm)

Weight percent of total sample 1

Composition:

Terrigenous rock fragments and mineral grains _____
Carbonate megafaunal shell fragments _____
Foraminifera 3
Volcanic ash 62
Siliceous spicules and shells 35

Fine fraction (<0.062 mm)

Weight percent silt (0.062 mm - 0.0039 mm) in total sample 61

Weight percent clay (<0.0039 mm) in total sample 38

Composition:

Clay minerals 43
Volcanic ash 45
Terrigenous mineral grains 5
Siliceous shells and spicules 7
Carbonate shells _____

SAMPLE NUMBER 354

Coarse fraction (>2 mm)

Weight percent of total sample _____

Composition:

Terrigenous rock fragments _____ granules _____ pebbles
Carbonate shells _____ cobbles _____ boulders

Sand fraction (2 mm - 0.062 mm)

Weight percent of total sample 1

Composition:

Terrigenous rock fragments and mineral grains _____
Carbonate megafaunal shell fragments Tr
Foraminifera Tr
Volcanic ash 55
Siliceous spicules and shells 45

Fine fraction (<0.062 mm)

Weight percent silt (0.062 mm - 0.0039 mm) in total sample 61

Weight percent clay (<0.0039 mm) in total sample 38

Composition:

Clay minerals 20
Volcanic ash 62
Terrigenous mineral grains 10
Siliceous shells and spicules 5
Carbonate shells 3

SAMPLE NUMBER 355

Coarse fraction (>2 mm)

Weight percent of total sample 10

Composition:

Terrigenous rock fragments 100 granules pebbles
Carbonate shells _____ cobbles boulders

Sand fraction (2 mm - 0.062 mm)

Weight percent of total sample 45

Composition:

Terrigenous rock fragments and mineral grains 99
Carbonate megafaunal shell fragments Tr
Foraminifera Tr
Volcanic ash Tr
Siliceous spicules and shells 1

Fine fraction (<0.062 mm)

Weight percent silt (0.062 mm - 0.0039 mm) in total sample 26

Weight percent clay (<0.0039 mm) in total sample 19

Composition:

Clay minerals 22
Volcanic ash 50
Terrigenous mineral grains 25
Siliceous shells and spicules Tr
Carbonate shells 3

SAMPLE NUMBER 356

Coarse fraction (>2 mm)

Weight percent of total sample 43

Composition:

Terrigenous rock fragments 100
Carbonate shells _____

granules pebbles
_____ cobbles _____ boulders

Sand fraction (2 mm - 0.062 mm)

Weight percent of total sample 49

Composition:

Terrigenous rock fragments and mineral grains 100
Carbonate megafaunal shell fragments TV
Foraminifera TV
Volcanic ash TV
Siliceous spicules and shells TV

Fine fraction (<0.062 mm)

Weight percent silt (0.062 mm - 0.0039 mm) in total sample 5
Weight percent clay (<0.0039 mm) in total sample 3

Composition:

Clay minerals 45
Volcanic ash 35
Terrigenous mineral grains 20
Siliceous shells and spicules TV
Carbonate shells _____

SAMPLE NUMBER 357

Coarse fraction (>2 mm)

Weight percent of total sample _____

Composition:

Terrigenous rock fragments _____
Carbonate shells _____

_____ granules _____ pebbles
_____ cobbles _____ boulders

Sand fraction (2 mm - 0.062 mm)

Weight percent of total sample 56

Composition:

Terrigenous rock fragments and mineral grains 80
Carbonate megafaunal shell fragments TV
Foraminifera 1
Volcanic ash 18
Siliceous spicules and shells 1

Fine fraction (<0.062 mm)

Weight percent silt (0.062 mm - 0.0039 mm) in total sample 30
Weight percent clay (<0.0039 mm) in total sample 14

Composition:

Clay minerals 45
Volcanic ash 30
Terrigenous mineral grains 19
Siliceous shells and spicules 6
Carbonate shells _____

SAMPLE NUMBER 358

Coarse fraction (>2 mm)

Weight percent of total sample 2

Composition:

Terrigenous rock fragments 100
Carbonate shells _____

____ granules pebbles
____ cobbles _____ boulders

Sand fraction (2 mm - 0.062 mm)

Weight percent of total sample 69

Composition:

Terrigenous rock fragments and mineral grains 70
Carbonate megafaunal shell fragments _____
Foraminifera Tr
Volcanic ash 30
Siliceous spicules and shells Tr

Fine fraction (<0.062 mm)

Weight percent silt (0.062 mm - 0.0039 mm) in total sample 16
Weight percent clay (<0.0039 mm) in total sample 13

Composition:

Clay minerals 50
Volcanic ash 40
Terrigenous mineral grains 5
Siliceous shells and spicules 5
Carbonate shells _____

SAMPLE NUMBER 359

Coarse fraction (>2 mm)

Weight percent of total sample _____

Composition:

Terrigenous rock fragments _____
Carbonate shells _____

____ granules _____ pebbles
____ cobbles _____ boulders

Sand fraction (2 mm - 0.062 mm)

Weight percent of total sample 49

Composition:

Terrigenous rock fragments and mineral grains 68
Carbonate megafaunal shell fragments _____
Foraminifera Tr
Volcanic ash 32
Siliceous spicules and shells Tr

Fine fraction (<0.062 mm)

Weight percent silt (0.062 mm - 0.0039 mm) in total sample 32
Weight percent clay (<0.0039 mm) in total sample 19

Composition:

Clay minerals 40
Volcanic ash 45
Terrigenous mineral grains 6
Siliceous shells and spicules 9
Carbonate shells _____

SAMPLE NUMBER 437

Coarse fraction (>2 mm)

Weight percent of total sample 80

Composition:

Terrigenous rock fragments 97
Carbonate shells 3

granules pebbles
 cobbles boulders

Sand fraction (2 mm - 0.062 mm)

Weight percent of total sample 18

Composition:

Terrigenous rock fragments and mineral grains 67
Carbonate megafaunal shell fragments 20
Foraminifera 5
Volcanic ash 7
Siliceous spicules and shells 1

Fine fraction (<0.062 mm)

Weight percent silt (0.062 mm - 0.0039 mm) in total sample 1
Weight percent clay (<0.0039 mm) in total sample 1

Composition:

Clay minerals 25
Volcanic ash 40
Terrigenous mineral grains 35
Siliceous shells and spicules TR
Carbonate shells TR

SAMPLE NUMBER 443

Coarse fraction (>2 mm)

Weight percent of total sample 71

Composition:

Terrigenous rock fragments 100
Carbonate shells TR

granules pebbles
 cobbles boulders

Sand fraction (2 mm - 0.062 mm)

Weight percent of total sample 18

Composition:

Terrigenous rock fragments and mineral grains 75
Carbonate megafaunal shell fragments 5
Foraminifera 4
Volcanic ash 15
Siliceous spicules and shells 1

Fine fraction (<0.062 mm)

Weight percent silt (0.062 mm - 0.0039 mm) in total sample 7
Weight percent clay (<0.0039 mm) in total sample 4

Composition:

Clay minerals 25
Volcanic ash 29
Terrigenous mineral grains 39
Siliceous shells and spicules 4
Carbonate shells 3

SAMPLE NUMBER 444

Coarse fraction (>2 mm)

Weight percent of total sample 39

Composition:

Terrigenous rock fragments 97
Carbonate shells 3

granules pebbles
 cobbles boulders

Sand fraction (2 mm - 0.062 mm)

Weight percent of total sample 59

Composition:

Terrigenous rock fragments and mineral grains 99
Carbonate megafaunal shell fragments 1
Foraminifera _____
Volcanic ash _____
Siliceous spicules and shells _____

Fine fraction (<0.062 mm)

Weight percent silt (0.062 mm - 0.0039 mm) in total sample 1
Weight percent clay (<0.0039 mm) in total sample 1

Composition:

Clay minerals 48
Volcanic ash 45
Terrigenous mineral grains 7
Siliceous shells and spicules _____
Carbonate shells _____

SAMPLE NUMBER 446

Coarse fraction (>2 mm)

Weight percent of total sample 10

Composition:

Terrigenous rock fragments 100
Carbonate shells _____

granules pebbles
 cobbles boulders

Sand fraction (2 mm - 0.062 mm)

Weight percent of total sample 76

Composition:

Terrigenous rock fragments and mineral grains 99
Carbonate megafaunal shell fragments _____
Foraminifera _____
Volcanic ash 1
Siliceous spicules and shells TK

Fine fraction (<0.062 mm)

Weight percent silt (0.062 mm - 0.0039 mm) in total sample 10
Weight percent clay (<0.0039 mm) in total sample 4

Composition:

Clay minerals 40
Volcanic ash 45
Terrigenous mineral grains 5
Siliceous shells and spicules 10
Carbonate shells _____

SAMPLE NUMBER 447

Coarse fraction (>2 mm)

Weight percent of total sample 9

Composition:

Terrigenous rock fragments 71 granules pebbles
Carbonate shells 29 cobbles boulders

Sand fraction (2 mm - 0.062 mm)

Weight percent of total sample 75

Composition:

Terrigenous rock fragments and mineral grains 62
Carbonate megafaunal shell fragments 25
Foraminifera 10
Volcanic ash 3
Siliceous spicules and shells Tr

Fine fraction (<0.062 mm)

Weight percent silt (0.062 mm - 0.0039 mm) in total sample 10

Weight percent clay (<0.0039 mm) in total sample 6

Composition:

Clay minerals 25
Volcanic ash 41
Terrigenous mineral grains 20
Siliceous shells and spicules 12
Carbonate shells 2

SAMPLE NUMBER 448

Coarse fraction (>2 mm)

Weight percent of total sample _____

Composition:

Terrigenous rock fragments _____ granules pebbles
Carbonate shells _____ cobbles boulders

Sand fraction (2 mm - 0.062 mm)

Weight percent of total sample 99

Composition:

Terrigenous rock fragments and mineral grains 100
Carbonate megafaunal shell fragments _____
Foraminifera _____
Volcanic ash _____
Siliceous spicules and shells _____

Fine fraction (<0.062 mm)

Weight percent silt (0.062 mm - 0.0039 mm) in total sample Tr

Weight percent clay (<0.0039 mm) in total sample 1

Composition:

Clay minerals 40
Volcanic ash 45
Terrigenous mineral grains 15
Siliceous shells and spicules Tr
Carbonate shells _____

SAMPLE NUMBER 449

Coarse fraction (>2 mm)

Weight percent of total sample 63

Composition:

Terrigenous rock fragments 100
Carbonate shells Tr

granules pebbles
 cobbles boulders

Sand fraction (2 mm - 0.062 mm)

Weight percent of total sample 30

Composition:

Terrigenous rock fragments and mineral grains 95
Carbonate megafaunal shell fragments _____
Foraminifera 3
Volcanic ash 1
Siliceous spicules and shells 1

Fine fraction (<0.062 mm)

Weight percent silt (0.062 mm - 0.0039 mm) in total sample 4
Weight percent clay (<0.0039 mm) in total sample 3

Composition:

Clay minerals 50
Volcanic ash 15
Terrigenous mineral grains 25
Siliceous shells and spicules 10
Carbonate shells Tr

SAMPLE NUMBER 452

Coarse fraction (>2 mm)

Weight percent of total sample 1

Composition:

Terrigenous rock fragments 75
Carbonate shells 25

granules pebbles
 cobbles boulders

Sand fraction (2 mm - 0.062 mm)

Weight percent of total sample 99

Composition:

Terrigenous rock fragments and mineral grains 100
Carbonate megafaunal shell fragments _____
Foraminifera _____
Volcanic ash _____
Siliceous spicules and shells _____

Fine fraction (<0.062 mm)

Weight percent silt (0.062 mm - 0.0039 mm) in total sample _____
Weight percent clay (<0.0039 mm) in total sample _____

Composition:

Clay minerals _____
Volcanic ash _____
Terrigenous mineral grains _____
Siliceous shells and spicules _____
Carbonate shells _____

SAMPLE NUMBER 453

Coarse fraction (>2 mm)

Weight percent of total sample 91

Composition:

Terrigenous rock fragments 97 granules pebbles
Carbonate shells 3 cobbles boulders

Sand fraction (2 mm - 0.062 mm)

Weight percent of total sample 9

Composition:

Terrigenous rock fragments and mineral grains 93
Carbonate megafaunal shell fragments 7
Foraminifera Tr
Volcanic ash Tr
Siliceous spicules and shells _____

Fine fraction (<0.062 mm)

Weight percent silt (0.062 mm - 0.0039 mm) in total sample Tr

Weight percent clay (<0.0039 mm) in total sample Tr

Composition:

Clay minerals 22
Volcanic ash 20
Terrigenous mineral grains 58
Siliceous shells and spicules Tr
Carbonate shells Tr

SAMPLE NUMBER 454

Coarse fraction (>2 mm)

Weight percent of total sample _____

Composition:

Terrigenous rock fragments _____ granules pebbles
Carbonate shells _____ cobbles boulders

Sand fraction (2 mm - 0.062 mm)

Weight percent of total sample 97

Composition:

Terrigenous rock fragments and mineral grains 99
Carbonate megafaunal shell fragments _____
Foraminifera _____
Volcanic ash 1
Siliceous spicules and shells _____

Fine fraction (<0.062 mm)

Weight percent silt (0.062 mm - 0.0039 mm) in total sample 1

Weight percent clay (<0.0039 mm) in total sample 2

Composition:

Clay minerals 26
Volcanic ash 49
Terrigenous mineral grains 20
Siliceous shells and spicules 3
Carbonate shells 2

ATTACHMENT B

Depositional Environments and Quaternary Sedimentary Units within
Lower Cook Inlet, Alaska -
A High-energy Tidally Dominated Embayment along the Pacific Margin
of the United States

by

M. L. Rapoport
U.S. Geological Survey
Menlo Park, California 94025

IN

Quaternary Depositional Environments of the Pacific Coast
edited by

M.E. Field, I.P. Colburn, and A.H. Bouma
The Pacific Section

Society of Economic Paleontologists and Mineralogist, Los Angeles, California

April 1980

Figures 3 through 7 have been omitted
from this report since they were not
of sufficient quality to reproduce.

DEPOSITIONAL ENVIRONMENTS AND QUATERNARY SEDIMENTARY UNITS
WITHIN LOWER COOK INLET, ALASKA -A HIGH-ENERGY TIDALLY DOMINATED EMBAYMENT ALONG THE
PACIFIC MARGIN OF THE UNITED STATES

by

M. L. Rapoport
U.S. Geological Survey
Menlo Park, California 94025

Abstract

Sedimentological studies conducted since 1976 within lower Cook Inlet, Alaska, a large tidally dominated embayment, have delineated six major depositional environments. The environments are: high-energy shoreface, trough-edge platform, trough slope, trough floor, trough-mouth plateau, and seaward progradational ramp. Common to these environments are sandy sediments concentrated in sand patches, sand ribbons and sand-wave fields as well as coarser sediments found as mixed cobble-sand 'hard bottom' and sand-shell-gravel complexes. The distribution of the modern surficial sediments is controlled primarily by the strength of the tidal current regime.

Sea level rise since the last major glacial advance has led to the modern high-energy tidal environment of lower Cook Inlet. Sand and gravel are being deposited while older glacial sediments are being winnowed. High-resolution seismic-reflection evidence indicates that Holocene sediments are deposited upon a strongly glaciated topography. Numerous buried or partly buried channels are present on the platform areas.

Four primary sedimentologic units are recognized in the shallow stratigraphy on the basis of high-resolution geophysical data. Unit D represents unsorted glacial sediments that overlie the glaciated basement and locally exceeds 75 meters in thickness. On high-resolution seismic records, Unit D is characterized by irregular discontinuous reflectors. Overlying Unit D is a thin unit, Unit C, which has a high acoustic reflectivity and is thought to be a layer of glacial outwash sediments. Unit B locally overlies Unit C and is composed of large-scale sand-wave complexes. Unit B appears to be limited to trough floor, trough-mouth plateau and seaward progradational ramp environments. The uppermost unit, Unit A, overlies Unit B or Unit C. It is acoustically identified by its pattern of flat-lying multiple reflectors and is considered to consist of intercalated layers of sand and silt. Unit A is present only where hydrodynamic energies are low.

INTRODUCTION

The microtopography of the seafloor of lower Cook Inlet, Alaska (Fig. 1) consists of small-, medium- and large-scale marine bedforms which overlie a glacially constructed depositional surface (Bouma and Hampton, 1976; Bouma and others, 1977a, 1977b, 1978, 1979; Rapoport and others, 1979). The extent to which the modern hydrodynamic regime within the inlet has constructed, maintained or is transporting these bedforms has been a matter of disagreement. Recent

bottom boundary layer measurements and bottom photography (Cacchione and Drake, 1979) have indicated that the smallest scale bedforms such as current ripples are probably actively migrating. Current ripples were observed during a period of low-energy fair-weather conditions to consistently reverse their asymmetry with the tide. However, recent studies by Whitney and others (1979) suggest that within navigational accuracy limits, the largest and medium-size bedforms have not appreciably changed position or morphology over the past seven years. To help resolve this problem, the role of the modern hydrodynamic regime within a region of very large bedforms and the role played by the glacial and post-glacial macrotopography in controlling the position and nature of these bedforms is being evaluated (Rapoport, unpub. data). This paper examines two interrelated geologic problems--the modern sedimentological characteristics and depositional environments within lower Cook Inlet and the characteristics of the glacial and neoglacial shallow stratigraphy.

Subsurface sedimentologic units were defined by their acoustic characteristics on high-resolution seismic records. Since 1976, uniboom high-resolution seismic data (800-joule hull mounted system), 3.5 kHz and 12 kHz high-resolution profiler data, mini-sparker, and sidescan sonar data has been collected along more than 5,000 km of tracklines in lower Cook Inlet. Surficial sediments were sampled with Van Veen and Soutar-Van Veen samplers, and some gravity cores and vibracores were also collected. Core samples were split, photographed, subsampled and described on board the R/V Sea Sounder. Over 20 hours of underwater television tapes and 70-mm bottom photographs were examined to aid in interpretation of sidescan records, the characteristics of the surface sediments, and sedimentologic lithofacies. Hydrodynamic information on flow conditions within the bottom boundary layer gained through several deployments of an instrumented tripod system (GEOPROBE) was presented by Cacchione and others (1979). Additional data were gained through shipboard current meter observations in 1978 (Rapoport, unpub. data). Other hydrodynamic information has been provided by industry sources (Dames and Moore, 1978) as well as recent mean flow observations within the inlet by the National Oceanic and Atmosphere Administration (NOAA), using Aanderaa current meters deployed on taut wire moorings (Muench and others, 1978; R. D. Muench, unpub. data).

Bathymetry

The bathymetry of lower Cook Inlet is dominated by a major glacial trough (Cook Trough) and several other large-scale depressions (Chisik Valley, Kachemak Trough). Most of the inlet, except for some minor

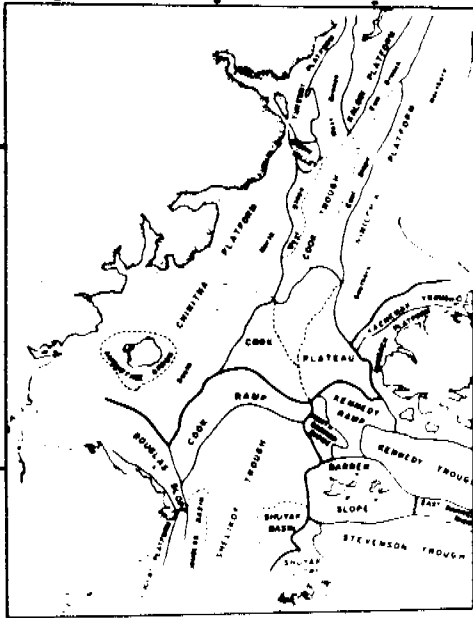


Figure 1. (a) Physiographic nomenclature proposed by A. H. Bouma.

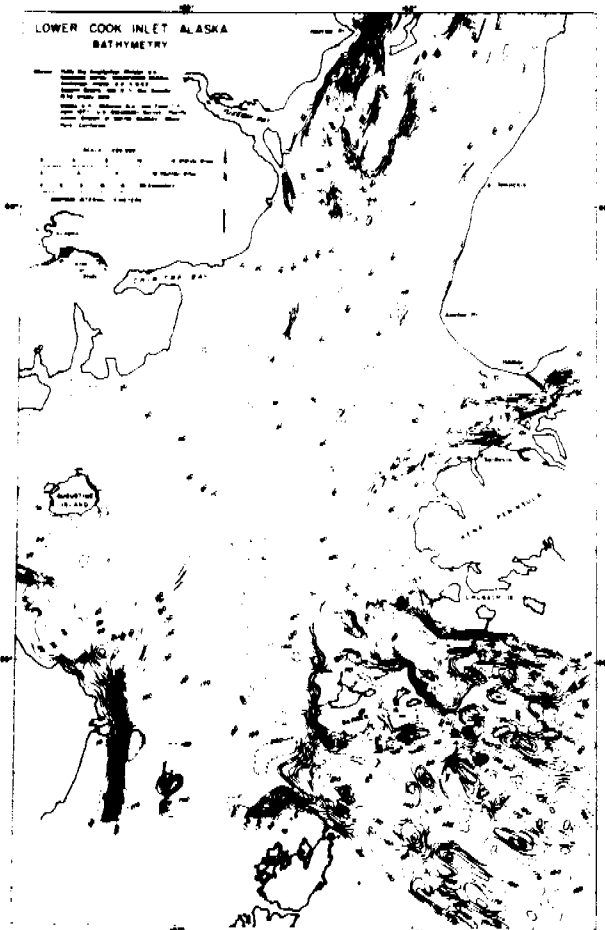


Figure 1. (b) Bathymetric map of lower Cook Inlet (contour interval 5 m).

depressions, channels and seafloor irregularities, shows a smooth southward slope toward Cook Ramp (Fig. 1). At the ramp there is a sharp increase in gradient where maximum depths rapidly increase from 70-80 m to over 200 m within the deep depressions in Kennedy and Stevenson troughs. A noteworthy feature of the ramp physiography is a major indentation in the ramp wall. This indentation is thought to be connected with Cook Trough (Bouma and others, 1978). Depths in lower Cook Inlet range from tidal flats down to 70-80 m at the ramp edge; the average depth is approximately 50 m. Except for the trough slopes and ramp slope, gradients are generally less than 2°.

The wide distribution of bedforms ranging up to 10 m in height and over 800 m in wavelength produces a complex meso- and microtopography. Low-amplitude sand waves and current ripples in the form of isolated sand patches, sand ribbons or isolated crests are found. Parts of the inlet have a smooth gravelly or sandy surface with isolated boulders resting upon the surface.

On the southwest edge of the Ninilchik platform, there is a north-trending reentrant into the platform wall that tapers out at about the 50-m isobath (A. H. Bouma, unpub. data). This reentrant is thought to be a glaciofluvial erosional feature postdating the formation of Kachemak Trough during a period of lower sea level. On the west side of the inlet the platform region is extremely flat; however, high-resolution seismic evidence indicates many buried channels and canyons. It may be that the two platform areas underwent a common period of erosion, but that the currently higher sedimentation rates (Hein and others, 1979) on the western side have subsequently smoothed out the erosional irregularities on that platform region.

Modern Current Regime

The mean circulation within lower Cook Inlet is controlled by sea surface slope currents generated by the west-flowing Alaskan current (Muench and others, 1978). Superimposed upon this mean circulation are strong tidal currents with near-surface velocities ranging from 0.5 m/s to 3.5 m/s. Swift currents are generated by large storms in late summer and early fall and again in February and March. Chinook winds blowing in excess of 100 knots (50 m/s) have been reported by marine operators in the inlet (Evans and others, 1972) and storms with 50-75-knot winds (25-38 m/s) occur nearly every winter (Carsola, 1975). Muench and others (1978) showed that one storm event generated residual near-surface currents flowing at 50 cm/s over a three-day period in the southwestern part of the inlet.

In general, flood tidal waters enter the inlet from the eastern edge of the Gulf of Alaska. A portion of this volume moves directly westward as a contour current along the ramp while other flood waters move northward along the Kenai Peninsula. At Kachemak Bay, some water moves into Kachemak Bay itself but most moves further northward toward Kalgin Island. At Kalgin Island the circulation becomes more confused as the flood water interacts with ebb water from upper Cook Inlet. The ebbing water diluted with fresh water and sediment from rivers that flow into upper Cook Inlet move southward along the western margin where they eventually join with the water flowing westward along the ramp. The combined flow then exits at Shelikof Strait. Local flow, crossflows and large semi-permanent gyres complicate this general picture.

QUATERNARY DEPOSITIONAL ENVIRONMENTS, LOWER COOK INLET, ALASKA

The mean diurnal tidal range is 4.2 m at the mouth of the inlet and more than 9 m at Anchorage. There is a mean tidal variation from east to west of approximately 0.8 m, with the eastern side being higher (Alaska OCS Office, 1976). According to Muench and others (1978) the eastern parts of the inlet absorb most of the tidal energies as the tidal currents propagate along isobaths. On the other hand, the western parts show higher mean current speeds. The nontidal currents are dominated by events in the 3- to 4-day range (Muench and others, 1978).

Sediments

Detailed grain-size analyses conducted on a representative suite of samples (Bouma and others, 1978) and supplemented with visual estimates suggest that sand and gravel are the dominant sediments of lower Cook Inlet. In the northern part of lower Cook Inlet the sediments range from gravel to sandy gravel. Southward the sediments grade into medium sand in the central parts and then to muddy sand south of the ramp. Sandy gravel is common along the margin of the inlet. The grain-size trend within the inlet suggests that current speeds decrease as width and depth increase. Sands are moderately to well sorted, with a Folk and Ward (1957) mean of 1.4 ϕ in the north and 2.4 ϕ in the area at the top of the ramp. Throughout the inlet gravel, cobbles or small boulders lie upon the sandy seafloor. These were probably ice-rafted. On parts of the seafloor, especially on the platform regions, sand is present primarily as small sand waves migrating over a lag surface consisting of gravel and shell hash.

Detailed sidescan sonar surveys, bottom television and bottom photography studies show that Cook Inlet has a wide and varied distribution of marine bedforms. A nearly complete morphological hierarchy is present (Fig. 2) including sand waves of all sizes and small to medium dunes, and sand patches, sand ribbons, and sand bands. Regions of interspersed sand ribbons and hard bottom are common as well as large areas of hard bottom with isolated boulders and cobbles. Underwater television and photographs show that smooth-appearing, acoustically very reflective seafloor actually is carpeted by small low-amplitude current ripples.

DEPOSITIONAL ENVIRONMENTS

Six depositional environments have been defined for lower Cook Inlet on the basis of areal extent, hydrodynamic energies, and sedimentological and bedform characteristics. These environments are: (1) high-energy shoreface, (2) trough-edge platform, (3) trough slope, (4) trough floor, (5) trough-mouth plateau, and (6) seaward progradational ramp. These names follow closely an as-yet unpublished physiographic nomenclature proposed by A. H. Bouma (Fig. 1).

High-energy shoreface

Coarse sediment, principally gravel and cobbles, characterizes the high-energy shoreface environment. This environment extends from the back-beach through the surf zone and is routinely affected by high wave energies. Long-period, high-energy waves propagate into the inlet through Shelikof Strait, Kennedy and Stevenson entrances or as 4- to 6-second waves generated during local storms (Carsola, 1975).

Hayes and others (1977) showed that approximately 41 percent of the coast of lower Cook Inlet is

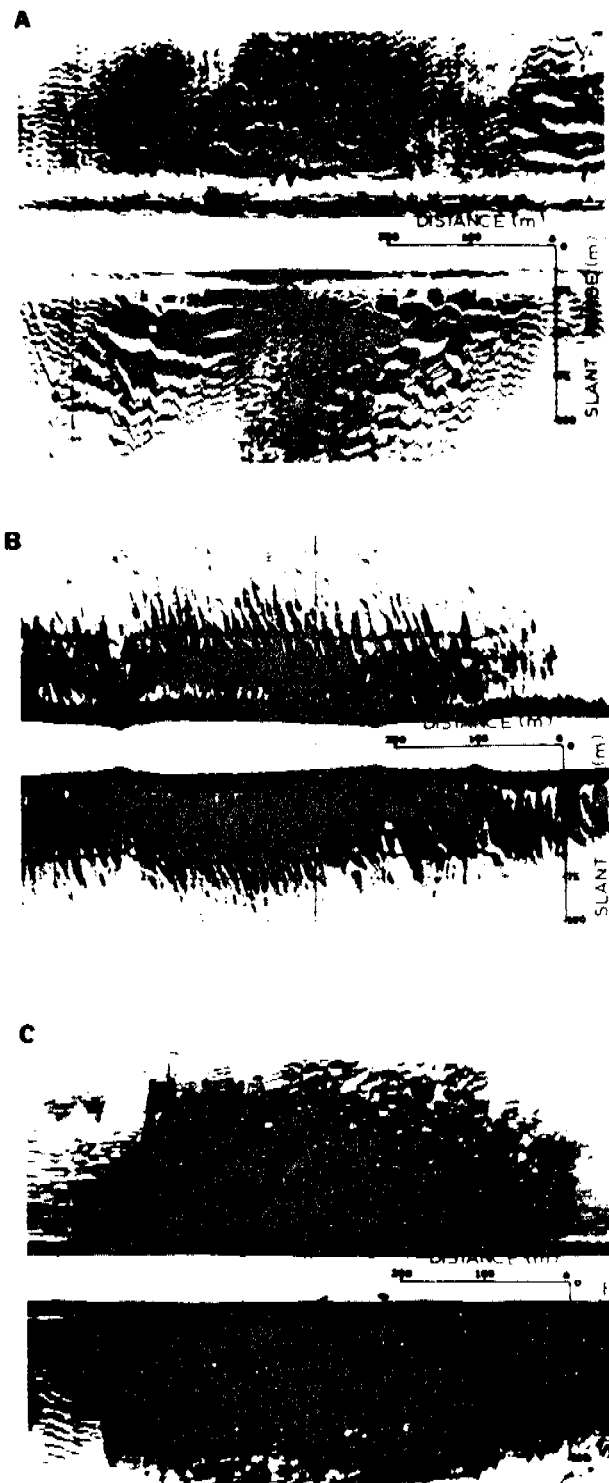


Figure 2. Representative sonographs from lower Cook Inlet. (a) Sand bands with small dunes within a field of continuous medium to small sand waves. (b) Large sand waves with medium sand waves superimposed. (c) Patchy sands and barchan-shaped sand patch grading into weakly developed sand ribbon.

dominated by rugged topography characterized by complex drowned mountain valleys and sheer erosional cliffs fronting the water's edge. The highest scarps front the southeastern side of Kenai Peninsula and the northern part of Kamishak Bay, where gravelly beaches and wave-cut bedrock platforms are found. The intertidal zone is usually small, consisting of a rock bench and a narrow mixed sand and gravel berm with a representative mean grain size of 1.8 mm (Hayes and others, 1977).

Other erosional scarp-bounded shorefaces are found all along the Kenai Lowlands and in small scattered areas along the western side of the inlet. Characteristic of this type of shoreface is a low vertical scarp composed of flat-lying sedimentary rocks abutting a relatively narrow series of multiple berms composed of mixed sand and gravel. A broad wave-cut rock platform usually occupies the middle and lower intertidal regions.

Locally, wave-cut platforms extend seaward some 400 to 500 m. Just seaward of the wave-cut rock benches, the seafloor slopes gradually and uniformly toward the trough-edge platforms. On the western shore edge, the high-energy shoreface environment is complicated by the presence of large bays in which low-energy, tidal-flat conditions exist (parts of Kamishak Bay and Tuxedni Bay), but in general the zone is one of high wave energies and swift offshore tidal currents. Most of the cobbly and gravelly surface or hard bottom that covers the seafloor of this zone has resulted from the winnowing of Holocene morainal sediments or by erosion of Tertiary and Pleistocene conglomeratic sandstone exposed along cliffs.

Few bedforms are observed within this zone except for the beach features themselves, but just offshore there are isolated sand and gravel patches containing small current ripples and poorly developed sand ribbons. In restricted waters such as behind Homer Spit and within Kamishak and Tuxedni Bays, intertidal and subtidal bedforms such as muddy sand waves, ripples and sand bars are found.

Trough-edge Platform

Seaward of the high-energy shoreface environment is the trough-edge platform. This broad, flat-lying region locally extends 10-15 km offshore. The region is characterized by a sedimentological suite of coarse gravel, pebbly sand, patchy clean sand, shell hash and some silt and clay.

The trough-edge platform has regional gradients of less than 1° . It is several kilometers wider on the western side than on the eastern shore; however, the eastern side is more heavily dissected by narrow channels and small canyons. Chisik Valley and an unnamed valley just south of Augustine Island are the only major channels that cut sharply through the western trough-edge platform.

Tidal currents are the dominant forces shaping and controlling the sediments within this environment; however, some wave effects can be expected during peak storms. The tidal currents are highly bidirectional. Water depths range from 5 m to 35 m over this zone. Near-bottom velocity estimates can be calculated using the method of Belderson and others (1978) in which near-surface tidal velocities are used to extrapolate near-bottom velocities. They suggest that tidal maximum near-bottom velocities are approximately 0.7 to 0.8 times the near-surface maximum current speed for a mean depth of 30 m, and

0.6 to 0.7 times the maximum near-surface speed for a depth of 100 m. Estimated bottom velocities based on the above ratios for the trough-edge platform, where near-surface velocities reach 100 cm/s to 200 cm/s, range from 77 cm/s to 155 cm/s. 1978 observations (D. A. Cacchione and others, unpub. data) of near-bottom current speeds at station 005 during neap tidal conditions and at sub-maximum tidal current speeds suggest that near-bottom velocities range from 20 to 40 percent of near-surface conditions. Station 005 was located on the eastern trough-edge platform. Observations at other sites within the inlet support that estimate; therefore the best estimate for near-bottom velocities for most of the tidal cycle is between 30 and 60 cm/s. These velocities are more than enough to move medium sand (Komar, 1976). Underwater television studies within the trough-edge platform show that the seafloor is often covered by low-amplitude current ripples of coarse sand (Fig. 3) and small sand waves (Fig. 4). Often the current ripples are found concentrated in sand ribbons and sand patches (Fig. 5).

Trough-slope

Sporadic thin sand ribbons and sand patches and the absence of most other bedform types characterize the trough-slope environment. The slopes of the trough are mantled with coarse gravel and cobble except for the lowermost levels, where increasing sand and fine sediment have accumulated. Winnowed glacial drift, as shown by large angular and subangular boulders protruding through the gravelly surface, is found in the upper parts of Cook Trough especially along the west side. Down the slope, the seafloor shows evidence of sand accumulation in the form of small ripples and isolated patches of sandy material. Occasionally there is sufficient sand to form sand ribbons. The sand ribbons run parallel to the isobaths and are concentrated at depths between 40 and 50 m. The eastern side of Cook Trough has a gentler slope and has some areas where sand waves are migrating down slope. These sand waves are generally small to medium in size and may also be migrating along the isobaths due to moderately strong axially directed tidal currents.

Current velocities were estimated from the drift speed of an instrument sled during a 1979 underwater television and 70-mm photography survey of the west slope of Cook Trough (A. H. Bouma, unpub. data). Surface currents during the survey reached 175 cm/s but averaged between 75 cm/s and 125 cm/s. Estimated bottom currents were in excess of 40 cm/s. Underwater television views of the large boulders and gravel carpet of the west trough slope show little vegetation or evidence of much sediment accumulation.

Trough Floor

Accumulations of sand in sufficient quantity to form large (>7 m high) sand waves are found along the axis of the major glacial trough of lower Cook Inlet. The large bedforms occur in patches and small depressions along the axis. Current speeds of sufficient strength to move sand-sized material has been documented by Rappeport and others (1979), Cacchione and Drake (1979) and Dames and Moore (1978). Bottom current measurements and visual evidence showed that near-bottom velocities in excess of 20 cm/s are quite common throughout the tidal cycle with a slight ebb flow dominance. Near-bottom currents are apparently affected by local topography and microtopography (Rappeport and others, 1979). Trough locations within a large sand wave field show a

sandy highly bioturbated surface with small irregular sand waves and ripples and high faunal activity as shown by the abundance of sand dollars, sea pens and concentrations of fine-grained organic materials. Crest and near-crest locations on these large sand waves show less biologic activity and are often covered with sharply formed sinuous to lunate ripples, small sand waves with steep lee slopes, and occasional ice-rafted large cobbles and rocks (Fig. 6). Currents near the crest are slightly swifter and are more strongly oriented up and down Cook Trough.

Other parts of the trough-floor environment show patchy sand and isolated sand ribbons. Elevated mesa-like platforms of till are present, over which are found small to medium sand waves. Sand bands are often formed in areas where there is a large sand accumulation.

Trough-mouth Plateau

The trough-mouth plateau is a relatively broad region of flat seafloor extending southward from Cook Trough. It is approximately triangular in plan view and has the gentlest slopes found anywhere in the inlet. A thick accumulation of sand covers this region. Average grain size is 2-2.5 ϕ , and nearly all of the region is covered by large sand waves or dense fields of medium-sized bedforms. Many sand bands have their principal axis parallel to contours. Faunal activity is intense; animal trails and small dimpled pockmarks are generally visible in bottom photographs (Fig. 7). Sea pens and sand dollars are common, but there is little shell hash.

The trough-mouth large sand waves are more regular in form and wavelength than large sand waves along the trough floor. Sand thickness measured from high-resolution seismic data exceeds 25 m. There is evidence of large shallow subsurface topographic irregularities.

Near-surface and near-bottom current velocities are weaker than those found elsewhere in the inlet. Because the average depth of the plateau region is between 60 and 70 m, there is little wave-motion interaction with the seafloor. Most of the small current ripples and sand waves covering the larger forms are poorly developed and appear degraded. They are primarily tidally controlled. Faunal activity may be one process of degradation, or the sand waves may develop during spring tides and be degraded during neap tides.

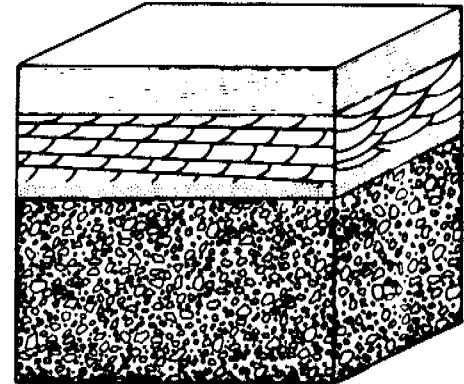
Seaward Progradational Ramp

This environment occurs where the seafloor of lower Cook Inlet slopes down from the trough-mouth plateau at water depths of 70-80 m to depths of 150-170 m (Fig. 1). This region encompasses some 150 km² of seafloor in the south-central prominent seaward bulge extending from the trough-mouth plateau. Surficial sediments are fine sand and muddy sand, which mantle the entire zone. The total thickness of this substrate is not completely known, but high-resolution seismic data suggest that it exceeds 40 m. Large sand waves are common as well as some areas of sand ridges (R. Orlando, pers. commun., 1980). Small-scale sand waves and current ripples are ubiquitous. These bedforms appear to be more poorly developed at the base of the ramp in contrast to those nearer the top. Intense faunal activity causes considerable bioturbation of the sediment. Principal fauna are sea pens and sand dollars (Fig. 7d).

Near-bottom current velocities are unknown, but the general mean currents follow along the ramp as contour currents (Muench and others, 1978). Further hydrodynamic studies are needed to delineate the roles played by the mean and tidal currents in this region.

SEDIMENTARY UNITS

Four major stratigraphic units have been identified from high-resolution uniboom data (Fig. 8).







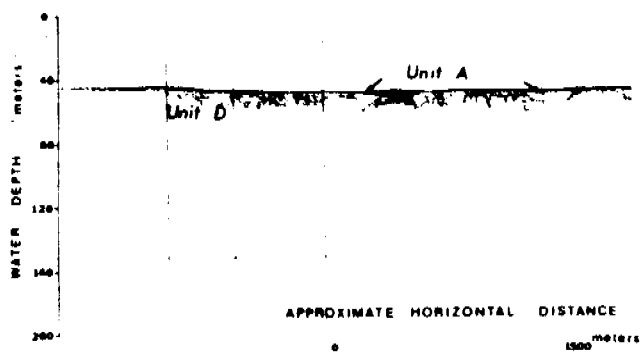
- Unit**
-  **A** Well-Laminated Sands And Silts
-  **B** Large-Scale Sand Wave Complex
-  **C** Gravel Outwash Lag
-  **D** Ground Moraine

Figure 8. Schematic of interpreted sedimentary stratigraphic units for shallow stratigraphy of lower Cook Inlet. Unit thickness not drawn to scale.

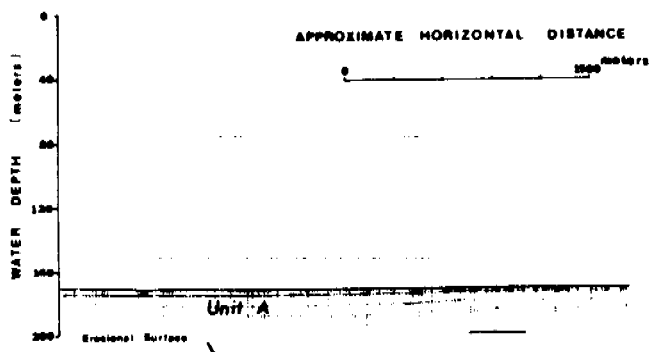
Unit A

Unit A is the uppermost unit that can be delineated in the shallow subsurface stratigraphy. Unit A ranges in thickness from 1-2 m to over 75 m within deep channels and troughs. On high-resolution uniboom records this unit is characterized by well-defined continuous horizontal reflectors. The lowest reflectors conform to the underlying surface as draped cover and as infilling of small channels and basins (Figs. 9a, 9b, 9c). The unit is considered to represent glaciomarine laminated watery sand and silty sand rapidly deposited as suspension load at the front of a wet-base retreating glacier (Anderson, 1972) or glacioluvial or glaciolacustrine sediments deposited during a time of lowered sea level when much of the inlet was subtidal or intertidal. Locally there are areas where fine-grained sediments may have been selectively winnowed from both the underlying glacial morainal material and from Unit A deposits such that a surface composed of coarse sand and gravel remains. Such a surface gives a characteristic acoustic signature showing considerable "ringing" (Fig. 9d).

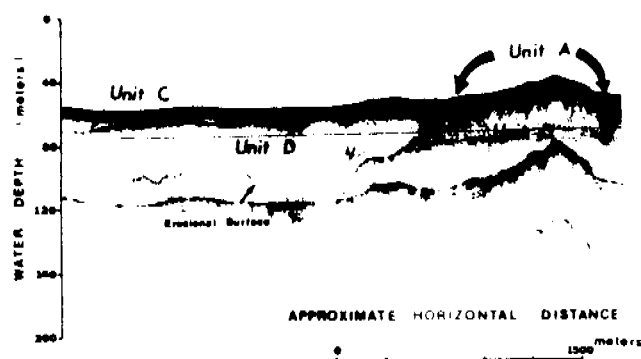
QUATERNARY DEPOSITIONAL ENVIRONMENTS, LOWER COOK INLET, ALASKA



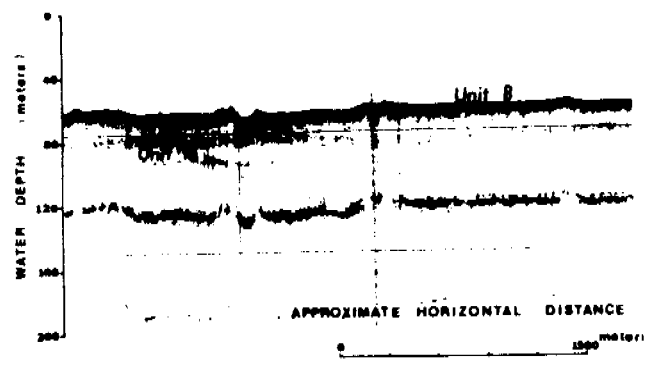
A



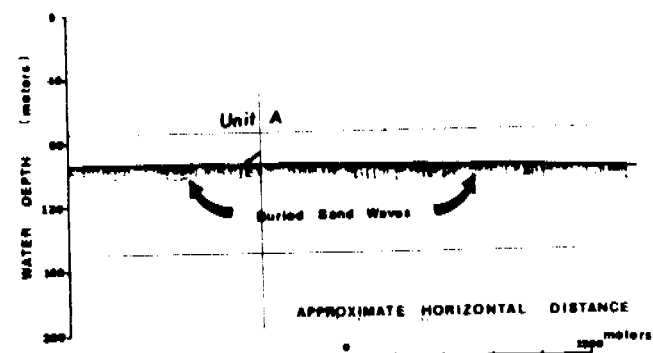
B



C



D



E

Figure 9. (a,b,c,d,e) Seismic-reflection records (uniboom) showing character of Unit A reflectors.

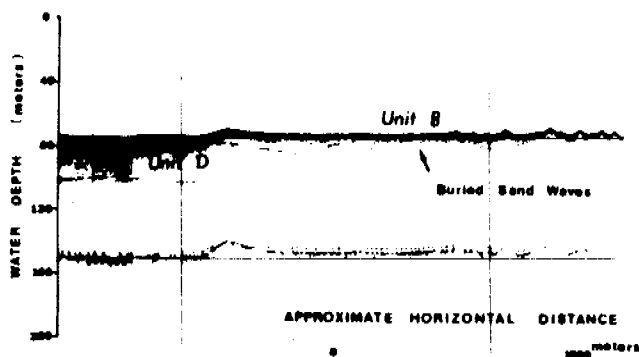
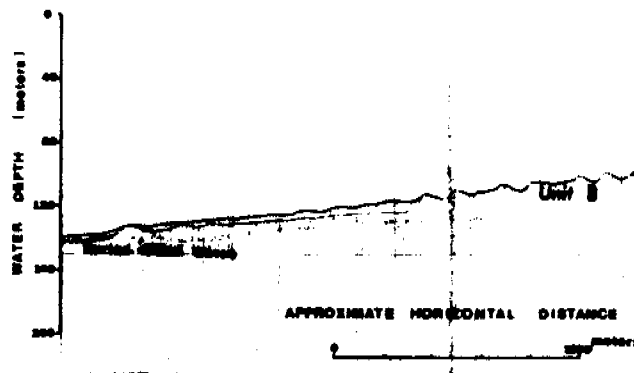
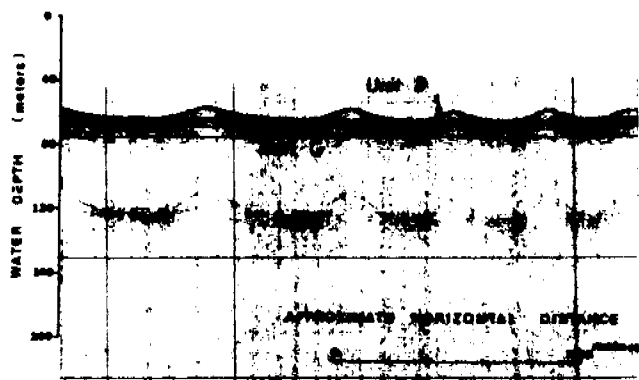


Figure 10. (a,b,c) Seismic-reflection records showing character of Unit B reflectors.

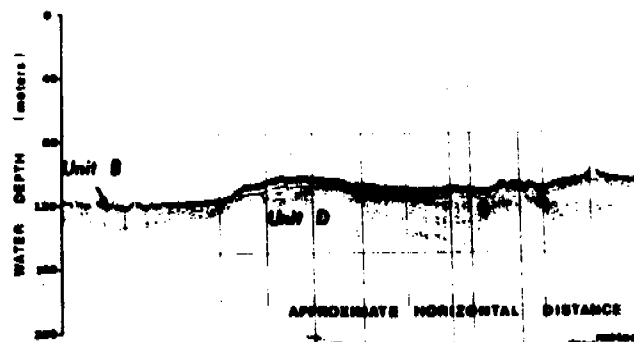
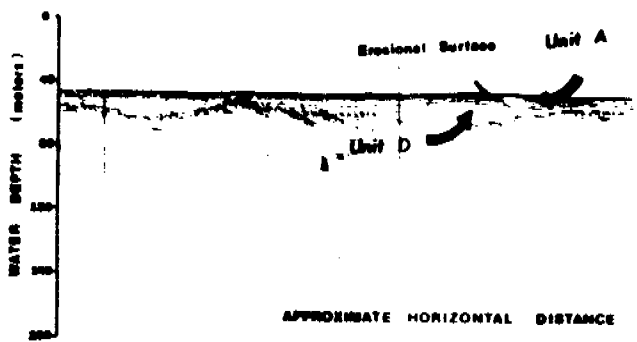


Figure 11. (a,b) Seismic-reflection records showing character of Unit C reflectors.

QUATERNARY DEPOSITIONAL ENVIRONMENTS, LOWER COOK INLET, ALASKA

Delta-like deposits showing large-scale foresets are visible at heads of small canyons incised into the northern slope of Kachemak Trough. These deposits appear to merge smoothly into the ringing-type deposits and are likely contemporaneous. In the southern part of Chinitna platform and along the western upper reaches of Cook Ramp are found the thickest accumulations of Unit A. Near the base of Cook Ramp the unit is over 44 m thick (Fig. 9b). Within the southwestern part of the inlet are found areas where 3-10 m of Unit A sediment overlies an undulating surface thought to represent the surface of buried large sand waves (Fig. 9e). Where Unit A sediments are very thick there are often small zones where reflectors generate such strong acoustic returns as to obscure lower reflectors.

Unit B

The next lowest unit is composed of large-scale sand-wave complexes. It generally occupies low swales and minor topographic depressions and ranges in thickness from 1-2 m to over 20 m.

This unit is readily observed on 3.5 kHz and uniboom seismic records as mappable bedform fields. On the southwestern side of the inlet, where tidal current strengths are generally weaker and where there is a much larger supply of fine sediment being carried southward out of upper Cook Inlet, these complexes are presently found as buried subsurface features (Fig. 9e). Where swift currents prevent deposition of fines, these complexes form part of the modern seafloor (Fig. 10a, 10b). Because buried sand wave fields are commonly found associated with surficial concentrations of large-scale sand waves (Figs. 10b, 10c), both exposed and buried sand wave complexes may have evolved under similar conditions. The presence of unit A overlying the sand-wave complexes in parts of the inlet suggests that post-glacial circulation within lower Cook Inlet was significantly different than the modern circulation pattern.

Unit B, where buried under Unit A sediments is recognized by its characteristic wavy reflector (Fig. 9e). This reflector is in turn sometimes seen to overlie a much flatter, deeper reflector thought to represent a depositional contact. The large-scale sand-wave complexes are composed of well-sorted medium to fine sand with little shell hash. The similarity of morphologic form of the modern exposed sand-wave complexes with the morphologic form of the buried complexes suggests that secondary smaller sand waves found on exposed large sand waves are probably also present in the subsurface buried sand waves. These small forms are not visible in seismic records due to their low heights and short wavelengths.

Unit C

Unit C is a thin but highly reflective unit composed of glacial outwash materials, deposited during lowered sea level, or glaciomarine and proglacial glaciofluvial sediments deposited at the front of retreating wet-base glaciers. These sediments are mostly coarse, as the fines were transported away by local currents or as suspended load in glacial outwash streams.

The sediments are poorly sorted coarse gravel and cobbles with some coarse sand. Many larger fragments were added to the sediments as ice-rafted materials. Acoustically this unit is recognized by its strong reflector, which overlies a glacially sculptured surface. It is very thin, ranging from 1 to 3 m in

thickness (Fig. 11a, 11b) and acoustically demonstrates no internal structure.

Unit D

Unit D is the lowest recognizable sedimentary unit. This basal unit is considered to be glacial drift sediments that have undergone partial erosion followed by renewed ground moraine deposition. It is best exposed in the northwest part of the inlet especially along the west wall of Cook Trough, Chisik sea valley and along parts of the Chinitna Platform. Where basement appears in the seismic records, this unit unconformably overlies it and the basement appears to be glacially scoured. The basement rocks are assumed to be late Tertiary or Pleistocene nonmarine conglomeratic sandstone and siltstone (Fisher and Magoon, 1978). Where the full thickness can be measured on seismic records, the total thickness of this unit is between 40 and 60 m. On the Ninilchik Platform region, on Cook Plateau and Cook Ramp the contact of this unit with basement was not observed. Acoustically this unit is characterized by the absence of well-layered horizontal reflectors.

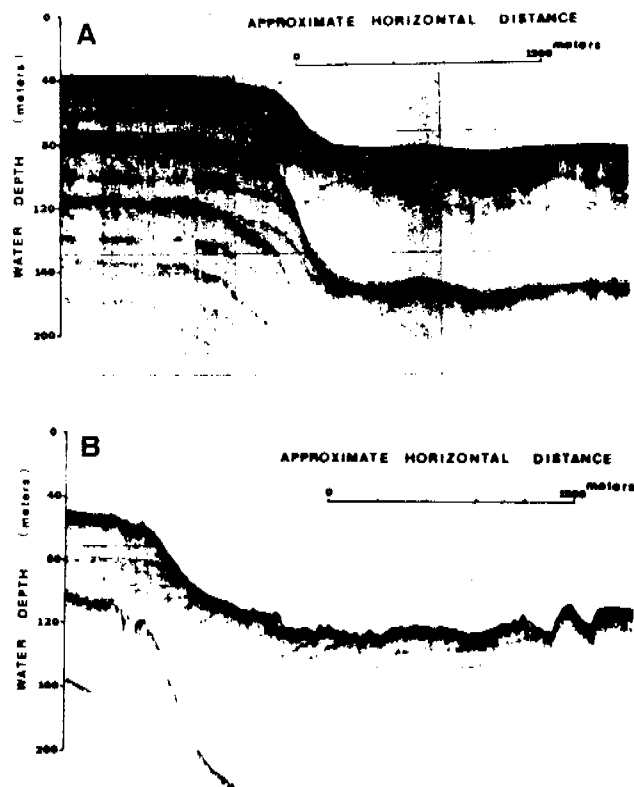


Figure 12. (a,b) Seismic-reflection records showing character of Unit D reflectors.

Most of this unit shows point reflector hyperbolae and a generally vague acoustic image. On the west wall of Cook Trough deposition of this unit appears to be interrupted by a period of Unit C deposition (Fig. 12a, 12b). The upper surface of this Unit D is sometimes marked by a highly irregular, blocky to wavy morphology. The layered association of Unit D and Unit C is suggestive of incomplete erosion of ground moraine sediments after glacial retreat, followed by

glacial outwash deposition, followed by renewed valley glacier advance onto the shelf and subsequent deposition of new ground moraine. Within the Cook Inlet structural trough there is evidence of over two major glacial advances over the last 20,000 years (Karlstrom, 1964). From shallow seismic data, it appears that the glaciofluvial erosion of the modern Cook Inlet Trough postdates deposition of this unit (Fig. 12b). Where glacially scoured bedrock is observed beneath Unit D, the total thickness of Units C and D stack approaches 75 m. Most of the platform areas of lower Cook Inlet may be composed of multiple layers of Unit D and Unit C representing the effects of repeated advances and retreats of glacier lobes extending out into the Cook structural trough. Similar acoustic facies have been identified as glacial ground moraine deposits (King, 1969, Jansen, 1976).

Buried Channels

A large part of lower Cook Inlet deposits shows partially or completely filled shallow channels and troughs. Multiple episodes of channelization, as shown by cut-and-fill structures, are observed in uniboom records taken over the platform areas of the inlet (Fig. 9a, 9b). In at least one area (at the head of a small canyon in the north wall of Kachemak Trough) there is evidence of local infilling from the platform surface into the canyon followed by a period of renewed canyon scour with subsequent infilling (Fig. 13). The process of channel infilling simulates delta formation, and large foresets are developed.

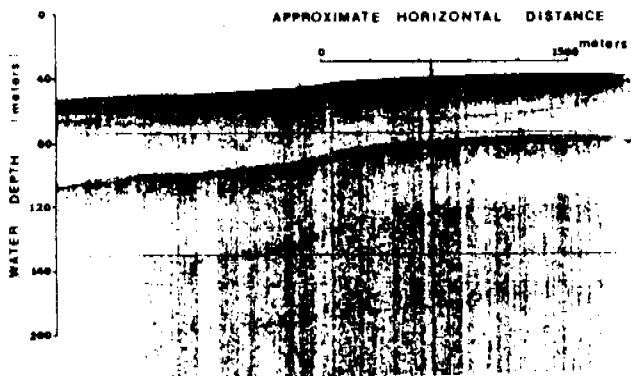


Figure 13. Seismic-reflection record of traverse of upper head of nearly filled small canyon on eastern platform. Well-developed foresets and truncated reflectors suggest erosion and renewed fill or change in sediment input direction.

The delta-like deposits may reach 400-500 m in length and some 30 m in thickness (Fig. 14a, 14b). McCabe (1977) in his studies on deep distributary channels and giant bedforms in deltaic sediments of the central Pennines, northern England, described giant crossbeds in deep channels (40 m) produced by side-attached alternate bar formation. These features are associated with a large distributary entering a fluvially dominated low-wave energy environment. A similar process of formation could account for the observed large-scale deltaic deposits.

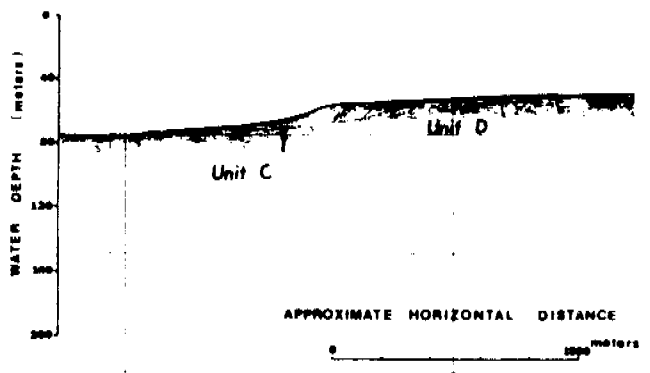
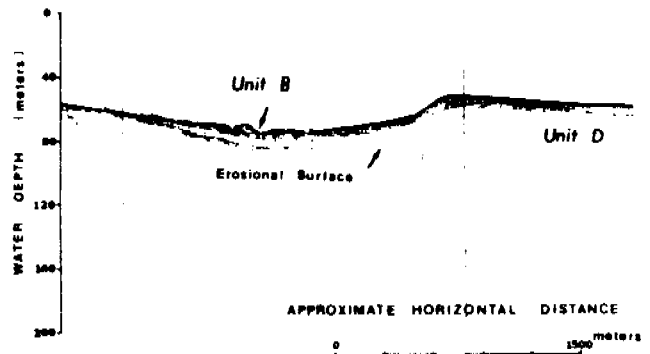


Figure 14. (a,b) Seismic-reflection records over the same canyon as in Figure 13 but lower down canyon and distinctly showing apparent deltaic-type deposition.

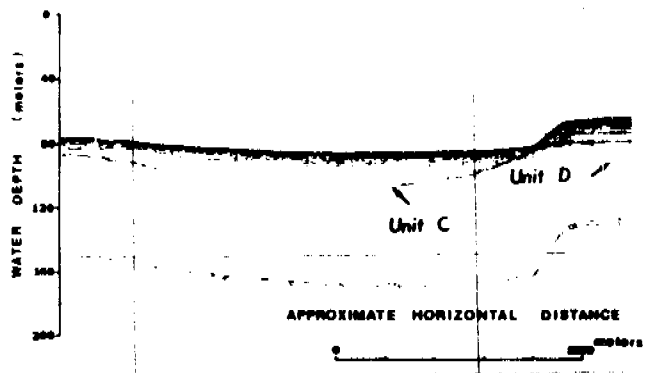


Figure 15. Seismic-reflection record of main glacial trough of lower Cook Inlet.

QUATERNARY DEPOSITIONAL ENVIRONMENTS, LOWER COOK INLET, ALASKA

Other parts of the inlet show various types of channel and trough fill. Within the main trough of the inlet there is 30-40 m of well-layered sediment filling the shallow lower part (Fig. 15), and over the eastern platform regions there is considerable fill within wide (1,000 m) channels (Fig. 16a, 16b). At the mouth of Chisik Valley there is evidence for multiple episodes of filling of a migrating trough exiting from Tuxedni Bay (Fig. 17). Chisik Valley is

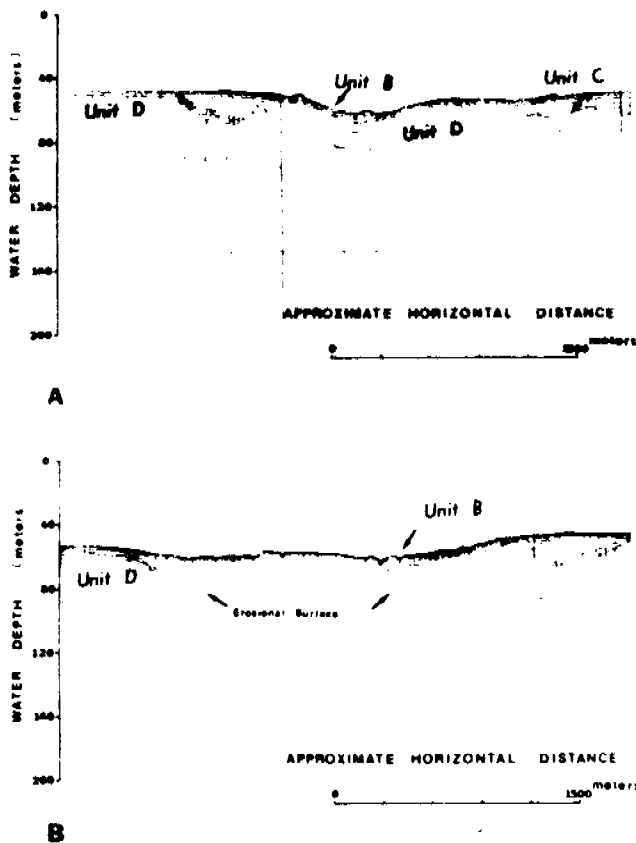


Figure 16. (a,b) Seismic-reflection records showing canyon fill on the eastern platform region.

floored with 10-20 m of apparently well-layered sand and sandy silt, and the north flank contains 30-45 m of fill. Farther north along the west side of Kalgin platform there is a deep depression that has over 50 m of fill. The massive fill appears to have been built rapidly from the north. Small sand waves presently migrate southward over the surface of this fill (Fig. 18).

Channelization is characteristic of glacial outwash plains. During retreat of the last major glacier in Cook Trough there was a period of channelization and contemporaneous or nearly contemporaneous infilling over a large outwash plain. The outwash sediments were then modified by the action of the increasing strong tidal currents as sea level rose. The observed deltaic deposition represents well-sorted sand infilling a channel at the front of the glacial lobe. Fine material has bypassed this infilling and been carried away by local currents along the glacier front.

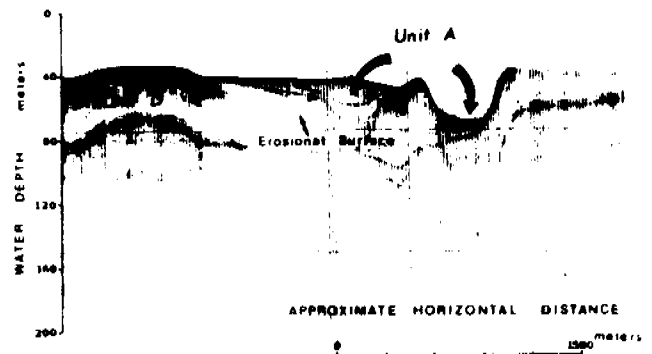


Figure 17. Seismic reflection record showing the character of the trough exiting from Tuxedni Bay with main channel fill and large-scale fill within apparent older channels.

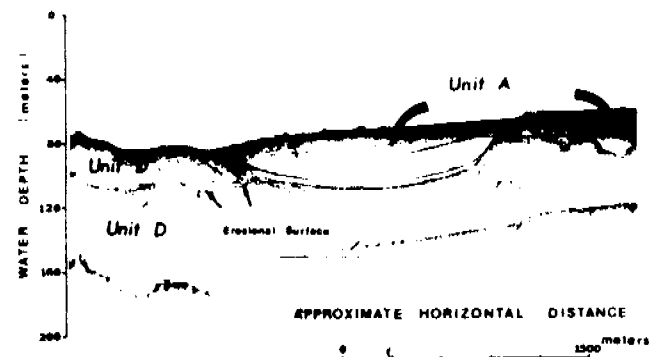


Figure 18. Detail of large-scale fill within a deep depression on the west flank of Kalgin Island showing migrating sand waves.

SUMMARY AND CONCLUSIONS

Surficial sediments of lower Cook Inlet are gravel, sandy gravel, sand and silty sand. Six depositional environments have been defined within the inlet on the basis of upon sedimentologic, hydrodynamic and morphologic characteristics. These six environments are: (1) high-energy shoreface, (2) trough-edge platform, (3) trough slope, (4) trough floor, (5) trough-mouth plateau, and (6) seaward progradational ramp. All of these environments have characteristics that reflect the complex glacial and post-glacial history of lower Cook Inlet.

Four major sedimentary units have been observed in uniboom seismic data and have been preliminarily identified as (1) Unit A - Holocene laminated sand and silty sand, (2) Unit B - large-scale sand-wave complexes, (3) Unit C - outwash gravel lag, and (4) Unit D - glacial drift tentatively identified as ground moraine. These units were identified on the basis of their acoustic characteristics. This procedure follows similar works by King (1969) on the Scotian shelf, Jansen (1976) in the North Sea and Amos (1978) in the Minas Basin, Nova Scotia.

Due to the complexity of the Quaternary glacial history of lower Cook Inlet, only the major characteristics of the above units have been described. Further research aimed toward correlations with the known glacial sediments of the surrounding shoreline may lead toward a more definitive glacial depositional time sequence. The data presently available are not sufficient to assess the relative ages of the various sedimentary units. It is clear, however, that multiple episodes of glacial deposition and erosion have occurred within the high-energy tidally dominated embayment of lower Cook Inlet. Each of these events has left a distinct imprint which is now preserved in the shallow stratigraphy.

Acknowledgments

This study was supported by the U.S. Bureau of Land Management through interagency agreement with the National Oceanic and Atmospheric Administration under which a multi-year program responding to needs of petroleum development of the Alaskan continental shelf is managed by the Outer Continental Shelf Environmental Assessment Program Office.

I thank Bruce F. Molnia and Arnold H. Bouma for their support, advice, and critical reviews.

References Cited

- Alaska OCS Office, 1976, Lower Cook Inlet, Final Environmental Impact Statement: Alaska Outer Continental Shelf Office, Anchorage, Alaska, 3 volumes.
- Amos, C. L., 1978, The post glacial evolution of the Minas Basin, N.S., a sedimentological interpretation: *Journal of Sedimentary Petrology*, v. 48, no. 3, p. 965-982.
- Anderson, J. B., 1972, Nearshore glacial-marine deposition from modern sediments of the Weddell Sea: *Nature Physical Science*, v. 240, Dec. 25, p. 189-192.
- Belderson, R. H., Johnson, M. A., and Stride, A. H., 1978, Bed-load partings and convergences at the entrance to the White Sea, U.S.S.R., and between Cape Cod and the Georges Bank, U.S.A.: *Marine Geology*, v. 28, p. 65-75.
- Bouma, A. H., and Hampton, M. A., 1976, Preliminary report on the surface and shallow subsurface geology of the lower Cook Inlet and Kodiak shelf, Alaska: U.S. Geological Survey, Open-File Report 76-695, 36 p.
- Bouma, A. H., Hampton, M. A., Wennekens, M. P., and Dygas, J. A., 1977a, Large dunes and other bedforms in lower Cook Inlet, Alaska: Ninth Offshore Technology Conference, Paper 2737, p. 79-85.
- Bouma, A. H., Hampton, M. A., and Orlando, R. C., 1977b, Sand waves and other bedforms in lower Cook Inlet: *Marine Geotechnology*, v. 2, p. 291-308.
- Bouma, A. H., Hampton, M. A., Rappeport, M. L., Whitney, J. W., Teleki, P. G., Orlando, R. C., and Torresan, M. E., 1978, Movement of sand waves in lower Cook Inlet, Alaska: Tenth Offshore Technology Conference, Paper 3311, p. 2271-2284.
- Bouma, A. H., Rappeport, M. L., Cacchione, D. A., Drake, D. E., Garrison, L. E., Hampton, M. A., and Orlando, R. C., 1979, Bedform characteristics and sand transport in a region of large sand waves, lower Cook Inlet, Alaska: Eleventh Offshore Technology Conference, Paper 3485.
- Bouma, A. H., Rappeport, M. L., Orlando, R. C., and Hampton, M. A., 1980, Identification of bedforms in lower Cook Inlet, Alaska: *Sedimentary Geology*, (in press).
- Cacchione, D. A., and Drake, D. E., 1979, Bottom and near-bottom sediment dynamics in lower Cook Inlet: Annual Report RU 430, Outer Continental Shelf Environmental Assessment Program (OCSEAP), 41 p.
- Carsola, A. J., 1975, Oceanographic/meteorological study of the lower Cook Inlet, Alaska: Lockheed Ocean Laboratory, Report to Shell Oil Company, 137 p.
- Dames and Moore, 1978, Drilling fluid dispersion and biological effects study for the lower Cook Inlet C.O.S.T. Well: Report to Atlantic Richfield Company, 309 p.
- Evans, C. D., Buck, E. H., Buffler, R. T., Fisk, S. G., Forbes, R. B., and Parker, W. B., 1972, The Cook Inlet environment - A background study of available knowledge: University of Alaska Resource and Science Center, Alaska SeaGrant Program, Anchorage, 137 p.
- Fisher, M. A., and Magoon, L. B., 1978, Geologic framework of lower Cook Inlet, Alaska: *American Association of Petroleum Geologists Bulletin*, v. 62, no. 3, p. 373-402.
- Folk, R. L., and Ward, W., 1957, Brazos River Bar: A study in the significance of grain size parameters: *Journal of Sedimentary Petrology*, v. 27, p. 3-26.
- Hayes, M., Brown, P., and Michel, J., 1977, Coastal morphology and sedimentation lower Cook Inlet, Alaska, in L. L. Trasky, ed., *Environmental studies of Kachemak Bay and lower Cook Inlet*: Alaska Department of Fish and Game, Anchorage, Alaska, 99 p.
- Hein, J. R., Bouma, A. H., Hampton, M. A., and Ross, C. R., 1979, Clay mineralogy, fine-grained sediment dispersal, and inferred current patterns, lower Cook Inlet and Kodiak Shelf, Alaska: *Sedimentary Geology*, v. 24, p. 291-306.
- Jansen, J. H. F., 1976, Late Pleistocene and Holocene history of the Northern North Sea, based on acoustic reflection records: *Netherlands Journal of Sea Research*, v. 10, p. 1-43.
- Karlstrom, T. N. V., 1964, Quaternary geology of the Kenai Lowland and glacial history of the Cook Inlet region, Alaska: U.S. Geological Survey, Professional Paper 443, 69 p.
- King, L. H., 1969, Submarine end moraines and associated deposits on the Scotian Shelf: *Geological Society of America Bulletin*, v. 80, p. 83-96.
- Komar, P. D., 1976, The transport of cohesionless sediments on continental shelves, in P. J. Stanley and D. J. P. Swift, eds., *Marine transport and environmental management*: Wiley, New York, p. 107-125.
- McCabe, P. J., 1977, Deep distributary channels and giant bedforms in the upper carboniferous of the central Pennines, northern England: *Sedimentology*, v. 24, p. 271-190.
- Muench, R. D., Mofjeld, H. O., and Charnell, R. L., 1978, Oceanographic conditions in lower Cook Inlet: Spring and summer, 1973: *Journal of Geophysical Research*, v. 83, p. 5070-5098.
- Rappeport, M. L., Cacchione, D. A., Bouma, A. H., and Drake, D. E., 1979, Seafloor microtopography, tidal current characteristics and bottom boundary layer time-series data, Cook Inlet, Alaska (abs.): EOS, American Geophysical Union, Transactions, v. 60, no. 18, p. 285.
- Whitney, J. W., Noonan, W. G., Thruston, D., Bouma, A. H., and Hampton, M. A., 1979, Lower Cook Inlet, Alaska: Do those large sand waves migrate?: Eleventh Offshore Technology Conference Paper 3484, p. 1071-1082.

RU 429:

FAULTING, SEDIMENT INSTABILITY, EROSION AND DEPOSITION HAZARDS

OF THE NORTON BASIN SEA FLOOR

ANNUAL REPORT OF THE PRINCIPAL INVESTIGATOR FOR THE FISCAL YEAR

ENDING MARCH, 1980

C. Hans Nelson

TABLE OF CONTENTS

	<u>Page</u>
SEDIMENTARY PROCESSES AND POTENTIAL GEOLOGIC HAZARDS OF NORTON BASIN SEA FLOOR, by Matthew C. Larsen, C. Hans Nelson and Devin R. Thor	183
Appendices:	
Hydrocarbon gases in nearsurface sediment of the northern Bering Sea by Keith A. Kvenvolden, George D. Redden and C. Hans Nelson	215
Biogenic and thermogenic gas in gas-charged sediment of Norton Sound, Alaska, by Keith A. Kvenvolden, C. Hans Nelson, Devin R. Thor, Matthew C. Larsen, George D. Redden, John B. Rapp and D. J. Desmarais	244
Thermogenic gas in sediment of Norton Sound, Alaska by C. Hans Nelson, Keith A. Kvenvolden and Edward C. Clukey	251
Distribution of gas-charged sediment in Norton Basin, northern Bering Sea by Mark L. Holmes and Devin R. Thor	261
Ice Gouging on the subarctic Bering shelf by Devin R. Thor and C. Hans Nelson	286
Areas of active, large-scale sand wave and ripple fields with scour potential on the Norton Basin sea floor, by C. Hans Nelson, Michael E. Field, David A. Cacchione and David E. Drake	315
Depositional and erosional features of the northeastern Bering Sea inner shelf, by Ralph Hunter and Devin R. Thor	332
Graded strom sand layers offshore from the Yukon Delta, Alaska, by C. Hans Nelson	368
Geotechnical characteristics of bottom sediments in the northern Bering Sea, by Harold W. Olsen, Edward C. Clukey and C. Hans Nelson	387
Report on surface and subsurface faulting in Norton Sound and Chirikov Basin, Alaska, by Janice L. Johnson and Mark L. Holmes	420
Distribution of trace elements in bottom sediment of northern Bering Sea by Bradley R. Larsen, C. Hans Nelson, Chris Heropoulos, and Jeffrey J. Patry	445
Miscellaneous geologic maps, by Devin R. Thor	568
The following two appendices of this annual report can be obtained as reprints from the indicated journals:	
Geologic implications and potential hazards of scour depressions on Bering Shelf, Alaska, by Matthew C. Larsen, C. Hans Nelson and Devin R. Thor, in <u>Environmental Geology</u> 3, p.39-47, 1979.	
Modern biogenic gas-generated craters (sea-floor "pockmarks") on the Bering shelf, Alaska, by C. Hans Nelson, Devin R. Thor, Mark W. Sandstrom and Keith A. Kvenvolden, in <u>Geological Society of America Bulletin</u> , Part I v.90, p.1144-1152, December 1979, Doc. no. 91208	

Sedimentary Processes and Potential
Geologic Hazards of Norton Basin Sea Floor

Matthew C. Larsen, C. Hans Nelson, and Devin R. Thor

ABSTRACT

A dynamic environment of strong bottom currents, storm waves, and sediment gas-charging on the shallow sea floor of northern Bering Sea creates several potential geologic hazards. Thermogenic gas seeps, sea-floor gas cratering, sediment liquefaction, ice gouging, scour-depression formation, coastal and offshore storm surge and associated storm-sand deposition, and large-scale bedform movement all are active sedimentary processes in this epicontinental shelf region.

Interaction between the processes of liquefaction and the formation of shallow gas pockets and craters, scour depressions, storm-sand deposits, and slumps results in sediment instability. Liquefaction of the upper 1-3 m of sediment can be caused by cyclic storm-wave loading of the Holocene coarse-grained silt and very fine-grained sand covering Norton Sound. The widespread occurrence of gas-charged sediment with small surficial craters (3-8 m in diameter and less than 1 m deep) in central Norton Sound indicates that the sea-floor sediment is periodically disrupted by escape of biogenic gas from the underlying peaty mud. During major storms, liquefaction not only may help trigger crater formation, but may also enhance erosional and depositional processes that create large-scale scour areas and prograde storm sand sheets in the Yukon prodelta area.

Erosional and depositional processes are most intense in the shallower parts of northern Bering Sea or as storm surge flooding along the coastline. Ice gouges are numerous and ubiquitous in the area of the Yukon prodelta, and

the sediment is scoured to depths of 1 m. Although much less common, ice gouges are present throughout the remainder of northern Bering Sea where water depths are less than 20 m. In the Yukon prodelta area and in central Norton Sound, where currents are constricted by shoal areas and flow is made turbulent by local topographic irregularities (such as ice gouges), storm-induced currents have scoured large (10 - 150 m diameter), shallow (less than 1 m deep) depressions. Abundant storm-sand layers in Yukon prodelta mud show that storm surge and waves have generated bottom transport currents that deposit layers of sand as thick as 20 cm as far as 100 km from land. Storm surge run-off also may reinforce the strong geostrophic currents near Bering Strait so that intermittent movement of even the largest sand waves (10-200 cm wavelength and up to 2 m height) results.

INTRODUCTION

Studies of potential geologic hazards on Norton Basin sea floor in northern Bering Sea have been conducted by the U.S. Geological Survey (USGS) to evaluate oil and gas lease tracts preparatory to Outer Continental Shelf (OCS) leasing. The data base for this evaluation included 9000 km of high-resolution geophysical tracklines, (Nelson, et al., 1978a; Thor and Nelson, 1978; Larsen, et al., 1979) 1000 grab samples, 400 box cores and 60 vibracores; in addition, hundreds of camera, hydrographic, and current meter stations have been occupied during the past decade by USGS, National Oceanic and Atmospheric Administration (NOAA), and University of Washington oceanographic vessels (Figs. 1 and 2).

The northern Bering Sea is a broad, shallow epicontinental shelf region covering 200,000 km² of subarctic sea floor between northern Alaska and the U.S.S.R. The shelf can be divided into four general morphologic areas: (1) the western part, an area of undulating, hummocky relief with glacial gravel and transgressive-marine sand substrate (Nelson and Hopkins, 1972); (2) the southeastern part, a relatively flat, featureless plain with fine-grained, transgressive-marine sand substrate (McManus, et al., 1977); (3) the northeastern part, a complex system of sand ridges and shoals with fine- to medium-grained transgressive sand substrate (Nelson, et al., 1978b); and (4) the eastern part, a broad, flat marine reentrant (Norton Sound) covered by Holocene silt and very fine sand (Nelson and Creager, 1977). A detailed discussion of bathymetry and geomorphology of northern Bering Sea is given by Hopkins and others, (1976) (Fig. 3).

The northern Bering Sea is affected by a number of dynamic factors: winter sea ice, sea level setup, storm waves and strong currents (geostrophic, tidal, and storm). The sea is covered by pack ice for about half the year,

from November through May. A narrow zone of shorefast ice (sea ice attached to the shore) develops around the margin of the sea during winter months. Around the front of the Yukon River Delta shorefast ice extends up to 40 km offshore (Thor, et al., 1978). During the open-water season, the sea is subject to occasional strong northerly winds, and in the fall strong south-southwesterly winds cause high waves and storm surges along the entire west Alaskan coast (Fathauer, 1975). Throughout the year a continual northward flow of water is present with currents intensifying on the east side of strait areas (Coachman, et al., 1976). Although diurnal tides are very minor (less than 0.5 m), strong tidal currents are found in shoreline areas and within central Norton Sound (Fleming and Heggarty, 1966; Cacchione, and Drake, 1978).

This paper reviews basic sedimentary processes of this epicontinental shelf region and discusses the following potential geologic hazards related to these processes: thermogenic gas seepage, biogenic gas-charged sediment and cratering, sediment liquefaction, ice gouging, current scouring, storm sand deposition, and mobile bedform movement (Fig. 4). These geologic hazards may pose problems for the future development of offshore resources in Norton Basin.

SEDIMENTARY PROCESSES

Coastal storm surge

A severe storm in November 1974 moved from southwest to northwest across the Bering Sea. Peak winds were up to 111 km per hour from the south and nearshore waves were reportedly 3 to 4 m in height (Fathauer; 1975). Coastal flooding along the Bering Sea coast extended from Kotzebue Sound (north of Bering Strait) to just north of the Aleutian Islands (Fathauer, 1975). The maximum sea level setup was measured by the elevation of debris lines along the coast of Norton Sound and ranged from 3 to 5 m above mean sea level

(Sallenger, et al., 1978). During this storm, extensive inland flooding occurred and erosion of 2 to 5 m high coastal bluffs took place near Nome. Irregular landward erosion, as much as 18 m, occurred west of Nome where bluffs are 3 to 5 m high. East of Nome bluffs are 1.5 to 2 m high and landward erosion was as much as 45 m. Water level in the Norton Sound area reached its peak on 12 November when up to 6 feet of water was standing in Unalakleet and the static high water line in Nome was 13.2 feet above mean low low-water.

Offshore storm surge

The transport of sediment in Norton Sound can be described in terms of distinctly different quiescent and storm regimes (Cacchione and Drake, 1978). The quiescent regime is characterized by generally low levels of sediment transport caused principally by tidal currents. Fine silt and clay move as "wash load" and bedload transport is negligible except in shallow areas where surface waves become important. Current speeds in this regime are no greater than 30 cm/sec.

Although calm weather conditions exist for about 90% of the year in the northern Bering Sea, less than 50% of the sediment transport occurs under these conditions (Cacchione and Drake, 1978). Norton Sound is commonly exposed to strong southerly and southwesterly winds generated by low pressure weather systems in September, October and November. A two-day storm in September 1977 transported sediment equal to the transport that would occur during four months of quiescent conditions. Current speeds were as much as 70 cm/sec during this storm.

Graded storm sand layers, up to 20 cm thick (Nelson, in preparation), occur in sea-floor stratigraphy of the northern Bering Sea and are widespread evidence of major storm surge events. The effects of storm surge are

magnified by two factors: 1) extremely shallow water depth (less than 20 m), and 2) strong bottom return currents that move large amounts of sediment northward to the Chukchi Sea. The thickness of Holocene sediment in Norton Sound, when compared to Holocene sediment input from the Yukon River indicates that significant amounts of sediment have been resuspended and transported out of Norton Sound (Nelson and Creager, 1977). About 10% of the Yukon River input into Norton Sound may be carried as suspended sediment through the Bering Strait into the Chukchi Sea (Cacchione and Drake, 1978). As much as 40% of Holocene sediment discharged from the Yukon River appears to be missing from Norton Sound. This difference of 30% may be material which has been resuspended and transported during storms (Cacchione and Drake 1978).

Storm surges not only resuspend and transport massive amounts of suspended sediment, but also appear to move large amounts of sand in bedload transport for significant distances offshore. Graded storm sand layers are widespread throughout southern Norton Sound, and thicken considerably toward the Yukon subdelta, the apparent source region. This suggests that there are massive movements of bedload sediment away from the delta toward the adjacent offshore region during storms (Nelson, in prep.; Nelson, 1977).

Yukon Delta sedimentation

The Yukon delta drains an area of almost 900,000 km² providing a water discharge of approximately 6000 m³ per second and a sediment load of 70-90 million metric tons per year (Dupré and Thompson, 1979; Cacchione and Drake, 1978). The sediment load represents almost 90 percent of all sediment entering the Bering Sea and is composed mainly of very fine sand and coarse silt with very little clay.

Yukon delta and offshore processes can be divided into seasonal regimens (Dupré and Thompson, 1979). The ice-dominated regimen begins with freeze-up

in late October or November. Shorefast ice extends 10 to 40 km offshore where it is terminated by a series of pressure ridges and shear zones formed by the interaction of shorefast ice with the highly mobile, seasonal pack ice.

River breakup typically occurs in May and this marks the beginning of the river dominated regimen. Once the shorefast ice melts or drifts offshore, sedimentation is dominated by normal deltaic processes under the influence of the high discharge of the Yukon River.

Increasingly frequent southwest winds and waves associated with major storms during late summer mark the beginning of the storm-dominated regimen. High wave energy and decreasing sediment discharge from the Yukon cause significant coastal erosion and reworking of deltaic deposits. The Yukon delta plain is fringed by prograding tidal flats and distributary mouth bars, similar to many previously described deltas. However, the delta front and prodelta are offset from the prograding shoreline by a broad platform (referred to as a sub-ice platform) up to 30 km wide. The broad sub-ice platform appears to be related to the presence of shorefast ice which fringes the delta for half the year. The term delta front describes the relatively steep margin of the offshore delta environment characterized by rapid deposition of sediment in water 2 to 10 m deep. The prodelta, with extremely gentle slopes, marks the distal edge of the deltaic sediments extending up to 100 km offshore.

Inner Shelf Wave Effects

Waves and wave-induced currents are the dominant geologic processes on the inner shelf of northwestern Norton Sound and in the approaches to Bering Strait (Hunter and Thor, 1979). Sedimentary features common to both areas include sand and gravel patches and ribbons, wave ripples, sand waves and ice gouges (Hunter and Thor, 1979).

Wave ripples with spacings of up to 2 m are common in both the Port Clarence and Nome areas, in zones where sediment is well sorted and grain size ranges from coarse sand to pebbly gravel. Ripples in the Port Clarence area trend northwest-southeast and can be explained as the result of storm waves from the southwest Bering Sea. Ripples in the Nome area have trends indicating dominant wave activity from south to southwest.

Ribbons of sand and gravel are well developed near the entrance to Port Clarence. These appear to be bedforms produced by wave action or by wave-induced net water motion in the direction of wave propagation.

A rich assemblage of depositional and erosional features is present in shallow water close to the southern shore of Seward Peninsula. Both wave-formed and current-formed features are present. However, wave-formed features are more common; some of the current-formed features imply considerable sediment transport by strong bottom tidal currents.

Only a preliminary understanding of wave and current patterns is known for southwestern Norton Sound. The major wave trains originate in the southern Bering Sea: waves move northward and refract clockwise around protruding Yukon shoals. Smaller waves with shorter periods are generated by northeasterly winds and move southwestward.

Liquefaction

Sediment derived from the Yukon River covers most of the bottom of Norton Sound (McManus et al., 1977). This sediment consists primarily of silt with significant amounts of very fine sand in some areas, and a generally minor content of clay-size material. The sediment thickness is generally less than 3 m, except near the Yukon Delta where accumulations are as thick as 10 m (Olsen et al., 1979). The material is generally dense; however, there are relatively loose soil zones in gas-charged sediment areas of Norton Sound. In

addition, relatively loose soil zones were observed above and between dense layers in the delta areas sampled by 6 m vibracores.

Freshwater peaty mud beneath Yukon marine silt is somewhat overconsolidated, and contains substantial amounts of organic carbon and gas. The presence of gas indicates that the pore pressures in the peaty muds may be high. If so, the strength of the material could be low in spite of its overconsolidated state.

The dominantly coarse-silt to fine-sand sized texture of the material, occurrence of loose soil zones, and theoretical calculations utilizing GEOPROBE cyclic wave loading data (Olsen et al., 1979; Clukey et al., in prep.) indicate that Yukon prodelta sediment in southwestern Norton Sound is susceptible to liquefaction. Liquefaction of the prodelta deposits is attributable to cyclic loading resulting from the exposure of the Yukon prodelta to large storm waves from the southwest. Water depths are sufficiently shallow so that much of the wave generated surface energy is imparted to the bottom sediment with resultant liquefaction of the upper 1-2 m of sediment during extreme storm surge events (Clukey et al., in prep). This liquefaction potential of prodelta sediment may be important to storm sand transport processes, scour depression formation and gas crater development.

Ice scour

Ice on the Bering shelf scours and gouges surficial sediment of the sea floor (Fig. 5). The annual ice cover in this subarctic setting is thin (less than 2 m); however, thick ice capable of gouging forms where pack ice collides with and piles up against stationary, shorefast ice, developing numerous pressure ridges (Thor and Nelson, this volume). A wide, well-developed shear zone forms in southwest Norton Sound because ice moving southward from the northeast Bering Sea and westward along southern Norton Sound converges in the shallow water of the Yukon prodelta. Consequently, numerous zones of pressure

ridges are formed and this region at 10 to 20 m water depth has the maximum ice gouge density. Gouges are found in water up to 30 m deep and the furrows are as much as 1 m deep. Ice gouging affects the sea floor under shorefast areas minimally, or not at all (Thor and Nelson, 1980).

Current Scour Depressions

Zones of large flat-floored scour depressions occur in two principal areas of Norton Sound, west of the Yukon prodelta and 50 km southeast of Nome, on the flank of a broad shallow trough (Fig. 6) (Larsen et al., 1980). Scour features range from individual more or less elliptical depressions, 10 to 30 m in diameter, to large areas of scour with irregular margins, 80 to 150 m in diameter. The depressions are 60 to 80 cm deep (Larsen et al., 1980).

Bottom current speeds in scour depression areas are 20 to 30 cm per second under non-storm conditions, and were measured at 70 cm per second during a typical autumn storm (Cacchione and Drake, 1978). Both zones of scour depressions are situated on flanks of gently sloping shoals, where strong tidal or geostrophic currents shear against the slopes. Small-scale ripple bedforms are associated with scour areas and mean grain size ranges from 4 phi to 4.5 phi (0.063 mm to 0.044 mm). Depressions in the Yukon delta area are associated with extensive ice gouging. The gouge furrows commonly expand into large shallow depressions.

Experiments in flumes containing fine sand and silt have shown that currents flowing over an obstruction will erode material immediately downcurrent from the obstruction. The large scour depressions observed in Norton Sound may be a characteristic erosional bedform developed during storms when strong currents and high wave energy are focused on silt-covered slopes with local topographic disruptions that set off flow separation and downcurrent scour.

Sandwave Dynamics

Strong dynamic currents are present throughout much of the northern Bering Sea, particularly where westward land projections interject into the northward flow, such as in the eastern Bering Strait area. In such regions large bedforms develop and migrate, forming an unstable sea floor (Nelson et al., 1978b). These large bedforms include large-scale sand waves 1 to 2 m high with wavelengths of up to 200 m, and small-scale sand waves 0.5-1 m high with wavelengths of 10 m. They occupy the crests and some flanks of a series of linear sand ridges 2 to 5 km wide and as much as 20 km long located between Port Clarence and King Island (Nelson et al., 1979)

Sand wave movement and bedload transport take place during calm weather. However, maximum change apparently occurs when major southwesterly storms generate sea level set-up in the eastern Bering Sea that enhances northerly currents. In contrast, strong north winds from the Arctic reduce the strength of the continuous northerly currents and thereby arrest bedform migration.

Gas-charged sediment

The distribution of acoustic anomalies suggests that almost 7000 km² of sea floor in Norton Sound and Chirikov Basin are underlain by sediment containing sufficient gas (biogenic and/or thermogenic) to affect sound transmission through these zones (Holmes, 1979a). Core penetration rates (Nelson et al., 1978c and Kvenvolden et al., 1979a) and sediment samples from 2 to 6 m vibracores confirm gas saturation of nearsurface sediment at several locations characterized by acoustic anomalies. The isotopic compositions of methane at four of the sites range from -69 to -80‰ (δ¹³C_{PDB}) (Kvenvolden et al., 1978, 1979b). This range of values clearly indicates that the methane is formed by microbial processes, possibly operating on nearsurface

Pleistocene peat deposits that underlie Holocene deposits throughout the northern Bering Sea.

At one site in Norton Sound, nearsurface sediment is apparently charged with CO₂ which is actively seeping from the sea floor accompanied by less than one percent hydrocarbon gases (Kvenvolden et al., 1979a). Methane in this gas mixture has an isotopic composition of -36‰, a value suggesting that it is derived mainly from thermal processes, probably operating at depth in Norton Basin (Kvenvolden et al., 1979a). Geophysical evidence indicates that the hydrocarbon gases migrate into the nearsurface sediments along a fault zone (Nelson et al., 1978c). Subbottom reflector terminations on continuous seismic profiles near the fault zone outline a large zone of anomalous acoustic responses about 9 km in diameter and at a 100 m depth caused by a thick subsurface accumulation of gas. Gas geochemistry and extensive expansion of vibracores suggest a high degree of gas saturation at the seep site (Kvenvolden et al., 1979b).

Biogenic gas-generated craters

Small circular pits on the sea floor are found over a 20,000 km² area of central and eastern Norton Sound (Fig. 7). The craters in the northern Bering Sea are very young features, as shown by their presence within modern ice-gouge grooves and by the fact that relict, buried craters have not been observed in seismic profiles. These craters range from 1 to 10 m in diameter, average 2 m in diameter and are probably less than 0.5 m deep. They are associated with numerous acoustic anomalies observed on seismic profiles and with subsurface Pleistocene peaty mud that often is saturated with biogenic methane (Nelson et al., 1980; Holmes 1979b). The extensive reflector-termination anomalies and peat with a high gas content in east-central Norton Sound suggest that gas-charged sediment is the cause of crater formation.

Two basic mechanisms for gas venting can be proposed. The first is that continuous local degassing may maintain craters as active gas vents on the sea floor. The second and more likely mechanism is that gas is intermittently vented, particularly during severe storms when nearsurface sediment may liquefy.

The occurrence of surface craters in overlying marine sediment and the presence of high quantities of methane trapped beneath cohesive marine mud in Norton Sound suggest that gas venting is episodic in this lithologic setting; however, lack of craters in the non-cohesive nearsurface fine to medium sand and gravel of Chirikov Basin indicates that gas diffuses gradually through this more porous sediment which overlies the peaty mud there. Further evidence for intermittent venting of gas is the broad, shallow shape of the craters, unlike the deep, conical, actively bubbling vents of the thermogenic seep. Lack of methane in bottom water also suggests that the craters are not continually active vents.

POTENTIAL GEOLOGIC HAZARDS

Thermogenic gas cap

The extent of active gas seepage into the water column and gas saturation in nearsurface sediment above a thick underlying sediment section with acoustic anomalies suggests a possible hazard for any future drilling activity in the thermogenic gas seep area south of Nome. Any artificial structures penetrating the large gas accumulation at 100 m or intersecting associated faults that cut the gas-charged sediment may provide direct avenues for uncontrolled gas migration to the sea floor.

Shallow gas pockets

Gas-charged sediment creates potentially unstable surficial-sediment conditions in Norton Sound. 7,000 km² of Norton Sound are underlain by

acoustic anomalies with potential shallow gas pockets everywhere except under the Yukon prodelta (Holmes, 1979a). Pipelines built across areas of these potential gas pockets may be damaged by stress induced from the unequal bearing strength of gas-charged and normal sediment, particularly if the nearsurface sediment is undergoing liquefaction caused by cyclic loading of storm waves. The gas saturation and lateral and subsurface extent of any shallow gas pockets will have to be detailed in any site investigations for platforms or pipelines.

Gas craters

Gas craters cover a large area of north-central Norton Sound. During non-storm conditions, nearsurface gas in this area may be trapped by a 1-2 m thick layer of impermeable Holocene mud. Apparently the gas escapes and forms craters during periodic storms that initiate rapid changes in pore-water pressures, because of sea-level setup, seiches, erosional unloading of covering mud, and sediment liquefaction from cyclic wave loading. Gas venting and sediment craters or depressions, apparently formed during peak storm periods, may be a potential hazard to offshore facilities because of rapid lateral changes in bearing strengths and sediment collapse which forms the craters. Sediment collapse also may expose pipelines to ice gouging hazards. The upper several meters of sediment at many locations during non-storm conditions also has reduced shear strength because of the nearsurface gas saturation and presence of peat layers. Siting of artificial structures will require extensive local substrate testing to determine the extent of gas craters in a given area.

Liquefaction

The assessment and prediction of sea-floor stability is affected by the potential of a sedimentary deposit to liquefy under cyclic loading and behave

as a viscous fluid. The liquefaction potential of Norton Sound sediment is great in central Norton Sound and in the vicinity of the western Yukon prodelta. Possible causes of liquefaction include upward migration of gas from thermogenic and biogenic sources, earthquakes, and ocean waves. Bottom features caused in part by liquefaction include scour depressions and abundant sediment cratering where Yukon sediment is thin. Loss of substrate support due to sediment liquefaction is a problem that must be faced in the construction of pipelines, drilling platforms, and other types of structures resting on the sea floor. Full assessment of this problem requires extensive future studies of in situ pore pressure, gas saturation, and wave cyclic loading during storms.

Ice scour

Ice gouging presents some design problems and potential hazards to installations in or on the sea floor. Pipelines and cables should be buried at a depth which allows for maximum ice gouging of 1 m, plus a safety factor for combined effects with current scour around the western Yukon prodelta front or gas cratering in central Norton Sound.

The maximum intensity of ice gouging occurs in central Norton Sound, at 10-15 m depths in an area surrounding the Yukon Delta. The remaining area of Norton Sound, less than 10 m deep, and greater than 20 m deep, has a low density of gouging, or none at all. Special studies of nearshore areas off Nome and Port Clarence were conducted because both are potential centers for commercial development and activity. Offshore from Nome, the focal point for N. Bering logistics, is an area of ice divergence and thus is not heavily gouged. Although several gouges were found offshore, none were in water shallower than 8 m. Several gouges were found near Port Clarence, but again none occurred in water less than 8 m deep. The gouges in the Port Clarence

area were found at the northern end of the Port Clarence spit and on the northern side of Port Clarence inside the tidal inlet.

Scour depressions

The highest density of scour depressions occurs in two areas of Norton Sound: 1) west and northwest of the Yukon delta and 2) southeast of Nome (fig. 6). Scour depression distribution indicates areas where artificial structures that disrupt current flow may cause extensive erosion of Yukon-derived silt or very fine-grained sand and create potentially hazardous undercutting of the structures. Even buried structures such as pipelines may be subject to scour because strong currents may greatly broaden and deepen naturally occurring ice gouges and thus expose the buried structures. The severity of scour depressions is greatest where it occurs with ice gouging in the Yukon delta areas. Replicate surveys have shown that scour depressions recur annually. However, full assessment of this geologic hazard requires long-term current monitoring in specific localities of scour to predict current intensity and periodicity, especially during major storms, since measured current speeds have increased >100% under moderate storm conditions (Cacchione and Drake, 1979).

Mobile Bedform Movement

Large migrating bedforms form an unstable sea floor in the area west of Port Clarence. Actual rates of bedform movement are not known, however development and decay of sand waves up to 2 m in height has been observed over a one-year period. Pipelines could suffer damaging stress if free spans developed where the structure crossed such areas of migrating 2-m high sand waves.

Studies to date indicate that the most extreme scour potential exists in regions of sand ribbons and gravel plus shell pavement within the strait

areas. The Port Clarence sand wave area has the most rapidly changing relief and the scour in sand wave troughs may reach depths of up to 2 m. Replicate surveys have shown that such scour may occur each year in some areas of the Port Clarence sand wave field. Longterm monitoring of currents and bedform movement is particularly important in determining actual rates of change in this area because Port Clarence is the only natural Alaskan harbor in the northern Bering Sea.

Coastal and offshore storm surge hazards

The northern Bering Sea has a known history of severe storm surges, which are accompanied by widespread changes in sea-floor sedimentation. These changes have complications for sea-floor installations and mass transport of pollutants. Severe storms, such as the November 1974 storm have caused extensive flooding along the Norton Sound coast between Nome and Unalakleet, and on the St. Lawrence Island coast. At Nome, storm surge and waves overtopped a sea wall and caused nearly 15 million dollars in damage (Fathauer, 1975). Storm surge periodicity and intensity will have to be carefully studied in planning where and if pipelines come ashore in this area. The November 1974 storm is the worst storm measured in historic times although severe storm damage also occurred in 1913 and 1946 (Fathauer, 1975).

Rapid sedimentation is a problem in the Yukon delta area where storm sand layers of 15 cm or more from a single event have been measured in some places. Pipelines, offshore facilities, or other structures impeding the extensive erosion, transport and re-deposition of sediment in southern Norton Sound will require careful design. Accurate monitoring of the storm surge process will require a longterm array of current meters and tide gauges in the northern Bering Sea.

ACKNOWLEDGMENTS

We thank Keith Kvenvolden for information concerning gas in Norton Sound sediment, David Cacchione and David Drake for data on current and sediment movement, William Dupré for information on deltaic processes, Abby Sallenger and Ralph Hunter for data concerning inner shelf processes, and Harold Olsen and Edward Clukey for data on geotechnical properties. We are grateful for assistance of Phyllis Swenson, Marybeth Gerin, and Joan Esterle for drafting and preparation of figures and Helen Ogle for typing the manuscript.

The cruises were supported jointly by the U.S. Geological Survey and the Bureau of Land Management through interagency agreement with the National Oceanic and Atmospheric Administration, under which a multiyear program responding to needs of petroleum development of the Alaska continental shelf is managed by the Outer Continental Shelf Environmental Assessment Program (OCSEAP) Office.

REFERENCES

- Cacchione, D.A., and Drake, D.E., 1978, Sediment transport in Norton Sound, northern Bering Sea: in: Environmental Assessment of the Alaskan Continental Shelf, Annual Report of Principal Investigators for the year ending March 1978, Environmental Research Laboratory, Boulder, Colorado, NOAA, U.S. Dept. of Commerce, v. 12, p. 308-450.
- Cacchione, D.A., and Drake, D.E., 1979, Bottom shear stress generated by waves and currents in the northern Bering Sea, in: Abstracts volume, International Association of Sedimentologists, International meeting on Holocene marine sedimentation in the North Sea Basin, paper no. 71.
- Clukey, E.C., Cacchione, D.A., and Olsen, H.W., (in prep.), Storm generated liquefaction in bottom sediment of Norton Sound, Alaska.
- Coachman, L.K., Aagaard, K., and Tripp, R.B., 1976, Bering Strait: The Regional Physical Oceanography, Seattle, Washington University Press, 186 p.
- Dupré, W.R., and Thompson, R., 1979, The Yukon delta: A model for deltaic sedimentation in an ice-dominated environment: Proc. Offshore Technical Conference, paper no. 3434, p. 657-661.
- Fathauer, T.F., 1975, The great Bering Sea storms of 9-19 November, 1974: Weatherwise Magazine, American Meteorological Society, v. 28, p. 76-83.
- Flemming, R.H., and Heggarty, D., 1966, Oceanography of the southeastern Chukchi Sea, in: Wilimovsky, N.J., and Wolf, J.M., eds., Environment of Cape Thompson Region, Alaska: U.S. Atomic Energy Commission, p. 679-694.
- Holmes, M.L., 1979a, Distribution of gas-charged sediment in Norton Basin, northern Bering Sea, in: Abstracts volume, International Association of Sedimentologists, International meeting on Holocene marine sedimentation in the North Sea Basin, paper no. 78.

- Holmes, M.L., 1979b, Distribution of gas-charged sediment in Norton Sound and Chirikov Basin: in Environmental Assessment of the Alaskan Continental Shelf, Annual Report of Principal Investigators for the year ending March 1979, Environmental Research Laboratory, Boulder, Colorado, NOAA, U.S. Dept. of Commerce (in press).
- Hopkins, D.M., Nelson, C.H., Perry, R.B., and Alpha, T.R., 1976, Physiographic subdivisions of the Chirikov Basin, northern Bering Sea: U.S. Geological Survey Professional Paper 759-B, 7 p.
- Hunter, R., and Thor, D.R., 1979, Depositional and erosional features of the northeastern Bering Sea inner shelf, in: Abstracts volume, International Association of Sedimentologists, International meeting on Holocene marine sedimentation in the North Sea Basin, paper no. 80.
- Kvenvolden, K.E., Rapp, J.B., and Nelson, Hans, 1978, Low molecular weight hydrocarbons in sediments from Norton Sound: Am. Assoc. Petroleum Geologists Bulletin., (abs.), v. 62, p. 534.
- _____, Weliky, K., and Nelson, Hans, 1979a, Submarine seep of carbon dioxide in Norton Sound, Alaska: Science, v. 205, p. 1264-1266.
- _____, Redden, G.D., Nelson, C.H., 1979b, Gases in nearsurface sediment of the northern Bering Sea, in: Abstracts volume, International Association of Sedimentologists, International meeting on Holocene marine sedimentation in the North Sea Basin, paper no. 82.
- _____, Nelson, Hans, Thor, D.R., Larsen, M.C., Redden, G.D., Rapp, J.B., and Des Marais, D.J., 1979c, Biogenic and thermogenic gas in gas-charged sediment of Norton Sound, Alaska: Proceedings Offshore Technical Conference, Paper No. 3412.
- Larsen, M.C., Nelson, Hans, and Thor, D.R., 1979, Continuous seismic reflection data, S9-78-BS cruise, northern Bering Sea: U. S. Geological Survey Open File Report 79-1673, 7 p.

_____, _____, _____, 1980, Geologic implications and potential hazards of scour depressions on Bering shelf, Alaska: *Environmental Geology*, v. 3, no. 1, p. 39-47 (in press).

McManus, D.A., Kolla, V., Hopkins, D.M., and Nelson, C.H., 1977, Distribution of bottom sediments on the continental shelf, northern Bering Sea: U.S. Geological Survey Professional Paper 759-C, 31 p.

Nelson, C.Hans, (in prep.), Graded storm sand layers offshore from the Yukon Delta, Alaska.

_____, 1977, Storm surge effects, in: Environmental assessment of the Alaskan continental shelf, Annual Report of the Principal Investigators for the year ending March 1977, Environmental Research Laboratory, Boulder, Colorado, NOAA, U.S. Department of Commerce, v. 18, p. 111-119.

_____, and Hopkins, D.M., 1972, Sedimentary processes and distribution of particulate gold in the northern Bering Sea: U.S. Geological Survey Professional Paper 689, 27 p.

_____, and Creager, J.S., 1977, Displacement of Yukon-derived sediment from Bering Sea to Chukchi Sea during the Holocene: *Geology*, v. 5, p. 141-146.

_____, Field, M.E., Cacchione, D.A., and Drake, D.E., 1978b, Activity of mobile bedforms on northeastern Bering shelf, in: Environmental Assessment of the Alaskan Continental Shelf, Annual Report of Principal Investigators for the year ending March 1978, Environmental Research Laboratory, Boulder, Colorado, NOAA, U.S. Dept. of Commerce, v.12 p. 291-307.

_____, _____, and Dupré, W.R., 1979, Linear sand bodies on the Bering epicontinental shelf, in: Abstracts volume, International Association of Sedimentologists, International meeting on Holocene marine sedimentation in the North Sea Basin, paper no. 90.

- _____, Holmes, M.L., Thor, D.R., and Johnson, J.L., 1978a, Continuous seismic reflection data, S5-76-BBS cruise, northern Bering Sea: U.S. Geological Survey Open File Report 78-609, 6 p.
- _____, Kvenvolden, K.E., and Clukey, E.C., 1978c, Thermogenic gas in sediment of Norton Sound, Alaska, Proceedings of Offshore Technical Conference, 1978, Paper No. 3354, p. 1612-1633.
- _____, Thor, D.R., Sandstrom, M.W., and Kvenvolden, K.A., (1980), Modern biogenic gas-generated craters (sea-floor "pockmarks") on the Bering shelf, Alaska. Geological Society of America Bulletin (in press).
- Olsen, H.W., Clukey, E.C., and Nelson, C.H., 1979, Geotechnical characteristics of bottom sediments in the northern Bering Sea in: Abstracts volume, International Association of Sedimentologists, International meeting on Holocene marine sedimentation in the North Sea Basin, paper no. 91.
- Sallenger, A.H., Dingler, J.R., and Hunter, R., 1978, Coastal processes and morphology of the Bering Sea coast of Alaska, in: Environmental Assessment of the Alaskan Continental Shelf, Annual Report of Principal Investigators for the year ending March 1978, Environmental Research Laboratory, Boulder, Colorado, NOAA, U.S. Dept. of Commerce, v. 12, p. 451-470.
- Thor, D.R., and Nelson, Hans, 1978, Continuous seismic reflection data. S5-77-BS cruise, northern Bering Sea: U.S. Geological Survey Open File Report 78-608, 8 p.
- _____, _____, and Williams, R.O., 1978, Environmental geologic studies in northern Bering Sea, in: Blean, K.M., ed., U.S. Geological Survey in Alaska, Accomplishments during 1977: U.S. Geological Survey Circular 772-B, p. B94-B95.

_____, _____, 1979, A summary of interacting surficial geologic processes and potential geologic hazards in the Norton Basin, northern Bering Sea: Proceedings Offshore Technical Conference, Paper No. 3400, p. 377-381.

_____, _____, (1980), Sea ice as a geologic agent on the subarctic Bering shelf, in: Hood, D.W., ed., The Eastern Bering Sea Shelf: Its Oceanography and Resources.

Figure Captions

- Figure 1. Sampling station locations occupied between 1967 and 1978.
- Figure 1a. Expanded version of cross-hatched area of Figure 1, showing closely spaced sampling grid offshore of Nome.
- Figure 2. Coverage of geophysical surveys in northern Bering Sea 1967-1978.
- Figure 3. Bathymetry of northern Bering Sea in 10-m contour intervals.
- Figure 4. Summary of potentially hazardous areas of northern Bering Sea (from Thor and Nelson, 1979).
- Figure 5. Distribution and density of ice gouging, movement direction of pack ice, and limits of shorefast ice in northern Bering Sea (from Thor and Nelson, 1979).
- Figure 6. Location of scour depressions, extensive scour and ripple zones, and strong bottom currents in Norton Sound, showing area of storm sand deposition (modified from Larsen et al., 1980).
- Figure 7. Distribution and density of craters on sea floor of Norton Sound, showing isopachs of Holocene mud derived from Yukon River and deposited since Holocene postglacial sea-level rise (from Thor and Nelson, 1979).

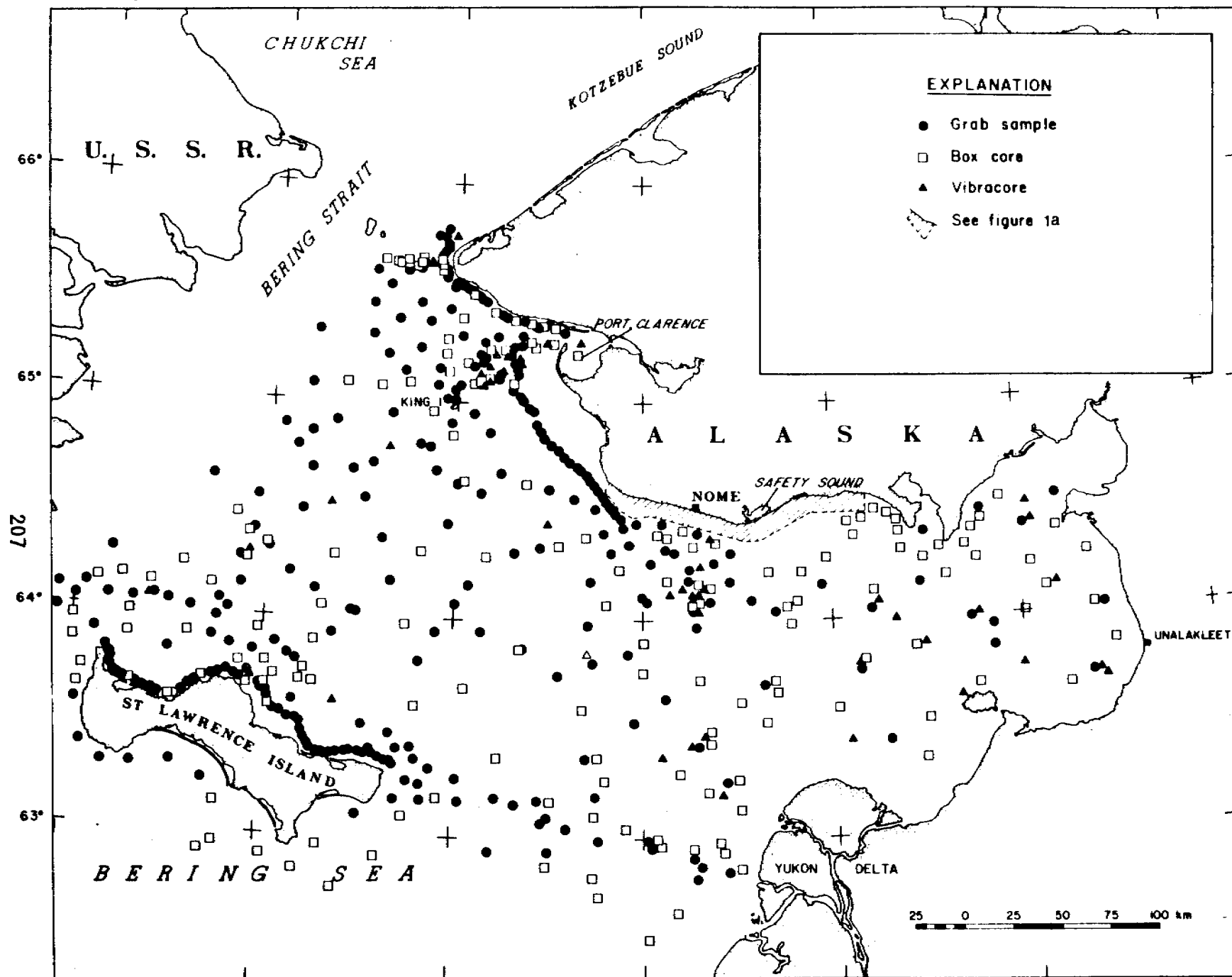


Fig. 1 - Sampling station locations occupied between 1967 and 1978.

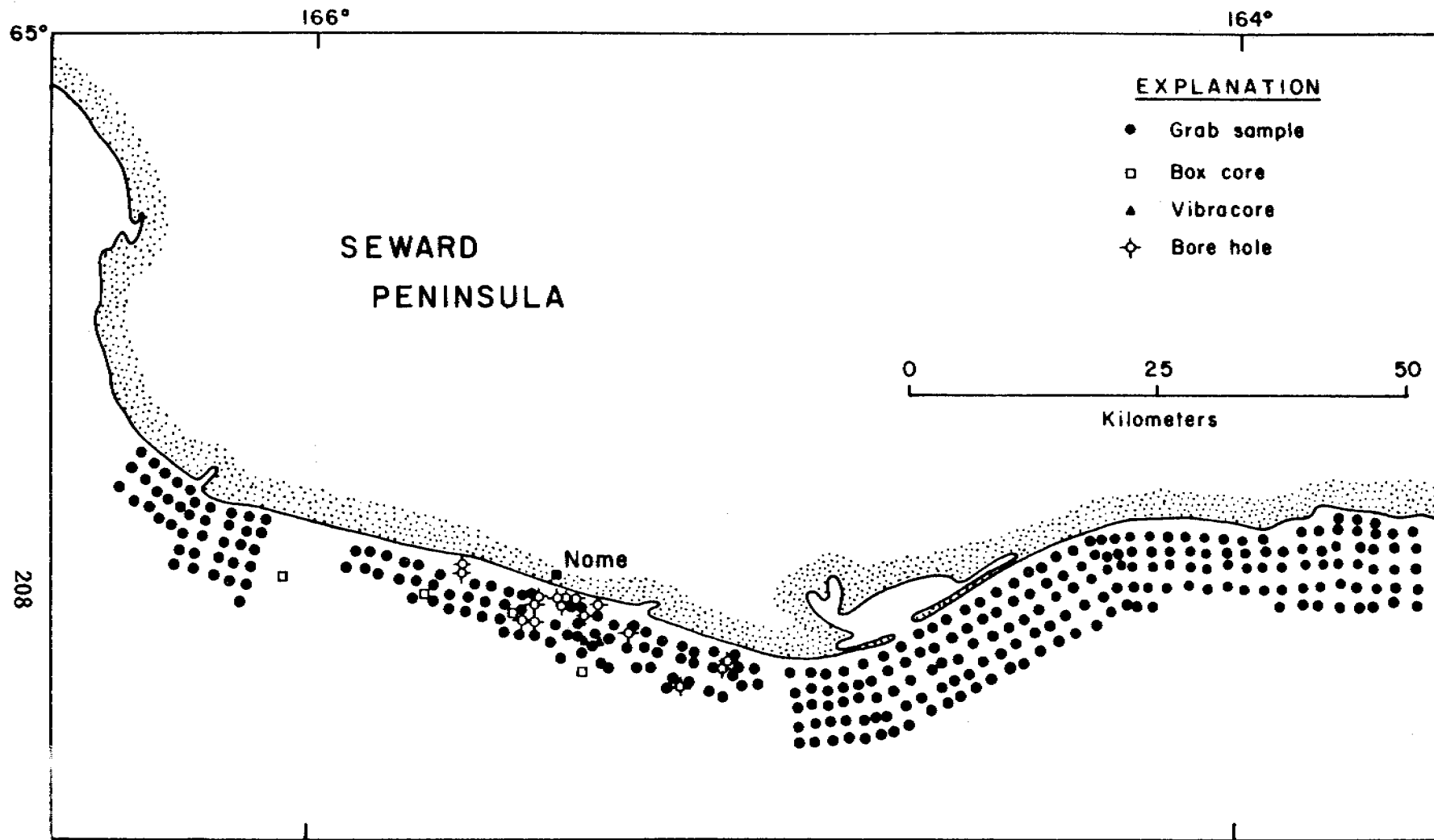


Fig. 1a - Expanded version of cross-hatched area of Figure 1, showing closely spaced sampling grid offshore of Nome.

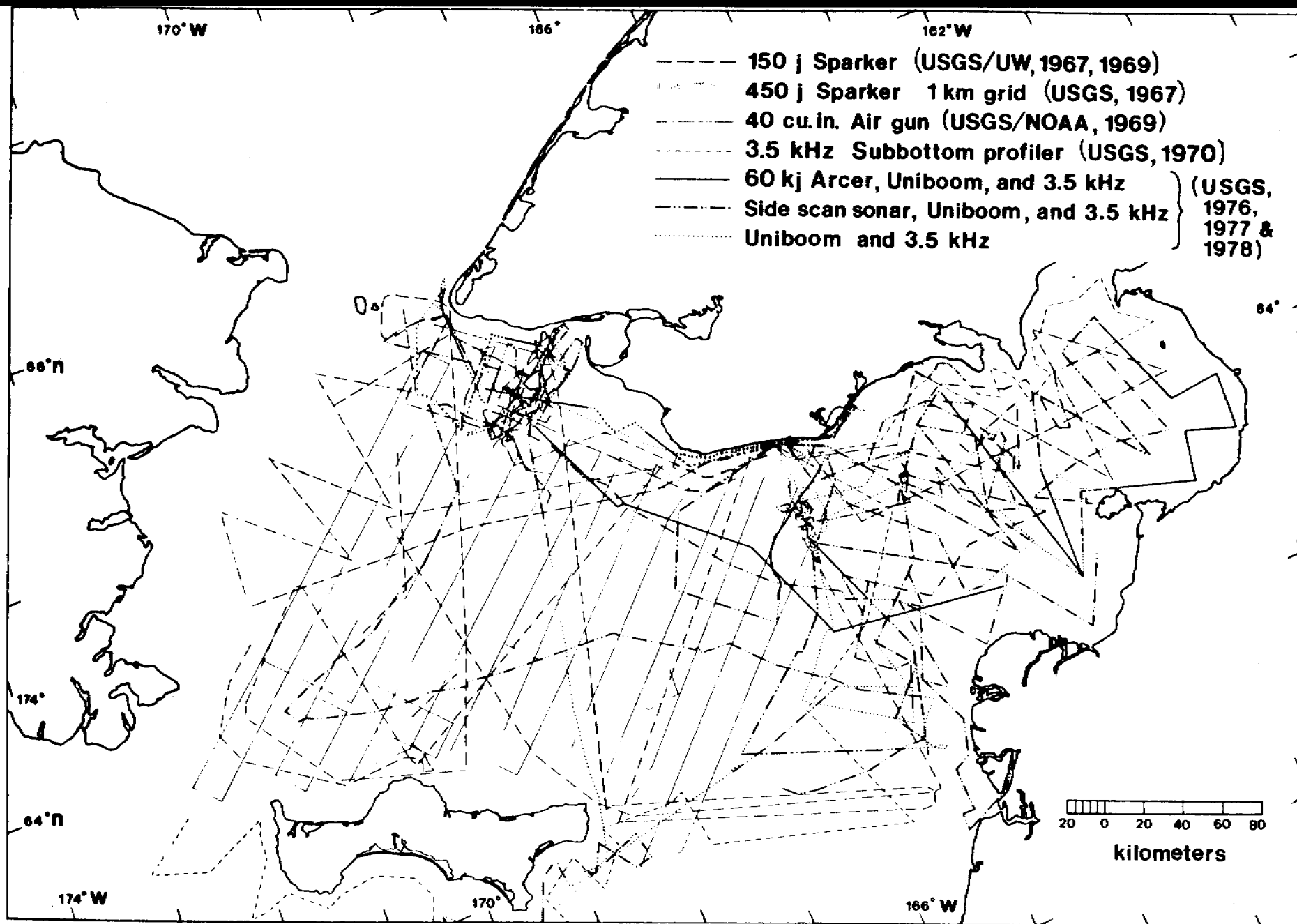


Fig. 2 - coverage of geophysical surveys in northern Bering Sea 1967-1978.

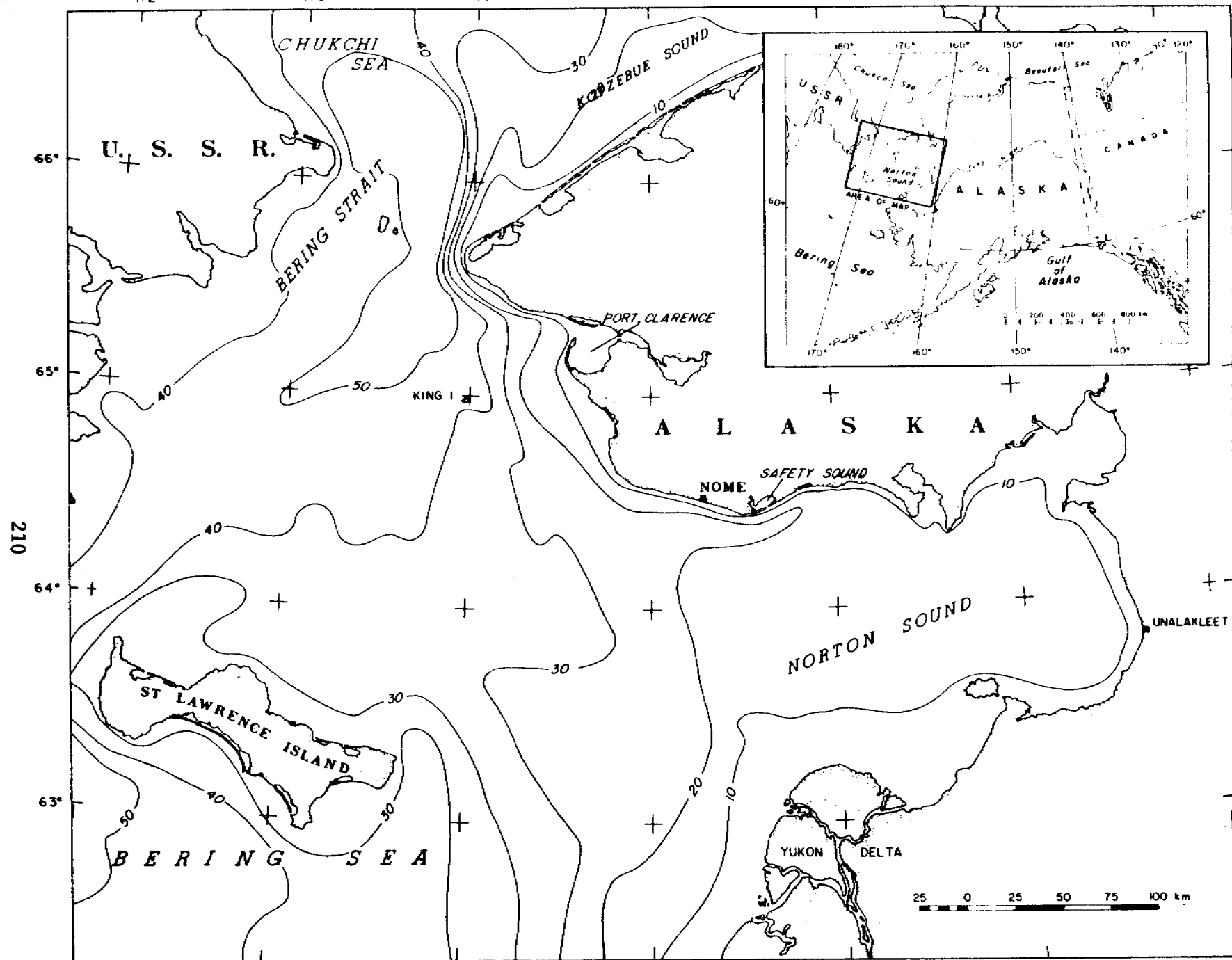


Fig. 3 - Bathymetry of northern Bering Sea in 10-m contour intervals.

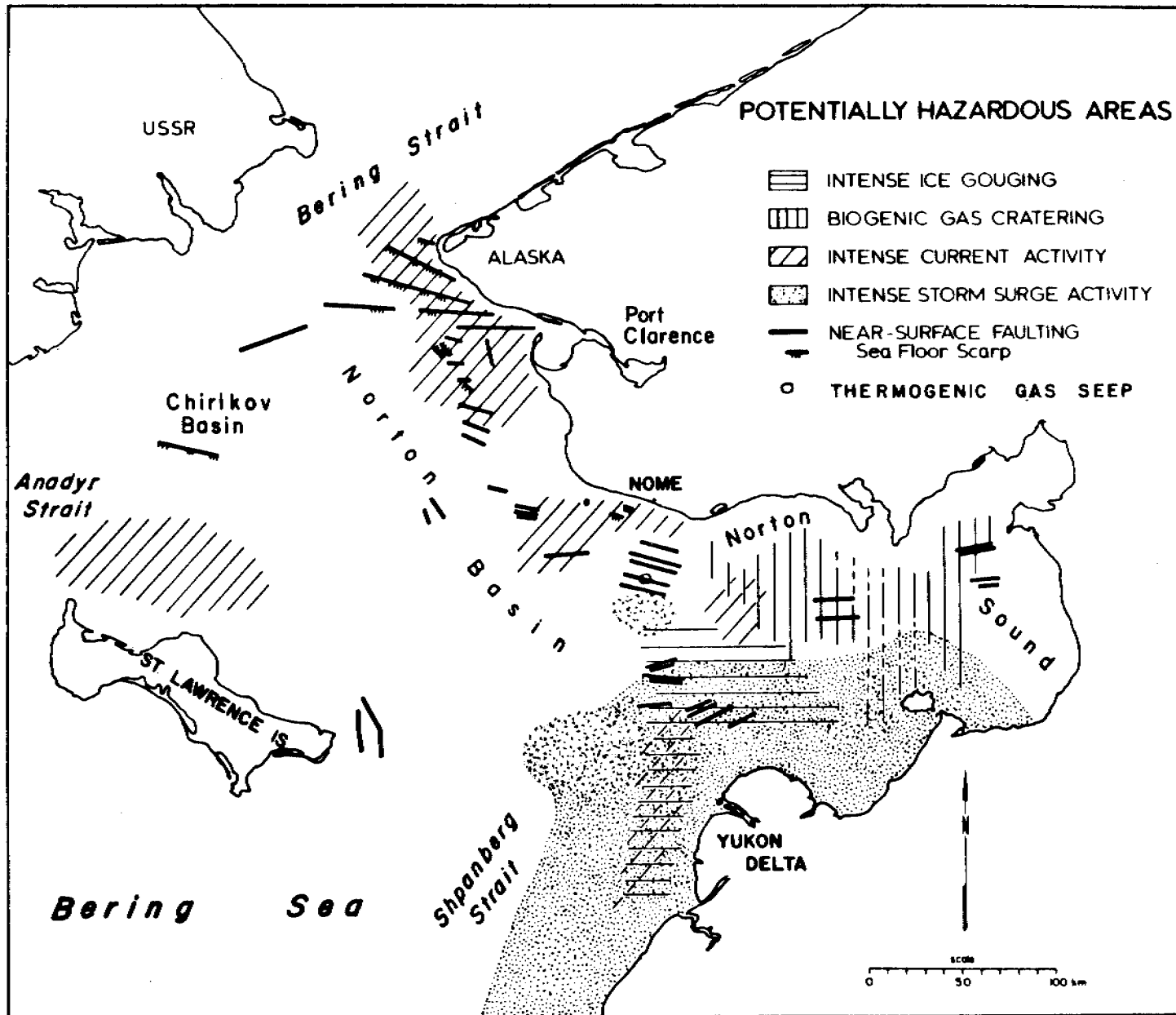


Fig. 4 - Summary of potentially hazardous areas of northern Bering Sea (from Thor and Nelson, 1979).

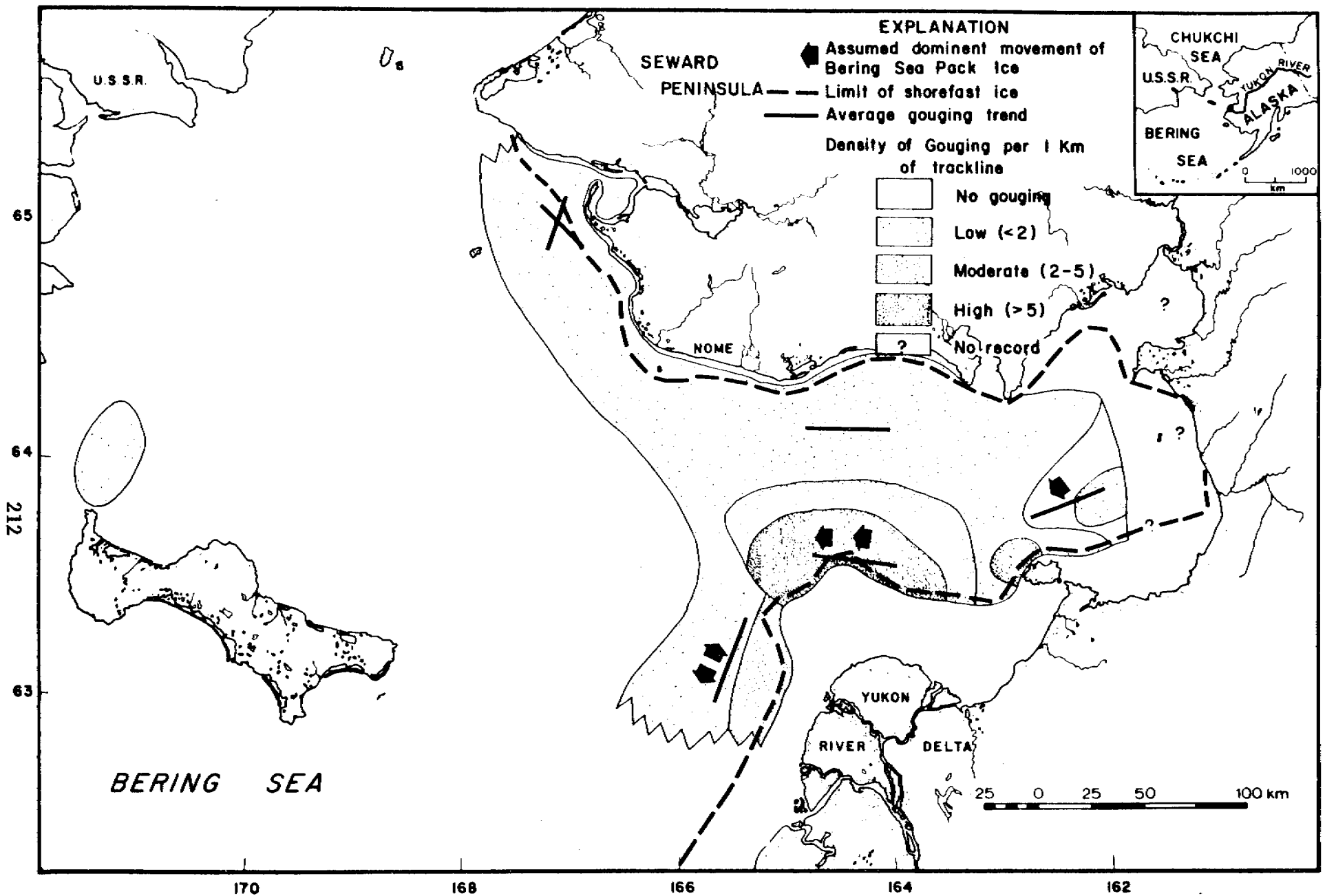


Fig. 5 - Distribution and density of ice gouging, movement direction of pack ice, and limits of shorefast ice in northern Bering Sea (from Thor and Nelson, 1979).

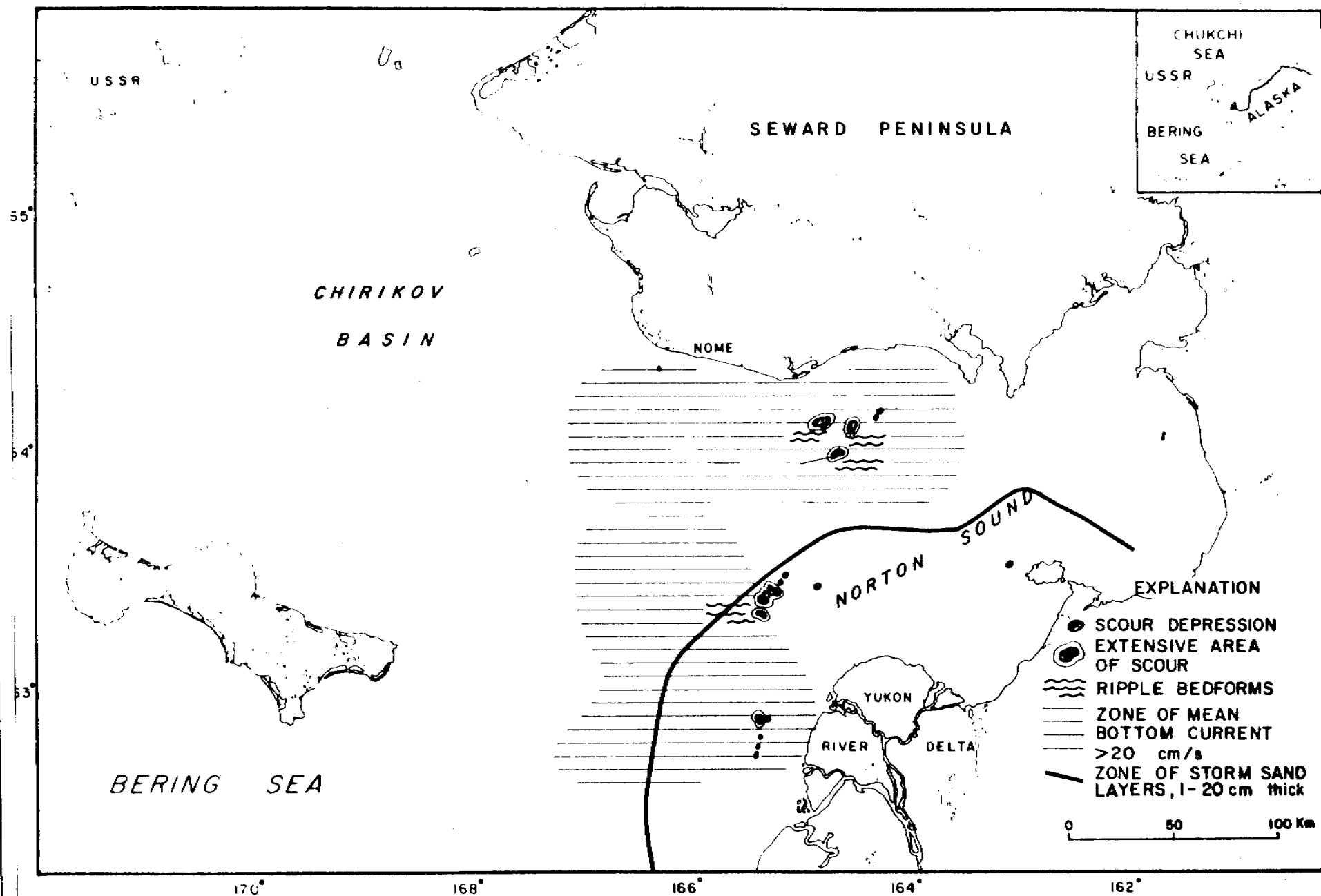


Fig. 6 - Location of scour depressions, extensive scour and ripple zones, and strong bottom currents in Norton Sound, showing area of storm sand deposition (modified from Larsen et al., 1980).

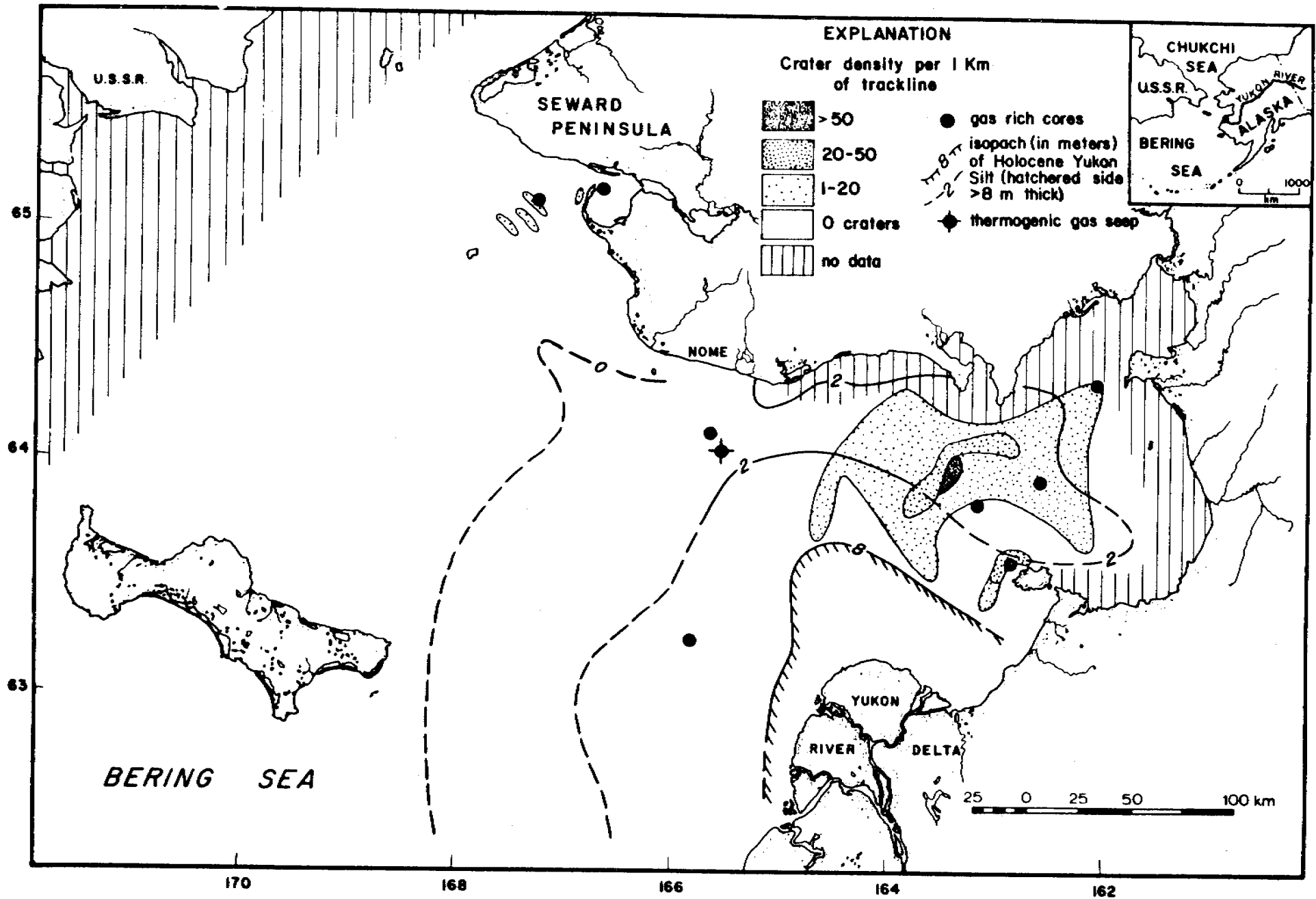


Fig. 7 - Distribution and density of craters on sea floor of Norton Sound, showing isopachs of Holocene mud derived from Yukon River and deposited since Holocene postglacial sea-level rise (from Thor and Nelson, 1979).

HYDROCARBON GASES IN NEAR-SURFACE SEDIMENT OF NORTHERN
BERING SEA (NORTON SOUND AND CHIRIKOV BASIN)

Keith A. Kvenvolden, George D. Redden,
Devin R. Thor, and C. Hans Nelson

U.S. Geological Survey, Menlo Park, California 94025

ABSTRACT

Methane, ethane, ethene, propane, propene, *n*-butane, and isobutane are common in bottom sediment of the northern Bering Sea. At eight sites the content of methane rapidly increases downward within the first four meters of sediment. These concentration gradients, and absolute methane concentrations, indicate that the interstitial water of the near-surface sediment at these sites may be gas saturated. These gas-charged sediments may be unstable, creating potential geologic hazards and, in certain areas, causing the formation of seafloor craters.

The isotopic compositions of methane at four of the sites range from -69 to -80‰ ($\delta^{13}\text{C}_{\text{PDB}}$). This range of values clearly indicates that the methane derives from microbial processes, possibly within the near-surface Pleistocene peat deposits that are common throughout the northern Bering Sea. At one site in Norton Sound, near-surface sediment is charged with CO_2 , accompanied by minor concentrations of hydrocarbons, that is seeping from the seafloor. Methane in this gas mixture has an isotopic composition of -36‰, a value that suggests derivation from thermal processes at depth in Norton Basin.

The presence of sediment charged with methane or CO_2 cannot in general be predicted from analyses of surface sediment, which usually contains hydrocarbon gases and CO_2 at low concentrations. Sampling beneath a sediment depth of about 0.5 m is generally required to detect high concentrations of gas. Acoustic anomalies detected on high-resolution seismic records indicate the presence of gas-charged sediment, but gas analyses of sediment samples from areas with these anomalies do not always confirm that high concentrations of gas are there. Conversely, high concentrations of methane are sometimes found at sites where no acoustic anomalies are obvious on high-resolution records.

INTRODUCTION

About twenty years ago Emery and Hoggan (1958) described the occurrence of hydrocarbon gases in near-surface marine sediment from Santa Barbara Basin, off southern California. These anoxic sediments contain methane, ethane, propane, butanes, pentanes, and hexanes, with methane being one to almost five orders of magnitude greater in concentration than any of the other hydrocarbons. Geochemical studies that followed have generally focused on methane and the processes that can account for its occurrence and distribution in a variety of aquatic sediments (Reeburgh, 1969; Whelan, 1974; Martens and Berner, 1974; Claypool and Kaplan, 1974; Oremland, 1975; Barnes and Goldberg, 1976; and Kosiur and Warford, 1979). Recently Bernard et al. (1978) described the distribution of methane, ethene, propane, and propene in sediment from shelf and slope sediment in the Gulf of Mexico, and Kvenvolden and Redden (1980) reported on the occurrence of these gases in sediment from the outer shelf, slope and basin of the Bering Sea. The present study examines inner shelf areas of the Bering Sea and considers the hydrocarbon gases methane (C_1), ethane (C_2), ethene ($C_{2:1}$), propane (C_3), propene ($C_{3:1}$), isobutane ($i-C_4$), and n -butane ($n-C_4$) in sediment of the inner Bering Shelf in Norton Sound and the adjacent eastern Chirikov Basin (Fig. 1).

Norton Sound is an elongate, east-west trending bay in the western coast of Alaska bounded on the north by the Seward Peninsula, on the east by the Alaskan mainland, on the south by the Yukon Delta, and on the west by the Chirikov Basin. The floor of the sound is very flat, and water depths average about 20 m. To the west into the Chirikov Basin water depths increase to about 50 m, especially in the northern part of the basin at the Bering Strait.

When sea level lowered in late Pleistocene time, the floor of Norton Sound and

eastern Chirikov Basin became exposed (Nelson and Hopkins, 1972). During this time fluvial processes and tundra vegetation characterized the area (Hopkins, 1967), and peaty mud was deposited over much of the region. This mud contains 2 to 8 percent organic carbon. As sea level rose during latest Pleistocene time, marine sedimentation resumed. In Holocene time, fine-grained, sandy silt derived mainly from the Yukon River blanketed the area with a cover up to 10 m thick (McManus et al., 1977; Nelson and Creager, 1977). In contrast to the nonmarine sediment, the organic content of the overlying sediment ranges from 0.5 to 1.0 percent (Nelson, 1977).

METHODS

The analytical procedures for this work have been described previously (Nelson et al., 1978; Kvenvolden et al., 1979a). Vibracores and surface samples were taken during three summer field seasons in 1976, 1977 and 1978. Hydrocarbon gases and carbon dioxide were extracted from sediment recovered from the surface and from various intervals in cores. Sediment samples were extruded into 0.95-L double-friction-seal cans which had two septa-covered holes near the top. Helium-purged distilled water was added to each can until a 100-mL headspace remained. Each can was closed with a lid, and the headspace was purged with helium through the septa. The cans were shaken for ten minutes to release gases into the headspace. Exactly one milliliter of the headspace gas mixture was analyzed by gas chromatography using both flame ionization (for hydrocarbons) and thermal conductivity (for carbon dioxide) detectors. Calculations of gas concentrations were determined by peak height measurements on chromatograms. Partition coefficients were used to correct for the different solubilities of the hydrocarbon gases. Concentrations are reported in nL, μ L, or mL per liter of wet sediment.

RESULTS

C_1 is the most abundant hydrocarbon gas found in the first five meters of

sediment in Norton Sound and the eastern Chirikov Basin. Figure 2 shows the geographic distribution of maximum concentrations of C_1 . At eight sites this concentration exceeds 1 mL/L, and at five of these sites (8-4, 8-8, 8-15, 8-21 and 8-22) concentrations exceed 10 mL/L. At the other stations the maximum amount of C_1 measured was less than 100 μ L/L with two exceptions at 7-33 and 8-6 where it was about 200 μ L/L at each site. The amount of C_1 found depends to some extent on the depth of core, for concentrations of C_1 generally increase with depth. Thus, surface samples and short cores usually have lower amounts of C_1 than do samples taken from greater depths. The vertical distribution of C_1 at the eight sites mentioned above is shown in Figure 3. For these sites the concentration of C_1 increases by 4 or 5 orders of magnitude within the top four or five meters of sediment. Also shown is the distribution of methane at Sites 7-17 and 8-3. The data for these sites are combined because the sites are at essentially the same location sampled during two different field seasons. Here the C_1 concentrations, especially in deeper samples, are much lower than at the eight sites. The major gas at 7-17/8-3 is not C_1 but CO_2 .

The second most abundant hydrocarbon gas in this area is C_2 ; C_3 concentrations are usually slightly lower and generally parallel C_2 concentration profiles with depth. The geographic distribution of $C_2 + C_3$ is shown in Figure 4. The maximum concentrations of these two hydrocarbons are usually less than 1 μ L/L. At two sites, 8-4 and 8-17, maximum $C_2 + C_3$ concentrations are slightly higher (1.2 and 1.1 μ L/L, respectively), but at Site 7-17/8-3, $C_2 + C_3$ maximum concentration is almost 8 μ L/L. At the eight sites where C_1 show 4-5 orders of magnitude increase in concentrations with depth, $C_2 + C_3$ increases by about two orders, but the profiles of concentration are more variable (Fig. 5) than the C_1 concentration profile (Fig. 3). The concentrations of $C_2 + C_3$ in samples from 7-17/8-3 are much higher than in all other samples.

Both $C_{2:1}$ and $C_{3:1}$ are present in all samples analyzed. Concentrations are variable, but as a general rule $C_{2:1}$ exceeds C_2 in surface samples and with increasing depth the reverse is observed. At Site 7-17/8-3, C_2 is much more abundant than $C_{2:1}$, with the $C_2/C_{2:1}$ ratio reaching a maximum of 340 at 60 cm depth. A similar relation holds for $C_{3:1}$ and C_3 . At the surface $C_{3:1}$ is usually more abundant than C_3 , and the reverse is true for deeper samples. At 7-17/8-3, C_3 is always more abundant than $C_{3:1}$ being larger by a factor of 47 at 200 cm depth.

The concentrations of $i-C_4$ and $n-C_4$ are lower in concentration than the lighter hydrocarbon gases and in many cases reach the limit of detection of the method, about 2 nL/L. In general the concentrations of $i-C_4 + n-C_4$ are less than 100 nL/L, and the distribution with depth is variable. In samples from 7-17/8-3, concentrations of $i-C_4 + n-C_4$ reach a maximum of 14 μ L/L at a depth of 200 cm.

Hydrocarbons from C_5 to C_7 are measured in a single backflush peak from chromatography and are designated C_{5+} . C_{5+} hydrocarbons commonly occur in low concentrations in surface samples from this area and in core samples from 7-17/8-3.

BIOGENIC METHANE

The occurrence in anoxic sediment of high concentrations of C_1 resulting from microbial decomposition of organic matter is well established (Emery and Hoggan, 1958; Barnes and Goldberg, 1976; Reeburgh and Heggie, 1977; and Kosiur and Warford, 1979). C_1 is both produced and consumed by microorganisms, and models for these processes have been devised (Claypool and Kaplan, 1974; Martens and Berner, 1974; Barnes and Goldberg, 1976; Kosiur and Warford, 1979). In less reducing sediments of open marine environments, C_1 is also present but at concentrations as much as five orders of magnitude less than those observed in

anoxic marine sediments (Bernard et al., 1978; Kvenvolden and Redden, 1980). Although there is much less C_1 in sediments of open marine environments, the processes that generate gas are probably similar to those in anoxic sediments, but much slower.

At eight sites in Norton Sound and the eastern Chirikov Basin abundances of C_1 increase by four or five orders of magnitude within the first five meters of sediment, reaching concentrations near or exceeding saturation of the interstitial water. These shallow sediments are likely anoxic, and the C_1 probably is being generated by the decomposition of peaty mud that contains 2 to 8 percent organic carbon, and is buried under marine sediment of lower carbon content (0.5 to 1.0 percent). This sediment cover is thickest near the front of the Yukon Delta and thins to the north (McManus et al., 1977; Nelson and Crea-ger, 1977; Nelson, 1977). The depth of burial of the peaty mud may account for the groupings of the C_1 concentration profiles shown in Figure 3. Seven of the sites (6-121, 6-125, 6-131, 8-4, 8-8, 8-15, and 8-21) have profiles that group together. These seven sites are located in the eastern and northern parts of Norton Sound and in the Chirikov Basin near Port Clarence (Fig. 2). In these areas, peaty sediment is buried under about 2 meters of sandy silt. The seven profiles show maximum concentrations below about 1.5 meters. Therefore, if peaty mud is the source of the methane, the depth of its burial accounts for the depth at which high C_1 concentrations are found. In contrast, one C_1 concentration profile (8-22) reaches maximum values below 3 meters. This site was located northwest of the Yukon Delta in the southern part of Norton Sound where the sediment cover is thicker and the peaty mud is more deeply buried. Thus there is a correlation between the depth of buried organic matter and the depth at which C_1 concentrations reach high values. At Site 7-17/8-3, C_1 concentrations follow a different trend to be discussed below.

That the high concentrations of C_1 at eight sites result from microbiological

processes is supported by both chemical and isotopic data. Higher molecular weight hydrocarbons accompany C_1 , and the ratio $C_1/(C_2 + C_3)$ can be used as a guide to interpret mode of formation. Likewise, the carbon isotopic composition of C_1 can be used to interpret process of formation (Bernard et al., 1976, 1977). Microbial degradation of organic matter produces hydrocarbon gases with $C_1/(C_2 + C_3)$ ratios greater than 1000, and with $\delta^{13}C_{1PDB}$ lighter than -60‰ . Table 1 shows these parameters for samples from the eight sites. Clearly, based on the criteria stated above, the C_1 at the eight sites was derived from microbiological processes, and the buried peaty mud, in which the organic carbon has an isotopic composition of -28‰ (Kvenvolden et al., 1979 a,b) is the likely source.

Other sites may exist in Norton Sound and eastern Chirikov Basin where C_1 concentrations exceed 1 mL/L. Finding these locations will require sampling below about one meter of sediment (three meters or more off the Yukon Delta), because the occurrence of high amounts of C_1 at shallow depths is not manifest at the surface. The surface layer of sandy silt either seals the C_1 preventing its migration to the surface or the rate of consumption or diffusion of C_1 in the upper meter is very rapid, leading to low concentrations of C_1 at the surface. At two sites, 8-6 and 7-33 (Fig. 2), maximum concentrations of C_1 of 224 and 196 $\mu\text{L/L}$, respectively, may hint that much higher concentrations are present at greater depths. At Site 7-33, the deepest sample (Fig. 1) came from 70 cm. If this sample, containing 196 $\mu\text{L/L}$, were plotted on Figure 3 it would fall within the envelope of C_1 -concentration profiles of cores in which C_1 exceeds 1 mL/L at depth. The case for Site 8-6 is not so clear. The sample containing 224 $\mu\text{L/L}$ comes from a depth of 220 cm (Fig. 1). If plotted on Figure 3, this value would fall below the envelope of C_1 -concentration profiles. At Site 8-6, peaty mud may be more deeply buried than at other sites in northern Norton Sound. Only deeper sampling can directly verify the presence of higher

Table 1.

$C_1/(C_2+C_3)$ ratios and $\delta^{13}C_1$ values for samples containing C_1 concentrations in excess of 1 mL/L

Site	Maximum $C_1/(C_2+C_3)$	$\delta^{13}C_1$ * (‰)
8-4	24000	-80 ¹
8-8	71000	nd
8-15	28000	nd
8-21	440000	nd
8-22	88000	nd
6-121	6500	-72 ²
6-125	28000	-69 ²
6-131	5400	-75 ²

* relative to the PDB standard

¹Kvenvolden et al. (1979a,b)

²Nelson et al. (1979)

amounts of C_1 . At other sites in Norton Sound and eastern Chirikov Basin, C_1 concentrations are below 100 $\mu\text{L/L}$ and at many sites below 10 $\mu\text{L/L}$ (Fig. 2).

POSSIBLE BIOLOGIC ORIGIN OF OTHER HYDROCARBONS

Besides C_1 , other hydrocarbon gases are present in these sediments, but quantitatively, they have much less significance than C_1 . The maximum concentrations of $C_2 + C_3$ are in the same range as the minimum concentrations of C_1 . At sites where C_1 increases rapidly with depth (Fig. 3), $C_2 + C_3$ also generally increases (Fig. 5) but much more slowly than C_1 . Concentrations of $i-C_4$ and $n-C_4$ are even lower than concentrations of $C_2 + C_3$, and the $i-C_4 + n-C_4$ concentrations are erratic with depth. As a generalization, however, the abundances of the higher hydrocarbons, C_2 , C_3 and C_4 , are greater in samples where concentrations of C_1 are larger. Therefore, the processes that produce C_1 may also be responsible in part for the generation of the higher hydrocarbons. Microbiological production and consumption provides a reasonable mechanism to account for C_1 at the eight sites where C_1 concentrations increase beyond 1 mL/L. Therefore, microbial processes may also explain the occurrence of the higher molecular weight hydrocarbons, although evidence for this process remains circumstantial. Laboratory experiments have demonstrated the microbial formation of C_2 and C_3 (Davis and Squires, 1954). Thus, there is support for the suggestion that the C_2 and the C_3 hydrocarbons at these sites can come from microbial processes, but there is no precedent in the literature on microbiology for the production of C_4 hydrocarbons.

The presence and distribution of $C_{2:1}$ is probably controlled by biological processes, but these processes likely differ from those which account for the very high C_1 concentrations. These unsaturated hydrocarbons have been formed by microbial action in the laboratory (Davis and Squires, 1954), and $C_{2:1}$ is produced in soils by bacteria (Primrose and Dilworth, 1976). In the sediment the process seems to take place uniformly, because there is no obvious concentration gradient with depth. In surface samples concentrations of $C_{2:1}$ and $C_{3:1}$ are

larger respectively than concentrations of C_2 and C_3 . With depth, concentrations of C_2 and C_3 increase slightly so that below the surface ratios of $C_2/C_{2:1}$ and $C_3/C_{3:1}$ are usually equal to or greater than one.

THERMOGENIC HYDROCARBONS

The above discussion focused mainly on sites where C_1 concentration increases rapidly with depth, and consideration has been given to the heavier

hydrocarbons associated with this C_1 . At one site, 7-17/8-3, however, C_1 concentrations are not unusually high, less than 100 $\mu\text{L/L}$ (Fig. 3), but concentrations of $C_2 + C_3$ (Fig. 5) and $i\text{-}C_4 + n\text{-}C_4$ are unusually large relative to concentrations seen elsewhere in the sediments of this area, or for that matter, anywhere else in marine sediments off Alaska.

Site 7-17/8-3 has been studied in great detail since anomalous hydrocarbon concentrations were first discovered in the water column at the site (Cline and Holmes, 1977). Nelson et al. (1978) showed that the sediments here also contain anomalous hydrocarbon concentrations. Kvenvolden et al. (1979a, b) confirmed the hydrocarbon chemistry and discovered that the major gas component within the sediment and escaping into the water column is CO_2 . The $C_1/(C_2+C_3)$ ratios in sediment at this site are less than 10 and the $\delta^{13}\text{C}_1$ is -36‰ . These numbers differ greatly from those discussed earlier where microbiological processes were inferred.

The hydrocarbons at Site 7-17/8-3 are likely derived from thermochemical processes, judging from the molecular distribution of C_1 , C_2 , and C_3 and the isotopic composition of C_1 . In addition, anomalously high concentrations of $i\text{-}C_4$, $n\text{-}C_4$ and C_{5+} (gasoline-range hydrocarbons) support the mechanism of thermochemical processes (Kvenvolden and Claypool, unpublished). Heat for this process must be available at depth in Norton Basin. The hydrocarbons resulting from the thermal decomposition of organic matter within the basin must migrate along with CO_2 up fault zones to the surface and escape as a seep. Although the hydrocarbon

chemistry indicates that the hydrocarbons at Site 7-17/8-3 likely migrate from depth, the concentration profiles (Figs. 3 and 5) indicate that special conditions of migration must exist. The fact that hydrocarbons are leaking into the water column suggests that surface sediments should contain large amounts of these hydrocarbons. On the contrary, surface samples at this site contain very low concentrations of hydrocarbons. In fact, surface samples (0-10 cm) at this site show no evidence of the high concentrations of hydrocarbons deeper in the sediment. The gradients of C_1 (Fig. 3), $C_2 + C_3$ (Fig. 5) and $i-C_4 + n-C_4$ decrease rapidly toward the sediment surface. This rapid decrease and lack of significant quantities of hydrocarbons at the sediment surface can be explained by rapid diffusion of hydrocarbons into the water column from the first few centimeters of sediment or the presence of discrete gas vents that pipe the hydrocarbons through the sediment leaving few hydrocarbons remaining in the sediment. The second explanation is more reasonable, because active gas vents were seen by television in 1978 (Kvenvolden et al., 1979a). The concentration profiles (Figs. 3 and 5) at Site 7-17/8-3 reach a maximum value at about 1 to 2 meters depth and then decrease. This profile suggests that migration from greater depths does not involve diffusion of hydrocarbons within the underlying sediment but rather that the hydrocarbons are following distinct conduits such as faults. Near the surface the hydrocarbons are dispersed into the sediment where they eventually vent along with CO_2 into the water. That the hydrocarbons from this seep are present in the water column has been documented by Cline and Holmes (1977). The waters of Norton Sound and the eastern Chirikov Basin also contain a regional distribution of hydrocarbon gases (Cline et al., 1978) whose sources, in part, may be the underlying surface and near-surface sediment.

GEOPHYSICAL EVIDENCE

The presence of gas in near-surface sediments can cause acoustic anomalies

on high-resolution geophysical records where the gas is no longer in solution in the interstitial water but takes the form of bubbles. Schubel (1974), for example, demonstrated how high concentrations of gas affect acoustic properties of sediments. At the eight sites where C_1 concentrations exceeded 1 mL/L and may have reached and exceeded interstitial water solubility, bubble-phase C_1 may be present. Acoustic anomalies would be expected on high-resolution records from these sites if free gas is indeed present.

Geophysical transects, utilizing 800-J boomer, 3.5 kHz subbottom profiler and 120 kJ sparker systems, indicate that near-surface acoustic anomalies are widespread in Norton Sound. Figure 6 shows those sites, sampled for hydrocarbon gases, at which acoustic anomalies are seen on geophysical records. At three sites (6-125, 8-4, and 8-21), acoustic anomalies correspond to samples having high concentrations of C_1 . The acoustic anomaly and associated C_1 at 8-4 were discussed in detail by Kvenvolden et al. (1979a,b). The characteristics of the acoustic anomaly at 8-21 suggest that the cause may be controlled more by the presence of glacial till deposits than by gas. At Sites 7-17/8-3, geophysical records show both near-surface and deeper acoustic anomalies. There the sediment is charged with CO_2 rather than C_1 , and the CO_2 is escaping from the seafloor as a submarine seep, observed acoustically and by television (Kvenvolden et al., 1979a). At five sites (6-121, 6-131, 8-8, 8-15, and 8-22) on Figure 6, where high concentrations of C_1 were measured, no acoustic anomalies were detected. At sites 6-121 and 6-131 no geophysical records were obtained; therefore, it is uncertain whether or not acoustic anomalies are present at these sites. At Sites 8-8, 8-15, and 8-22, high-resolution geophysical records show no evidence of acoustic anomalies although the geochemical measurements indicate high concentrations of C_1 (Figs. 2 and 4). Apparently the gas concentrations at these sites were not in the proper range to produce anomalies on the records of the geophysical systems employed. On the other hand, acoustic anomalies were observed on

records at Sites 8-1, 8-9, and 8-10, but maximum C_1 abundances in cores at these sites were only 6, 4, and 15 $\mu\text{L/L}$, respectively. Concentrations this low are not expected to produce acoustic anomalies. In addition, acoustic anomalies were found in geophysical records at Sites 6-168, 7-22, and 7-25, but sampling at these sites was not deep enough (Fig. 1) to test the presence of high C_1 or CO_2 concentrations at depth.

High concentrations of C_1 in near-surface sediment may cause instability and may lead to crater formation whenever the gas vents abruptly into the water column. Nelson et al. (1978) discussed some preliminary engineering information related to the stability of gas-charged sediment in Norton Sound, and Nelson et al. (1979) proposed that the craters found in central Norton Sound may result from the rapid escape of gas from gas-charged sediments.

SUMMARY

Hydrocarbon gases, methane, ethane, ethene, propane, propene, isobutane, and n-butane are common in surface and near-surface sediment of Norton Sound and eastern Chirikov Basin. From a quantitative standpoint methane is the most important hydrocarbon gas. At eight sites in this area methane abundances increase with depth in the sediment by four or five orders of magnitude, reaching concentrations near or exceeding saturation of the interstitial water. The highest value measured is about 55 mL/L. This methane is probably being generated by microbial decomposition of peat that is buried with mud under a cover of fine-grained, sandy silt derived from the Yukon Delta. Maximum ratios of methane to ethane plus propane at the eight sites are large, ranging from about 5×10^3 to 440×10^3 . Carbon isotopic compositions range from -69 to -80‰ (relative to the PDB standard). These molecular and isotopic compositions strongly suggest that microbiological processes are involved in the production of at least methane. Higher molecular weight hydrocarbons are present in much lower concen-

trations than methane, but, as a general rule over the area, the trends in concentrations of the hydrocarbons, at least through propane, are roughly the same. Therefore, microbiological processes may also be responsible for the hydrocarbon gases heavier than methane.

At one site in Norton Sound the concentrations of all hydrocarbon gases are anomalous. For example, methane is anomalously low in concentration relative to the methane at the eight sites mentioned above. On the other hand, ethane, propane, and the butanes are all anomalously high in concentration. The ratios of methane to ethane plus propane are less than 10 and the isotopic composition of methane is about -36‰ . The magnitude of these parameters sharply contrasts with the values obtained elsewhere in the area and indicates that thermochemical rather than biochemical processes are at work. The maximum concentration of hydrocarbons from samples at this site is about 100 $\mu\text{L/L}$.

The major component is carbon dioxide. The carbon dioxide and hydrocarbons are actively seeping from the sediment into the water column.

A number of geological consequences result from the presence of gases in near-surface sediment of this area. Where gas concentrations approach and exceed their solubilities in the interstitial water, free gas in the form of bubbles occurs. This gas modifies the acoustic properties of the sediments, and near-surface acoustic anomalies are detected on high-resolution geophysical records. Acoustic anomalies were observed at three of the eight sites where methane is very abundant and also at the site where carbon dioxide was observed along with hydrocarbons. On the other hand, acoustic anomalies were also seen in geophysical records from three sites where maximum gas concentrations in core samples were too low to cause anomalies. At three other sites there was no geophysical evidence for acoustic anomalies although geochemical measurements indicated high methane concentrations in the sediment. The presence of high gas concentrations in near-surface sediments can lead to sediment instability and the

possibility of seafloor cratering. Finally, the thermochemical hydrocarbons, observed at one site, may have been produced deep within Norton Basin and be migrating to the surface. These hydrocarbons have petroleum-like characteristics and may be indicative of petroleum generation and accumulation at depth.

REFERENCES CITED

- Barnes, R.O. and Goldberg, E.D. (1976) Methane production and consumption in anoxic marine sediments: Geology 4, 297-300.
- Bernard, B.B., Brooks, J.M., and Sackett, W.M. (1976) Natural gas seepage in the Gulf of Mexico. Earth and Planet. Sci. Lett. 31, 48-54.
- Bernard, B.B., Brooks, J.M., and Sackett, W.M. (1977) A geochemical model for characterization of hydrocarbon gas sources in marine sediments: Proc. 9th Offshore Tech. Conf., 1, 435-438.
- Bernard, B.B., Brooks, J.M., and Sackett, W.M. (1978) Light hydrocarbons in recent Texas continental shelf and slope sediments. Jour. Geophys. Res., 83, 4053-4061.
- Claypool, G.E. and Kaplan, I.R. (1974) The origin and distribution of methane in marine sediments. In Natural Gases in Marine Sediments, Kaplan, I.R., ed., Plenum, New York, 99-139.
- Cline, J.D., Feely, R.A., and Young, A. (1978) Identification of natural and anthropogenic petroleum sources in the Alaskan shelf areas utilizing low molecular weight hydrocarbons: Environmental Assessment of the Alaskan Continental Shelf, Ann. Report, v. 8, NOAA, BLM, p. 73-198.
- Cline, J.D. and Holmes, M.L. (1977) Submarine seepage of natural gas in Norton Sound, Alaska: Science, 198, 1149-1153.

David, J.B. and Squires, R.M. (1954) Detection of microbially produced gaseous hydrocarbons other than methane. Science, 119, 381-382.

Emery, K.O. and Hoggan, D. (1958) Gases in marine sediments. Am. Assoc. Petrol. Geol. Bull., 42, 2174-2188.

Hopkins, D.M. (1967) Quaternary marine transgression in Alaska. In The Bering Land Bridge, Hopkins, D.M., ed., Stanford University Press, Stanford, California, 47-90.

Kosiur, D.R., and Warford, A.L. (1979) Methane production and oxidation in Santa Barbara Basin Sediments: Estuarine and Coastal Marine Science, 8, 379-385.

Kvenvolden, K.A., Nelson, C.H., Thor, D.R., Larsen, M.C., Redden, G.D., Rapp, J.B., and DesMarais, D.J. (1979a) Biogenic and thermogenic gas in gas-charged sediment of Norton Sound, Alaska. Proc. 11th Offshore Tech. Conf. 1, 479-486.

Kvenvolden, K.A., Weliky, K., Nelson, C.H., and DesMarais, D.J. (1979b) Submarine seep of carbon dioxide in Norton Sound, Alaska: Science, 205, 1264-1266.

Kvenvolden, K.A. and Claypool, G.E. (1980) Migration of gasoline-range hydrocarbons by solution in carbon dioxide as observed in Norton Basin, Alaska: (unpublished).

Kvenvolden, K.A. and Redden, G.D. (1980) Hydrocarbon gas in sediment from the shelf, slope and basin of the Bering Sea: Geochim. Cosmochim. Acta, (submitted).

Martens, C.S. and Berner, R.A. (1974) Methane production in the interstitial waters of sulfate-depleted marine sediments. Science, 185, 1167-1169.

McManus, D.A., Venkatarathan, K., Hopkins, D.M., and Nelson, C.H. (1977) Distribution of bottom sediments on the continental shelf, northern Bering Sea: U.S. Geol. Survey Prof. Paper 759-C, 31 pp.

Nelson, C.H. (1977) Potential seafloor instability from gas-rich sediments and sediment depression craters. In Environmental Assessment of the Alaskan Continental Shelf, Ann. Rept. Prin. Inv. for 1977, NOAA, Env. Res. Lab, U.S. Dept. of Commerce, Boulder, Colo., 79-92.

Nelson, C.H. and Creager, J.S. (1977) Displacement of Yukon-derived sediment from Bering Sea to Chukchi Sea during Holocene time: Geology, 5, 141-146.

Nelson, C.H. and Hopkins, D.M. (1972) Sedimentary processes and distribution of particulate gold in northern Bering Sea: U.S. Geol. Survey Prof. Paper 689, 27 pp.

Nelson, C.H., Kvenvolden, K.A., and Clukey, E.C. (1978) Thermogenic gases in near-surface sediments of Norton Sound, Alaska. Proc. 10th Offshore Tech. Conf. 4, 2623-2633.

Nelson, C.H., Thor, D.R., Dandstrom, M.W., and Kvenvolden, K.A. (1979) Modern biogenic gas-generated craters (seafloor "pockmarks") on the Bering Shelf. Geol. Soc. Am. Bull. (accepted).

Oremland, R.S. (1975) Methane production in shallow-water, tropical marine sediments. Appl. Microbiol. 30, 602-608.

Primrose, S.B. and Dilworth, M.J. (1976) Ethylene production by bacteria: Jour. General Microbiology, 93, 177-181.

Reeburgh, W.S. (1969) Observations of gases in Chesapeake Bay sediments. Limnol. Oceanog. 14, 368-375.

Reeburgh, W.S. and Heggie, D.T. (1977) Microbial methane consumption reactions and their effect on methane distributions in freshwater and marine environments. Limnology and Oceanography 22, 1-9.

Schubel, J.R. (1974) Gas bubbles and the acoustically impenetratable, or turbid, character of some estuarine sediment. In Natural Gases in Marine Sediments, Kaplan, I.R., ed., Plenum Publ. Corp., New York, 275-298.

Whelan, T. (1974) Methane, carbon dioxide and dissolved sulfide from interstitial water of coastal marsh sediments: Estuarine and Coastal Marine Science 2, 407-415.

FIGURE CAPTIONS

Figure 1. Location of hydrocarbon gas sampling sites in Norton Sound and Chirikov Basin (dots). Sites are designated with the last digit of the year when the site was occupied followed by the station number. In parentheses is the interval in centimeters from which samples were taken. After the colon is the number of samples analyzed for hydrocarbon gases in that interval.

Figure 2. Distribution of maximum concentrations of C_1 in $\mu\text{L/L}$ and mL/L of wet sediment at each site.

- 1-10' $\mu\text{L/L}$
- 10'-10² $\mu\text{L/L}$
- 10²-10³ $\mu\text{L/L}$
- 1-10 mL/L
- > 10 mL/L




Figure 3. Graph of concentration of C_1 in $\mu\text{L/L}$ and mL/L of wet sediment vs. depth (cm) for sediment samples from cores taken at nine sites in Norton Sound and eastern Chirikov Basin. Site 7-17 and 8-3 are the same location; results are combined into one curve.

Figure 4. Distribution of maximum concentrations of $C_2 + C_3$ in nL/L and $\mu\text{L/L}$ of wet sediment at each site.

- 1-100 nL/L
- 100-500 nL/L
- 500-1000 nL/L
- 1-5 $\mu\text{L/L}$
- > 5 $\mu\text{L/L}$

Figure 5. Graph of concentrations of $C_2 + C_3$ in nL/L and $\mu\text{L/L}$ of wet sediment vs depth (cm) for sediment samples from cores taken at nine sites in Norton Sound and eastern Chirikov Basin.

Figure 6. Distribution of acoustic anomalies and sites with high concentrations of gas.

-  Sites where high-resolution geophysical records indicate acoustic anomalies.
-  Sites where geochemical measurements on sediment core samples show concentrations of C_1 exceeding 1 mL/L.
-  Site where geochemical measurements on sediment core samples show concentrations of CO_2 exceeding 10 mL/L.

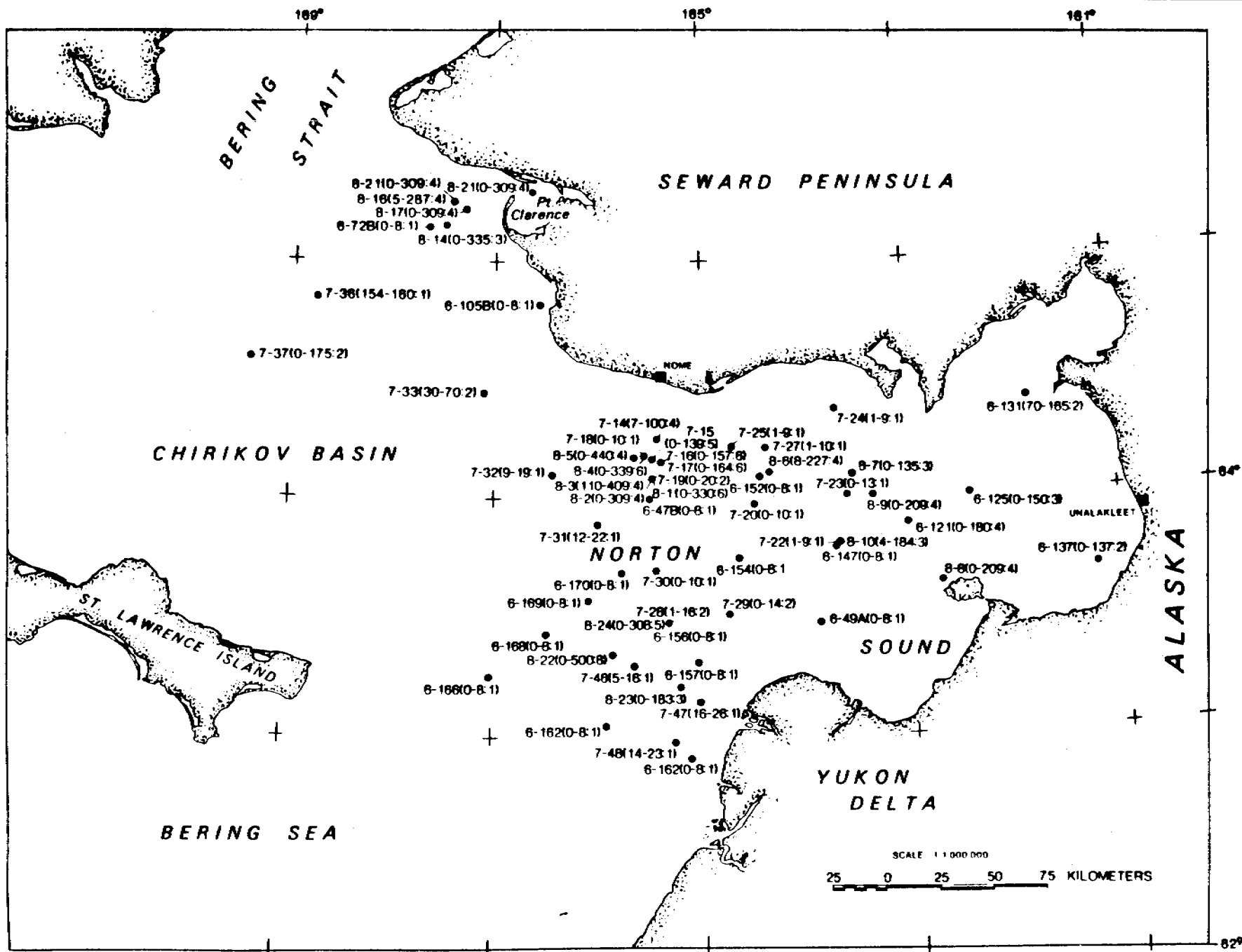


Fig. 1 - Location of hydrocarbon gas sampling sites in Norton Sound and Chirikov Basin (dots). Sites are designated with the last digit of the year when the site was occupied followed by the station number. In parentheses is the interval in centimeters from which samples were taken. After the colon is the number of samples analyzed for hydrocarbon gases in that interval.

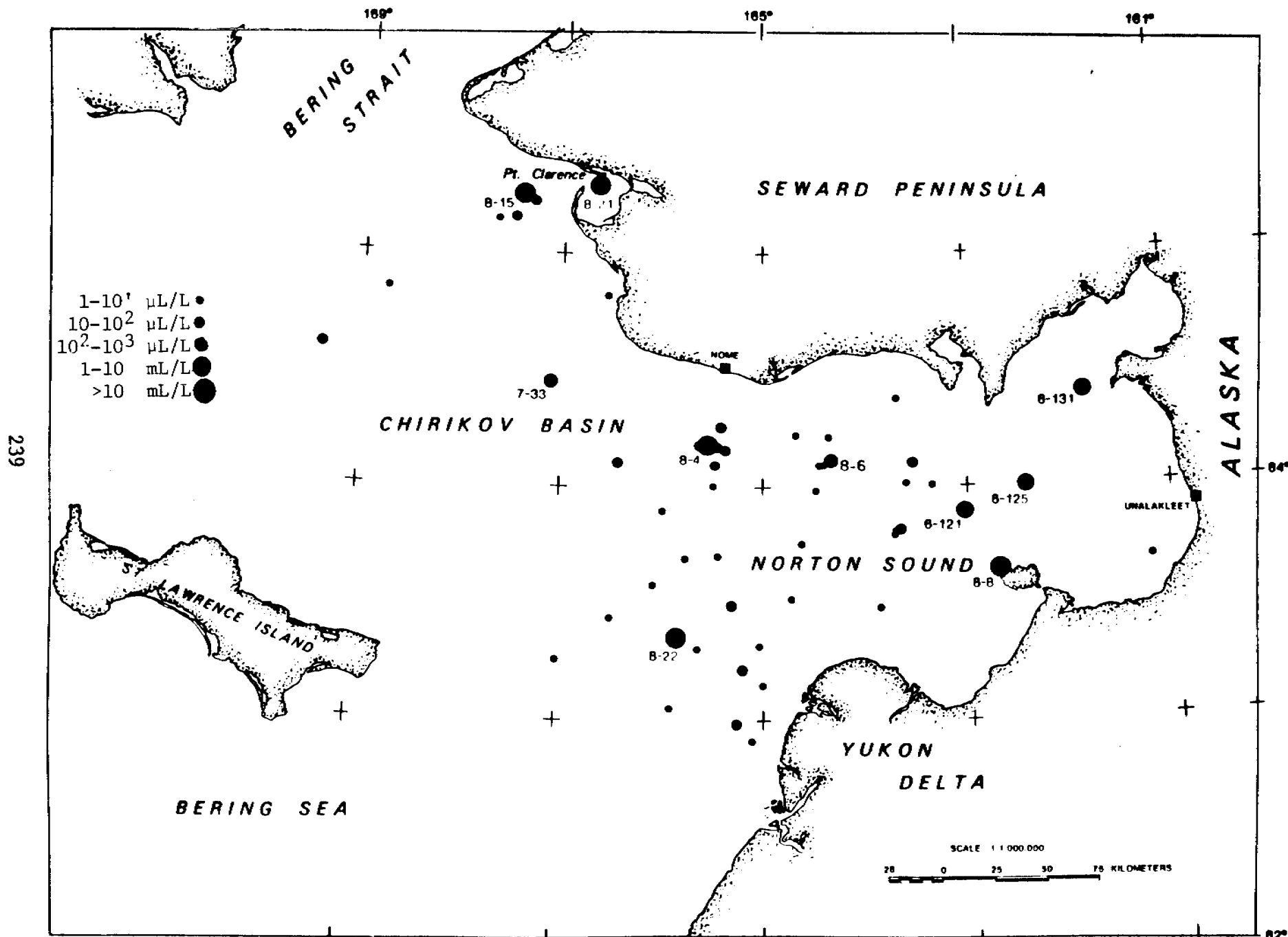


Fig. 2 - Distribution of maximum concentrations of C_1 in $\mu\text{L/L}$ and mL/L of wet sediment at each site.

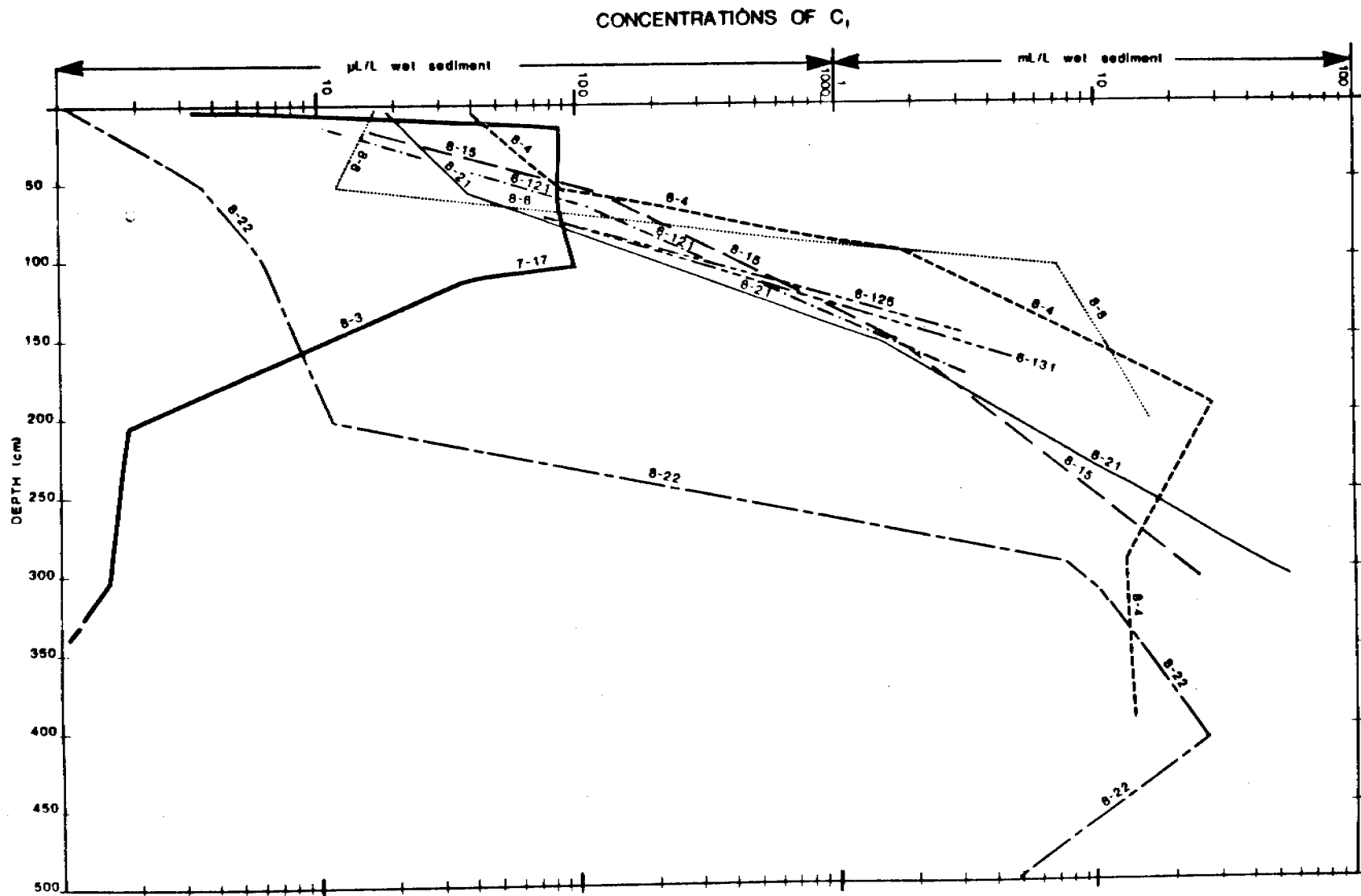


Fig. 3 - Graph of concentration of C_1 in $\mu\text{L/L}$ and mL/L of wet sediment vs. depth (cm) for sediment samples from cores taken at nine sites in Norton Sound and eastern Chirikov Basin. Site 7-17 and 8-3 are the same location; results are combined into one curve.

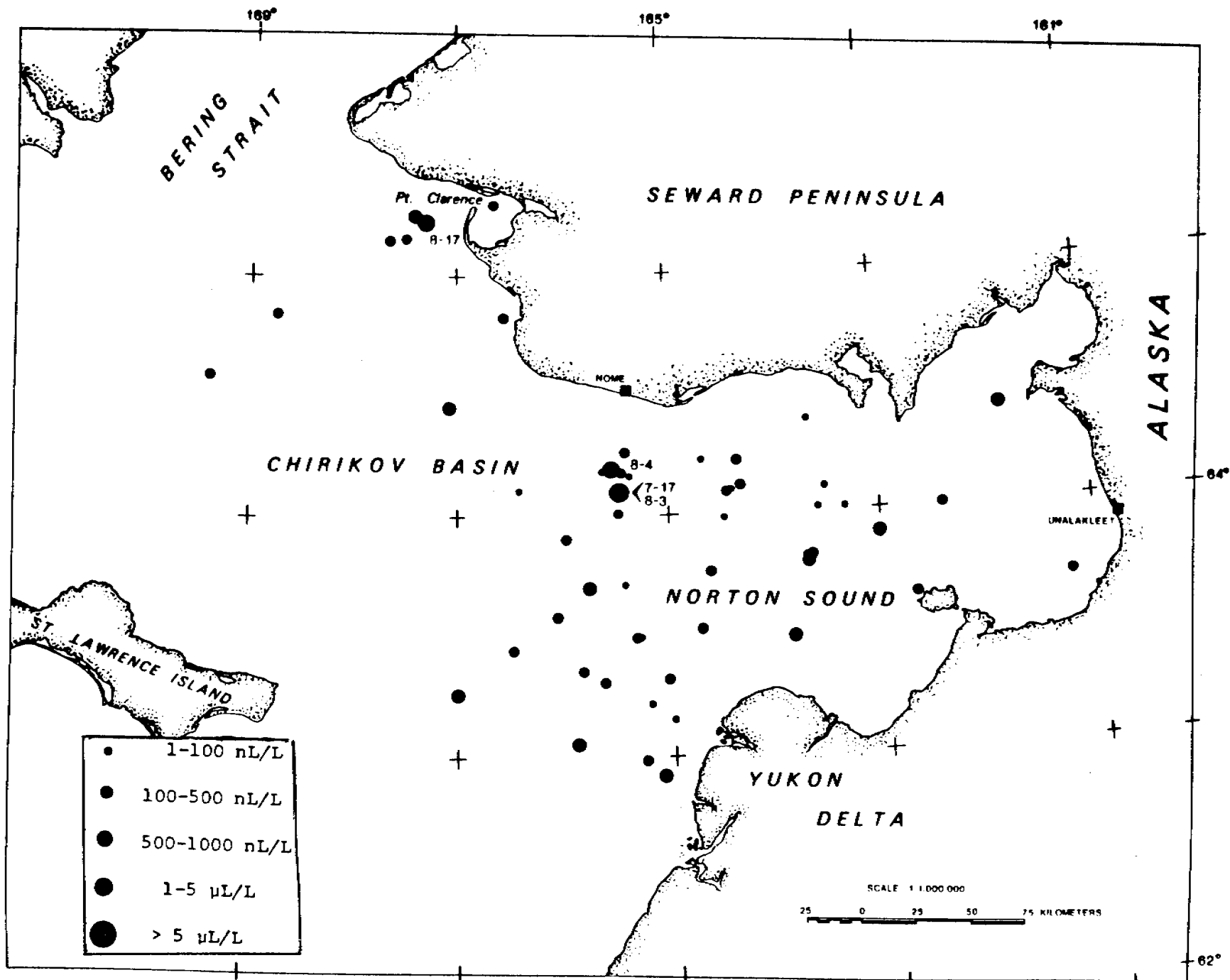


Fig. 4 - Distribution of maximum concentrations of $C_2 + C_3$ in nL/L and $\mu L/L$ of wet sediment at each site.

CONCENTRATIONS OF C₂ + C₃

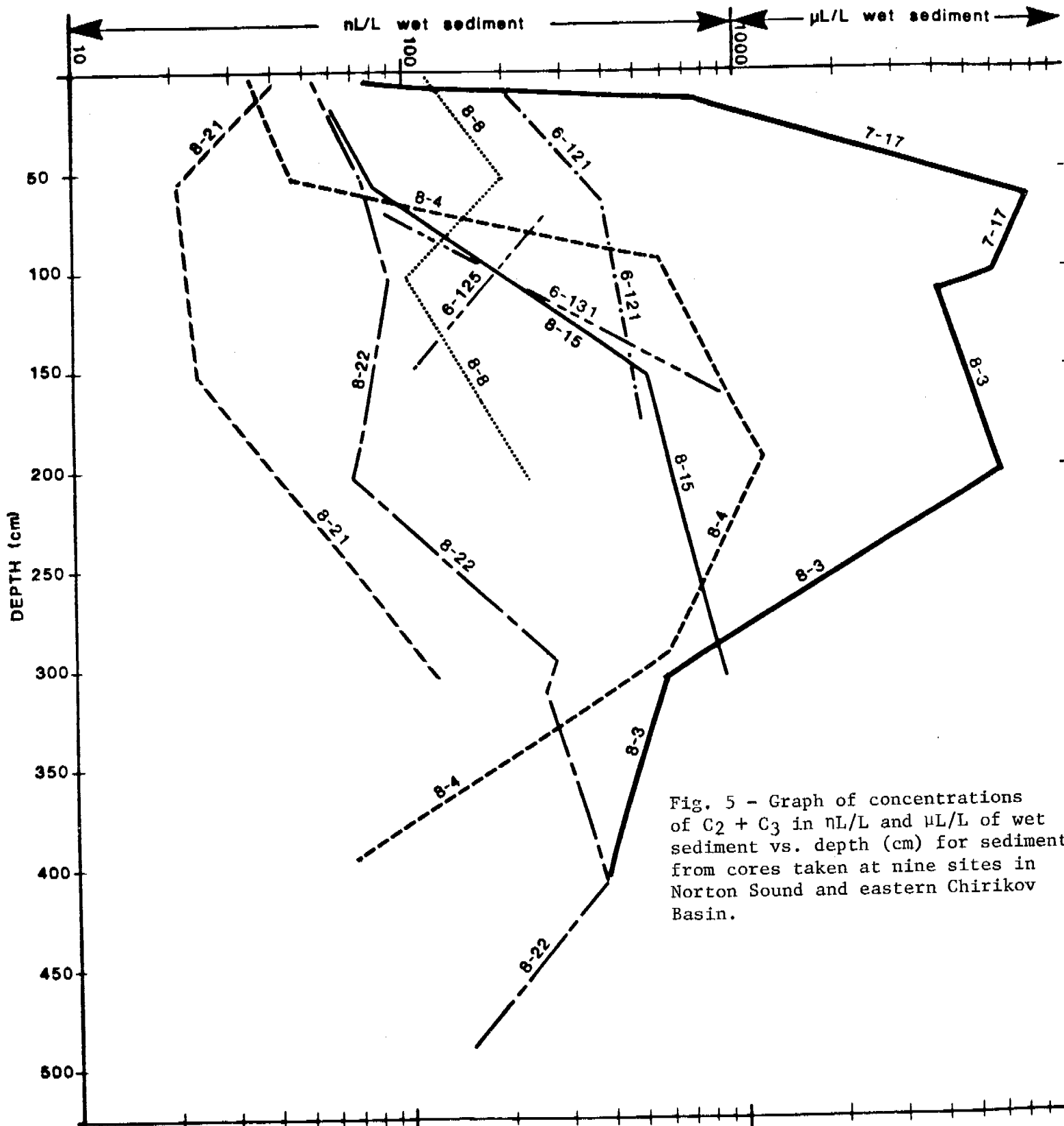


Fig. 5 - Graph of concentrations of C₂ + C₃ in nL/L and μL/L of wet sediment vs. depth (cm) for sediment from cores taken at nine sites in Norton Sound and eastern Chirikov Basin.

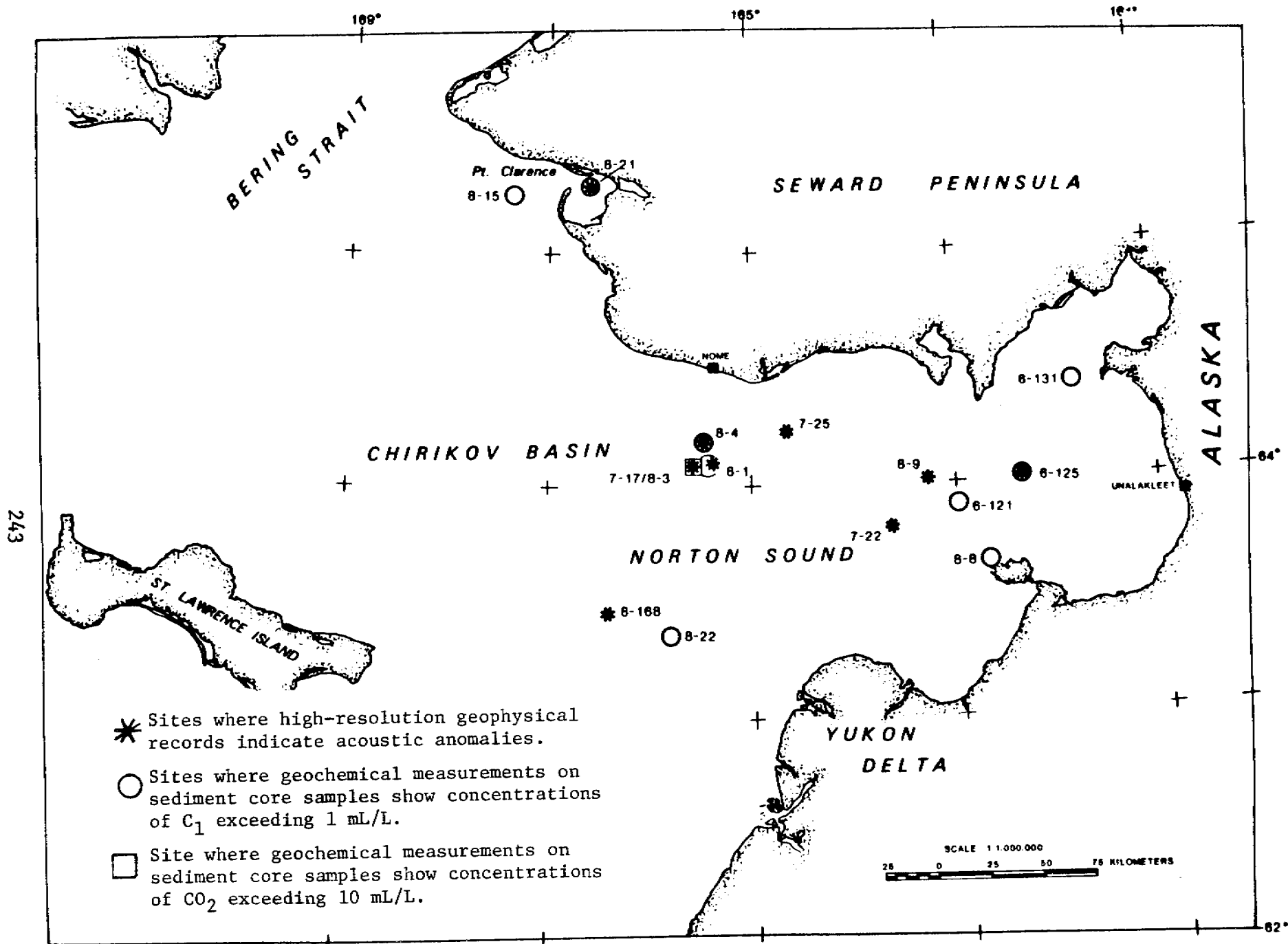


Fig. 6 - Distribution of acoustic anomalies and sites with high concentrations of gas.

OTC 3412

BIOGENIC AND THERMOGENIC GAS IN GAS-CHARGED SEDIMENT OF NORTON SOUND, ALASKA



by K. A. Kvenvolden, C. H. Nelson, D. R. Thor,
M. C. Larsen, G. D. Redden, J. B. Rapp, U.S.
Geological Survey; and D. J. Des Marais, NASA,
Ames Research Center

This paper was presented at the 11th Annual OTC in Houston, Tex. April 30-May 3, 1979. The material is subject to correction by the author. Permission to copy is restricted to an abstract of not more than 300 words.

ABSTRACT

Chemical and isotopic compositions of sediment gas from Norton Sound have been determined for near-surface, gas-charged sediments at two sites identified in acoustic profiles and bottom observations. At one site our air-driven vibrocorer penetrated sediment saturated with methane that has a carbon isotopic composition ($\delta^{13}\text{C}_{\text{PDB}}$) of -80‰ . This isotopic value suggests that the methane originated from active biological processes operating on peat in the top 4 m of sediment. At the other site, characterized by a large subsurface acoustic anomaly, smaller near-surface acoustic anomalies and active seepage of gas, our vibrocorer obtained sediment saturated with gas composed of 98% CO_2 which had a $\delta^{13}\text{C}_{\text{PDB}}$ value of -2.7‰ . Associated with the CO_2 are minor concentrations of petroleum-like light hydrocarbons. Methane in this mixture has a $\delta^{13}\text{C}_{\text{PDB}}$ value of -36‰ . The carbon isotopic compositions of CO_2 and methane along with the chemical distribution of gaseous hydrocarbons indicate that at this site these gases are derived from thermal processes operating at depth in Norton Basin. Apparently CO_2 from the decarbonation of marine limestone acts as a carrier for hydrocarbon gases that have been generated from organic matter buried in the basin. The gases reach the surface by faults and escape at the seafloor as a submarine seep. The presence of near-surface gas-charged sediment in Norton Sound reduces the stability of the seafloor. Areas where sediments are charged with gas may pose potential hazards for engineering developments.

INTRODUCTION

Previous investigations in Norton Sound describe acoustic anomalies that are attributed to the presence of near-surface gas-charged sediment.¹⁻⁴ One anomaly in particular has been studied in detail because of the discovery in 1976 of submarine seepage of petroleum-like gaseous hydrocarbons into the water column.¹ The gas seep comes from sediment that is inferred to be saturated with hydrocarbons.¹⁻⁴ In the summer of 1977 a geochemical investigation of the seep site showed that near-surface sediment contains

References and illustrations at end of paper.

petroleum-like gas and gasoline-range hydrocarbons;² However, the measured concentrations of hydrocarbons in the sediment, although unusually high, were well below saturation. The contradiction between geophysical evidence suggesting gas-saturated sediment and the geochemical analyses showing concentrations of hydrocarbons greatly below saturation led to the work described in this paper.

A major objective was to determine the chemical composition and concentration of the gas in the sediment and to indicate possible sources for this gas. We focused on two areas (Fig. 1) where geophysical, geological and geochemical information indicates that the sediment is charged with gas. One area, approximately 50 km south of Nome, is designated Site 3 from the core number of our 1978 survey. This area corresponds in location to the seep mentioned above.¹⁻⁴ About 12 km northwest of Site 3 we investigated a second area, designated Site 4. At Site 4 there is evidence of gas-charged sediment, but there is no indication of surface seepage of gas. At both sites the depth of water is 19 m. The geophysical, geologic and geochemical results obtained at these two contrasting sites have explained the earlier contradictory evidence from the seep area.

METHODS

The following high-resolution reflection-profiling multisensor system defined the acoustical responses of the anomalies: (1) 800-J boomer; (2) 3.5-kHz subbottom profiling system; (3) 12-kHz echo sounder tuned to detect bubbles in the water column; and (4) 200-kHz echo sounder also tuned to detect bubbles. In addition to the high-resolution systems, deep-penetration reflection profiling was obtained with a 120-kJ sparker system. Side-scan sonar with a 100-m sweep was used to detail the seafloor. About 200 km² of seafloor surrounding Sites 3 and 4 has been crossed by about 400 km of geophysical tracklines. The multisensor acoustic system obtained a sequence of acoustic profiles from which we constructed a detailed grid of geologic cross sections.⁵⁻⁷

Geologic observations consisted of underwater television and photography and detailed examination of sediment cores. A sled carrying a 70-mm underwater camera and a television camera was deployed at Site 3

(the seep site) to obtain a direct view of the features on the bottom. Time constraints prevented underwater camera and television coverage at Site 4. Sediment cores were taken with an air-driven vibrator which monitored its rate of sediment penetration. The vibrator had a barrel 6 m long and contained an 8.5-cm diameter plastic core liner. From every meter of core, segments about 9 cm long were removed for gas analysis. Also, where a gas expansion pocket developed within the core, analyses were made on gases directly removed through the core liner. The remaining core segments were preserved for later engineering studies. A duplicate core was split, described geologically and sampled for organic carbon, moisture content, and radiocarbon dating.

Geochemical studies consisted of analyses for hydrocarbons and CO₂ on board ship and measurements of total gas composition and of carbon isotopic compositions of CO₂ and methane in shore-based laboratories.⁸ One gas expansion pocket in the core at Site 3 was sampled as follows: the core liner was partially penetrated with an awl, and a rubber septum was strapped over the partial penetration with a hose clamp. Gas samples were recovered by penetrating the septum, with a needle on a gas-tight syringe and with double-ended needles, to fill 20-mL vacutainers. Also, sediment from the samples removed from the cores were extruded from the liners into 1-qt. paint cans. Each can was immediately filled with helium-purged water. From each can 100 mL of water was withdrawn and the can was sealed. The resulting headspace was purged with helium thru septa-covered holes in the can. The can was shaken for 10 minutes in a paint can shaker to release interstitial gas into the headspace. One-milliliter samples of the gas mixture from the gas pocket, the vacutainers and the paint can headspace were analyzed on a gas chromatograph having both flame ionization and thermal conductivity detectors. More detailed compositional information on the gas in the vacutainers was obtained by shore-based gas chromatography. Methane and CO₂ from the vacutainers were separated in a vacuum-line combustion apparatus and their carbon isotopic composition determined by mass spectrometry using methods modified after Craig.⁹ Results are reported relative to the PDB (Peedee Belemnite) standard. $(\delta^{13}\text{C}/\text{‰} = \frac{^{13}\text{C}/^{12}\text{C} (\text{sample}) - ^{13}\text{C}/^{12}\text{C} (\text{standard})}{^{13}\text{C}/^{12}\text{C} (\text{standard})} \times 1000.$

GEOPHYSICAL RESULTS

Geophysical studies have defined the general geologic setting for the area where Sites 3 and 4 are located.³ The sites are on the northeastern side of Norton Basin, a major subsurface northwest-southeast-trending synclinorium. The upper stratigraphic section of the basin fill consists of folded and faulted Tertiary rocks unconformably overlain by horizontally bedded Quaternary units.¹⁰ Tertiary strata dip generally southwest by several degrees or less into the synclinorium. Broad anticlinal arches within the Tertiary section are formed by dip reversals of less than 0.5° toward the northeast.

The geology of the area is characterized by faults, folds, acoustic anomalies, and gas seepage. Faults are subparallel, trend northwest-southeast, and dip southwest (Fig. 1). These faults occur in zones which splay from deeper master faults that offset the acoustic basement.³ The fault system displaces Tertiary and Quaternary units but does not seem to cut through surficial sediment.

Near-surface acoustic anomalies on seismic pro-

files are common in the area of this investigation. Two types of anomalies are recognized on sparker records. One type of acoustic anomaly, seen at Site 3, is an acoustic-termination anomaly, characterized by sharp termination of subbottom seismic reflectors with an intervening zone lacking coherent reflections (Fig. 2A). The other type of anomaly, observed at Site 4, is characterized by near-surface "pull-downs" of seismic reflectors. The pull-down effect continues to depth (Fig. 2D). The anomalies are attributed to the attenuation and scattering of seismic signals due to gas bubbles in the sediment.²

The 120-kJ sparker profile over Site 3 (Fig. 2A) shows dipping reflectors terminating at regions where the acoustic return signals are highly attenuated. This anomaly is probably caused by a large continuous gas accumulation about 100 m below the surface.^{2,3} The boomer profile (Fig. 2B) shows an apparent near-surface extension of the large gas accumulation.² The 12-kHz (Fig. 2C) and 200-kHz profiles show gas-bubble trains in the water column that indicate active gas seepage above the near-surface acoustic anomaly.

At Site 4 the 120-kJ sparker profile (Fig. 2D) reveals a series of reflector "pull-downs". The source of acoustic disturbance is very near the surface. The anomaly on the boomer record at Site 4 is patchy (Fig. 2E) in contrast to the more continuous response shown on the record at Site 3 (Fig. 2B). The 12-kHz (Fig. 2F) and 200-kHz profiles at Site 4 show a clear water column with no evidence of gas bubbles.

GEOLOGIC OBSERVATIONS

The presence of active gas seepage at Site 3, as indicated on the 12-kHz and 200-kHz profiles, is documented by underwater television and photographs. Intermittent and rapid streams of bubbles come from small vents. Bubbles are easy to see on television but difficult to see in plan-view photographs (Fig. 3A). Apparent gas vents were videotaped in 1977, but no bubbles were seen.² These vents, plus those seen in 1978, range from 5 to 40 cm in diameter, are too small to appear on side scan sonar records, and are conical in shape with depth to width ratios about 1:1. This shape differs from the shapes produced by biological activities which tend to be infilled and much smaller in size.¹¹ Gas-seep vents sometimes occur at the crest of ripple fields (Fig. 3B). There is no mounding around small vents. The vents do not resemble mud volcanoes that have been described at other places and that have generally been attributed to gas venting with mixtures of liquid and mud.¹² The Norton Sound seep vents are quite different from the apparent biogenic gas craters commonly found elsewhere in the sound.¹³ These craters are large (3-10 m in diameter) and shallow (depth to width ratio about 1:10), and are evident on side scan sonar records, and do not exhibit bubbling gas.

At Site 4 no video or photographic record of the seafloor was obtained; thus, there is no evidence of vents. High resolution (12-kHz and 200-kHz) records do not show gas bubbles in the water column; therefore, gas vents are probably absent on the seafloor. Side scan sonar records do not show craters like the ones elsewhere in Norton Sound.¹³

Relations between sediment ripples and vents indicate that dynamic processes are operating at Site 3. Sediment at the two sites consists of very fine sand and coarse silt derived from the Yukon River. This material can be worked into small ripples (Figs. 3A and 3B) by either intermittent storm waves or strong bottom currents that reach speeds of up to 30 cm/s during

daily tidal fluxes.¹⁴ Photographs taken in 1977 show a generally smooth, highly bioturbated seafloor at the seep site.² In 1978, however, the seafloor was rippled. The ripples were well preserved and generally symmetrical, like ripples attributed to wave effects. Some of the ripples, however, were modified by bottom currents and were formed into more asymmetric bedforms. The presence of gas vents superposed on these dynamic mobile bedforms suggests that vents form quite frequently. Furthermore, the absence of bubble emanations at most vents indicates that gas movement in near-surface sediment is episodic and rapidly changes pathways to the surface.

Gas in the sediment significantly changes sediment geotechnical properties and internal structures. When the 2-m vibrocorer penetrated gas-charged sediment in 1977, rates of penetration were much higher than at locations that did not show geophysical evidence of gas-charging.² With the 6-m-long vibrocorer used in 1978, penetration was as much as three times faster at Sites 3 and 4 than at locations where no anomalies exist. These data on rates of penetration emphasize the loss of shear strength in near-surface, gas-charged sediment.

When cores in gas-charged sediment are removed from the seafloor, the gas begins to expand rapidly and causes a number of secondary phenomena in the sediment core. At Site 3 the core expanded in an explosive manner so that nearly a meter of sediment was blown out the end of the liner when it was removed from the vibrocorer. In addition, several 5-10-cm gas pockets formed in the core from the bubble phase gas (Fig. 3C).

The rapid expansion of the core disrupted internal sedimentary structures. Cores at both sites showed a number of cracks (Fig. 3D) which have been noted in other cores affected by gas expansion. The core at Site 3 contained a number of gas cavities in the lower part, so that the sediment resembled a honeycomb (Fig. 3E). The gas apparently streamed rapidly up through the core causing longitudinal gas streaming structures in the lower part of the core (Fig. 3D, top). A large honeycomb structure then formed above where this gas became trapped beneath a cohesive peat layer. At Site 4 sediment expansion cracks also were observed in the core; however, no large gas expansion pockets developed, and the core extruded only a few centimeters out of the core barrel.

Seismic profiles suggest that the region near Sites 3 and 4 is characterized by 1-2 m of Holocene sediment 5-7,¹⁵ and lithologic studies indicate that the sediment is coarse silt derived from the Yukon River.¹⁶ The stratigraphy in the vibrocore shows Holocene sediment slightly over 3 m thick at Site 3, and about 1.5 m thick at Site 4. Because of necessary compensation for gas expansion, the true thickness of the overlying Yukon mud in this area is probably like the 2-m thickness found elsewhere in Norton Sound. Yukon mud, 1.5 to 2 m thick, overlies Pleistocene freshwater peaty mud deposited before the Holocene marine transgression.¹⁵ The peats or peaty muds that characterize Pleistocene sedimentation contain large amounts of organic carbon (8 to 34 percent). This organic-rich mud may generate high quantities of methane as observed at several places in Norton Sound.¹³

GEOCHEMICAL ANALYSES

The gases extracted from sediments at Sites 3 and 4 (Table 1) were analyzed by gas chromatography

on board ship. The measurements should be considered semiquantitative because our standards required large multiplication factors to calculate the unusually high concentrations of gases found at both these sites. At Site 3, CO₂ is the dominant gas being about 4 to 5 orders of magnitude higher in concentrations than methane, which is the most abundant hydrocarbon gas. Of special interest is the fact that the hydrocarbon gases heavier than methane, namely ethane, propane, and the butanes, are especially abundant relative to methane. The ratios of methane/ethane + propane (C₁/(C₂ + C₃)) are all less than 10 and in fact, in one sample, this ratio is less than 1. Ethene and propene are also present but always in lower concentrations than their saturated homologues. Gas chromatograms also show that gasoline-range hydrocarbons are present. Generally, the overall concentrations of hydrocarbons appear to decrease with depth in the vibrocore.

The dominant gas in sediment at Site 4 is methane and CO₂ is usually subordinate by a factor of about 3. Hydrocarbons heavier than methane are present, but their concentrations relative to methane are small. For example, the ratios of C₁/(C₂ + C₃) range from about 1000 to 24,000. Near the surface ethene and propene are in greater concentrations than ethane and propane but at depth saturated hydrocarbons are more abundant. The concentration of hydrocarbons increases with depth. Methane reaches concentrations near saturation in the interstitial water.

Geochemical analyses of the gases present in a gas expansion pocket (Fig. 3C) in the core at about 178-187 cm depth provided a good estimate of the bubble-phase composition of the gas at Site 3. Carbon dioxide constitutes about 98% by volume of the total gas mixture. Other gases measured are: N₂, 1.9%; O₂, 0.5%; Ar, 0.3%; H₂, 0.1%; and H₂O, trace. Only 0.04% of the mixture is hydrocarbons. Concentrations of individual hydrocarbons in parts per million by volume of total gas are: methane, 362; ethane, 39; propane, 18; n-butane, 4; and isobutane, 20. Ethene and propene were not detected. The ratio C₁/(C₂+C₃) is 6.4, in the same range of values shown in Table 1 for Site 3.

Carbon isotopic compositions were determined for CO₂ and methane from the gas expansion pocket and for organic carbon at 325 cm in the core at Site 3. For Site 4, carbon isotopic compositions were measured for CO₂ and methane from the headspace of the canned sample from 190 to 199 cm and for organic carbon from Pleistocene sediment at 212 cm in the core. The results, summarized in Table 2, clearly show that the sources of the gases at Sites 3 and 4 must be distinctly different. On the other hand, the organic carbon in the Pleistocene peaty mud has the same isotopic composition at both sites, and, therefore, the peat probably is of the same source.

DISCUSSION

Our geophysical and geologic observations indicate that gas is present at high concentrations in the sediment at Sites 3 and 4. The geochemical data confirm these observations but show that the gas composition differs at the two sites, with CO₂ leaking into the water at Site 3 and methane trapped in the Pleistocene sediment at Site 4.

Many of the geophysical features at the two sites are similar, but there are a few differences between the sites. Similarities between Sites 3 and 4 include (1) a thin veneer of Holocene sediment covering

Pleistocene peaty mud; (2) higher rates of vibracorer penetration at both sites than at adjacent locations not exhibiting near-surface acoustic anomalies. (These penetration data help substantiate that the acoustic anomalies at Sites 3 and 4 indicate gas-charged sediment); and (3) gas expansion cracks in cores from both sites. The core from Site 3 also exploded at the top and developed large gas expansion pockets within the core liner, suggesting a higher sediment gas content at Site 3 than at Site 4.

Differences between the two sites appear mainly in geophysical records. For example, the sparker records for Site 3 show an acoustic anomaly at about 100 m depth that has sharp terminations of subbottom seismic reflectors with an intervening lack of coherent reflections; high-resolution records indicate bubbles leaking from the sediment into the water column. At Site 4 the sparker records show near-surface pull-downs of the seismic reflectors, and high-resolution records indicate no bubbles in the water. The acoustic anomaly at Site 3 is interpreted to be caused by an accumulation at 100 m and deeper of gas, mainly CO₂. Some CO₂ apparently is escaping from the accumulation and breaks through the seafloor as a seep. At Site 4 the acoustic anomaly is believed to be due to trapping of gas, mainly methane, generated in the near-surface sediment.

The chemical and isotopic compositions of the gases at Sites 3 and 4 provide information for interpreting possible sources. Bernard *et al.*¹⁷ utilize two parameters, the ratio of C₁/(C₂ + C₃) and the δ¹³C value of methane, to determine the origin of natural hydrocarbon gases in submarine seeps. They point out that microbial degradation produces hydrocarbons with C₁/(C₂ + C₃) ratios greater than 1000 and with methane having δ¹³C values less than -60‰. On the other hand, thermal sources produce hydrocarbons with C₁/(C₂ + C₃) ratios of 0 to 50 and δ¹³C values of methane heavier than -50‰. The hydrocarbon gases at Site 3, where C₁/(C₂ + C₃) ratios are less than 10 and the δ¹³C value of methane is -36‰, clearly are from thermogenic sources according to the criteria of Bernard *et al.*¹⁷ The dominant CO₂ at this site has a carbon isotopic composition of -2.7‰. This value suggests that the CO₂ is probably derived from the thermal decomposition of marine carbonates, which are believed to underlie large parts of the Bering Sea Shelf.¹⁸ Thus, the isotopic evidence for both organic and inorganic carbon indicates that thermal processes are involved in the formation of gases at Site 3. In contrast, the gases from Site 4 are dominated by methane and are apparently produced by microbial activity as suggested by the C₁/(C₂ + C₃) ratios ranging from 1000 to 24,000 and by the δ¹³C of methane of -80‰. The CO₂ at Site 4 has a δ¹³C value of -14‰ that is in the range consistent with biologically produced CO₂ but we do not know if the method of collecting samples from canned sediment affects the isotopic fractionation of the CO₂. Carbon isotopic compositions of bacterially generated CO₂ and methane in sediment from the Deep Sea Drilling Project¹⁹, however, are similar to isotopic compositions at Site 4. The presence of high concentrations of methane in Norton Sound sediment is fairly common¹³, but the occurrence of a CO₂ seep at Site 3 is unique.

At Site 3 the predominant gas, CO₂, carries with it a small component of gas and gasoline-range hydrocarbons. These hydrocarbons may be related to petroleum. As an example, in the petroleum province offshore southern California, submarine gas seeps are common. At two of these seeps the chemical and carbon isotopic compositions of hydrocarbon gases have been

determined. The results are similar to those we obtained for gas at Site 3. For example, seeps at Coal Oil Point and Carpenteria have C₁/(C₂ + C₃) ratios of 36 and 10 respectively and δ¹³C values of methane of -38.7‰ and -40.3‰.¹⁹ Thus, the hydrocarbons at Site 3 may be derived from processes similar to or the same as those involved in the origin and maturation of petroleum. Even if these hydrocarbons are derived from petroleum, they probably constitute less than 0.1% of the gas in the accumulation at 100 m depth indicated by the sparker records. We cannot yet define precisely the sources and processes by which CO₂ and the hydrocarbon gases are produced at Site 3, but a number of alternatives have been considered and are discussed elsewhere.⁸

The occurrence of near-surface sediment charged with biogenic or thermogenic gas has direct implications for sediment stability.²¹ The presence of high concentrations of gas in the sediment of Norton Sound causes a reduction in stability as suggested by the rapid rates of vibracorer penetration into the gas-charged sediment. Areas with near-surface, gas-charged sediment may be potentially hazardous to any engineering developments requiring firm and stable footings.

CONCLUSIONS

Geophysical, geologic, and geochemical evidence all indicate that gas-charged, near-surface sediment is present in Norton Sound, Alaska. Some sediment is charged with methane that is probably derived from microbial processes operating on Pleistocene peaty mud beneath a thin veneer of Holocene sediment from the Yukon River. At Site 3 sediment is charged with CO₂, which seeps into the water column. This CO₂ carries with it a minor component of hydrocarbon gases and gasoline-range hydrocarbons. The chemical and isotopic compositions of the sediment gases indicate that they are derived from thermal sources operating at depth within Norton Basin. The gases probably migrate up faults eventually reaching the surface as a seep. The hydrocarbons apparently are derived through processes similar to or the same as those that produce petroleum. Our data do not indicate whether a significant accumulation of petroleum is present at depth. The ease of penetration by the vibracorer into the gas-charged sediment suggest that the presence of gas reduces the stability of the sediment. Areas where sediments are charged with biogenically and thermogenically derived gas may be hazardous for any future engineering developments in the area.

ACKNOWLEDGMENTS

We thank the scientific staff and crew of the R/V SEA SOUNDER for assistance in collecting and processing samples at sea. Particularly we are grateful to E.C. Clukey for geotechnical information, W.C. Evans for compositional analysis of the total gas mixture, K. Weliky for help in preparing samples for carbon isotopic measurements, and J. Henning for typing and assembling the manuscript.

The cruise was supported jointly by the U.S. Geological Survey and by the Bureau of Land Management through an interagency agreement with the National Oceanic and Atmospheric Administration, under which a multiyear program responding to the needs of petroleum development of the Alaskan continental shelf is managed by the Outer Continental Shelf Environmental Assessment Program (OCSEAP) Office.

REFERENCES

1. Cline, J.D. and Holmes, M.L.: "Submarine seepage of natural gas in Norton Sound, Alaska", Science [1977] 198, 1149-1153.
2. Nelson, C.H., Kvenvolden, K.A. and Clukey, E.C.: "Thermogenic gases in near-surface sediments of Norton Sound", OTC 3354, 10th Annual Offshore Technology Conference, Houston, Texas [1978] 2623-2633.
3. Holmes, M.L., Cline, J.D. and Johnson, J.L.: "Geological setting of the Norton Basin gas seep", OTC 3051, 10th Annual Offshore Technology Conference, Houston, Texas [1978] 73-80.
4. Cline, J.D. and Holmes, M.L.: "Anomalous gaseous hydrocarbons in Norton Sound: biogenic or thermogenic?", OTC 3052, 10th Annual Offshore Technology Conference, Houston, Texas [1978] 81-86.
5. Nelson, C.H., Holmes, M.L., Thor, D.R. and Johnson, J.L.: "Continuous seismic reflection data, SEA 5-76-BS cruise, northern Bering Sea", U.S. Geol. Survey, Open-file Rept. 78-609 [1978] 6 p.
6. Thor, D.R. and Nelson, C.H.: "Continuous seismic reflection data, SEA 5-77-BS cruise, northern Bering Sea", U.S. Geol. Survey, Open-file Rept. 78-608 [1978] 8 p.
7. Larsen, M.C., Nelson, C.H. and Thor, D.R.: "Continuous seismic reflection data, SEA 9-78-BS cruise, northern Bering Sea", U.S. Geol. Survey, Open-file Rept. (in press).
8. Kvenvolden, K.A., Weliky, K., Nelson, H. and Des Marais, D.J.: "Submarine carbon dioxide seep in Norton Sound, Alaska", submitted for publication.
9. Craig, H.: "The geochemistry of the stable carbon isotopes", Geochim. Cosmochim. Acta [1953] 3, 53-92.
10. Nelson, C.H., Hopkins, D.M. and Scholl, D.W.: "Cenozoic sedimentary and tectonic history of the Bering Sea", Oceanography of the Bering Sea, Hood, D.W. and Kelley, E.J. (eds.), University of Alaska, Inst. Marine Sciences [1974] 485-516.
11. Nelson, C.H., Rowland, R.W., Stoker, S.W. and Larsen, B.B.: "Interplay of physical and biological sedimentary structures of the Bering epicontinental shelf", in review for Jour. Sed. Pet., 53 p.
12. Newton, R.S.: Personal communication, D'Appolonia, Houston, Texas [1978].
13. Nelson, C.H., Thor, D.R. and Sandstrom, M.W.: "Modern biogenic gas craters (seafloor "pockmarks") on the Bering Shelf, Alaska", Environmental Assessment of the Alaska Continental Shelf, Ann. Rept. of Principal Investigators for the year ending March 1978, Env. Res. Lab., Boulder, Colo., NOAA, U.S. Dept. of Commerce, (in press).
14. Cacchione, D.A. and Drake, D.E.: "Sediment transport in Norton Sound - northern Bering Sea", Environmental Assessment of the Alaskan Continental Shelf, Ann. Rept. of Principal Investigators for the year ending March 1978, Env. Res. Lab., Boulder, Colo., NOAA, U.S. Dept. of Commerce (in press).
15. Nelson, C.H. and Creager, J.S.: "Displacement of Yukon-derived sediment from Bering Sea to Chukchi Sea during Holocene", Geology [1977] 5, 141-146.
16. McManus, D.A., Venkataratham, K., Hopkins, D.M. and Nelson, C.H.: "Yukon River sediment on the northernmost Bering Sea shelf", Jour. Sed. Pet. [1974] 44, 1052-1060.
17. Bernard, B.B., Brooks, J.M. and Sackett, W.M.: "Natural gas seepage in the Gulf of Mexico", Earth and Planet. Sci. Lett. [1976] 31, 48-54.
18. Patton, W.W., Jr. and Dutro, J.R., Jr.: "Preliminary report on the Paleozoic and Mesozoic sedimentary sequence on St. Lawrence Island, Alaska", Geological Survey Research, U.S. Geol. Survey Prof. Paper 650-D [1969], D138-D143.
19. Claypool, G.E., Presley, B.J. and Kaplan, I.R.: "Gas analyses in sediment samples from Legs 10, 11, 13, 14, 15, 18 and 19", Initial Reports of the Deep Sea Drilling Project, Creager, J.S. and Scholl, D.W. (eds.) U.S. Govt. Printing Office, [1973] 19, 879-884.
20. Reed, W.E. and Kaplan, I.R.: "The chemistry of marine petroleum seeps", Jour. Geochemical Exploration [1977] 7, 255-293.
21. Whelan, T., Coleman, J.M., Roberts, H.H. and Suhayda, J.N.: "The occurrence of methane in recent deltaic sediments and its effect on soil stability", Bull. Int. Assoc. Engr. Geol. [1976], n. 14, 55-64.

Table 1
Content of Gases in Sediment
nL/L of Interstitial Water*

Interval (cm)	Methane (x 10 ³)	Ethane	Ethene	Propane	Propene	n-Butane	Isobutane	CO ₂ (x 10 ⁶)	Methane Ethane+Propane	Ethane Ethene
Site 3										
110 - 119	68	7300	63	220	48	50	640	61	9	120
200 - 209	4.0	3000	290	9300	200	5600	24000	110	< 1	13
300 - 309	2.1	500	56	330	56	280	240	47	3	9
400 - 409	1.5	340	180	440	130	240	94	52	2	2
Site 4										
0 - 9	69	28	81	35	68	14	-	0.072	1100	0.4
50 - 59	220	66	170	45	66	-	-	1.4	2000	.4
90 - 99	3500	820	99	320	28	34	40	4.6	3100	8
190 - 199	33000	830	62	560	30	170	400	11	24000	13
290 - 299	41000	1100	330	760	140	290	640	17	20000	3
390 - 399	38000	1000	330	910	230	170	230	12	20000	3

* Concentrations are calculated on the basis of interstitial water determined from moisture content. Hydrocarbons are corrected for partitioning effects between the headspace and the sediment-water mixture in the paint cans.

Table 2
Carbon Isotopic Composition of Gases and
Organic Carbon in Sediments of Norton Sound ($\delta^{13}\text{C}^{\text{‰}}$)

	Site 3	Site 4
CO ₂	-2.7±0.1, -2.6±0.1	-14.0±0.1, -14.4±0.1
Methane	-37±2, -35±2	-80.5±0.2, 80.4±0.2
Organic Carbon	-27.9, -27.4	-27.8, -27.8

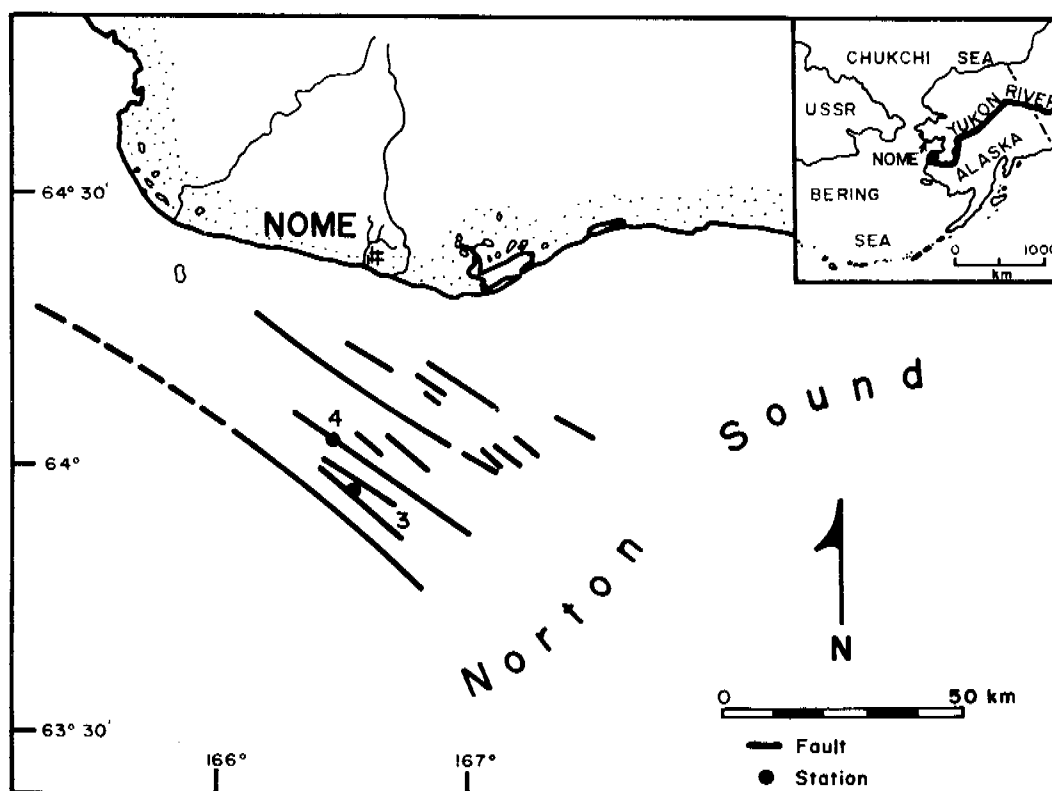


FIG. 1 - LOCATION MAP OF SITES 3 AND 4 IN NORTON SOUND, ALASKA. NEAR-SURFACE FAULT TRACES ARE MAPPED NEAR THESE SITES.

Map coordinates are incorrect
Correct locations are:
Site 3 64°05.3'N; 165°29.5'W
Site 4 64°10.9'N; 165°32.4'W

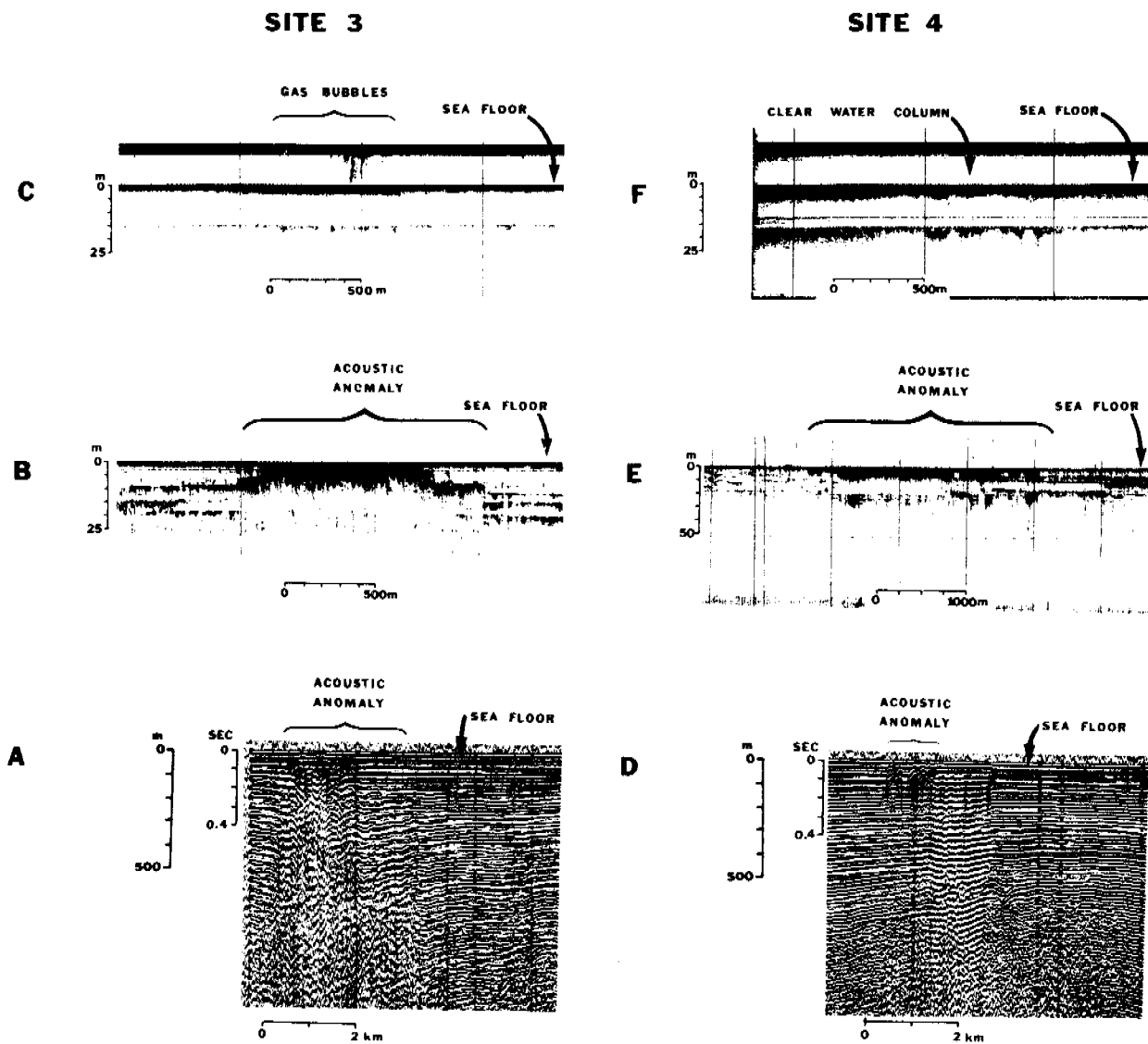


Fig. 2 - Geophysical profiles taken over site 3 (A-C) and site 4 (D-F). A--120-kJ sparker record showing reflector terminations and intervening lack of coherent reflections. B--boomer record showing reflector terminations and continuous zone lacking acoustic definition. C--12-kHz record showing V-shaped gas bubble trains in the water column. D--120-kJ sparker record showing reflector "pull-downs". E--boomer record showing reflector terminations and patchy acoustic response. F--12-kHz record showing a clear water column without bubble trains.

Fig. 3 - This figure has not been included in this report since it was not of sufficient quality for reproduction.



OTC 3354

THERMOGENIC GASES IN NEAR-SURFACE SEDIMENTS OF NORTON SOUND, ALASKA

by Hans Nelson, Keith A. Kvenvolden, and Edward C. Clukey, U.S. Geological Survey

© Copyright 1978, Offshore Technology Conference

This paper was presented at the 10th Annual OTC in Houston, Tex., May 8-11, 1978. The material is subject to correction by the author. Permission to copy is restricted to an abstract of not more than 300 words.

ABSTRACT

A plume of hydrocarbon gases, assumed to be of thermogenic origin based on chemical compositions, has been noted by others in the water column of Norton Sound about 40 km south of Nome, Alaska. We used detailed geophysical transects, side-scan sonar, underwater television, and chromatographic analyses of gases in near-surface sediments to define a probable source area of hydrocarbon gases at the southern apex of the water plume epicenter. Geophysical, geotechnical, and geochemical evidence together indicate that hydrocarbon gases of subsurface, thermogenic origin apparently migrate into the near-surface sediments along a fault zone.

Subbottom reflector terminations on continuous seismic profiles outline a large zone of anomalous acoustic responses about 9 km in diameter and at 100-m depth that may be caused by a subsurface accumulation of gas. Gas migration from the accumulation to the surface sediment is indicated by smaller zones of reflector terminations observed in high-resolution profiles and by seafloor craters seen on underwater television at one station. The presence of gas-charged surface sediment also is suggested by low percent pore water saturation, greater penetration of the penetrometer, and more rapid penetration of the vibracorer in sediment at the station with near-surface acoustic anomalies and seafloor craters.

Analyses of hydrocarbon gases in sediments from a 1.6-m vibracore taken at this station showed unusually high concentrations of hydrocarbon gases heavier than methane; the ethane, propane, *n*-butane, and isobutane were 76, 4, 6, and 52 times greater than in other near-surface sediments in this region, and also significant quantities of gasoline-range hydrocarbons were present. The gas composition and presence in near-surface sediments above a thick underlying section with acoustic anomalies points to the possibility of petroleum at depth in this region. Our work indicates that surface and near-surface studies of the continental shelf may contribute significantly to petroleum-resource evaluations in addition to defining areas of potential hazard from gas-charged sediment.

INTRODUCTION

In the summer of 1976, Cline and Holmes¹ discovered unusual concentrations of hydrocarbon gases, particularly gases heavier than methane, in the water column of Norton Sound (fig. 1). The epicenter of the gas plume is coincident with a near-surface zone of northwest-trending faults about 40 km south of Nome, Alaska. The distribution of these gases, coupled with an assessment of the geochemistry, geology, and geophysics of the area, indicated the nearby presence of a seep of thermogenically derived gases from a possible petroleum reservoir.^{1,2}

In the field season of 1977, we investigated the gas content of the bottom sediment beneath the hydrocarbon-rich plume. We wanted to know where and how the possible seepage would manifest itself in the surface and near-surface sediments and whether such a seepage into sediment presented a geologic hazard. We anticipated that a combination of detailed deep-penetration and high-resolution geophysical techniques together with geotechnical properties and the organic geochemical characteristics of the sediment could precisely define the source of the water column anomaly and the location of a potential petroleum resource. This paper describes application of these techniques to outline (a) the presence of an apparent large (9 km diameter) subsurface gas accumulation, (b) several locations where leakage into near-surface sediments presumably is occurring, and (c) one location where apparent gas craters and thermogenic hydrocarbons are found.

A potential source of the major hydrocarbon accumulation from which the near-surface manifestations are derived is provided by an underlying Tertiary basin, Norton basin. This basin contains up to 5.5 kilometers of marine and continental sediment (fig. 1) (Holmes et al., this volume, OTC no. 3051)³. A thin layer of mixed Pleistocene marine, glacial, and lacustrine deposits overlies the Tertiary deposits;^{4,5} Holocene silty sand 1-3 m thick covers Pleistocene deposits at the seep site 5 where the depth of water is about 20 m. Detailed characteristics of the oceanographic and geologic setting are not given in this paper because companion papers of Holmes et al., and Cline and Holmes (in this volume, OTC no. 3051 and 3052) provide that specific information.

METHODS

A detailed grid of high-resolution reflection profiling and side-scan sonographs, and a limited amount of deep-penetration seismic profiling, was obtained in the region of the gas plume epicenter (fig. 1). The geophysical instruments consisted of an EG&E side-scan sonar with a 100-m sweep, an 800-joule EG&G Uniboom utilizing 4 hull-mounted transducers, a 3.5-kHz Raytheon subbottom profiling system with 12 hull-mounted transducers, a 12-kHz echo sounder, an extra recorder displaying the Uniboom signal filtered at 1500 to 5,500 Hz to detect bubbles in the water column, and a 160-kJ arcer system. This array of profiling systems was used to map patterns of acoustic anomalies and also to detect any associated seafloor gas craters or water column bubble streams caused by leaking gas.

Because no point sources of leaking gas (bubbles) were observed in side-scan sonar, bubble detector, or other high-resolution profiling records, a general reconnaissance grid of vibracorer holes was drilled along the trace of a near-surface fault close to the epicenter of the water column anomaly (fig. 1); some cores were positioned in specific locations of acoustic anomalies and others outside them for background data (figs. 1 and 2). Kiel vibracores with a maximum penetration of 2 m were taken at stations 14 through 17. The vibracorer failed at station 18, thus terminating the coring program. Van Veen surface samples were taken at stations 15, 17, and 18; a box core was obtained at station 16. Station 14 was located to the north of the expected seep location, and thus served as a control. Stations 15, 16, and 18 were located above a fault that was thought to be a possible conduit for the gas seep. Station 17 was positioned south of the locus of the seep as mapped in 1976, but was located within a newly outlined fault and acoustic anomaly zone. At all vibracoring sites except station 18, approximately 30 minutes of underwater television scanning of the seafloor was videotaped, and 20 bottom photos were taken with a 70-mm film camera.

At selected sites throughout Norton Sound, a seafloor penetrometer was deployed to map relative penetration and determine regions of anomalously deep penetration. The penetrometer measured the relative stiffness of the upper meter of sediment by dropping a probe of known weight (5.3 kg) a known distance (6-7 cm) above the seafloor to provide a standardized measurement of penetration at each site.

At all five coring sites, the rate of penetration of the vibracorer was recorded. Thus, the rate of penetration in sediment associated with acoustic anomalies could be compared with those normal sediments without anomalies, and effects from the possible presence of gas could be judged.

To test for unusual amounts of gas in cores, measurements for shear strength and subsamples of known volume were taken in vertical sequence down the cores immediately upon retrieval. Water contents, percent pore water saturation, and bulk densities of the samples were calculated from the measured appropriate weight-volume relations. The percent pore water saturation was evaluated by subtracting the volume of the solid particles in each sample from the total volume of the sample, to determine the volume of pore space, and then dividing the measured volume of water by that difference. If the measured volume of water was not equal to the available pore space (i.e., saturation < 100 percent), then part of

the pore space may have been occupied by hydrocarbon gas. Some pore water may have been lost by drainage after core retrieval and by evaporation before sampling. Effects due to drainage appear to be noticeable near the base of most cores, where there were commonly marked decreases in percent pore water saturation (fig. 3b).

Although physical disturbance of sedimentary structures and stratigraphy in vibracores is minimal, loss of gas, like loss of pore water, may be significant. Unlike pore water, gas may be lost at the seafloor because of the vibracoring process. Once the core reaches the sea surface, any drainage of pore water also will cause loss of gas. The mid-section in the vertical sequence will be the most reliable for gas content, although even these samples will not be quantitative and can only provide a qualitative estimate of the gases. Because of the greater loss of pore water and exposure of the open ends of the core barrel to ambient conditions, the top and bottom samples of a core will be the least reliable for geotechnical and geochemical samples.

The rectangular cores recovered with the Kiel vibracorer were split so that the central part could be sampled in 5-9-cm-long segments at several intervals down the core for gas analyses. Loss of hydrocarbon through this sampling procedure is likely, and the recovered samples probably do not contain quantities of *in situ* gas. The volume of the sample segments from the core was measured for use in determining gas concentrations. Van Veen and box cores, which have the greatest exposure to ambient conditions of any samples, were subsampled with a stainless steel tube that recovered a 10-cm-long core of 0.42 L volume. Sediment splits from all sampling devices were analyzed for hydrocarbon gases by the following procedure:

A sediment sample was placed in a 1-qt. paint can which was immediately filled with helium-purged water. From the can, 100 mL of water was withdrawn, the can was sealed, and the resulting 100 mL headspace was purged with helium through septa previously attached to the can. The can was shaken for ten minutes on a paint-can shaker to release interstitial gas into the 100 mL headspace. Exactly 1 mL of this gas mixture was analyzed on a Carle Model 311 analytical gas chromatograph equipped with both flame ionization and thermal conductivity detectors to obtain complete separation of common hydrocarbon gases containing as many as four carbon atoms. Hydrocarbons with five and more carbon atoms (C_5+) were analyzed as a single backflush peak. Gas concentrations were calculated from the chromatograms by measuring the heights of peaks representing the various gases present in the mixture. Partition coefficients were used to correct for the differences in solubilities of the gases. Concentrations of methane are reported in $\mu\text{L/L}$ wet sediment; the other gases are reported in nL/L wet sediment (Table 1).

RESULTS

The high-resolution records show that near-surface anomalies are common throughout this general region¹ and can be of two general types. Profiling records in figures 2b and 2c over station 17 exhibit an acoustic response consisting of sharp termination of subbottom seismic reflectors and an absence of surface multiple reflectors on the record, indicating nearly complete absorption of the seismic signal. Profiling records near stations 15 (fig. 2d) and 16 and numerous other locations in Norton Basin²

(Nelson, unpub. data) show acoustic anomalies of the second type, where the subbottom record is acoustically turbid, but strong surface multiple reflectors occur in the lower part of the record beneath the upper anomaly zone. This second type of acoustic anomaly appears to be generated by highly reflective surface sources in contrast to the first type of anomaly. In the seismic profile shown in figure 2d it also is apparent that subbottom reflectors outline the edges of buried channels, and that the acoustic anomaly occurs directly beneath the channel floor. In this region of glaciated terrain⁴, it is quite likely that such buried channel floors contain gravel layers producing "reflective" type anomalies rather than "absorptive" types.

The deep-penetration geophysical records from the 160-kJ arcer system exhibited a widespread subsurface "absorptive" type acoustic anomaly in the vicinity of station 17 (figs. 1 and 2a). Our records and also those of Holmes et al. (this volume, OTC no. 3051) show a reflector termination anomaly about 100 m below the seafloor; this acoustically turbid zone is about 9 km wide. Near station 17 is a narrow zone where an upward continuation of this anomalous acoustic response extends close to the seafloor (fig. 2a).

The 3.5-kHz and Uniboom high-resolution seismic profiling records show "absorptive" acoustic anomalies at station 17 (figs. 2b and c) which appear to be a near-surface continuation of the same "absorptive" type anomalies seen in the deep-penetration arcer records. The greater resolution in these records shows that, in some areally restricted zones, the surface of the large, deeper, acoustically anomalous zone rises suddenly to within a meter of the seafloor (figs. 1 and 2a, b, and c). Vibracore samples penetrating only two meters into the seafloor can therefore provide significant information about the cause of the smaller near-surface anomalies as well as their possible relations to the much deeper and wider anomaly patterns observed in the deep-penetration arcer profiles.

The sequence of high-resolution and deep-penetration geophysical records also disclosed previously undetected faults (B and C in figs. 1 and 2e) south of fault A, which was known from previous work (Nelson, unpub. data)⁶. Correlation between seismic records from adjacent tracklines revealed near-surface "absorptive" acoustic anomalies associated with the projected fault traces in the vicinity of stations 17 and 18 (fig. 1). The high-resolution records crossing the projected trace of the newly defined fault C show an "absorptive" type of anomaly covering a 1 x 2 km area around station 17 (fig. 1). Station 18, on the westward projection of a well-defined near-surface fault to the east (A, figs. 1 and 2e), is located over a surficial acoustic anomaly similar in size and type to that at station 17. Unfortunately, we have no deep-penetration records to define the possible occurrence of a deeper and larger associated subsurface acoustic anomaly near station 18, or between stations 17 and 18 where a series of smaller "absorptive" type anomalies occur close to the seafloor (fig. 1).

Geotechnical properties also are anomalous at stations 17 and 18 (fig. 3). At these locations, the rate of penetration of the vibracorer (fig. 3A) was much greater than that encountered at stations 14, 15, and 16 even though all five sites are covered by the same type of Yukon mud. The penetrometer readings at stations 17 and 18 were three times

greater than that of surrounding areas. Penetrometer readings elsewhere in Norton Sound are low except in the east-central region where near-surface peat layers and high quantities of biogenic gas are found⁷, and in the southeastern area where the sediment has a high clay content.

Water saturation percent below the 20-cm-thick surface mixed layer⁸, where bioturbation and other physical and chemical processes may have affected gas contents, also appeared to be consistently lower in sediment at station 17 compared to sediment at stations 14, 15, and 16 (fig. 3B). Coring artifacts (evaporation and drainage at the ends of the barrel) also may have masked true relations of water saturation percent except in the middle parts of the cores.

At stations 14, 15, and 16, the concentrations of hydrocarbon gases from sediment showed no distinctive trends, nor were the concentrations anomalous in any way (Table 1); $C_1/(C_2 + C_3)$ was always greater than 50.* At station 17, however, the $C_1/(C_2 + C_3)$ ratio showed a minimum value of 6*, and the sediment contained anomalous gas concentrations and compositions compared to sediment at other stations. For example, the maximum amounts of methane, ethane, propane, n-butane, and isobutane, were 2.3, 76, 4, 6, and 52 times greater, respectively, than in samples from the other three stations.

Representative gas chromatograms from sediment at approximately the same depth at stations 17 and 14 emphasize the marked difference in concentration and composition of gases at the two sites (fig. 4). Of particular interest at station 17 is the C_5+ peak; this peak represents gasoline-range hydrocarbons that are present in anomalous amounts at all depths below the mixed layer at station 17. The C_5+ peak was not measured because of the lack of a suitable standard.

Although the compositions and the concentrations of gases in sediments at station 17 are anomalous, the amounts measured are well below saturation. For example, we estimate that the solubility of methane in the interstitial water of these samples at a water depth of 20 m is about 50 mL/L of wet sediment. The maximum concentration of methane measured was only about 0.1 mL/L.

DISCUSSION

The geophysical and geotechnical observations, coupled with data on composition of hydrocarbon gases in the bottom sediments (especially the low $C_1/(C_2 + C_3)$ ratios and the presence of gasoline-range hydrocarbons), suggest that thermogenic gas has leaked into near-surface sediment of Norton Sound. The occurrence of hydrocarbon gases of anomalous composition at station 17 coincides with the presence of acoustically turbid zones on seismic-reflection records. A principal cause for such acoustically turbid zones ("absorptive" acoustic anomalies) may be the presence of gas bubbles in the sediment¹⁰. The higher penetration rates of the vibracore and the greater penetration of the bottom penetrometer are a result of lower shearing resistance of the sediment that may

* This ratio has been used as a measure to determine the possible sources of hydrocarbon gases (see ⁹ for discussion). Ratios less than 50 suggest that hydrocarbon gases may be from thermogenic sources, i.e., they result from the same kind of thermal processes which generate petroleum. On the other hand, ratios greater than 50 suggest that gases from biogenic, microbial processes are present.

be due in part to included gas. Lower shearing resistance is related to the development of excess pore pressures (i.e., pressures greater than hydrostatic) that may be a consequence of gas in bubble phase within interstitial pore spaces¹¹. The lower pore water saturation percentages in sediment at station 17 are believed to indicate that gas bubbles may occupy part of the pore space within the sediment (fig. 3).

In addition to acoustic anomalies and geotechnical measurements, television observations of numerous seafloor pits, 10 - 40 cm in diameter at station 17, also suggest the presence of gas that may have vented from sediment into the water (fig. 5). The lack of pits at all stations except 17, and the size, irregular shapes, and lack of ridges or sediment mounding around the pits negate a biological origin and suggest an origin as gas vents. Some pits contain vertical holes descending to unknown depths and resemble underwater fumaroles observed in the bottom of Crater Lake, Oregon (Nelson, unpub. data). No core samples, videotape recordings of underwater television scans, or bottom photographs were taken at station 18, where geophysical and geotechnical data also suggest that gas in bubble phase may be present in surficial sediment.

The geophysical, geotechnical, and geological evidence suggests that the sediment at station 17 is gas-charged. However, the measured concentrations of hydrocarbon gases, although anomalously high, are well below saturation and the formation of free gas bubbles in sediment pore space. In part this contradiction may be explained by loss of gas and pore water during coring and sample processing. Another contributing factor may be inhomogeneity of gas distribution in the sediment as shown by the sporadic occurrence of gas pits on the seafloor and variable gas concentrations down the core.

In the sediments at station 17, the hydrocarbon gases are distributed irregularly, suggesting they are being selectively oxidized, metabolized, or fractionated by some process. Of the gases measured, only propane and n-butane increase continuously with depth (Table 1). Contents of ethane and iso-butane are erratic both in concentration and distribution. The highest concentrations of these gases as well as methane are found in the middle interval of the core, where the lowest water saturation values occur. Contents of ethene and propene remain nearly constant with depth and are comparable to concentrations found in most sediments from other station locations. These unsaturated gases are probably biologically derived and are not significant components of the actual seep gas.

The variable gas concentrations with depth in the sediment may relate to the sampling procedure itself. It was very difficult to recover samples efficiently from the vibracore in a manner that assured minimum loss of gases. The sediment is silty sand that could not be recovered as discrete blocks of material. Even if there has been selective loss of gases in some samples from core 17, this loss has not overshadowed the primary observation that the gases remaining were clearly anomalous in composition relative to the gases in sediments at the other station locations.

Cline and Holmes¹ showed that the gases in the hydrocarbon-rich plume in the water had a minimum $C_1/(C_2 + C_3)$ ratio of about 40 and they used a dynamic model¹ to predict a C_2/C_3 ratio of 1.7 for the

initial gas phase in the sediment. On the basis of these calculations and other considerations, they suggested that the hydrocarbon deposit from which the gas is leaking contains liquid petroleum as well as natural gas. Our data show a minimum $C_1/(C_2 + C_3)$ ratio of 6 and a minimum C_2/C_3 of about 3. Also, gasoline-range hydrocarbons are present as indicated by the C_2+ peak (fig. 4). Therefore, our data point in the same direction as those of Cline and Holmes¹. Apparently, much of the hydrocarbon gas in sediments at station 17 is of thermogenic origin, and it is likely that the gas source is associated with a liquid petroleum occurrence in Norton Basin.

The general appearance of the large (9 km diameter), subsurface (-100 m) acoustic anomaly associated with the Norton Sound gas seep is similar to features observed on seismic records taken over large subsurface gas caps of petroleum reservoirs in developed offshore oil fields (Holmes et al., this volume, OTC no. 3051). In Norton Sound, the seep at station 17 over this acoustic anomaly is located beneath the southern apex of a large gas plume observed in the water column (fig. 1)¹. The highest hydrocarbon concentrations measured in the plume were at a station 5.5 km north of station 17; concentrations decreased northward and westward from this station, as would be expected in a region with north-northwest water currents¹². This relation and the highly pitted seafloor (fig. 5) surrounding station 17 suggest that gas leaking into the water column around this site is a major source of the gas plume observed in the water. The presence of other local, surficial acoustic anomalies and abnormal geotechnical properties indicate that several other possible seep sources for the water plume exist between stations 17 and 18.

Our work indicates that high-resolution profiling, together with geotechnical and geochemical techniques can aid petroleum prospecting. High-resolution seismic profiles may be used in conjunction with deep-penetration seismic records to trace acoustic anomalies from deep, large subsurface sources to surface locations. Regions with near-surface "absorptive" type acoustic anomalies merit additional testing but those with "reflective" type anomalies, for example stations 15 and 16 along the eastern half of fault A (fig. 2d), do not because they are unrelated to anomalous gas concentrations. Scans over "absorptive" anomaly sites with bubble detectors, side-scan sonar, underwater television, and bottom camera can help detect specific gas vents. Geotechnical probes may be deployed to locate areas of anomalous soil engineering properties indicating potential gas-charged sediment. Shallow cores for gas samples should be taken only in areas exhibiting a combination of (a) "absorptive" acoustic anomalies on deep-penetration and high-resolution seismic records, and (b) characteristics of gas-charged sediment such as seafloor pitting, low shearing resistance and low water-saturation values.

Cores for gas and geotechnical sampling need to reach depths greater than one-half meter to obtain a representative subsurface sample and to note sequential changes in gas types and concentrations with depth. For example, normal (background) gas concentrations and pore water saturation values were measured in surface samples at station 17, although they were clearly anomalous deeper in the sediment (Table 1). Apparently, the surface mixed layer, up to one-half meter in depth⁸ and actively reworked by biological, chemical, and physical processes, yields

samples unsuitable for reliable identification of gases and geotechnical properties of surficial sediment.

Gases from submarine seeps have been sampled previously^{9, 13, 14} by capturing and analyzing gas bubbles emanating from the seafloor. We know of only one published report, by Carlisle, Bayliss, and Van Delinder¹⁵, in which marine bottom sediments contained evidence for a seep of thermogenic gas. We used their general approach and with modified methods have apparently confirmed that potential seeps of thermogenic gas can be identified by analyses of hydrocarbons dissolved in the pore waters of marine sediment.

Application of our combined geophysical, geotechnical, and geochemical techniques suggests that the seafloor at station 18 in northern Norton Sound exhibits the desirable criteria for further testing by coring. Seismic records show an area of acoustically turbid sediment at station 18 equal in size to that at station 17 (fig. 1). Sediments with a high degree of penetrability also occur there (fig. 3A). Unfortunately, television and bottom camera data are absent, and lack of core recovery prevented gas analysis of subsurface samples at station 18 in 1977. However, a high priority will be put on collection of bottom surface imagery and of deeper sediment for analysis during the next field season. Smaller acoustic anomaly zones representing potential targets also exist in the area between stations 17 and 18 (fig. 1).

If indeed gas is seeping into the sediments at station 17 from a possible large subsurface accumulation at relatively shallow depths (-100 m)², a potential hazard to petroleum development may exist in the broad 9-km-diameter area over the gas accumulation (fig. 1). Observed patterns of near-surface acoustic anomalies indicate that the subsurface gas may be seeping out of several seafloor locations associated with near-surface faults; these steeply dipping faults may act as pathways for upward migration of gas from the subsurface accumulation (figs. 1 and 2)². Because there appears to be a thick subsurface sequence of gas-charged sediment (Holmes et al., this volume, OTC no. 3051), penetration or even near-penetration of this large accumulation by artificial structures may provide direct avenues for uncontrolled gas migration to the seafloor.

The presence of gas also may cause a reduction in the strength and bearing capacity of the near-surface sediments and present potential hazards for offshore gravity structures and pipeline installations. Soil engineering anomalies have already been measured at stations 17 and 18 where gas seeps are suspected.

CONCLUSIONS

1. One source of a large hydrocarbon-gas plume previously observed in the water column of Norton Sound¹ has been identified in sediment at station 17 (fig. 1). The gas apparently migrates to the seafloor surface along faults dipping steeply toward a large subsurface gas accumulation². Significant geophysical and geotechnical anomalies at station 18 suggest additional potential seep sites over a fault trace 12 km northwest of station 17. All evidence points to a possible new petroleum resource area 45 km south of Nome.

2. Our combination of several geophysical systems, geotechnical probes, and shipboard chromatography provides an effective means for resource exploration. Geophysical methods permit mapping of anomalous acoustic responses that might be caused by gas-charged sediment. These targets can then be tested for (a) "absorptive" acoustic anomalies suggesting near-surface gas, (b) low shear resistance of the sediment possibly indicating gas charging, (c) composition of dissolved hydrocarbons to discriminate between biogenic and thermogenic gas sources. Near-surface core sampling must, however, penetrate beneath the surface mixed layer of sediment to obtain representative gas and geotechnical samples.

3. A potential hazard to development of this possible petroleum resource in Norton Basin is presented by the observed shallow, subsurface (about -100 m) occurrence of a possible large gas accumulation (9 km diameter)². Any artificial structures penetrating the gas accumulation or associated faults may provide direct avenues for uncontrolled gas migration to the seafloor. Near-surface, gas-charged sediments associated with the large, subsurface accumulation, may seriously reduce the bearing capacity for offshore structures and pipelines.

ACKNOWLEDGMENTS

We thank the scientific staff and crew of the R/V Sea Souder for assistance in collection and processing of samples at sea, and particularly we thank J.B. Rapp for help in gas chromatographic analyses. Numerous beneficial discussions on acoustic anomalies in seismic profiles were held with M.L. Holmes, M.S. Marlow, and D.R. Thor. Devin Thor also assisted with figure compilation and drafting along with R.O. Williams, M.C. Larsen, J.J. Patry, and S.A. Bailey. Beneficial review comments were provided by M.L. Holmes and G.E. Claypool.

The cruises were supported jointly by the U.S. Geological Survey and by the Bureau of Land Management through interagency agreement with the National Oceanic and Atmospheric Administration, under which a multiyear program responding to needs of petroleum development of the Alaska continental shelf is managed by the Outer Continental Shelf Environmental Assessment Program (OCSEAP) Office.

REFERENCES

1. Cline, J.D., and Holmes, M.L.: "Submarine seepages of natural gas in Norton Sound, Alaska", *Science* [1977], 198, 1149-1153.
2. Holmes, M.L., Cline, J.D.: "Acoustic anomalies and seeping gas in Norton Basin" [1977], *Geol. Soc. America Abs. with Programs*, 9, no. 7, 1022.
3. Nelson, C.H., Hopkins, D.M., and Scholl, D.W.: "Cenozoic sedimentary and tectonic history of the Bering Sea", In: Hood, D.W., and Kelley, E.J. (eds.) *Oceanography of the Bering Sea* [1974], University of Alaska, Inst. of Marine Sciences, Occasional Pub. No. 2, 485-516.
4. Nelson, C.H., and Hopkins, D.M.: "Sedimentary processes and distribution of particulate gold in northern Bering Sea" [1972], *U.S. Geol. Survey Prof. Paper* 689, 27 p.
5. Nelson, C.H., and Creager, J.S.: "Displacement of Yukon derived sediment from Bering Sea to Chukchi Sea during the Holocene" [1977], *Geology*, 5, 141-146.

6. Walton, F.W., Perry, R.B., and Greene, H.G.: "Seismic reflection profiles northern Bering Sea" [1969], U.S. Dept. Commerce, ESSA, Operational Data Rep., C&GS DR-8.
7. Nelson, C.H.: "Potential seafloor instability from gas-rich sediments and sediment depression craters", In: Environmental Assessment of the Alaskan Continental Shelf, Ann. Rep. of Principal Investigators for Year Ending March 1977 [1978], Environmental Research Lab., NOAA, U.S. Dept. Commerce, Boulder, Colorado, 18, 79-92.
8. Nittrouer, C.A., Sternberg, R.W., Carpenter, R., and Bennett, J.T.: "The use of Pb-210 geochronology as a sedimentological tool: Application to the Washington continental shelf" [in press], Marine Geology.
9. Bernard, B.B., Brooks, J.M., and Sackett, W.M.: "Natural gas seepage in the Gulf of Mexico" [1976], Earth and Planetary Sci. Letters, 31, 48-54.
10. Schubel, J.R., and Scheimer, E.W.: "The cause of the acoustically impenetrable, or turbid, character of Chesapeake Bay sediments" [1973], Marine Geophys. Researches, 2, 61-71.
11. Sangr y, D.A.: Marine geotechnology-state of the art [in press], Marine Geotech., 2, no. 1.
12. Coachman, L.K., Aagaard, K., and Tripp, R.B.: Bering Strait: The regional physical oceanography [1976], Univ. Washington Press, Seattle, 186 p.
13. Clifton, H.E., Greene, H.G., Moore, G.W., and Phillips, R.L.: Methane seep off Malibu Point following the San Fernando earthquake", [1971], In: The San Fernando, California earthquake of February 9, 1971, U.S. Geol. Survey Prof. Paper 733, 112-116.
14. Reed, W.E., and Kaplan, I.R.: "The chemistry of marine petroleum seeps" [1977], Jour. Geochem. Explor., 7, 255-293.
15. Carlisle, C.T., Bayliss, G.S., and Van Delinder, D.G.: "Distribution of light hydrocarbon in seafloor sediments: Correlations between geochemistry, seismic structure, and possible reservoir oil and gas" [1975], In: Proceedings of the 1975 Offshore Technology Conference, 3, 65-70.
16. Cline, J.: "Distribution of light hydrocarbons, C₁-C₄, in Norton Sound and Chuckchi Sea" [1976], In: Environmental Assessment of the Alaskan Continental Shelf, Quarterly Reports, Oct. 1, 1976 - Jan. 1, 1977, Environmental Research Laboratory, NOAA, U.S. Dept. Commerce, Boulder, Colorado, 46 p.

Table 1 - Content of Low Molecular Weight Hydrocarbons in Core Sediment Samples

Interval Sampled (cm)		Content of Low Molecular Weight Hydrocarbons							
		$\mu\text{L/L}$			nL/L				
		C ₁	C ₂	C _{2:1}	C ₃	C _{3:1}	n-C ₄	iC ₄	$\frac{C_1}{C_2 + C_3}$
V= vibracore VV= Van Veen B= box core									
Station 14									
7-12	V	10.7	51	34	27	10	11	11	138
40-45	V	13.8	56	46	31	15	tr	tr	158
80-85	V	8.2	90	52	43	31	tr	tr	62
95-100	V	5.7	73	54	41	24	tr	tr	51
Station 15									
0-10	VV	9.9	53	166	70	72	26	9	81
10-15	V	50.3	33	34	22	19	10	10	928
70-75	V	28.8	38	28	18	9	-	-	514
115-120	V	31.7	70	50	43	24	21	10	279
135-139	V	35.5	114	53	164	22	38	19	128
Station 16									
0-10	B	8.6	21	31	26	15	-	-	183
10-15	V	5.1	38	34	22	9	-	-	86
50-55	V	7.8	27	28	18	9	-	-	175
90-95	V	9.3	27	39	18	9	-	-	205
130-135	V	12.0	60	67	40	24	10	-	121
152-157	V	14.6	60	62	54	24	-	-	128
Station 17									
0-10	VV	3.9	55	48	34	22	8	-	44
10-18	V	101	857	27	21	8	12	8	115
60-69	V	99	8626	24	24	7	tr	946	11
100-109	V	113	6600	-	64	14	28	982	17
145-159	V	6.7	770	44	313	14	187	286	6
160-164	V	18	2005	45	620	22	231	433	7
Station 18									
0-10	VV	0.74	26	43	17	11	-	16	17

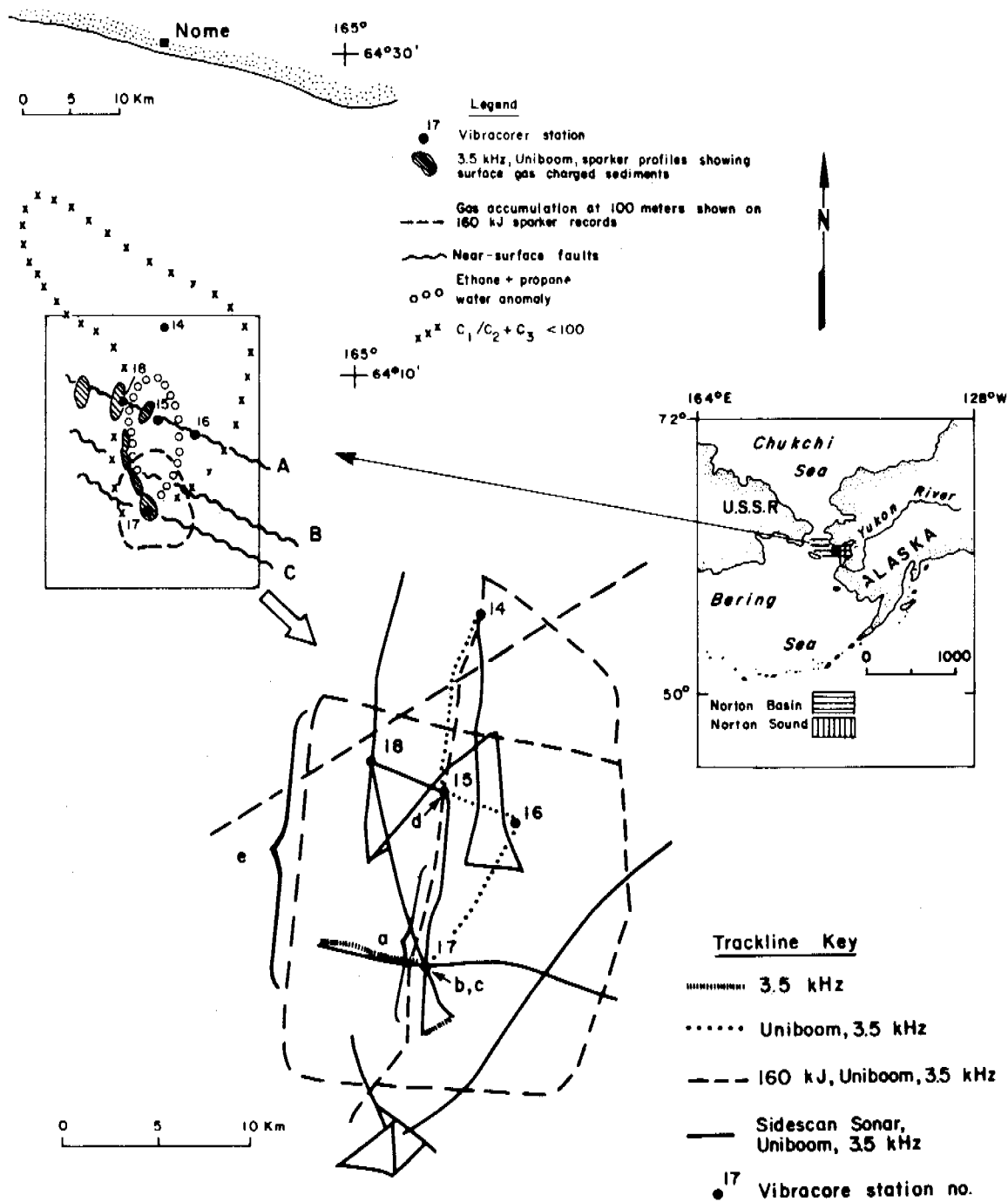


Fig. 1 - Location of region of thermogenic gas-rich sediment and water in Norton Sound showing geophysical tracklines and vibracore station locations. Outline of possible gas cap is after Holmes et al. (OTC paper no. 3051, Volume 1), and data on gas content in water is after Cline (16). Capital letters key near-surface fault traces discussed in this paper. Small letters key locations of seismic profiles in Fig. 2.

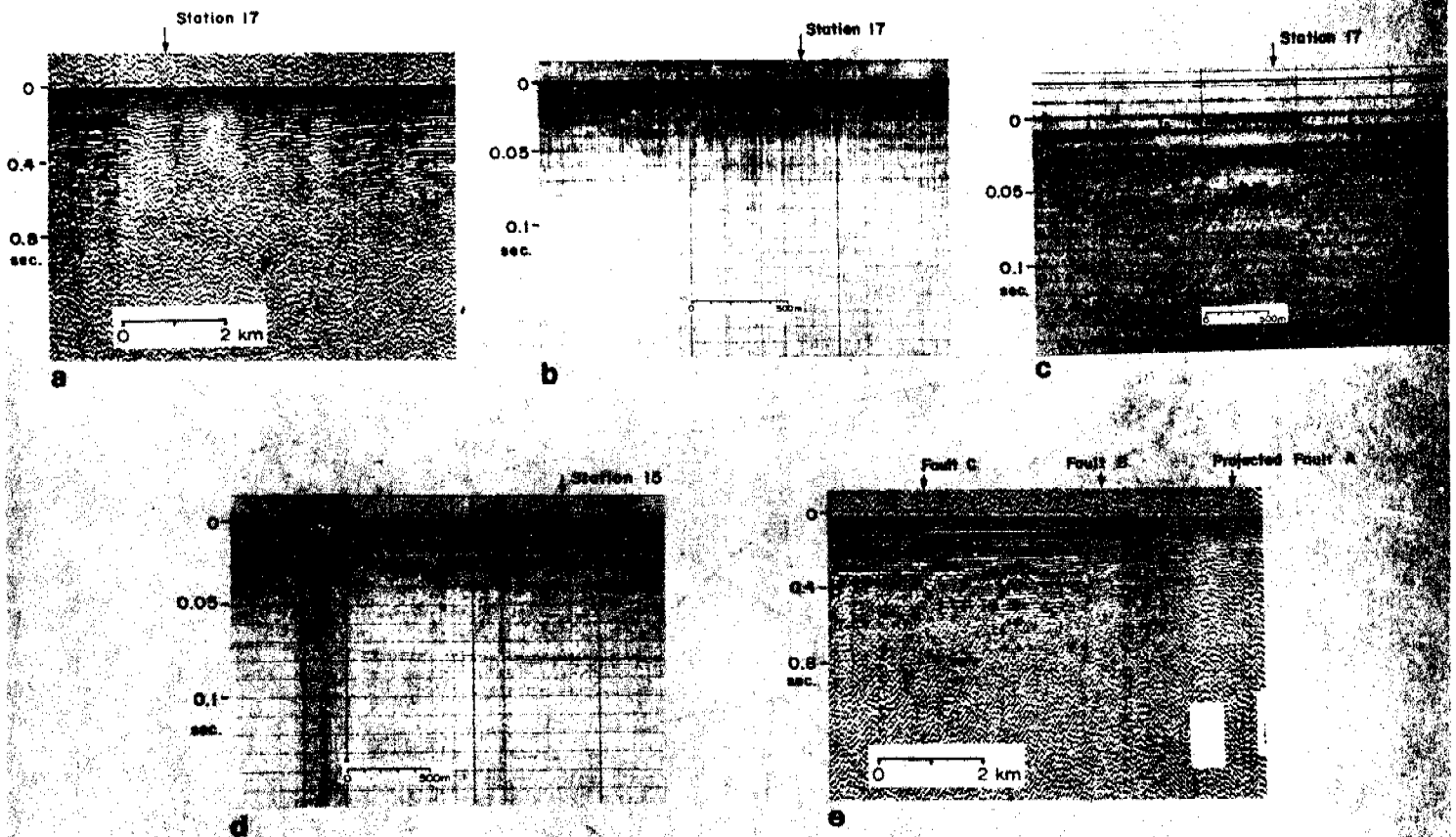


Fig. 2 - Acoustic anomalies observed in continuous seismic profiles from the gas-seep region. The station number above the records indicates the vibracore station locations shown in Fig. 1; the locations of seismic record examples are keyed to the trackline map in Fig. 1.

- (a) Small near-surface acoustic anomaly connecting to a large subsurface acoustic anomaly (possible gas accumulation at -100 m) shown on our 120 kJ arcer record closest to vibracore station 17.
- (b) Acoustic anomaly in Uniboom profile at vibracore station 17.
- (c) Acoustic anomaly in 3.5-kHz profile at vibracore station 17.
- (d) Acoustic anomalies in Uniboom profile over buried channels near fault A and vibracore station 15.
- (e) Arcer profile across faults A, B, and C. Acoustic anomalies obscure apparent location of fault A projected from other adjacent records.

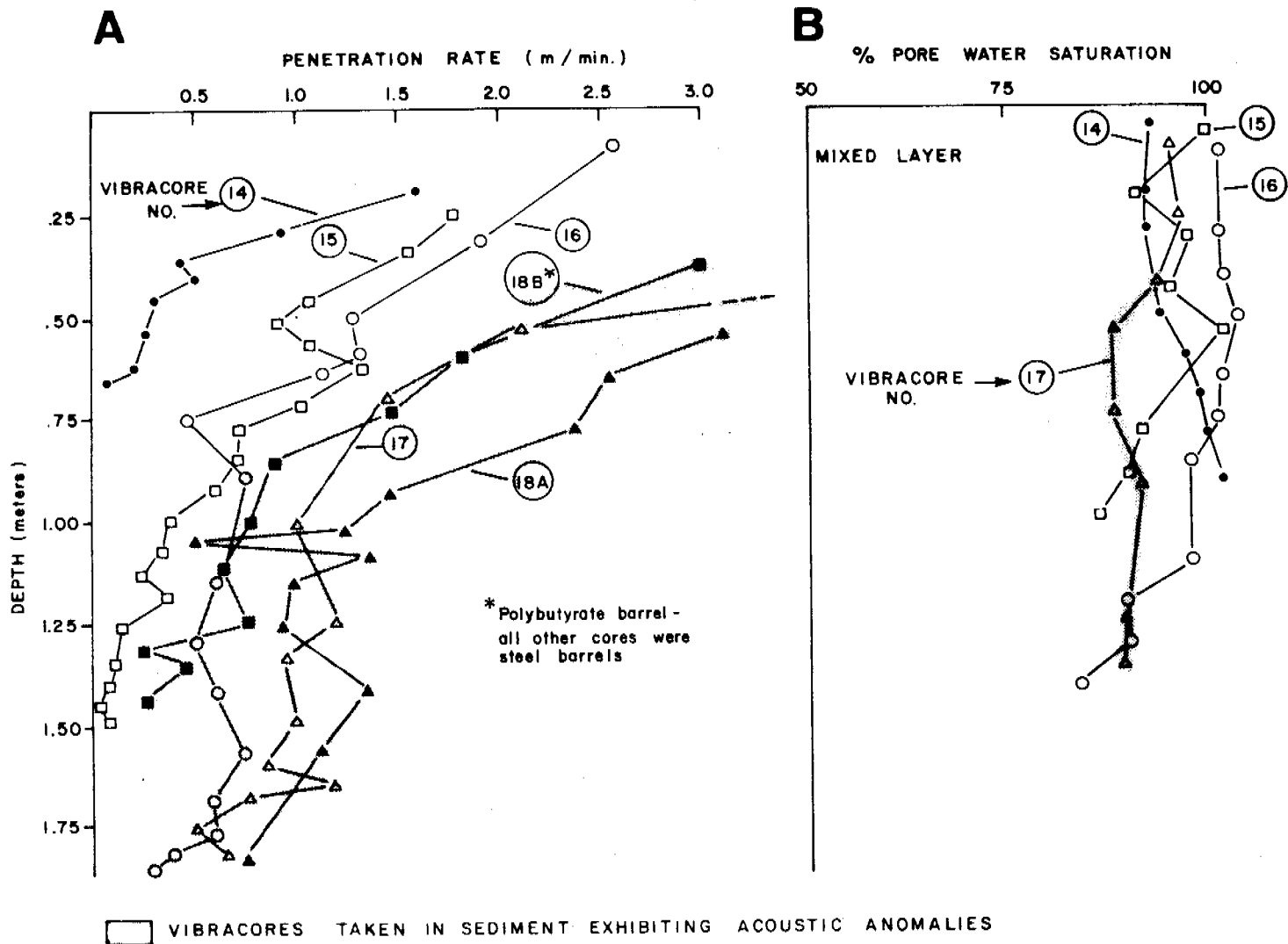


Fig. 3 - (A) Vibracore penetration rates, and (B) percent pore water saturation at sites in the thermogenic seep area of Norton basin (see Fig. 1 for vibracore station location.) Profiles in Part B were constructed by using three-point moving averages of original values.

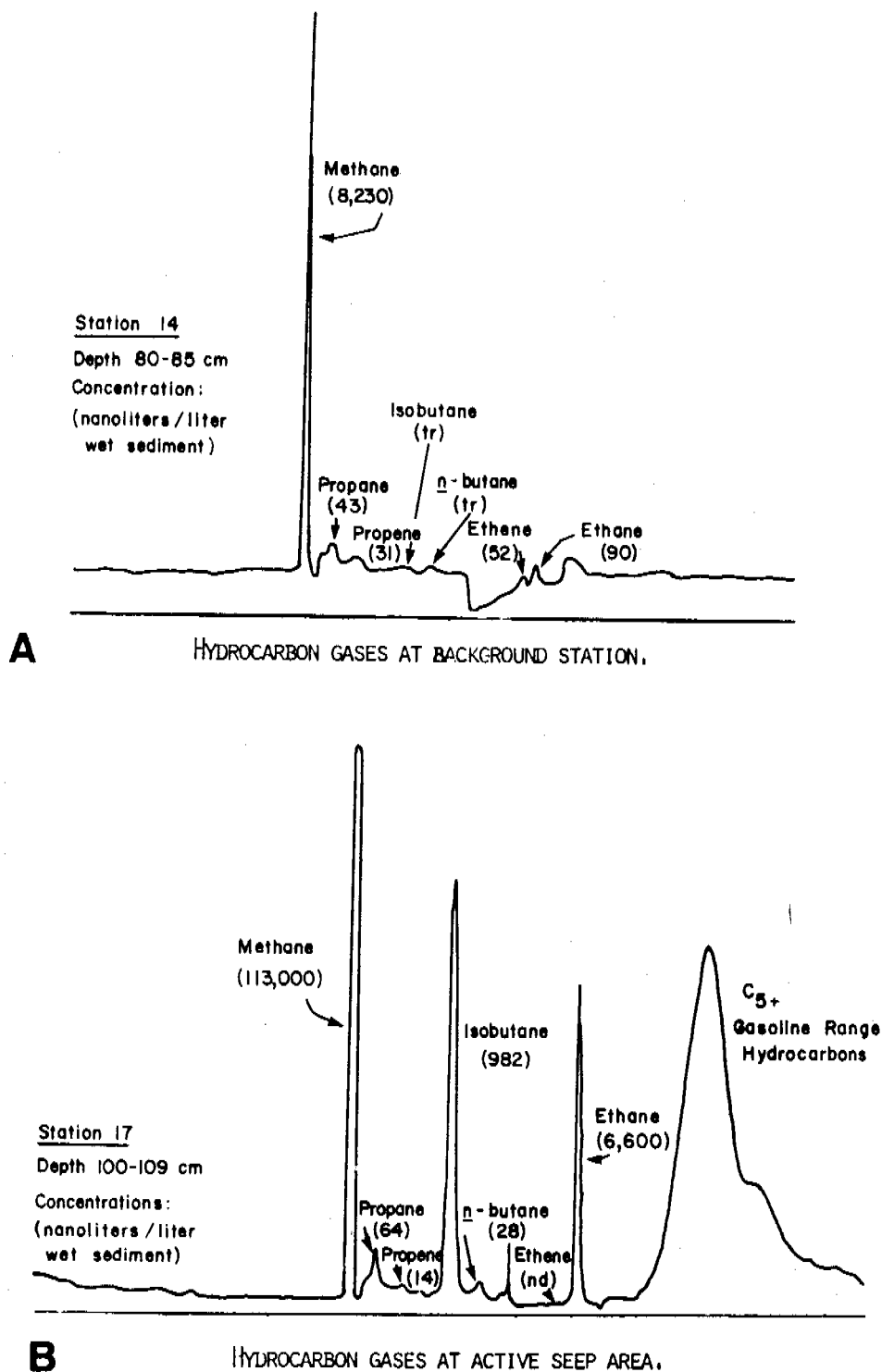


Fig. 4 - Representative hydrocarbons gas chromatograms (A) at background site of vibracore station 14 and (B) at thermogenic gas-rich site of station 17 (see Fig. 1 for location of vibracore stations.)

Fig. 5 - This figure has not been included in this report since it was not of sufficient quality for reproduction.

DISTRIBUTION OF GAS-CHARGED SEDIMENTS IN NORTON BASIN,
NORTHERN BERING SEA

M. L. Holmes and D. R. Thor

ABSTRACT

Seismic reflection records from Norton Sound and Chirikov basin contain numerous zones of anomalous acoustic responses caused by gas in the subsurface sediment layers. These acoustic anomalies have been detected using sound sources ranging in size and power from 3.5 kHz transducers to 1326 cubic inch air gun arrays. The frequency and distribution of these zones suggest that up to 7000 km² of the northern Bering Sea (Norton basin) may be underlain by gas-charged sediment. Much of the gas is of shallow biogenic origin, having been generated in buried peat deposits. Compressional velocity is about 1.5 km/sec in these layers, or 7 per cent below the velocity in gas free areas as determined from seismic refraction studies. Seismic velocity beneath a large gas seep south of Nome decreases to about 1.2 km/sec in the interval from 250-440 m below the sea floor. Here, thermogenic gases of deeper origin are migrating upwards along a system of basin margin faults.

INTRODUCTION

Discovery of the submarine seepage of natural gas south of Nome, Alaska, in 1976 (Cline and Holmes, 1977) prompted a comprehensive review of seismic reflection data from the Norton basin area (Fig. 1). The same types of anomalous acoustic responses associated with the seep zone (Cline and Holmes, 1977; Holmes and Cline, 1978; Nelson et al., 1978) were first encountered by Grim and McManus (1970) in the course of a high-resolution seismic study of the northern Bering Sea in 1967. They interpreted the zones of acoustically impenetrable sea floor on their sparker records as representing a Yukon River deposit very near the surface of the present-day sea floor. The highly reflective nature of this surficial deposit was thought to cause the sudden termination of deeper reflectors observed along portions of the seismic track (Grim and McManus, 1970). Air gun reflection records collected in Chirikov basin during a cruise by NOAA (then ESSA) in 1968 (Walton et al., 1969) also crossed a few of these reflector termination anomalies.

Cline and Holmes (1977) first suggested that these acoustic responses were caused by the presence of bubble phase gas in the near-surface sediment; Holmes and Cline (1978), Nelson et al. (1978), and Kvenvolden et al. (1979) presented detailed analyses of the deep penetration and high resolution seismic reflection records collected over the seep zone and the geochemistry of sediment samples from Norton Sound and Chirikov basin on USGS cruises in 1977 and 1978.

The main objective of this study was to determine the geographic extent and distribution of zones showing anomalous acoustic responses on seismic reflection records from Norton Sound and Chirikov basin. Certain

characteristics of these acoustic anomalies could then be analyzed to determine the most probable cause of the anomaly (gas, change in sediment type, etc.). Seismic records used for this study were collected aboard U.S. Geological Survey and University of Washington research vessels during the past 12 years along some 27,000 km of trackline (Fig. 2). Sound sources used in these geophysical studies included medium- and high-resolution sparker, 40 to 1300 cubic inch air gun, Uniboom, and subbottom profilers.

GEOLOGIC SETTING

The floor of the northern Bering Sea is a broad, shallow epicontinental shelf (Fig. 1). Water depths in Chirikov basin in the western part of the survey area range from 20-50 m. Norton Sound is bounded on the north by Seward Peninsula, on the east by the Alaska mainland, and on the south by the Yukon Delta. Water depths in Norton Sound range from 10-25 m. The surficial sediment of Norton Sound is primarily derived from the Yukon River and consists of coarse silt to very fine sand underlain by organic rich, nonmarine, peaty mud. Surficial sediment in Chirikov basin consists mostly of glacial gravel and transgressive fine sand (Nelson and Hopkins, 1974; McManus et al., 1974).

DESCRIPTION AND CAUSE OF ACOUSTIC ANOMALIES

Figures 3 and 4 show the locations of acoustically anomalous zones along more than 20,000 km of seismic reflection lines in Norton basin. The distribution of the many crossings of these zones suggests that they occur in large patches beneath much of the sea floor of Norton Sound; the total area may be as much as 7000 km². Two distinct types of acoustic anomalies were observed on the seismic reflection records: Reflector pull-downs and

reflector terminations (Holmes and Cline, 1978). Reflector pull-downs similar to those shown in Fig. 5 have been observed and described by several other investigators from both deep and shallow water areas where gas had accumulated in the subsurface strata (Lindsey and Craft, 1973; Cooper, 1978). The low compressional velocity in gas-charged horizons causes the recorded time section (seismic record) to be distorted relative to the true depth section. The greater travel time through the gassy sediment produces a zone of pulled down reflectors beneath it on the seismic record. The gas does not necessarily have to be in the free state (bubble phase) to produce this phenomenon; gas-water or oil-water solutions have compressional velocities less than water alone (Craft, 1973), although the decrease is much greater if gas is present in the sediment interstices. The strong horizontal reflector exhibiting a 180° phase shift which is associated with the observed pull-downs (Fig. 5) could be the result of reflections from interfaces between gas-charged zones and strata where water alone fills the pore spaces. The decrease in both compressional velocity and density due to the presence of gas in the sediment results in a large negative reflection coefficient at the top of the gas-charged layer (Craft, 1973; Savit, 1974). Such a condition would produce acoustic responses similar to the strong horizontal reflectors above the reflector pull-downs (Fig. 5).

Crossings of the acoustic anomaly associated with the gas seep south of Nome are shown in Figs. 5 and 6. The anomaly covers an area of about 50 km^2 ; it is characterized by a sudden termination of subbottom reflectors, and by a dramatic pull-down of the reflectors at its margins (Fig. 6). The depth to the top of the feature causing the anomalous acoustic signature appears to be quite shallow, on the order of 50-200 m. In places the surface of the acoustically opaque zone rises abruptly to within a few meters

of the sea floor (Nelson et al., 1978). These zones may indicate the locations of the active seeps (Kvenvolden et al., 1979).

Calculations by Cline and Holmes (1977, 1978) indicated that the concentrations of the low molecular weight hydrocarbons which had accumulated in the sediment beneath the seep zone were far below theoretical saturation values. This finding was in conflict with the seismic reflection data, which strongly suggested the presence of bubble phase gas in the sediment. The paradox was resolved by the recent discovery that the seep consists primarily of CO₂ rather than hydrocarbons, and that CO₂ is present in the free state in the sediment interstices (Kvenvolden et al., 1979).

Examples of other reflector termination anomalies observed on air gun records in Norton basin (Fig. 7) are quite different from the one associated with the gas seep. They exhibit only slight reflector pull-downs at their margins, and lack the dramatic "wipe-out" appearance of the seep anomaly. Low frequency reflections at 0.6, 0.9, and 1.2 seconds can be traced across the acoustic anomaly zone (Fig. 7); these reflectors show distinct pull-down relative to the corresponding reflectors in the normal section. The attenuation of all but the low frequency energy is a distinctive characteristic of the reflector termination zones (Figs. 3 and 4).

Other indirect evidence indicating abnormally low compressional velocities in these shallow zones is provided by the multichannel seismic reflection data collected by the USGS in August 1978. An oscillographic camera is used to monitor the signal from the hydrophone streamer every 50 shots. A "normal" shot record is shown in Figure 8. This is not a "gather" in the true sense of the word, but merely a recording of the output from each of the 24 streamer channels for one shot from the 1326 cubic inch (21.7ℓ) air gun array. Refracted arrivals (head waves), the water wave, and

reflected arrivals are clearly visible. In sharp contrast is a shot record over the gas seep reflector termination zone (Fig. 9). Little reflected energy is returned to the streamer over the gas-charged zone. Severe attenuation of the reflected arrivals is apparent, and the only arrival beyond trace 22 is the direct water wave (D). This phenomenon can easily be explained by invoking the model of near-surface gas-charged sediment; attenuation of the reflected arrivals, especially the high frequencies, will be pronounced (Mavko and Nur, 1979), as in the case of Figure 9.

Anomalous acoustic responses were also observed on mini-sparker and Uniboom reflection records (Grim and McManus, 1970; Nelson et al., 1978; Kvenvolden et al., 1979). Small reflector pull-downs observed on the air-gun records usually appear as abrupt reflector terminations on the high resolution profiles. Anomalies on Uniboom and mini-sparker records characteristically are near the surface (10 meters or less) and in some cases the top of anomalies are in the energy pulse of the record. Core-sample gas analysis substantiates that the top of gas-charged sediment zone is within a couple tens of centimeters of the surface (Kvenvolden et al., in press). The thickness of these near-surface gas zones is unknown, because only the top of the zone acts as a reflector, no energy is returned from lower reflectors. A minimum thickness of 5 m is set by the continuously high gas contents in a 5-m-long core.

Figure 10 shows a portion of a mini-sparker (800 joules) record over an anomaly approximately 20 km east of the Norton basin gas seep. The near surface zone of diffractions (point source reflectors) was at first thought to be related to the acoustic anomaly; this diffraction layer is commonly observed on high-resolution records over the reflector wipe-outs. However, careful examination of the seismic data (Fig. 10) shows that the diffractions are also present outside of the acoustic anomaly zones. The presence of

gas in the near-surface sediment apparently attenuates energy reflected from deeper horizons in the gas-charged zone, thereby making the zone of diffractions more apparent on records over the gas-charged zones. The patches of diffracted arrivals observed on the high resolution records in Norton Sound and Chirikov basin are probably caused by coarse sediment (cobbles and pebbles) buried in or a few meters beneath the Holocene section.

The extensive reflector termination anomalies observed throughout Norton basin (Figs. 3 and 4) are probably caused by a subsurface accumulation of gas in sufficient quantity that scattering and attenuation of the seismic signal, even from large sources, is almost complete. The drastic reduction in apparent amplitude of both the reflected and direct arrivals was observed over virtually all of the reflector termination anomalies crossed in the course of the geophysical surveys. It is indicative of an unusually low impedance mismatch at the sea floor; the most likely explanation is the presence of free (bubble-phase) gas in the sediment.

Geochemical analyses by Kvenvolden and others (1979) have shown that biogenic methane and thermogenic carbon dioxide are present at saturation volumes in near-surface sediment at many station sites in Norton basin. At many of the sampled sites, but not all, acoustic anomalies are associated with known saturated gas conditions.

Reflector Pull-Down Analysis

In an effort to gain more quantitative estimates of the velocity changes due to the presence of gas, a method was developed for computing the compressional velocity in gas-charged zones over which single channel seismic reflection records show a distinct pull-down of reflectors. Compressional velocity data obtained from sonobuoy refraction profiles (Holmes and Fisher, 1979) were first used to construct an average thickness versus reflection time curve for the "normal" gas-free section in Norton basin.

The next step was to carefully measure reflection times to several marker horizons which can be traced across a pull-down zone. The reflection times measured from the single channel seismic sections were first corrected for source to receiver offset using the formula

$$T_v^2 = T_r^2 - \frac{x^2}{V_o^2}$$

where T_r = apparent reflection time from the record, x = source to receiver offset, V_o = compressional velocity just beneath the sea floor (1.60 km/sec), and T_v = corrected (normal incidence) reflection time.

The depth to a given reflector could then be determined using the equation for the depth (thickness) versus reflection time curve derived from the sonobuoy measurements:

$$D = 0.80 T_v + 0.167 T_v^2$$

It was then possible to construct average velocity curves for both the normal zones and the gas-charged zones:

$$\frac{2}{V} = \frac{4D^2 + x^2}{T_v^2}$$

where T_v = corrected vertical reflection time to a given reflector in the normal zone and to that same reflector in the pulled-down (gas-charged) section. These average velocity curves can then be used to compute interval velocities in each zone.

In actual practice, reflectors were picked at time increments of 0.1 sec, and these intervals were carried through the entire chain of calculations. Figure 11 is an example of such an analysis of the pull-down zone over the gas seep shown in Figure 6. The analysis extends only to

a subbottom depth of 640 m; the extent and character of the acoustically anomalous zone beneath the seep area prevents accurate picking of pulled-down reflectors below that depth. However, the general trend of the average and interval velocity curves for the gas-charged zone beneath the seep suggest that the entire section above basement (about 1.3 km) probably contains enough gas to significantly lower compressional velocity.

The interval velocity curve can also be used as a qualitative indicator of gas concentration in the sedimentary section. Figure 11 shows that compressional velocity reaches a minimum of 1.21-1.24 km/sec between 250-440 m subbottom depth. This represents a decrease of about 35 per cent from the velocity one would expect at that depth in a normal sedimentary section. If the interval velocity curve could be constructed for the entire section down to basement, it might exhibit several minima similar to the one shown in Figure 11. These minima are probably an expression of a change in sediment or rock type which allows gas to be concentrated in those horizons.

POSSIBLE SOURCES OF GAS

The distribution of acoustic anomalies (Figs. 3 and 4) suggests that near-surface accumulations of gas are most common in the central part of Norton basin northwest of the Yukon River delta. The apparent gas-free zones along the southern and eastern shores of Norton Sound (Fig. 3) are due to the absence of data from these very shallow water areas. Such is not the case for western Norton basin, however. Seismic reflection coverage is good (Fig. 2); there are simply few occurrences of acoustic anomalies.

The possible sources of the gas are still being investigated. The gas seep south of Nome is the only well-substantiated source of low

molecular weight hydrocarbon gases and carbon dioxide indicative of a deep thermogenic origin (Cline and Holmes, 1978; Nelson et al., 1978; Kvenvolden et al., 1979).

Carbon isotope measurements on the CO₂ and CH₄ components yielded $\delta^{13}\text{C}$ values (relative to PDB) of -0.27% and -3.6% , respectively (Kvenvolden et al., 1979). Holmes and Cline (1979) have used these data to estimate the source depth of these seep gases. A $\delta^{13}\text{C}$ value of -3.6% is characteristic of methane from a depth of about 2500 m (Galimov, 1969). This greatly exceeds basement depth (850-1450 m) beneath the seep, suggesting that the gas has migrated to the seep area from the deeper central portion of Norton basin. The southerly dip of beds and unconformities as well as numerous faults observed on the reflection records over the seep also support such an interpretation.

The location of many of the other reflector termination zones, especially in Norton Sound, coincides with known occurrences of buried tundra-derived peat deposits which were formed during low sea-level stands in the Quaternary (Nelson and Creager, 1977). Biogenic methane and carbon dioxide generated in these peat beds could cause the observed anomalous acoustic responses (Kvenvolden et al., in press); the peat layers themselves could also act to trap upward migrating petroleum-derived gases. A velocity analysis similar to the one previously discussed for the seep zone was performed for an acoustic anomaly associated with a suspected peat deposit. Although the reflector termination anomalies usually associated with this type of gas accumulation make it difficult to trace reflector pull-downs, preliminary results suggest that the gas has accumulated in near surface horizons up to a few tens of meters thick. Compressional velocity in these layers is approximately 1.5 km/sec, or about 7 percent less than in the surrounding gas-free sediment.

The absence of acoustic anomalies (gas-charged sediment) in western Chirikov basin is probably due to the different types of Quaternary deposits. Chirikov basin was extensively glaciated during the Pleistocene (Grim and McManus, 1970); the boundary between the glaciated and unglaciated terrain corresponds closely with the eastern limit of acoustic anomalies in Figs. 3 and 4. The Quaternary glacial and glacio-marine sediments deposited in Chirikov basin do not have a high potential for biogenic gas generation because advance and retreat of the ice sheets evidently destroyed or prevented the growth of tundra-derived peats common to Norton Sound. Also, the relatively thin Tertiary sedimentary section beneath Chirikov basin has not attained sufficient thickness to subject the basal sediments to the temperatures and pressures required for the generation of hydrocarbon gases.

SUMMARY

The distribution of acoustic anomalies indicates that almost 7000 km² of seafloor in Norton Sound and Chirikov basin is underlain by sediments containing sufficient gas to affect sound transmission through these zones. A method of indirectly determining compressional velocity in the gas-charged zones gave values from 7 to 35 per cent lower than would be expected in the case of gas-free sediment. The cause of one of the anomalies, that associated with the Norton basin gas seep, is well documented. Here thermogenic gases are seeping to the surface along a system of basic margin faults. Although other undiscovered seeps of the thermogenic gas may exist in Norton Sound or Chirikov basin, most of the acoustic anomalies in this area are probably caused by biogenic gases generated in buried peat layers. Further detailed processing and analysis of the seismic data will possibly permit quantitative estimates to be made of the amounts of gas present in these acoustically anomalous zones.

REFERENCES

- Cline, J.D., and Holmes, M.L. (1977) Submarine seepage of natural gas in Norton Sound, Alaska. Science 198, 1149-1153.
- _____ (1978) Anomalous gaseous hydrocarbons in Norton Sound: Biogenic or thermogenic? Proceedings, Offshore Technology Conference, Houston, p. 81-86.
- Cooper, A.K. (1978) Hydrocarbon prospects for the frontier abyssal areas of the Bering Sea. The Oil and Gas Journal, Oct. 23, p. 196-201.
- Craft, C.I. (1973) Detecting hydrocarbons--for years the goal of exploration geophysicists. The Oil and Gas Journal, Feb. 19, p. 122-125.
- Galimov, E.M. (1969) Isotopic composition of carbon in gases of the crust. International Geology Review 11, 1092-1104.
- Grim, M.S., and McManus, D.A. (1970) A shallow seismic-profiling survey of the northern Bering Sea. Marine Geology 8, 293-320.
- Holmes, M.L., and Cline, J.D. (1978) Geological setting of the Norton basin gas seep. Proceedings, Offshore Technology Conference, Houston, p. 73-80.
- _____ (1979) Source depth and geologic setting of the Norton basin gas seep. Journal of Petroleum Technology 31, 1241-1248.
- Holmes, M.L., and Fisher, M.A. (1979) Sonobuoy refraction measurements from Norton basin, northern Bering Sea. Program, Amer. Assoc. Petroleum Geologists Annual Convention, Houston, p. 104 (abs).
- Kvenvolden, K.A., Nelson, C.H., Thor, D.R., Larsen, M.C., Redden, G.D., and Rapp, J.B. (1979) Biogenic and thermogenic gas in gas-charged sediment of Norton Sound, Alaska. Proceedings, Offshore Technology Conference, Houston, p. 479-486.

- Lindsey, J.P., and Craft, C.I. (1973) How hydrocarbon reserves are estimated from seismic data. World Oil, Aug. 1, p. 23-25.
- Mavko, G.M., and Nur, A., (1979) Wave attenuation in partially saturated rocks. Geophysics 44:161-178.
- McManus, D.A., Venkatarathnam, K., Hopkins, D.M., and Nelson, C.H. (1974) Yukon River sediment on the northernmost Bering Sea shelf. Journal of Sedimentary Petrology 44, 1052-1060.
- Nelson, C.H., Hopkins, D.M., and Scholl, D.W. (1974) Cenozoic sedimentary and tectonic history of the Bering Sea. In D.W. Hood and E.J. Kelley (eds.) Oceanography of the Bering Sea, University of Alaska, Inst. Marine Sciences, p. 485-516.
- Nelson, C.H., and Creager, J.S. (1977) Displacement of Yukon-derived sediment from Bering Sea to Chukchi Sea during Holocene time. Geology 5, 141-146.
- Nelson, C.H., Kvenvolden, K., and Clukey, E.C. (1978) Thermogenic gases in near-surface sediments of Norton Sound, Alaska. Proceedings, Offshore Technology Conference, Houston, p. 2623-2633.
- Savit, C.H. (1974) Bright spot in the energy picture. Ocean Industry, Feb., p. 60-65.
- Walton, F.W., Perry, R.B., and Greene, H.G. (1969) Seismic reflection profiles, northern Bering Sea. Environmental Science Services Administration Operational Data Report C & GS DR-8, 26 p.

FIGURE CAPTIONS

- FIGURE 1. Location map of study area showing Norton Sound, Chirikov basin, and the Norton basin gas seep (Cline and Holmes, 1977; Holmes and Cline, 1979).
- FIGURE 2. Seismic reflection tracklines in the northern Bering Sea. Cruise dates and sound sources used are also shown.
- FIGURE 3. Location of anomalous near-surface acoustic responses observed on single channel air-gun and minisparker seismic reflection records from Norton Sound and Chirikov basin. Also shown are the locations of the Norton basin gas seep (Cline and Holmes, 1977), and the seismic record sections shown in Figures 5,6,7,10.
- FIGURE 4. Location of anomalous near-surface acoustic responses observed on Uniboom reflection records from Norton Sound and Chirikov basin.
- FIGURE 5. Seismic reflection record across the Norton basin gas seep zone. Location of line shown in Figure 3. This record shows two types of acoustic anomalies indicative of gas in the sediment: Reflector terminations and reflector pull-downs.
- FIGURE 6. Single channel reflection record across the Norton basin gas seep area. Location of line shown in Figure 3. Reflector termination zone and marginal pull-downs are clearly shown.
- FIGURE 7. Single channel seismic reflection record from eastern Norton basin showing "normal" reflector zones and typical reflector termination anomalies. Location of line is shown in Figure 3.
- FIGURE 8. Multichannel shot record over "normal" reflector sequence shown in Figure 7. Refracted head waves (H), and reflected arrivals (R) are clearly visible.
- FIGURE 9. Multichannel shot record over the gas seep reflector termination anomaly shown in Figure 6. All arrivals are markedly attenuated due to gas in the near surface sediment. Amplifier settings slightly higher than in Figure 8.
- FIGURE 10. Minisparker (800 joules) record from Norton basin showing reflector termination anomaly with near-surface diffractions. Location of line is shown in Figure 3.
- FIGURE 11. Velocity analysis of reflector pull-down zone beneath the Norton basin gas seep (Fig. 6). The two right hand curves show average and interval velocity versus depth in the gas-free reflector sequence outside the seep zone. The two curves on the left are for the gas-charged section beneath the seep itself.

Fig. 1 - Location map of study area showing Norton Sound, Chirikov basin, and the Norton basin gap seep (Cline and Holmes, 1977; Holmes and Cline, 1979).

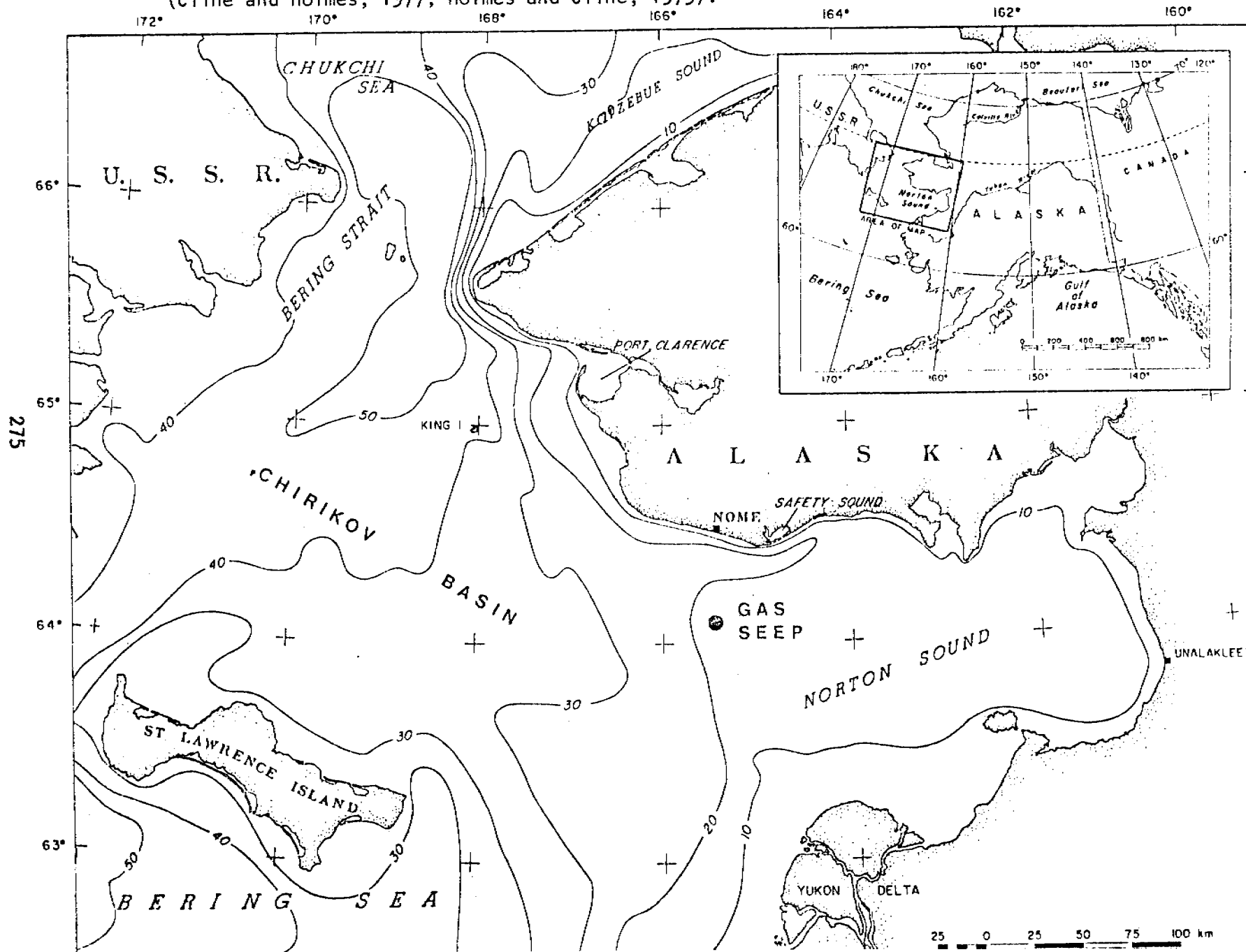


Fig. 2 - Seismic reflection tracklines in the northern Bering Sea. Cruise dates and sound sources used are also shown.

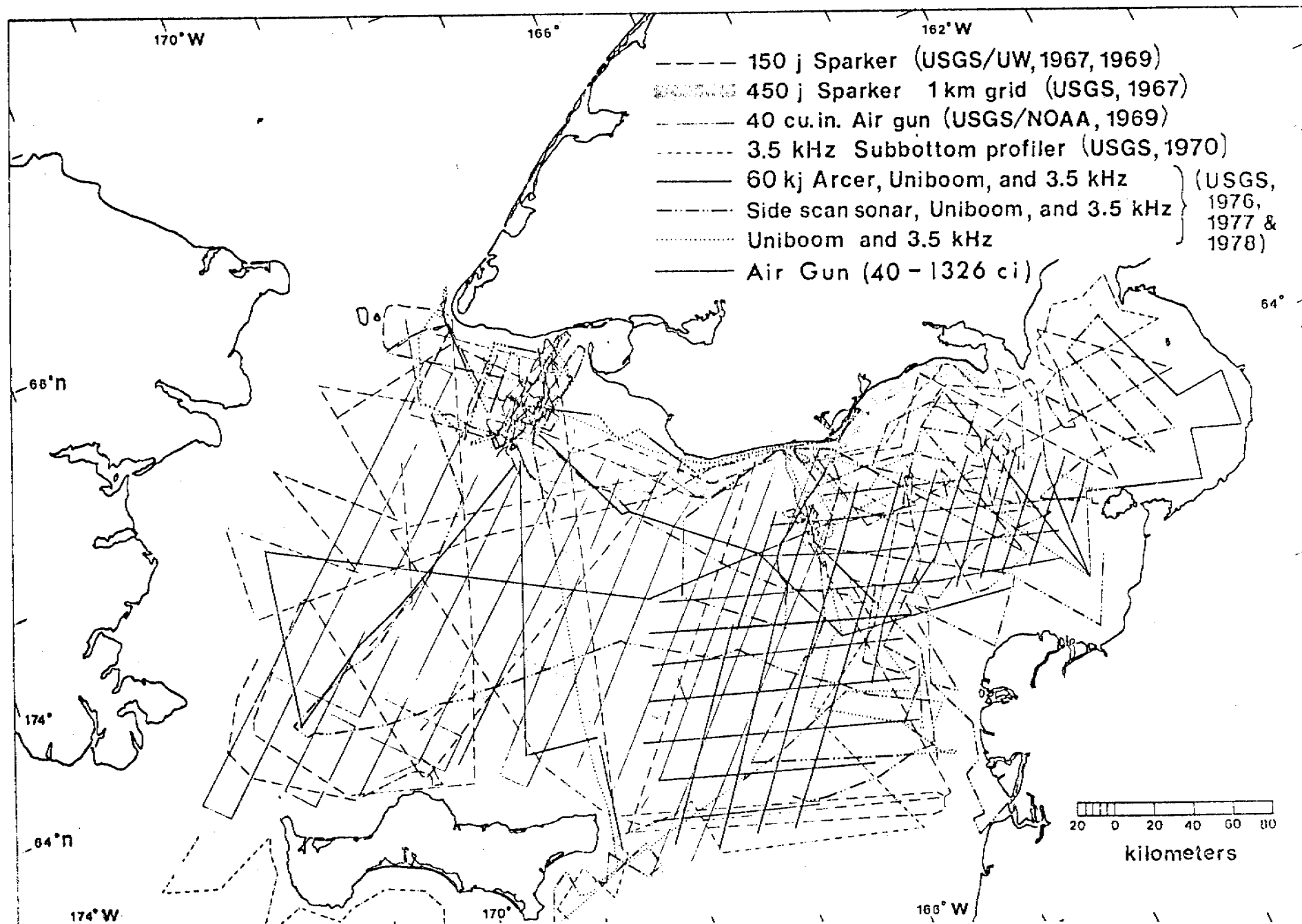


Fig. 3 - Location of anomalous near-surface acoustic responses observed on single channel air-gun and minisparker seismic reflection records from Norton Sound and Chirikov basin. Also shown are the locations of the Norton basin gas seep (Cline and Holmes, 1977), and the seismic record sections shown in Figures 5, 6, 7 and 10.

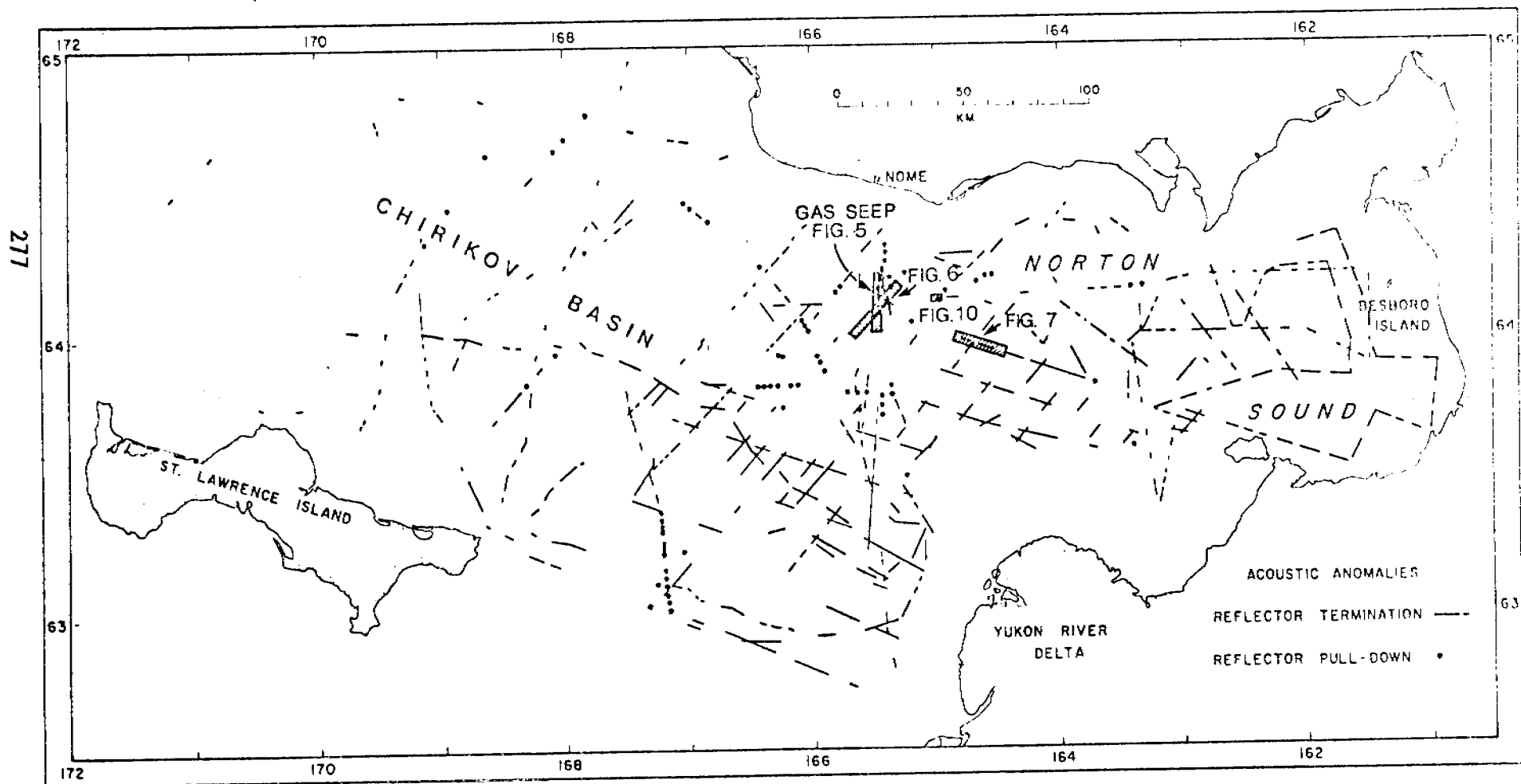


Fig. 4 - Location of anomalous near-surface acoustic responses observed on Uniboom reflection records from Norton Sound and Chirikov basin.

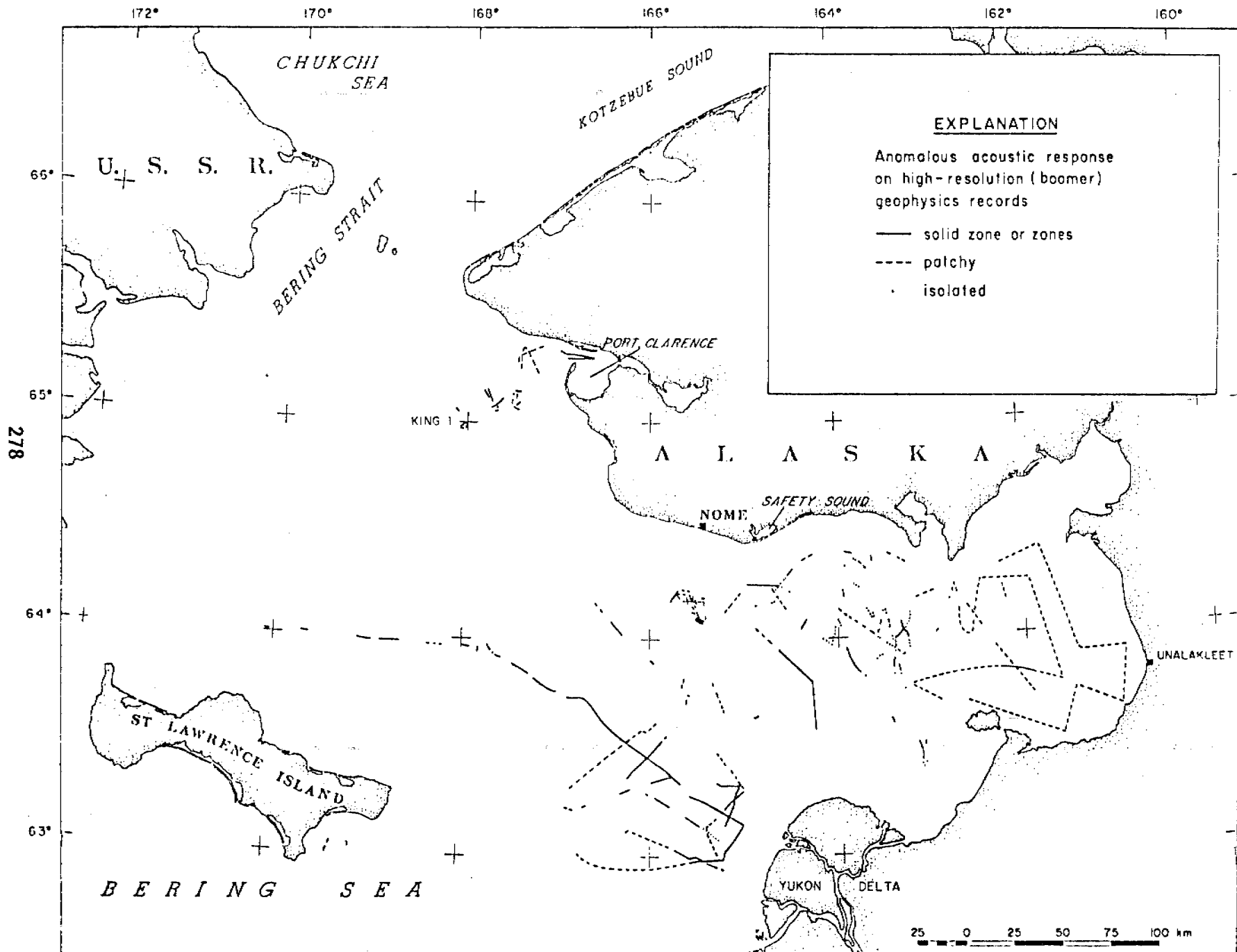


Fig. 5 - Seismic reflection record across the Norton basin gas seep zone. Location of line shown in Figure 3. This record shows two types of acoustic anomalies indicative of gas in the sediment: Reflector terminations and reflector pull-downs.

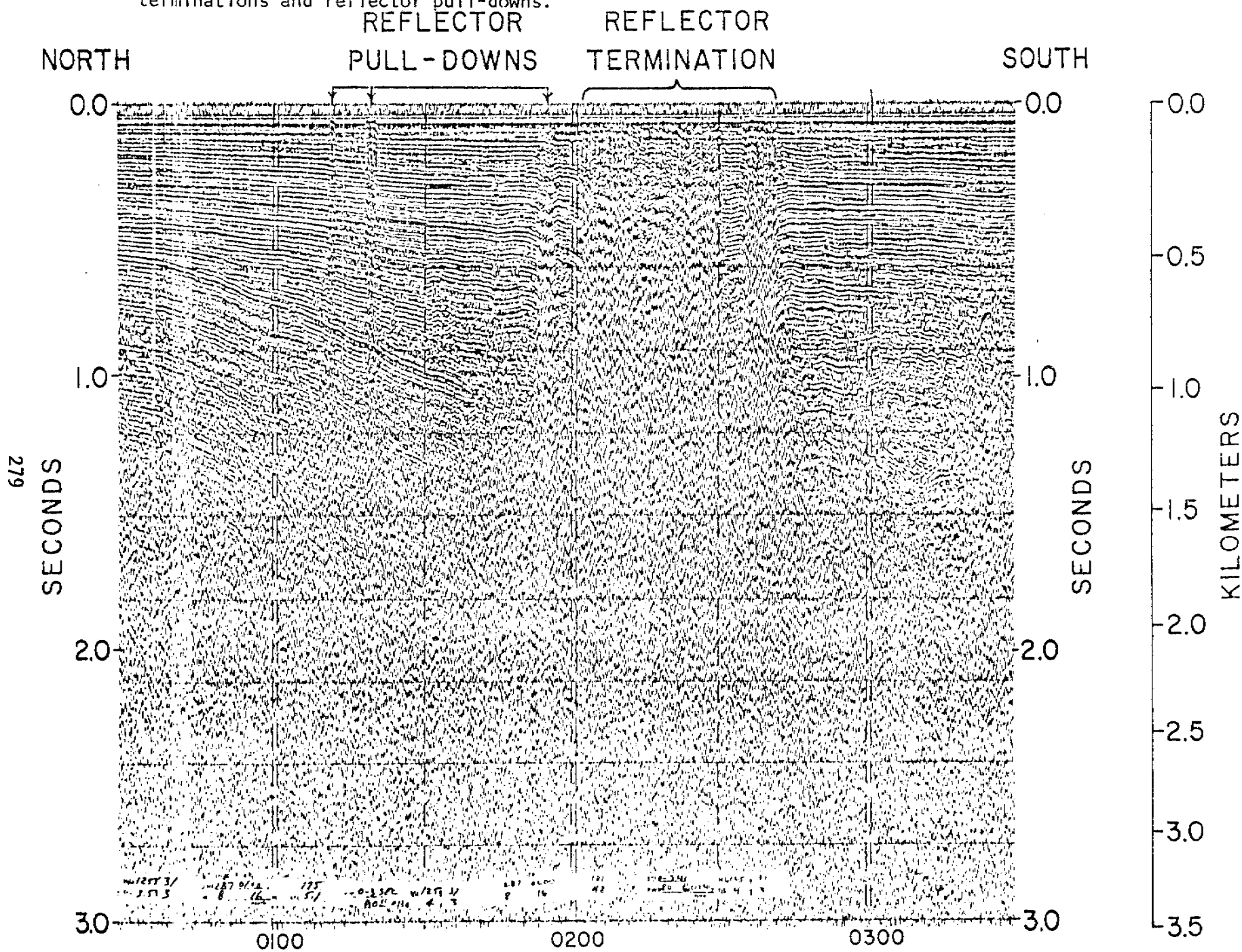


Fig. 6 - Single channel reflection record across the Norton basin gas seep area. Location of line shown in Figure 3. Reflector termination zone and marginal pull-downs are clearly shown.

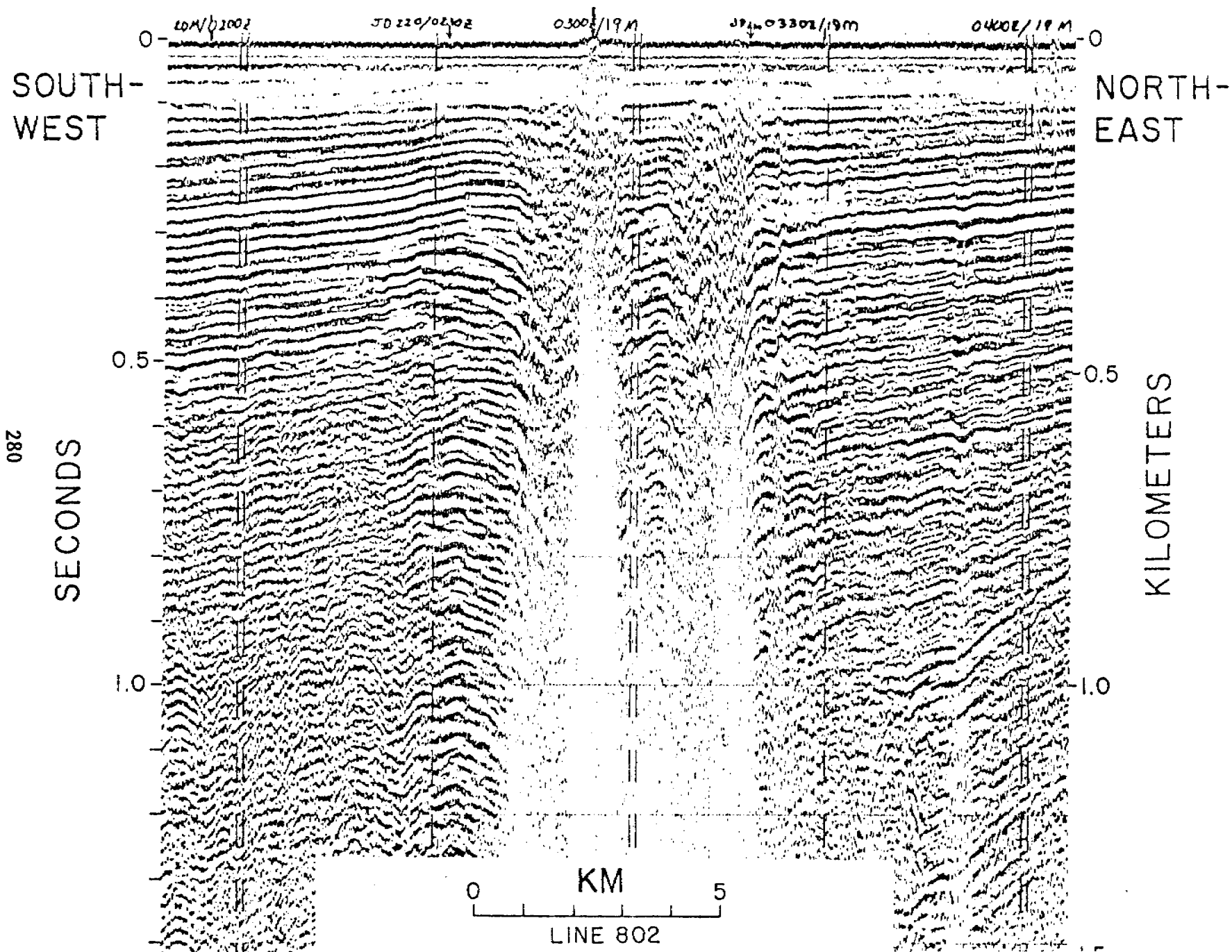


Fig. 7 - Single channel seismic reflection record from eastern Norton basin showing "normal" reflector zones and typical reflector termination anomalies. Location of line is shown in Figure 3.

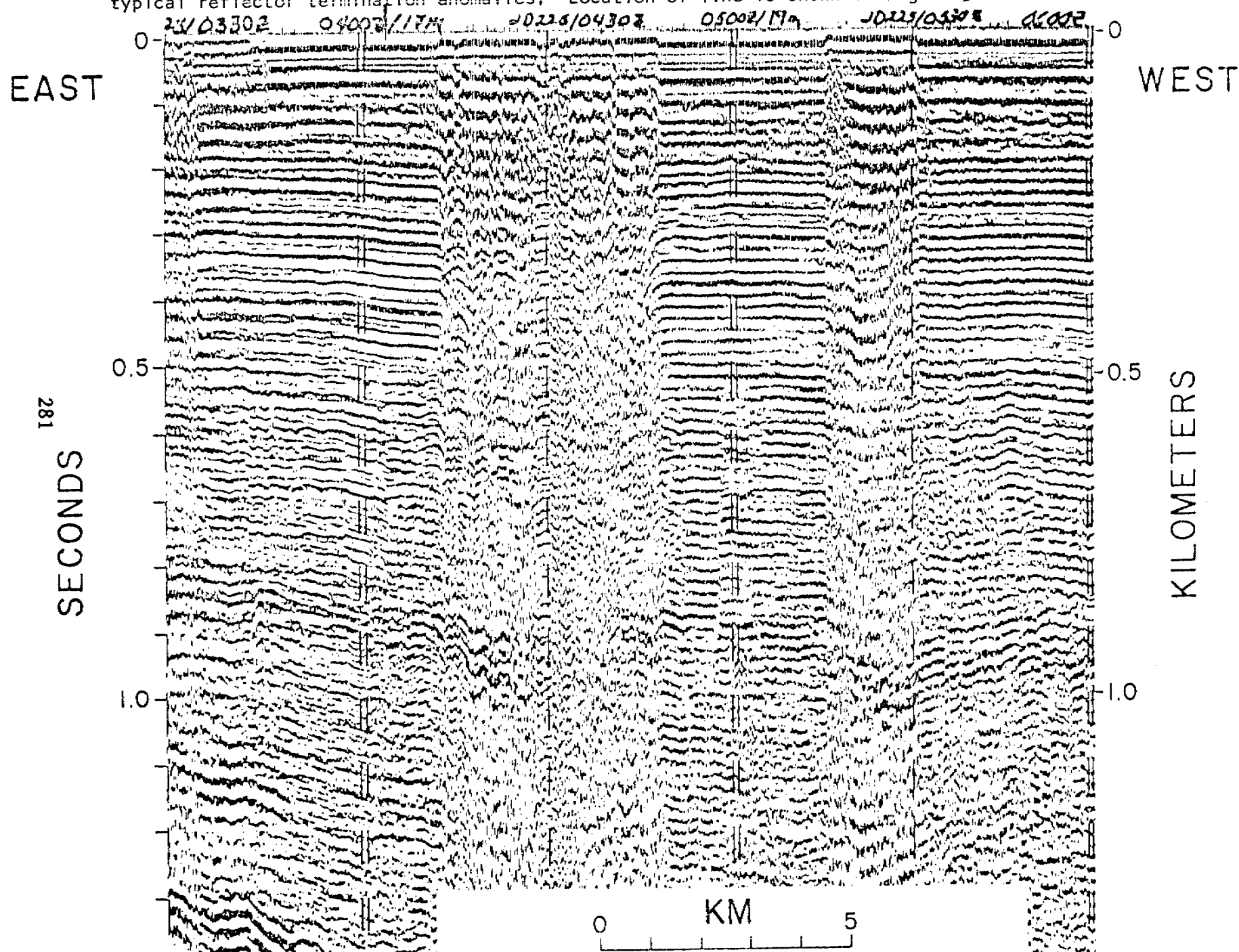


Fig. 8 - Multichannel shot record over "normal" reflector sequence shown in Figure 7. Reflected head waves (H), and reflected arrivals (R) are clearly visible.

SHOT RECORD

CRUISE: L4-78-BS
DATE / TIME: 225 / 0404
LINE: 812

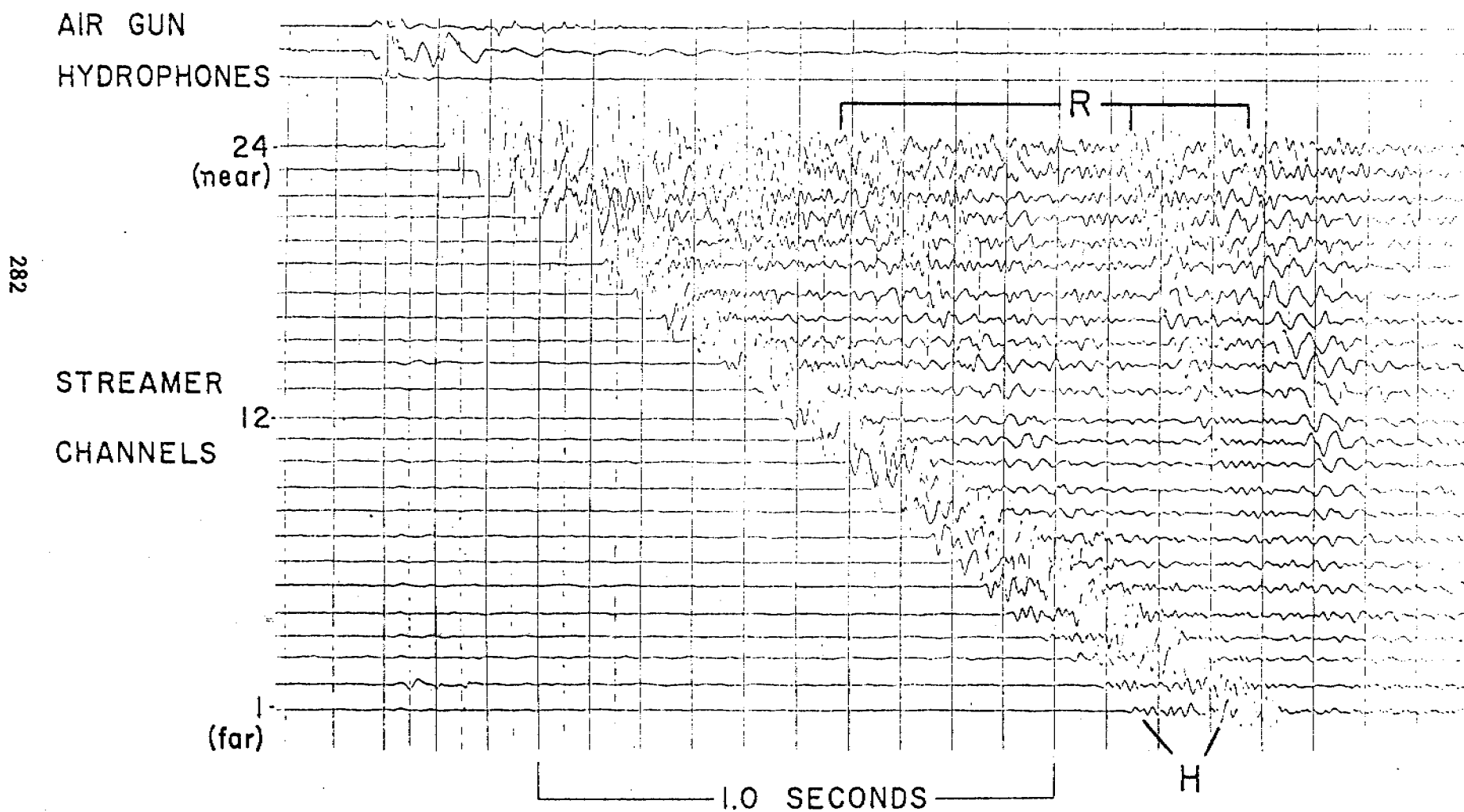


Fig. 9 - Multichannel shot record over the gas seep reflector termination anomaly shown in Figure 6. All arrivals are markedly attenuated due to gas in the near surface sediment. Amplifier settings slightly higher than in Figure 8.

SHOT RECORD

CRUISE: L4-78-BS

DATE / TIME: 220 / 0254

LINE: 802

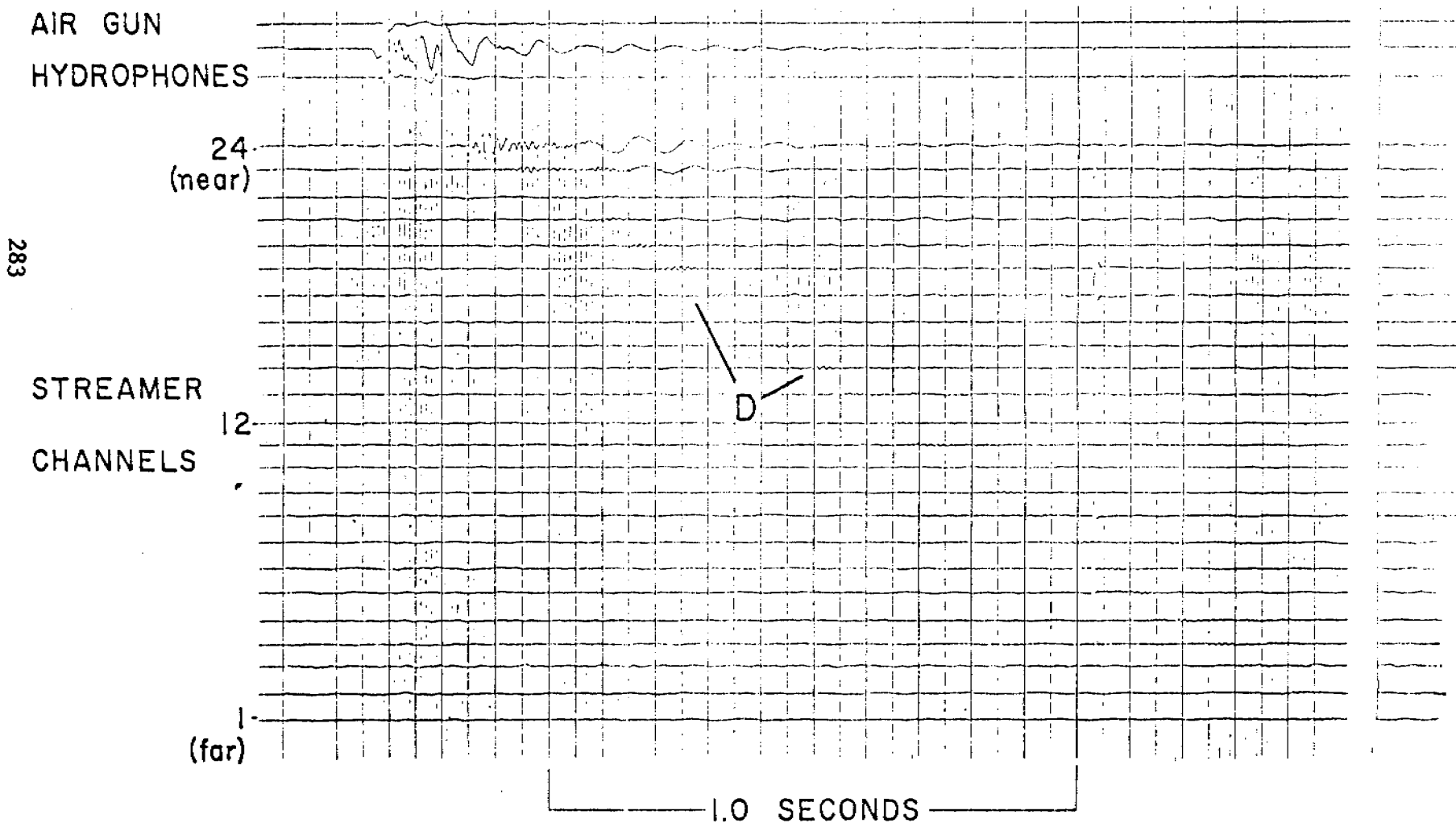


Fig. 10 - Minisparker (800 joules) record from Norton basin showing reflector termination anomaly with near-surface diffractions. Location of line is shown in Figure 3.

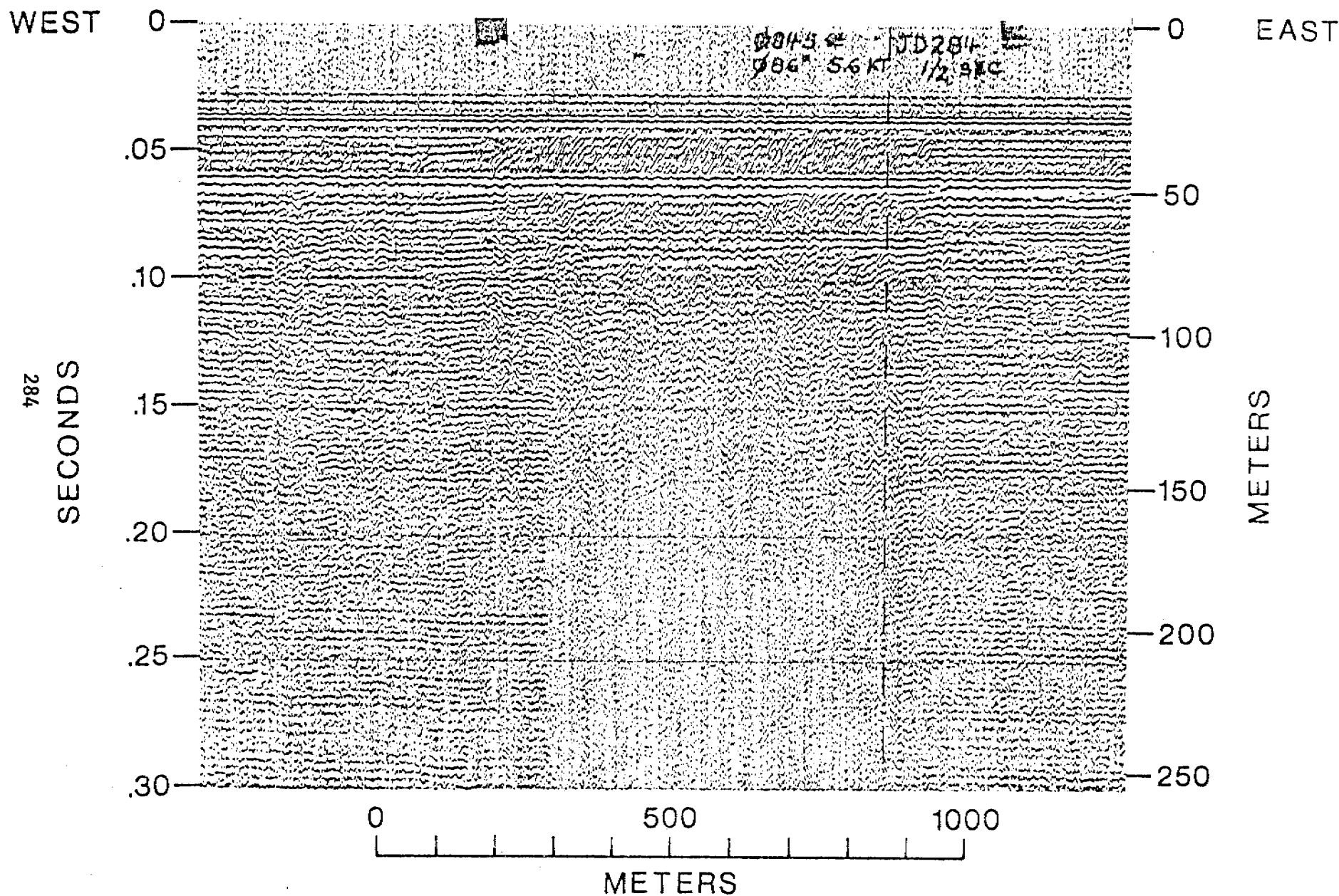
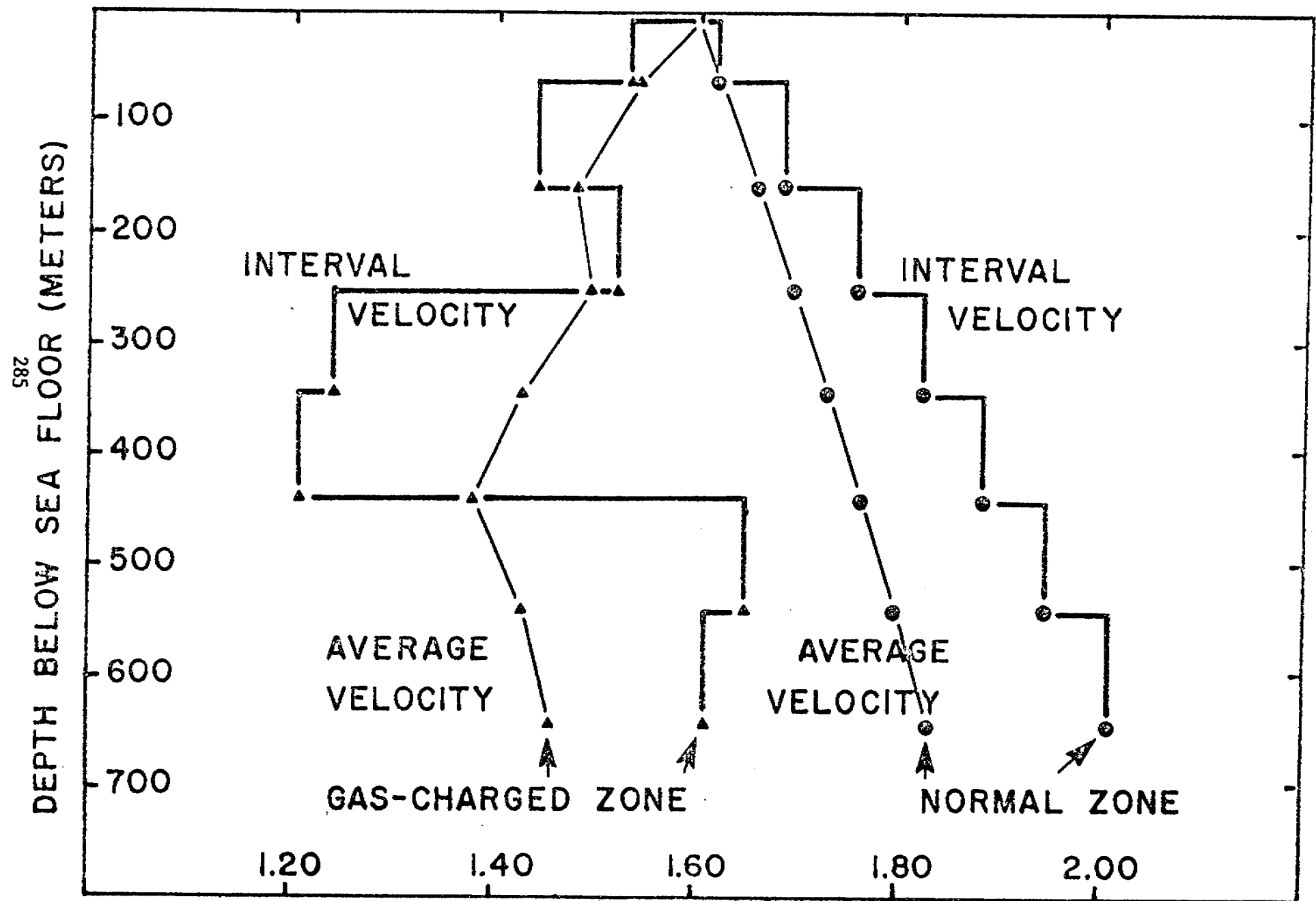


Fig. 11 - Velocity analysis of reflector pull-down zone beneath the Norton basin gas seep (Fig. 6). The two right hand curves show average and interval velocity versus depth in the gas-free reflector sequence outside the seep zone. The two curves on the left are for the gas-charged section beneath the seep itself.

GAS SEEP PULL-DOWN ANALYSIS



ICE GOUGING ON THE SUBARCTIC BERING SHELF

Devin R. Thor and C. Hans Nelson

U. S. Geological Survey, Menlo Park, California 94025

ABSTRACT

Ice impacting the sea floor gouges surficial sediment of the shallow, Bering epicontinental shelf, Alaska. Two types of ice gouge have been recognized: the single gouge, a single gouge furrow, and multiple gouges or raking, a wide zone of numerous, subparallel gouge furrows. Single gouges, the most common type, are cut by single-keeled pieces of thick ice, whereas multiple gouges are formed by multikeeled, thick, pressure-ridge ice. Gouges occur in water depths of 30 m or less, but are most dense in water 10 to 20 m deep. Although some gouge incisions are as deep as 1 m, most gouges are 0.5 m or less. Ice gouges trend parallel to pack ice movement, which in turn generally moves parallel to isobaths and coastline configuration. Mean gouge trend in Norton Sound is west-east, in northeastern Bering Sea north-south.

The annual ice cover in this subarctic setting is thin (less than 2 m). Ice thick enough to gouge the substrate forms in compression and in shear zones; there moving pack ice collides with and piles up against other pack ice or stationary shorefast ice to develop numerous pressure ridges. Southward-moving pack ice in northeastern Bering Sea and westward-moving pack ice in Norton Sound converge with, and shear past, a 10-30-km wide shorefast ice zone that covers the shallow water offshore of the Yukon Delta. The intensity of ice deformation in this zone causes the highest gouge density in the study area. In contrast, northeastern Norton Sound is an area of ice divergence and only minimal ice gouging. The rest of Norton Sound and northeastern Bering Sea is either in ice-divergence areas or water depths are too great for ice to touch bottom, thus ice gouge density in these places is low. Gouging is extremely rare inshore of the shear zone, because shorefast ice is relatively static and protects inshore areas from the dynamics of the shear or compression zone and consequent ice gouging.

INTRODUCTION

Development of natural resources in northern latitudes has led to increased research on the effects of ice on shelf sediment in arctic regions such as the Beaufort Sea (Reed and Sater, 1974; Reimnitz and others, 1973; Reimnitz and others, 1977; Barnes and others, 1978). Until recently, however, research on ice gouging had not been done in subarctic regions such as the Bering Sea. A variety of gouge features are found in many areas of northeastern Bering Sea, even though ice conditions there are not as severe as in high-latitude arctic regions. Ice gouging into the sea floor is a potential hazard to future resource development and sea-floor installations such as pipelines and wellheads.

This paper discusses general ice conditions and ice movement in northeastern Bering Sea, the effect of ice as an erosional and depositional agent that influences the geomorphology and depositional history of the shallow subarctic Bering Sea shelf, and ice gouging as a potential hazard to resource development in and around Norton Basin. Terminology used is adopted from Barnes and others (1978), particularly in the use of the word "gouge" to describe the feature and the process of ice interacting with the sea floor.

Geographic Setting

The floor of northeastern Bering Sea is a broad, shallow epicontinental shelf (Figs. 1 and 2). Water depths in Chirikov Basin range from 20 m on the eastern side to 50 m in the central part. The shelf is generally flat and featureless except for a prominent series of ridges and swales that subparallel the coastline off Port Clarence. A large, elongate marine re-entrant forms Norton Sound, bounded on the north by Seward Peninsula, on the east by the Alaskan mainland, and on the south by the Yukon Delta. Except in

a broad trough in the northern part of the sound, where depths are as great as 27 m, water depths in Norton Sound range from 10 to 20 m. The offshore part of the Yukon Delta is a zone of extensive shoals covering about 8000 km² (Fig. 2). Water depths 10 to 30 km offshore do not exceed 3 m, at which point there is a gentle break in slope and the depth increases to 10 m as far as 50 to 70 km from shore. The substrate of the Yukon prodelta, derived from the Yukon River, consists of coarse silt to very fine sand, whereas sediment in Chirikov Basin consists mostly of glacial gravel and transgressive fine sand (Nelson and Hopkins, 1972; McManus and others, 1977).

Ice Conditions and Movement

Ice overlies northern Bering Sea annually from November through June (Muench and Ahlnas, 1976; Shapiro and Burns, 1975). Depending on the severity of the winter, multiyear ice may migrate into Bering Sea from southern Chukchi Sea. Keel depth of 90% of the pack ice (any free-floating ice regardless of origin) is less than 1 m, although depths to 20 m have been reported (Arctic Research Laboratory, 1973).

Ice in open sea pans in Norton Sound is 0.7 to 1.2 m thick (Brower, and others, 1977), but can get as thick as 2 m (Carole Pease, 1979, pers. comm.). Shorefast ice (ice anchored to the land) extends seaward to about the 10 m isobath and is best developed in the southern part of Norton Sound, around the Yukon Delta (Ralph Hunter, written comm., 1976; Duprè, 1977, Stringer and others, 1977) (Fig. 2).

Analysis of Landsat photographs (Dupr  and Ray, Sec. II, this volume; Stringer and others, 1977; Muench and Ahlnas, 1976; Shapiro and Burns, 1975) has contributed to a preliminary understanding of ice dynamics in the Bering Sea. Pack ice in the northern Bering Sea originates from (1) in situ northeastern Bering Sea ice and (2) advected Chukchi Sea ice. Chukchi Sea ice can move through the Bering Strait and into the northern Bering Sea during episodes of rapid deformation and subsequent rapid southerly movement of pack ice caused by episodes of strong northerly winds (Shapiro and Burns, 1975).

Ice movement in the northeastern Bering Sea is controlled by the interplay of: (1) prevailing winter northeasterly geostrophic wind (Muench and Ahlnas, 1976), (2) erratic onshore wind (NOAA, 1974), (3) northward-flowing water current on the eastern side of the Bering Sea (Coachman and others, 1976) (Fig. 2), and (4) a counterclockwise current gyre in Norton Sound (Nelson and Creager, 1977) (Fig. 2). Late winter and early spring winds tend to push ice generally southward in northeastern Bering Sea, whereas waning late spring winds allow pack ice to be increasingly influenced by the northward-flowing water currents (Fig. 2).

In Norton Sound the dominant direction of ice movement is southwestward out of the sound. This drift creates a zone of divergence in the northeastern part of the sound and a zone of convergence in the southwestern or Yukon prodelta area of the sound (Dupr  and Ray, Sec. II, this volume; Stringer and others, 1977) (Fig. 2). Periodic changes in wind and water current tend to move ice in and out of the sound, thereby making it possible for Bering Sea ice, or even advected Chukchi Sea ice, to work its way into the sound.

Zones of convergence can be zones of pressure-ridge or shear-ridge formation characterized by colliding, piling up, and deforming of the edges of

fast ice and of pack ice (Reimnitz and Barnes, 1974). The best-developed pressure ridges in northeastern Bering Sea form around the Yukon Delta, where Bering Sea pack ice on the western prodelta and Norton Sound pack ice on the northern prodelta collides with the Yukon Delta fast ice (Dupr  and Ray, Sec. II, this volume; Stringer and others, 1977).

Methods

Data for this study were gathered by the U.S. Geological Survey during September 1976, July 1977, and September 1978 aboard R/V SEA SOUNDER and during June and July 1978 aboard R/V KARLUK. Approximately 5,100 km of side-scan sonar trackline was obtained (Fig. 1). Normally, seismic units with energy sources of 200 kHz, 12 kHz, 7 kHz, 3.5 kHz, and 2 kHz were run simultaneously with side scan for additional bottom and subbottom information. The 6-m keel depth of the R/V SEA SOUNDER limited ship operations to water deeper than 8 m, whereas the shallow draft of the R/V KARLUK (1 m) allowed surveying in nearshore areas and in the shallow waters off the Yukon Delta. Geophysical and navigational operations are described in Thor (1978).

An EG and G side-scan sonar system*, consisting of a dual-channel graphic recorder and a towed transducer fish, was used to survey the sea floor. Side-scan sonar, an alternative method to conventional vertical echo sounding, employs a 105 kHz acoustic beam whose axis is slightly below horizontal. This acoustic beam can resolve topographic irregularities and objects on the sea

*Any use of trade names and trademarks in this publication is for descriptive purposes only and does not constitute endorsement by the U.S. Geological Survey.

floor with as little as 10 cm of relief. Reflected echoes are graphically recorded in a form that approaches a plan view map. Discussions on theoretical and practical aspects of side-scan operation and interpretation can be found in Belderson and others (1972) and Flemming (1976). Normally the side-scan was operated at 100-m sweep (the scan range on either side of the ship); although at times, the 50-m sweep was used to help resolve details of the gouging. In addition, a 200 kHz high-resolution fathometer was operated to measure the incision depth of ice gouges (Fig. 3). Vertical relief of gouges on the fathometer record or on the horizon line of sonographs is generally masked by the recording of sea swell or ship's motion on the chart paper.

Gouge data were collected from the sonographs by counting the number, measuring the trend, and noting the time of occurrence of all gouges seen on the records. Distortion of sea floor features on the sonograph occurs parallel to the line of travel because of the difference in ship's speed and the recorder's paper-advance speed. To obtain absolute compass trend of gouges, a distortion ellipse protractor, which corrects for the apparent angle produced by ship paper speed, was used to measure gouge angle with respect to ship's track. This information was then normalized at 10-km intervals. Normalization entailed two procedures: (1) correction of the number of observed gouges and (2) averaging of observed gouge trends. The number of observed gouges per 10-km interval was multiplied by $1/\sin$ (where angle equals the angle between ship's course and gouge trend) to correct for the fact that ship's course usually was not normal to the gouge trend. Any angle other than 90° between ship's course and gouge trend will give a false picture of gouge density (Barnes and others, 1978). Averaging observed gouge trends

involved graphing the measured trends for the 10-km intervals and noting the average dominant and subordinate trend or trends. Each average trend per 10-km interval was then plotted on the base map to define areas of similar gouge trend.

GEOMETRY AND TYPE OF ICE GOUGING

Two basic types of ice gouge have been recognized on the sea floor of northeastern Bering Sea: (1) single gouges and (2) multiple gouges or raking. A single gouge, the dominant type of ice-produced mark on the Bering Sea floor, is a groove produced by a single ice keel plowing through the surficial sediment (Figs. 3-A, 3-B, 4-A, 4-B, and 4-C) (Reimnitz and others, 1973; Reimnitz and Barnes, 1974). Single gouges are ubiquitous throughout Norton Sound; although the highest density occurs around the prodelta of the Yukon River (Fig. 5).

Single gouge widths range from 5 to 60 m; a width of 15 to 25 m is most common. Gouge patterns range from straight, through sinuous, to sharp-angled turns (Fig. 4). Incision depths of gouges, as measured on the sea-floor profile of sonographs (Fig. 4-E) and on the 200 kHz fathometer record (Fig. 3-B), can be as deep as 1 m. Most gouges range in depth from 0.25 to 0.5 m or less. These figures may be conservative because of the geometric relation between the narrow width of the gouge and the spread of the acoustic cone of the fathometer transducer (Reimnitz and others, 1977). The original incision depth is impossible to determine unless the gouge is seen as the keel plows the bottom, because the gouge has subsequently been infilled.

Multiple gouges or raking (Figs. 4-F and 4-G) are produced when multi-keeled floes (such as pressure ridges) plow or rake the bottom sediment, creating numerous parallel furrows (Reimnitz and others, 1973; Reimnitz and

Barnes, 1974). Unlike single gouges, raking is not ubiquitous, but in the Yukon prodelta area the raking process is locally more prevalent than single gouging. Zones of raking are 50-100 m to several kilometers wide. The deepest incisions caused by raking observed on the records are about 1 m; but raking, like single gouges, usually produces incisions less than 0.25-0.5 m deep.

TREND AND DISTRIBUTION OF GOUGES

Analysis of the trend and distribution of gouges allows recognition of five areas of gouging with similar trends (areas I - V), and two large areas almost devoid of gouges (VI and shorefast ice zone) (Fig. 5). Absolute direction of ice movement cannot be predicted because criteria needed to make certain distinctions, such as gouge terminations, were not seen on the sonographs.

In areas I and II (Fig. 5), the dominant trend of gouges is distinctly subparallel to isobaths and the coastline. There is more data scatter in areas III, IV, and V, but gouges again are generally parallel to isobaths and the coastline. The greatest data scatter is seen in area V, but this may reflect the irregular bathymetry of ridge and swale topography off Port Clarence. Except for a couple of gouges off the northwestern end of St. Lawrence Island, area VI is devoid of ice gouges.

Density of ice gouges is as much as 25 times higher around the Yukon Delta area, where the water is 10 to 20m deep, than in other areas of northeastern Bering Sea (Table I and Fig. 5, areas I and II). Not coincidentally, the Yukon prodelta is the largest expanse of shallow water in the study region. Here density of ice gouges can be as high as 75 gouges/km². Density of ice gouging is 60 times higher in water 10 to 20 m deep than in water 5 to 10 m deep or in water 20 to 39 m deep (Table II). Gouging has not been seen in water shallower than 5 m or deeper than 30 m.

Table I

Gouge Density by Area

Area	km ²	Trackline km	Total number of gouges	Average density (gouges/km ² *)
I	5,500	530	1,684	3.18
II	8,000	1,005	5,080	5.05
III	9,500	1,100	917	0.83
IV	15,500	400	993	2.48
V	7,900	1,120	216	0.19
VI	50,400	766	4	0.03

*Assuming 1 km trackline of side-scan sonar is representative of 1 km².

Table II
Gouge Density by Water Depth Interval

Depth interval (m)	km ²	Trackline km	Total number of gouges	Gouges/km ² *
0-10	16,500	480	147	0.31
10-20	24,600	2100	8,593	4.09
20-30	32,700	1300	143	0.11
30-40	26,000	750	0	0
40-50	12,600	450	0	0
>50	5,400	170	0	0

*Same as Table 1.

GEOLOGICAL SIGNIFICANCE

Trend and Density of Gouges

The interplay of geomorphology, water depth, oceanic conditions, and location of compression or of shear zones (Fig. 2) determines the pattern of ice gouging in northern Bering Sea (Figs. 5 and 6). The orientation of ice gouges is dependent on the direction of ice drift under the influence of wind and water current. The dominant trend of ice gouges, therefore, in Norton Sound is east-west and in the Bering Sea north-south (Figs. 5 and 6).

Land promontories, such as the Yukon Delta, tend to block ice movement and to cause the formation of compression and shear zones. Formation of ice ridges around the Yukon Delta by the collision and shearing of moving pack ice with stationary shorefast ice accounts for the high density of ice gouges in areas I and II (Fig. 5). Areas within the zone of shorefast ice, such as the large area around the Yukon Delta (Fig. 5), are devoid of gouges. This is because only the edge of the shorefast ice is deformed by the pack ice, and subsequent deformation occurs continually seaward through a process of migration of the compression/shear zone through time (Dupré, 1978). Areas III and IV are characterized by low density of ice gouges (Fig. 5). Gouging in areas III and IV is the product of ridges formed in an ice-divergence zone by intercollisions of pack ice. Density of ice gouges in area V is low because this area is not in a convergence zone and at most places water depth exceeds normal ice-keel depths. Area VI does not seem to have any ice gouging because water depths (Fig. 2) exceed normal ice-keel depths (Fig. 5).

Age of Ice Gouges

Although no specific studies were made to determine the age and longevity of gouges, the gouges seem to be modern ephemeral phenomena that recur annually. West of Port Clarence and in the nearshore area of Nome, ice gouges cut through ripple- and sand-wave fields that are in dynamic equilibrium with present wave or current motion (Nelson and others, 1978; Hunter and Thor, 1979) (Figs. 4-A and B). Here old gouges, highly modified by ripples or sand waves and new gouges suggests that gouges are being formed each winter.

A number of geologic processes act to rapidly destroy gouges once they have formed. Initial smoothing of ice gouges can be enhanced by: (1) the saturated, silty substrate that tends to seek a minimum relief equilibrium

with sides of the gouge flowing or slumping toward the center of the gouge, and (2) the constant oscillatory pounding of wave motion on the sea floor that causes shear failure in the soft sediment (Henkel, 1970), causing gouge sides to collapse toward the center. The 'dish-shape' profiles of most gouges (Figs. 4-E and G) indicate that these are normal factors in the process of gouge destruction.

Repeated surveys of ice gouges in water less than 20 m deep in the Beaufort Sea have shown that gouges are frequently smoothed over completely in one season (Barnes and Reimnitz, 1979). In the Bering Sea, the ice-free season is 3 to 4 months longer than in the Beaufort Sea, allowing more time for considerably stronger open-water wave and current regimes of the Bering Sea to destroy gouges. In Norton Sound, storm waves and currents caused by advance and retreat of storm-surge water, in addition to normal tidal and geostrophic currents, resuspend and transport large quantities of surficial sediment (Cacchione and Drake, 1978; Nelson and Creager, 1977). Destruction of gouges is augmented by biological reworking of surficial sediment, an active process in Norton Sound (Nelson and others, in press). In summary, gouges will tend to be either eroded or buried because they are not in equilibrium with the dynamic physical processes on the sea floor. This reinforces the hypothesis that gouges in Bering Sea are present-day phenomena involving development of some new gouges each ice season.

Ice/Sediment Interaction

Ice acts as both an erosional and a depositional agent. Ice gouges, mixes, and deforms the substrate, and promotes current scour. Ice partially controls the geomorphology of the Yukon Delta (Dupré and Thompson, 1979).

Sediment mixing and deformation of the substrate are important processes in densely gouged areas such as the Yukon prodelta where pressure-ridge raking can gouge 1 m into the sediment. One event of pressure ridge raking can affect several square kilometers of sea floor.* Such an event can mix or disrupt several million cubic meters of sediment. A zone of deformed sediment in box core No. 48 (11-18 cm interval, Fig. 3-C) possibly represents an ice-gouge event.

Sharpness of gouge morphology is highly dependent on the type of substrate being gouged. The sediment of the Yukon prodelta is a moderately cohesive sandy silt that will hold a shape better than the coarser-grained sediment of central Norton Sound or offshore from Port Clarence (Clukey and others, 1978; Nelson and Hopkins, 1972; McManus and others, 1977). The gouge shown in figure 5-A and some gouges shown in figure 4 are examples of forms with sharp relief in a competent substrate. Gouges shown in figure 4-A are smoother in form because they cut into a cohesionless sand substrate in the Port Clarence area.

Prominent broad (50-150 m wide), shallow (0.6-0.8 m deep) depressions on the western Yukon prodelta are associated with areas of intense ice gouging and strong bottom currents (Larsen and others, 1979). Topographic disruption by ice gouges in these areas apparently causes flow separation in the strong

*Area of gouging times depth of gouging. Ex. 2000 m (length of gouged zone) x 1000 m (width of gouged zone) x 0.5 m (depth of gouge) = 1,000,000 m³.

currents, thereby initiating scour depression for extensive distances downstream. Consequently, large regions of scour may continue to expand away from intensely gouged areas (Fig. 4-H).

The extensive depositional sand shoals of the Yukon Delta front coincide with the seaward extent of shorefast ice, stamukhi (grounded pressure ridges) and zones of dense ice gouging (Figs. 2 and 6). Reimnitz and Barnes (1974) have noted this relation in the Colville Delta area of the Beaufort Sea. They postulate that pressure ridges and stamukhi act as sediment traps or dams, channelize winter currents, or bulldoze sediment to form shoals. Thus, a cycle is formed in the sense that shoal areas determine the extent of shorefast ice and the location of a shear zone and pressure ridges, which in turn cause shoals to develop. Duprè (1979) hypothesizes that the geomorphology of onshore and offshore parts of the Yukon Delta are similarly controlled by ice.

RESOURCE DEVELOPMENT: POTENTIAL HAZARDS

To summarize, gouges are ubiquitous throughout northeastern Bering Sea in water depths of 5 to 30 m. Ice-gouge density varies from rare to sparse in northeastern Bering sea and northern Norton Sound; maximum density is around the Yukon Delta (Fig. 6). Depth of ice gouges is fairly uniform throughout northeastern Bering Sea and seems to be independent of gouge density. Although maximum observed ice-gouge depth is about 1 m and maximum observed current scour about 1 m, the combination of these forces could affect the bottom to depths of several meters, thus presenting some design problems and potential hazards to installations in or on the sea floor. Pipelines and

cables should be buried below the combined effective depth of ice gouging and current scour, plus a safety factor.

Special studies of nearshore areas off Nome and Port Clarence were conducted because both are potential centers for commercial development and activity. Nome, already a well established small city, is the focal point for barge traffic in the northern Bering Sea. Port Clarence, the only natural harbor in the northern Bering Sea has high potential for development as a site for future shipping activity.

Offshore Nome, being an area of ice divergence, is not heavily gouged. Although several gouges were found offshore, none were in water shallower than 8 m. Several of these gouges are probably not related to ice. They are very narrow (less than 1 m) compared to typical ice gouges (more than 5 m wide) and are possibly produced by anchor, anchor chain, or cable drag from the tugs and barges that frequent the port of Nome.

Several gouges were found near Port Clarence at the northern end of the Port Clarence spit and on the northern side of Port Clarence inside the tidal inlet. But, none occurred in water less than 8 m deep.

ACKNOWLEDGMENTS

We thank William Dupré, University of Houston, for data concerning pack ice movement and shorefast ice limits; Ralph Hunter, U. S. Geological Survey, for data on shorefast ice limits; and David Drake U. S. Geological Survey, for data on ice thickness. Jim Evans and Ron Williams compiled data on gouges from sonographs. Valuable discussions on ice processes and interpretation of sonographs were held with Peter Barnes, Erk Reimnitz, and Larry Toimil, U.S. Geological Survey. Marybeth Gerin helped with figure layout and drafting. Erk Reimnitz and Harry Cook, U.S. Geological Survey, made helpful comments on

the manuscript. The officers, crew, and technical staff of the R/V SEA SOUNDER made data collection a successful and enjoyable endeavor.

The cruises were supported jointly by the U.S. Geological Survey and by the Bureau of Land Management through interagency agreement with the National Oceanic and Atmospheric Administration, under which a multi-year program responding to the needs of petroleum development of the Alaska continental shelf is managed by the Outer Continental Shelf Environmental Assessment Program (OCSEAP) Office.

REFERENCES CITED

Arctic Resesearch Laboratory

1973 Ice Character in Bering and Chukchi Seas

Naval Oceanic Systems Center, Dept. of Navy, San Diego, CA.

Barnes, P.W., David McDowell, and Erk Reimnitz

1978 Ice gouging characteristics: Their changing patterns from 1975-

1977, Beaufort Sea, Alaska: U. S. Geological Survey Open File

Report 78-730, 42 pp.

Barnes, P.W., and Erk Reimnitz

1979 Ice gouge obliteration and sediment redistribution event;

1977-1978, Beaufort Sea, Alaska, U.S. Geological Survey Open

File Report 79-848, 22 pp.

Belderson, R.H., N.H. Kenyon, A.H. Stride, and A.R. Stubbs

1972 Sonographs of the sea floor: Elsevier Pub. Co., New York,

185 pp.

Brower, W.A., and others

1977 Climatic atlas of the outer continental shelf waters - coastal

region of Alaska: v. 2 - Bering Sea, Arctic Environmental

Information and Data Center, Anchorage, Alaska.

Cacchione, D.A., and Drake, D.E.

1978 Sediment transport in Norton Sound, Northern Bering Sea, in

Environmental Assessment of the Alaskan Continental Shelf,

Annual Report of Principal Investigators for the year ending

March 1978, Environmental Research Laboratory, Boulder, Colorado,

NOAA, U.S. Department of Commerce, 12: 308-450.

Clukey, E.C., Hans Nelson, and J.E. Newby,

1978 Geotechnical properties of northern Bering Sea sediment: U.S.

Geological Survey Open File Report 78-408, 48 pp.

Coachman, L.K., K. Aagaard, and R.B. Tripp

1976 Bering Strait: The regional physical oceanography:

Washington University Press, Seattle, 186 pp.

Dupré, W.R.

1977 Yukon Delta coastal processes study: Environmental Assessment of

the Alaskan Continental Shelf, Annual Report of Principal

Investigators for the year ending March 1977, Environmental

Research Laboratory, Boulder, Colorado, NOAA, U.S. Department of

Commerce, 14: 508-553.

Dupré, W.R.

1978 Yukon Delta coastal processes study: Environmental Assessment of

the Alaskan Continental Shelf, Annual Report of Principal

Investigators for the year ending March 1978, Environmental

Research Laboratory, Boulder, Colorado, NOAA, U.S. Department of

Commerce, 11: 384-446.

Dupré, W.R., and R. Thompson

1979 The Yukon Delta: A model for deltaic sedimentation in an ice

dominated environment: Proceedings Offshore Technology

Conference, v. 1, paper no. 3434: 657-664.

FATHAUER, T.F.

1975 The great Bering Sea storms of 9-19 November, 1974: Weatherwise

Magazine, American Meterological Society, 28: 76-83.

Flemming, B.W.

1976 Side-scan sonar: A practical guide, in Side Scan Sonar, A comprehensive presentation: E.G. and G. environmental Equipment Division, Waltham, MA, A-1 - A-45.

Fleming, R.H., and Heggarty, D.,

1966 Oceanography of the southeastern Chukchi Sea, in: Willimovsky M.H., and J.M. Wolfe, eds., Environment of Cape Thompson region Alaska: Washington, D.C., U.S. Atomic Energy Commission 697-754.

Goodman, J.R., Lincoln, J.H., Thompson, T.G., and Zeusler, F.A.

1941 Physical and chemical investigations: Bering Sea, Bering Strait, Chukchi Sea during the summers of 1937 and 1938: Washington University publications in Oceanography, v. 3, no. 4 105-169 and appendix 1-117.

HENKEL, D.J.,

1970 The role of waves in causing submarine landslides: Geotechnique, v. 10, 75-80.

Hunter, R. E., and Thor, D.R.

1979 Depositional and erosional features of the northeastern Bering Sea inner shelf (abs.): Amsterdam, International Association of Sedimentologists, Program and Abstracts, Eleventh International Congress in Sedimentology, (in press).

Husby, D.M.

1969 Report of oceanographic cruise U.S.C.G.C. NORTHWIND, northern Bering Sea-Bering Strait-Chukchi Sea, July 1969: U.S. Coast Guard Oceanographic Report, no. 24, 75 pp.

Husby, D.M.

1971 Oceanographic investigations in the northern Bering Sea and Bering Strait, June-July 1969: U.S. Coast Guard Oceanographic Report no. 49, 50 pp.

LARSEN, M.C., HANS NELSON, and D.R. THOR

1979 Geologic implications and potential hazards of scour depressions on Bering shelf, Alaska: Environmental Geology, v. 3, 39-47.

McManus, D.A., V. Kolla, D.M. Hopkins, and C.H. Nelson,

1977 Distribution of bottom sediments on the continental shelf, northern Bering Sea: U.S. Geological Survey Professional Paper 759-C, C1-C31.

McMANUS, D.A., and C.S., SMYTH

1970 Turbid bottom water on the continental shelf of northern Bering Sea: Journal of Sedimentary Petrology, v. 40, 869-877.

MUENCH, R.D., and K. AHLNAS

1976 Ice movement and distribution in the Bering Sea from March to June 1974: Journal of Geophysical Research, v. 81, no. 24, 4467-4476.

National Oceanic and Atmospheric Administration

1974 Local climatological data - annual summary with comparative data for Nome, Unalakeet, Shismaref and Wales, Alaska.

NELSON, HANS, and J. CREAGER

1977 Displacement of Yukon-derived sediment from Bering Sea to Chukchi Sea during Holocene time: Geology, v. 5, 141-146.

Nelson, Hans, M E. Field, D.A. Cacchione, and D.E. Drake

1978 Areas of active large-scale sand wave and ripple fields with scour potential on the Norton Basin sea floor, in: Environmental Assessment of the Alaskan Continental Shelf, Annual Report of Principal Investigators for the year ending March 1978, Environmental Research Laboratory, Boulder, Colorado. NOAA. U.S. Department of Commerce, v. 12, 291-307.

Nelson, Hans, and D.M. Hopkins

1972 Sedimentary processes and distribution of particulate gold in the northern Bering Sea: U.S. Geological Survey Professional Paper 689, 27 pp.

Nelson, Hans, R.W. Rowland, Sam Stoker, and B.R. Larsen

1980 Interplay of physical and biological sedimentary structures of the Bering Sea epicontinental shelf, in Hood, D. (ed.), Bering Sea Shelf: Oceanography and Resources: NOAA, (in press).

Pratt, R., and F. Walton,

1974 Bathymetric map of the Bering shelf: Boulder, Colorado, Geological Society of America, scale 1:1,440,000.

Reed, J.C., and J.E. Sater, (eds.)

1974 The coast and shelf of the Beaufort Sea: Arlington, Virginia Arctic Institute of North America, 750 pp.

Reimnitz, Erk, and P.W. Barnes

1974 Sea ice as a geologic agent on the Beaufort Sea shelf of Alaska in Reed, J.C., and J.E. Sater (eds.), The coast and shelf of the Beaufort Sea: Arlington, Virginia, Arctic Institute of North America, 301-351.

Reimnitz, Erk, P.W. Barnes, and T.R. Alpha

1973 Bottom features and processes related to drifting ice: U.S.
Geological Survey Miscellaneous Field Studies Map MF-532.

REIMNITZ, ERK, P.W. BARNES, L.J. TOIMIL, and JOHN MELCHIOR

1977 Ice gouge recurrence and rates of sediment reworking,

Beaufort Sea, Alaska: *Geology*, v. 5, 405-408.

Sackinger, W.M., and J.C. Rogers

1974 Dynamics of break-up in shorefast ice in Reed, J.C., and J.E. Sater

(eds.), *The coast and shelf of the Beaufort Sea*: Arlington

Virginia, Arctic Institute North America, 367-376.

Shapiro, L.H., and J.J. Burns

1975 Satellite observations of sea ice movement in the Bering

Strait region: *Climate of the Arctic, Report*, University of

Alaska, Fairbanks, 379-386.

Stringer, W.J., S.A. Barrett, Nita Blavin, and Diane Thomson

1977 Morphology of Beaufort, Chukchi, and Bering Seas nearshore ice

conditions by means of satellite and aerial remote sensing:

Environmental Assessment of the Alaskan Continental Shelf, Annual

Report of Principal Investigators for the year ending March 1977,

Environmental Research Laboratory, Boulder, Colorado, NOAA, U.S.

Department of Commerce, v. 15, 42-150.

Thor, D.R., and Hans Nelson

1978 Continuous seismic reflection profile records, SEA 5-77-BS Cruise

northern Bering Sea: U.S. Geological Survey Open File Report

78-608, 8 pp., 2 pls.

List of Figures

- Figure 1. Index map and chart of high-resolution geophysical and side-scan sonar tracklines covered by the R/V SEA SOUNDER and R/V KARLUK in northeastern Bering Sea during 1976, 1977, and 1978.
- Figure 2. Northeastern Bering Sea and southern Chukchi Sea, showing water circulation and bathymetry. Compilation sources include Goodman and others (1942), Fleming and Heggarty (1966), Husby (1969, 1971), McManus and Smyth (1970), Nelson and Hopkins (1972), Pratt and Walton (1974), and Coachman and others (1976). Drift directions of pack ice in northern Bering Sea adapted from Muench and Ahlms (1976) and Duprè (1978).
- Figure 3. A - solitary gouge on a sonograph. B - 200 kHz fathometer profile and diagrammatic representation of gouge shown in A. Features of gouge include a) incision depth as measured from gouge bottom to a horizontal line projected across sediment surface, b) height of sediment mounded on the gouge edge, c) width of incision, d) width of disruption zone caused by the gouging process. C - box core slab showing subsurface (11-18 cm interval) disruption possibly caused by a past gouge event.
- Figure 4. Sonographs showing ice gouges of the northeastern Bering Sea. A and B - solitary gouges in sand-wave and ripple fields. C, D, and E - solitary gouges. Example E shows depth of incision on the sonograph horizon line. F and G - examples of pressure ridge raking. Example G shows depth of incision on the sonograph horizon line. H - example of depressions associated with ice gouging.
- Figure 5. Rose diagrams representing trend and density of gouges. Division into areas I - V based on zones of similar trending gouges. Zone of shorefast ice based on evaluation of Landsat imagery (Duprè, 1977, 1978; Ralph Hunter, pers. comm., 1977).
- Figure 6. Summary of ice gouging: density, shorefast ice limits, and ice movements in northeastern Bering Sea.

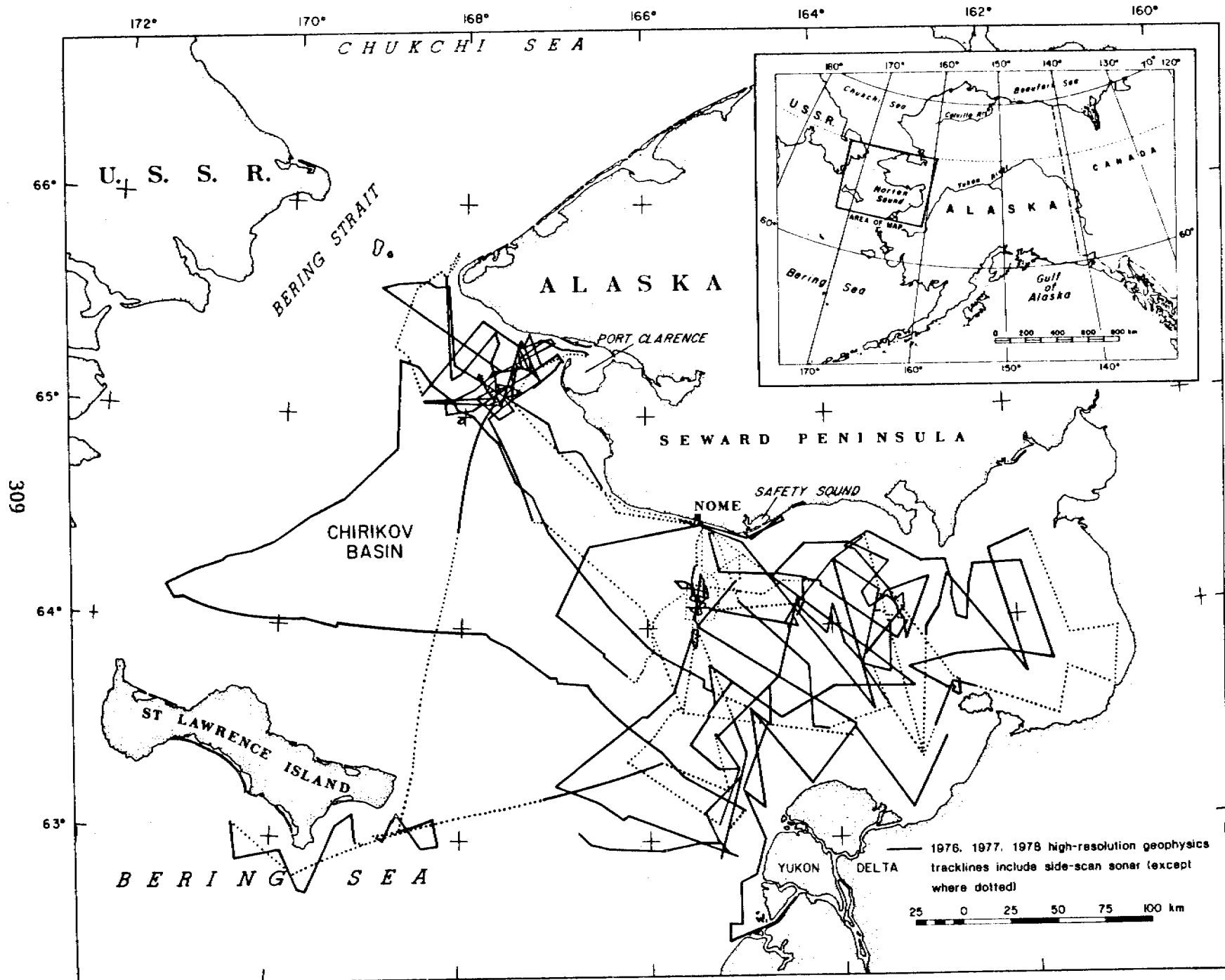


Fig. 1 - Index map and chart of high-resolution geophysical and side-scan sonar tracklines covered by the R/V SEA and R/V KARLUK in northeastern Bering Sea during 1976, 1977, and 1978.

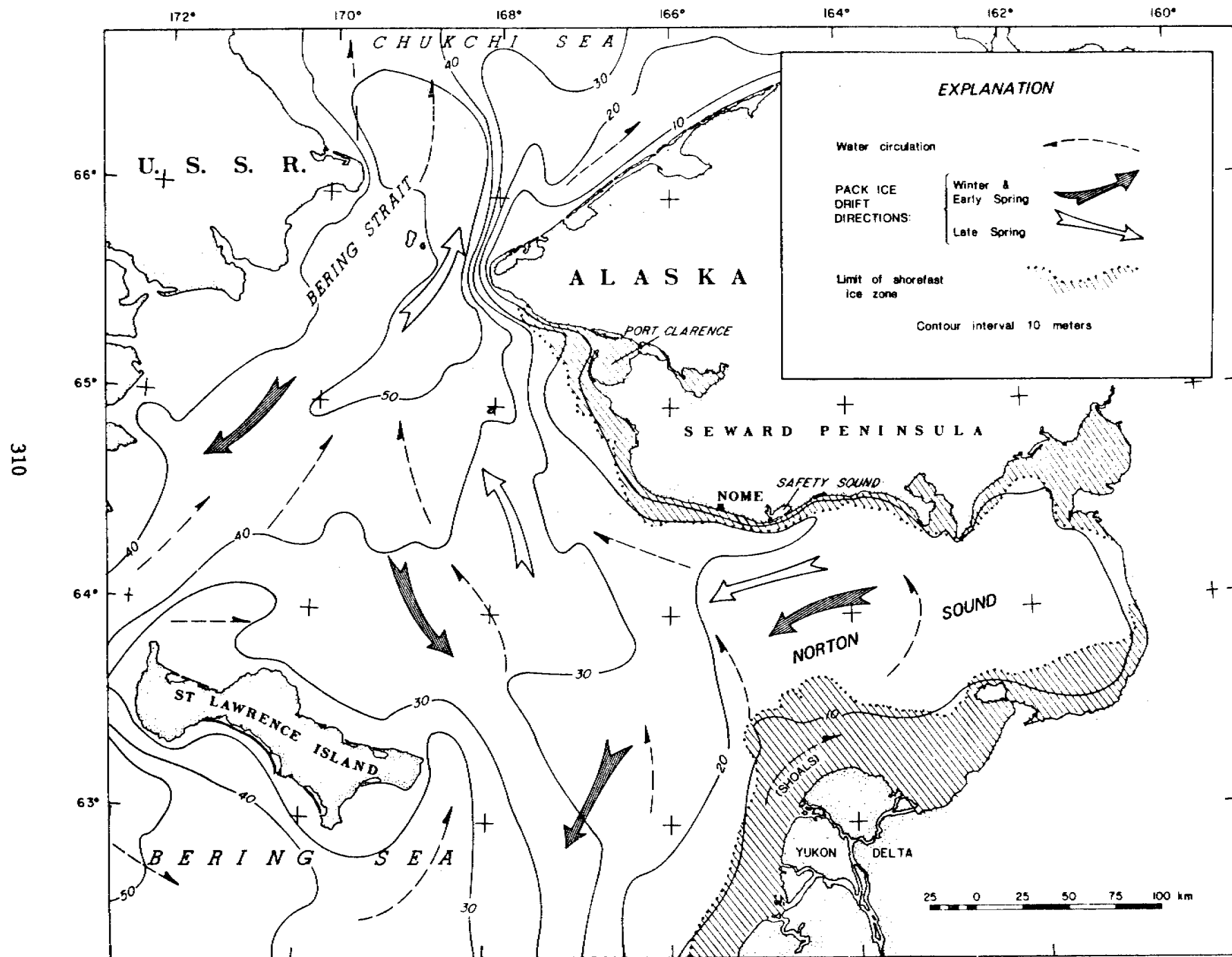


Fig. 2 - Northeastern Bering Sea and southern Chukchi Sea, showing water circulation and bathymetry. Compilation sources include Goodman and others (1942), Fleming and Heggarty (1966), Musby (1969, 1971), McManus and Smyth (1970), Nelson and Hopkins (1972), Pratt and Walton (1974), and Coachman and others (1976). Drift directions of pack ice in northern Bering Sea adapted from Muench and Ahlmas (1976) and Duprè (1978).

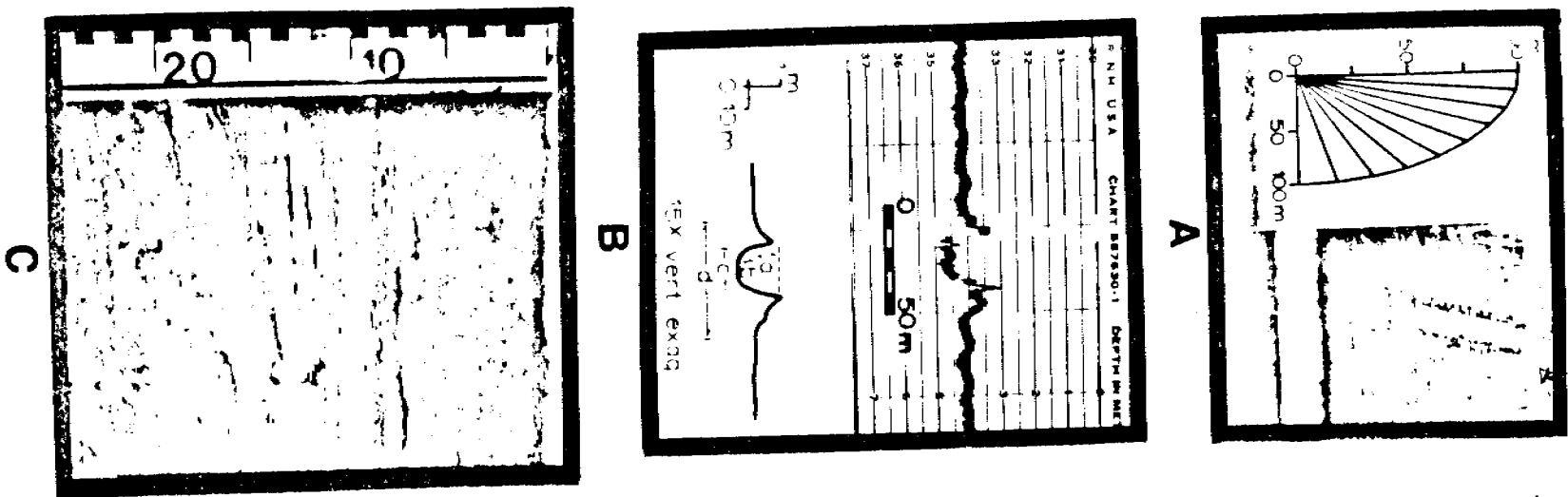
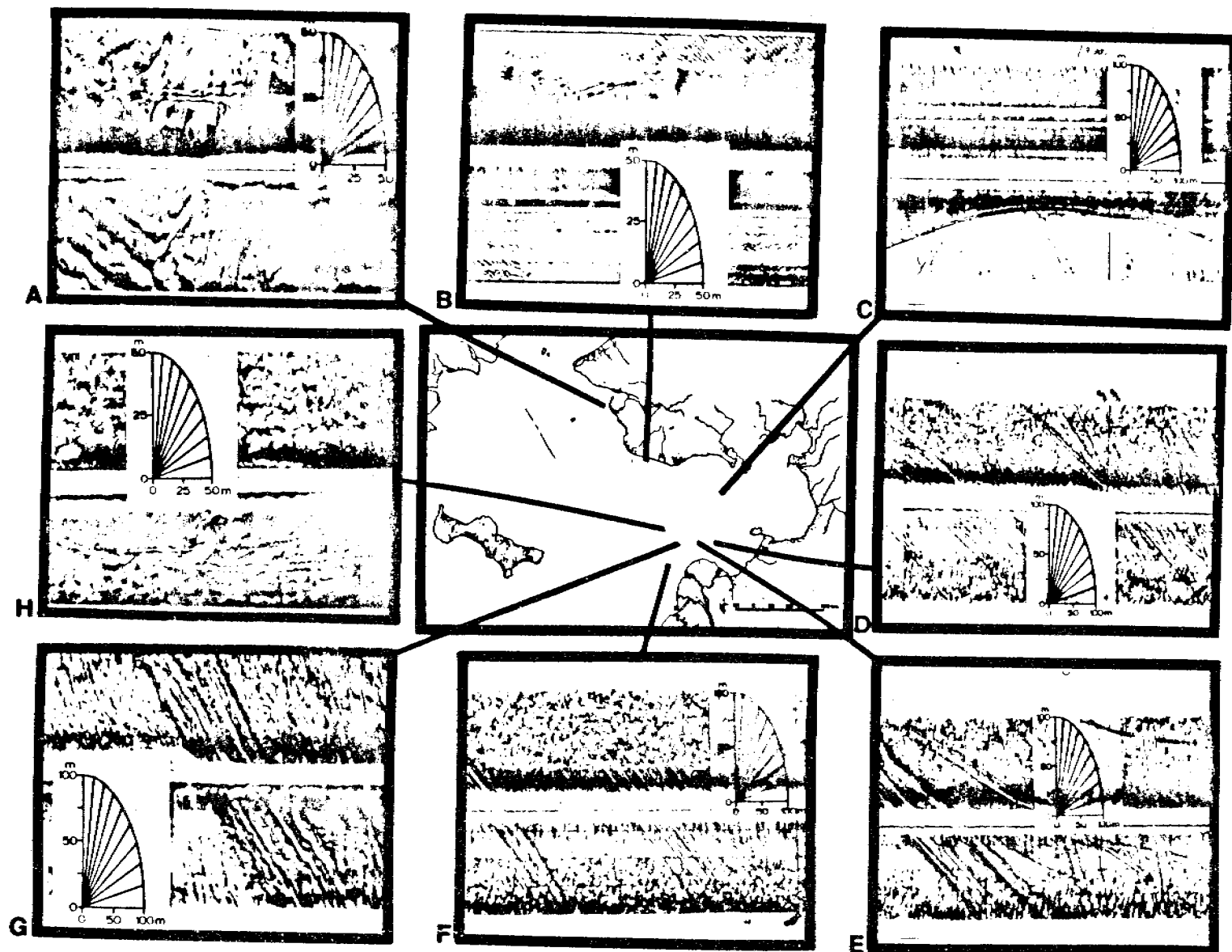


Fig. 3 - A. Solitary gouge on a sonograph. B. 200 kHz fathometer profile and diagrammatic representation of gouge shown in A. Features of gouge include (a) incision depth as measured from gouge bottom to a horizontal line projected across sediment surface, (b) height of sediment mounded on the gouge edge, (c) width of incision, (d) width of disruption zone caused by the gouging process. C. Box core slab showing subsurface (11-18 cm interval) disruption possibly caused by a past gouge event.

Fig. 4 - Sonographs showing ice gouges of the northeastern Bering Sea. A and B - solitary gouges in sand-wave and ripple fields. C, D, and E - solitary gouges. Example E shows depth of incision on the sonograph horizon line. F and G - examples of pressure ridge raking. Example G shows depth of incision on the sonograph horizon line. H - example of depressions associated with ice gouging.



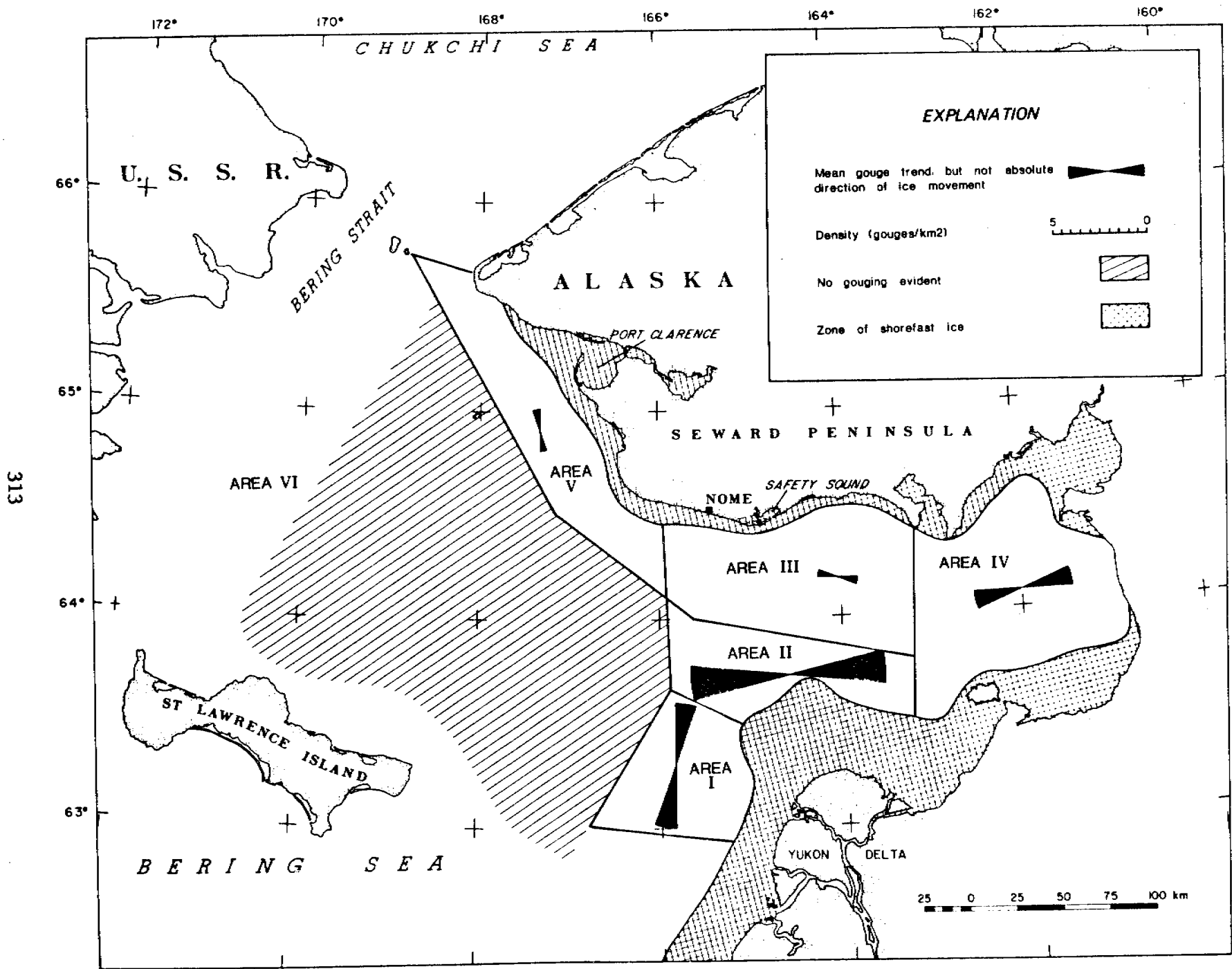


Fig. 5 - Rose diagrams representing trend and density of gouges. Division into areas I - V based on zones of similar trending gouges. Zone of shorefast ice based on evaluation of Landsat imagery (Duprè, 1977, 1978; Ralph Hunter, pers. comm., 1977).

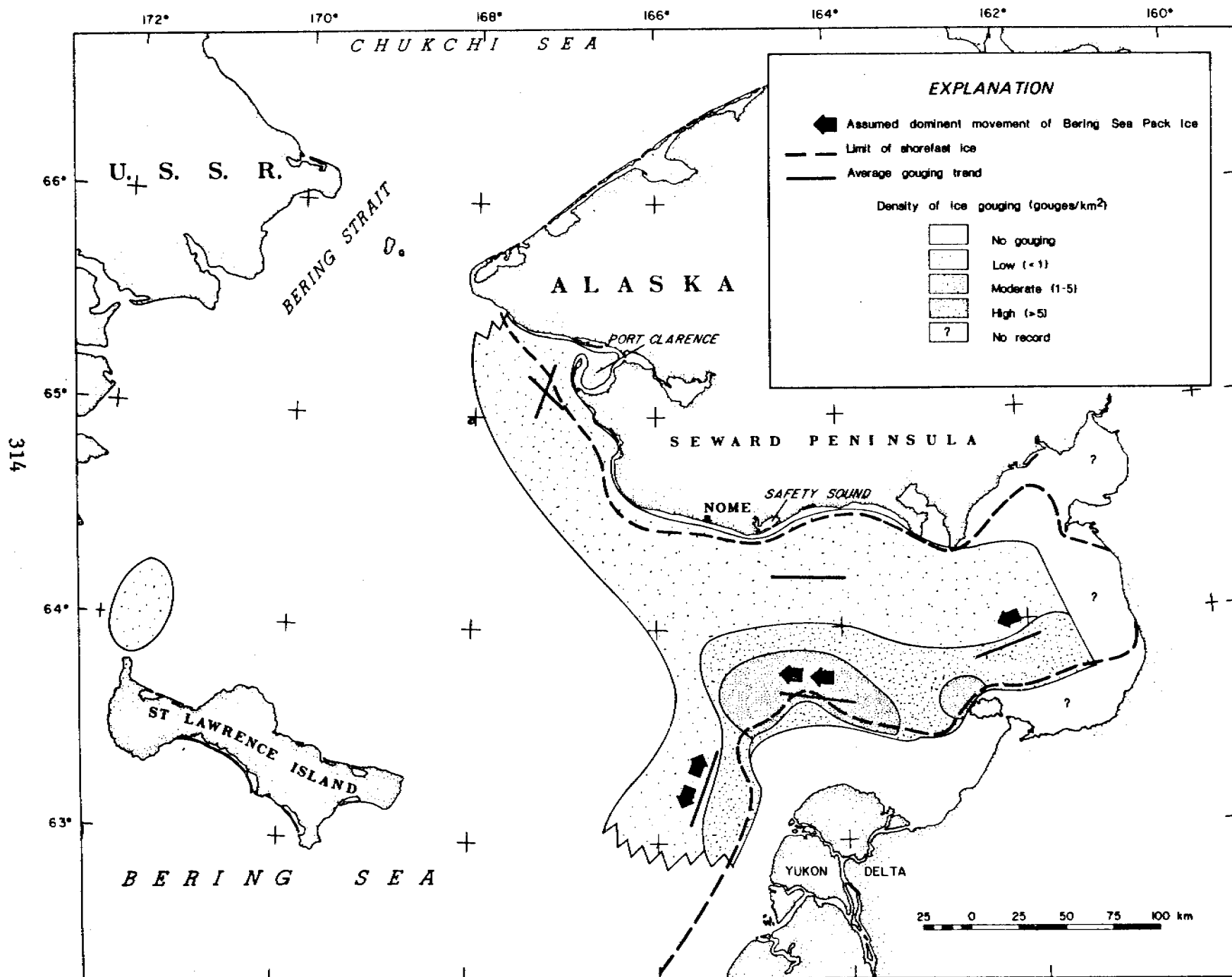


Fig. 6 - Summary of ice gouging: density, shorefast ice limits, and ice movements in northeastern Bering Sea.

Areas of Active, Large Scale Sand Wave and Ripple Fields with Scour Potential on the Norton Basin Sea Floor

Hans Nelson, Michael E. Field, David A. Cacchione, and
David E. Drake

Introduction

Strong dynamic currents are present throughout much of the northern Bering Sea, particularly where westward land projections interject into the northward flow, such as in the eastern Bering Strait area (fig. G-1) (Fleming and Heggarty, 1966). In such regions large bedforms develop and migrate to form an unstable sea floor that can be a potential hazard to platform foundations and pipelines. Such potentially hazardous areas must be identified, their history assessed, and magnitude of future problems predicted. This paper outlines regions of mobile bedforms (fig. G-1) and presently known aspects of their dynamic activity.

Identification and Distribution of Bedform and Scour Features

Large bedforms and scour features can be recognized and mapped with side-scan sonar profiles and basic internal structure sometimes can be determined by high-resolution profiles (fig. G-2; see Methods in sections B-D for a description of techniques). Detailed surficial observations can be made with underwater television and bottom photos, and subsurface stratigraphic history may be determined by analyses of vibracores and box cores (figs. G-3 and 4).

In general, only small scale bedforms and large scale scour features (fig. F-1) are found in Norton Sound (fig. G-1). Chirikov Basin on the other hand is characterized by coarser grain size than Norton Sound (fig. F-5) (Nelson and Hopkins, 1972; McManus et al., 1974 and 1977), and numerous fields of mobile bedforms. In the vicinity of Sledge Island, most of the sea floor has been stripped bare of sediment (Nelson and Hopkins, 1972), suggesting intense current scour. Just east and west of the scoured region and extending across the nearshore area of the Nome coastal plain, extensive sand wave and ripple fields are found (fig. G-1).

From Pt. Spencer spit west to King Island a series of sand ridges and swales exist (fig. G-2). The crest of each shoal is covered with sand waves of varying types and sizes (fig. G-5). To the north of the ridge and swale area toward Bering Strait, extensive sand ribbon fields are found with occasional sand dune areas (fig. G-1); however, the area is not completely surveyed. The sand ribbon fields indicate a sediment-starved region and possibly one prone to current scour as the current speeds intensify toward Bering Strait (fig. E-3). Further north within Bering Strait itself, gravel and shell pavements are noted (Nelson and Hopkins, 1972) in addition to sporadic occurrences of extremely large sand waves (Grim and McManus, 1970).

Off the eastern and western ends of St. Lawrence Island, major sand ridge and swale topography is known (Hopkins et al., 1976), and ripple fields are common to the northwest off St. Lawrence Island (fig. G-1).

Character and Origin of Mobile Bedform Features

In the ridge and swale area between King Island and the mainland, swale areas appear to undergo erosion periodically. Generally, a thin veneer of fine, modern mud at the surface overlies Pleistocene peaty mud (fig. G-6). Fine mud, signifying sluggish currents, typically deposit rapidly in depressions (fig. G-7). The lack of thick deposits, and very old radiocarbon dates close to the surface, however, suggest that muds periodically are swept away so that there has been no net mud accumulation for thousands of years. In fact, a radiocarbon date on peat 20 cm below the surface of the swale between Tin City and York Shoal was >30,000 BP, indicating that significant quantities of younger sediment had been stripped away, possibly by currents (fig. G-6).

In contrast to swales, sand ridges are definitely constructive as is shown in the sparker seismic profiles (figs. G-8 and 9). The morphology of inner shoals mirrors the shape of the modern Pt. Spencer spit and these shoals may be ancient analogues (fig. G-3). Indeed, depths of shoal crests coincide with proposed still-stand depths of ancient submerged strandlines noted elsewhere in northern Bering Sea (Nelson and Hopkins, 1972). Sand ridges behind large obstructions to the northward current flow, such as King Island and Cape Prince of Wales (see area north of 88 in fig. G-3), may be lee side accumulations of sediment unrelated to past paralic environments.

Although formation of the basic ridge structures (15-30 km long, see cross-hatched areas in fig. G-3), may relate to past transgressive history, these structures also have a modern history of modification by development of sand waves and ripple fields. Sand waves are 1 to 2 m high and have crest spacings of either 10 to 20 m or 150 to 200 m (figs. G-9 and G-10E). Superimposed on the sand waves are smaller scale current asymmetric (figs. G-10B and C) and wave oscillation (fig. 10A) ripples with heights approximately 4 to 10 cm and wavelengths approximately 20 to 100+ cm. Except for the oscillation ripples, bedforms of all sizes are asymmetric to the north, and their asymmetry coincides with the prevailing northward flowing dynamic currents (fig. E-3) (Coachman et al., 1976).

Growth and movement of the sand wave fields on crests is definitely intermittent, just like the apparent erosional history of the swales. Ice gouges observed to cut sand wave fields on inner shoals in the summer of 1976 proved that no change in the sand wave fields had occurred at a minimum since the previous winter, or possibly for many years before, depending on how recently the gouge occurred. At the time we studied the area in the fall of 1976, only low speed oscillatory bottom currents up to 15 cm/sec (fig. G-11) were measured. Underwater television observation showed only the development of oscillation ripples (Fig. G-10A) and only decayed, inactive sand wave bedforms were seen on sonographs (figs. G-10D and E). Thus, sand wave movement was active neither then nor apparently for some time before. However, a piece of wood found at 30 cm depth in a sand wave had an age of 1155 BP (Teledyne Isotopes #I-9773). This date proved that sand wave scour had been active to this depth since sea level has reached its present height, and that sand waves are not relict features from some past time of lower sea level.

Data collected in the field season of 1977 indicates that significant activity has occurred since the 1976 survey. In some areas with replicate side-scan lines, large scale sand waves have reformed from decayed fields and developed subsets of smaller scale sand waves offset at an angle (fig. G-10E); however, sand waves on some other ridges remained unmodified from 1976 to 1977 (fig. G-10D). Underwater television videotapes show that small scale ripple fields were undergoing active modification at the time of observation in 1977. Instead of oscillation ripples observed during the storm conditions in 1976, there were actively migrating asymmetric straight-crested ripples in the troughs (fig. G-10C) and linguoid ripples on the upcurrent face of sand waves (fig. G-10B). Northward flowing bottom current speeds measured with the shipboard profiling current meter ranged from 20-40 cm/sec, and near bottom average current speed was 24 cm/sec (fig. G-12).

Observations of a series of ice gouges also confirms that there has been recent, active migration of sand waves near Port Clarence (fig. G-13). Ice gouges range from fresh to highly modified by sand wave migration (fig. G-12 F); thus, extensive movement of some sand wave fields has occurred recently. Lack of modification of gouges (fig. G-13) and continued presence of decayed bedforms in some locations indicate that current activity in the Port Clarence area varies both in time and space. Only long term current measurements from several locations will solve the complexity of current regimes and allow predictability of mobile bedform activity.

Conclusions and Needs for Further Study

Surveys in September 1976 during a period of subsiding storm waves from the north showed only oscillatory movement of sand on ripple crests. A maximum speed of the north-flowing coastal current of about 15 cm/sec was measured near the bottom and no net bedload movement was observed. Fresh-looking ice gouges cutting inshore ripples indicated that bedload movement had been negligible in this zone since ice break-up in the spring. The second survey, in July 1977, was made during very calm weather, yet significant bedload movement was observed on ridge crests at water depths of 10 to 30 m. Northward flowing bottom currents measured up to 40 cm/sec. Linguoid ripples were observed moving on the stoss slope of sand waves and straight-crested ripples in the troughs. Ice gouges on deeper ridge crests in varying states of preservation indicated active bedload transport.

Sand wave movement and bedload transport apparently occur during calm weather and maximum change apparently occurs when major southwesterly storms generate sea level set-up in the eastern Bering Sea that enhances northerly currents. Strong north winds from the Arctic, however, reduce the strength of the continuous northerly currents and thereby reduce the amount of bedload transport.

Studies to date indicate that the most extreme scour potential exists in regions of sand ribbons and gravel plus shell pavement within straits areas (fig. G-1). The Port Clarence sand wave area has the most rapidly changing relief and the scour in sand wave troughs may reach depths of up to 2 m (Fig. G-9). Data from replicate lies in 1976 and 1977 show that such scour may occur in some areas of the Port Clarence sand wave field each year (fig. G-10).

Future studies require reoccupation of key sites within the sand wave field to determine stability. Long measurements for several months must be made of current velocity and suspended sediment, especially during times of storm stress. Detailed side-scan profiling is required at locations of suspected current scour and stratigraphic history must be investigated with deep vibracoring to determine depth of active scour, and periodicity and extent of bedform movement.

Acknowledgements

Devin Thor, Mathew Larsen, Terry Hallinan, William Richmond, Jeff Patry and James Evans compiled data and prepared figures. We thank the officers, crew, and shipboard scientific staff for their concerted effort in the detailed study of sand wave areas.

References Cited

- Coachman, L.K., Aagaard, Knut, and Tripp, R.B., 1976, Bering Strait: The regional physical oceanography; Univ. of Washington Press, 186 p.
- Fleming, R.H., and Heggarty, D., 1966, Oceanography of the southeastern Chukchi Sea, in Wilimovsky, N.J., Wolie, J.M., (eds.), Environment of Cape Thompson Region, Alaska: U.S. Atomic Energy Commission, p. 697-754.
- Grim, M.S., and McManus, D.A., 1970, A shallow seismic profiling survey of the northern Bering Sea: Marine Geology, v. 8, p. 293-320.
- Hopkins, D.M., Nelson, Hans, Parry, R.B., and Alpha, Tau Rho, in press, Physiographic subdivisions of the Chirikov Basin, northern Bering Sea; U.S. Geol. Survey Prof. Paper 759-B, (published in cooperation with) National Ocean Survey, National Oceanographic and Atmospheric Administration.
- McManus, D.A., Venkataratham, K., Hopkins, D.M., and Nelson, C.H., 1974, Yukon River sediment on the northernmost Bering Sea shelf: Jour. Sed. Pet., v. 44, no. 4, p. 1052-1060.
- McManus, D.A., Venkataratham, Kolla, Hopkins, D.M., and Nelson, Hans, 1977, Distribution of bottom sediments on the continental shelf, northern Bering Sea: U.S. Geol. Survey, Prof. Paper 759-C, p. C1-C31.
- Nelson, C.H., and Hopkins, D.M., 1972, Sedimentary processes and distribution of particulate gold in the northern Bering Sea: U. S. Geol. Survey Prof. Paper 689, 27 p.
- Nelson, C. H., and Creager, J.S., 1977, Displacement of Yukon-derived sediment from Bering Sea to Chukchi Sea during Holocene time: Geology, v. 5, pp. 141-146.

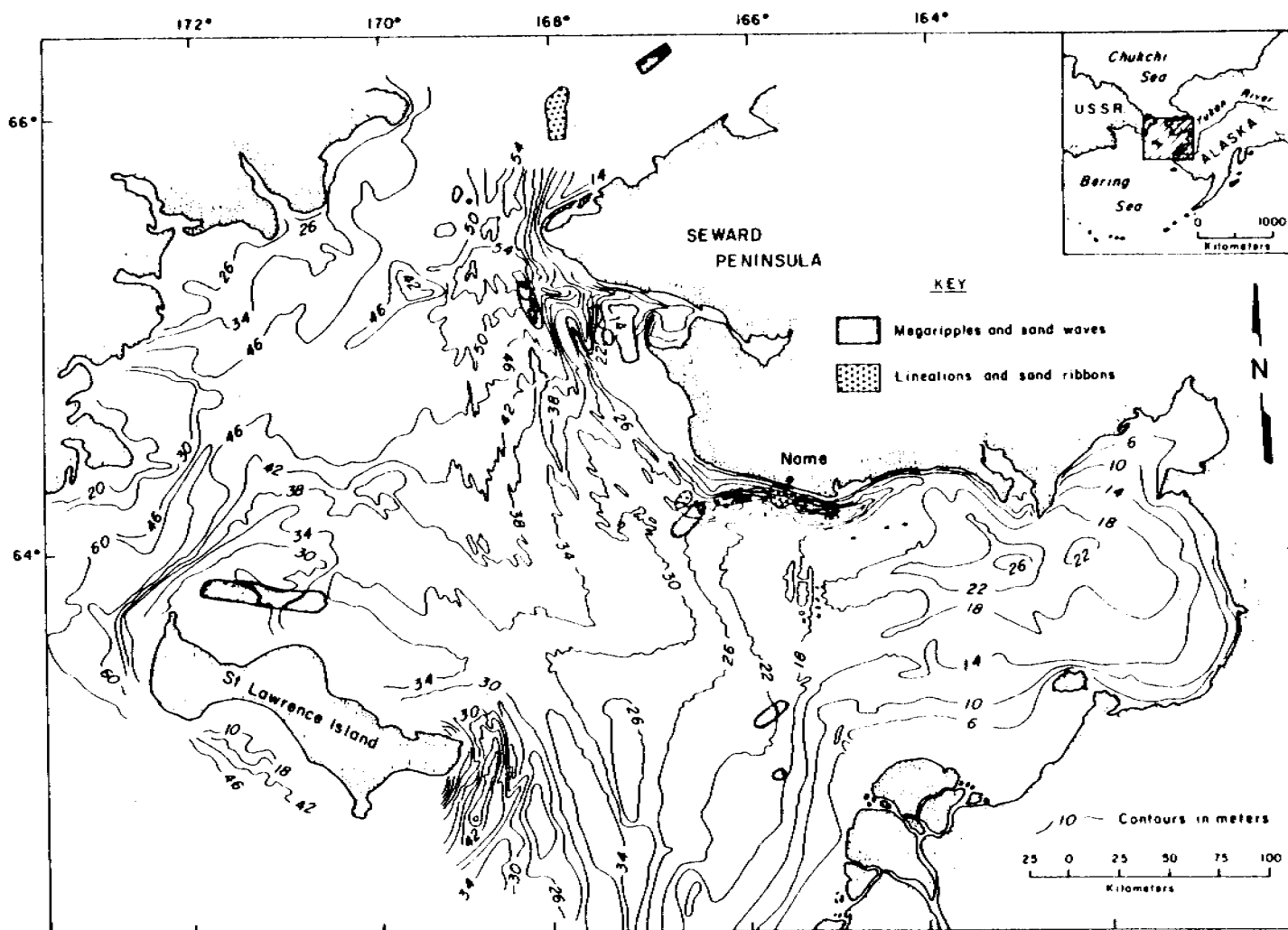


Figure G-1. Index map of Northern Bering Sea showing major areas of mobile bedforms.

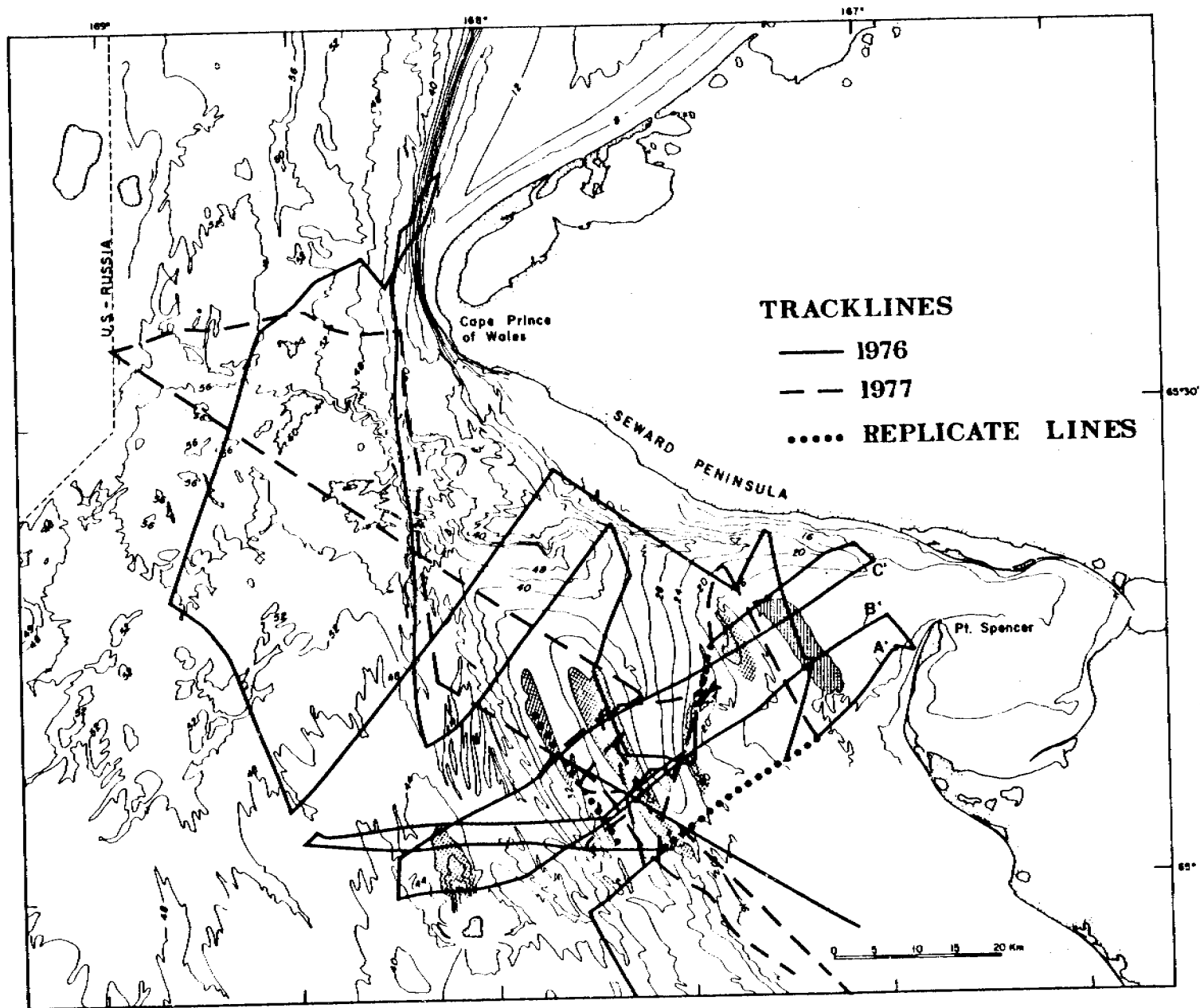


Figure G-2. Detailed high-resolution seismic profile and side scan tracklines collected in 1976 and 1977 in northeastern Chirikov Basin. Miniranger precision navigation was used to replicate tracklines. Bathymetric contours are in meters; hatched areas outline major sand ridges that exhibit sand-wave fields.

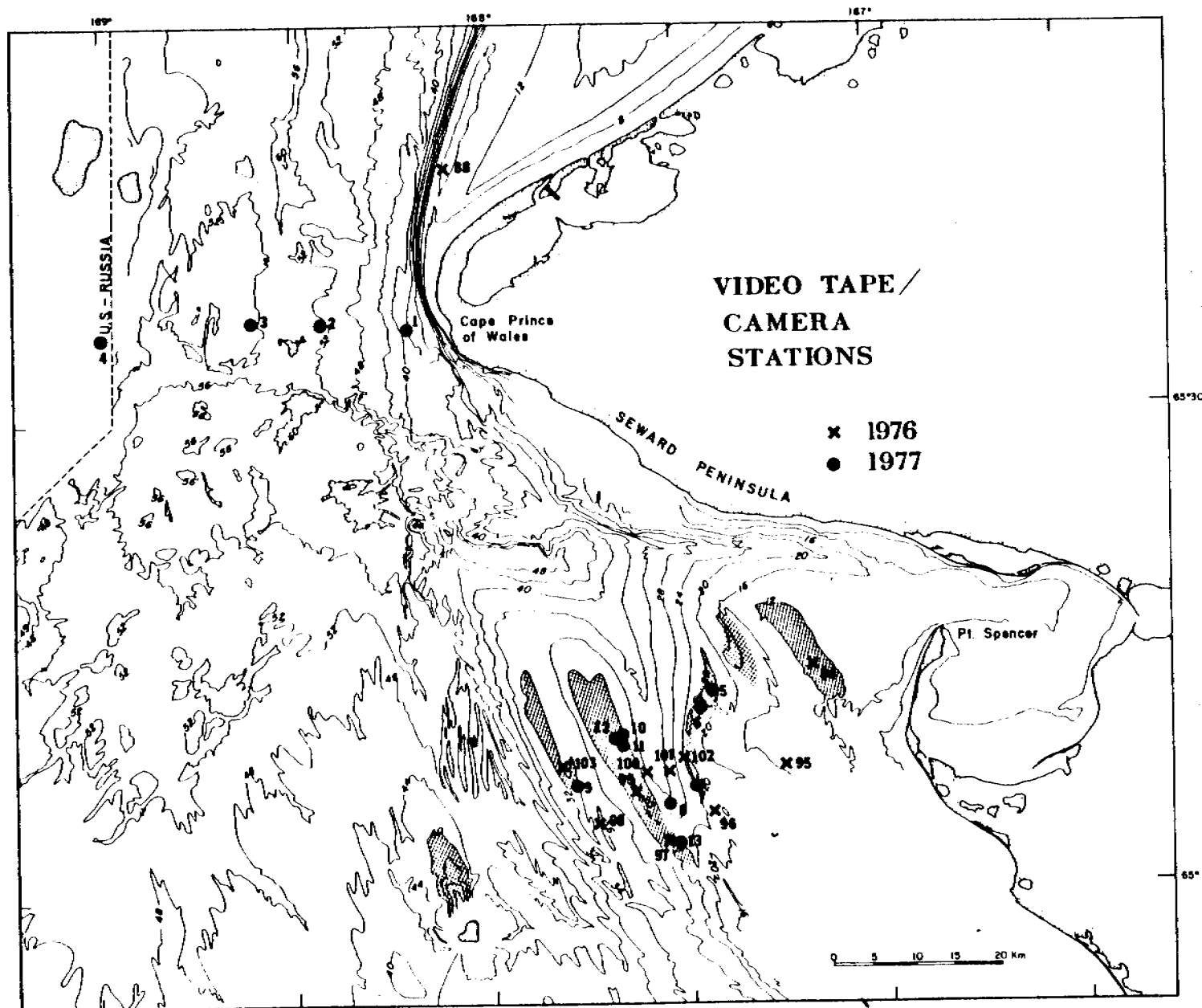


Figure G-3. Detailed transects of underwater television and bottom camera stations taken in northeastern Chirikov Basin. Bathymetric contours are in meters; hatched areas outline major sand ridges that exhibit sand-wave fields.

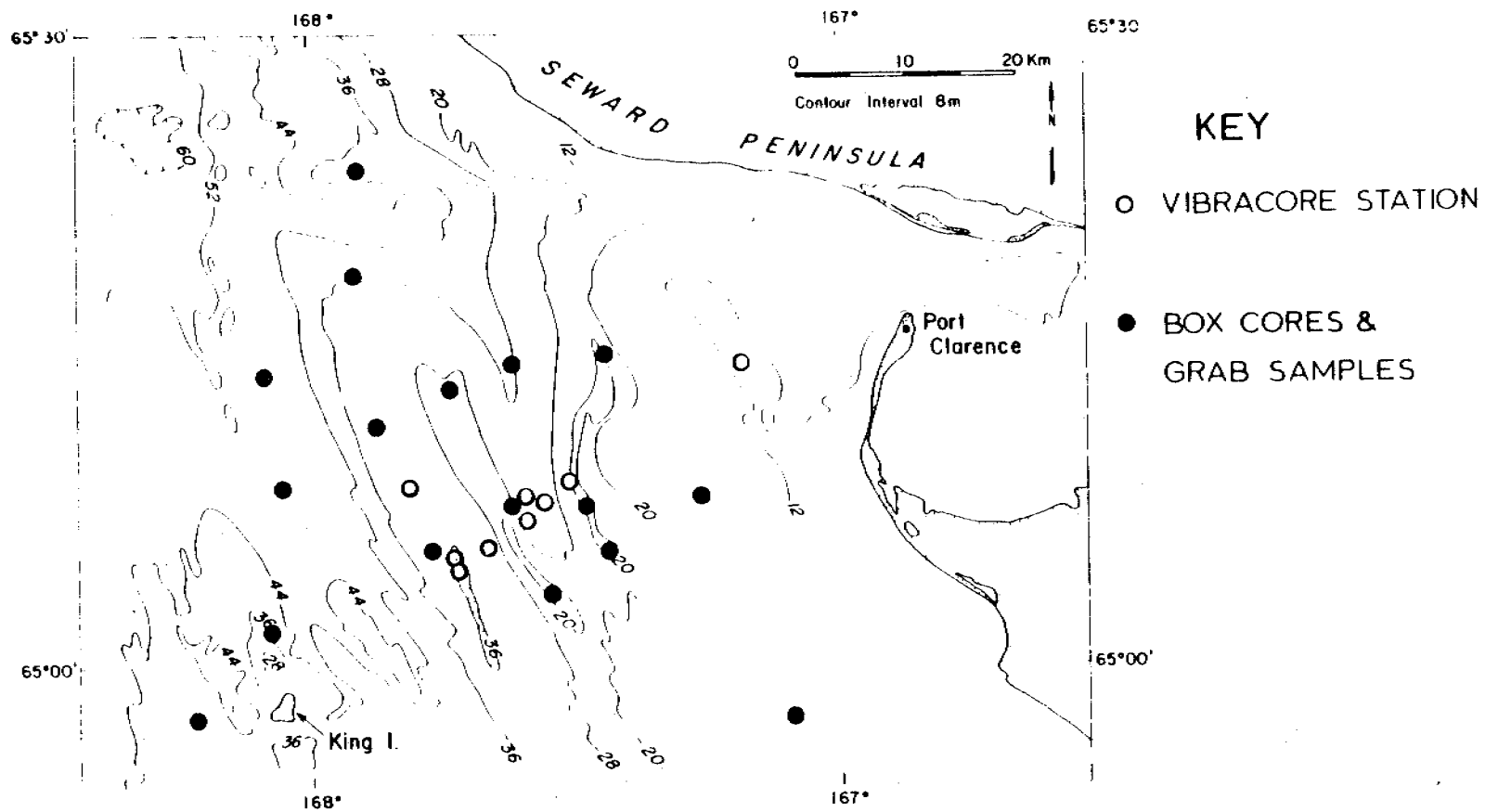


Figure G-4. Location of detailed sampling stations in area of sand ridges west of Port Clarence, Alaska.

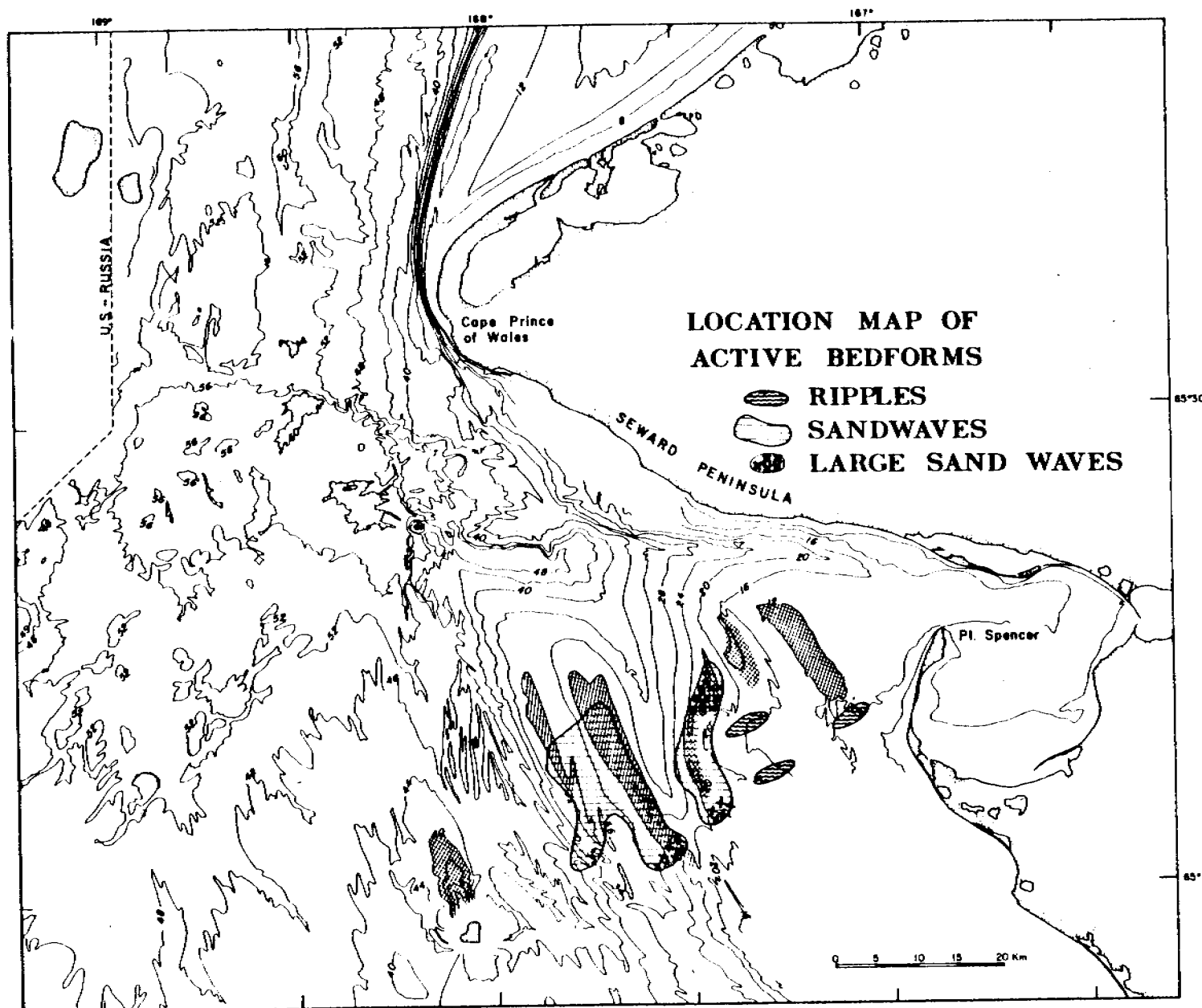


Figure G-5. Location of active bedforms in northeastern Chirikov Basin. Bathymetric contours are in meters; hatched areas outline major sand ridges that exhibit sand-wave fields.

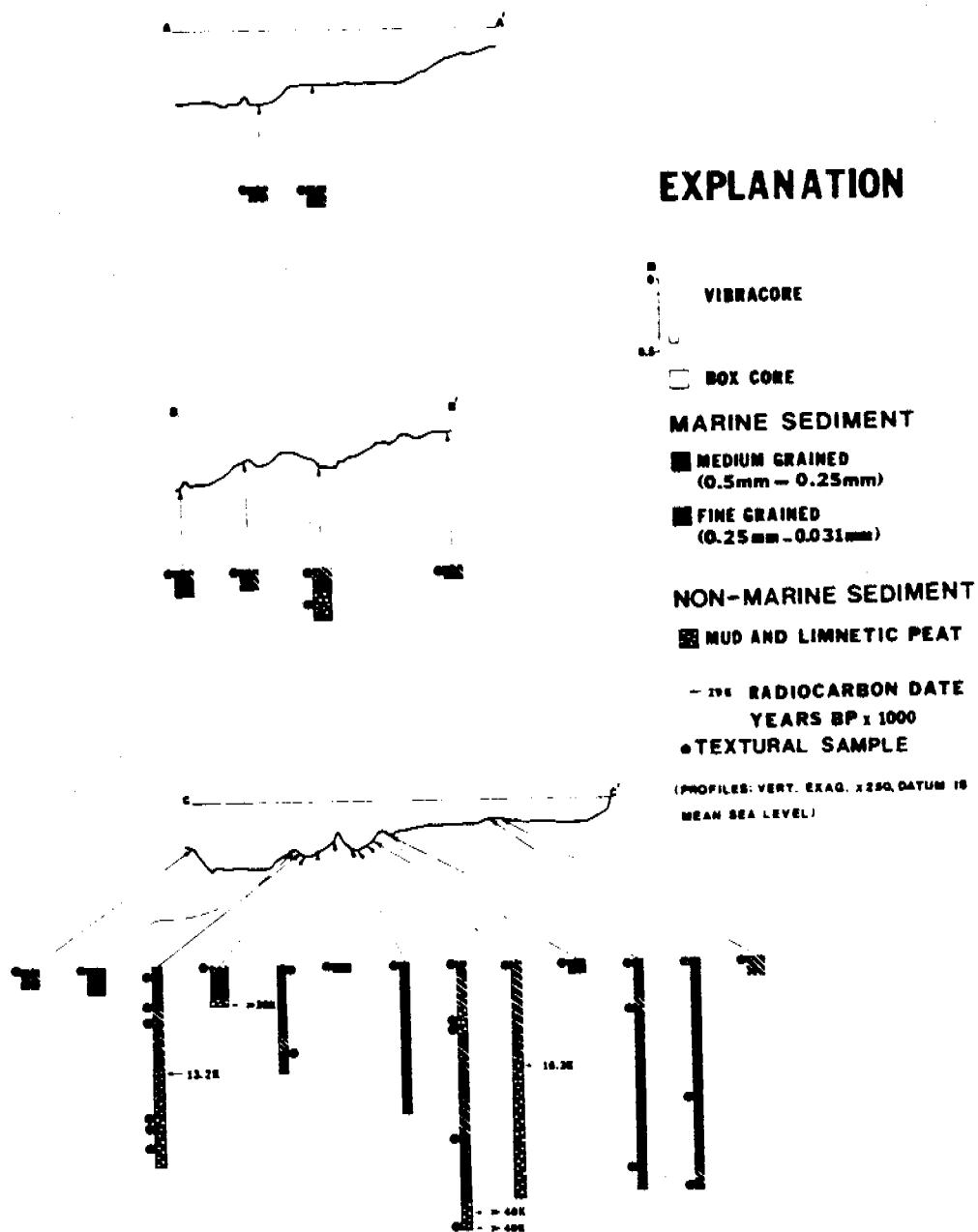


Figure G-6. Stratigraphy of near-surface sediment observed in box and vibracores from sampling transects across sand ridges near Port Clarence. Location of transects is shown in figure G-2.

SEDIMENT DISTRIBUTION

325

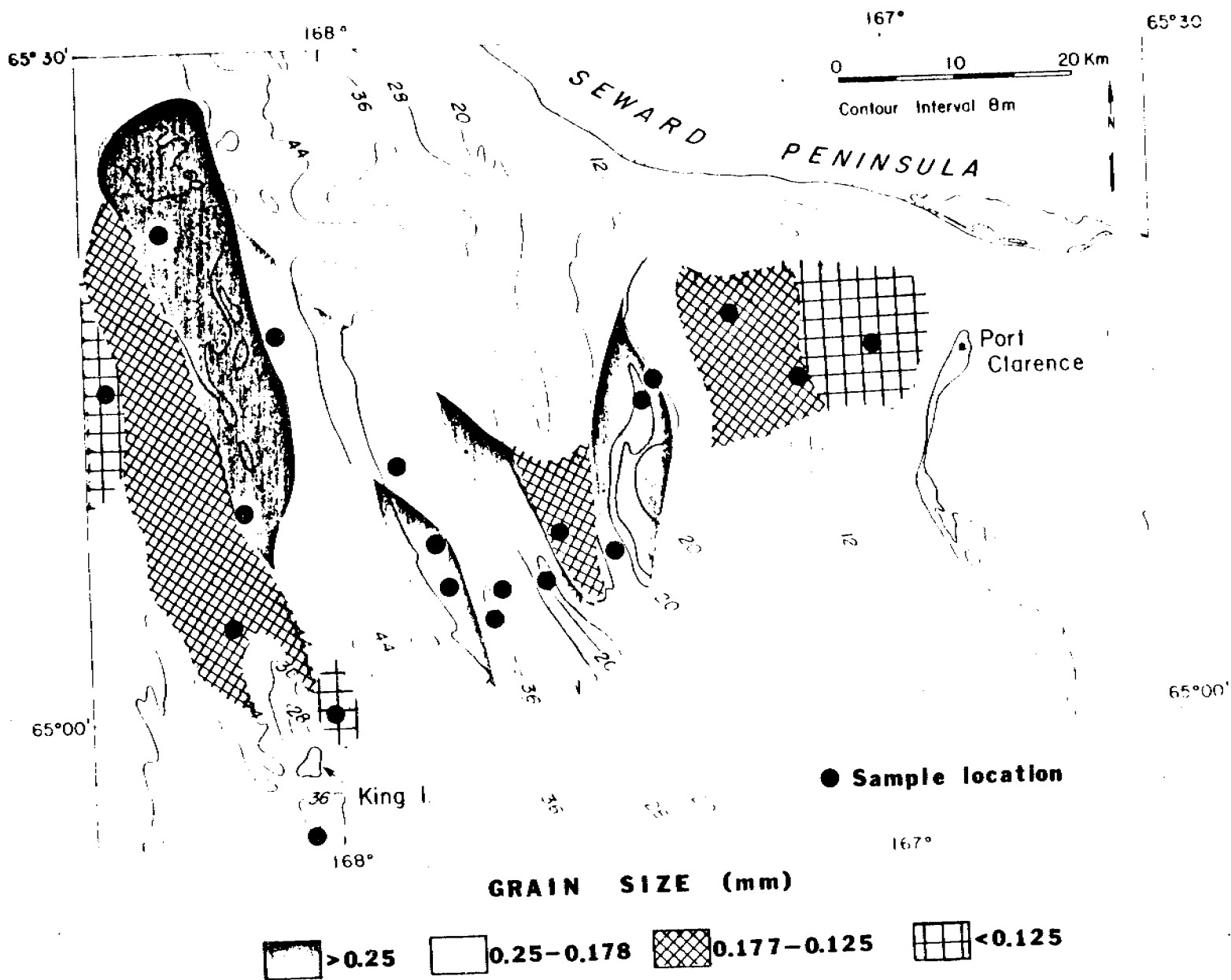


Figure G-7. Grain-size distribution in sand ridge area west of Port Clarence.

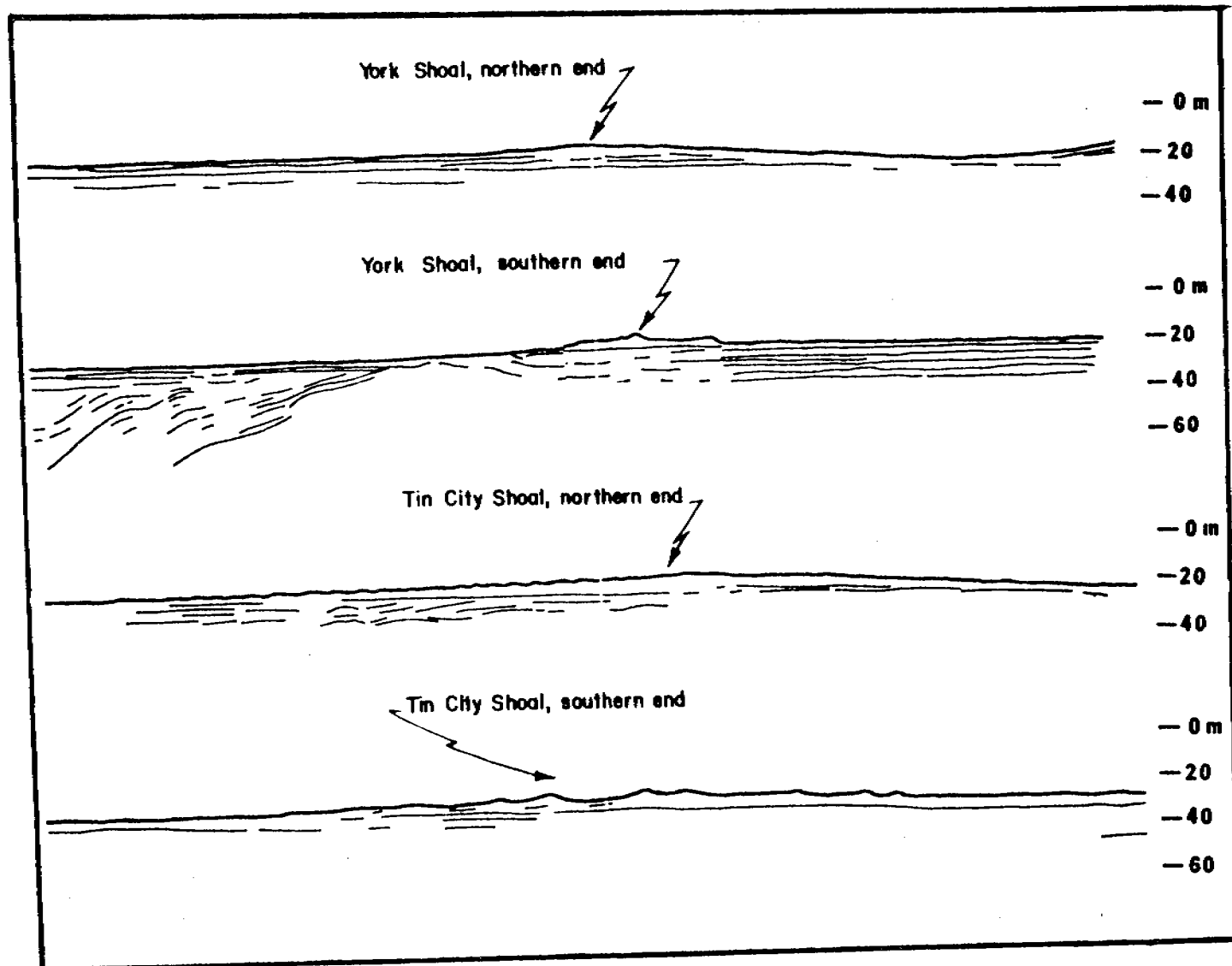


Figure G-8. Line drawings of high-resolution seismic profiles across major sand ridges shown in figure G-2. Note that the "sand ridges" are constructional features overlying parallel or folded, older sediment. Names of ridges are given in figure A-2.

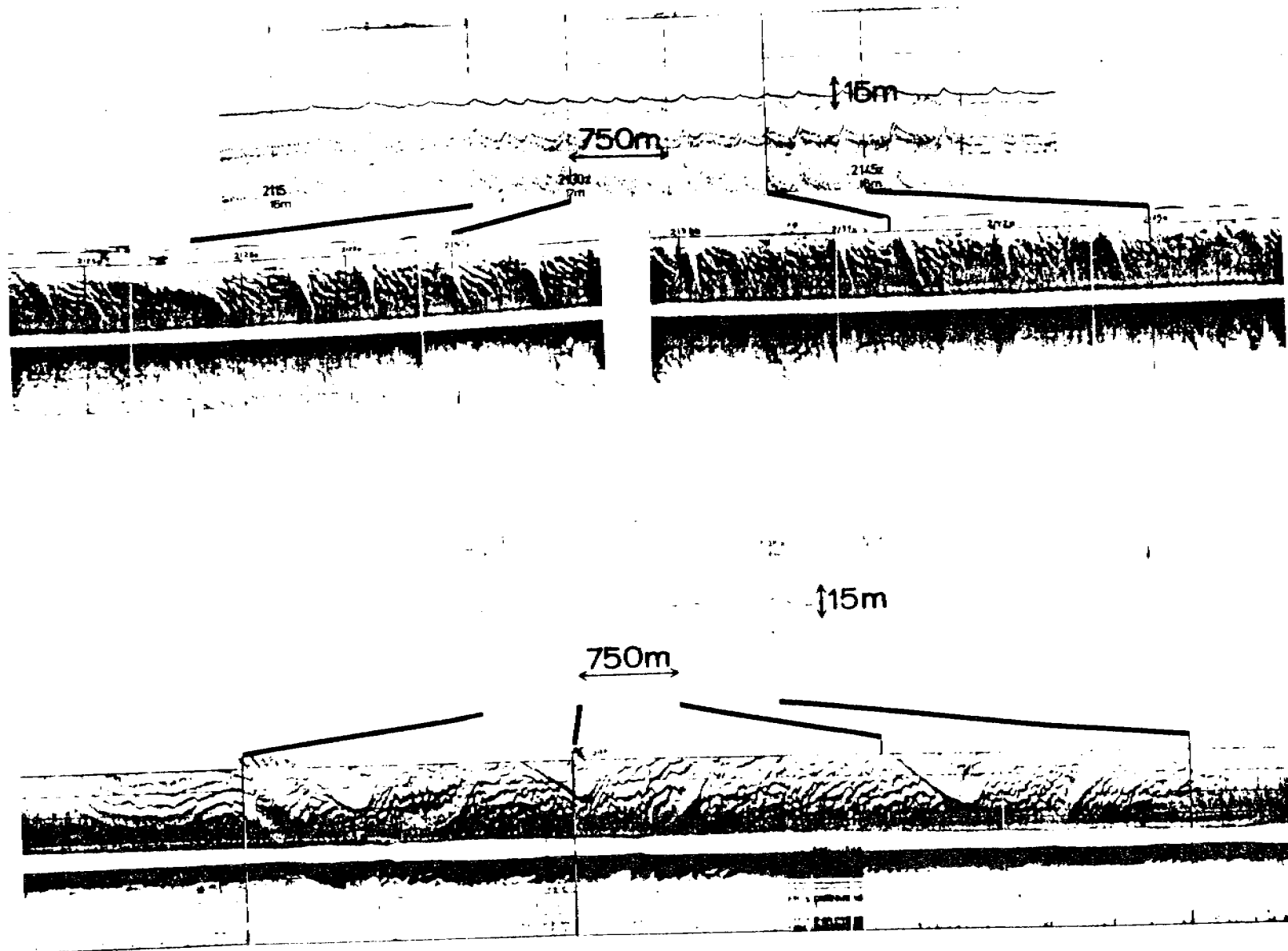


Figure G-9. 3.5 kHz seismic profiles with associated sonographs taken over sand ridges covered by large and small-scale, active sand waves. Records are from the York Shoal area shown in Figure A-2.

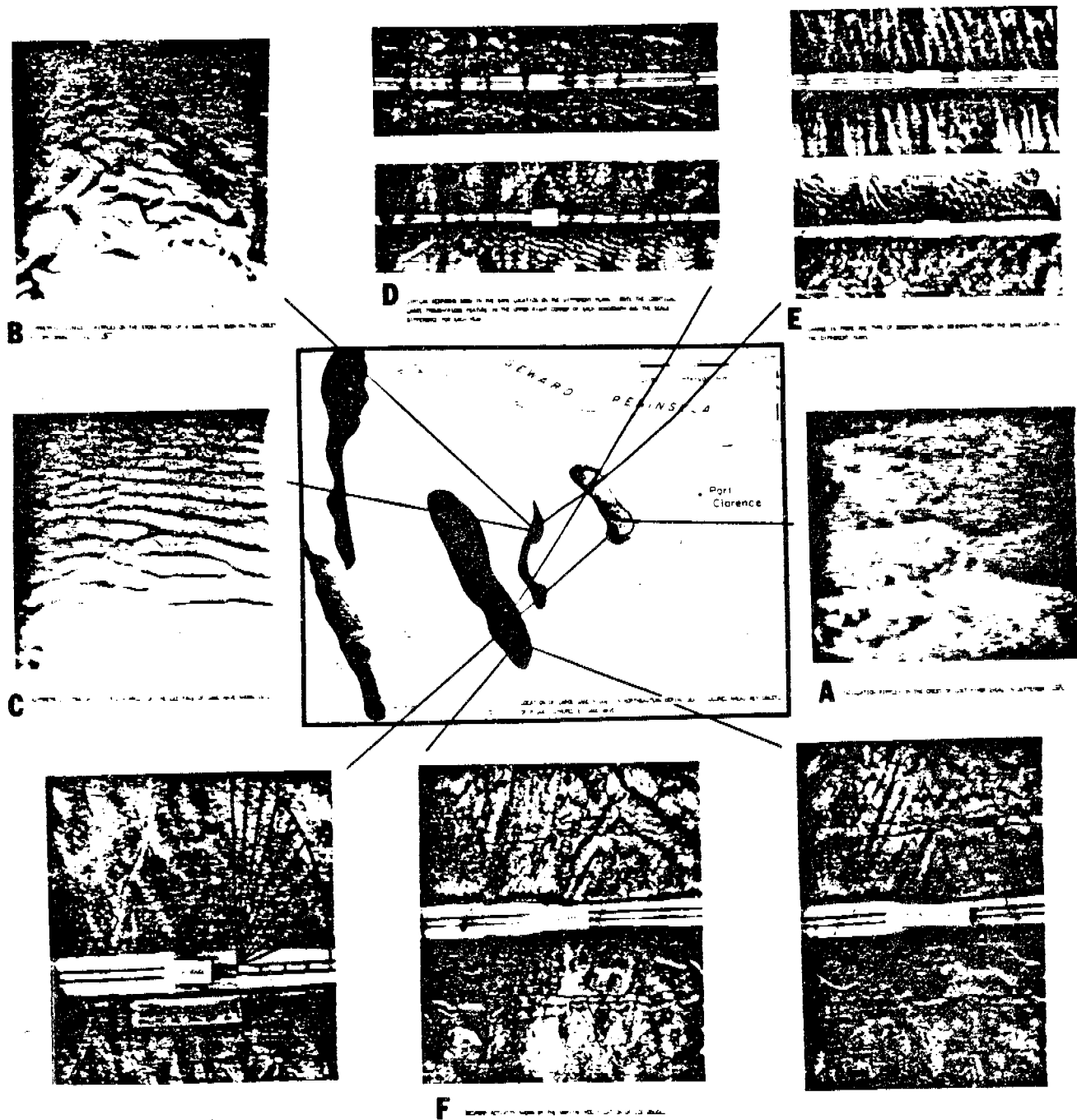


Figure G-10. Bedforms and ice gouges observed on sand ridges west of Port Clarence. A- videotape photo of oscillation ripples taken on the crest of Lost River Shoal in September, 1976 (ripple height approximately 4 cm and wave length about 20 cm; water depth 12 m). B- Bottom camera photo of asymmetric linguoid ripples on the stoss face of a sand wave on York Shoal taken in July, 1977 (ripple height approximately 2-3 cm and wave length about 10 cm; water depth 20m). C- Bottom camera photo taken at same location as B showing asymmetric straight-crested ripples of the same scale, but located in a trough between sand waves of .5m wave height, approximately. D- Sonographs of unchanged sand waves on the crest of Tin City Shoal. E. Sonographs of sand waves on York Shoal that changed from decayed bedforms in 1976 to two active sets of bedforms in 1977 (large-scale waves 2m high and 150-200 m wave length; small-scale waves .5 m high and 10-20m wave length). F-Series of sonographs showing different stages of ice gouge modification by actively migrating sand wave fields.

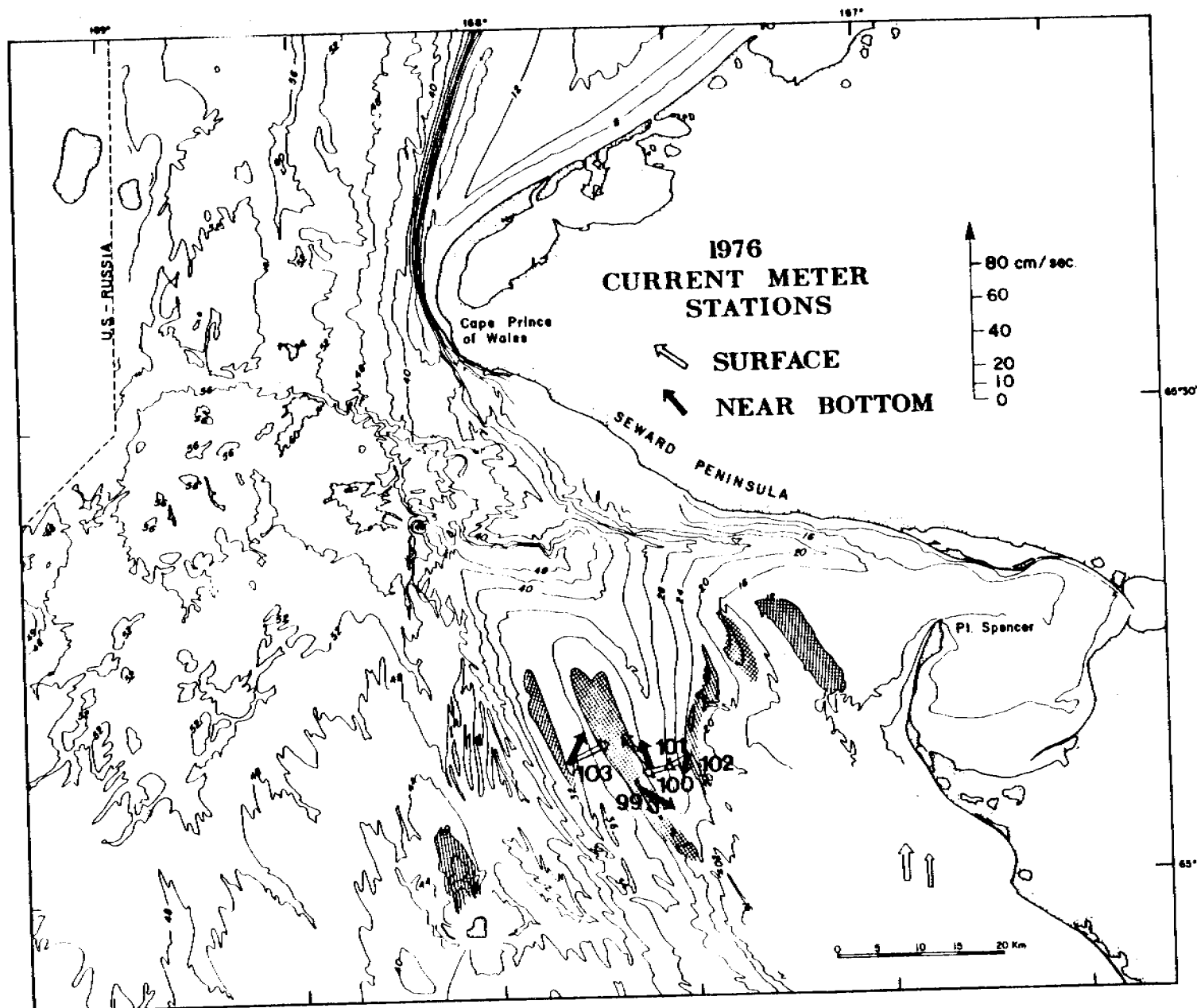


Figure G-11. Summary of profiling current meter data collected at stations in the sand wave fields west of Port Clarence in September, 1976. Hatched area depicts region of major sand ridges with sand wave fields; contour interval is 4 meters.

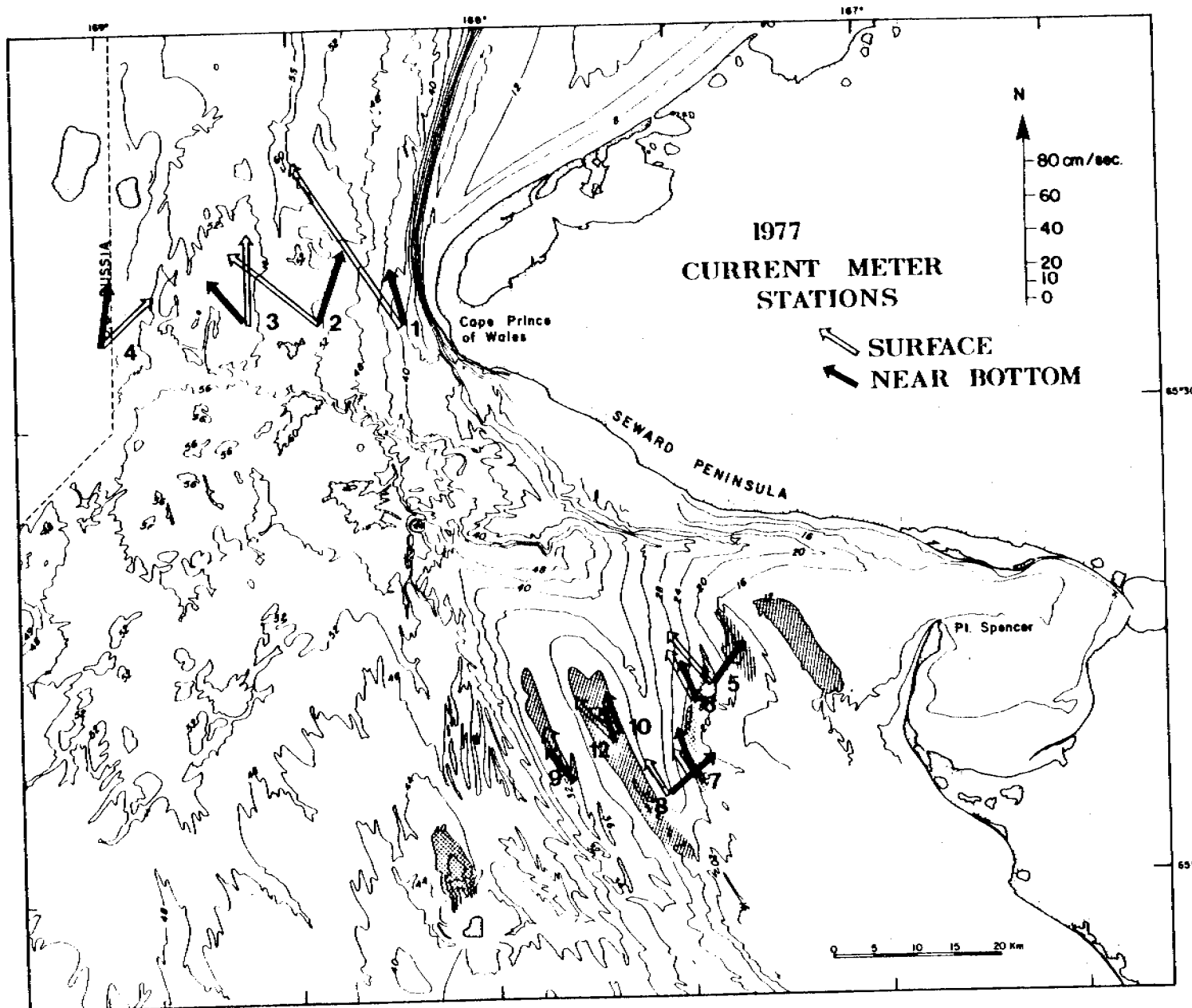


Figure G-12. Summary of profiling current meter data collected at stations in the sand wave fields west of Port Clarence and in Bering Strait during July, 1977. Hatched area depicts region of major sand ridges with sand wave fields; contour interval is 4 meters.

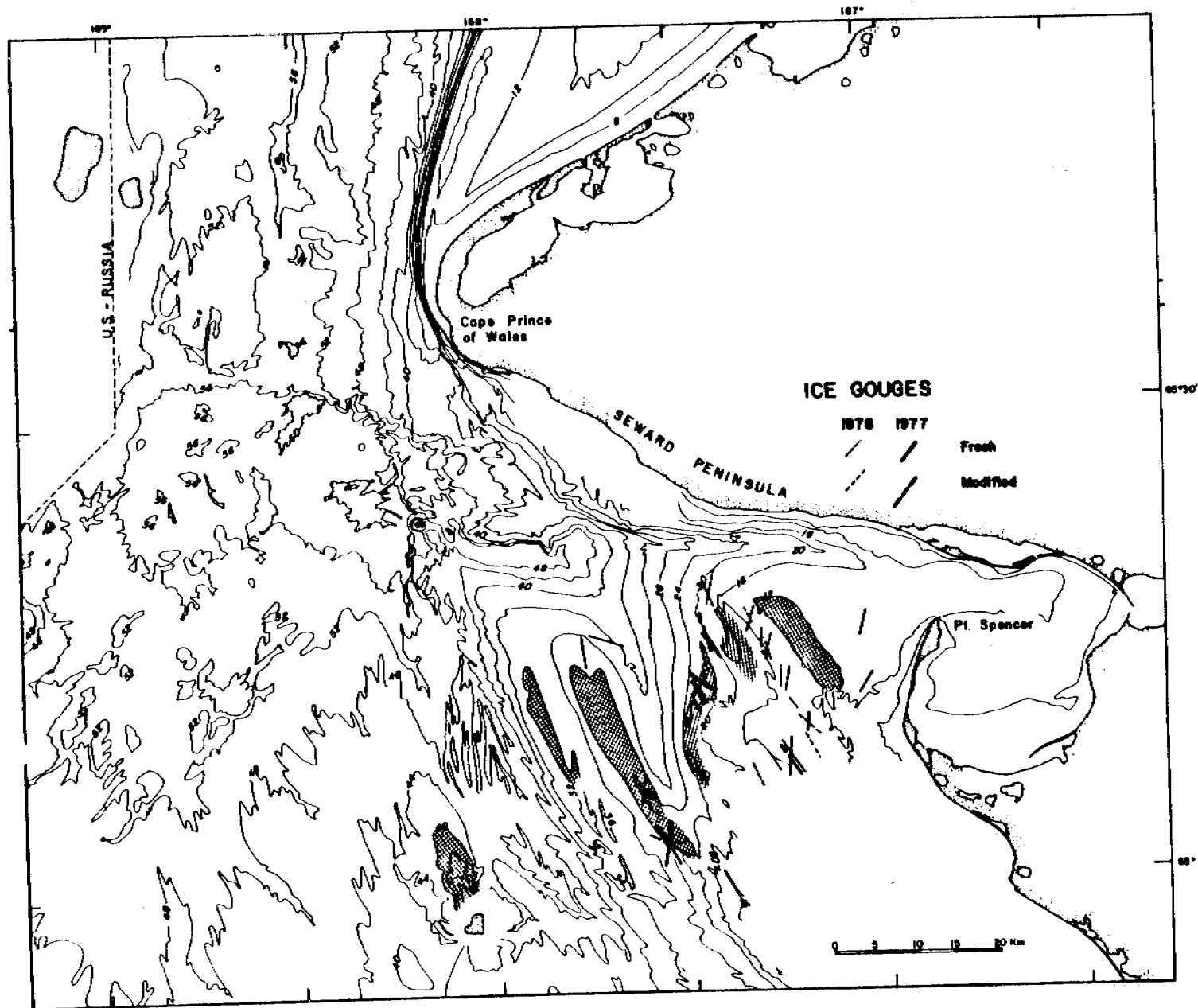


Figure G-13. Modification of ice gouges by actively migrating sand waves that is observed in sonographs taken in the area west of Point Spencer, Alaska. Hatched areas depict sand ridge crests with sand waves ; contour interval is 4 meters.

DEPOSITIONAL AND EROSIONAL FEATURES OF THE
INNER SHELF, NORTHEASTERN BERING SEA

Ralph E. Hunter, Devin R. Thor, and Mary Lou Swisher

U. S. Geological Survey
Menlo Park, California 94025

ABSTRACT

Sonographs and bathymetric profiles from water depths less than 15 m in the Nome-Solomon, Port Clarence, and Yukon delta areas of the Alaskan Bering Sea coast show features generated by waves, currents, and drifting ice. The surficial sediments in the Nome-Solomon and Port Clarence areas range in grain size from sand to boulder gravel and have many surface features visible on sonographs, whereas the sediments of the Yukon delta are fine sands and silts that have few such features.

Materials in the Nome-Solomon and Port Clarence areas have been segregated by grain size into ribbons and irregular, elongate, and lobate patches. The sand patches commonly have convex-up profiles and probably rest on gravel lag deposits that are exposed in adjacent gravel patches. Coarse sand and fine gravel patches and ribbons are characterized by symmetrical ripples, spaced 0.5 to 2 m apart, that could only have been generated by storm waves. Gravelly sand waves in the Nome-Solomon area were formed by westward shore-parallel currents. Boulder gravel ridges in this area are of unknown origin.

Sand and gravel ribbons are common near the entrance to Port Clarence. Unlike ribbons elsewhere, which have been attributed to tidal or other currents, the ribbons in the Port Clarence area show features suggesting generation by storm waves. These ribbons are oriented approximately normal to the associated large wave ripples, and both the ripples and ribbons vary in orientation in ways that can be explained as effects of wave refraction over a shoaling bottom. Ribbonlike features of unknown origin occur locally on the Yukon delta front.

Ice-gouged furrows, though less common than in areas farther offshore, occur in all the nearshore areas studied. The gouges are 5 to 15 m wide, as much as hundreds of meters long, and usually less than 0.25 m deep. Some gouges off Nome and Safety Sound are caused by tugboat cables, barge cables, or anchors dragging on the bottom.

INTRODUCTION

Strong currents are known to occur in parts of the northern Bering Sea, particularly in the approaches to Bering Strait. These currents include a semipermanent northward drift toward Bering Strait and fluctuating tidal and wind-driven currents (Coachman et al., 1975). The geologic importance of these currents in areas more than a few kilometers from shore has been shown in studies by Nelson and Hopkins (1972), Moore and Welkie (1976), Field et al. (1977), Nelson et al. (1977), Cacchione et al. (this volume), and Drake et al. (in press). Studies by Hunter et al. (1979), in contrast, have shown that waves and wave-induced currents are the dominant geologic agents on the beaches during the ice-free season. The shoreface, from the shoreline to a depth of 15 m, seemed likely to include the zone of transition from wave dominance to current dominance, and this previously little studied depth zone was the target of the present study.

We selected for detailed study three areas that offer a wide variety of sediment grain sizes and exposures to waves and currents: Port Clarence and vicinity, the stretch of coast from Nome to Solomon, and the Yukon delta (Fig. 1).

Data on these areas were gathered aboard the R/V KARLUK during June and July 1978. Data collected while underway include side-scan sonar, 7 kHz, and 200 kHz records; data collected at stations include underwater television

tapes, observations made while diving with scuba, and a few sediment samples to supplement those gathered during previous studies by Nelson and Hopkins (1972), Moore and Welkie (1976), and McManus et al. (1977).

SETTING

Port Clarence

Port Clarence is an embayment 25 to 30 km across (Fig. 2), protected from the Bering Sea by a Holocene gravel spit (Black, 1958). On the north, a Holocene gravel barrier separates Port Clarence from Brevig Lagoon. The inlet to Port Clarence is 7.3 km wide, has a maximum depth of 16 m, and is floored by mud (Moore and Welkie, 1976; McManus et al., 1977). The margins of the inlet, where most of the features visible on sonographs are located, are floored by sand and gravel. The surficial sediments are presumably Holocene, but the thickness of Holocene deposits is not known.

The mean tidal range in Port Clarence is 0.4 m. Currents through the inlet have not been studied, but the small tidal range and large cross-sectional area of the inlet ensure that the tidal currents are not extremely strong. Storm surges, known to be as high as 3.25 m (Sallenger et al., 1978), undoubtedly create stronger currents. The northward drift of the Alaskan Coastal Water toward Bering Strait (Coachman et al., 1975) may not affect the embayed coast near Port Clarence very strongly. The only long fetch for waves is to the southwest.

Nome-Solomon Area

The coast in the Nome area has developed by erosion of Pleistocene glacial and associated deposits (Hopkins et al., 1960; Nelson and Hopkins, 1972; Tagg and Greene, 1973). In the area from Safety Sound to Solomon,

Holocene barriers of sand and gravel have formed in front of the mainland (Fig. 3). The shoreface in the Nome-Solomon area slopes steeply to a depth of 12 m. Beyond the shoreface, the seafloor slopes more gently. The only Holocene deposits off Nome are gravel lag deposits and thin sand patches. Sand and gravel of presumed Holocene age occur off the Safety Sound-Solomon area, but the thickness of Holocene deposits is not known.

The mean tidal range at Nome is 0.3 m. Strong westward currents, tidal in part but reinforced by a net drift, are known to occur in northern Norton Sound (Nelson and Hopkins, 1972; Coachman et al., 1975). Currents associated with storm surges, which are as high as 4.75 m at the east end of Norton Sound (Sallenger et al., 1978), may be very strong. Fetches for waves are fairly long to the south and southeast and longest to the southwest.

Yukon Delta

The Yukon River debouches into the northern Bering Sea and forms a large arcuate delta complex in southwestern Norton Sound. The offshore part of this complex comprises three major components: (1) a sub-ice platform, (2) a delta front, and (3) a prodelta (Dupré, this volume) (Fig. 4). The sub-ice platform extends 10 to 30 km offshore as a featureless plain at water depths of 1 to 3 m. Dissecting the platform are several subaqueous distributary channels. The delta front, which is relatively steep and locally irregular, extends from the break in slope at the outer edge of the sub-ice platform to a water depth of 10 m. The prodelta slopes gently seaward from the toe of the delta front. Sediment of the delta complex is silt to fine sand.

Wave and current patterns in southwestern Norton Sound are poorly known. The major wave trains move northward from the southern Bering Sea and refract clockwise around the protruding Yukon shoals (Sallenger et al., 1978). Fetches are shorter to the north and northeast. The mean tidal range varies from 0.5 to 1.2 m around the delta margin.

Marine Climate

The coastal waters of the northeastern Bering Sea are usually free of ice from middle or late May to late October or early November. During the ice-free season the wind and wave regimens are variable; no distinctly dominant wind or wave direction is evident in data from the northeastern Bering Sea (Brower et al., 1977). The largest storms usually occur around the time of freeze-up in the fall, and the winds and waves during these storms are mostly from the east, northeast, or north. These storms may or may not affect the coastal waters, depending on the fetch in the direction of the storm winds and the timing of the storm with respect to freeze-up. In general, the direction of the dominant waves along a given stretch of shore is closely related to the direction of greatest fetch.

FEATURES PRODUCED BY WAVES AND CURRENTS

Areas off Southern Seward Peninsula

Features in the Port Clarence and Nome-Solomon inner shelf areas off the southern Seward Peninsula are similar, largely because of the similarly coarse sediment in the two areas. Wave- and current-produced features in these areas include sand and gravel patches and ribbons, wave ripples, and large current-produced transverse bedforms.

Patches

Irregular segregations of sand and gravel are ubiquitous in the Nome-Solomon area (Fig. 5). On sonographs, the sand patches are light toned and the gravel patches dark toned. The patches are extremely variable in width, ranging from 10 to 500 m. In the shallowest water depths studied, 4 to 8 m, the sand patches are sharply separated from gravel, which consists of cobbles and boulders. These shallow-water patches range in shape from very irregular (Fig. 5a) to roughly elongate at high angles to shore (Fig. 5b). Locally the sand patches are smoothly curved seaward-convex lobes spaced an average of 450 m apart (Fig. 6). On some of the bathymetric profiles, sand patches can be distinguished from gravel patches by differences in acoustic signature (Fig. 5c, d). The sand patches have smooth convex-up surfaces that typically rise above the intervening gravel, and with little doubt the sand forms lenses resting on a gravel substrate. Where the gravel surface is irregular, gravel ridges or mounds commonly rise above the sand lenses (Fig. 5).

In water deeper than 10 m, the patches become less distinct because patches of pebbly sand and pebble gravel commonly occur between the coarser gravel and the sand. Much of the pebbly sand and pebble gravel is visibly rippled on sonographs (Fig. 7). Many textural segregations are recognizable more by differences in ripple size and trend than by tonal differences on the sonographs (Fig. 7b).

The tendency for the patches to be elongate at high angles to shore and to have straighter boundaries at high angles to shore than at low angles represents a tendency toward ribbonlike forms. No well-developed ribbons are found in the Nome-Solomon area, however. The possible significance of the ribbonlike forms will be discussed in connection with the well-developed ribbons in the Port Clarence area. The lobate form and regular spacing of

some of the nearshore sand patches suggest an origin by stationary rip currents or edge waves.

Wave Ripples

Ripples with spacings of 0.5 to 2.0 m are commonly visible on sonographs in both the Nome-Solomon and Port Clarence areas (Fig. 7). These ripples were identified as wave generated by their symmetry as seen on the sonographs, by underwater television, and by diving. They occur wherever the sediment is moderately to well sorted and of a suitable grain size, in the very coarse sand to pebble gravel grades. Wave ripples of similar size in similarly coarse sediment are known from many areas (Trask, 1955; Vause, 1959; Newton and Werner, 1972; Channon and Hamilton, 1976). All of the large wave ripples were inactive when seen by television camera or by diving and must have formed during storms. In addition to the large inactive ripples, active ripples too small to be visible on sonographs were present in medium-grained sand.

All wave ripples in the Port Clarence inlet area trend northwest-southeast and can be explained as products of storm waves propagating northeastward out of the Bering Sea. In the Nome area, at least three sets of wave ripples can be seen at a depth of 12 m (Fig. 7d). The largest ripples (spacing 1.3 m) were formed by waves from the southwest, the middle-sized ripples (spacing 0.7 m) were formed by waves from the south, and the smallest ripples visible on the sonographs (spacing 0.4 m) were formed by waves from the south-southwest. Ripples of successively smaller size occur in successively finer sediment. Waves generated during a major storm must have formed the largest ripples in the coarsest rippled sediment. This large storm presumably formed ripples in finer sediment as well, but only the ripples in the coarsest sediment remained inactive and unmodified until the time of

observation. After the largest ripples were formed, successively smaller ripples were formed in successively finer material by what must have been successively smaller waves at successively later times.

In more detailed hydrodynamic terms, the wave ripples may be classified as vortex ripples because of their steepness (Dingler and Inman, 1977). At least the larger ripples are probably of orbital type, having a spacing similar to the orbital diameter of the waves (Clifton, 1976, Figs. 11-13). Calculations based on threshold velocities for grain movement (Rance and Warren, 1969; Komar, 1976; Dingler, 1979) and on the upper limit for the existence of orbital ripples (Mogridge and Kamphuis, 1972) suggest that the largest ripples (ripple spacing of 2.0 m in gravel having a median diameter of 2 to 8 mm at a water depth of 12 m) were formed by waves 2 to 5 m high having a period of 6 to 11 s.

Ribbons

Linear segregations or ribbons of sand and gravel are well developed at water depths of 4 to 8 m on the north side of Port Clarence, just outside and inside the inlet (Fig. 8). The ribbons are developed in three sizes of material with distinct side-scan sonar signatures similar to those in the Nome-Solomon area: unrippled cobble and coarse-pebble gravel, pebbly sand and fine-pebble gravel with wave ripples visible on sonographs, and sand with wave ripples too small to be visible on sonographs. Commonly the three materials lie next to one another in order of grain size (Fig. 8a, c). The ribbons show little regularity of spacing or width, but the average spacing is roughly estimated at 60 m. No relief is detectable on the bathymetric profiles, but underwater television suggests that the sand lies on the gravel.

Ribbons in other areas have been interpreted as longitudinal current-produced bedforms (Kenyon, 1970). The currents that produce most ribbons are tidal, though wind-driven currents have apparently produced some ribbons or similar textural bands (Stride and Chesterman, 1973; McKinney et al., 1974). For the Port Clarence area, however, a strong though not conclusive argument can be made that the ribbons are produced by wave action and are oriented parallel to the direction of wave propagation.

The evidence for a wave origin of the ribbons is in part negative. The ribbons are not parallel to the expected east-west direction of tidal or storm-surge currents through the inlet (Fig. 9). Nor are the ribbons approximately parallel to shore, as would be expected for Ekman currents driven by winds at almost any angle to shore in very shallow water (Neumann and Pierson, 1966, p. 202-203). The ribbons do not change in orientation significantly along irregularly curving isobaths on the north side of the inlet, as might be expected if the ribbons were parallel to currents that were deflected around seafloor irregularities.

Several positive kinds of evidence suggest an origin by wave action. The general northeast-southwest trend of the ribbons is parallel to the direction of greatest fetch and roughly normal to the trend of the accompanying wave ripples. Both the ribbons and the ripples curve in ways consistent with wave refraction; that is, the ribbons become more nearly perpendicular to shore as the bottom shoals and the ripples become more nearly parallel to shore.

Exactly how waves might produce ribbons is not known, though several mechanisms are conceivable. Originally irregular textural segregations produced by other causes might become streaked out by sediment transport caused either by wave-induced net water motion in the direction of wave propagation or, if net water motion is absent, by the time-velocity asymmetry

of wave orbital motion (short but strong pulses in the direction of wave propagation and longer but weaker pulses in the opposite direction). Langmuir circulation induced by waves or by wave-current interaction (Faller and Caponi, 1978) might be capable of forming linear textural segregations where no segregations had existed previously.

The hypothesis of ribbon generation by wave action is complicated by the fact that some of the ribbons in very shallow water are parallel to, and possibly bounded by, ice gouges (Fig. 8d). These ribbons may have somehow been produced by gouging. The occurrence of straight parallel ribbons through a depth range of 4 to 15 m, however, is difficult to reconcile with an origin by gouging, given the probability of ice grounding somewhere in that depth range.

An origin by wave action may explain the ribbonlike tendencies of the elongate textural segregations in the Nome-Solomon area. The poorer development of ribbonlike forms in that area than in the Port Clarence area could be explained by a greater variability of wave directions, as suggested by the greater variability in orientation of wave ripples.

Ribbons or elongate textural patches oriented at high angles to shore or normal to wave ripples have been observed elsewhere. McKinney and Pilkey (1969) observed textural bands oriented normal to large wave ripples on the Atlantic shelf of the southeastern United States. Newton et al. (1973) observed bands oriented at high angles to shore at relatively shallow depths (30-40 m) on the Atlantic shelf of northwest Africa. Swift et al. (1976) and Swift and Freeland (1978) observed textural bands oriented at high angles to shore off the northeastern United States but were not certain whether the bands were parallel to or transverse to the currents. Reimnitz et al. (1976) interpreted shore-normal rippled and unrippled bands off the west coast of

Mexico as products of rip currents. Such an interpretation is not feasible for the Port Clarence ribbons, which extend to water depths of 15 m, more than 3 km from shore. Textural bands tentatively interpreted as a product of Langmuir circulations generated by a combination of wind and waves have been observed on the San Pedro shelf off southern California (Karl, 1980).

Current-Produced Transverse Bedforms

Bedforms that can definitely be interpreted as produced by currents are not common in the Port Clarence and Nome-Solomon areas. Asymmetric sand waves having spacings of 2 to 4 m occur in the deeper parts of the inlet to Port Clarence (Fig. 9). Asymmetric transverse bedforms composed at least partly of pebble gravel occur in water depths of 12 to 15 m off Safety Sound (Fig. 10a). These bedforms are as much as 2.5 m in height, average 200 m in spacing, trend at a high angle to shore (N 12°E), and face westward.

Boulder ridges in water depths of 12 to 15 m off Nome trend at high angles to shore (trend N 33-60°E) and have relatively steep west-facing slopes (Fig. 10b). Underwater television showed that the west-facing slopes are composed of boulders and the more gentle east-facing slopes are composed of sand and relatively fine gravel.

The direction of asymmetry of the bedforms off Safety Sound is in accord with the dominance of westward currents in northern Norton Sound (Nelson and Hopkins, 1972; Coachman et al., 1975). These bedforms were probably produced by westward tidal currents reinforced by the semipermanent net westward drift, by storm-surge relaxation currents, or by a combination of these currents. The origin of the boulder ridges off Nome is not known. If they were produced by modern currents, only storm-surge relaxation currents could possibly be of adequate strength, and even these currents may not be capable of moving

boulders. An alternative explanation is that the boulder ridges were produced during the Holocene transgression at water depths shallower than present. If so, they may be similar in origin to the boulder ridges at water depths of 4 to 8 m off Nome (Fig. 5c) except that sand and finer gravel have been banked up against their east sides. Even assuming an origin in shallower water, it remains unknown whether the ridgelike form of the boulder masses was produced by wave and current action or resulted from the original distribution of boulders in the glacial or glaciofluvial material eroded during the Holocene transgression.

Areas Off Yukon Delta

Rolling and hummocky topography

Irregular rolling and hummocky topography characterizes the seaward edge of the sub-ice platform and the upper part of the delta front (Fig. 4b). North of the delta, the topography consists of east-west-trending sediment shoals that form a transition zone between the sub-ice platform and the delta front. Water depths over the shoal crests are 1 to 2 m and over the intervening troughs are 4 to 6 m. The shoal crests are 3 to 6 km apart. Seaward of the shoals, on the upper part of the delta front, the surface is undulatory or rolling. Relief is as much as 1 m, and the crests are 100 to 300 m apart. Below a water depth of about 5 m, the undulations disappear and the delta front slopes smoothly down to the nearly flat prodelta.

The morphologic character of the offshore part of the delta changes from the northern to the western side. The sub-ice platform on the western side is narrower than the platform on the northern side, and the slope of the delta front and prodelta on the western side is twice as steep as the slope on the northern side. The western delta front is irregular and hummocky but does not

have the shoals or rolling topography characteristic of the northern delta front. Locally, the western delta front has seaward-facing steps, which may be slump scarps, with as much as 0.5 m relief. Possible slump features are shown in Figure 11a. Current-scour depressions and erosion into underlying competent beds are also seen on the lower part of the western delta front or upper prodelta (Fig. 11b). Two major and numerous minor subaqueous distributary channels cut through the sub-ice platform and delta front. In contrast, the northern parts of the sub-ice platform and delta front have no channels. Scour in the channels (Fig. 11c) is proof that the channels are modern and active.

The differences in topographic features between the northern and western sides of the offshore delta complex suggest different processes or differences in degree and intensity of the processes at work. Unlike the northern side, which faces Norton Sound, the western side faces the open Bering Sea and is strongly affected by the north-flowing Alaskan Coastal Water Current. The northern delta front and sub-ice platform are in a destructive or erosive phase characterized by wave and current reworking of sediment into features such as shoals, ripples, and rolling topography. The western delta front and sub-ice platform are in a constructive phase characterized by rapid sedimentation and associated processes such as channeling, current scour, and slumping.

Sand waves and ripples

Sand waves and ripples are found on the upper parts of the delta front and on the flanks and bottoms of the major subaqueous distributary channels on the western side of the delta (Fig. 4b). Wavy bedforms on the upper part of the delta front have heights of 10 to 50 cm and wavelengths of 10 to 200 m.

These bedforms progressively increase in height toward the tops of the transition-zone shoals. The bedform crests trend generally east-west, subparalleling the trend of the shoals.

Asymmetric ripples on the flanks of subaqueous distributary channels have wavelengths of 3 to 5 m. Sand waves in the channels are strongly asymmetrical seaward-facing bedforms with wavelengths ranging from 25 to 200 m and heights of 0.5 to 1 m (Fig. 10c, d).

The sand waves and ripples are interpreted to be in equilibrium with the present wave and current regimes. Bedforms on the delta front are caused by waves and/or currents impacting the shoals of the delta front. Ripples on the flanks of subaqueous distributary channels are possibly caused by overbank flow during times of high river discharge. Sand waves on channel bottoms are caused by high flow velocities during times of high river discharge.

Ribbons

Features interpreted as sediment ribbons (Fig. 11d) are visible on sonographs from an area north of the Yukon delta, on the upper part of the delta front (Fig. 4b). The ribbons occur on the crests, flanks, and troughs of the broadly rolling ridges characteristic of the upper part of the delta front. The ribbons trend N 60-90° W, generally parallel to the trend of the rolling topography. Spacing between ribbons varies from 10 to 150 m. The wider spaced ribbons tend to occur more commonly in the trough areas. Associated with the ribbons are wavy bed-relief features, visible on depth profiles, that have wavelengths similar to ribbon spacing, but the lack of a one-to-one correspondence in location or spacing between these two features obscures their relations. As ribbon and interribbon areas were not sampled, the grain size of these features is not known. The character of the ribbons

on the sonographs, however, requires some acoustic difference (probably grain size) between ribbon and interribbon areas. The lack of correspondence between relief features and ribbons eliminates the possibility that the ribbon features are simply bedform shadows.

The ribbons occur in shallow water on the south side of the entrance to Norton Sound. This area is highly susceptible to southern Bering Sea storm waves, storm-surge run-off, the Alaskan Coastal Water Current, and tidal currents that would pass through the area either in a westward or an eastward direction. The ribbons here are subparallel to known or probable current directions and are possibly longitudinal features produced by one or more of these currents.

FEATURES PRODUCED BY ICE

Furrows produced by gouging of the seafloor are found in parts of the study area (Fig. 12). Three types of gouging occur: two are formed naturally by ice plowing the bottom sediment and one is formed artificially by anchors, anchor chains, or cables dragging the bottom. Single ice gouges are produced by a single ice keel plowing the bottom sediment. These gouges range in width from 5 to 20 m and are as much as one meter deep, although most are less than one-half meter deep (Fig. 12a, b). Multiple gouges are produced by multikeel ice plowing or "raking" the bottom sediment, creating numerous parallel furrows (Fig. 12c). Zones of raking are as much as 100 m wide. Artificial gouges are straighter and narrower (2 m or less) than most ice gouges (Fig. 12d).

Both single and multiple gouges are related to ice dynamics in Norton Sound. Landsat imagery has been used to study ice movement in northeastern Bering Sea (Dupré, 1978). Pack ice usually moves in a southwestward or

westward direction, pushed by the prevailing northeasterly winds. When this pack ice collides with other floes or with stationary shorefast ice, ice keels are forced deeper into the water. These keels keep moving with the ice pack but extend down far enough to plow the bottom. Gouges in Norton Sound generally trend subparallel to the shore (Fig. 4b), in agreement with ice movement directions as determined by satellite imagery. Ice-gouge trends in and around Port Clarence are more randomly oriented (Fig. 9), suggesting more complex ice movement in this embayed area.

Gouge furrows are not a common feature in the Nome/Safety Sound area because of ice movement patterns and because of current and wave action. Ice generally moves in a southwestward direction, making northern Norton Sound an area of ice divergence, not conducive to intense or dense gouging. Southwestern Norton Sound (Yukon prodelta area) is an area of ice convergence and consequently of high gouge density. Gouges are probably ephemeral features in this area because storm waves and tidal currents are capable of eroding the gouges or burying them by sediment.

Artificial gouges (Fig. 12d) have been found off Nome and off Safety Sound. They differ from ice gouges in that they are narrower, usually trend at a high angle to shore, and are found only in areas that have high barge traffic. Potential gouging tools are: (1) anchors and anchor chains that drag the bottom during deployment or recovery, (2) long tow cables between barges and tugboat, which tend to drag bottom even while underway, and (3) stabilization cables that trail from barge sterns.

CONCLUSIONS

A rich assemblage of wave- and current-produced features visible on sonographs is present in shallow water close to the southern shore of Seward Peninsula. The richness of the assemblage is dependent on the textural variability and general coarseness of the sediment. Few features were seen on sonographs from the fine sand and silt areas of the Yukon delta except in channels subject to river discharge.

In general, features known or thought to be produced by waves are more common than current-formed features. Where current-formed features do occur, they tend to be restricted to deeper parts of the shallow depth zone investigated here. Although the current-formed features are not common, some of them imply considerable sediment transport by strong currents. In the Nome-Solomon area, the current-formed features indicate westward sediment transport, opposite from the wave-induced net sediment transport along the beaches.

The more problematical features described here clearly need to be investigated further. Among such features are the lobate sand patches off Safety Sound, the ribbons interpreted to be produced by wave action in the Port Clarence area, the boulder ridges off Nome and Safety Sound, and the ribbons on the Yukon Delta.

ACKNOWLEDGMENTS

This study was supported jointly by the U.S. Geological Survey and the Bureau of Land Management through an interagency agreement with the National Oceanic and Atmospheric Administration, under which a multiyear program responding to needs of petroleum development of the Alaskan continental shelf is managed by the Outer Continental Shelf Environmental Assessment Program (OCSEAP) Office.

We wish to thank Tom Barnett, Captain of the R/V KARLUK, Bob Novak, Harry Hill, Jim Howard, Matt Larsen, Mark Holmes, and Dave McCulloch for their assistance during the cruises. We also thank Bill Dillon and Herman Karl for their reviews of the manuscript.

REFERENCES

- Black, R. F. (1958) Permafrost, water-supply, and engineering geology of Point Spencer Spit, Seward Peninsula, Alaska. *Arctic*, 11, 102-116.
- Brower, W. A., Jr., Diaz, H. F., Prechtel, A. S., Searby, H. W. & Wise, J. L. (1977) Climatic atlas of the outer continental shelf waters and coastal regions of Alaska. Vol. II, Bering Sea. Arctic Environ. Inf. and Data Center, Anchorage, Alaska, and Natl. Climatic Center, Asheville, N. C.
- Cacchione, D. A., Drake, D. E. & Wiberg, Patricia (this volume) Bottom shear stress generated by waves and currents in the northern Bering Sea. Spec. Pub. Internat. Assoc. Sedimentologists.
- Channon, R. D. & Hamilton, D. (1976) Wave and tidal current sorting of shelf sediments southwest of England. *Sedimentology*, 23, 17-42.
- Clifton, H. E. (1976) Wave-formed sedimentary structures - a conceptual model. In (Ed. by R. A. Davis, Jr. & R. L. Ethington) Beach and nearshore sedimentation. Spec. Pap. Soc. econ. Paleont. Miner. 24, 126-148.
- Coachman, L. K., Aagaard, Knut & Tripp, R. B. (1975) Bering Strait: the regional physical oceanography. Univ. Washington Press, Seattle.
- Dingler, J. R. (1979) The threshold of grain motion under oscillatory flow in a laboratory wave channel. *J. sedim. Petrol.* 49, 287-294.
- Dingler, J. R. & Inman, D. L. (1977) Wave-formed ripples in nearshore sands. Conf. Coastal Engring., 15th, Proc. 2109-2125.
- Drake, D. E., Cacchione, D. A., Muench, R. D. & Nelson, C. H. (in press) Sediment transport in Norton Sound, Alaska. *Mar. Geol.*

- Dupré, W. R. (1978) Yukon delta coastal processes study, in Environmental assessment of the Alaskan continental shelf, Annual reports of principal investigators for the year ending March 1978. Vol. XI, Hazards. Natl. Oceanic and Atmospheric Admin. and Bur. Land Management, 384-446.
- Dupré, W. R. (this volume) Seasonal variations in deltaic sedimentation on a high-latitude epicontinental shelf. Spec. Pub. Internat. Assoc. Sedimentologists.
- Faller, A. J. & Caponi, E. A. (1978) Laboratory studies of wind-driven Langmuir circulations. Jour. Geophys. Res. 83, 3617-3633.
- Field, M. E., Nelson, Hans, Cacchione, D. A. & Drake, D. E. (1977) Dynamics of bedforms of an epicontinental shelf: northern Bering Sea (abs.). Am. geophys. Union Trans. (EOS), 58, 1162.
- Hopkins, D. M., McNeil, F. S. & Leopold, E. B. (1960) The coastal plain of Nome, Alaska. Internat. geol. Cong., XXI Sess., 4, 46-57.
- Hunter, R. E., Sallenger, A. H. & Dupré, W. R. (1979) Maps showing directions of longshore sediment transport along the Alaskan Bering Sea coast. Misc. Field Studies Map U. S. geol. Surv. MF-1049.
- Karl, H. A. (1980) Speculations on processes responsible for mesoscale current lineations on the continental shelf, Southern California. Mar. Geol. 34, M9-M18.
- Kenyon, N. H. (1970) Sand ribbons of European tidal seas. Mar. Geol. 9, 25-39.
- Komar, P. D. (1976) Beach processes and sedimentation. Prentice-Hall, Englewood Cliffs, N. J.
- Larsen, M. C., Nelson, Hans & Thor, D. R. (1980) Geologic implications and potential hazards of scour depressions on Bering shelf, Alaska. Environmental Geol. 3, 39-47.

- MacIntyre, I. G. & Pilkey, O. H. (1969) Preliminary comments on linear sand-surface features, Onslow Bay, North Carolina continental shelf: problems in making detailed sea-floor observations. *Maritime Sediments*, 5, 26-29.
- McKinney, T. F., Stubblefield, W. L. & Swift, D. J. P. (1974) Large-scale current lineations on the central New Jersey shelf: investigations by side-scan sonar. *Mar. Geol.* 17, 79-102.
- McManus, D. A., Kolla, Venkatarathnam, Hopkins, D. M. & Nelson, C. H. (1977) Distribution of bottom sediments on the continental shelf, northern Bering Sea. *Prof. Pap. U. S. geol. Surv.* 759-C.
- Mogridge, G. R. & Kamphuis, J. W. (1972) Experiments on bed form generation by wave action. *Conf. Coastal Engring., 13th, Proc., 2*, 1123-1142.
- Moore, J. R. & Welkie, C. J. (1976) Metal-bearing sediments of economic interest, coastal Bering Sea. *Alaska geol. Soc. Symposium on recent and ancient sedimentary environments of Alaska, Proc.* K1-K17.
- Nelson, C. H., Cacchione, D. A., Field, M. A., Drake, D. E. & Nilsen, T. H. (1977) Complex ridge and trough topography on a shallow current-dominated shelf, northwest Alaska (abs.). *Bull. Am. Assoc. Petrol. Geol.* 61, 817.
- Nelson, C. H. & Hopkins, D. M. (1972) Sedimentary processes and distribution of particulate gold in the northern Bering Sea. *Prof. Pap. U. S. geol. Surv.* 689.
- Neumann, Gerhard & Pierson, W. T., Jr. (1966) Principles of physical oceanography. Prentice-Hall, Englewood Cliffs, N. J.
- Newton, R. S., Seibold, E. & Werner, F. (1973) Facies distribution patterns on the Spanish Sahara continental shelf mapped with side-scan sonar. "Meteor" *Forsch-Ergebnisse, Reihe C.*, 15, 55-77.
- Newton, R. S. & Werner, Friedrich (1972) Transitional-size ripple marks in Kiel Bay (Baltic Sea). *Meyniana*, 22, 89-94.

- Rance, P. J. & Warren, N. F. (1969) The threshold of movement of coarse material in oscillatory flow. Conf. Coastal Engring., 11th, Proc. 1, 487-491.
- Reimnitz, Erk, Toimil, L. J., Shepard, F. P. & Gutierrez-Estrada, Mario (1976) Possible rip-current origin for bottom ripple zones to 30 m depth. Geology, 4, 345-400.
- Sallenger, A. H., Jr., Dingler, J. R. & Hunter, R. E. (1978) Coastal processes and morphology of the Bering Sea coast of Alaska, in Environmental assessment of the Alaskan continental shelf, Annual reports of principal investigators for the year ending March 1978. Vol. XII. Hazards. Natl. Oceanic and Atmospheric Admin. and Bur. Land Management, 451-502.
- Stride, A. H. & Chesterman, W. D. (1973) Sedimentation by non-tidal currents around northern Denmark. Mar. Geol., 15, M53-M58.
- Swift, D.J.P., Freeland, G. L., Gadd, P. E., Han, G., Lavelle, J. W. & Stubblefield, W. L. (1976) Morphologic evolution and coastal sand transport, New York-New Jersey shelf. In Middle Atlantic Continental Shelf and the New York Bight (Ed. by M. G. Gross). Am. Soc. Limnol. Oceanog. Special Symposia, 2, 69-89.
- Swift, D. J. P. & Freeland, G. L. (1978) Current lineations and sand waves on the inner shelf, Middle Atlantic Bight of North America. J. sedim. Petrol. 48, 1257-1266.
- Tagg, A. R. & Greene, H. G. (1973) High-resolution seismic survey of an offshore area near Nome, Alaska. Prof. Pap. U. S. Geol. Survey 759-A.
- Trask, P. D. (1955) Movement of sand around southern California promontories. U. S. Corps Engrs. Beach Erosion Board Tech. Memo. 76.
- Vause, J. E. (1959) Underwater geology and analysis of recent sediments off the northwest Florida coast. J. sedim. Petrol. 29, 555-563.

FIG. 1 -- Index map showing areas studied in the northeastern Bering Sea.

FIG. 2 -- Map showing tracklines and locations of illustrated features in the Port Clarence area.

FIG. 3 -- Map showing tracklines and locations of illustrated features in the Nome-Solomon area.

FIG. 4 -- a. Map of tracklines in Yukon delta area.

b. Map of morphologic features, and of features shown on sonographs in Yukon delta area.

FIG. 5 -- Irregular to elongate sand and gravel patches in the Nome-Solomon area. Distinctive points allowing comparison of a sonograph and its accompanying bathymetric profile are labelled x and y.

a. Sonograph of irregular patches.

b. Sonograph of elongate patches.

c. Bathymetric profile of area shown in a.

d. Bathymetric profile of area shown in b.

FIG. 6 -- Sonograph of cusped sand and gravel patches off Safety Sound.

FIG. 7 -- Sonographs of wave ripples and associated features.

a. Sand (light-toned), gravel (dark-toned), and rippled fine gravel patches off Nome.

b. Patches off Nome distinguished by differences in ripple size and trend.

c. Sand, gravel, and rippled fine gravel patches in Port Clarence area.

d. Sand and rippled fine gravel patches off Nome. Note: the three areas distinguished by differences in ripple size and trend.

- a. Sand (light-toned), gravel (dark-toned), and rippled fine gravel ribbons.
- b. Sand and rippled fine gravel ribbons.
- c. Elongate patches of sand surrounded by gravel, with narrow transitional zones of rippled fine gravel.
- d. Sand and gravel ribbons oriented parallel to ice gauge (lower right); note gauge-like features at boundaries between sand and gravel.

FIG. 9 -- Map of features shown on sonographs in vicinity of Port Clarence entrance.

Fig. 10 -- Bathymetric profiles of sound waves and similar features.

- a. Large transverse bedforms composed partly of gravel, off Safety Sound.
- b. Somewhat asymmetric ridges whose steep west faces are of boulder gravel, off Nome.
- c. Large sand waves in a channel that crosses the sub-ice platform, Yukon delta.
- d. Small sand waves in a channel that crosses the sub-ice platform, Yukon delta.

FIG. 11 -- Features shown on sonographs in Yukon delta area.

- a. Probable slump features.
- b. Current-scour depressions and ice gouges.
- c. Scour features in a channel that crosses the sub-ice platform.
- d. Ribbon-like features.

FIG. 12 -- Sonographs of ice gouges and similar features.

- a. Solitary gouge in the Port Clarence area.
- b. Solitary gouges in the Port Clarence area.
- c. Pressure-ridge raking off Safety Sound.
- d. Artificial gouges off Nome; one is marked by arrows.

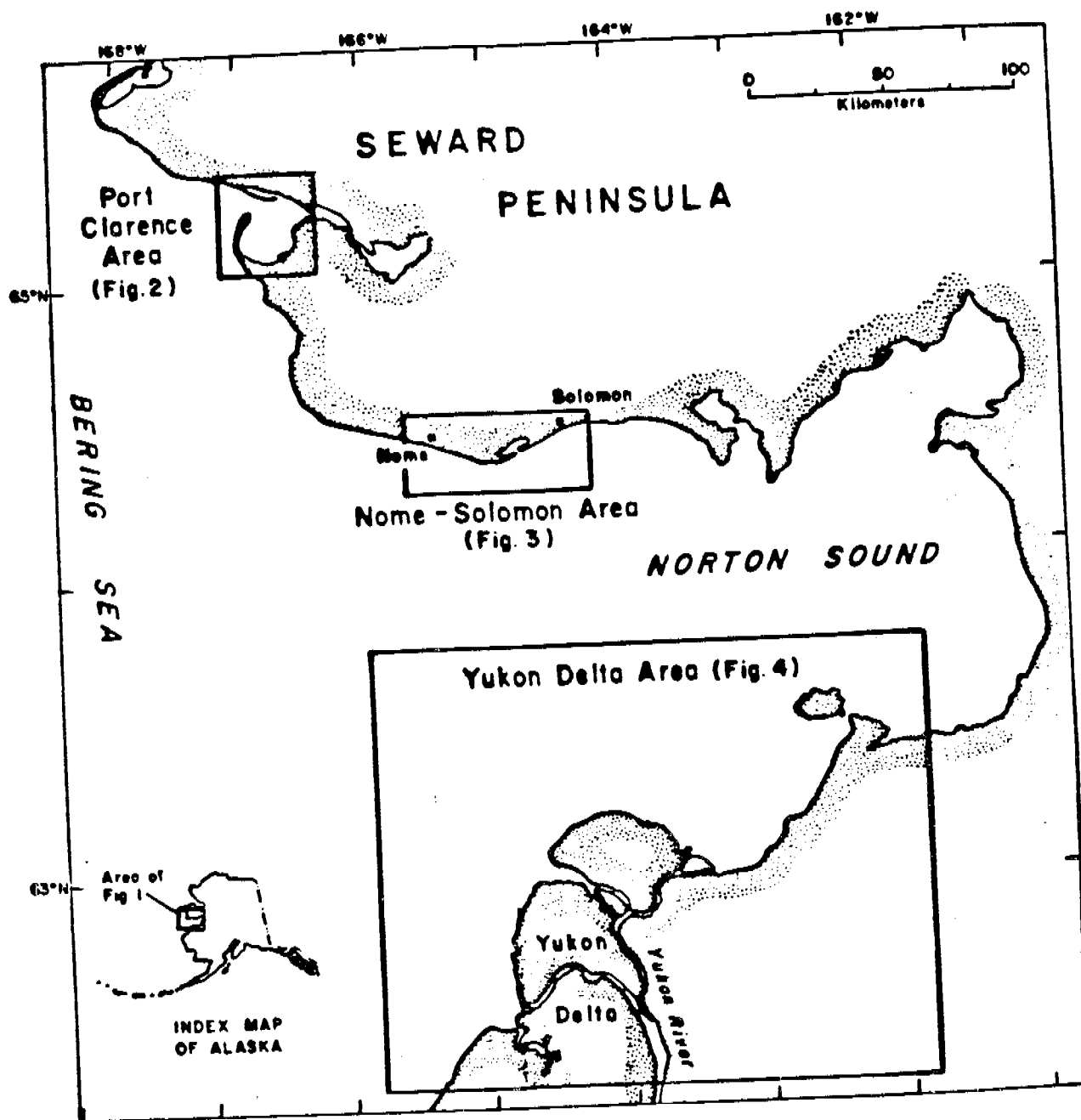


Fig. 1 - Index map showing areas studied in the northeastern Bering Sea.

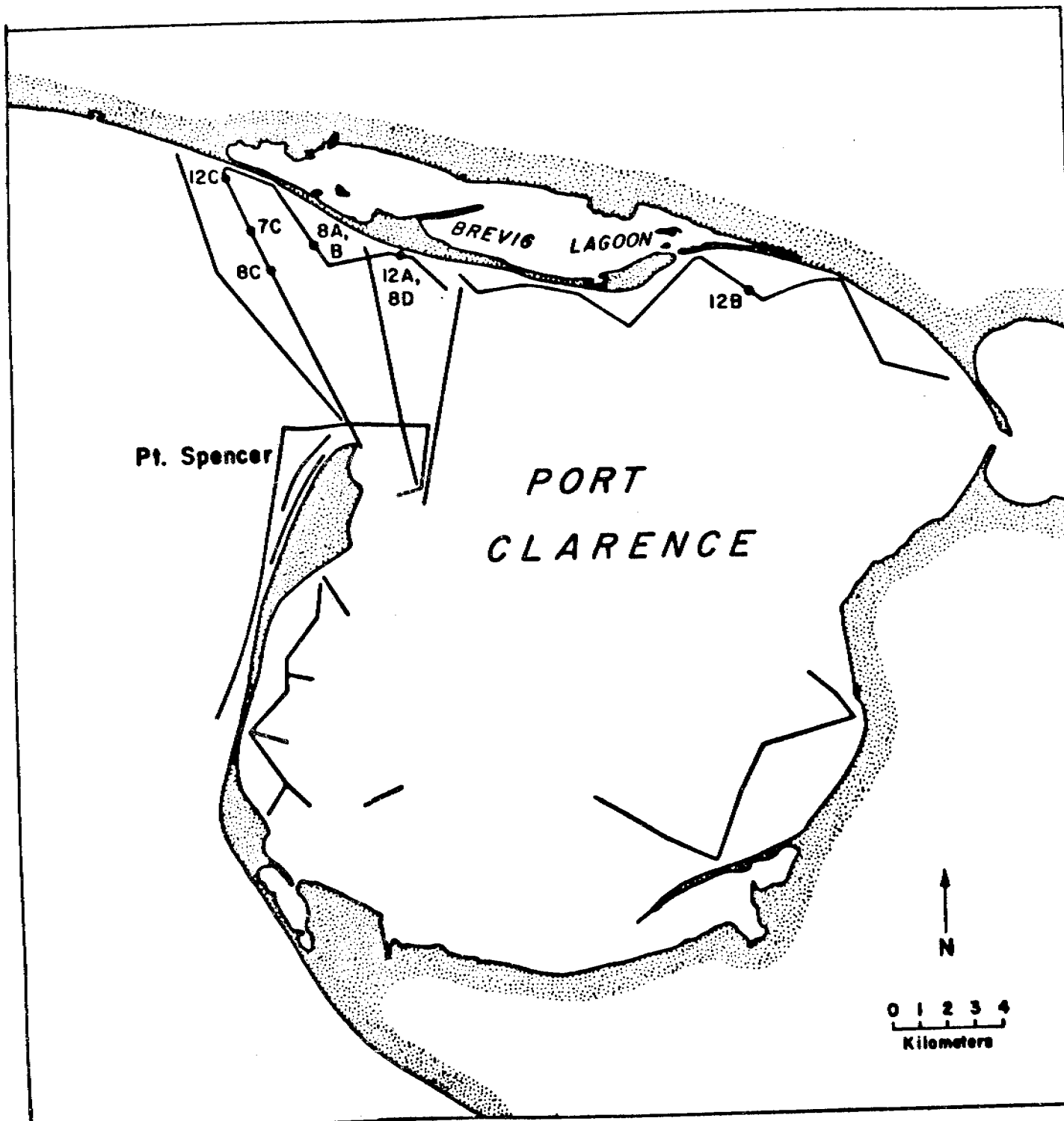


Fig. 2 - Map showing tracklines and locations of illustrated features in the Port Clarence area.

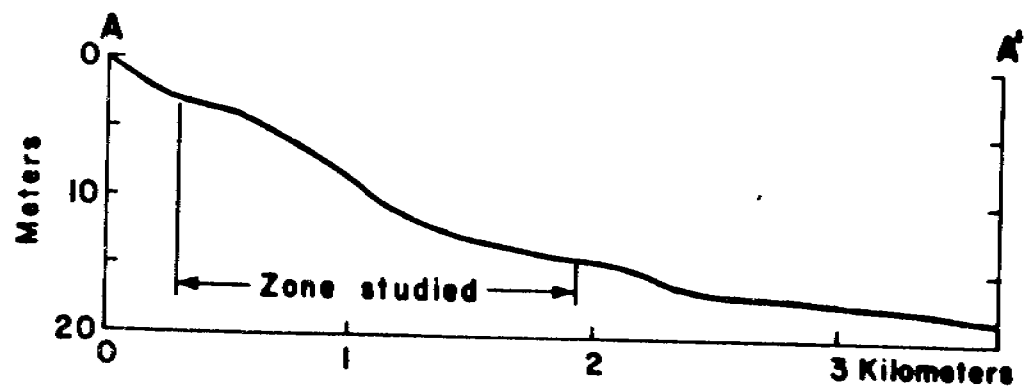
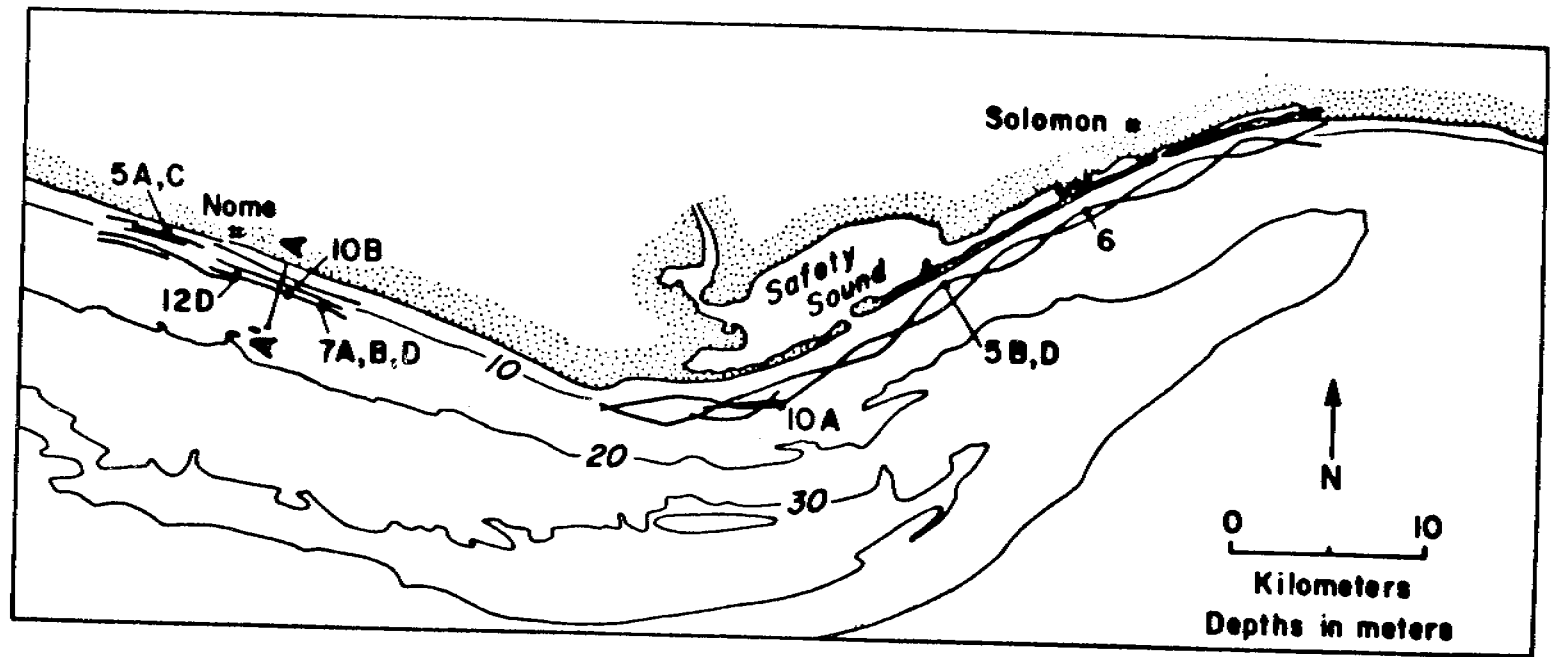


Fig. 3 - Map showing tracklines and locations for illustrated features in the Nome-Solomon area.

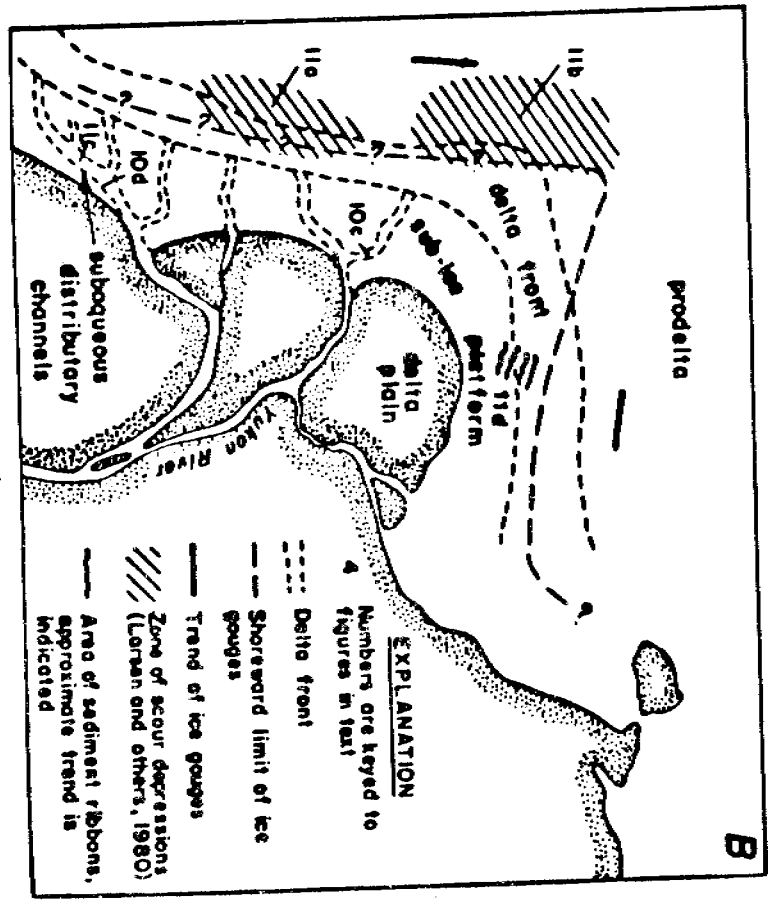
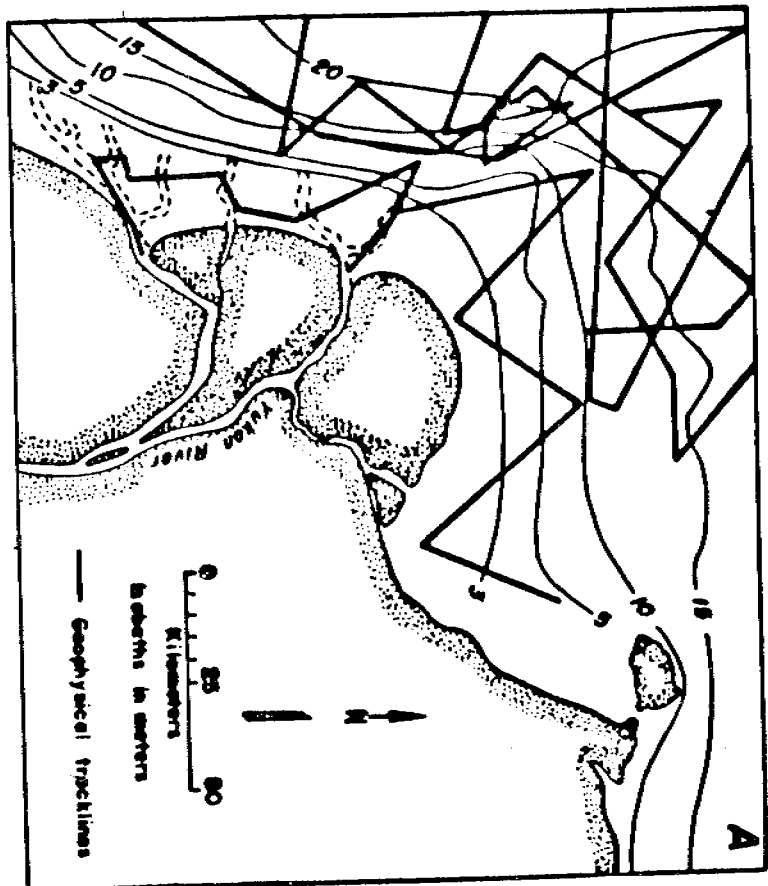


Fig. 4 - a. Map of tracklines in Yukon delta area.
 b. Map of morphologic features, and of features shown on sonographs in Yukon delta area.

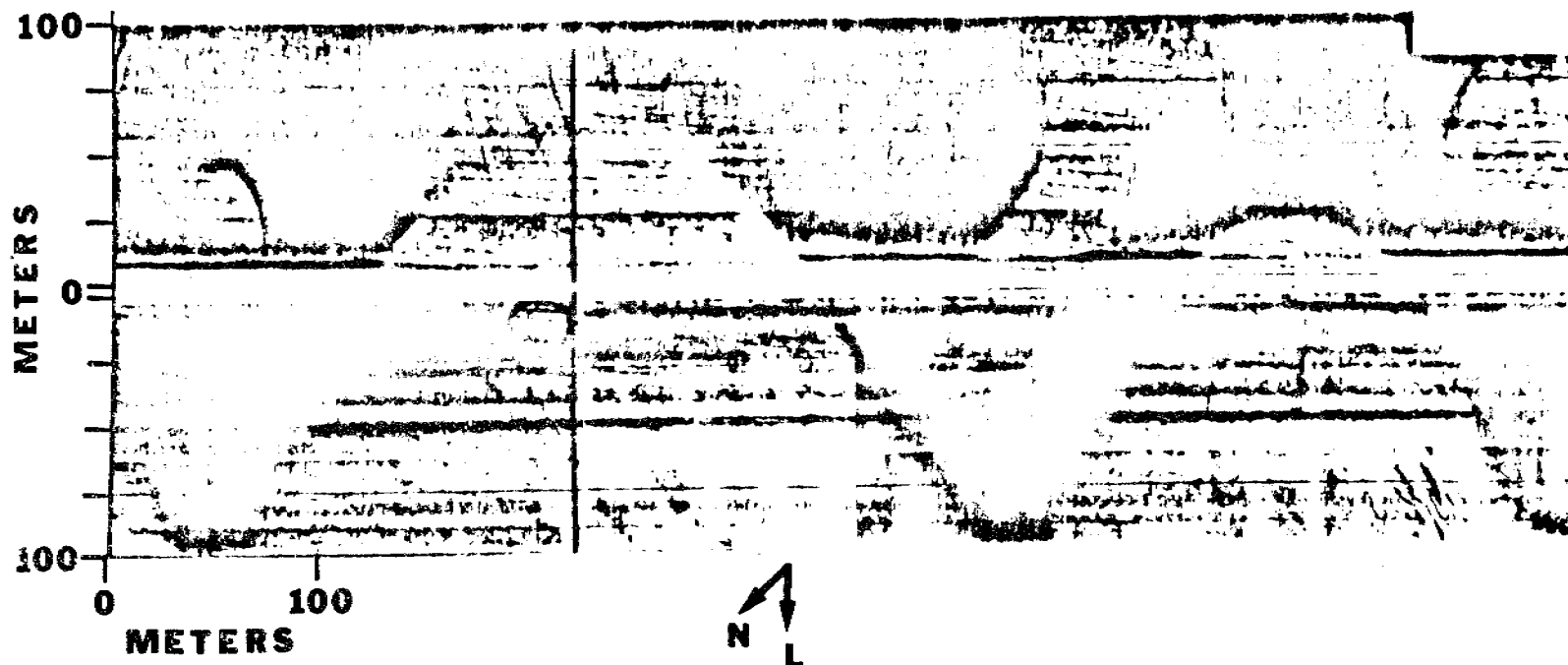


Fig. 5 - Not included for publication.

Fig. 6 - Sonograph of cusped sand and gravel patches off Safety Sound.

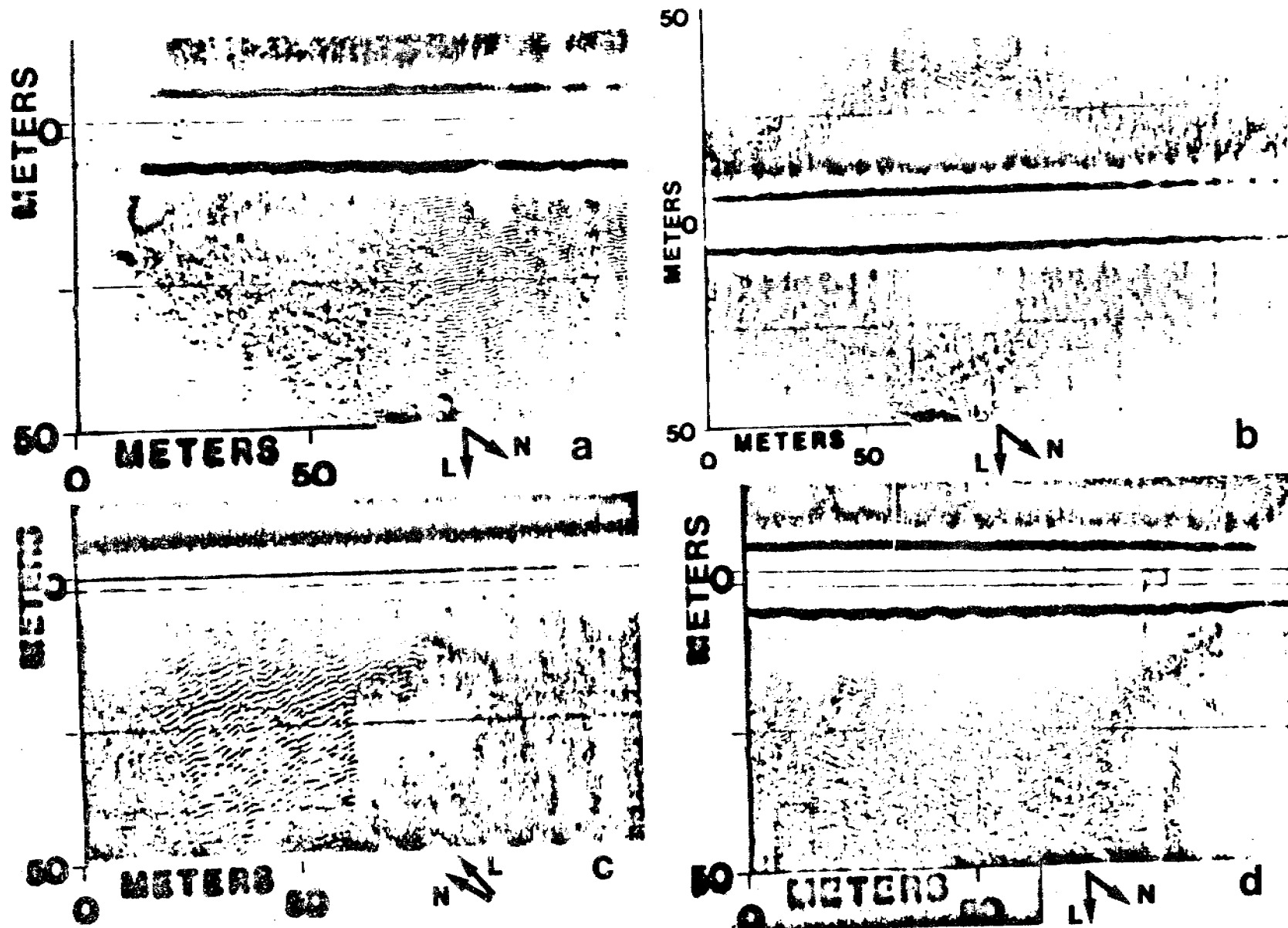


Fig. 7 - Sonographs of wave ripples and associated features.

- a. Sand (light-toned), gravel (dark-toned), and rippled fine gravel patches off Nome.
- b. Patches off Nome distinguished by differences in ripple size and trend.
- c. Sand, gravel, and rippled fine gravel patches in Port Clarence.
- d. Sand and rippled fine gravel patches off Nome. Note: The three areas distinguished by differences in ripple size and trend.

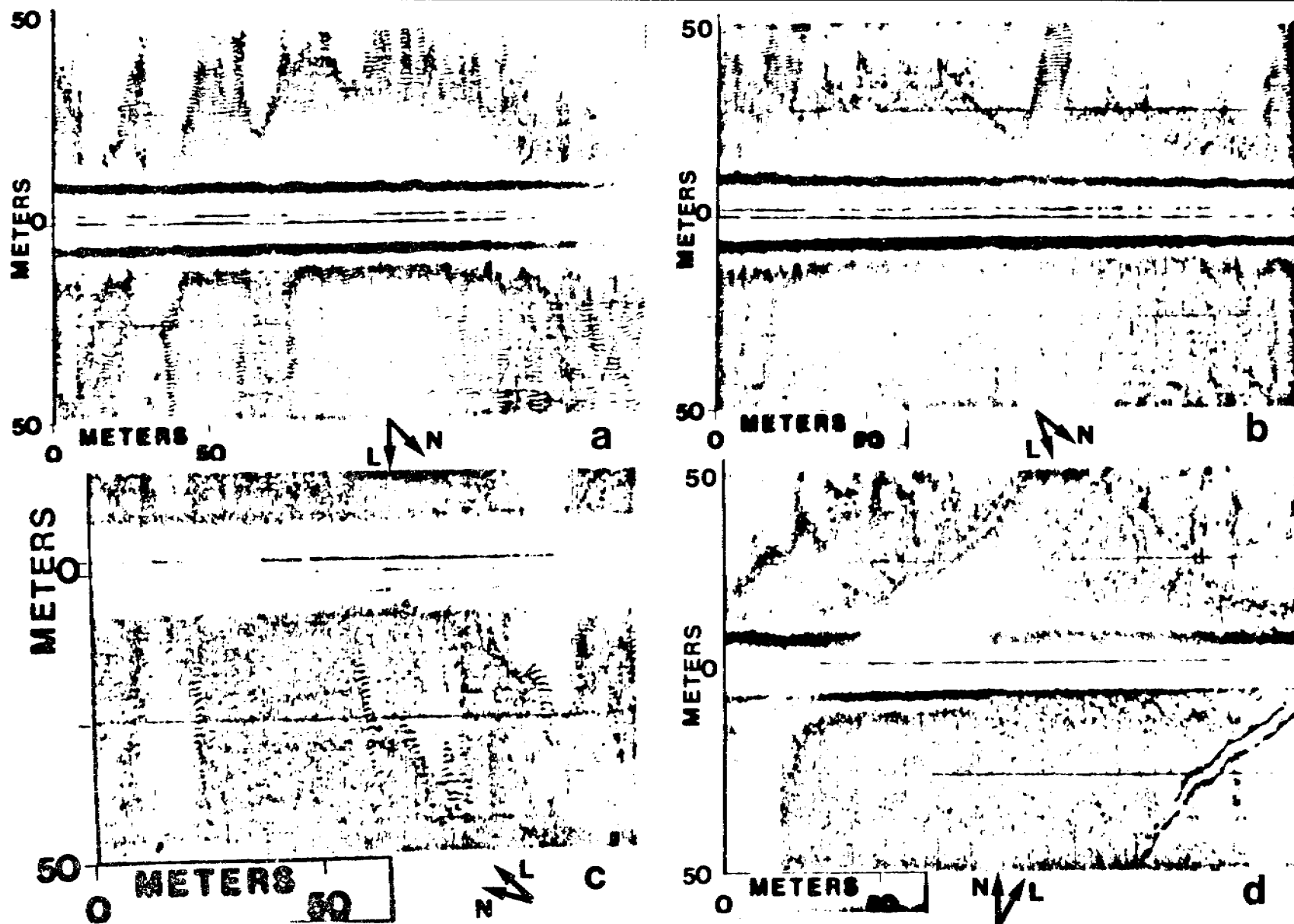


Fig. 8 - Sonographs of ribbons in the Port Clanence area.

- a. Sand (light-toned), gravel (dark-toned), and rippled fine gravel ribbons.
- b. Sand and rippled fine gravel ribbons.
- c. Elongate patches of sand surrounded by gravel, with narrow transitional zones of rippled fine gravel.
- d. Sand and gravel ribbons oriented parallel to ice guage (lower right); note guage-like features at boundaries between sand and gravel.

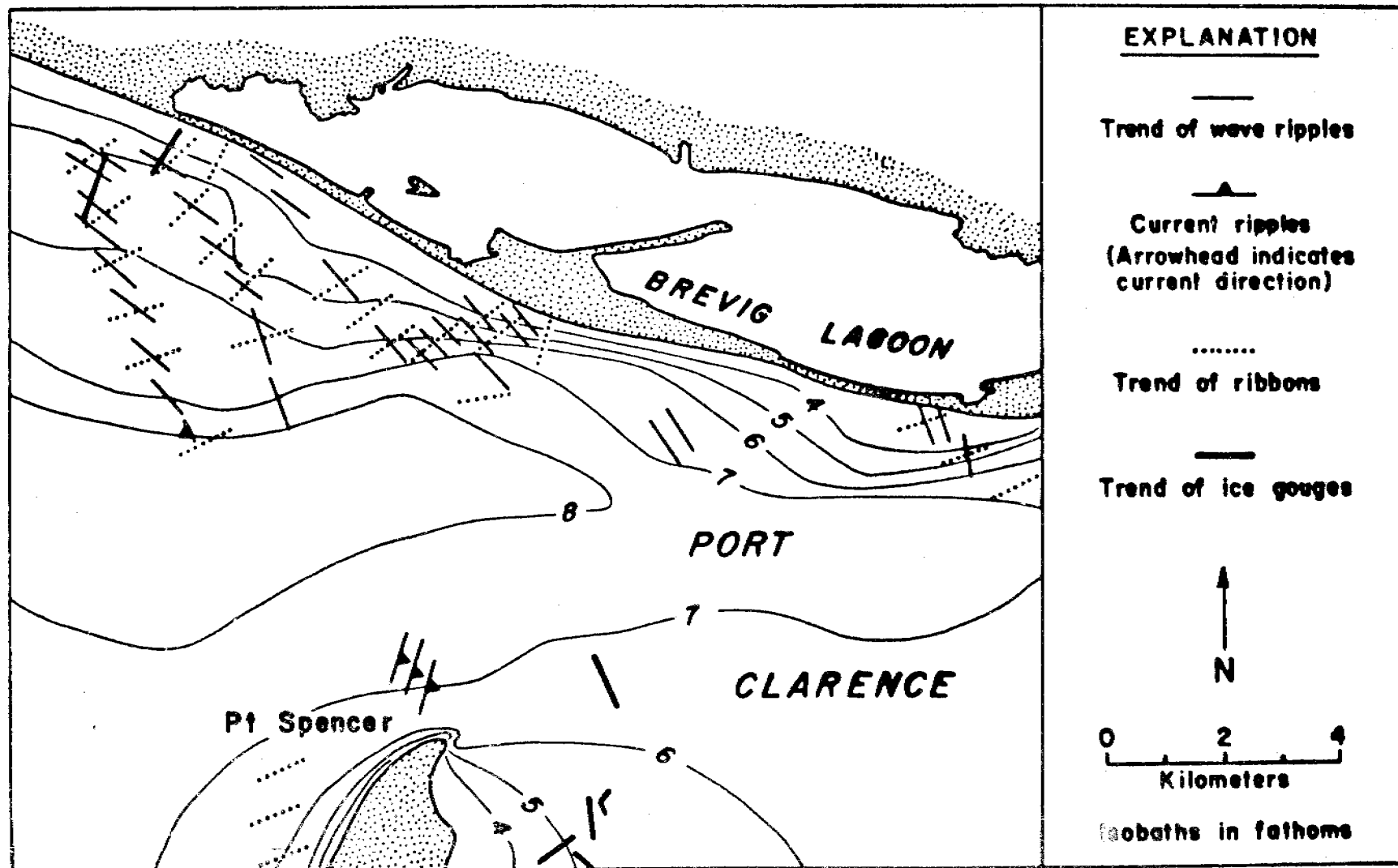


Fig. 9 - Map of features shown on sonographs in vicinity of Port Clarence entrance.

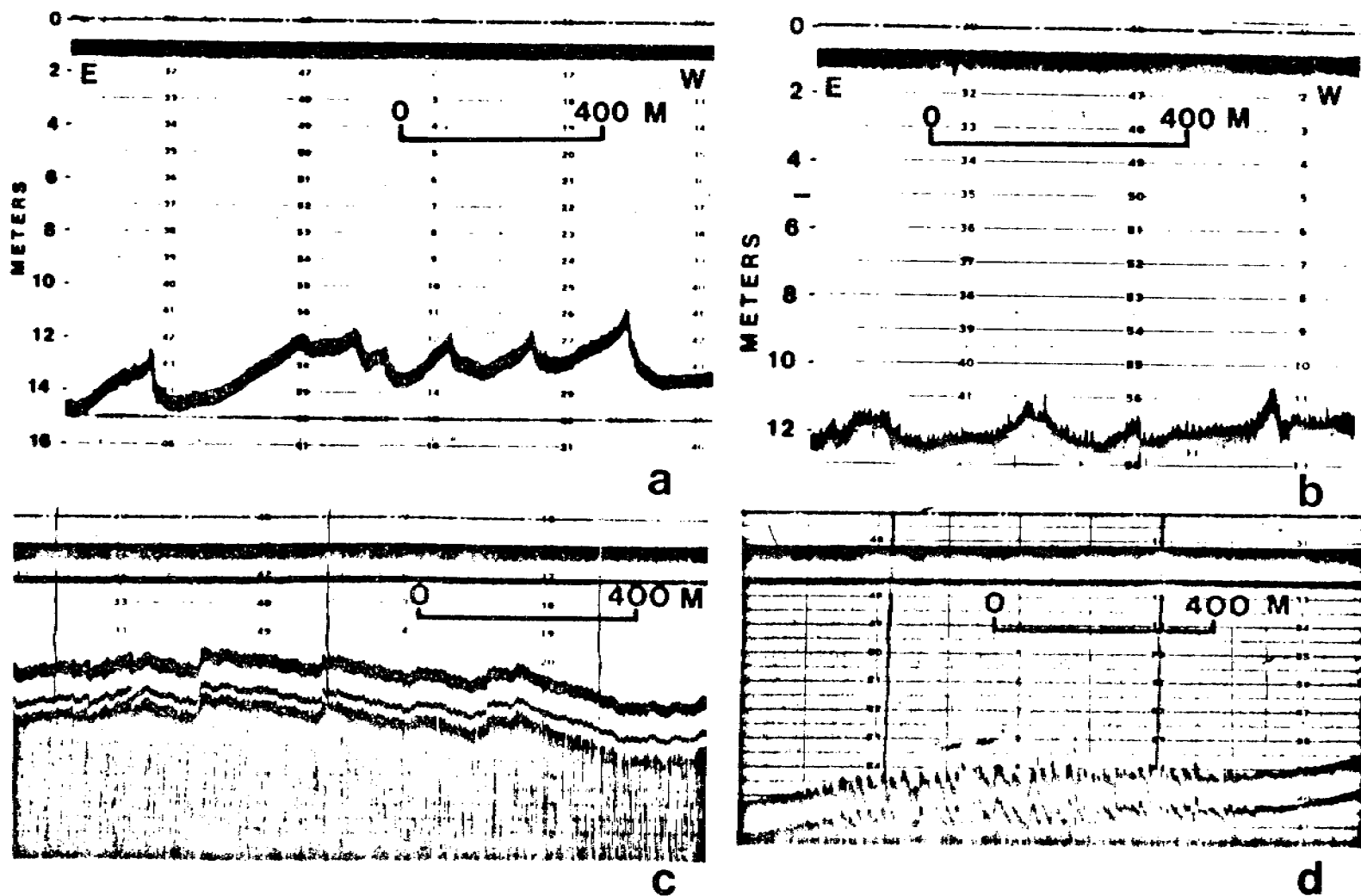


Fig. 10 - Bathymetric profiles of sound waves and similar features.

- Large transverse bedforms compared partly of gravel, off Safety Sound.
- Somewhat asymmetric ridges whose steep west faces are of boulder gravel, off Nome.
- Large sand waves in a channel that crosses the sub-ice platform, Yukon delta.
- Small sand waves in a channel that crosses the sub-ice platform, Yukon delta.

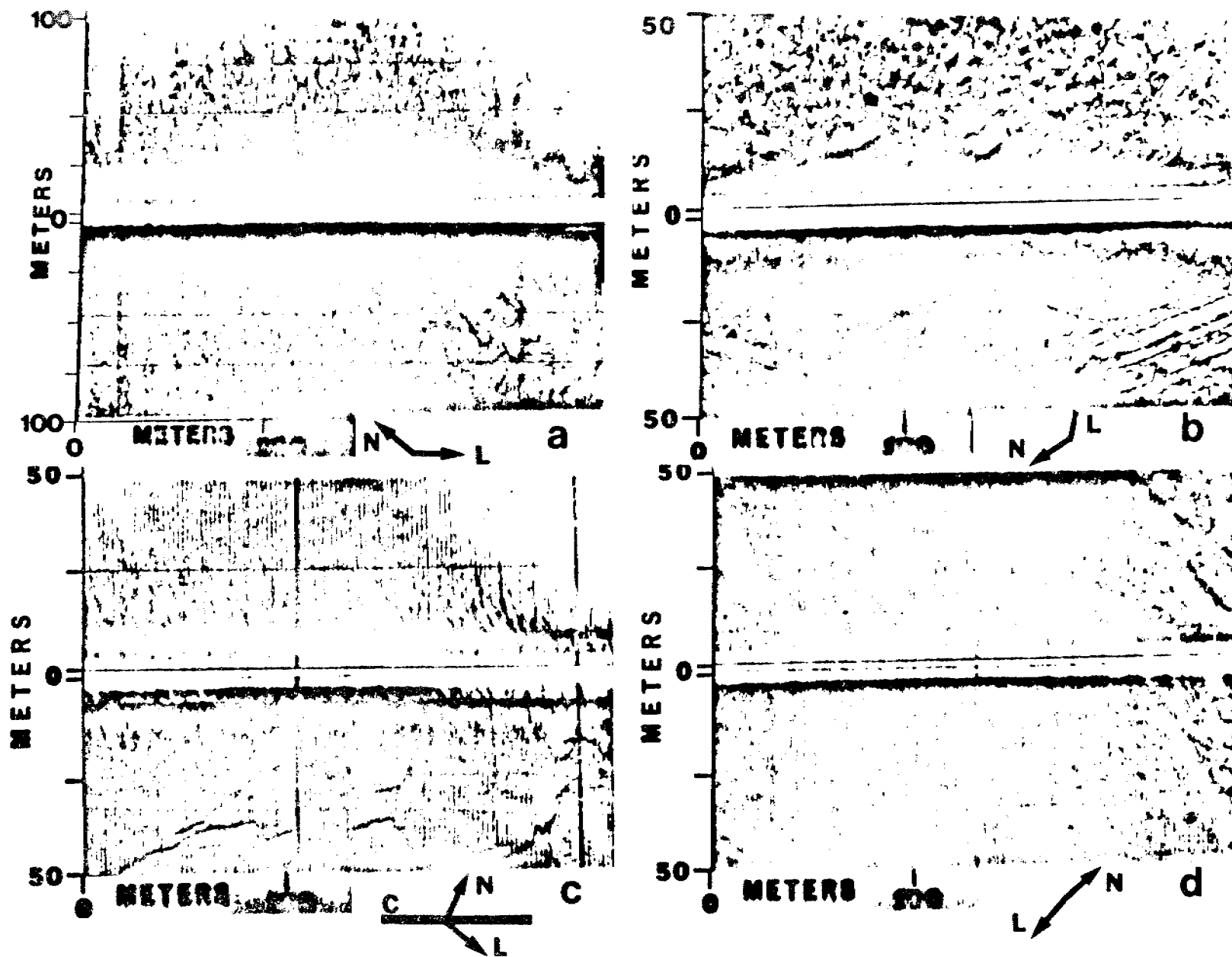


Fig. 11 - Features shown on sonographs in Yukon delta area.

- a. Probable slump features.
- b. Current-scour depressions and ice gouges.
- c. Scour features in a channel that crosses the sub-ice platform.
- d. Ribbon-like features.

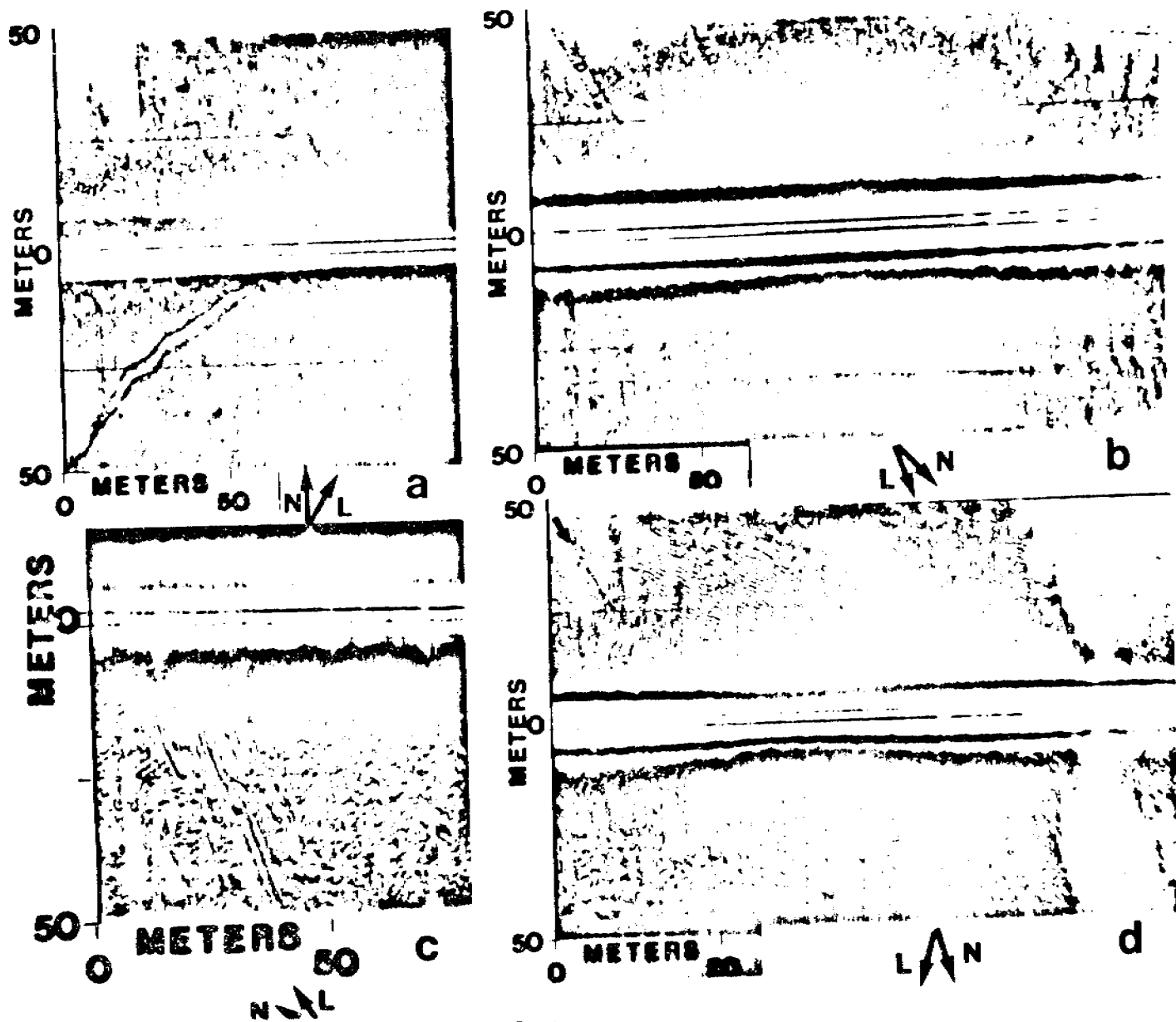


Fig. 12 - Sonographs of ice gouges and similar features.
 a. Solitary gouge in the Port Clarence area.
 b. Solitary gouges in the Port Clarence area.
 c. Pressure-ridge raking off Safety Sound.
 d. Artificial gouges off Nome; one is marked by arrows.

Graded Storm Sand Layers Offshore from the Yukon Delta, Alaska

C. Hans Nelson

Introduction

The northern Bering Sea has a history of severe storm surges. The most recent, and perhaps the worst in historical times, occurred in November, 1974 (Fathauer, 1975). Evidence of storm surge events is exhibited in sea-floor stratigraphy as well as shoreline flooding and indicates that significant widespread changes in sea-floor sedimentation take place (Nelson and Creager, 1977). These changes have implications for installations on the sea floor and for mass transport of pollutants.

This paper describes the interbedded sand layers found in southern Norton Sound off the modern Yukon Delta that are deposited by the storm surge events. Such deposits are evident in both modern and ancient deposits of epicontinental shelves (Hays, 1967; Howard and Reineck, in press; Anderton, 1976). These graded sand layers in very shallow water mimic many of the features of thin-bedded turbidite sands, although we propose that the shallow water deposits have a very different mechanism of deposition related to storm surge processes.

Two factors in the oceanographic setting of northern Bering Sea magnify the effects of storm surge. The sea floor is very shallow (less than 20 m deep over wide areas) particularly in Norton Sound. Consequently there is intensive wave reworking which causes extensive sea-floor erosion, mass movement, displacement, and offshore progradation of significant amounts of sediment during storm surges. The second factor is a system of strong dynamic bottom currents that can move large amounts of sediment northward to Chukchi Sea during normal weather. Much more sediment is moved when the current is reinforced by relaxing of the sea surface set-up caused by storm surge

(Fig. 1) (Flemming and Heggarty, 1966; Coachman et al., 1976; Cacchione and Drake, 1979).

Characteristics of Graded Sand Storm layers

Over 10,000 km³ of southern Norton Sound display graded sand layers interbedded with silty muds. In this paper we have focused on the prominent interbedded very fine sand and coarse silt layers that show definite vertical gradation of grain size and sedimentary structures. In addition to the vertical gradation within individual beds, there are several aspects of areal gradation patterns observed in grain size, thickness of layers, and completeness of vertical sequences of sedimentary structures. Other subtle areal gradations are found in types of sedimentary structures as well as general lobes and patterns of grain size and layer thickness variation from west to east across the front of the Yukon Delta. These characteristics are found in a common surface sand layer and at each location the entire sequence of graded beds is similar to the surface layer (Fig. 2).

Onshore to offshore, the graded sand beds become finer grained, thinner in total thickness, contain a smaller percentage of graded sand layers, and show less complete sequences of vertical sedimentary structures. Inshore the graded sand layers make up 50-100 percent of the total sedimentary section (Fig. 3); they range from 10-20 cm thick and the basal part of the layer is made up of fine-grained sand. Approximately 60-75 km from the Yukon Delta shoreline, the graded sands are generally 1-2 cm thick, less than 35 percent of the total section, and very fine sand or coarse silt at the base of the layers (Figs. 2-4).

The graded layers typically contain a vertical sequence of sedimentary structures (S_b - S_e see Fig. 5). The base of the layer may or may not contain flat-laminated medium to fine sand (S_b). In the center section of the sand

layer, cross lamination and convolute lamination are dominant (S_c). In the upper part of the layer, in the very fine sand or coarse silt, flat lamination again predominates and often laminated beds of epiclastic plant fragments become very prominent (S_d). The upper flat-laminated sequence of the individual sand beds grades into normal, continuous mud deposition (S_e) in most instances, although this mud cap may be lacking.

Going from nearshore graded sand layers to offshore layers, there is a less complete sequence of vertical structure (Fig. 5). Often on the onshore layers flat lamination is present whereas in distal graded layers, flat lamination at the base is not encountered (Fig. 5). In addition, in the most distal layers, occasionally both the lower flat lamination and cross lamination are missing leaving only flat laminated sands. Another areal change in sedimentary structures is that trough cross lamination characterizes the nearshore graded sand beds and ripple lamination or starved ripple drift prevails in the distal graded sand beds (Fig. 5).

A surface sand layer is present in many of the cores and could potentially be a correlative layer from the 1974 storm surge (Fathauer, 1975) (Fig. 2). Such a continuous layer was not encountered in samplings in field seasons prior to 1974. Oxidized grain coatings are present, giving the thicker sands a yellowish color rather than the usual olive drab hue. Such coatings suggest a subareal source and that sediment movement offshore may correlate with extensive shoreline erosion. Such shoreline erosion extended up to several hundred meters inland in the 1974 storm (Sallenger et al., 1978). Offshore movement of extensive sand masses from delta source areas from the 1974 storms is also indicated by the grading of thicker to thinner layers offshore. It is not possible to confirm the dating of this upper sand layer, but it does exhibit a consistent pattern of trends in thickness, grain

size and vertical sequence of sedimentary structures that is the same as the average of these characteristics throughout the entire core sequences. Thus, the surface layer appears to be a verification of the areal patterns of gradation in these vertical sequences of graded sand beds.

In addition, presence of a post 1974 extensive change in surface texture of the sediment can be shown in certain areas of the sea floor (Fig. 6). Change is most prominent nearshore off the modern Yukon subdelta where storm sand layers are thicker than they are far offshore. Coarser texture is found in most inshore areas where pre and post 1974 data is available. A 30-50 percent increase in sand content is noted in these regions. In the furthest offshore region of the central sound, no change is apparent, as would be expected in this distal region where storm sands are poorly developed at best and are subject to more intense bioturbation (Nelson et al., in press).

Characteristics of graded sand beds also vary from the western side of the delta to the eastern nearshore area of the delta. In the western delta the sand layers are approximately 18 cm thick whereas in the eastern area most sand layers are 8-9 cm thick with occasional layers of up to 20 cm in thickness. Similarly, in the distal areas off the western delta, sand layers average 5-10 cm thick whereas off the eastern area sand layers average 1-2 cm thick.

Local areal variation also is apparent from the morphological study of the cores and the stratigraphic variation in the graded sand layers. Some cores change from thicker to thinner layers from base to top (Fig. 5) and others change from thinner to thicker layers from base to top. The cores taken in channels consist almost entirely of sand and may or may not contain thick graded sands, whereas cores taken on the flanks of the channels and on the delta front platform are those which present well-developed graded beds; these become thinner at greater distances from the channels.

Depositional Processes of the Graded Sand Layers

The vertical and areal trends of graded sand layers permits speculation concerning the method of deposition. The well-developed vertical sequence of sedimentary structures and vertical gradation of grain size in the individual beds suggests that a rapidly waning current deposits these beds. It is apparent that this rapidly waning current is stronger inshore and gradually relaxes offshore, as shown by the pronounced change to thinner beds, fewer beds, and finer-grained beds offshore. In addition, it is apparent that sources vary and that pathways of the rapidly waning current are influenced by the sub-ice channel system (Duprè, 1979). It seems that the western delta, where 90 percent of the sediment is introduced, has a much more vigorous transport of the prograded sand beds from onshore to offshore. In contrast, the eastern delta is a region with much less effective sand transport from onshore to offshore.

The mechanism of deposition for these prograding sand beds is thought to be a storm surge runoff current that develops from the relaxation of sea level set-up after passage of the strong south to southwesterly winds that usually accompany the low-pressure storms in this region (Fathauer, 1975) (Fig. 7). In small storms, sea surface set up of a meter and current speed increases of over 100% have been measured in central Norton Sound (Cacchione and Drake, 1979; Schumacher and Tripp, 1979). Measurement of offshore set-up nearly equal to shoreline set-up and known occurrences of up to 5 m of shoreline set-up (Sallenger et al., 1978) indicate storm surge runoff currents several orders of magnitude greater than normal current speeds are possible.

The progradation of sand from onshore to offshore is potentially enhanced by cyclic wave loading on the delta front that can interact with the favorable grain size that is present. The possibility of cyclic wave loading and

liquefaction potential appears to be verified by theoretical calculations based on wave pressures measured at the GEOPROBE site by Cacchione and Drake (1979). Consequently, a synergistic effect of sea level set-up, wave cyclic loading and liquefaction, and strong bottom return flow onshore toward offshore, is reinforced by the relaxing of the sea surface set-up. The pathway of the bottom return flow is apparently affected by the onshore channel systems whereas offshore, beyond the 30 km reach of the channel, sheet flow apparently gives a uniform distribution of thin sands (Fig. 7).

Another possible gradational process may be due to the greater effect of waves inshore. There, trough cross lamination predominates, whereas offshore current ripple lamination and starved ripple drift are apparent as the sand progradation process may be dominated mainly by bottom current flow with lesser influence of waves and a waning source of sand in the distal regions.

Isopach thicknesses of Holocene sediment in Norton Sound (Nelson and Creager, 1977) and comparison of these thicknesses with total sediment input from the Yukon River during the Holocene, indicate that significant amounts of sediment have been removed from the sea floor by sediment resuspension (Nelson and Creager, 1977). Detailed stratigraphy and lithology suggest the same conclusion. The section of Yukon Holocene muds is exceptionally thin in many places adjacent to the delta source region and this indicates sediment removal. Numerous lag layers of pebbles and shells and thin sands are apparent in the distal areas of Yukon muds of central and northern Norton Sound (Fig. 5). These form when storm waves resuspend the bottom mud but leave behind coarse ice-rafted pebbles, shell fragments, and coarse fraction in the bottom muds.

Additional new evidence of resuspension appears in the form of a thick storm sand layer now observed on the surface of southern Norton Sound; a layer

of this thickness is not apparent in the past thousands of years of stratigraphy. This suggests that originally thick sand layers of major storms are eroded away due to resuspension by smaller storm events subsequent to the major event, so that the stratigraphic record may preserve storm sand layers that are thinner than those originally deposited. A generally thicker surface sand, compared to the other sand layers in each individual core, verifies the model of sediment resuspension.

Resuspension of bottom sediment by waves is also suggested by side-scan sonar and underwater television videotapes which show large scour depressions and formation of oscillation ripples by storm waves (Larsen et al., 1979). Ice gouges covered by sediment in regions of intense ice scouring again suggest significant sediment resuspension and movement in southern Norton Sound (Thor and Nelson, 1980).

Potential Hazards and Storm-surge Deposition and Erosion

All evidence indicates that unusually large amounts of sediment are resuspended and then transported from Bering Sea to Chukchi Sea (Nelson and Creager, 1977) consequently any structure impeding this movement requires careful design. Data on suspended sediment verifies that about 10 percent of the Yukon River input to Norton Sound may be carried as part of the normal suspended sediment load that is bypassing through the Bering Strait. Because as much as 40 percent of the late Holocene discharge of the Yukon River appears to be missing from Norton Sound (Nelson and Creager, 1977), then, up to 20 million metric tons of sediment per year, on the average, may be suspended and carried to Chukchi Sea by the strong northward flowing currents. The several hundred percent increase of suspended sediment transport, observed during a small storm in 1977, by Cacchione and Drake (1979), suggests that most of the 40 percent displacement of the suspended sediment occurs during storm events.

In summary, there are extremely large amounts of suspended sediment moving rapidly in the coastal waters along Alaska, often in intermittent large concentrations generated by storms and the early summer seasonal runoff. The fall storm season consequently could cause extremely wide dispersal of any oil spill material residing on the sea floor. Recent data by Drake (in press) suggest sediment resuspension may also be vigorous, even during the season of ice cover, because of greater constriction of currents in the delta region where the most rapid deposition occurs. Thus, any pollutants residing on the sea floor face extremely wide dispersal from northern Bering Sea to distances as far as a thousand kilometers to the north into the Arctic Ocean.

Storm surges generally dominate the mass movements of suspended sediment and also can be seen to move large amounts of rapidly prograding sand in bedload transport for distances of up to 60 km offshore. This intensive transport and deposition could affect offshore facilities, especially pipelines. Storm sand layers deposited by such events could be impeded in their transport by any structures that protrude on the sea floor. These protruding structures could act as a dam, holding back the sediment transport and of course, would be put under severe stress if the sediment piled up rapidly against any feature such as a pipeline on the sea floor.

Conclusions and Suggestions for Future Work

A complex and vigorous set of sedimentary processes are apparent in the shallow Yukon Delta front platform and prodelta regions. A major depositional sequence of graded sands may prograde offshore in storm surges. These graded sand beds with a vertical sequence of structures that mimic those of turbidites (Bouma, 1962) provide an example of shallow water deposition from rapidly waning storm surge currents that is very much like that of turbidity currents.

Storm surges and their concomitant wave and current activity have important effects on this basin that must be considered in planning for offshore development. Extensive erosion of the sea floor, resuspension of sediment, and transport of materials and any attached pollutants is one aspect. The second potential effect is movement of extensive sand sheets from shoreline and nearshore sources to offshore areas. Rapid deposition of 15 cm or more of sand can smother biota immediately and alter texture of the substrate over extensive areas for a number of years. Thus, a sea-floor baseline measured at one time, alters markedly in post-storm conditions. Future studies should monitor conditions with an instrument such as the GEOPROBE which can help to determine the severity of sea-floor erosion in different locations during a storm. A number of deep vibracores are needed to determine recurrence intervals of such events and characteristics before and after such a catastrophic episode.

Acknowledgments

Discussion with Hans Reineck, Ed Clifton, Bill Duprè, and Jim Howard has enhanced my conceptual development of storm sand layer sedimentation. Collection of inshore cores and preparation of excellent peel structures by James Howard, Devin Thor, and Rick Brokaw was a key to complete assessment of this storm sand system. Brad Larsen, Devin Thor, Jeff Patry, Carol Hirozawa, Joan Esterle, and Carol Madison have assisted in preparation of figures and compilation of data.

References Cited

- Anderton R., 1976, Tidal shelf sedimentation: an example from the Scottish Dalradian: *Sedimentology*, v. 23, no. 4, p. 429-458.
- Cacchione, D.A., and Drake, D.E., 1979, Sediment transport in Norton Sound, Alaska, Regional Patterns and GEOPROBE SSystem measurements: U.S. Geological Survey Open-File Report 79-1555, 88 p.
- Coachman, L.K., Aagaard, Knut, and Tripp, R.B., in press, Bering Strait: The regional physical oceanography: University of Washington Press.
- Dupfe, W.R., and Thompson, R., 1979, The Yukon Delta: A model for deltaic sedimentation in an ice-dominated environment: Proc. Offshore Technical Conference, Paper no. 3434, p. 657-661.
- Fathauer, T.F., 1975, The Great Bering Sea Storms of 9-12 November 1974: Weatherwise Magazine, Am. Meteorological Society, v. 28, pp. 56-84.
- Fleming, R.H., and Heggarty, D., 1966, Oceanography of the southeastern Chukchi Sea, in Wilimovsky, N.J., Wolfe, J.M., eds., Environment of Cape Thompson Reigon, Alaska: U.S. Atomic Energy Commission, p. 697-754.
- Howard, J.D., and Reinick, H., 1980, Sedimentary structures of a "high energy" beach-to-offshore sequence; Ventura-Port Hueneme area, California, U.S.A., University of Georgia Marine Institute, contribution no. 371. (in press).
- Hayes, M.O., 1967, Hurricanes as geological agents: case studies of Hurricane Carla, 1961 and Cindy, 1963: Report Inves. No. 61, Bur. Econ. Geol., University of Texas, Austin, Texas, 54 p.

- Larsen, M.C., Nelson, C. Hans, and Thor, D.R., 1979, Geologic implications and potential hazards of scour depressions on Bering shelf, Alaska: *Environmental Geology*, v. 3, p. 39-47.
- McManus, D.A., Venkatarathnam, K., Hopkins, D.M., and Nelson, C.H., 1974, Yukon River sediment on the northernmost Bering Sea shelf: *Jour. Sedimentary Petrology*, v. 44, no. 4, p. 1052-1060.
- Nelson, C. Hans, and Creager, J.S., 1977, Displacement of Yukon-derived sediment from Bering Sea to Chukchi Sea during Holocene time: *Geology*, v. 5, p. 141-146.
- Nelson, C.H., Rowland, R.W., Stoker, S.W., and Larsen, B.R., 1980, Interplay of physical and biological sedimentary structures: in: Hood, D.W., ed., *The Eastern Bering Shelf: its Oceanography and Resources*, in press.
- Sallenger, A.H., Dingler, J.R., and Hunter, R., 1978, Coastal processes and morphology of the Bering Sea coast of Alaska, in: *Environmental Assessment of the Alaskan Continental Shelf, Annual Report of Principal Investigators for the year ending March 1978*, Environmental Research Laboratory, Boulder, Colorado, NOAA, U.S. Dept. of Commerce, v. 12, p. 451-470.
- Schumacher, J.D., and Tripp, R.B., 1979, Response of northeast Bering Sea shelf waters to storms: *EOS*, v. 60, p. 856.
- Thor, D.R., and Nelson, H., 1980, Sea ice as a geologic agent on the subarctic Bering shelf, in: Hood, D.W., ed., *The Eastern Bering Sea Shelf: Its Oceanography and Resources* (in press).

Figures

- Figure 1. Bottom-water currents and bathymetry of the northern Bering Sea.
- Figure 2. Thickness and distribution of a surface sand layer in samples taken after the 1974 storm surge.
- Figure 3. Amount and distribution of graded sand layers and types of sedimentary structures.
- Figure 4. Mean grain size change in graded sand layers with distance from the Yukon Delta shoreline.
- Figure 5. Sedimentary structures of storm sand layers
A. Inshore (5 km from shoreline) graded sand layers off the southwest distributary showing lower flat lamination S_b , cross lamination S_c , upper flat lamination and S_e mud cap.
B. Offshore graded sand showing S_{c-e} and $S_{d,e}$ sequences from a 2 m vibracore 22 km from shoreline off the northeastern part of the delta.
C. Radiograph of distal graded sands and pebble and shell lags from a box core 115 km from Yukon Delta shoreline.
- Figure 6. Change in surface texture, pre- and post-1974 storm surge in Norton Sound.
- Figure 7. Model depicting sedimentary processes of a storm surge runoff current that may deposit graded storm sand layers off the Yukon Delta in Norton Sound.

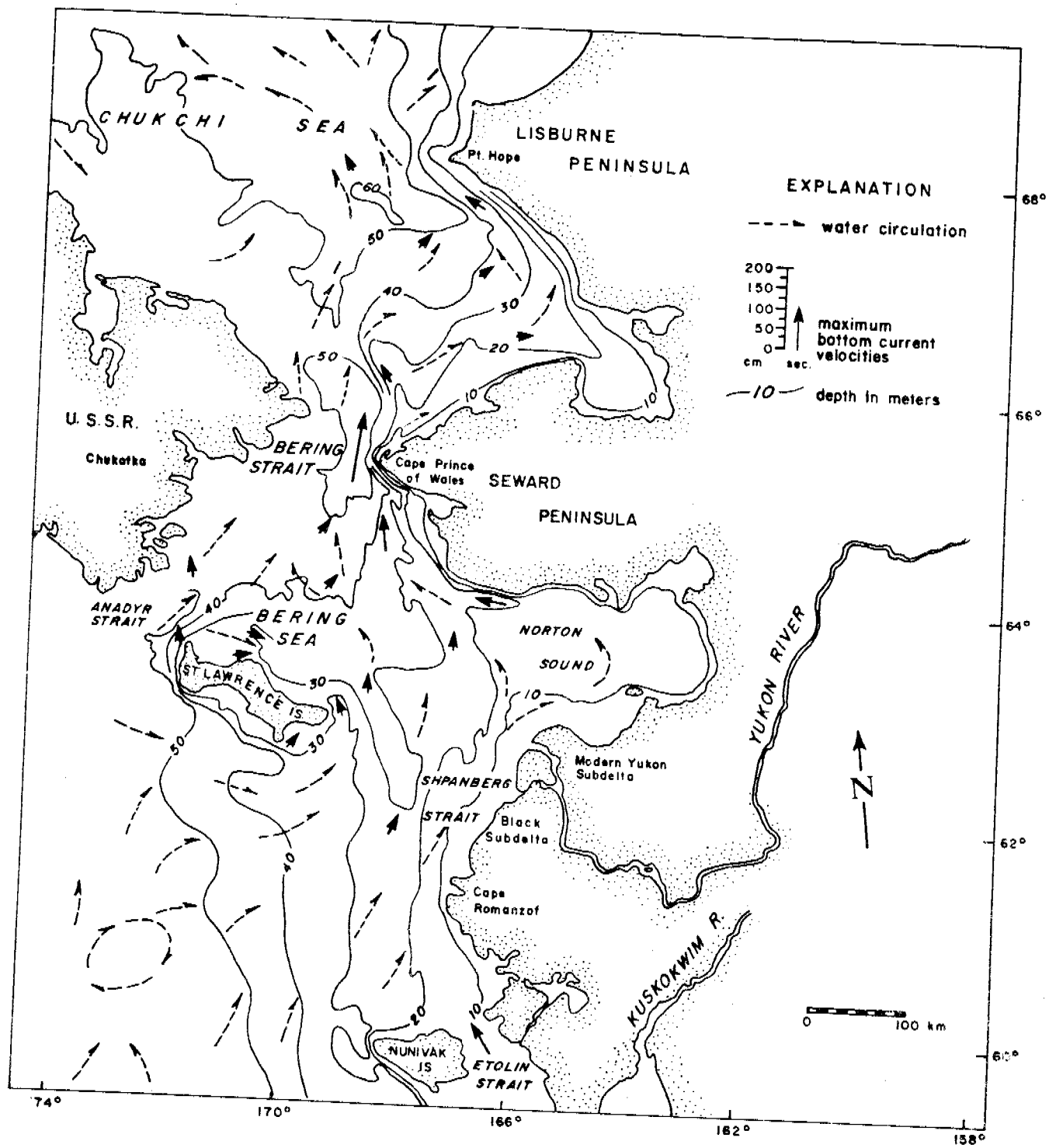


Fig. 1 - Bottom-water currents and bathymetry of the northern Bering Sea.

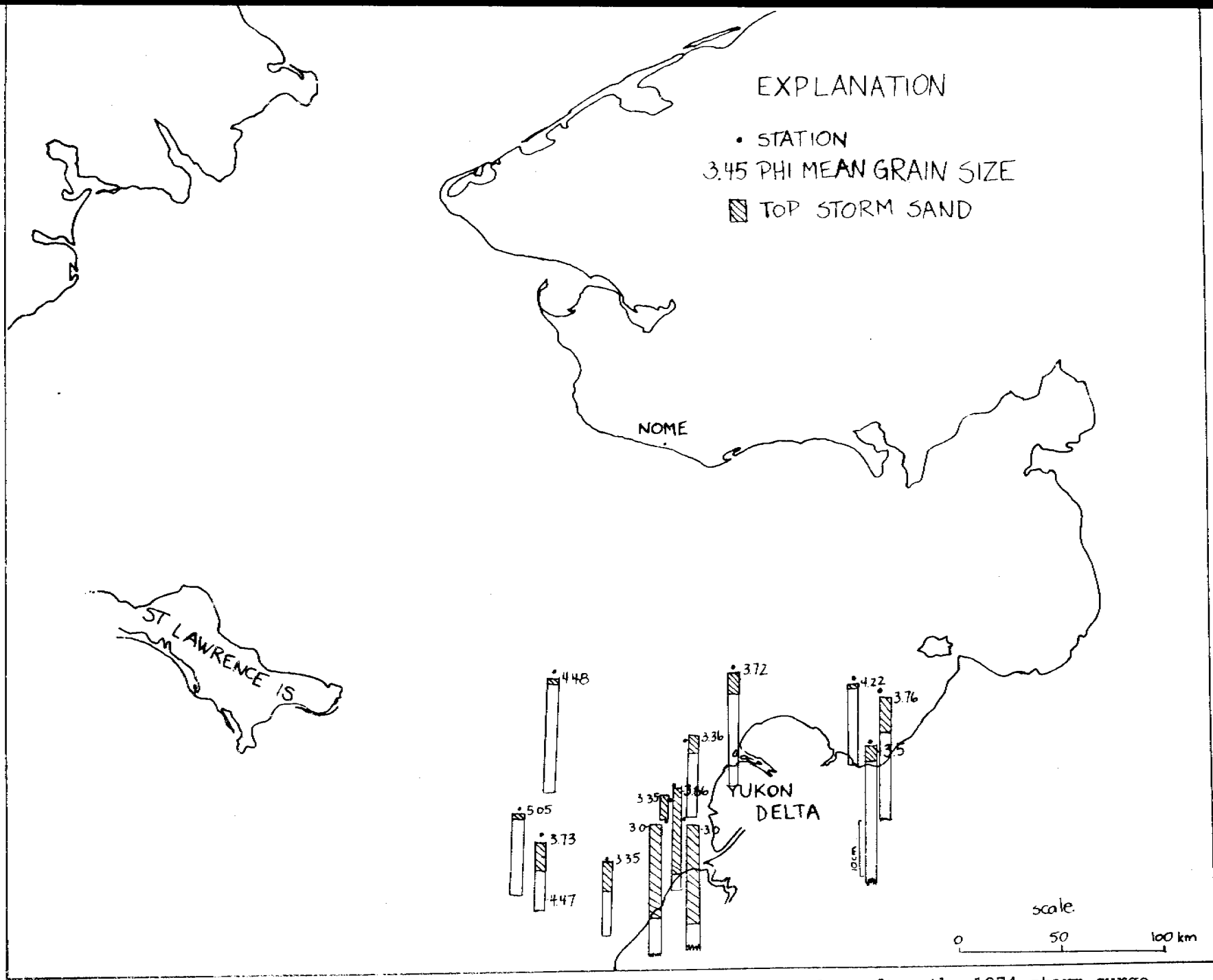


Fig. 2 - Thickness and distribution of a surface sand layer in samples taken after the 1974 storm surge.

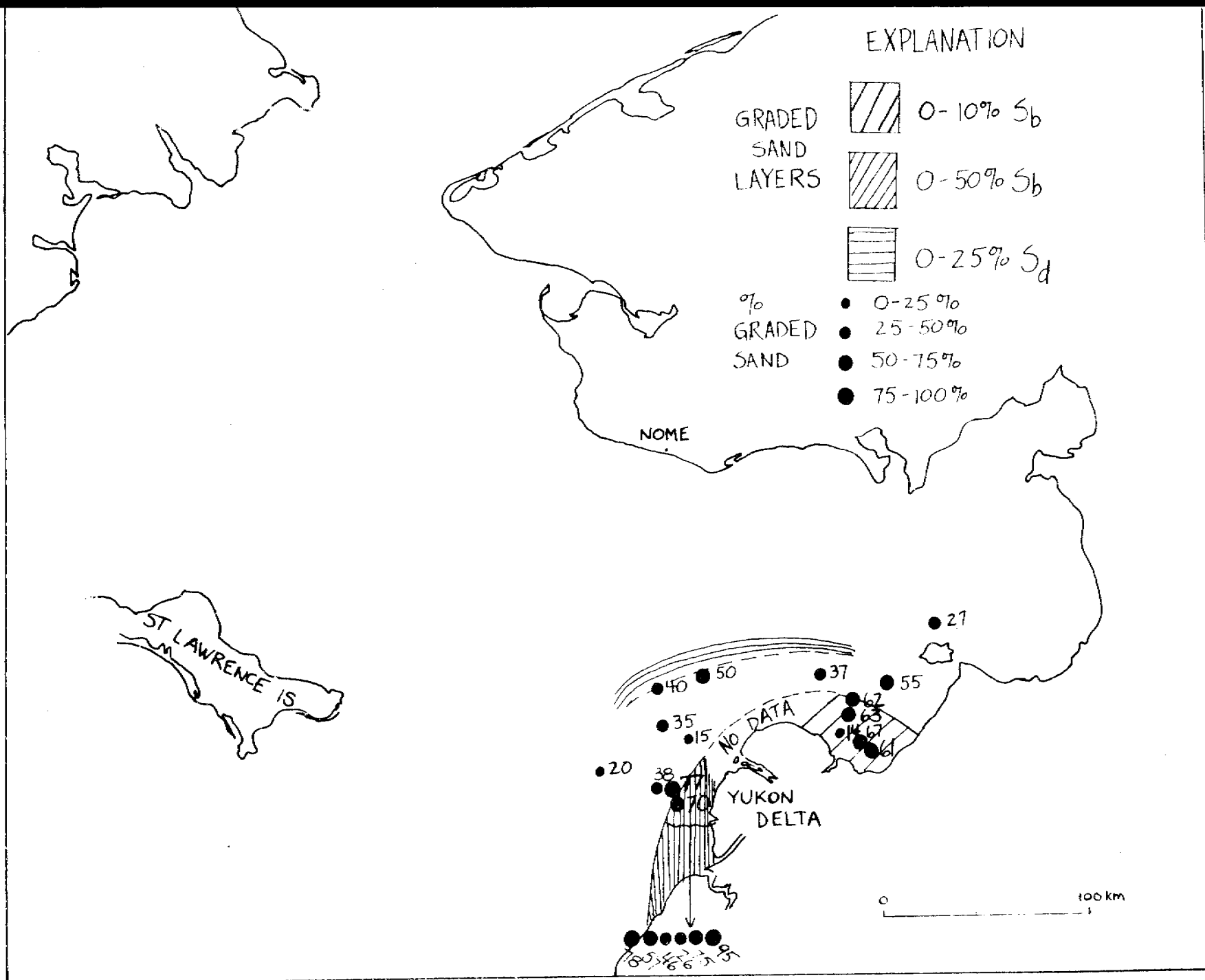
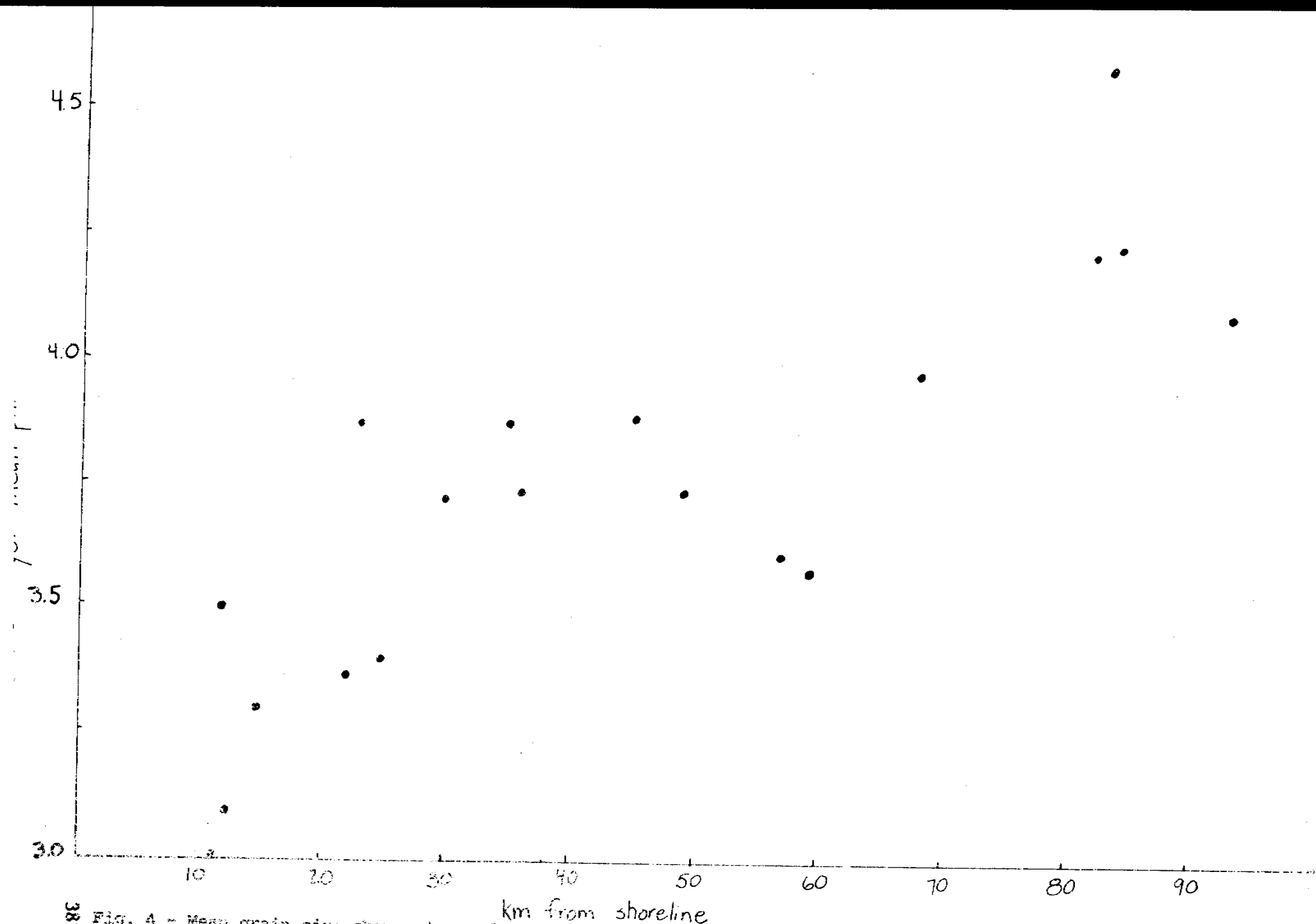


Fig. 3 - Amount and distribution of graded sand layers and types of sedimentary structures.



383 Fig. 4 - Mean grain size change in graded sand layers with distance from the Yukon Delta shoreline.

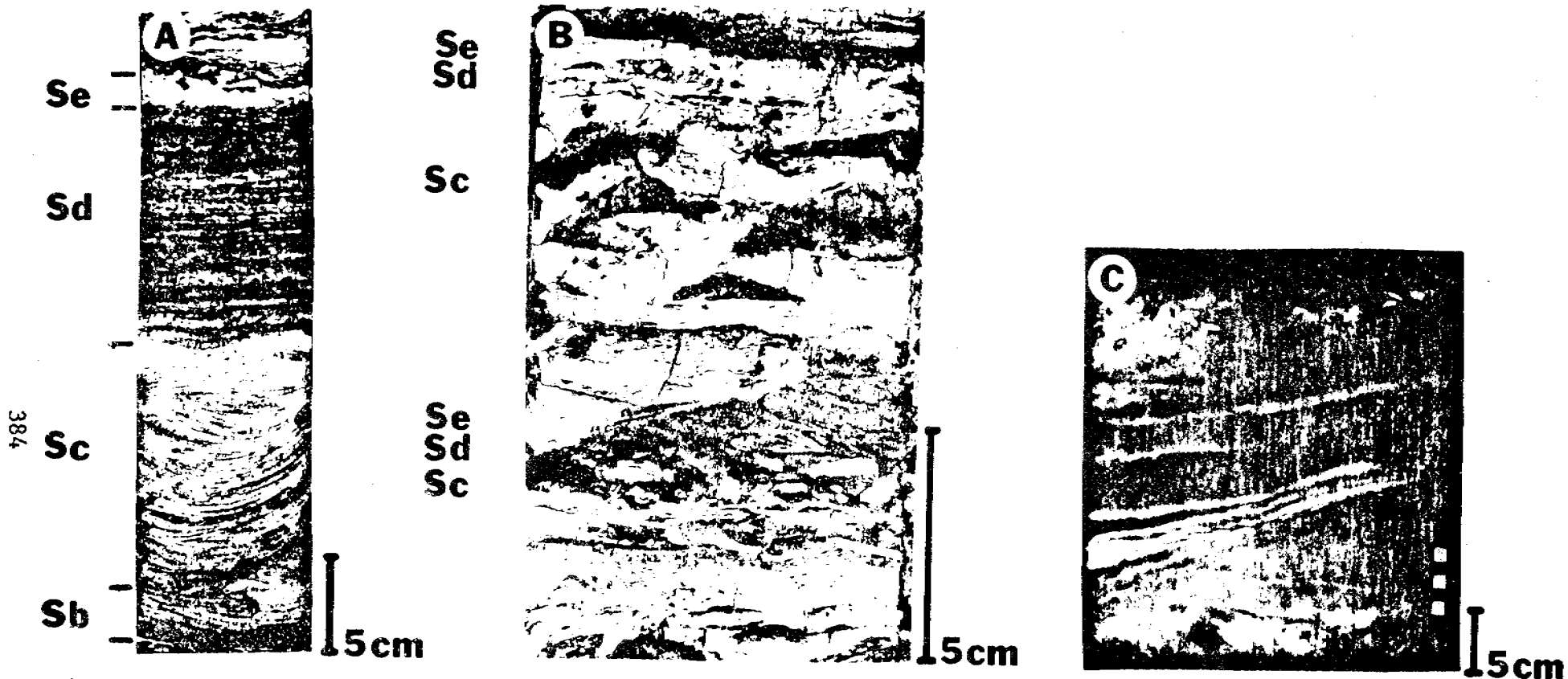


Fig. 5 - Sedimentary structures of storm sand layers:

- A. Inshore (5 km from shoreline) graded sand layers off the southwest distributary showing lower flat lamination S_b , cross lamination S_c , upper flat lamination and S_e mud cap.
- B. Offshore graded sand showing S_{c-e} and $S_{d,e}$ sequences from a 2 m vibrocorr 22 km from shoreline off the northeastern part of the delta.
- C. Radiograph of distal graded sands and pebble and shell lags from a box core 115 km from Yukon Delta shoreline.

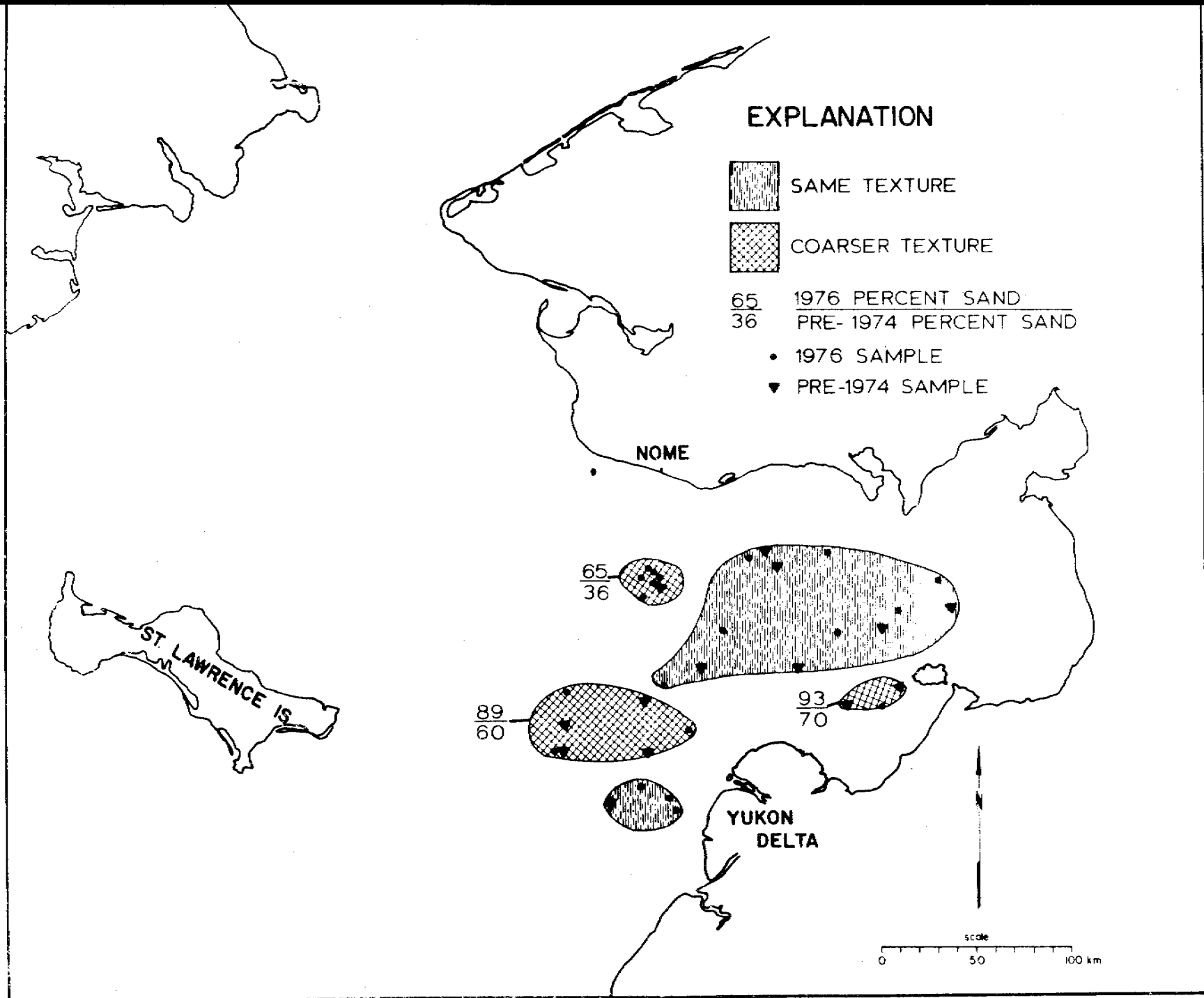
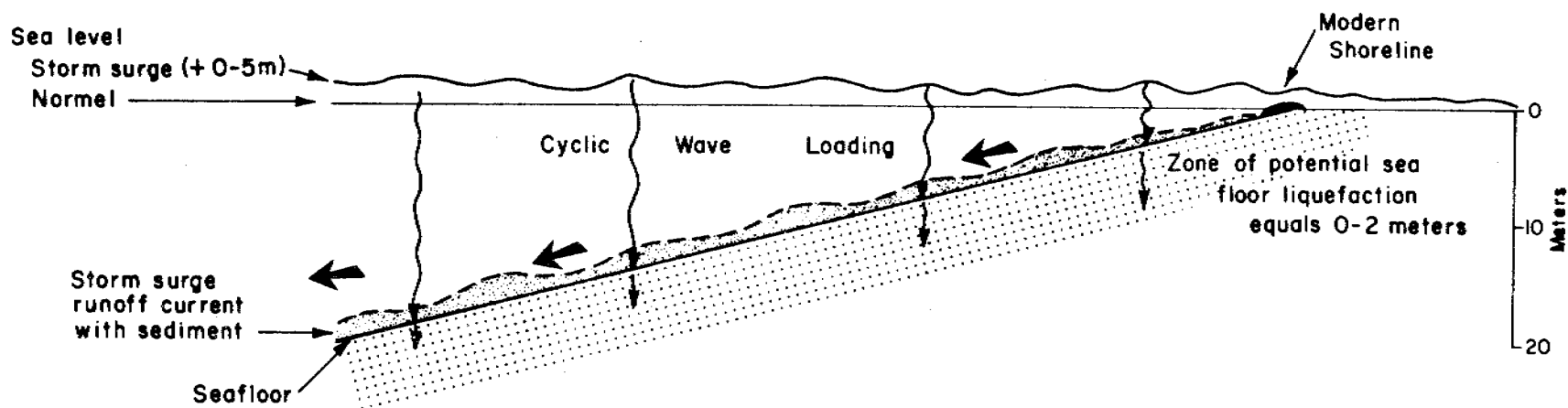


Fig. 6 - Change in surface texture, pre- and post-1974 storm surge in Norton Sound.

STORM SURGE PROCESSES



386

Fig. 7 - Model depicting sedimentary processes of a storm surge runoff current that may deposit graded storm sand layers off the Yukon Delta in Norton Sound.

UNITED STATES DEPARTMENT OF THE INTERIOR
GEOLOGICAL SURVEY

Geotechnical Characteristics of Bottom
Sediment in the Northern Bering Sea

By

Harold W. Olsen, Edward C. Clukey,
and C. Hans Nelson

Contents

	Page
Abstract.....	389
Introduction.....	390
Geologic and environmental framework.....	391
Geotechnical profiles.....	393
Consolidation and static triaxial data.....	398
Discussion of potential hazards.....	400
Acknowledgments.....	404
References.....	405

Table

Table 1.--Geologic and environmental framework for geotechnical studies in the northern Bering Sea.....	410
--	-----

Geotechnical Characteristics of Bottom Sediment
in the Northern Bering Sea

By

Harold W. Olsen¹, Edward C. Clukey², and
C. Hans Nelson²

Abstract

Yukon sediment of Holocene age, consisting dominantly of silty fine sand and sandy silt, covers the bottom of central and western Norton Sound, which is a high energy environment involving extensive ice loading, high waves, and strong bottom currents. The sediment contains significant amounts of sand in some areas and a generally minor amount of clay-size material ranging from 0 to 20 percent. Moreover, it is generally dense although loose and weak zones occur at the surface and also at depth between relatively dense layers. These characteristics, evidence of storm sand layers and scour depressions, and the results of preliminary analytical studies indicate this sediment is susceptible to liquefaction during major storms.

Substantially finer grained, weak, and highly compressible sediment of Holocene age, derived from the Yukon River and from local rivers and streams, covers eastern Norton Sound and the Port Clarence embayment, which are low

¹U.S. Geological Survey, Box 25046, Mail Stop 903, Denver, Colorado
80225.

²U.S. Geological Survey, 345 Middlefield Road, Menlo Park, California
94025.

energy environments with negligible ice loading, low waves, and weak bottom currents.

Transgressive deposits of late Pleistocene age that cover the bottom of Chirikov Basin include an inner-shelf fine sand underlain by a basal transgressive medium sand that is exposed on the north and east flanks of the basin. Geotechnical data on the latter, obtained in the sand-wave fields near Port Clarence, show the material is loose near the surface but becomes firm rapidly with depth and could not be penetrated more than about 3 m with the Alpine vibratory sampler.

Pleistocene peaty deposits underlie the Holocene and late Pleistocene deposits in both Norton Sound and Chirikov Basin and are somewhat overconsolidated, probably because of subaerial desiccation during low sea level stands in the late Pleistocene. These materials have a higher clay content than the overlying deposits and they contain substantial amounts of organic carbon and gas. The presence of gas suggests that in situ pore pressures may be high. If so, the strength of the material could be low even though the material is generally overconsolidated.

Introduction

During the last few years the U.S. Geological Survey (USGS) has been acquiring geotechnical data on bottom sediment in the Northern Bering Sea. This effort has been part of a broad group of USGS studies in this region aimed at clarifying and evaluating those geologic conditions and processes that may be hazardous to offshore resource development activities (Thor and Nelson, 1979; Larsen, Nelson, and Thor, 1980).

Previous reports concerning this geotechnical effort include the papers by Clukey, Nelson, and Newby (1978); Nelson, Kvenvolden, and Clukey (1978); Nelson et al. (1979); and Sangrey et al. (1979). These reports describe near-

surface data on samples obtained during 1976 and 1977 with box corers, Soutar Van Veen samplers, and a Kiel vibracore sampler capable of penetrating 2 m beneath the ocean floor^{3/}. The data also include penetration rate measurements during vibracorer sampling operations. During 1978, additional samples and penetration records were obtained with an Alpine vibratory corer system equipped to obtain 8.89 cm diameter continuous samples to a maximum depth of 6 m. All of the data obtained to date have been compiled for the Bureau of Land Management in a USGS open-file report by Larsen, B. R., et al. (1980).

The purpose of this paper is to summarize the geotechnical information obtained in the above studies in relation to the geologic and environmental conditions in the northern Bering Sea and to assess the implications of these data with regard to potential hazards to offshore resource development activities in the region.

Geologic and environmental framework

The bottom of Norton Sound consists of silty fine sand and sandy silt of Holocene age discharged from the Yukon River, except for nearshore areas where Pleistocene (>10,000 years B.P.; Hopkins, 1975) transgressive deposits remain and tidally scoured troughs where transgressive and Holocene deposits are mixed (Fig. 1; Nelson, this volume, Fig. 6). In southern Norton Sound, the Holocene sediment is interbedded with fine sand layers as much as 20 cm thick near the Yukon Delta. Pleistocene freshwater silt interbedded with peaty muds and peat layers underlies the Holocene sediment.

³Use of brand names in this report is for descriptive purposes only and does not constitute endorsement by the U.S. Geological Survey.

Most of Chirikov Basin is covered by an inner shelf fine sand deposited by the late Pleistocene shoreline transgression across this region (Fig. 1; Nelson, this volume, Fig. 6). This deposit is underlain by a basal transgressive medium sand that is exposed on the north and east flanks of the basin. Lag gravels are exposed near the basin margins where the late Pleistocene shoreline transgression has reworked pre-Quaternary bedrock and glacial moraines and where strong modern currents have prevented subsequent deposition. Strong bottom currents and water circulation patterns have inhibited deposition of Holocene sediment from the Yukon River throughout Chirikov Basin, except for some accumulations with ice-rafted pebbles in local depressions in eastern and southern Chirikov Basin (McManus, Hopkins, and Nelson, 1977).

Prior to the deposition of the transgressive sand layers, tundra-derived peat deposits formed during several Pleistocene low sea-level stands that periodically exposed the entire northern Bering shelf until 12,000-13,000 years ago. These Pleistocene limnic peaty muds generally overlie Pleistocene glacial and alluvial deposits that are underlain by pre-Quaternary bedrock.

The Pleistocene peaty mud is a source of biogenic gas throughout the region. Seismic profiles showing acoustic anomalies associated with these materials indicate gas concentrations are of sufficient magnitude to affect sound transmission throughout Norton Sound (Holmes and Thor, this volume). The presence of shallow craters in the thin Holocene sediment in east-central Norton Sound suggests venting of biogenic gas accumulations from the underlying peaty muds. Generally low background levels of dissolved hydrocarbons in the waters of Norton Sound and high gas contents in the underlying peaty mud suggest venting is episodic, while the Holocene sediment generally acts as a seal preventing the biogenic gas from diffusing freely to

the sea floor as it appears to do through the transgressive sand in Chirikov Basin (Nelson et al., 1979).

A large submarine seepage of thermogenic gas in west-central Norton Sound was discovered in 1976 (Cline and Holmes, 1977; Kvenvolden et al., 1979b). Acoustic investigations indicate the presence of bubble-phase gas associated with the sediment in the seep in an area of 50 km² (Nelson et al., 1978). Detailed geophysical and geochemical studies indicate that hydrocarbons and CO₂ are migrating upward along a major growth fault in the sedimentary section (Kvenvolden et al., 1979a).

Bottom sediment in the northern Bering Sea is exposed to ice loading, cyclic stress from waves, and drag from bottom currents (Table 1). Ice loading is extensive in the vicinity of the Yukon Delta (Thor and Nelson, 1979). High waves and strong bottom currents occur in central and western Norton Sound and in Chirikov Basin. Storm waves and bottom currents cause significant reworking and erosion of the sediment in Norton Sound (Larsen, Nelson, and Thor, 1979) and also cause the transport of sediment from Norton Sound to the Chukchi Sea, almost 1000 km to the northwest (Cacchione, Drake, and Weiberg, this volume; Duprè and Thompson, 1979; Nelson and Creager, 1977; Drake et al., 1980). Two areas in this study, Port Clarence and eastern Norton Sound, are protected from large waves and strong bottom currents.

Geotechnical profiles

Methods

The geotechnical profiles (Figs. 2-6) present, for each of the regions outlined in Table 1, information concerning the composition and the relative density or consolidation state of the materials. Direct evidence concerning the composition of the materials includes the data on lithology, texture, Atterberg limits, and gas content. The other data on moisture content,

density, strength indices, and vibrocore penetration resistance reflect the combined influences of the composition and the relative density or consolidation state. The latter can usually be inferred on a qualitative basis from the suites of information presented.

The data in Figs. 2-6 were obtained with shipboard and laboratory procedures as follows: penetration rates were derived from vibratory corer penetration rates during sampling; gas content data were obtained on shipboard from 10- to 15-cm sample tube sections using the procedures described by Kvenvolden et al. (1979a); bulk densities of tube sections were calculated from shipboard measurements of their volume and weight; visual descriptions, shear strength index measurements, and subsamples for moisture content, density, Atterberg limits, and texture analyses were obtained on shipboard from split tube sections of all cores except 78-1 through 78-5. The latter cores were preserved on shipboard and were subsequently extruded, logged, and tested in the USGS geotechnical laboratory in Denver. The Holocene-Pleistocene boundaries noted on Figs. 2-6 were derived from lithologic logging and radiocarbon dates (Nelson, this volume), and from microfaunal analyses (McDougall, this volume). Texture analyses were run with geologic (Larsen, B. R., et al., 1980), and engineering standard (American Society for Testing and Materials, 1977) sieving and sedimentation column techniques. Moisture content and density data were obtained on subsamples taken with the miniature coring device described by Clukey et al. (1978). Atterberg limits were run in accordance with ASTM Standards using the wet preparation method, D 2217 (American Society for Testing and Materials, 1977). Strength index data were obtained with laboratory vane, hand vane, pocket penetrometer, and unconfined compression test equipment. Circumstances did not generally allow these measurements to be made under controlled conditions with standardized

procedures that must be employed for the data to have quantitative significance regarding shear strengths. Nevertheless, these data show differences in strength that reflect variations in the composition and the relative density or consolidation states of the materials tested. The absence of strength index data in some of the profiles is also significant in that materials, such as clean sands that do not possess any apparent cohesion, cannot be tested with the strength index test methods used in this study.

Yukon Prodelta

The three profiles in the vicinity of the Yukon Delta (Fig. 2) show mostly Holocene materials that are dominantly silty fine sand, and sandy silt with occasional thin beds of organic clayey silt having clay contents generally less than 20 percent. Gas contents vary over a wide range at station 78-22 from about 0.2 to 70 ml/l of interstitial water; the range at stations 78-23 and 78-24 is considerably less, from about 0.8 to 4.0 ml/l. The relative density of the material varies over a wide range. Moderately dense to dense zones predominate. However, loose zones, indicated by a watery appearance and very low strengths, are particularly evident at a depth of 2-3 m at station 78-22, and from the surface to a depth of about 1.5 m at station 78-24. The watery appearance of the loose zones emerged fairly rapidly after the core was split, apparently because the material densified in response to vibrations generated by the ship engines. The variations of penetration resistance with depth generally correlate with the presence of loose or dense zones. The variations in gas content with depth do not show a close association either with relative density as inferred above or with the variations in texture, density, and strength with depth.

West-central Norton Sound

The five profiles in west-central Norton Sound (Fig. 3) are located in

the thermogenic (Kvenvolden et al., 1979a) gas seep acoustic anomaly (stations 78-1, 78-2, and 78-3), within a nearby biogenic (Kvenvolden et al., 1979a) gas acoustic anomaly (station 78-4), and adjacent to the biogenic gas acoustic anomaly (station 78-5). Very high gas contents occur at one location in the thermogenic anomaly (station 78-3) and in the biogenic anomaly (station 78-4). Much lower gas contents occur at stations 78-1 and 78-2 in the thermogenic anomaly and at station 78-5 adjacent to the biogenic anomaly. These profiles penetrate silty fine sand and sandy silt that are similar to the materials in the Yukon Delta region (Fig. 2) and that are probably Holocene deposits because of their lithology, texture, and consistently low moisture contents. The two profiles with very high gas contents also penetrate Pleistocene peaty muds at depths of about 3 m and 1 m at stations 78-3 and 78-4, respectively. Note that the high water contents and low densities are clearly associated with the peaty muds. The relative density of the materials varies over a wide range, which is similar to the range observed in the Yukon Delta region (Fig. 2) as indicated by watery-appearing zones and the wide variations in strength. The vibracore penetration resistance appears to correlate in general with the strength data, although not below 3 m depth at station 78-4. Low penetration resistance is associated with very high gas contents in the profile at station 78-3 and above 3 m in the profile at station 78-4. However, the increase in penetration resistance below 3 m at station 78-4, and the low penetration resistance at station 78-5 are not associated with changes in, or high values of, gas contents, respectively.

East-central Norton Sound

In east-central Norton Sound (Fig. 4) four of the five profiles (stations 78-6, 78-9, 76-121, 76-125) penetrate thin deposits of Holocene silty fine sand and sandy silt and extend into the underlying Pleistocene deposits which

include freshwater peaty mud. The profile at station 78-10 appears to penetrate only the Holocene material. Compared with the west-central Norton Sound and Yukon Delta regions (Figs. 2 and 3), these profiles show similar materials with relative densities that are low near the surface, but that increase much more rapidly with depth. In fact, the Alpine vibratory corer was unable to penetrate deeper than about 3 m in this region. The rapid increase in penetration resistance with depth occurs in both Holocene and Pleistocene materials, even though their gas contents are similar to those in weaker materials at other locations such as in the station 78-5 profile in west-central Norton Sound (Fig. 3).

Eastern Norton Sound and the Port Clarence embayment

The profiles from eastern Norton Sound, near Stuart Island, and from the Port Clarence embayment (Fig. 5) penetrate materials that are generally finer grained and have relatively high moisture contents, high plasticity, low density, low strength, and low penetration resistance compared with the materials in the regions previously discussed. The characteristics of these profiles (Fig. 5) appear to be associated with their low-energy environments. Station 78-21 is located in Port Clarence, the most protected environment in the region. The materials in this profile have substantially higher water contents (~90 percent) and lower strengths (~10 kPa) than other materials encountered in the northern Bering Sea. The very low strengths and their uniformity with depth suggest the Holocene materials in Port Clarence may be somewhat underconsolidated; i.e., not yet in equilibrium with the weight of the material.

Sand-wave fields near Port Clarence

Four profiles in the sand-wave fields near Port Clarence in the Chirikov Basin are shown in Fig. 6. Stations 78-14 and 78-16 are located on one sand-

wave crest, and the profiles penetrate medium sand that appears to be the basal transgressive deposit described by Nelson (this volume, Fig. 6). Station 78-15 is located in the adjacent sand-wave trough to the east, and penetrates the Pleistocene peaty mud that underlies the basal transgressive deposits in the region. The profile at station 78-17 is located on the adjacent sand-wave crest to the east. It penetrates the basal transgressive sand to a depth of about 1.5 m and the Pleistocene peaty mud from 1.5 to 2.2 m. The materials from 2.5 to 3.5 m are poorly to moderately sorted medium to fine sand with abundant pebbles and some silt- and clay-sized material. Below a sharp contact at 3.5 m the material appears to be glacial till consisting of a firm muddy sand with scattered pebbles.

The relative density of the basal transgressive sand is low near the surface but increases rapidly with depth, as indicated by the strength and penetration resistance data in the profiles for stations 78-14 and 78-16. The peaty mud at stations 78-15 and 78-17 is comparatively weak and has a very wide range of water contents due to the intermittent distribution and variable character of the peaty material. At station 78-17 the sand beneath the peaty mud appear to be firm and dense with a moderate to high resistance to vibracore penetration.

Consolidation and static triaxial data

Consolidation data (Fig. 7) on three box core samples of Holocene sediment show a wide range in the initial void ratio and compressibility of materials from the Yukon Delta and central regions of Norton Sound (Fig. 1; stations 76-154, 76-156). The wide range in these properties is consistent with the high variability in the strength and penetration resistance of these materials as shown in Figs. 2, 3, and 4. The compressibilities of the samples from station 76-156 may be high compared with other materials in these

regions, because this station is located near vibracore station 78-24, whose profile (Fig. 2) shows a very loose and weak zone at the surface.

Triaxial data on vibracore samples of Holocene Yukon sediment from stations 78-22 and 78-23 (Fig. 8) show moderate to high static strengths with friction angles in the range of 35° to 40° . The variation in friction angle is small for the samples from station 78-22, consistent with the small variations in texture and density among the samples. The wider variation in friction angle for the samples from station 78-23 appears to be associated with variations in both the texture and density of the samples tested.

Soils that tend to contract during shear (contractive) weaken and may liquefy during cyclic loading from earthquakes and ocean waves (Sangrey, et al., 1978). The stress paths in Fig. 8 show the materials tested are generally contractive at low deviator stress levels and become dilative (tend to dilate during shear) as they approach the yield surface. Moreover, with the exception of the sample from 2.34 m depth at station 78-22, the stress paths become less contractive and more dilative at decreasing initial volumetric stress levels. This behavior pattern is normal for homogeneous material. The in situ stresses at the depths from which the samples were obtained are on the order of 10 kPa to 30 kPa. These stresses are very low compared to the initial volumetric stresses used to obtain the data in Fig. 8. Therefore, the behavior of the materials in situ should be less contractive and more dilative than that shown by the stress paths in Fig. 8.

The stress path for the sample from 2.34 m depth at station 78-22 (Fig. 8) is of particular interest in that it shows this sample is more contractive at low stress levels than any of the samples tested. This behavior is consistent with the data in Fig. 2 which shows this sample represents the loosest zone in the profiles at stations 78-22 and 78-23. Thus

the data indicate that loose zones within the Holocene Yukon sediment are of the most concern with regard to strength loss and liquefaction during cyclic loading from earthquakes and ocean waves. Work in progress is aimed at defining the potential for strength loss in these materials on a more quantitative basis (Clukey, Cacchione, and Nelson, 1980).

Discussion of potential hazards

Potential hazards associated with the geotechnical characteristics of bottom sediment in the northern Bering Sea include the liquefaction of bottom sediments in response to ocean waves, earthquakes, and the upward migration of gas from thermogenic and biogenic sources; the scour and transport of bottom sediments and mobile bed forms in response to bottom currents; low strength and high compressibility of materials in low relative density and consolidation states; and gas-charged sediment.

Liquefaction is of particular concern in central and western Norton Sound because the area is exposed to strong cyclic loading from storm waves and is underlain by gas-charged material. Moreover, the susceptibility of the Holocene Yukon sediment in these regions to liquefaction is suggested by its dominantly silty fine sand and sandy silt texture and by the occurrence of relatively loose zones within it (Figs. 2, 3, 4). In addition, historic occurrences of wave-induced liquefaction are suggested by evidence of widespread storm-sand layers and scour depressions in the vicinity of the Yukon Delta (Nelson this volume; Larsen et al., 1979).

Work in progress is aimed at assessing on a quantitative basis the susceptibility of the Holocene Yukon sediment to liquefaction during storm waves. The approach involves the measurement of storm waves to define the cyclic bottom stresses induced during major storms; laboratory cyclic shear tests on Yukon Prodelta materials to determine the dynamic properties that

govern the rate of pore pressure increase and associated degradation of strength during cyclic loading; and analyses of these measurements with a finite-element model that takes into account both the buildup of pore pressure induced by cyclic loading and the concomitant dissipation of pore pressure that is governed by the permeability of the material.

Preliminary analyses have been completed (Clukey et al., 1980) for a semi-infinite half-space model of the Yukon prodelta using dynamic property and permeability data estimated from the geotechnical characteristics reported in this paper together with 3-m and 6-m sinusoidal surface waves. The 3-m wave represents worst-case conditions for a storm recorded in July 1977, and the 6-m wave corresponds to a 1-percent occurrence interval for storms in September and October (Arctic Environmental Information and Data Center, 1977). The results indicate the prodelta will not liquefy in response to the 3-m storm wave even for the extreme case when zero dissipation of pore pressure is assumed. However, the results for the 6-m storm wave, presented in Fig. 9, indicate the sediment will liquefy to a depth of approximately 3.5 m. The results in Fig. 9 further indicate that the depth of liquefaction varies with storm duration but does not increase significantly for durations greater than 1 hour. This relation is suggested by the 4-m pore pressure contour, which is increasing at a very slow rate at the end of the 1-hour storm assumed in the analysis.

Materials with low strength and high compressibility are present in eastern Norton Sound and the Port Clarence embayment. Comparison of Fig. 5 with Figs. 2, 3, and 4 shows that these materials are substantially finer grained and weaker than those in central and western Norton Sound. Because eastern Norton Sound and the Port Clarence embayment are protected from strong bottom currents and large waves, deposition has taken place in a low energy

environment. Also the materials have not been subjected to cyclic shear stresses associated with large waves, which have probably densified much of the sediment in other parts of the northern Bering Sea. The organic sandy clayey silt in the Port Clarence embayment is particularly weak and highly compressible because the very low strengths indicate the material may be somewhat underconsolidated.

Scour and transport of bottom sediment depend on the drag associated with bottom currents and the strength of the bottom sediment. Bottom currents are strong in central and western Norton Sound (Table 1). The bottom sediment is loose and weak at some locations in these regions (Figs. 2, 3, 4) and also in the sand waves near Port Clarence in Chirikov Basin (Fig. 6). In addition, the bottom sediment in central and western Norton Sound appear to be susceptible to liquefaction during major storms. These conditions are consistent with evidence of scour depressions in the vicinity of the Yukon Delta and also evidence for the large-scale transport and modification of sand waves near Port Clarence in the Chirikov Basin (Nelson, this volume; Larsen et al., 1979; Larsen et al., 1980).

The importance of gas in sediment depends on whether it is present in the bubble phase and whether the amount present is sufficient to cause significantly elevated pore fluid pressures. Elevated pore pressures can induce liquefaction in overlying materials, and they are associated with reductions in the strength of sediment in situ (Sangrey, 1977).

Seismic and core studies in Norton Sound suggest bubble phase gas is present in the anomaly associated with the thermogenic gas seep south of Nome and at several other locations where biogenic gas is being generated in the Pleistocene peaty mud beneath the Holocene silt (Kvenvolden et al., 1979a;

Holmes and Thor this volume; Kvenvolden et al., 1980; Nelson et al., 1978; Nelson et al., 1979).

Previous work that suggests bubble phase gas may be causing elevated pore pressures in situ includes: limited data showing an association of low vibracore sample penetration resistance with very high gas contents (Nelson et al., 1978); and studies of shallow craters on the bottom of east-central Norton Sound which attribute their origin to episodic venting of biogenic gas generated in the Pleistocene peaty mud and trapped by the overlying Holocene Yukon sediment (Nelson et al., 1979).

The geotechnical profiles in this paper (Figs. 2-6) show additional data concerning the association of vibracore penetration resistance and gas contents. Low penetration resistance is associated with very high gas contents in some of the profiles (see stations 78-3, 78-4, 78-8, and 78-15), but not in general as noted in the section on geotechnical profiles above. For example, the penetration resistance at station 78-5 is about the same as that at station 78-3 even though the gas contents in the two profiles differ substantially.

However, the lack of consistent correlations between gas content and penetration resistance in all the profiles does not eliminate the possibility that gas is causing elevated pore pressures in situ. The relative density or consolidation state of the materials also influences the penetration resistance and may be masking the effects of gas. In this regard the association of the shear strength and penetration resistance data in the profiles is of interest because both measurements are influenced by the relative density or consolidation state, but only the penetration resistance is influenced by in situ elevated pore pressures. The strength data were obtained from samples on shipboard and in the laboratory where elevated pore

pressures would have easily dissipated prior to the measurements.

The importance of the relative density or consolidation state of the material on penetration resistance is clearly evident in the geotechnical profiles from eastern Norton Sound and the Port Clarence embayment (Fig. 5). As noted in the discussion above very low strengths occur because these locations are not exposed to significant ice loading and waves that can densify and consolidate sediment. The penetration resistance is correspondingly low, it varies with the shear strength, and it does not appear to be influenced by variations in gas content. Similarly, in the profiles from the Yukon Delta region (Fig. 2), the penetration resistance is more closely associated with relative density, as indicated by the strength data, than with the gas content.

Hence the question remains whether significant elevated pore pressures associated with biogenic and thermogenic gas exist in the bottom sediment of the northern Bering Sea. Additional work is needed to determine the magnitudes of in situ pore pressures and their regional distribution.

Acknowledgments

The cruises for this study were supported jointly by the U.S. Geological Survey and the U.S. Bureau of Land Management through an interagency agreement with the U.S. National Oceanic and Atmospheric Administration, under which a multiyear program responding to the needs of petroleum development of the Alaska continental shelf is managed by the Outer Continental Shelf Environmental Assessment Program (OCSEAP) Office.

References

- American Society for Testing and Materials (1977) Annual Book of ASTM Standards: Part 19, Philadelphia.
- Arctic Environmental Information and Data Center, University of Alaska, Anchorage, and National Climatic Center, Environmental Data Service, NOAA, Asheville, North Carolina, (1977) Climatic Atlas of the Outer Continental Shelf waters and coastal regions of Alaska, vol. 2, Bering Sea.
- Bishop, A. W., and Henkel, D. J. (1962) The measurement of soil properties in the triaxial test, 2d ed. Edward Arnold (Publishers) Ltd., London.
- Cline, J. D., and Holmes, M. L. (1977) Submarine seepage of natural gas in Norton Sound, Alaska. Science, 198, 1149-1153.
- Clukey, E. C., Cacchione, D. A., and Nelson, C. H. (1980) Liquefaction of Yukon Prodelta. Offshore Technology Conference Proceedings, Paper 3773.
- Clukey, E. C., Nelson, H., and Newby, J. E. (1978) Geotechnical properties of Northern Bering Sea sediment. U.S. Geological Survey Open-File Report 78-408.
- Drake, D. E., Cacchione, D. A., Meunch, R. D., and Nelson, C. H. (1980) Sediment transport in Norton Sound, Alaska. Marine Geology (in press).
- Duprè, W. R., and Thompson, R. (1979) A model for deltaic sedimentation in an ice-dominated environment. Offshore Technology Conference Proceedings, Paper 3434, 2, 657-661.
- Hopkins, D. M. (1975) Time-stratigraphic nomenclature for the Holocene Epoch. Geology, 3, 10.

- Kvenvolden, K. A., Nelson, C. H., Thor, D. R., Larsen, M. C., Redden, G. D., Rapp, J. B., and DesMarais, D. J. (1979a) Biogenic and thermogenic gas in gas-charged sediment of Norton Sound, Alaska. Offshore Technology Conference Proceedings, Paper 3412, 1, 479-483.
- Kvenvolden, K. A., Redden, G. D., Thor, D. R., and Nelson, C. H. (1980) Hydrocarbon gases in near-surface sediment of northern Bering Sea (Norton Sound and Chirikov Basin). In: Hood, D. W., editor, The Eastern Bering Sea Shelf, Chapter 19: Oceanography and Resources (in press).
- Kvenvolden, K. A., Weliky, K., Nelson, C. H., and DesMarais, D. J. (1979b) Submarine seep of carbon dioxide in Norton Sound, Alaska. Science, 205, 1264-1266.
- Larsen, B. R., Nelson, C. H., Larsen, M. C., Thor, D. R., Olsen, H. W., Clukey, E. C., and Esterlee, J. S. (1980) Physical properties of Norton Basin sediment. U.S. Geological Survey Open-File Report (in press).
- Larsen, M. C., Nelson, H., and Thor, D. R. (1979) Geologic implications and potential hazards of scour depressions on Bering Shelf, Alaska. Environmental Geology, 3, 39-47.
- Larsen, M. C., Nelson, C. H., and Thor, D. R. (1980) Sedimentary processes and potential geologic hazards of Norton Basin sea floor. In: Hood, D. W., ed., The Eastern Bering Sea Shelf, Chapter 19: Oceanography and Resources (in press).
- McManus, D. A., Hopkins, D. M., and Nelson, C. H. (1977) Distribution of bottom sediments on the continental shelf, northern Bering Sea. U.S. Geological Survey Professional Paper 759-C.
- Nelson, H., and Creager, J. S. (1977) Displacement of Yukon derived sediment from Bering Sea to Chukchi Sea during Holocene time. Geology, 5, 141-146.

- Nelson, H., Kvenvolden, K. A., and Clukey, E. C. (1978) Thermogenic gases in near-surface sediments of Norton Sound, Alaska, 10th Offshore Technology Conference Proceedings, Paper 3354, 3, 2623-2633.
- Nelson, C. H., Thor, D. R., Sandstrom, M. W., and Kvenvolden, K. A. (1979) Modern biogenic gas-generated craters (sea-floor "pockmarks") on the Bering Shelf, Alaska. Geological Society of America Bulletin, 90, 1144-1152.
- Sangrey, D. A. (1977) Marine Geotechnology--State-of-the-Art. Marine Geotechnology, 2, 45-80.
- Sangrey, D. A., Bouma, A. H., Hampton, M. A., Carlson, P. R., Molnia, B. F., Clukey, E. C., Nelson, C. H., and Olsen, H. W. (1979) Geotechnical engineering characteristics of the outer continental shelf lease areas in Alaska, Proceedings. 5th International Conference on Port and Ocean Engineering Under Arctic Conditions, August 13-18, 1979, 2, 963-976.
- Sangrey, D. A., Castro, G., Poulos, S. J., and France, J. W. (1978) Cyclic loading of sands, silts, and clays. Proceedings of the ASCE Geotechnical Engineering Division Specialty Conference on Earthquake Engineering and Soil Dynamics, 11, 836-851.
- Thor, D. R., and Nelson, C. H. (1979) A summary of interacting surficial geologic processes and potential geologic hazards in the Norton Basin, northern Bering Sea. Offshore Technology Conference Proceedings, Paper 3400, 377-381.
- Wissa, A. E. Z., Christian, J. T., Davis, E. H., and Heiberg, S. (1971) Consolidation at constant rate of strain. American Society of Civil Engineers, Journal of Soil Mechanics and Foundation Engineering, 97, SM 10, 1393-1412.

Figure Captions

1. Location map of northern Bering Sea showing regions and sampling stations cited in this paper.
2. Geotechnical profiles from the Yukon Prodelta.
3. Geotechnical profiles from west-central Norton Sound. Stations 78-1, 78-2, and 78-3 are in the thermogenic gas seep acoustic anomaly south of Nome. Station 78-4 is on a nearby biogenic gas acoustic anomaly. Station 78-5 is adjacent to the biogenic gas acoustic anomaly.
4. Geotechnical profiles from east-central Norton Sound where shallow gas craters are associated with thin deposits of Holocene Yukon silt overlying Pleistocene freshwater peaty mud.
5. Geotechnical profiles from eastern Norton Sound, including Stuart Island (78-8), and the Port Clarence embayment (78-21).
6. Geotechnical profiles from the sand-wave fields near Port Clarence in the Chirikov Basin. Stations 78-14 and 78-16 are located on one sand-wave crest. Station 78-17 is located on the adjacent sand-wave crest. Station 78-15 is in the trough between these sand-wave crests.
7. Consolidation data on samples of Holocene Yukon silt from box cores in the vicinity of the Yukon Delta and central Norton Sound. (See Fig. 1.) Box core station 78-156 is adjacent to vibracore station 78-24 whose geotechnical profile is shown in Fig. 2. w = moisture content in percent dry soil weight; γ_t = bulk density in g/cm³; C_c = compression index. Tests run according to procedures described by the American Society for Testing and Materials (1977) and Wissa et al. (1971).

8. Consolidated-undrained triaxial data on samples of Holocene Yukon silt from Alpine vibracores at stations 78-22 and 78-23 near the Yukon prodelta (see Fig. 2). ϕ' = effective friction angle. σ_1 and σ_3 are the total vertical and horizontal stresses, respectively. σ_1' and σ_3' are the effective vertical and horizontal stresses, respectively. w and γ_t are defined in the caption for Fig. 7. d_{50} and $<2\mu$ are the median grain size and minus 2 micron fraction, respectively. Tests run according to procedures described by Bishop and Henkel (1962).
9. Results of preliminary analyses of wave-induced liquefaction potential of Holocene Yukon silt near the Yukon prodelta, assuming a wave height of 6 m, a period of 10 seconds, a relative density of 54 percent, and a coefficient of permeability of 1.50×10^{-6} cm/s. U/σ = ratio of pore pressure to total overburden stress. The figure shows the variation of pore pressure ratio with time at depths below the sediment surface ranging from 0.25 m to 6 m.

Table 1.--Geologic and environmental framework for geotechnical studies in the northern Bering Sea

Region	Geologic units	Origin	Gas	Environmental Loading		
				Waves	Bottom currents	Ice
Yukon prodelta.	Holocene silty fine sand and sandy silt with interbedded storm sand layers less than 20 m thick.	Yukon River. High energy deposition and redeposition.	Biogenic	High	Strong	Extensive
West-central Norton Sound.	Holocene silty fine sand and sandy silt, bioturbated, 1-2 m thick, over	Yukon River. Medium energy deposition,	Thermogenic and biogenic	Medium to strong	Medium to strong	Low
	Pleistocene freshwater peaty mud.	Freshwater deposition; tundra-derived peat; subaerial desiccation.				
East-central Norton Sound.	Holocene silty fine sand and sandy silt, bioturbated, 1-2 m thick, over	Yukon River. Medium energy deposition,	Biogenic	Medium	Medium	Low
	Pleistocene freshwater peaty mud.	Freshwater deposition; tundra-derived peat; subaerial desiccation.				
Eastern Norton Sound and Port Clarence Embayment.	Holocene sandy clayey silt, over	Yukon River and streams discharging from nearby shorelines. Low energy. deposition.	Biogenic	Low	Low	Low
	Pleistocene freshwater peaty mud and (or) glacial till.	Origin of Pleistocene peaty mud, same as above.				
Sand-wave fields near Port Clarence in Chirikov Basin	Late Pleistocene transgressive sands, over	Sand derived from pre-Quaternary bedrock and glacial moraines.	Biogenic	High	Very strong	Low
	Pleistocene freshwater peaty mud and (or) glacial till.	Origin of Pleistocene peaty mud, same as above.				

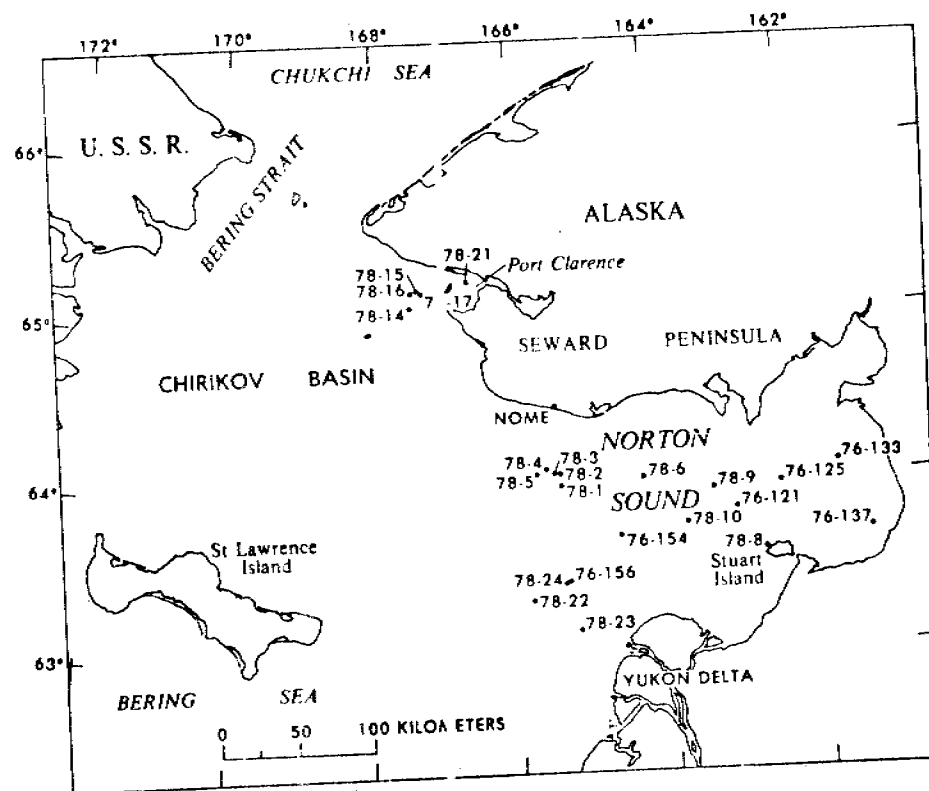


Fig. 1 - Location map of northern Bering Sea showing regions and sampling stations cited in this paper.

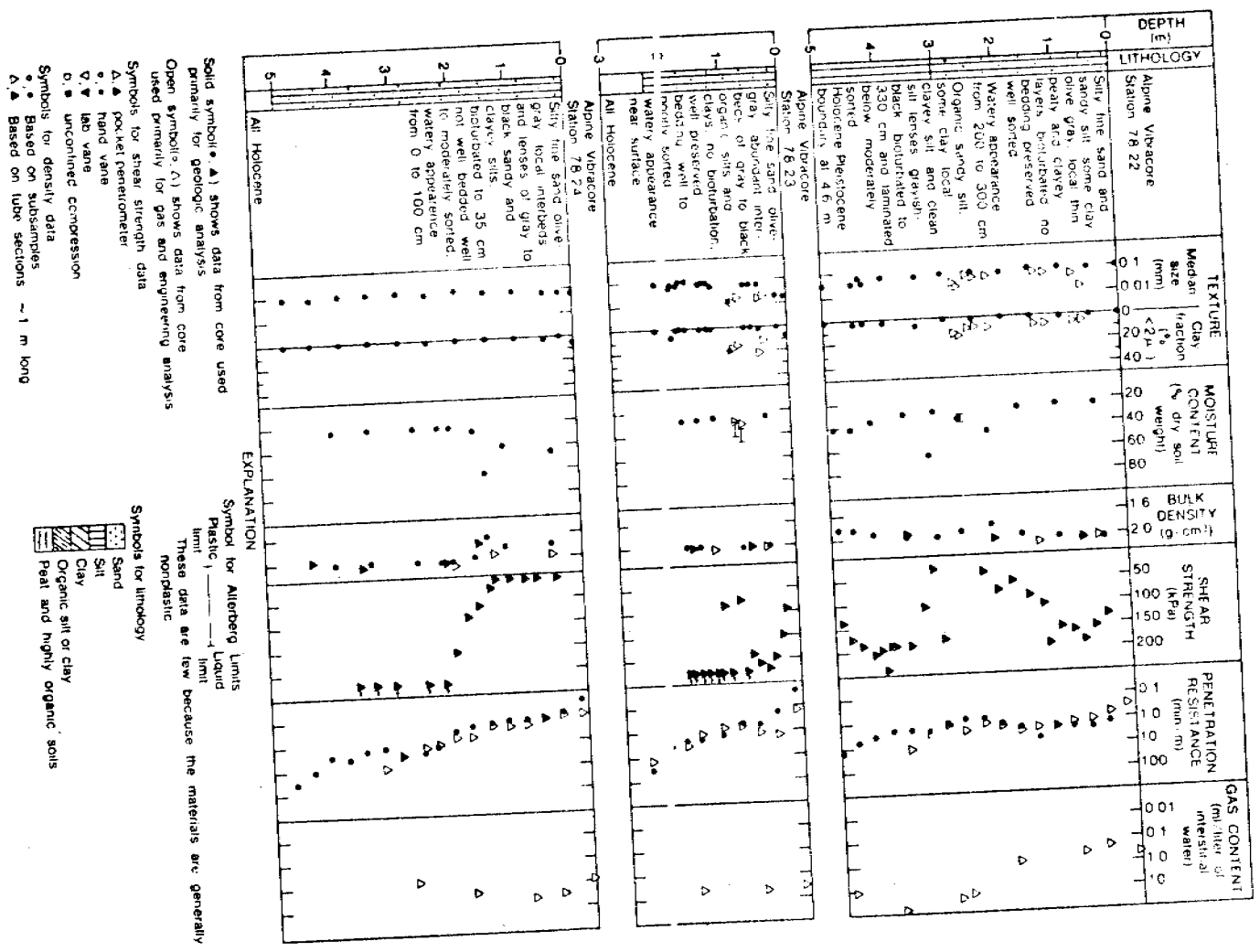


Fig. 2 - Geotechnical profiles from the Yukon Prodelta.

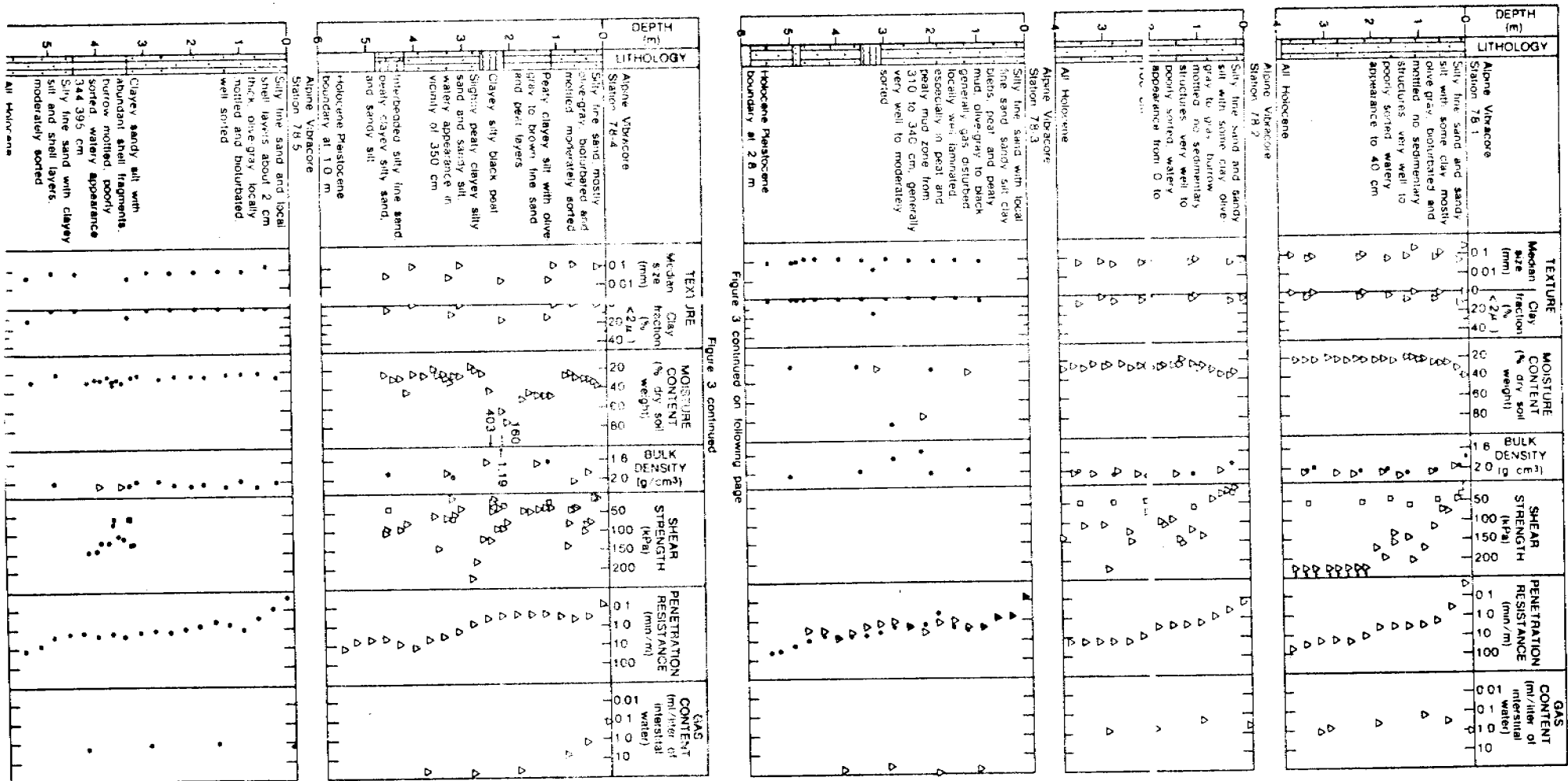


Figure 3 continued on following page

Fig. 3 - Geotechnical profiles from west-central Norton Sound. Stations 78-1, 78-2, and 78-3 are in the thermogenic gas seep acoustic anomaly south of Nome. Station 78-4 is on a nearby biogenic gas acoustic anomaly. Station 78-5 is adjacent to the biogenic gas acoustic anomaly.

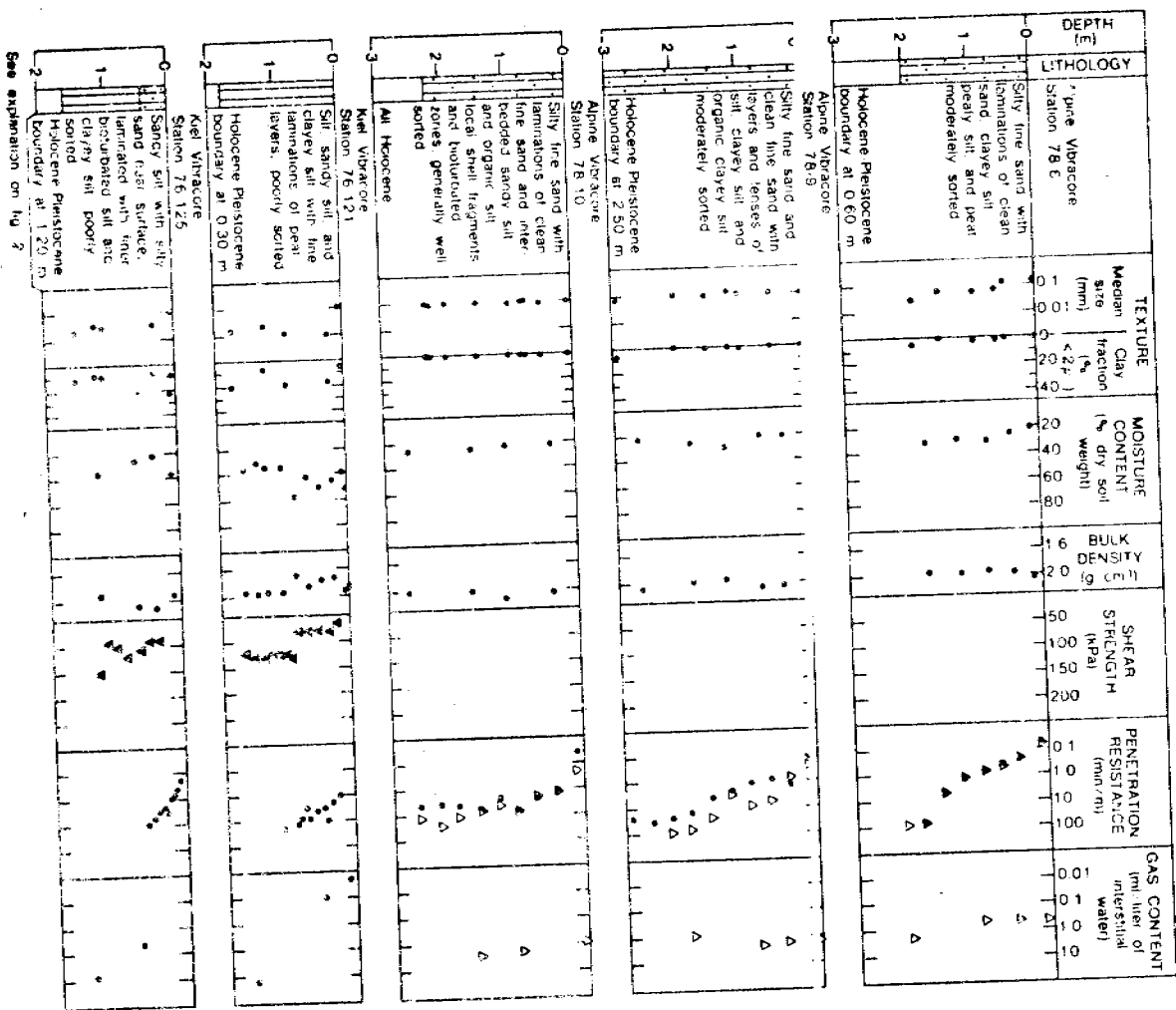
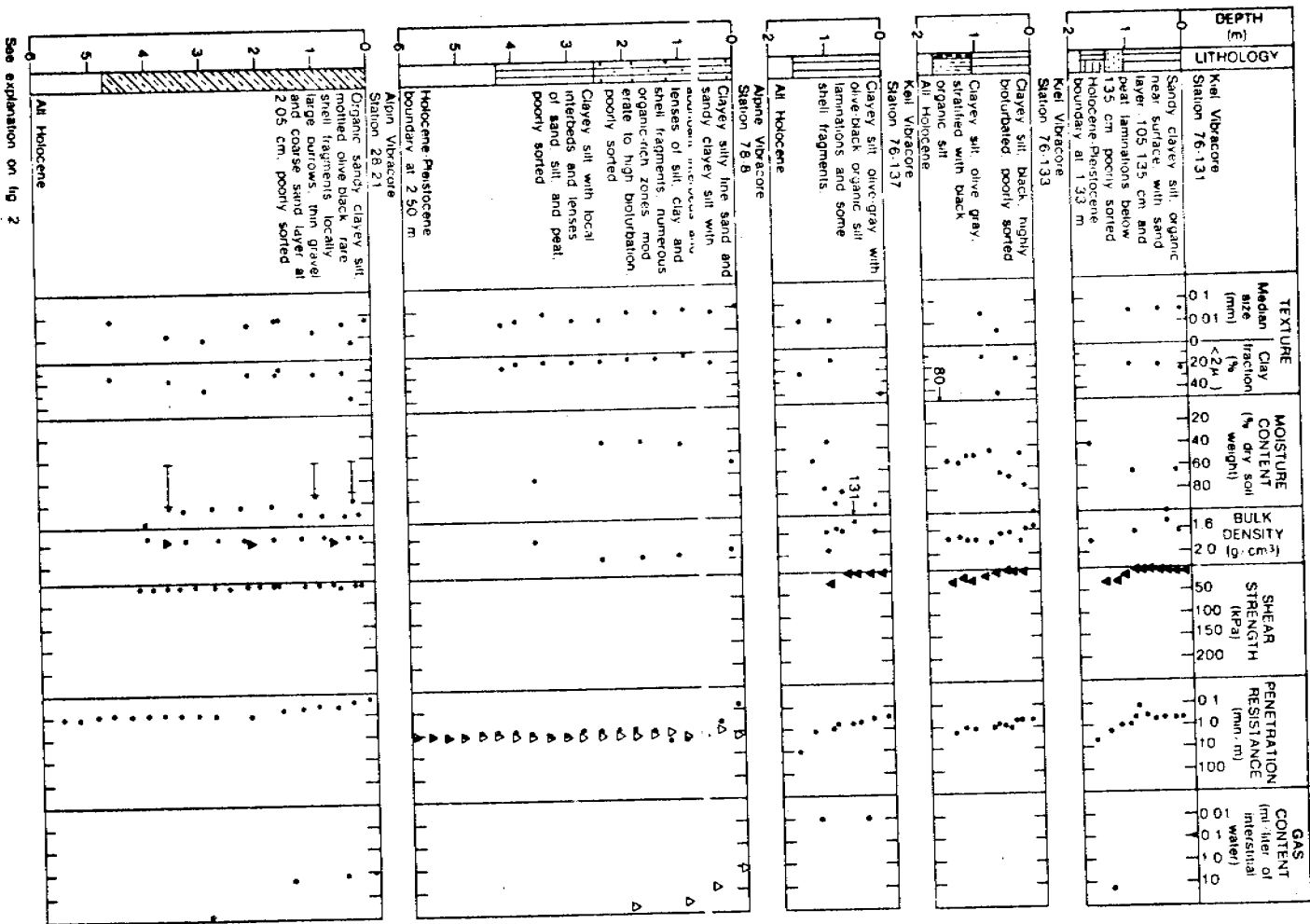


Fig. 4 - Geotechnical profiles from east-central Norton Sound where shallow gas craters are associated with thin deposits of Holocene Yukon silt overlying Pleistocene freshwater peaty mud.



See explanation on fig 2

Fig. 5 - Geotechnical profiles from eastern Norton Sound, including Stuart Island (78-8), and the Port Clarence embayment (78-21).

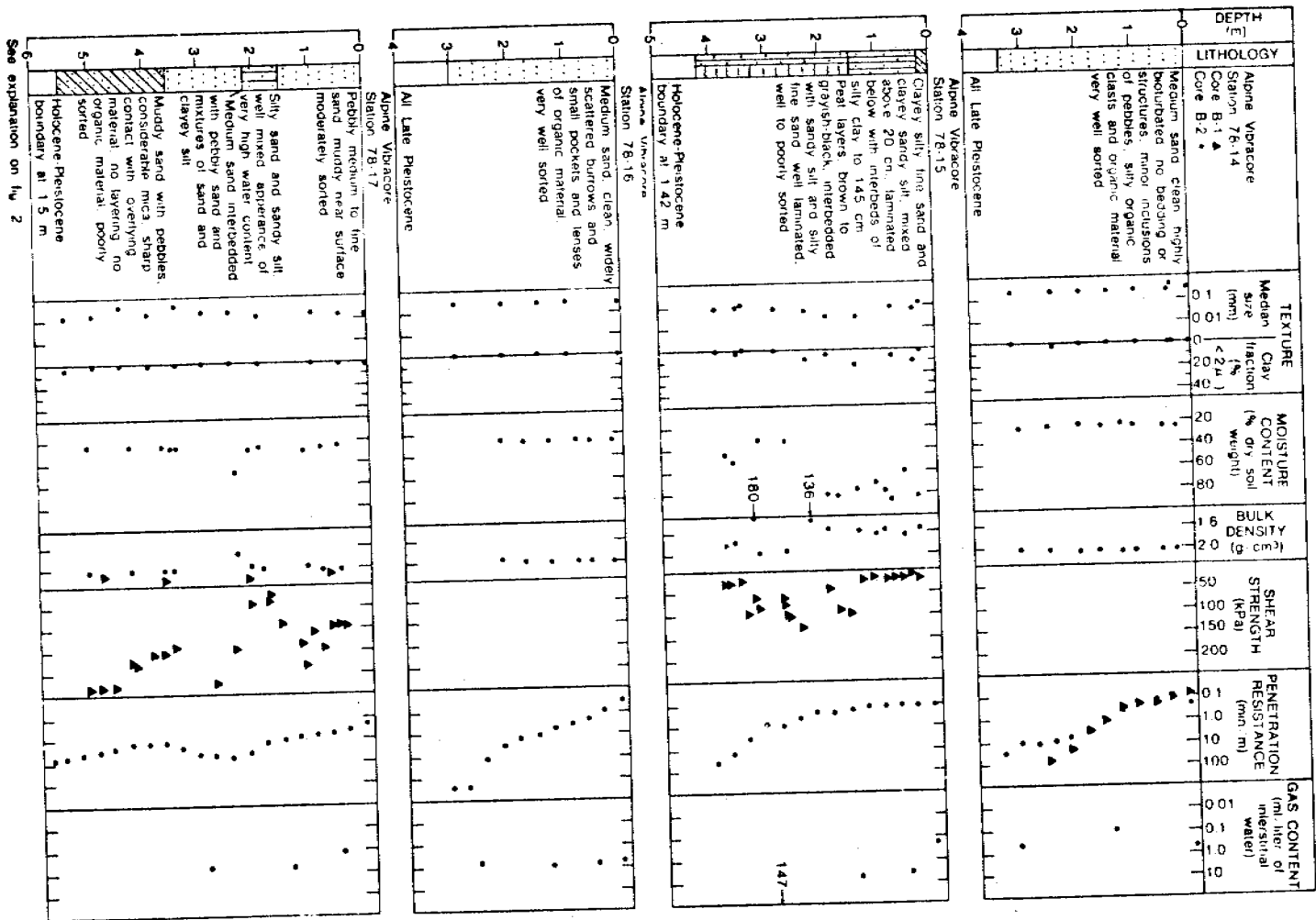


Fig. 6 - Geotechnical profiles from the sand-wave fields near Port Clarence in the Chirikov Basin. Stations 78-14 and 78-16 are located on one sand-wave crest. Station 78-17 is located on the adjacent sand-wave crest. Station 78-15 is in the trough between these sand-wave crests.

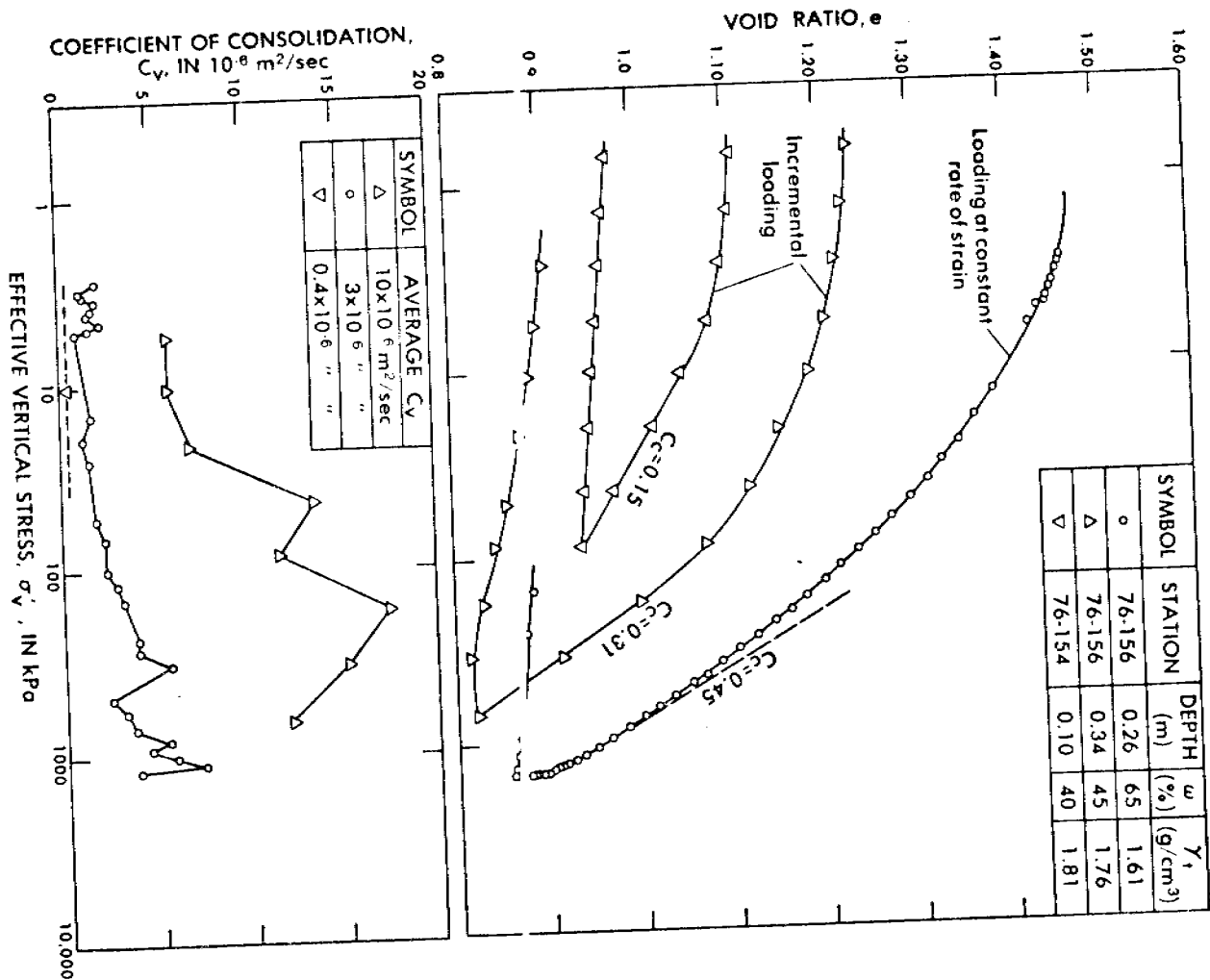


Fig. 7 - Consolidation data on samples of Holocene Yukon silt from box cores in the vicinity of the Yukon Delta and central Norton Sound. (See Fig. 1.) Box core station 78-156 is adjacent to vibrocore station 78-28 whose geotechnical profile is shown in Fig. 2. w = moisture content in percent dry soil weight; γ_+ = bulk density in g/cm^3 ; C_c = compression index. Tests run according to procedures described by the American Society for Testing and Materials (1977) and Wissa et al. (1971).

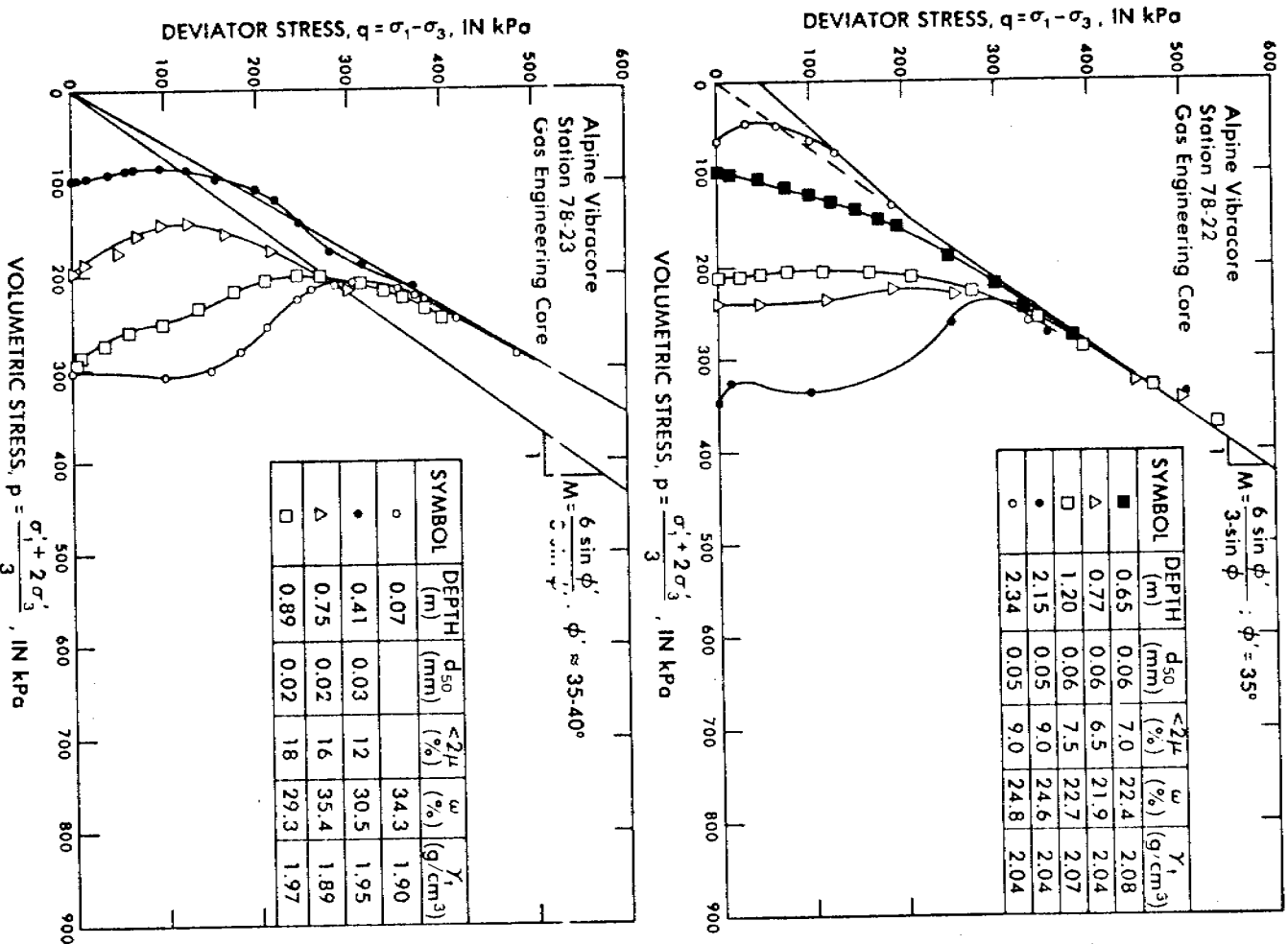


Fig. 8 - Consolidated-undrained triaxial data on samples of Holocene Yukon silt from Alpine vibracores at stations 78-22 and 78-23 near the Yukon prodelta (see Fig. 2). ϕ' = effective friction angle. σ_1 and σ_3 are the total vertical and horizontal stresses, respectively. σ_1' and σ_3' are the effective vertical and horizontal stresses, respectively. ω and γ_t are defined in the caption for Fig. 7. d_{50} and $<2\mu$ are the median grain size and minus 2 micron fraction, respectively. Tests run according to procedures described by Bishop and Henkel (1962).

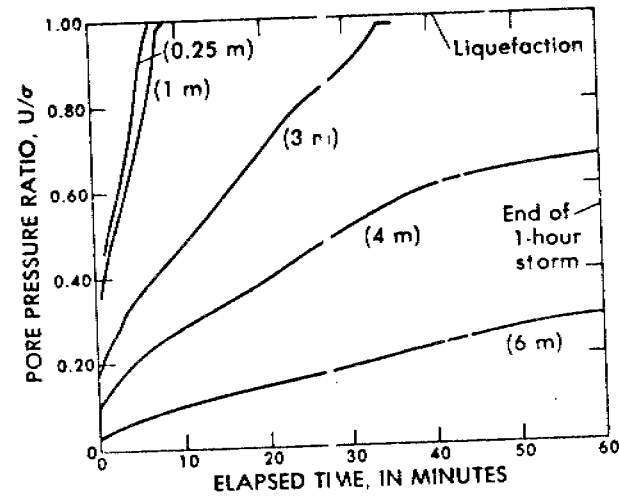


Fig. 9 - Results of preliminary analyses of wave-induced liquefaction potential of Holocene Yukon silt near the Yukon prodelta, assuming a wave height of 6 m, a period of 10 seconds, a relative density of 54 percent, and a coefficient of permeability of 1.50×10^{-6} cm/s. U/σ = ratio of pore pressure to total overburden stress. The figure shows the variation of pore pressure ratio with time at depths below the sediment surface ranging from 0.25 m to 6 m.

REPORT ON SURFACE AND SUBSURFACE FAULTING IN NORTON SOUND AND
CHIRIKOV BASIN, ALASKA

By

Janice L. Johnson and Mark L. Holmes

SUMMARY

Seismic reflection data were obtained in July 1977 by the U. S. Geological Survey aboard R/V SEA SOUNDER along 2800 km of track in Norton Sound and northeastern Chirikov basin. These data and records from several previous surveys were analyzed in order to determine the location, extent, and possible age and activity potential of offshore faulting. Acoustic reflection records were obtained using sparkers (160 and 0.8 kilojoule), Uniboom (1200 joule), and 3.5 kHz subbottom profiler. Sidescan sonar measurements were made along some of the tracklines whenever the large sparker was not deployed.

Maps showing the distribution of surface, near-surface, and deeper subbottom faults show that faulting occurs most commonly within 50 km of the margins of Norton basin, the deep sedimentary trough which underlies Norton Sound and Chirikov basin. A smaller number of faults were detected in the central regions of the basin.

Surface fault scarps were seen in several places in northern Chirikov basin. These sea-floor offsets ranged in height from 5 to 15 m along several west-trending faults which may be associated with some of the major transcurrent faults in Alaska. The existence of these scarps

indicates possible disturbance of sedimentary deposits over the fault, although the scarps may have been maintained by non-deposition. Evidence from both onshore and offshore field studies indicate that movement along these faults may have occurred between 12,000-120,000 years ago.

Many northwest-trending faults were mapped around the margins and in the central regions of Norton basin; they appear to show increasing displacement with depth and a thickening of the strata as they dip basinward away from the fault. These characteristics indicate a more or less continual movement along the faults as Norton basin was subsiding. The lack of recorded earthquakes in Norton basin during historical time implies that either activity along the offshore faults has ceased, or that movement is taking place at a slow but steady rate, preventing a buildup of strain and consequent earthquake-producing ruptures.

The west-trending faults in northern Chirikov basin appear to offset, and therefore postdate, the northwest trending faults which parallel the Norton basin axis. These two intersecting trends may have resulted from a change in the direction of regional compression during late Tertiary or early Quaternary time.

Considerable sea-floor relief hampered identification of surface scarps associated with offshore faults near St. Lawrence Island; and horizontal (transcurrent) motions along these faults may have taken place during Quaternary time in conjunction with movements on the Kaltag Fault which displaced Pleistocene deposits in western Alaska.

CONTENTS

	Page
INTRODUCTION-----	423
METHODS-----	425
Navigation-----	425
Acoustic Survey Techniques-----	426
Sparker-----	426
Uniboom-----	427
Bathymetry/Subbottom Profiler-----	428
Sidescan Sonar-----	428
GEOLOGIC SETTING-----	429
Tectonic Framework-----	429
Regional Geology-----	430
Norton Basin-----	430
Acoustic Basement-----	432
RESULTS AND DISCUSSION-----	432
Observed Faults and Structures-----	432
Fault Activity and Hazard Potential-----	435
CONCLUSIONS-----	438
REFERENCES-----	440

INTRODUCTION

Geological and geophysical studies were carried out by U. S. Geological Survey personnel aboard R/V SEA SOUNDER in Norton Sound and Chirikov basin during July 1977 (Fig. B1). Acoustic survey systems used included 160 and 0.8 kilojoule sparkers, a 1200 joule (four transducer) Uniboom, a 3.5 kHz bathymetric/subbottom profiling system, and sidescan sonar. This section of the annual report deals primarily with an interpretation of the extent and hazard potential of the surface and subsurface faults shown on the sparker and Uniboom records. Discussions of the 3.5 kHz and sidescan sonar data will be found in other sections.

The geophysical data obtained on this recent USGS cruise has been supplemented in places by seismic reflection information which was collected on previous expeditions by the USGS, NOAA, and the University of Washington (Fig. B1). In 1967 a joint USGS/University of Washington cruise obtained 4200 km of 150 joule sparker data (Grim and McManus, 1970), and 3200 km of 120 kilojoule sparker records (Schoil and Hopkins, 1969). High-resolution seismic reflection surveys were conducted in 1967 in the nearshore region south of Nome between Sledge Island and Cape Nome (Tagg and Greene, 1973). Walton et al. (1969) shot 3840 km of single channel 40 in³ air gun records during a joint USGS/NOAA (then ESSA) survey in 1969, and that same year an additional 800 km of 150 joule sparker records were collected in Chirikov basin on a joint USGS/University of Washington cruise. Johnson and Holmes (1977) reported on preliminary results of a study of recent faulting in the northern Bering Sea, based primarily on examination of approximately 3000 km of seismic reflection data collected aboard R/V SEA SOUNDER in September and October 1976. Holmes

et al. (1978) obtained an additional 675 km of single channel air gun reflection data and 13 refraction profiles in Norton Sound during a survey conducted by the USGS aboard R/V LEE in October 1977.

All seismic records, sidescan records, and navigational data from the 1976 and 1977 R/V SEA SOUNDER cruises are on microfilm. Copies can be obtained from the National Geophysical and Solar-Terrestrial Data Center, EDS/NOAA, Boulder, Colorado 80302, or from the Alaska Technical Data Unit, USGS, 345 Middlefield Road, Menlo Park, California 94025.

METHODS

This section discusses the instrumentation and procedures used in collecting navigation and acoustic survey data on the R/V SEA SOUNDER cruise in July 1977.

Navigation

Navigational information was obtained by two independent systems. A Magnavox satellite navigator with integrated Teledyne Loran C received inputs from the ship's speed log and gyro. This system computed dead reckoning positions every two seconds and the data were stored on magnetic tape and a teleprinter. Performance of the system was degraded somewhat by proximity to the Loran C master station at Port Clarence and the high elevation of many of the satellites during transit.

A Motorola mini-Ranger system was used to obtain fixes every seven and one-half minutes which were recorded on paper tape in digital form. This system measures the range to two or more shore-based transponders which were maintained by survey personnel on land. On a few occasions the included angle between the transponders was too small to permit obtaining reliable fix information.

Fixes were plotted at least every fifteen minutes on the navigational charts with appropriate notations made at the time of major course and speed changes. Radar and line-of-sight bearings were sometimes used to augment the other navigational information, and navigational accuracy probably averaged ± 150 m.

Acoustic Survey Techniques

Figure B1 shows the tracklines for the 1977 R/V SEA SOUNDER cruise, as well as those of previous expeditions on which seismic reflection data were collected. The figure also notes which acoustic systems were used during the various cruises. The bathymetry-subbottom profiler and sidescan sonar systems used aboard R/V SEA SOUNDER will be briefly discussed, although interpretation of these data will be, as previously mentioned, found in other sections of the report.

Seismic profiling operations aboard R/V SEA SOUNDER were carried out at speeds ranging from 4-6 knots. It was found that speeds greater or less than this range resulted in generation of "ship noise" by the propulsion machinery which produced a significant amount of interference on the records.

Sparker. A Teledyne SSP (Seismic Section Profiler) was used to obtain 325 km of single channel seismic reflection records in Norton Sound and northeastern Chirikov basin. Power output was normally 160 kilojoules, but was reduced to 120 kilojoules at times because of equipment casualties. The signals were received by a Teledyne 100-element Hydrostreamer and processed through a Teledyne seismic amplifier before being printed off a modified Raytheon PFR (Precision Fathometer Recorder). Frequency pass band was normally set at 20-98 Hz, and sweep and fire rate was 4 seconds. The records were annotated at 30 minute intervals with date, time (GMT), line number, water depth, and appropriate instrument settings. Changes in course, speed, or instrumentation were noted when they occurred.

Maximum penetration achieved by the sparker was approximately 2.1 km. The quality of the records was affected adversely by the shallow water and the generally flat nature of the bottom and subbottom reflectors. The shallow depth caused the water bottom multiple to appear at small distances below the initial sea-floor reflection, thus partially obscuring signals from deeper reflectors. The flat subbottom layering produced intra-formational or "peg-leg" multiples which also obscured or interfered with the primary reflections. In only a few places was an acoustic basement detected; more commonly the reflection amplitudes slowly decreased as the signal was attenuated in the sedimentary section.

Uniboom. Approximately 2800 km of high-resolution records were obtained using a hull-mounted EG & G Uniboom system consisting of four transducer plates. Total power level for this array was 1200 joules. An EG & G model 265 hydrophone streamer (10-element) was used as a receiver. Records were printed on an EPC 4100 recorder after passing through a Krohn-Hite filter. Sweep and fire rate was normally 1/4 second, although a 1/2 second sweep was used on occasion. The filter pass band was typically set from 400-4000 Hz. Time marks were made at 5 minute intervals and record annotations similar to those for the sparker were made at 15 minute intervals.

The quality of the Uniboom records was most affected by sea state, surficial bottom sediment type, and machinery generated ship noise. The hydrophone streamer was towed alongside the ship and only 20-30 cm below the surface. Consistently choppy seas were responsible for a significant amount of noise on the record which sometimes totally obscured subbottom

reflectors. Maximum penetration achieved was approximately 100 m, but was typically less than 75 m. Whenever coarse-grained and hard sediments were encountered penetration was severely reduced, and in some instances, such as near the Yukon Delta, the records are very poor.

Bathymetry/Subbottom Profiler. These data were collected along 2800 km of track using a Raytheon 3.5 kHz CESP II system. A hull-mounted transducer array consisting of 12 TR-109A units was used to send and receive the signals. Pulse generation and correlation functions were done by a CESP II (Correlator Echo Sounder Processor) and a PTR-105B (Precision Transmitter Receiver) was used as a tone burst amplifier during pulse transmission. Sweep and fire rates were normally 1/2 second. Time marks were made every 5 minutes and the records were annotated and depth measurements taken at 15-minute intervals.

Clarity of the records and amount of penetration varied considerably over the survey area. This system seemed less sensitive to ship-generated noise than the Uniboom, but the 3.5 kHz records were more adversely affected by hard bottom sediment. The long (50 msec) pulse generated during transmission also created an internal "ringing" in the transducer array which masked not only the weak subbottom reflections but sometimes the bottom echo as well in shallow water. Penetration ranged from 0-20 m.

Sidescan Sonar. An EG & G sidescan sonar system was used to record 1000 km of good to high quality data. Scales (sweeps) of 50 m and 100 m were used, and the "fish" altitude above the sea-floor was maintained at approximately 10 percent of the scale being used. The sidescan system was used in shallow water areas of known or suspected sand waves and ice-gouge features, and at such times the sparker system was shut down and its associated arc cables and hydrostreamer were brought aboard to prevent their fouling the sidescan cable.

GEOLOGIC SETTING

Tectonic Framework

The structural features and evolution of the Bering Sea continental shelf have been discussed by Scholl and Hopkins, 1969; Scholl et al., 1968; Pratt et al., 1972; Churkin, 1972; Lathram, 1973; Nelson et al., 1974; and Marlow et al., 1976. Figure B2 shows the major Cenozoic structures of western Alaska and eastern Siberia.

The general tectonic framework is characterized by large scale oroclinal bending forming two distinct flexures in central Alaska and eastern Siberia concave toward the Pacific Ocean. The Bering and Chukchi continental shelves are part of the broad intervening structural arc which is concave toward the Arctic Ocean.

This large scale oroclinal folding appears to have been completed before Oligocene time (Nelson et al., 1974), but continued activity along the major Alaskan transcurrent faults has displaced upper Tertiary and Quaternary sediment in several places on land and beneath the shelf areas (Patton and Hoare, 1968; Scholl et al., 1970; Grim and McManus, 1970). Total horizontal (right-lateral) movement along some of these large transcurrent faults has been approximately 130 km since the beginning of the Tertiary (Grantz, 1966; Patton and Hoare, 1968).

Regional Geology

Norton Basin. The geology of Norton basin has been discussed by Moore, 1964; Scholl and Hopkins, 1969; Grim and McManus, 1970; Tagg and Greene, 1973; Nelson et al., 1974; and Holmes et al., 1978. A submarine seepage of natural gas 40 km south of Nome has been described by Cline and Holmes (1977). Seismic reflection data suggest that the basin area is about 130,000 km²; maximum basin depth has recently been estimated to be approximately 5.5 km (Anon., 1976). The basin probably contains as much as 180,000 km³ of sediment.

The basin fill consists of three major stratified units (Homes et al., 1978), which are in turn covered by a thin mantle of Quaternary sediment (Grim and McManus, 1970; Tagg and Greene, 1973; Nelson and Creager, 1977). The lowermost unit in the basin, with a velocity of 4.9 km/sec (Holmes et al., 1978), may consist of Cretaceous nonmarine sandstones similar to those mapped onshore in the Koyukuk geosyncline (Patton and Hoare, 1968; Cobb, 1974). A velocity discontinuity at the top of this unit indicates that this interface may be an erosional unconformity.

Two other units of the basin fill can also be distinguished on the basis of compressional velocities (Holmes et al., 1978). A strong reflector on the reflection records corresponds to an apparent unconformity separating those units; the unconformity lies at a depth of about 1.2 km near the basin axis and approaches to within a few tens of meters of the sea floor near the basin margins. The compressional velocities above this unconformity are low, ranging from 1.6 to 2.1 km/sec; this section is probably composed of recent marine and glaciomarine sediment and loosely cemented sandstones and shales. The higher velocities (2.3-3.7 km/sec) below the

unconformity are more characteristic of compact or indurated sandstones and shales (Grant and West, 1965; Gardner et al., 1974). The unconformity was probably formed during the late Miocene marine transgression which inundated the northern Bering Sea continental shelf (Nelson et al., 1974). Strata of the unit below the unconformity form a broad synclinorium whose principal axis trends generally northwest; the beds of the upper unit are more nearly flat-lying.

Although younger Quaternary deposits everywhere cover the older Cenozoic and Mesozoic basin fill, some onshore outcrops and drill-hole data give clues as to the nature of the two upper units. Nonmarine coal-bearing strata of late Oligocene age are exposed on northwestern St. Lawrence Island (Patton and Csejtey, 1970), and several offshore holes drilled by the U.S. Bureau of Mines near Nome encountered marine sands and clayey silts of early Pliocene age at a subbottom depth of approximately 18 m (Scholl and Hopkins, 1969; Nelson et al., 1974). Late Miocene or early Pliocene marine limestone was recovered from a dredge haul 30 km south of St. Lawrence Island, just outside the basin.

These facts and the regional stratigraphic patterns indicate that the basin fill probably consists of late Cretaceous and lower to middle Tertiary sedimentary rock in the lower two units and upper Tertiary and Plio-Pleistocene sedimentary rocks and sediment in the upper unit. All direct evidence suggests that the lower units are nonmarine, but the size of the basin is such that unseen transitions to marine facies could occur within this sequence.

Acoustic Basement. The high compressional velocity contrast across the acoustic basement is indicative of a marked lithologic change at this interface (Holmes et al., 1978). Velocities of 5.5 to 6.5 km/sec are characteristic of igneous and metamorphic rocks (Grant and West, 1965), indicating that Norton basin is probably floored by a basement surface formed on strata which are analogous to the diverse older rocks which occur on land around the basin margins. Sedimentary, metamorphic, and igneous rocks of Precambrian through Mesozoic age are exposed on the Chukotka Peninsula (Nalivkin, 1960); and Seward Peninsula is formed primarily of Paleozoic sedimentary and metamorphic units with some Mesozoic and Cenozoic intrusive and extrusive rocks. Mesozoic sedimentary rocks (some slightly metamorphosed) and Cenozoic volcanics have been mapped onshore in the Yukon-Koyukuk basin east and southeast of Norton Sound (Miller et al., 1959; Patton and Hoare, 1968). At the southern margin of Norton basin, St. Lawrence Island is constructed mainly of Paleozoic, Mesozoic, and Cenozoic intrusive and extrusive rocks with some Cenozoic sedimentary deposits (Miller et al., 1959; Scholl and Hopkins, 1969; Patton and Csejtey, 1970). The acoustic basement probably represents an erosional surface which has been steepened by tectonic subsidence during development of Norton basin.

RESULTS AND DISCUSSION

Observed Faults and Structures

Locations of faults observed on seismic reflection profiles from Norton Sound and Chirikov basin are shown in Fig. B3. The majority of faults, especially those extending close to the sea floor, occur within 50 km of the basin margins. Most faults in Chirikov basin and western

Norton Sound trend northwest in alignment with the major axis of Norton basin. Synclinal and anticlinal axes mapped by Greene and Perry (unpub.), and shown in Johnson and Holmes (1977, Fig. B3), reflect this same trend. In eastern Norton Sound, the structural grain is nearly east-west.

Seismic records from the basin margins generally show sediments of the upper two units of basin fill, the Main Layered Sequence of Scholl and Hopkins (1969), resting with onlap unconformity against the eroded surface of the acoustic basement. The single channel seismic reflection systems were unable to resolve acoustic basement in the deeper basin areas where sediment thickness exceeded 2 km. Numerous faults offset the acoustic basement, often displacing overlying sediments. Many normal and antithetic faults displace the basin fill and extend to within 100 meters of the sediment surface. A few of these have topographic expression as fault scarps.

Faulting appears to be most complex, and the fault density is highest, in the area west of Port Clarence (Fig. B3). Several west-trending faults appear to intersect, and can be seen to offset, the dominant pattern of northwest-trending faults. These west-trending faults must therefore be younger than the others, and may be indicative of a change in the direction of regional compression during Quaternary time.

One of the major faults comprising this major east-west trend is the Bering Strait Fault (BSF) of Hopkins (unpub.). It forms the northern boundary of the Bering Strait Depression (BSD) named by Greene and Perry

(unpub.) and appears to extend for over 90 km west from Port Clarence (Fig. B3). A south-facing scarp 5 meters high marks the fault near the Bering Strait Depression. The scarp decreases in height eastward; no trace of the fault has been found beneath Port Clarence. This fault appears to have been active as recently as 12,000 years ago (Hopkins, unpub.).

The Port Clarence Rift (PCR) (Hopkins, unpub.) is a narrow fault-bounded depression extending eastward from the Bering Strait Depression; the fault along the northern margin of the depression is probably equivalent to the Cape York Fault of Greene and Perry (unpub.). This northern fault has a scarp 9 meters high near the Bering Strait Depression, which decreases to the east. No trace of this fault has been observed beneath Port Clarence, but displacement of bedrock beneath Grantley Harbor has been suggested as evidence for extension of the Port Clarence Rift further to the east. The Rocks beneath Grantley Harbor have experienced 16 km of left-lateral movement (Hopkins, unpub.). Several other west-trending faults with scarps up to 15 m high have been observed in the area west of Port Clarence (Fig. B3).

The rough seafloor topography north of St. Lawrence Island made identification of fault scarps difficult, but a few have been tentatively mapped (Fig. B3). A large west-trending fault has been inferred by Hopkins (unpub.) to parallel the northern coast of St. Lawrence Island and bend northward before reaching the western end of the island (Fig. B3). Existence of the St. Lawrence Fault Zone (SLF) is based on swarms of volcanic vents which trend N80°W through the axis of the Kookooligit

Mountains, and on the extension of these volcanic rocks into offshore regions. Hopkins has suggested that movement along this fault has been left-lateral. Possibly it is related to movement along the Kaltag Fault (KF), a large transcurrent fault in western Alaska that has been known to displace Pleistocene sediments onshore.

Many deep-seated and near-surface normal faults occur in the central part of Norton basin, although no surface expressions of these have been identified. An increase in displacement with depth, and apparent thickening of beds on the downthrown side of these faults, indicates that they are probably growth faults along which movement has taken place more or less continuously during the major episodes of basin subsidence.

Several subbottom faults occur along the southern and eastern margins of Norton Sound (Fig. B3). Short line segments indicate faults have been observed on one crossing, and therefore, their exact orientation is unknown. However, several faults appear to parallel the trend of the Kaltag Fault; others may represent splays of the Kaltag Fault. No surface scarps were associated with the near-surface faults along the eastern margin of Norton Sound.

Fault Activity and Hazard Potential

Surface fault scarps in northern Chirikov basin are associated with the Bering Strait Fault, the Port Clarence Rift, and other nearby faults (Fig. B3). The Bering Strait Fault and Port Clarence Rift may represent extensions or splays of the large transcurrent faults which have been mapped in western Alaska and Seward Peninsula (Fig. B2). The scarps may have been caused by recent vertical movement on these faults, and therefore would indicate a definite hazard to man-made structures placed over

or near these fault zones. There is also the possibility, that the faults have been inactive for some time, and the scarps have been maintained by nondeposition or lack of erosion. Currents west of Port Clarence flow almost normal to the trend of these scarps, and carry almost one third of the Yukon River sediment load into the Chukchi Sea (Nelson and Creager, 1977). The persistence of the surface expression of the faults in spite of apparently vigorous erosional agents would argue for the fault scarps to be recently formed features.

The Bering Strait Fault must have formed between 12,000 and 120,000 years ago; evidence exists that a lake was formed during the Wisconsin glaciation when development of the fault scarp dammed a northward-flowing river west of present day Port Clarence. Marine terraces on Seward Peninsula may have been uplifted during the Illinoian glaciation as a result of movement along the fault 130,000 years ago. Although no specific age can be given to movements along these faults in northern Chirikov basin, the area should definitely be considered as potentially hazardous to placement of structures on the bottom in the vicinity of the fault scarps.

Only a few surface scarps have been noted in association with faults along the northern side of the St. Lawrence Island or in southern and eastern Norton Sound; the rough sea-floor topography in this area makes identification of fault scarps difficult. Movement may have occurred along these faults during Tertiary and Quaternary time in conjunction with known displacement in western Alaska along the large transcurrent Kaltag Fault. Further study is necessary to determine if this represents a hazard to resource development.

Earthquake records show an almost complete lack of epicenters beneath Norton basin. This lack of seismicity can be interpreted to indicate either inactivity or, conversely, that strain release is being accomplished by small but frequent adjustments along the faults. The growth nature of most of the northwest trending faults which parallel the Norton basin axis support the latter interpretation, although the rate of basin subsidence may have decreased since the end of Pleistocene time when rising sea-level opened Bering Strait and resulted in a significant change in deposition patterns in the northern Bering Sea.

CONCLUSIONS

Based on the foregoing discussion, the following conclusions may be made regarding the faulting observed in Norton Sound and Chirikov basin:

1. Faults are most numerous in a belt approximately 50 km wide around the margins of Norton basin. Near surface faults are more numerous in central Norton basin than previously reported, but are still less prevalent than around the periphery of the basin. Most of the faults trend generally northwest, with the basinward sides down-dropped; antithetic faults are also common, resulting in series of narrow horsts and grabens along the basin margins. These faults and the many associated anticlinal and synclinal folds involving the basin fill and acoustic basement are the result of tectonic activity which occurred during subsidence and filling of the 5.5-km deep Norton basin. Initial subsidence of the basin probably began during late Cretaceous time, and has continued to the present with two apparent major interruptions during early and late Tertiary time.

2. Surface scarps up to 15 m high are associated with some of the long west-trending faults in northern Chirikov basin. These scarps can indicate either recent activity or persistence due to lack of erosion or burial by sedimentation since the last movement. Scarps occur on the Bering Strait Fault and on the northern side of the Port Clarence Rift, and movement along these faults possibly occurred as recently as 12,000 years ago in conjunction with uplift of marine terraces on Seward Peninsula.

3. The west-trending faults in northern Chirikov basin intersect and appear to offset the northwest-trending faults and structures south of Bering Strait. This relationship implies that the west-trending features postdate the main Norton basin structures; the different trends could also be indicative of a shift in regional compressive axes.

4. None of the faults can definitely be classed as historically active, however the area of northern Chirikov basin west of Port Clarence should be considered potentially hazardous to any bottom mounted structures. The fault scarps in this region are still well defined in spite of the swift currents and bottom sediment transport which occur normal to the trend of the fault zones. Basin subsidence is probably still taking place, and the lack of recorded earthquakes beneath Norton basin may indicate that strain release is being accomplished by small but frequent movement along some of these faults.

5. West-trending subbottom faults without surface fault scarps occur along the southern margin of Norton basin. These may represent splays or displacements related to the Kaltag Fault, one of the major transcurrent faults in western Alaska. Movement along onshore portions of the Kaltag Fault have displaced Pleistocene deposits, but data regarding age of movements along the offshore portion are inconclusive.

REFERENCES

- Anonymous, 1976, Prospective basins included in Alaska OCS sale plans: *The Oil and Gas Journal*, v. 74, p. 126-130.
- Churkin, M., Jr., 1972, Western boundary of the North American continental plate in Asia: *Geol. Soc. America Bull.*, v. 83, p. 1027-1036.
- Cline, J. D., and M. L. Holmes, 1977, Submarine seepage of natural gas in Norton Sound, Alaska: *Science*, v. 198, p. 1149-1153.
- Cobb, E. H., 1974, Synopsis of the mineral resources of Alaska: U.S. Geological Survey Bull. 1307, 53 p.
- Gardner, G.H.F., L. W. Gardner, and A. R. Gregory, 1974, Formation velocity and density--the diagnostic basis for stratigraphic traps: *Geophysics*, v. 39, p. 770-780.
- Grant, F. S., and G. F. West, 1965. Interpretation theory in applied geophysics: McGraw-Hill, New York, p. 8.
- Grantz, A., 1966, Strike-slip faults in Alaska: U.S. Geol. Survey Open-File Report, 82 p.
- Grim, M. S., and D. A. McManus, 1970, A shallow seismic-profiling survey of the northern Bering Sea: *Marine Geology*, v. 8, p. 293-320.
- Holmes, M. L., J. D. Cline, and J. L. Johnson, 1978, Geological setting of the Norton basin gas seep: *Proceedings, 1978 Offshore Technology Conference* (in press).
- Johnson, J. L., and M. L. Holmes, 1977, Preliminary report on surface and subsurface faulting in Norton Sound and northeastern Chirikov basin, in *Environmental Assessment of the Alaskan Continental Shelf*, v. XVIII, Hazards and Data Management, Annual Reports of Principal Investigators: U.S. Dept. of the Interior, Bureau of Land Management, p. 14-41.
- Lathram, E. H., 1973, Tectonic framework of northern and central Alaska, in Pitcher, M. G., ed., *Arctic Geology*: Tulsa, Okla., American Assoc. Petroleum Geologists Mem. 19, p. 351-360.
- Marlow, M. S., D. W. Scholl, A. K. Cooper, and E. C. Buffington, 1976, Structure and evolution of Bering Sea shelf south of St. Lawrence Island: *American Assoc. of Petroleum Geologists Bull.*, v. 60, p. 161-183.

- Miller, D. J., T. G. Payne, and G. Gryc, 1959, Geology of possible petroleum provinces in Alaska: U.S. Geol. Survey Bull. 1094, 131 p.
- Moore, D. G., 1964, Acoustic reconnaissance of continental shelves: Eastern Bering and Chukchi Seas, in Miller, R. L., ed., Papers in Marine Geology, Shepard commemorative volume: New York, MacMillan Co., p. 319-362.
- Nalivkin, D. V., 1960, The geology of the U.S.S.R.: New York, Pergamon Press, 170 p.
- Nelson, C. H., D. M. Hopkins, and D. W. Scholl, 1974, Tectonic setting and Cenozoic sedimentary history of the Bering Sea, in Herman, Y., ed., Marine Geology and Oceanography of the Arctic Seas: New York, Springer-Verlag, p. 119-140.
- Nelson, C. H., and J. S. Creager, 1977, Displacement of Yukon-derived sediment from Bering Sea to Chukchi Sea during Holocene time: Geology, v. 5, p. 141-146.
- Patton, W. W., Jr., and J. M. Hoare, 1968, The Kaltag fault, west-central Alaska: U.S. Geol. Survey Prof. Paper 600-D, p. D147-D153.
- Patton, W. W., Jr., and B. Csejtey, Jr., 1970, Preliminary geologic investigations of western St. Lawrence Island, Alaska: U.S. Geol. Survey Prof. Paper 684, 15 p.
- Pratt, R. M., M. S. Rutstein, F. W. Walton, and J. A. Buschur, 1972, Extension of Alaskan structural trends beneath Bristol Bay, Bering shelf, Alaska: Jour. Geophys. Research, v. 77, p. 4994-4999.
- Scholl, D. W., E. C. Buffington, and D. M. Hopkins, 1968, Geologic history of the continental margin of North America in Bering Sea: Marine Geology, v. 6, p. 297-330.
- Scholl, D. W., and D. M. Hopkins, 1969, Newly discovered Cenozoic basins, Bering Sea shelf, Alaska: Amer. Assoc. Petroleum Geologists Bull., v. 53, p. 2067-2078.
- Scholl, D. W., M. S. Marlow, J. S. Creager, M. L. Holmes, S. C. Wolf, and A. K. Cooper, 1970, A search for the seaward extension of the Kaltag fault beneath the Bering Sea: Geol. Soc. America, Abs. with Program, Cordilleran Sect., v. 2, p. 141-142.
- Tagg, A. R., and H. G. Greene, 1973, High-resolution seismic survey of an offshore area near Nome, Alaska: U.S. Geol. Survey Prof. Paper 759-A, 23 p.
- Walton, F. W., R. B. Perry, and H. G. Greene, 1969, Seismic reflection profiles, northern Bering Sea: ESSA Operational Data Report C+GS DR-B

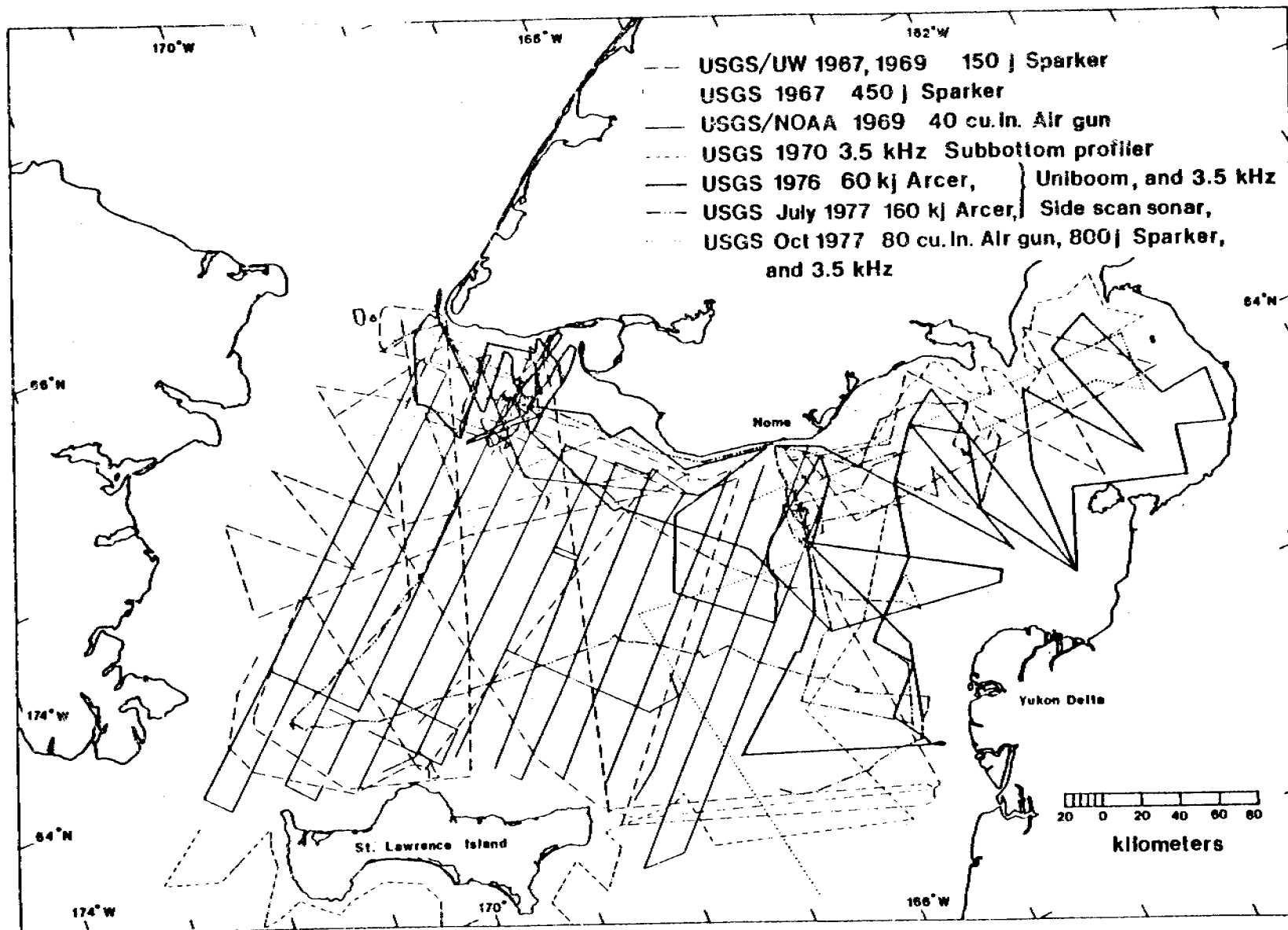


Figure B1. Coverage of geophysical studies conducted in northeastern Bering Sea.

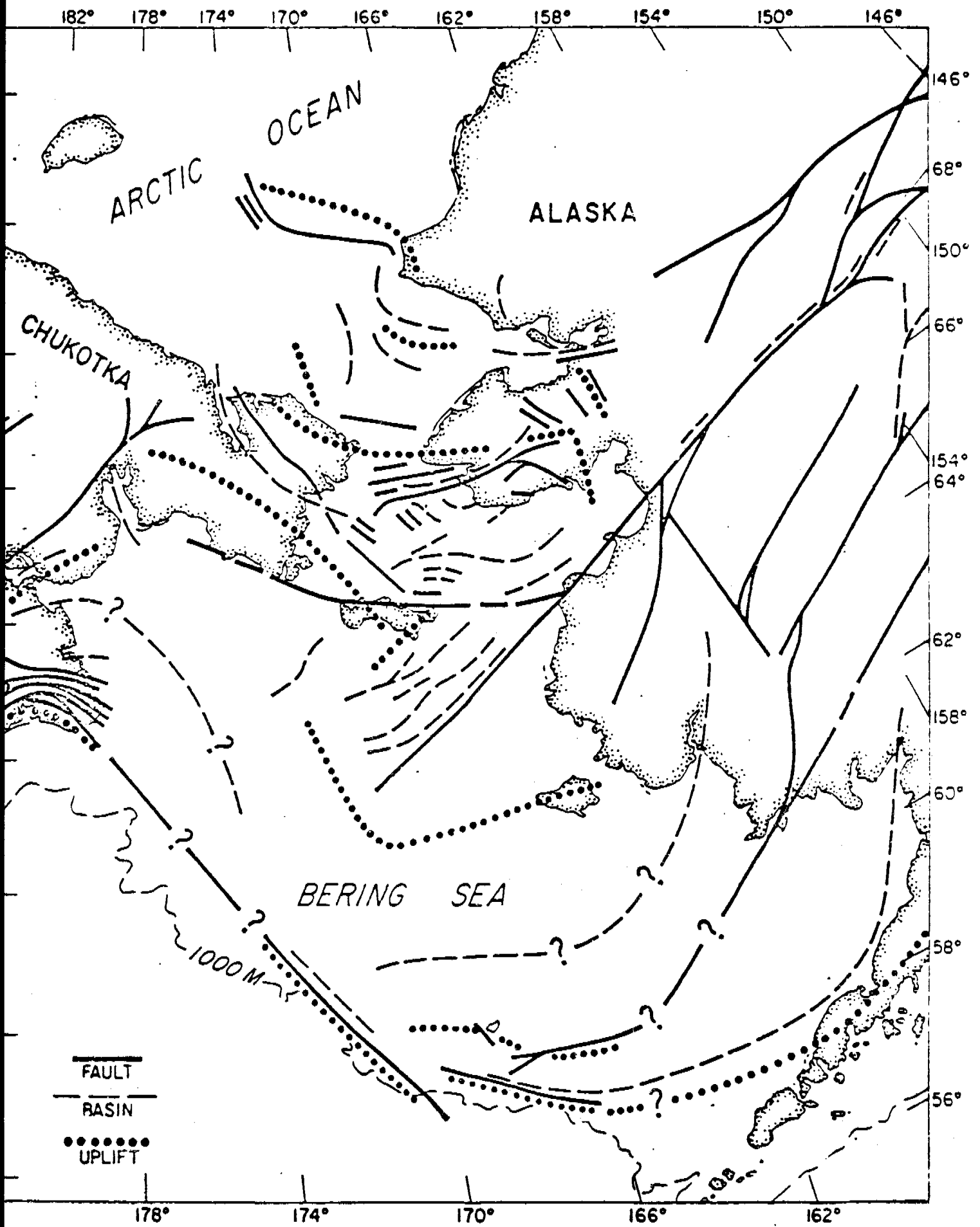


Figure B2. Regional tectonic map of northern Bering Sea area.

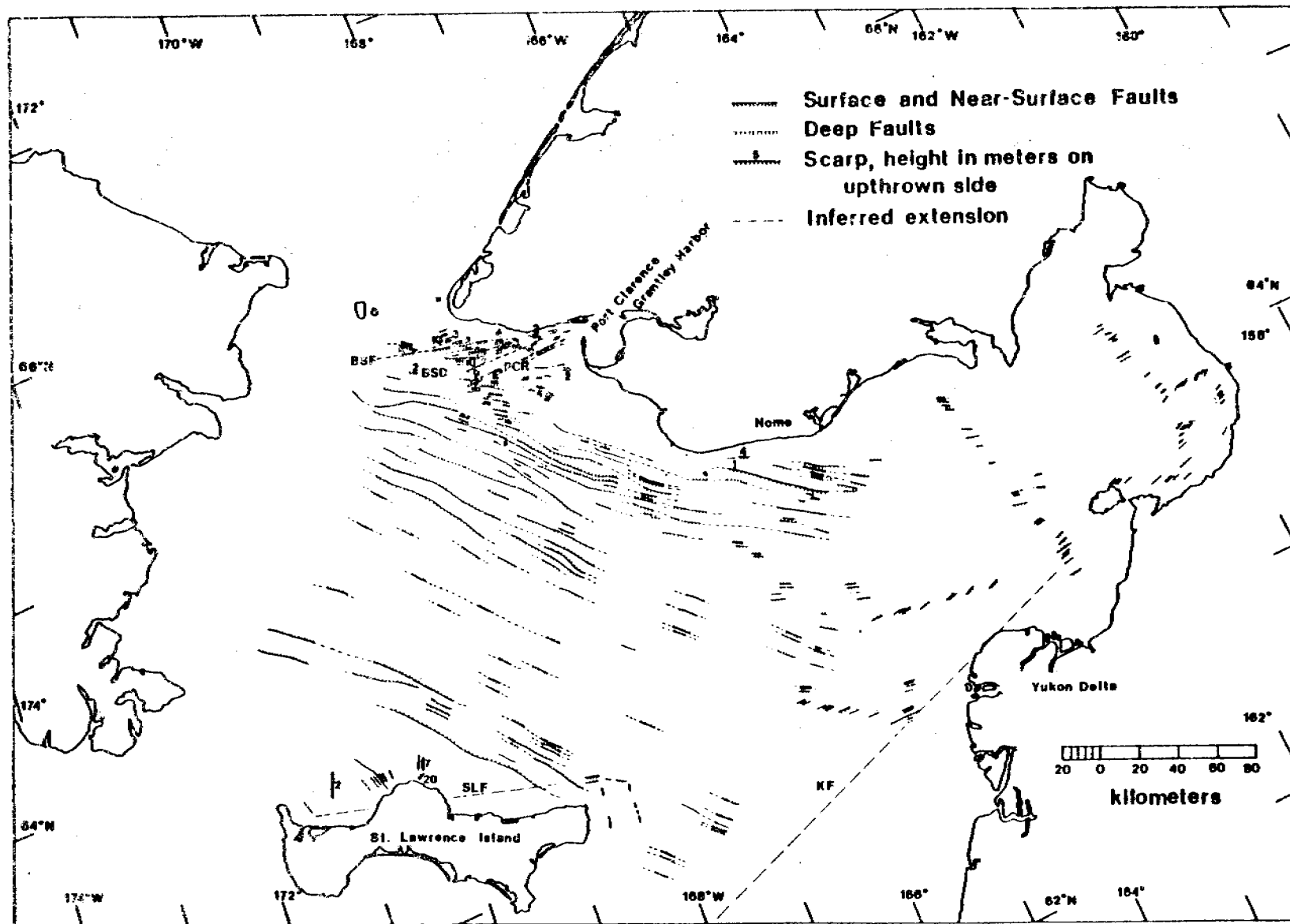


Figure B3. Faults in Chirikov Basin and Norton Sound.

Distribution of Trace Elements in Bottom Sediment
of Northern Bering Sea

Bradley R. Larsen
C. Hans Nelson
Chris Heropoulos
Jeffrey J. Patry

U.S. Geological Survey
345 Middlefield Rd.
Menlo Park, California 94025

I. SUMMARY

2-dimensional contour and 3-dimensional value surface maps of semi-quantitative emission spectographic analyses for over 50 elements from 180 sampling stations are presented. For purposes of discussion, certain of these elements have been grouped into the following categories: petroleum indicators, heavy metals, potentially toxic elements, chemically sensitive elements, major elements, minor trace elements, and a group of elements of economic interest.

Of the petroleum indicator elements, Ni and V, Ni showed only average values near a gas seep 35 km south of Nome, Alaska, while V showed slightly lower values in samples taken recently and relatively high values in samples collected earlier. 40 km west of the south tip of St. Lawrence Island, high amounts of V and Ni were found, suggesting that potential petroleum seeps should be searched for in this area. All other anomalous values for Ni and V correlate with general sediment type or nearby onshore sources.

The elements Zr, Sn, Cr, and Ce were categorized as heavy metals. Zr is found in high amounts in an area surrounding the Yukon Delta and in Norton Sound. It is generally low in the region of the Chirikov Basin. Very high Zr values are found off NE Cape of St. Lawrence Island as well as off the western and southern portions of St. Lawrence Island. These high values are probably derived from zircon containing quartz-monzonite plutons widely dispersed throughout the island. Sn was detected in only 23 samples. High values were found off Cape Prince of Wales, in Anadyr Strait; and in the areas of King Island, Port Clarence, Bluff, Cape Rodney, and off the north central coast of St. Lawrence Island. It is possible that the high values in Anadyr Strait, Port Clarence and King Island are hydraulically concentrated. Values in other areas appear to be derived from immediate land sources. Cr is rather evenly

distributed except for high values close to Stuart Island, at locations south and north of St. Lawrence Island, and off Cape Prince of Wales. These high values appear to be closely related to the mafic rock types found on adjacent land areas. Cerium is found in few raw-bulk samples but where present it is associated with lanthanum and neodymium which suggests the presence of the heavy mineral monazite. The highest values for Zn, Cr and Ce were found in a sample taken from 30 km south of Cape Prince of Wales. Because this sample also contains the highest values for Ti, Mn, La, Sc, Y, Yb and Nd, it is probably representative of a region of considerable placering.

Of the potentially toxic elements, Sb, As, Cu, Pb and Zn, Sb was detected in only a few samples from the Bluff, NE Cape of St. Lawrence Island, and Stuart Island beaches. As was detected only in samples from Bluff beach where lode cinnabar deposits occur. High values for Cu, Pb, and Zn occur together in the same areas off St. Lawrence Island, along the southern coast of the Seward Peninsula and in Norton Sound. These high values seem directly related to highly mineralized areas in adjacent land areas. Cu and Zn also show the same trend as Zr, with high values off the Yukon Delta in Norton Sound and low values in the Chirikov Basin.

Value surface maps for the chemically or environmentally sensitive elements Fe, Mn, Co and Ba are quite similar in having high values off the volcanogenic areas of north-central St. Lawrence Island and Stuart Island. They also exhibit high values off Yukon delta and low values within Chirikov Basin, with Co showing this relationship least of all. Ba is singled out in this group because of its use in drilling muds. It also exhibits high values surrounding Yukon Delta, near Stuart Island and along the southern coast of the Seward Peninsula. Maximum values occur off the southern edge of St. Lawrence Island and in the middle of Anadyr Strait. The elevated Ba values

off the Yukon probably originate in sediment from the Yukon drainage as do high values for Zr, Cu, Zn, Fe, and Mn. The anomalies near Stuart Island and Seward Peninsula appear to be derived from specific land sources.

Of the major elements, generally the highest values for Ti, as with Fe and Mn discussed above, are found close to the volcanics of Stuart Island and St. Lawrence Island, though the highest value of Ti is from the sample from 30 km south of Cape Prince of Wales. High quantities of Ti, Fe and Mn are typically found in regions associated with mafic rock types. Ca and Mg also exhibit elevated values in these areas but are in greatest abundance south of Port Clarence and offshore from Cape Prince of Wales, a site of paleozoic limestone formations. Value surface maps for Na, K, and Al do not show strong trends. K shows highest values off NE Cape of St. Lawrence Island and is probably related to the granitic bodies there. Al shows highest values in the Stuart Island area and eastern Norton Sound. Mn, Fe, Ti and to a lesser degree Ca, Mg, Na and to a slight degree K and Al all have high values in the region of the Yukon Delta and in Norton Sound. The highest P value was from an enclosed basin northeast of St. Lawrence Island. The relative percent composition profiles for these elements in sediment off the Yukon Delta are very similar to profiles for average granites. A profile from Chirikov Basin is closer to the profile of a typical sandstone than to profiles for average granites.

In the minor element category, Sr correlates closest with K, Na, and Ba, but the highest Sr values have a closer visual correlation with the highest Ca values. Sc correlates closest to Ti, Fe, V, La, and Mn and shows the same broad high anomaly surrounding the Yukon Delta and the low anomaly in the Chirikov Basin already mentioned for Ti, Fe, and Mn. Ga correlates closest with La, Sc and Ti and has high values in Anadyr Strait and the eastern end of

Norton Sound. Nb has a significantly high value east of Cape Darby. It is probably related to the high values of Nb reported in stream sediments from Cape Darby peninsula. Nd correlates closely with Ce and La. Y follows the trend of high values in the Yukon Delta/Norton Sound area and low values in Chirikov Basin. Yb correlates closest to Mn, Zn, and Y and also correlates with the Holocene sediment distribution. Ag is found in 8 samples close to areas of St. Lawrence Island known to have silver mineralization, close to Stuart Island, the Yukon Delta, and off Cape Nome, and Bluff. The highest values for Mo were found close to Stuart Island off Cape Prince of Wales in a sample containing a high amount of Sn, and in a Bluff beach sample.

Q-mode factor analysis came up with 4 factors which explain 92% of the variance between samples. A plot of the most significant factor grouping (Factor III) covers an area roughly the area of Yukon Holocene sediment deposition but also an area NW of St. Lawrence Island. Elements that are related to Factor III are La, Na, Ga, Ba, Sr, Sc, K, V and Al. A plot of the next most significant factor grouping (Factor I) corresponds approximately to the extent of relict sediment cover in Chirikov Basin. Related elements are B, V, Yb, Ba and Al. These two factors seem to explain the trend exhibited by many of the elements with generally high values surrounding the Yukon Delta and Norton Sound area and generally low values in the Chirikov Basin. However, some of the elements that show this trend most conspicuously do not seem to be related to Factor III very closely, but instead are better related to Factor II. Factor II corresponds roughly to the highly mineralized areas along the southern Seward Peninsula and the highest element values for these areas are the ones closely related to Factor II. Elements related to Factor II are Y, Yb, Ti, Fe, Sc, Co, V and Mn. Factor IV doesn't seem to correlate with any obvious sedimentological, mineralogical or depositional characteristic of the area. The one correlative element is Nb.

II. INTRODUCTION

A. General Nature and Scope of Study

This study has been undertaken to assess the element and trace element content of bulk bottom sediment in the northern Bering Sea. The values arrived at are useful as geochemical baseline data that can be compared with similar data from bottom sediment in the same region and elsewhere. The data are also useful for monitoring possible changes in chemistry of the bottom sediments that might result from future development in the region. Present anomalously high element and trace element values are mapped and related to highly mineralized sources on land so that these high values will not be mistaken at some future time as sites of contamination caused by mineral resource development.

B. Specific Objectives

More specifically, this study considers 7 groups of elements of varying environmental significance and resource potential; we map their areal distribution in surface sediments and relate these to probable sediment source. The 7 groups of elements include: V and Ni as possible petroleum indicators; the heavy metals Sn, Zr, Ce, and Cr as possible indicators of placer deposits (Hg and Au are considered in separate studies, see Nelson et al., 1975; and Nelson and Hopkins, 1972); the potentially toxic elements Pb, Cu, Zn, As, Sb, and Cd (Hg is considered elsewhere, see above); Fe, Mn, Co, and Ba as signposts for change in the sediment chemistry, with Ba as a particular indicator of petroleum drilling muds; a suite of major and minor trace elements, and a miscellaneous group of economic elements.

The data are both graphically and statistically displayed. Computer maps have been generated that show element value locations and that display both contoured and 3-dimensional mesh value surfaces for each element. Geometric

means and deviations as well as value ranges are found in Tables I and II. Results of correlation analyses are found in Tables III and IV. Plots of significant Q-mode factor analyses sample groupings are found in Fig. 5.

III. CURRENT STATE OF KNOWLEDGE

The toxic and heavy metal, Hg, has been previously studied in the sediments of this area by Nelson, et al., 1975. Gold placer deposits in the nearshore areas of Nome-Bluff and in the offshore areas of Chirikov Basin have been extensively studied by Nelson and Hopkins, 1972. Work done by McManus, et al., 1977; Venkatarathnam, 1971; and Sheth, 1971, discuss in detail the related topic of heavy mineral and sediment distribution, dispersal and provenance in the northern Bering Sea shelf region. W. Dean, et al., 1978, have completed a study similar to this one in the central and southern Bering Sea shelf regions.

IV. STUDY AREA

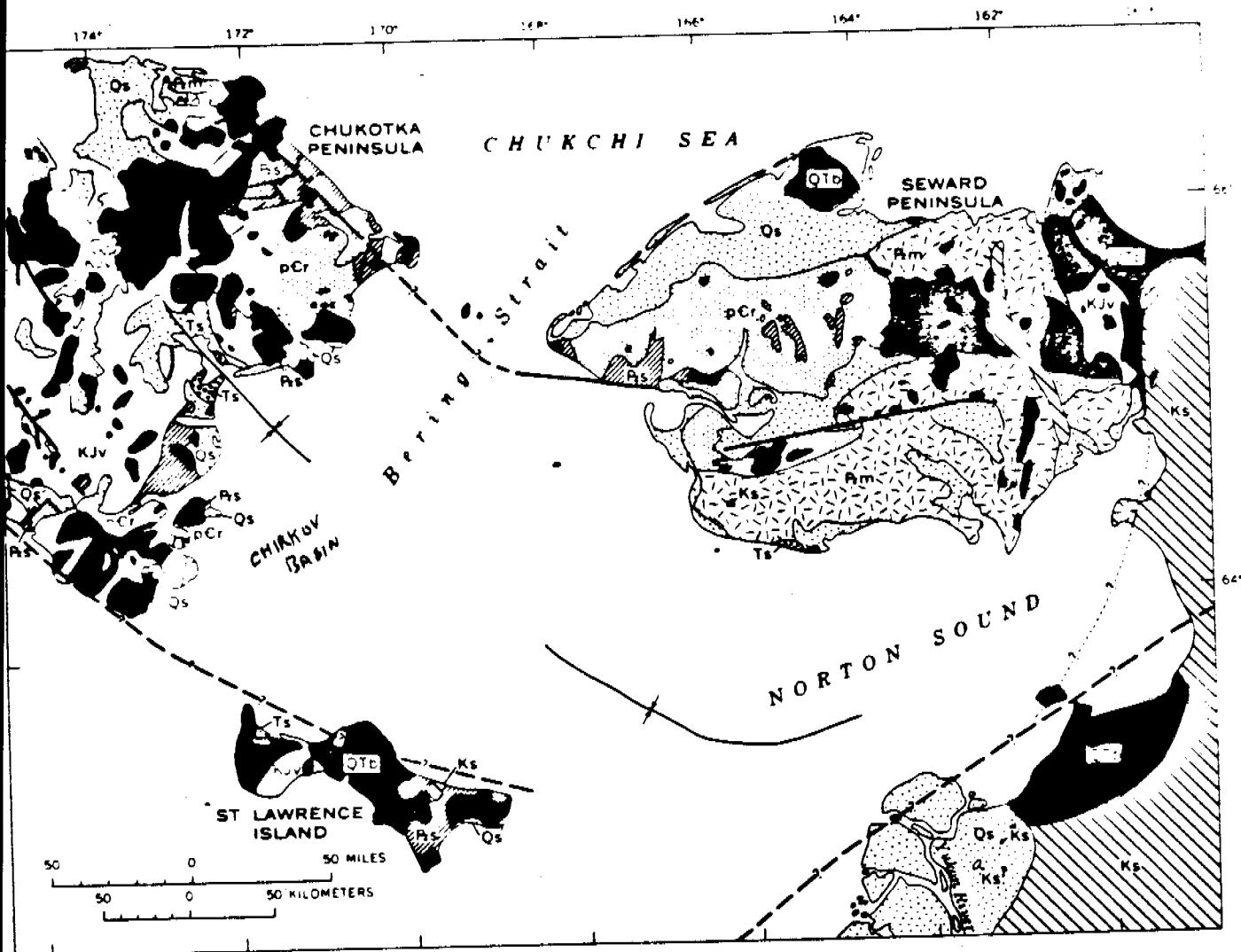
The bottom surface sediment analyzed for this study came from 180 sampling stations spread randomly over Norton Basin (Figs. 1 and 2). The western portion of the area, Chirikov Basin, is covered with what is thought to be a relict covering of medium-fine sand (Fig. 2) (Nelson and Hopkins, 1972). The region surrounding the Yukon Delta as well as much of Norton Sound, and sporadic depressions in an eastern corridor extending up to the Bering Strait, is generally covered with more recent sediment grading from coarse silt to fine sand. The major source of Holocene sediment in this region is the Yukon River (Nelson and Creager, 1977). There are some areas where the relict and modern sediments intersect creating a palimpsest mixture of the two (McManus et al., 1977). Much of the sediment coming from the Yukon and deposited in Norton Sound is thought to be re-suspended periodically and then flushed through the Bering Strait and deposited in the Chukchi Sea by

normal and storm tides (Nelson and Creager, 1977). This is helped by currents which trend generally northwards to the Bering Strait and have measured velocities as high as 190 cm/sec in the Strait itself (Coachman, et al., 1976).

Water in the region is characterized by two fairly distinct masses. Colder, more saline waters are found to dominate the central and western portions of the region. These are surrounded by a shoreward hugging mass of Alaskan coastal water which is warmer, less dense and moving generally along the eastern coast northward to the Bering Strait.

Significant mineralized deposits are found in several areas bounding this region (Fig. 2); (from Cobb, 1960a,b,c, 1962, 1964; Eberlein and Menzie, 1978; Hudson and DeYoung, 1978, Hudson, et al., 1977; Hummel, 1977, Nelson and Hopkins, 1972, Nelson, et al., 1972; Patton and Csejtey, 1971, 1972; and Sainsbury, 1969, 1975). Of particular importance are the gold placer deposits found in the Nome Bluff area. Gold placers are also located in various relict beach ridges or reworked glacial moraines presently submerged off the coast from Nome as well as off Chutkotka Peninsula and St. Lawrence Island (Nelson, Hopkins, 1972).

Lode deposits of economic interest occur in many areas surrounding Norton Basin. They include copper, lead, zinc, silver and molybdenum. Occurrences in western and eastern St. Lawrence Island; the tin and beryllium deposits of the Lost River mining district on the western tip of Seward Peninsula which also occur with high amounts of copper, lead, zinc, antimony, gold and molybdenum; the general area of the southern Seward Peninsula where there are numerous occurrences of gold, copper, lead, zinc, mercury, antimony, iron, and some tungsten and niobium; the lands to the east of Norton Sound where gold, tungsten, antimony, tin, copper, silver, lead, zinc, molybdenum, platinum,



EXPLANATION

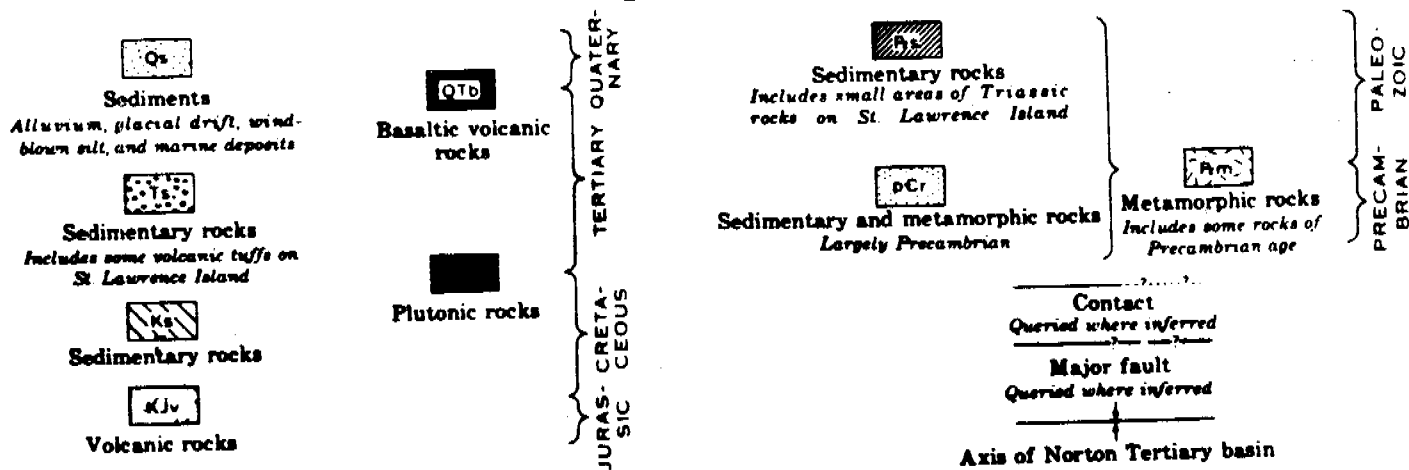


Figure 1. Generalized map of the northern Bering Sea region, (Nelson and Hopkins, 1972).

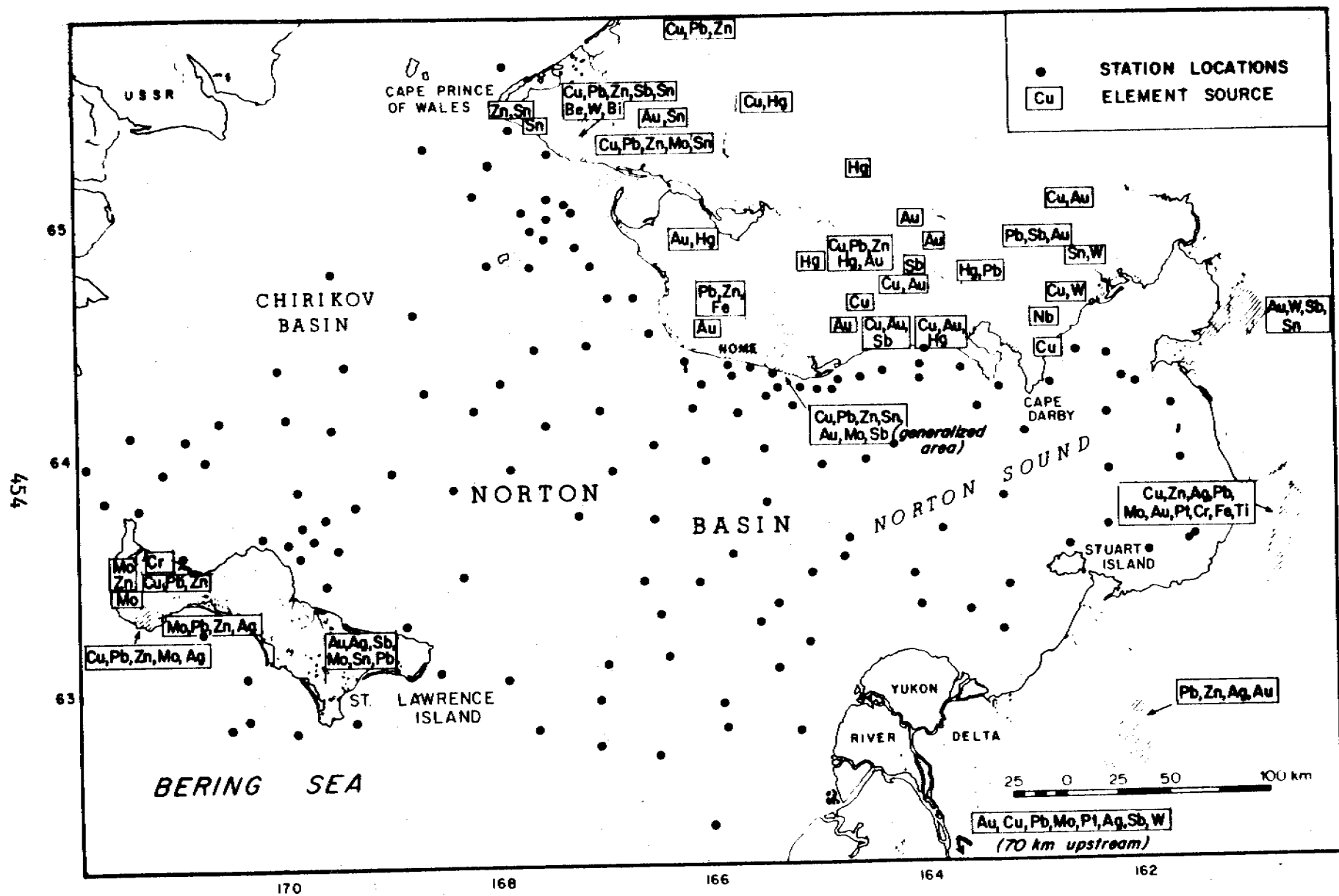


Figure 2. Offshore sampling locations and terrestrial sites of known mineralization for various elements.

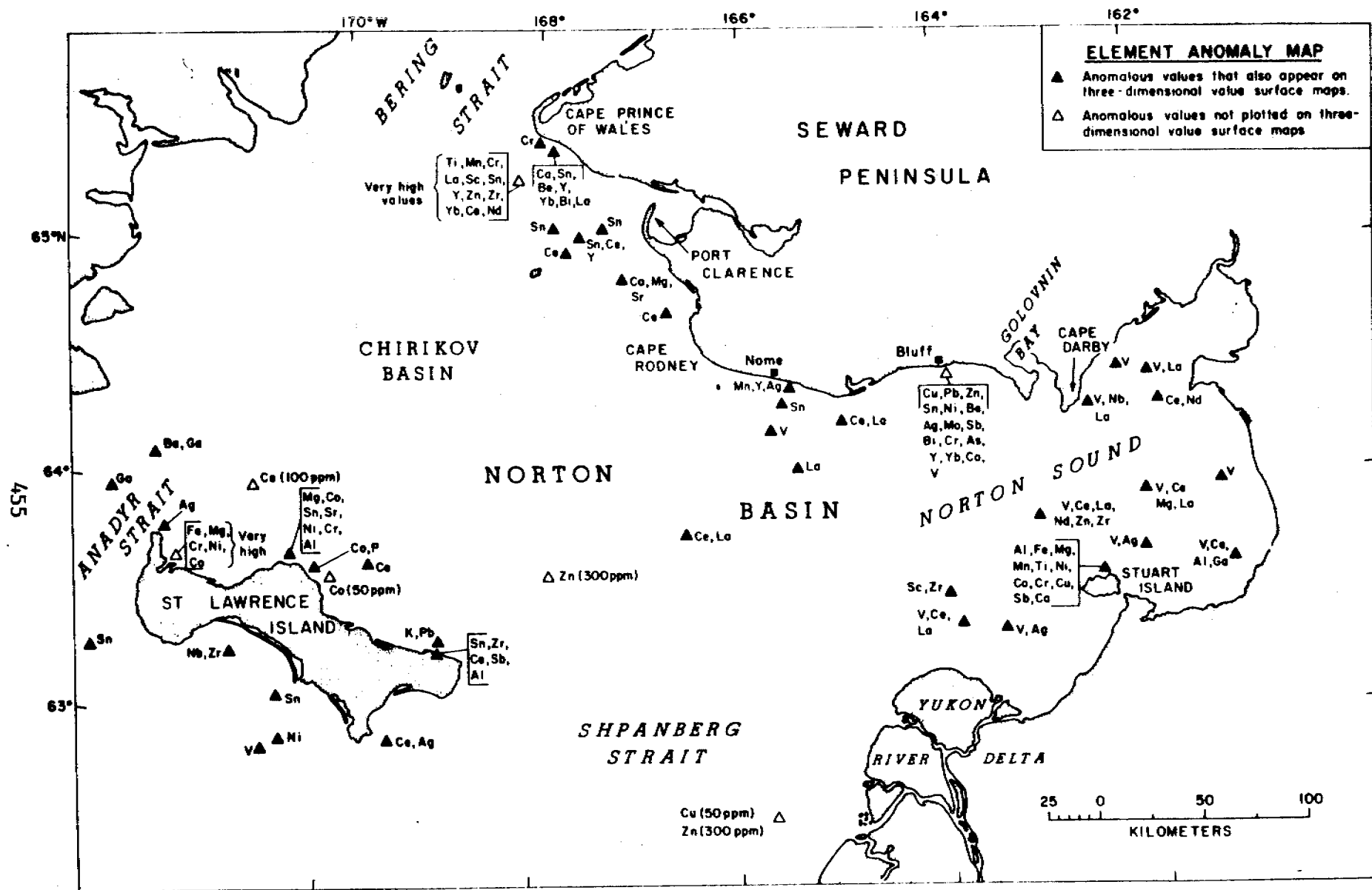


Figure 3. Map depicting significant anomalies defined as values falling outside the upper limit of the expected value range or as the highest few values (see Table I).

chromium and titanium are found; and the entire Yukon drainage basin where mineral concentrations containing anomalous amounts of most of the aforementioned elements are located.

All of the areas mentioned are drained by streams and rivers that have undoubtedly been contributing substantial amounts of mineralized sediment to the sediment regime of Norton Basin for the past several thousand years.

V. SOURCES, METHODS AND RATIONALE OF DATA COLLECTION

Two groups of samples were utilized for this study. The first group consists of samples collected on 3 different expeditions during the years 1968, 1969, and 1970. These samples were originally collected to delineate sediment characteristics and faunal distributions in the region and to assess placer gold dispersal from Seward Peninsula sources (Nelson and Hopkins, 1972). They were taken using a 5 gallon galvanized steel Van Veen grab sampler which would normally penetrate the top 5-10 cm of bottom sediment. The resulting samples were given no special treatment and were stored at room temperature. The second group of samples were collected using a 'Soutar' Van Veen grab sampler during the 1976 and 1977 U.S.G.S. cruises: S5-76-BS and S5-77-BS. The Soutar grab sampler is a chemically clean device that causes minimal disturbance of surface samples. Subsamples were selected for trace element analysis from the top 1-2 cm of each sample collected using the Soutar sampler and were immediately frozen and preserved in that manner until analysis in Menlo Park, California. This sampling technique duplicates that developed by Ian Kaplan of UCLA for their BIM/NOAA trace element study of the western North American outer continental shelf. No significant difference in trace element values was found between samples taken with these two different types of Van Veen sampler.

The average distance between samples is approximately 30 km. In an analysis of variance in samples from the central and southern Bering Sea, Dean, et al., 1978, found this distance to be adequate in showing statistically significant trends and changes in sediment element and trace element content.

A one gram split of each sample was analyzed by the Analytic Laboratories Branch, U.S.G.S, for a suite of over 50 elements using semi-quantitative emission spectroscopy techniques (Grimes and Marinizino, 1968).

To verify the quality of the data, measures were taken to assess the precision and accuracy of the 6-step semi-quantitative emission spectrographic technique used in this study. Replicate analyses were done on both U.S.G.S. rock standards and on 4 or 5 subsamples of the sediment samples being studied. Additionally, several replicate subsamples were analyzed using the technique of neutron activation.

VI. ANALYTIC RESULTS

6-step emission spectroscopy, although not as exact as other analytic techniques, yields values that are adequate to delineate regional trends. Care must be taken, however, to establish the limits of precision and accuracy for the technique as used with a particular type of sample to detect a particular element.

The precision of the 6-step emission spectroscopy technique is influenced by two factors: variability of the substance being analyzed and the variability introduced by the imprecision in the use of the technique or in the technique itself. To reduce errors due to sample variability, samples were ground to 230 mesh and homogenized. Sub-splits from the sample were then used for replicate analyses. The overall precision of the 6-step emission spectrographic technique was determined by running 5 to 8 replicate analyses

on each of three samples. The subsamples used for the replicate analyses were submitted randomly along with the other samples analyzed. The precision was calculated by averaging the percent difference between each replicate analysis and the mean value for all of the replicate analyses. Additional replicate analyses were run on subsamples from the same set of test samples using the completely different technique of neutron activation as a further test of both the precision and accuracy of the emission spectrographic technique. Values of replicate analyses for all elements except zinc, were found to fall with 25 percent of the mean values for the replicate analyses. Replicate values for most of the elements fall within 15 percent of their mean (Patry, et al., 1977).

The accuracy of the 6-step emission spectrographic analyses was tested by analyzing four U.S.G.S. standard rock samples of known element composition. Two analyses were made on each rock sample and the average of the two values was calculated for each of 30 elements. Then the percent difference between these values and the actual values for each rock was determined. Next, the percent differences for all four rock standards were averaged to give the average percent error between values yielded by the 6-step emission spectrographic technique and the known values for the rocks. Element values for Y, Ca, Ba, K, Cr, Cu, Na, Co, Nb, Ni, V, and Zn, as determined by emission spec, were within 30 percent of the established values for the rock standards. This group of elements is almost entirely within the bounds of the 'accepted' error for this analytic technique and would thus be very good baseline data for the area. Values for eleven elements including Sr, Al, Sc, Zr, Ti, Ga, Pb, Fe, Mn, and Mg, were within 35 to 65 percent of the actual values for the rock standards and could still be considered as giving reasonable baseline data. Two elements, Yb and B, had values varying by more

than 80% from the known values. Values for these elements should be regarded as only gross estimates of their actual content in the sediment. Data on the eight elements Ag, As, Bi, Mo, Nd, Sb, Sn, and Ce were too sparse to say anything about the accuracy because quantities present were too low to be detected by the analytic method. These elements were not statistically analyzed but where present, were plotted as anomalous values. Si was left out of the statistics and plotting because its values were all greater than the upper limit of detection of the analytic technique (Patry, et al., 1977).

The analytic results were organized into a data matrix called the 'STATPAC format' to enable the data to be analyzed in a series of statistical programs (STATPAC). The data was transformed into base 10 logarithms and Fisher-K statistics which include calculations of the mean, variance, and the third and fourth moments about the mean. The log transform step was performed because most geochemical element value distributions are log-normal. The arithmetic mean of the log values of a log-normal distribution is equivalent to the geometric mean of the original values. Insofar as the distribution approximates log normality, the geometric mean is the best measurement of the central tendency of the distribution (Miesch, 1970). Correlation analyses relating element pairs were also run on the logs of the data values. Q and R mode analyses were performed to get an idea of significant sample and element groupings (Fig. 5, Tables VI, VII, and VIII). Most of the elements had no values less than the lower limit of detection used by the analytic method. Where an element had only one to three values outside the limits of detection these values were substituted with values one or two class intervals above or below the value of the limit of detection. Then statistics based on a straight Fisher-K program-run were generated for the altered data set. Nine of the elements examined (Ag, As, Bi, Mo, Nd, Si, Sb, Sn, and Ce) had too few

values for statistical treatment. However, Ag, Mo, and Sn were graphically plotted. Twenty-six elements had no values at all (TABLE II). Two elements, Ga and P, had a considerable number of values that were less than the lower limits of detection. In this case, the distribution was statistically analyzed in conjunction with Fisher-K statistics using a method developed by Sichel, 1947; and Cohen, 1959, to determine an accurate statistic on distributions which may have a certain number of indeterminate values.

Computer software developed by the Dynamic Graphics Company, Berkeley, California (Dynamic Graphics Surface Display Library) was used to display the geochemical values. For each element (Figs. 3-93) there is a two-dimensional contour map of the value surface and a three-dimensional mesh plot of the value surface shown at an oblique perspective to the land surface. A single viewing perspective of 20° degrees to the horizontal and looking NNW was chosen for all of the three-dimensional mesh plots because the uniformity was found to enhance the ease with which one can compare plots for different elements. The value surface of each three-dimensional plot was made to drop off to a zero value as it impinged on a rough polygonal outline of surrounding coastlines. To further help viewer orientation, a planar plot showing the coastal outline in the very same perspective as the three-dimensional plot was generated a few inches above the three-dimensional plot.

The Dynamic Graphics software used to generate the plotting grids from which the two- and three-dimensional map plots are made, employ an iterative technique to solve biharmonic equations which produces a surface of least tension passing through all the data points. It is this surface which is contoured or graphically represented by a mesh pattern. Contour intervals for the two-dimensional contour plots are chosen automatically by the program which makes the selection based on the maximum and minimum and the distribution of the values encountered.

VII. DISCUSSION

This study is an attempt to say something about the distribution of elements, trace elements, and groups of these elements in the Norton Basin.

A. Petroleum Indicators

High values of V and Ni in sediments near petroleum seeps have been attributed to contamination of the sediments by high concentrations of these elements existing as chelated porphyrins in the oils and tars of the seeps (Reed and Kaplan, 1977; Yen, 1975). Therefore, relatively high concentrations of V and Ni together in a particular area might indicate the presence of thermogenic hydrocarbons.

The one known gas seep in Norton Basin is located roughly 35 km south of Nome. At this site the surface values for Ni are not anomalously high but V has values up to 200 ppm, a value greater than two geometric deviations from the geometric mean for V in the northern Bering Sea region (Figs. 6,7,8,9; Table I). The high V values may be controlled strictly by the sediment type because equally high values are found over broad areas in sediments surrounding the Yukon Delta and the eastern portions of Norton Sound. It is not unexpected that Ni and V show no anomalies, since the Norton Sound Seep is not a petroleum seep but is mainly a CO₂ gas seep with only traces of low molecular weight thermogenic hydrocarbons (Kvenvolden, et al., 1979).

Recently, additional sediment samples were collected in a tight grid surrounding the suspected gas seep in order to take a closer look at possible chemical differences between the gas seep sediments and surrounding sediments. The samples were analyzed for 54 elements including V and Ni. The average ppm values for V and Ni in these samples are 68.8 and 18.8 which are lower than background V and Ni values for this region (Table I).

It is clear that the V and Ni values for the detailed sampling 'grid' give no clear support for the thermogenic origin of the anomalous hydrocarbons found in this area. If the higher Ni and V values found in the sample group collected earlier are indicative of sediment contamination by thermogenic hydrocarbons, it may be that the lower values found in the later 'grid' samples are due to changes in the sediment between the two sampling periods. A large storm surge occurred in 1974 and may have been strong enough to flush V and Ni contaminated sediment from the area of the gas seep (Fathauer, T. F., 1975).

One area located approximately 40 km west of the southern tip of St. Lawrence Island had high V and Ni values of 200 and 100 ppm (Fig. 3). Both of these values fall outside the expected value ranges for V and Ni (Table I). These relatively high values coupled with the fact that the sample locations are at some distance from any possible land source could be taken as sufficient evidence to warrant a closer look at this area in terms of its gas/petroleum potential.

B. Heavy Metals

General Characteristics

Sn, Cr, Zr, and Ce are treated as a group because they are found in minerals which are heavy and stable enough to be mechanically concentrated into placer deposits. Au and Hg, etc., are not considered in this report because their distribution is described in other published reports (Nelson and Hopkins, 1972; Nelson et al., 1975-1977).

Previous studies including those by Venkatrathnam, 1971; Sheth, 1971; and McManus et al., 1976, have looked at the distribution of heavy minerals in the Norton Basin region but these studies were either limited to a small area or involved only mineral concentrates from a portion of the sand-size range.

The degree to which a heavy mineral concentrates in placers is dependent on winnowing forces and the magnitude of the density and size differences between the heavy mineral and the containing sediment. For example, if the heavy mineral particles in a sediment are relatively uniform in size, the mineral may be evenly distributed throughout hydraulically equivalent sediment. Concentration can begin to take place only when the hydraulic balance between the particle size and density for the various mineral constituents of a sediment begin to break down. An example would be when mechanical and chemical forces wear down heavy mineral particles in a sediment at a slower rate than the other mineral constituents of the sediment.

Once a given heavy mineral has been concentrated, the main factor influencing whether the concentration will be detected is the sampling interval. If the sampling interval was chosen primarily to detect significant areal variability in an average suite of elements, it may be too large to detect significant variability in specific heavier elements that tend to change in concentration over shorter distance intervals. Also, the sampling interval may be entirely adequate to pick up general variability of the heavy element as it is distributed in sediments from a particular provenance but it may miss smaller scale variability caused by localized hydraulic fractionation (Flores and Shideler, 1978). It is left to ^{future} studies to examine the more detailed variability in the distribution of these elements that closer-spaced sampling and sample concentrating might detect.

Zr

Relatively high values for Zr are found surrounding the Yukon Delta and in Norton Sound and around St. Lawrence Island (Figs. 10 and 11). This contrasts with the much lower values in Chirikov Basin. The presence of relatively higher values of Zr in Yukon-derived sediment probably reflects

that the Yukon River passes through a terrain which is composed on the average of sialic rock types, a predominant contributor of zircon (Mason and Berry, 1968). A comparison of our 2-dimensionally contoured value surface map for Zr with Venkatarathnam's percentage distribution maps (1971) of the heavy mineral zircon in the 1-2.75 and 2.75-4.0 phi size range show that his areas of high values correspond generally with the high value areas of our 2-dimensional map. This is particularly true off the NE Cape of St. Lawrence Island where his values as well as ours are highest. Our data also show persistently high values for Zr off the western and southern portions of St. Lawrence Island. Probable sources for these high values are sediments derived from quartz-monzonite plutons which are found over much of St. Lawrence Island.

A strong Zr anomaly occurs in the central portion of Norton Sound, relatively far from land. Sediment analyzed at this locale was taken from a depth of roughly 10 meters and, according to McManus et al., 1976, in an area of generally higher sand content than the rest of Norton Sound. The lack of a nearby land source and the lack of generally high values in similar surrounding sediments might indicate that this sample may contain hydraulically concentrated zircon in a zone of coarser sediment. Strong tidal currents pass through this area (Cacchione and Drake, 1978) and ^{may} concentrate ₁ the heavier zircon grains.

Another strong Zr anomaly was found 30 km south of Cape Prince of Wales (see Fig. 3; this sample is not represented on the value-surface maps). The Zr content in sediment from this location is as great as in any other sample in this study and the amounts of Ti, Mn, Cr, La, Sc, Y, Zr, Yb, Nd, Ce, Sn and Zn are also greater or much greater than the expected value range.

Venkatarathnam reports high concentrations of heavy minerals in the 2.75-4.0 phi size range from this area, especially further south and east in the

sand wave region west of Port Clarence. Similar concentrations are found in Anadyr and Shpanberg Straits. It is probable that the high speed currents in these areas have concentrated heavy minerals there. The anomaly south of Cape Prince of Wales represents a very significant anomaly and may point to deposits heretofore undetected and of considerable economic potential.

Sn

Sn values in 156 of the 180 samples analyzed were below the limit of detection of 2 ppm. The highest values occurred close to Tin City on the southwest coast of Cape Prince of Wales; lesser anomalies were found in the area of King Island, Port Clarence, Bluff, Cape Rodney, the western and north-central coast of St. Lawrence Island, half way between Cape Prince of Wales and St. Lawrence Island, plus the aforementioned from the sample from 30 km south of Cape Prince of Wales (Figs. 12 and 13). The highest values for Sn, near Tin City, are obviously derived from the same mineralized formation which gave Tin City its name. Anomalies near Bluff, north central St. Lawrence Island, and Cape Rodney-Nome areas also appear to be related to adjacent onshore mineralization. The isolated high values off of the NW tip of St. Lawrence Island may have been hydraulically concentrated. High values off Pt. Clarence and in the area of King Island are in an area of high currents and sand dune fields that also may represent an area of tin placering.

Cr

The distribution of Cr in the Norton Basin is quite uniform except in the areas of Stuart Island, St. Lawrence Island, and Cape Prince of Wales (Figs. 14 and 15). These locations have relatively high values of Cr that are in some cases greater than one geometric deviation from the geometric mean.

All these anomalies, except the sample site 30 km south of Cape Prince of Wales discussed earlier, are located close to igneous outcrops on land. Cape

Prince of Wales is the site of granitic plutons that are cut by occasional mafic dikes. Gabbro and metagabbro bodies are also found throughout the same region. Stuart Island, the adjacent peninsula and the central portion of St. Lawrence Island are composed largely of alkali olivine basalts. Because chromite (FeCr_2O_4), which is the principal mineral of chromium, is thought to form as a magmatic segregation in ultrabasic rocks and is usually associated with olivine, there is probably a direct connection between anomalous values of Cr offshore, and the adjacent mafic igneous outcrops on land.

One area in this entire region at which very high Cr amounts have been reported in the past did not show similar high values in this study. Nelson and Hopkins found an abundance of harzburgite among rock fragments collected in dredge hauls in Akeftapak Bay off the NNE end of St. Lawrence Island (Patton and Csejtey, 1972). Semi-quantitative emission spectrographic analysis of some of these harzburgite samples yielded chromium values as high as 2,000 to 10,000 ppm. Patton and Csejtey similarly reported very high chromium values in the lower reaches of streams feeding into Akeftapak Bay. From this evidence, Patton infers the presence of an ultramafic body existing just below a thin veneer of sediment at this location.

The distance between the dredge haul site and the nearest sampling site used in this study is 14 km. The fact that our study did not pick up the dredge haul anomalies illustrates the importance of selecting the right sampling interval when attempting to delineate concentrations of heavy minerals and their associated heavy metals.

Ce

Ce (cerium) is a heavy metal classified with a group of chemically similar elements called the lanthanides. The lanthanides usually occur together and their most common source mineral is monazite which is a fairly

rare and complex phosphate occurring as an accessory mineral in granites, gneisses, aplites, and pegmatites. Monazite is resistant to chemical attack and is often concentrated in sands, particularly beach placers (Bateman, 1965; Sienko and Plane, 1961). The presence of cerium and other lanthanide elements in the same samples would be strong evidence then for the presence of monazite in the samples.

La (lanthanum) and Ce anomalies on our maps (Figs. 16, 17, and 50,51) generally coincide. The only real difference is that La has a much lower limit of detection than Ce and therefore shows much greater definition in the lower value range. Neodymium (Nd), another lanthanide, was detected in three raw bulk samples and these three samples also had anomalously high values for La and Ce. It is clear that these three elements occur together. Strong evidence that the containing mineral for these elements is monazite is the occurrence of Ce and Nd in concentrates from replicate samples. Analyses from raw bulk samples of the same sample set show either an absence of Ce or Nd or much lower values. This indicates that these elements are present in a heavy mineral like monazite that may be hydraulically concentrated.

The highest values for Ce as well as for La and Nd are from the sample 30 km south of Cape Prince of Wales. Their presence together lends support to the probability that the sample had indeed been placered.

C. Potentially Toxic Elements

Of the potentially toxic elements considered in this report, only Cu, Pb, and Zn have sufficient numbers of values greater than their lower limits of detection to calculate meaningful statistics or to plot their value surfaces. Cd (cadmium) was not detected in any sample analyzed. Sb (antimony) was detected only in beach samples taken near the Bluff, the NE Cape of St. Lawrence Island, and from Stuart Island, while As (arsenic) was

detected only in the beach samples from Bluff. Anomalous values are not found offshore from these beach areas. The values for Sb and As in these samples are several orders of magnitude higher than their limits of detection by the 6-step emission spectrographic technique and can therefore be considered to be anomalous. The map depicting source areas (Fig. 2) for some of the more economically important elements of this study shows Bluff as a known area of concentration for As.

Distribution of Cu, Pb, and Zn surface values in shelf sediments of Norton Basin have broad similarities including anomalously high values off St. Lawrence Island, along the southern coast of the Seward Peninsula, and throughout Norton Sound. The maps for Cu and Zn show much greater similarity to each other, however, than to the map for Pb (Figs. 18, 19, 20, 21, 22, and 23). Statistically, Pb correlates better with Cu and Zn than with any other element represented in the study (Table III), but Cu and Zn have a much higher correlation between themselves (.8023) than with Pb which supports the relative visual similarity between the maps of these elements.

A significant trend that shows up in both the Cu and Zn maps is the generally higher values in Norton Sound compared to Chirikov basin. High values for Cu and Zn form a halo surrounding the Yukon Delta and in both cases the western edge of the halo trends due north along a line extending from the southern edge of the Yukon Delta towards the Bering Strait. The location of this halo coincides quite closely to the area of maximum deposition of Yukon-derived sediment in Norton Sound (Nelson and Creager, 1977). The gradation of Cu and Zn values away from the delta and the generally higher values for these elements in Norton Sound suggest a source and dispersal with Yukon-derived flows through an area highly mineralized in these elements and thus appears to be the dominant source for minerals bearing these elements.

Another significant aspect of the Cu, Zn and Pb distribution is localized high values found generally close to certain coastal areas. All three elements have their highest values in beach samples taken near Bluff, Alaska (not completely represented on value surface maps.) Pb and Cu show a continuation of these high values up to 20 km offshore from Bluff. Unlike Cu and Zn, except for values from the Bluff beach samples, Pb deviates little from the geometric mean; though fairly high values can be seen adjacent to Stuart Island and the eastern tip of St. Lawrence Island. Cu also shows high values near Stuart Island and the eastern tip of St. Lawrence Island. In addition, high values are found off the southern coast of eastern St. Lawrence Island and off the north-central projection of the island as well as off Nome and in an area around King Island. High Zn content occurs off south-central St. Lawrence Island as well as off the north-central part. Zn also has relatively high values off Nome, in a sample taken 30 km south of Cape Prince of Wales, and along the eastern edge of Norton Sound, but has its greatest quantities (except for the Bluff beach samples) in the central portion of eastern Norton Sound. This last Zn anomaly is rather puzzling and does not appear to be related to dispersal with Yukon sediment or to the nearshore high values that seem to be caused by concentration in sediment derived from immediately adjacent land areas.

In summary, the 'toxic' elements discussed here apparently have their highest values in relatively localized beach areas close to known terrestrial sources or are clearly derived from the sediments eroding from nearshore areas close to probable higher concentrations of these elements. Other elevated contents offshore are probably related to general sediment dispersal within the region and the possible placer concentration of those elements aggregated in 'heavy minerals'. An example of high values over a broad area which are

probably related to sediment type/source terrains are the regionally high values of Cu and Zn over Norton Sound.

D. Chemical-Environmental Change Indicators

The elements of Fe, Mn, and Co are singled out here because they are more apt to be chemically dissociated from the minerals and sediment in which they originate than most of the other elements under discussion. Ba is included because of its use as a drilling mud and the resulting potential contamination of sediment where it is used.

Fe and Mn are quite responsive to changing oxidation/reduction environments and as a result often dissociate from their originating minerals. Co is less sensitive but is subject to co-precipitation and co-solution at the same time as Fe and Mn.

An example of this kind of Fe/Mg cycle taking place is in sediments rich in these elements that are deposited with much organic debris. The organic debris creates a reducing environment which can cause the Fe and Mn to be reduced and to go into solution. The Fe⁺⁺- and Mn⁺⁺-rich solutions then tend to rise and to be precipitated at the sediment-water interface by the oxidation environment existing there (Kennedy, oral commun., 1978).

The value surface maps for Fe, Mn and Co are quite similar (Figs. 24, 25, 26, 27, 28, and 29). The most obvious correlations are the high anomalous values each map shows in the areas of the north-central St. Lawrence Island volcanics and the volcanics of the Stuart Island area. Anomalies in these volcanogenic areas have also been found for Cu, Ni, and Cr (other mafic-associated elements) as has already been pointed out. The other obvious correlation is the wide area with high values surrounding the Yukon Delta in particular and Norton Sound in general; however, Co does not show this pattern to the degree that Fe and Mn do.

Fe, Mn and Co anomalies in sediments off the volcanic areas obviously have been derived from the nearby volcanic terrain. The anomalous values for Mn and Fe in these areas are almost exact reflections of the content of these elements as determined for an average suite of basalts. For instance, the value of Mn in the Stuart Island area is 1,700 ppm. This is equivalent to .17% which is the approximate average value measured for a variety of basalts from different parts of the world. The value of Fe surrounding Stuart Island is 10-12% which is also the average content for Fe in the basalts mentioned (Carmichael et al., 1974).

High values surrounding the Yukon Delta, much of Norton Sound, and northward toward the Bering Strait seem to fall mainly within the area defining the prevalence of modern Yukon sediment. The generally high values in this region probably are directly related to Yukon source sediment which is in part derived from the input of mafic volcanic terrain in the river drainage basin. Anomalous values of Fe, Mn or Co resulting from concentrated precipitates of these elements are not readily apparent. This could only be determined by taking a closer look at the exact mineral species containing Fe and Mn.

The highest Mn value was detected in a sample from 30 km south of Cape Prince of Wales that has been previously discussed. This sample is considerably removed from land and it is probable that its high Mn values are due to mechanical concentration rather than having been directly derived from volcanic terrain.

The value surface maps for Ba show slightly anomalous values surrounding the Yukon Delta, in addition to high values near Stuart Island and at various locations along the southern coast of the Seward Peninsula (Figs. 30 and 31). The highest anomalies are just off the southern edge of St. Lawrence

Island and in the middle of Anadyr Strait. The general elevation of values surrounding the delta has already been noted for other elements and seems to be related to the Yukon sediment source and dispersal pattern. The anomalies near Stuart Island and the southern coast of Seward Peninsula appear as lobes coming off the land and may be correlated with sediment sources from igneous rocks in those areas. The origin of the high values close to St. Lawrence Island are more obscure. None of the elements that correlate with Ba have outstanding anomalies in the Anadyr Strait and only Sr has high values off the southern edge of St. Lawrence Island. The value of 1500 ppm in Anadyr Strait is equal to .15% and could reflect a source for Ba mineralization on the point of the Chukotka Peninsula.

E. Major Elements

The samples used in this study were analyzed for all of the major elements (Si, Ti, Al, Fe, Mn, Mg, Ca, Na, K, and P). Values for Si, however, were higher than the upper limit of detection (10%) in every sample analyzed and are not represented here.

Value surface maps for these elements show some of the general element distribution patterns already discussed. Mn, Fe, and Ti appear to have higher values surrounding the Yukon Delta and in Norton Sound as opposed to the Chirikov Basin (Figs. 24, 25, 26, 27, 32, and 33). Ca, Mg, and Na show a similar trend to some degree and it is slightly noticeable for K and Al (Figs. 34, 35, 36, 37, 38, 39, 40, 41, 42, and 43). Each element also has its anomalously high values near what appear to be clearly defined land sources.

The higher Ti values generally correspond with those for Mn and Fe which have already been shown to be associated with the volcanics of Stuart Island and St. Lawrence Island. This is expected because Ti content is relatively high in basaltic rock types (Fig. 4). The highest Ti value is from the sample

previously discussed that comes from 30 km south of Cape Prince of Wales. This sample does not appear to be derived directly from a volcanic terrain. Ca and Mg also exhibit high values near the Stuart Island and St. Lawrence volcanics for the same reason, but they are highest offshore from the southern coast of Cape Prince of Wales and south of Port Clarence. Their high values in these last areas probably are related to the limestone formations found on Cape Prince of Wales and in outcrops reported on the sea floor south of Port Clarence (Nelson et al. in preparation,; Nelson and Hopkins, 1972). Sr anomalies, normally associated with limestone, exist in the same areas.

Na, K and Al exhibit more variegated value surfaces than the other major elements. Their value surface maps consist of alternating high and low values and show only slight regional differences. The anomalies that do seem to originate from land sources appear broader in areal extent than some of the less common elements already discussed. The highest value for K is off of the NE Cape of St. Lawrence Island and is probably related to the granitic bodies that are found there. Al has highest values in the Stuart Island and eastern Norton Sound areas and is probably related to basalts.

P (phosphorus) was found in only 54 samples. It was not used in the correlation analysis. The lower limit of detection is .10% which is somewhat higher than amounts found in average shales and sandstones (Mason, 1966). Elevated values are found in the eastern portion of Norton Sound, in a few patches surrounding the Yukon Delta and in a swath running through eastern Anadyr Strait and hooking to north of St. Lawrence Island. The highest value is found in an enclosed basin just off the northeast coast of St. Lawrence Island. This high value may be related in some way to the reducing conditions of the enclosed basin (Mason, 1966).

Percent composition of the major elements in sediment just off the Yukon

Delta is intermediate between the average profiles for these elements in granite and monzonites and is very close to the profile for average shales. Al is an exception (Fig. 4) because its content is closer to the average in sandstones. In contrast, a percentage composition profile taken in the middle of Chirikov Basin sands shows less Al, much less Fe, and less than half as much of the other major elements compared to Yukon silts and, except for more abundant Ca, is very close to that of the average sandstone.

F. Minor Elements

The minor elements Sr, Sc, La, Ga, Nb, Nd, B, Y, Yb, and Be show correlations with other element distributions. Sr, as previously mentioned, has anomalous values that correspond quite closely to the Ca anomalies. However, the correlation coefficients, which measure the degree of relation between Sr and other elements, are higher between Sr and K, Na, Ba, and Al than between Sr and Ca (see Tables III and IV). The association of Sr with Ba is a common one but the association of Sr with K, Na, and Al is puzzling and does not seem to be borne out by a visual comparison of the value surface maps of these elements (Figs. 46, 47, etc).

Sc (scandium) has relatively high correlation coefficients with Ti, Fe, V, La and Mn and exhibits the same general distribution with higher values grading off the Yukon to lower values in Chirikov Basin (Figs. 48 and 49). The association of Sc with La and Nd is common and the usual mineral containing them is monazite (Figs. 50 and 51). Ga (galium) also shows some association with La, Sc, and Ti. The highest values of Ga are in Anadyr Straits and the eastern end of Norton Sound (Figs. 52 and 53).

Nb (niobium) exhibits no correlation with any other Norton Basin elements but typically is associated with Ta (tantalum) in the oxides of columbite and tantalite. Tantalum has not been detected however, because of a relatively

high lower limit of detection of 50 ppm as opposed to 7 ppm for Nb. The greatest values are located off Cape Darby in Norton Sound and southwest of St. Lawrence Island (Figs. 54 and 55). The anomaly off Cape Darby correlates with the highest Nb anomalies detected in western Alaska found on the Darby Peninsula (Miller and Grybeck, 1973).

B (boron) has a correlation coefficient closer to K and Ba than any other element. High values are located at the eastern end of Norton Sound, off Cape Darby, off the coast from Bluff, off Cape Rodney, and southwest of St. Lawrence Island (Figs. 56 and 57).

Y (yttrium) follows the pattern of elements with generally high values surrounding the Yukon Delta and Norton Sound and with low values in the Chirikov Basin (Figs. 58 and 59). It correlates most closely with Mn, Fe, and Ti which also follow this pattern. Very localized high anomalies are found off Cape Prince of Wales, Nome, and Bluff.

Yb (ytterbium) correlates most closely to Mn, Zn, and Y but has no pronounced trends except for the general trend of high values in Norton Sound, and low values in Chirikov Basin (Figs. 60 and 61). A few very high values are found off Cape Prince of Wales, at various localized points off the southern coast of Seward Peninsula, in the general area of eastern Norton Sound, and NNE of St. Lawrence Island.

Beryllium (Be) correlates closest to La, Yb, and Sc and shows elevated values in eastern Norton Sound, along the southern coast of the Seward Peninsula, and off the southwest and southeast coasts of St. Lawrence Island. Highest values are just off Tin City at Cape Prince of Wales and one close to Stuart Island. These two high values as well as other high values that appear as lobes coming off the land indicate that specific mineralized terrain are probable sources. This is confirmed in the case of the Cape Prince

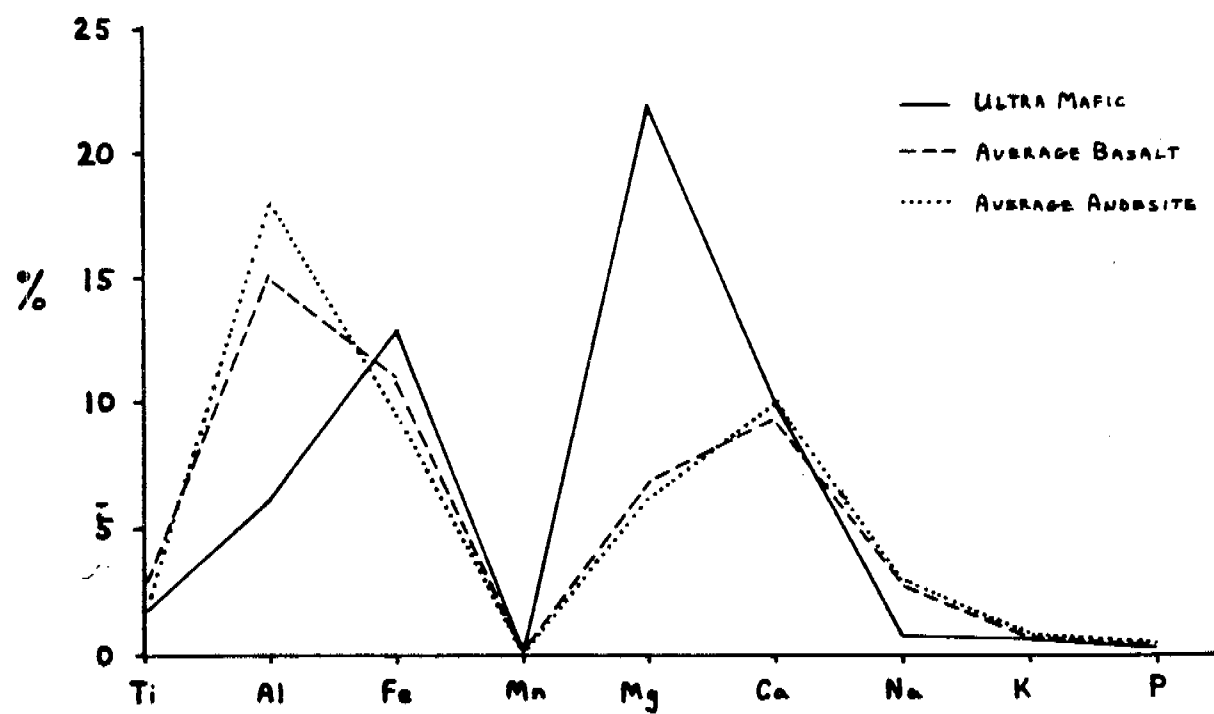
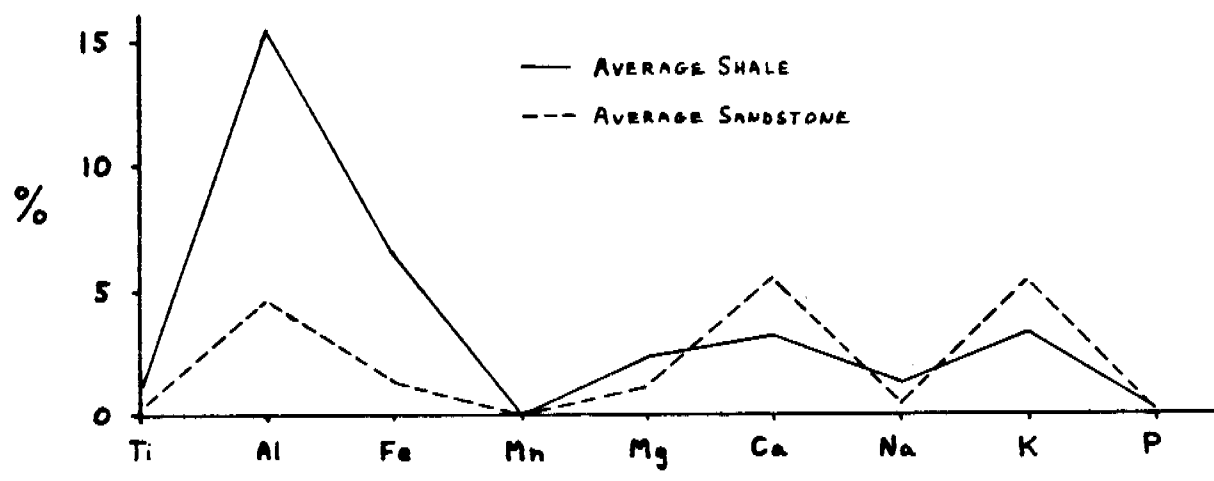
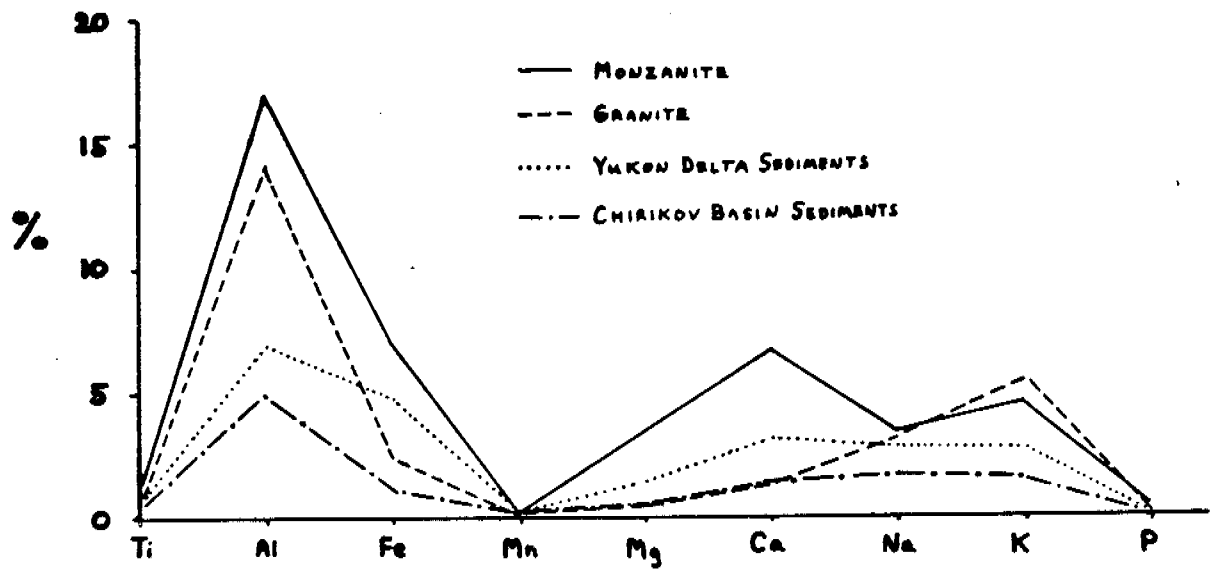


Figure 4. Relative abundance of major elements in standard rock types and in sediment off the Yukon Delta and from the Chirikov Basin

of Wales anomaly, where extensive economic grade beryllium deposits have been reported by Sainsbury, 1969, in the central York Mountains. The variance of Be values is quite small.

G. Other Miscellaneous Economic Elements

Au was not detected in any of the samples analyzed. This was to be expected because the lower limit of detection for Au using the emission spectographic method, is 7 ppm. A study by Nelson and Hopkins, 1972, has shown that average Au values in open Bering Sea sediments are roughly 2-3 parts per billion (ppb). The highest nearshore values found in relict gravel and selected ruby sands ranged from 556 to 2,118 ppb. These values are quite a bit lower than 7 ppm which is equivalent to 7000 ppb.

Ag was detected in only 8 of the 180 samples and 3 of these samples were below the limit at which a reasonable quantitative estimate can be made (7. ppm). High values showed up off the NW Cape and the southern tip of St. Lawrence Island (Figs. 64 and 65). Mineralization containing appreciable amounts of Ag has been reported on both ends of St. Lawrence Island and could be the source for these anomalies. Relatively high values were also found near Stuart Island and close in to the Yukon Delta. In addition, Ag was detected in a few places off Nome and Cape Nome. Bluff had very high values in beach samples whose element values were not plotted on the value-surface maps.

Mo was detected in only 5 of the 180 samples. Mo in all the other samples was below the limit of detection of 2 ppm. The highest values were detected in the vicinity of Stuart Island (Figs. 66 and 67). Another high value was found off Bluff and the presence of Mo was detected off Cape Rodney. Mo has been reported in mineralization inland from the coast of eastern Norton Sound and in the Nome area.

Bi was below the limit of detection of 7 ppm in all but 2 samples. The highest value of 70 ppm was from sediment close to the Lost River Mining District on Cape Prince of Wales that also had an anomalously high Sn value. Bi is often found in association with Sn ores and has been shown by Sainsbury, 1969, to occur, in the form of bismuthinite, as one of the main mineral constituents of a skarn zone associated with the Sn and Be deposits at Lost River. The other value was detected off the known mineralized area of Bluff which also exhibits high values for Cu, Pb, Zn, Mn, Sb, and As.

H. Q- and R- Mode Factor Analysis

General

Q-mode analysis was employed to discover possible relationships between groups of samples. R-mode analysis was used to determine relationships between groups of elements. The results of the two types of factor analyses may be linked if significant sample groups, as defined by Q-mode analysis, are found to contain characteristic groups of elements as defined by R-mode analysis.

Four factors from the Q-mode varimax factor matrix were found to explain 92% of the variance between samples (see Table VII). Of these factors, Factor III was judged to include the most important sample group because it explained 33.4% of the variance between samples. Factor I explained 24.3%, Factor IV explained 22.5% and Factor II with a variance of 11.8%, encompassed the fewest samples.

The highest factor loading values for Factor III were found in an apron around the Yukon Delta and in patches in the west-central part of Norton Sound and NNW of St. Lawrence Island and in Anadyr Strait (Fig. 5). Intermediate high values were found to exist in a wide apron around the Yukon Delta and throughout most of Norton Sound; around the northern, eastern, and southern coasts of St. Lawrence Island, and south of Cape Prince of Wales.

The highest loading values for Q-mode Factor I, which explained the next highest number of samples, were in an area that generally covers the low value areas for Factor III, namely the Chirikov Basin region (Fig. 5). The highest loading values for Factor II were found along the coast between Cape Rodney and Golovnin Bay, just off Cape Prince of Wales and near King Island. The highest loading values for Factor IV are located in patches north of St. Lawrence Island, at random spots throughout Norton Basin, and at spots just off the south coast of the Seward Peninsula.

Scaled varimax factor scores (Table VI) were computed for each element during the Q-mode analysis in order to determine the elements that are most correlative with each factor group. As an additional check of elements vs. Q-mode factor relationships, correlation coefficients were computed between element values and factor loadings for all the samples (Tables III and V). Both the Q-mode scaled varimax factor scores and the correlation coefficients between varimax factor loadings and element values indicate that Factor III samples contain strong relations between the elements Ba, Na, Sr, La, K, Ga, Al, and Sc. B and V were best represented in Factor I; Factor II was correlative with Y, Fe, Mn, Ti, Yb, Zn, Co, Sc, Cu, and V. The only element that seems to correlate somewhat with Factor IV is Nb.

Only the first two factors of the R-mode analysis were large enough to be significant (Tables VI and VIII). Factor IV related only three elements: Ca, Mg, and Sr; an expected correlation. The other R-mode factor grouping was not significant.

Factor II of the R-mode analysis groups contains the elements K, B, Na, Sr, Al, and La. This grouping is almost identical to Factor III of the Q-mode analysis. Factor I from the R-mode analysis groups Fe, Zn, Cu, Mn, Ti, Ni, Co, Sc, Yb, and Y. This factor is about the same as the group of elements

that were found to be correlative with Factor II of the Q-mode analysis. The other R-mode element groups do not bear any relation to the two other significant Q-mode sample groups.

The plot of the high factor loadings from Factor III of the Q-mode analysis (0.5 and above) is significant in that the plotted area corresponds quite closely to the area of predominant Yukon Holocene sediment deposition; though high values are also found north of St. Lawrence Island and in Anadyr Strait. The element grouping in this factor is important because it relates elements that are most abundant in sialic rock types. This fits the observation made earlier about the general composition of Yukon sediment indicated by the percent-composition profiles of the 'major' elements in the sediment (Fig. 4). The occurrence of high Factor III values elsewhere probably indicates that the sediment in these areas is similar to Yukon-type sediment and that they also originate in terrain dominant in sialic rock types.

High factor loadings for Factor I of the Q-mode analyses correspond to areas where modern Yukon sediment is absent but where Holocene transgressive sands of mixed origin are found. This general area covers the region of Chirikov Basin, but there does not seem to be any significant element grouping in this factor.

Factor II of the Q-mode analysis has its highest values very close to the Nome-Bluff strand line. Other regions with high values exist off of Cape Prince of Wales and King Island. Significantly, these areas are highly mineralized and the heavy metal elements that are shown to group in these samples bear this out. The elements also are mainly associated with the mafic end of an acidic-mafic composition spectrum.

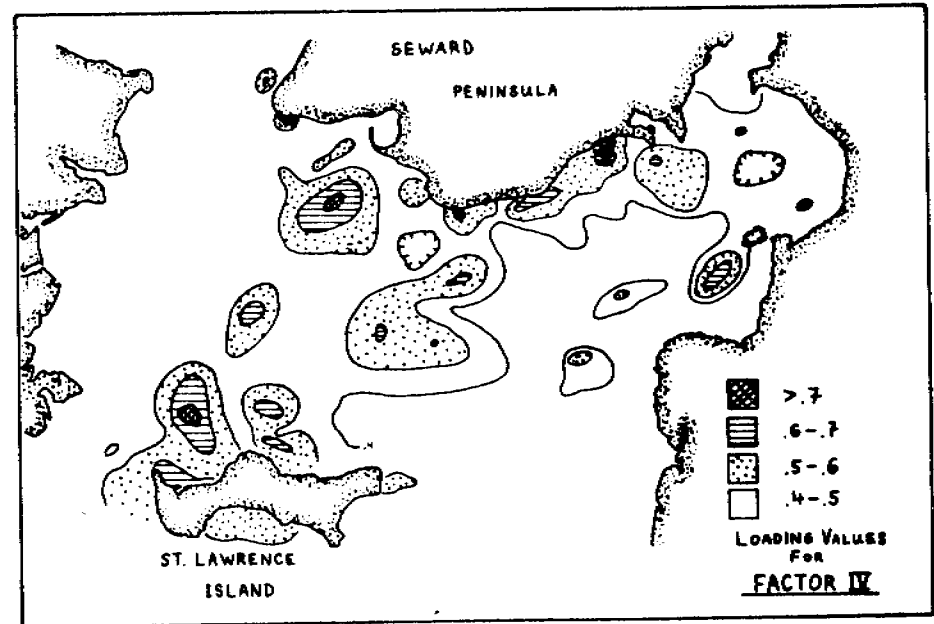
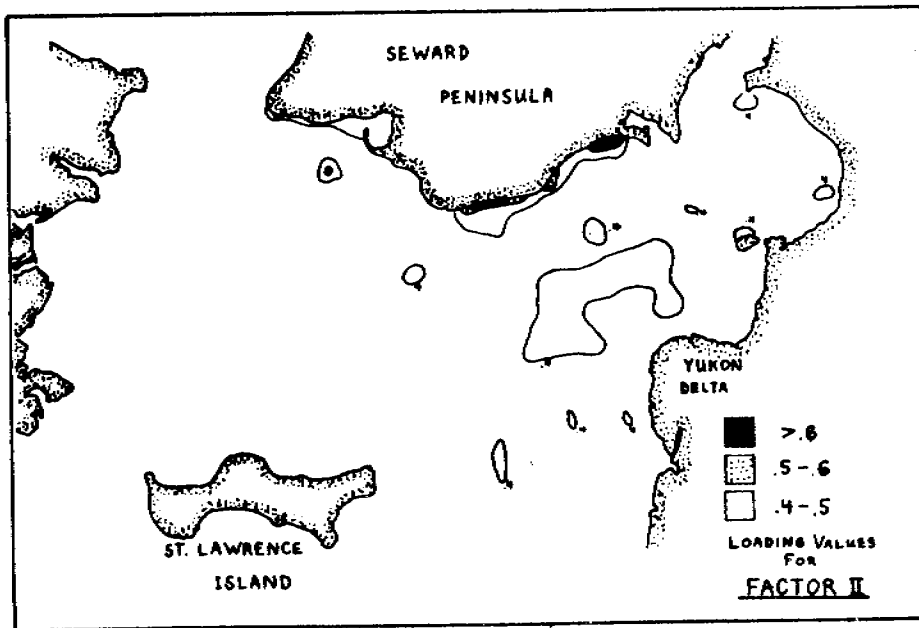
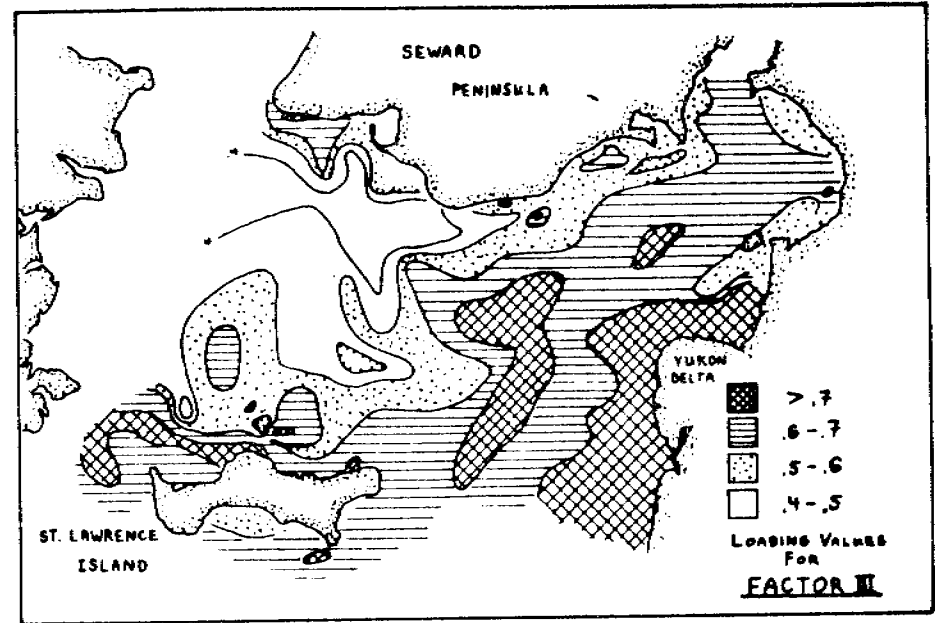
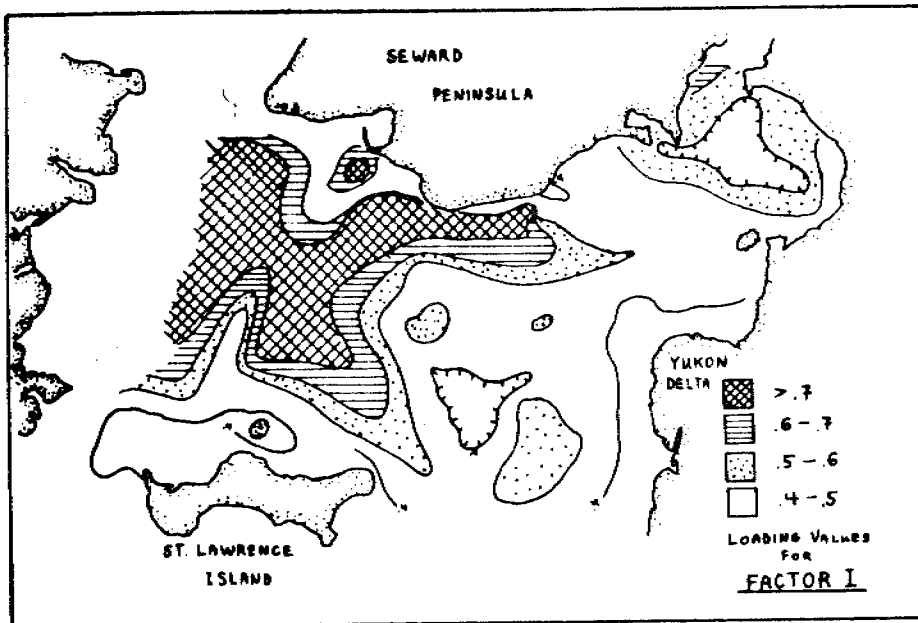


Figure 5. Distribution of Q-mode Factor loadings for the first four factors.

The contoured surface of Factor IV shows a rough correlation with areas reported to be covered by relict glacial debris and lag gravel, particularly in a lobe extending NE of St. Lawrence Island (McManus et al., 1977). Otherwise, its significance is not readily apparent.

VII. CONCLUSIONS AND NEED FOR FURTHER STUDY

Accuracy determinations for each element analyzed by this method indicate that element values for Y, Ca, Ba, K, Cr, Cu, Na, Co, Nb, Ni, V, and Zn fall within 30% of established values for rock standards. Values for these elements thus are good as baseline data. Values for Sr, Al, Sc, Zr, Ti, Ga, Pb, Fe, Mn, and Mg were within 35-65% of the actual values for rock standards and can therefore be regarded as providing reasonable baseline data. The elements Ag, As, Bi, Mo, Sb, Sn, P, Ce, and Nd had too few values to say anything about their accuracy. Values for Si were higher than the upper limit of detection in every sample. No values were found for Au, Cd, Pd, Pt, Te, U, W, Ge, Hf, In, Li, Re, Ta, Th, Tl, Pr, Sm, Eu, Gd, Tb, Dy, Ho, Er, Tm, and Lu because either the sensitivity of the analytic technique was not great enough or because these elements were not present in the samples analyzed.

High V and Ni values have been noted in sediment in the areas of petrogenic seeps. Values for these elements from a grid of samples covering a probable thermogenic gas seep 35 km south of Nome were no different than background values for these elements in the northern Bering Sea. Lack of V and Ni anomalies for this gas seep may only mean that the seep source is of a light hydrocarbon gas type that does not show high Ni and V values as do some heavy hydrocarbon petroleum seep sources. A location 40 km west of the southern tip of St. Lawrence Island has high values V and Ni and warrants a closer study of its petroleum potential. Other high values for Ni located in the vicinity of Stuart Island and off the north and south coasts of St.

Lawrence Island are related to the basaltic volcanics in these areas, not petroleum sources.

Pb, Cu, Zn, As, Sb, and Cd are considered to be potentially toxic when found in sufficient concentrations. Presently, the highest values of any of these elements are derived from highly mineralized onshore locations, for example, Cu and Zn off St. Lawrence Island, Nome, and Bluff beaches, and high Cu values off Stuart Island. The few values detected for Sb and As can be regarded as derived from anomalous onshore mineralization near Bluff, the NE tip of St. Lawrence Island, and just off Stuart Island. Both Cu and Zn have relatively high values off the Yukon Delta and in Norton Sound that correspond to the coverage of Yukon Holocene sediment.

Pb varies little from its geometric mean but does show relatively high values off the Bluff beach, Stuart Island, and the eastern tip of St. Lawrence Island.

Because the elements Zr, Sn, Cr, and Ce are commonly found in heavy minerals, anomalous values may well indicate placer as well as primary lode occurrences of these minerals. Anomalously high Zr values were found off the NE Cape and the western portions of St. Lawrence Island and probably originated from zircon-containing quartz monzonitic rocks on the island. Regionally elevated values were found coincident with Yukon sediment distribution. The highest values for Sn are found close to Tin City and originate in the tin mineralization there. Detection of Sn near Bluff and Cape Rodney-Nome areas again may be related to tin mineralization known to exist in these areas. The presence of Sn in the areas of King Island, Port Clarence, and in the Anadyr Strait may be examples of tin placering caused by the relatively high currents there. The high Cr values were found off Stuart Island, Cape Prince of Wales and northcentral St. Lawrence Island. appear to

be related to basalts or granites containing ultra-mafic dikes that are sources of chromite. Samples with high Ce values have high La values and often high Nd values, suggesting a source from the heavy mineral monazite--concentrated as a placer mineral. Because monazite is probably the primary carrier of Ce and related elements and because it placers, it promises to be a good indicator of sediment dispersal trends.

Sediment from 30 km south of Cape Prince of Wales was found to contain the greatest amounts of Cr, Zr, Ce, Ti, Mn, La, Sc, Y, Yb, and Nd of all the samples analyzed and also contained high tin values. Because of these high values and because the sample contains high values of La and Nd which are commonly found with Ce in the heavy mineral monazite, this sample may represent an area where extensive placering occurs. The existence and extent of a potential placer field should be explored in this area. Future studies of Sn, Zr, Cr, and Ce and their containing heavy minerals should use sampling intervals close-spaced enough to detect significant variations in their values caused by hydraulic concentration. Care should also be taken to mechanically concentrate samples before analysis.

Fe, Mn, Co, and Ba were considered together as chemically or environmentally sensitive elements. Fe, Mn, and Co all show high values near the volcanics of Stewart Island and north-central St. Lawrence Island. The actual Fe and Mn content of these samples is equal to their content in average element suites for various types of basalt. These elements also correlate with value trends of Cu, Zn, V, Y, and Zr showing generally high values in the areas of Yukon Holocene sedimentation and generally low values in Chirikov Basin. Co, however, does not follow this trend as closely as Fe and Mn. Elevated Ba values correlate with Yukon sediment distribution but also are found close to Stuart Island and at various locations along the southern coast

of the Seward Peninsula. The maximum value (.15%) is found in the Anadyr Strait and is unique in that other elements that usually correlate with Ba are not similarly high at this location.

Of the major elements, Ti is closely associated with Fe and Mn, discussed above, all of which show the trend of generally high values in Yukon sediment with very high values in areas close to the volcanics of Stuart Island and St. Lawrence Island. Ca and Mg values are relatively high in Yukon sediment and are elevated close to the volcanic areas mentioned. The highest values of Ca and Mg are probably related to the limestone formations of Cape Prince of Wales to Port Clarence areas. Values for Na, K, and Al exhibit more erratic variation than values for the other major elements and the anomalies of Na, K and Al that appear to originate from land sources are broader in areal extent. P occurred sporadically in eastern Norton Sound, Anadyr Strait, and surrounding the Yukon Delta. The highest value was from an enclosed basin NE of St. Lawrence Island and could be a result of reducing conditions in the basin. The relative percent composition of the major elements in sediment around the Yukon Delta is very close to the relative percent composition for these elements in granites and monzonites. The relative percent composition of these elements in sediment from the Chirikov Basin region is similar to that of granites and monzonites but is much closer to average sandstones.

Of the minor trace elements that are not usually regarded as potentially toxic, Sc correlates closest with Ti, Fe, V, La, and Mn. Yttrium correlates closest with Mn, Fe, and Ti. Yb correlates closest with Mn, Zn, and Y. Sc, Y, and Yb all follow the general trend of high values in Yukon sediment and low values in the Chirikov Basin. Nb exhibited minimum values off Cape Darby where the highest Nb anomalies on land in western Alaska have been found. Nd was detected in two places in Norton Sound and in sediment north of King

Island and correlates with high La and Ce values. These elements probably exist in the mineral monazite. Slightly higher values of Be can be found just off the coasts enclosing Norton Basin but maximum offshore values near Cape Prince of Wales correlate with economic Be deposits there.

Of the economically important elements, Ag, Mo, and Bi, high Ag values showed up off St. Lawrence Island, near Stuart Island, and close to the Yukon Delta offshore from terrestrial Ag mineralization sites; significant Mo was found off the Bluff beach mineralization; and Bi was detected off the Cape Prince of Wales mineralization area that has associated Bi.

A contour map of the Q-mode factor loading values for Factor III outlines an area corresponding to the distribution of Yukon Holocene sediment plus areas in Anadyr Strait and north of St. Lawrence Island. Scaled varimax factor scores and cross correlation between factors and element values indicate that Factor III is best represented by the elements Ba, Na, Sr, La, K, Ga, Al, and Sc. These elements are also associated in Factor II of an R-mode analysis of the data. The significance of this element grouping is that it is weighted toward the silicic end of the rock-type spectrum which agrees with the general element profile for Yukon sediment described elsewhere in this report. Factor I of the Q-mode analysis corresponds generally with the Chirikov Basin relict sediment area. Factor II of the Q-mode analysis occurs off the coast from Bluff, Nome, and Tin City, suggesting a strong correlation with the high mineralization in these areas. This is confirmed by high correlation of Fe, Mn, Ti, Co, Zn, Sc, Cu, Y, and V with this factor as shown by correlation analysis and scaled varimax factor scores. R-mode Factor I loadings encompass these same elements. Factor IV of the Q-mode analysis does not have any clear-cut relation to sedimentological or mineralogical characteristics but shows some correlation with areas of known glacial debris.

REFERENCES

- Bateman, A.M., 1965, *Economic Mineral Deposits*: John Wiley and Sons, Inc., New York, 916 p.
- Cacchione, D.A., and Drake, D.E., 1978, Sediment transport in Norton Sound-Northern Bering Sea, Alaska, in: *Environmental Assessment of the Alaskan Continental Shelf, Annual Report of Principal Investigators for the year ending March, 1978*: Environmental Research Laboratory, Boulder, Colorado, NOAA, U.S. Dept. of Commerce, v. 12, p. 308-450.
- Carmichael, I.S.E., Turner, F.J., Verhoogen, J., 1974, *Igneous Petrology*: McGraw Hill Book Company, New York, 739 pages.
- Coachman, L.K., Aagaard, K., and Tripp, R.B., 1976, *Bering Strait: The regional physical oceanography*: Seattle, Washington, University Press, 186 p.
- Cobb, E.H., 1960, Sb, bismuth and mercury occurrences in Alaska: U.S. Geological Survey, Mineral Investigations, Resource Map MR-11.
- _____, 1960a, Chromite, cobalt, nickel, and platinum occurrences in Alaska: U.S. Geological Survey, Mineral Investigations Resource Map MR-8.
- _____, 1960b, Copper, lead, and zinc occurrences in Alaska: U.S. Geological Survey, Mineral Investigations, Resource Map, MR-9.
- _____, 1960c, Molybdenum, tin, tungsten occurrences in Alaska: U.S. Geological Survey, Mineral investigations, Resource Map MR-10
- _____, 1962, Lode gold and silver occurrences in Alaska: U.S. Geological Survey, Mineral Investigations, Resource Map MR-32.
- _____, 1964, Iron occurrences in Alaska: U.S. Geological Survey, Mineral Investigations, Resource Map MR-40.

- Cohen, A.C., Jr., 1959, Simplified estimators for the normal distribution when samples are singly censored or truncated: *Technometrics*, v. 1, no. 3, p. 217-237.
- Dean, W., Gardner, J., and Vallier, T., 1978, Inorganic geochemistry and sedimentology of surface sediments, outer continental shelf, southern Bering Sea, Alaska: International Sedimentological Congress, Israel.
- Eberlein, G.D., Chapman, R.M., Foster, H.L., Gassaway, J.S., 1977, Map with table showing known metalliferous and non--metalliferous mineral deposits in central Alaska: U.S. Geological Survey Open-file Report 77-168-D.
- _____, Menzie, W.D., 1978, Maps and tables describing areas of metalliferous mineral resource potential of central Alaska: U.S. Geological Survey Open-file Report 78-1-0.
- Fathauer, T.F., 1975, The great Bering Sea storms of 9-19 November, 1974 Weatherwise Magazine, American Meteorological Society, v. 28, p. 76-83.
- Flores, R.M., Shideler, G.L., 1978, Factors controlling heavy-mineral variations on the south Texas outer continental shelf, Gulf of Mexico: *Journal of Sedimentary Petrology*, v. 48, p. 269.
- Grimes, D.J., and Marinizino, A.P., 1968, U.S. Geological Survey, Circular 591.
- Hudson, T., Miller, M.L., Pickthorn, W.J., 1977, Map showing metalliferous and selected non-metalliferous mineral deposits, Seward Peninsula, Alaska: U.S. Geological Survey, Open-file Report 77-796B, 46 p.
- _____, DeYoung, J.H., Jr., 1978, Maps and tables describing areas of mineral resource potential, Seward Peninsula, Alaska: U.S. Geological Survey, Open-file Report 78-1-C, 62 p.

- Hummel, C.L., 1977, Review of exploration geochemical surveys on Seward Peninsula, Western Alaska: U.S. Geological Survey Open-file Report 77-796D, 28 p.
- Kvenvolden, K.A., Weliky, K., Nelson, C.H., DesMarais, D.J., 1979, Submarine seep of carbon dioxide in Norton Sound, Alaska: Science, v. 205, No. 4412, p. 1264.
- Mason, B., 1966, Principles of Geochemistry: John Wiley and Sons, Inc., New York, 329 p.
- _____, Berry, L.G., 1968, Elements of Mineralogy: W. H. Freeman and Company, San Francisco, California, 550 p.
- McManus, D.A., Venkatarathnam, K., Hopkins, D.M., Nelson, C.H., 1977, Distribution of bottom sediments on the continental shelf, northern Bering Sea: U.S. Geological Survey Professional Paper 759-C, p. C1-C31.
- Meisch, A.T., 1967, Methods of computation for estimating geochemical abundance: U.S. Geological Survey Professional Paper 574-B, p. B1-B15.
- Miller, T.P., Grybeck, D., 1973, The geochemical survey of the eastern Solomon and southeastern Bendeleben Quadrangles, Seward Peninsula, Alaska: U.S. Geological Survey Open-file Report.
- Nelson, C.H., Hopkins, D.M., 1972, Sedimentary processes and distribution of partiulate gold in the northern Bering Sea: U.S. Geological Survey Professional Paper 689, 27 p.
- _____, Pierce, D.E., Leong, K.W., Wang, F., 1975, Mercury distribution in ancient and modern sediment of northeastern Bering Sea: Marine Geology 18C, p. 91-104.
- _____, and Creager, J.S., 1977, Sediment budgets and displacement of Yukon River sediments from Bering Sea in the late Holocene.

- _____, Larsen, B.R., Larsen, M., Thor, D.R., Sedimentary characteristics of the Norton Basin sea floor, U.S. Geological Survey Open-file Report (in prep.).
- Patry, J.J., Larsen, B.R., Nelson, C.H., Heropoulos, C., 1977, Trace metal content of bottom sediment in northern Bering Sea: Quarterly Report of Principal Investigators, April-June 1, in: Environmental Assessment of the Alaskan Continental Shelf, Environmental Research Laboratory, Boulder, Colorado, NOAA, U.S. Dept. of Commerce, Contract RK6-6074, 10 p.
- Patton, W.W., Jr., and Csejtey, B., Jr., 1971, Preliminary Geologic Investigations of eastern St. Lawrence Island, Alaska: U.S. Geological Survey Open-file report 52 p.
- _____, _____, 1971, Preliminary Geologic Investigations of western St. Lawrence Island, Alaska: U.S. Geological Survey Professional Paper 684-C, p. C1-C15.
- _____, _____, 1972, Analysis of stream-sediment and rock samples from St. Lawrence Island, Alaska, 1966-1971: U.S. Geological Survey Open-file Report, 78 p.
- Peratis, A., et al., 1978, User Manual for the Surface Display Library: Dynamic Graphics, Inc., Berkeley, California.
- _____, et al., 1978, User Manual for the Surface Gridding Library: Dynamic Graphics, Inc., Berkeley, California.
- Reed, W.E., Kaplan, I.R., 1977, The chemistry of marine petroleum seeps: Journal of Geochemical Exploration, No. 7., p. 255-293.
- Sainsbury, C.L., 1969, Geology and Ore Deposits of the Central York Mountains, western Seward Peninsular, Alaska: U.S. Geological Survey Bulletin 1287, 101 pages.

- _____, 1975, Geology, ore deposits, and mineral potential of the Seward Peninsula, Alaska: U.S. Bureau of Mines, Open-file Report, 108 p.
- Sheth, M., 1971, A heavy mineral study of Pleistocene and Holocene sediments near Nome, Alaska: U.S. Geological Survey Open-file Report, 82 p.
- Sichel, H.S., 1947, An experimental and theoretical investigation of bias error in mine sampling, with special reference to narrow gold reefs: London, Inst. Mining Metallurgy Trans., v. 56, p. 403-474.
- Sienko, M.J., Plane, R.A., 1961, Chemistry: McGraw Hill Book Company, Inc., New York, 673 p.
- Venkatarathnam, K., 1971, Heavy minerals on the continental shelf of the northern Bering Sea: U.S. Geological Survey Open-file report, 93 p.
- Yen, T.F., 1975, The role of trace metals in petroleum: Ann Arbor Science Publishers, Ann Arbor, Michigan, 221 p.

Figures

- Figure 1. Generalized map of the northern Bering Sea region, (Nelson and Hopkins, 1972).
- Figure 2. Offshore sampling locations and terrestrial sites of known mineralization for various elements.
- Figure 3. Map depicting significant anomalies defined as values falling outside the upper limit of the expected value range or as the highest few values (see Table I).
- Figure 4. Relative abundance of major elements in standard rock types and in sediment off the Yukon Delta and from the Chirikov Basin
- Figure 5. Distribution of Q-mode Factor loadings for the first four factors.
- Figure 6-67 shown on plates

TABLE IV

Correlation coefficients between element log values

TABLE V

Correlation coefficients between Q-mode Factor loading values and non-log element values.

TABLE VII

Q-mode varimax factor matrix associating samples into factor groupings.

TABLE VIII

R-mode varimax factor matrix associating elements into factor groupings.

TABLE I

Geometric means, geometric deviations, central and expected value ranges, and maximum and minimum values for different element groups in the Northern Bering Sea.

Element Group	Element	Geometric Mean	Geometric Deviation	Central Range*	Expected range**	Minimum Values	Maximum Values	
Petroleum Index Elements	Ni	22.7 ppm	2.01	11.3 - 45.6	5.6 - 91.6	7.0	1500.0	
	V	87.3 ppm	1.51	57.8 - 131.8	38.3 - 198.9	30.0	200.0	
Heavy Metal Element	Sn	too few values				N	100.0	
	Zr	162.4 ppm	1.56	104.2 - 253.1	66.8 - 394.5	50.0	2000.0 G	
	Cr	45.2 ppm	1.82	24.8 - 82.5	13.6 - 150.4	10.0	1000.0	
	Ce	too few values			N	300.		
Toxic Elements	Pb	20.5 ppm	1.66	12.3 - 34.0	7.4 - 56.5	N	500.0	
	Cu	12.6 ppm	2.17	5.8 - 27.4	2.7 - 59.5	3.0	700.0	
	Zn	72.8 ppm	1.70	42.8 - 124.0	25.1 - 211.0	N	1000.0	
	As	too few values				N	3000.0 ppm	
	Sb	too few values				N	1000.0 ppm	
Indicators or Change in Chemical Environment	Fe	2.29%	1.63	1.4 - 3.7	.86 - 6.1	.7	10.0 G	
	Mn	462.5 ppm	1.88	245.7 - 870.6	130.5 - 1638.8	150.0	7000.0	
	Co	11.6 ppm	1.80	6.4 - 20.9	3.6 - 37.7	5.0	100.0	
	Ba	551.3 ppm	1.70	323.6 - 939.3	189.9 - 1600.3	100.0	1500.0	
Major Elements	Al	5.6%	1.40	4.0 - 7.9	2.9 - 11.0	.7	10.0	
	Na	1.7%	1.72	1.0 - 3.0	.6 - 5.2	.07	3.0	
	K	1.5%	1.74	.9 - 2.7	.5 - 4.6	.1	5.0	
	Ca	1.6%	2.06	.8 - 3.4	.4 - 7.0	.2	10.0 G	
	Mg	.8%	2.08	.4 - 1.7	.2 - 3.5	.15	10.0 G	
	Ti	.4%	1.59	.3 - .7	.2 - 1.1	.1	2.0	
	P	too few values				N	.7%	
Minor Elements	Sr	222.7 ppm	1.81	123.1 - 402.5	68.2 - 727.5	30.0	1000.0	
	Y	26.9 ppm	1.50	17.9 - 40.5	11.9 - 60.9	10.0	150.0	
	Sc	12.1 ppm	1.50	8.0 - 18.2	5.3 - 27.4	5.0	50.0	
	Nb	11.3 ppm	1.47	7.6 - 16.6	5.2 - 24.5	N	30.0	
	B	73.7 ppm	1.72	42.8 - 126.9	24.9 - 218.6	N	150.0	
	La	41.4 ppm	1.63	25.5 - 67.3	15.7 - 109.5	10.0	100.0	
	Ga	10.3 ppm	2.45	4.2 - 25.3	1.7 - 62.1	N	30.0	
	Yb	3.4 ppm	1.52	2.2 - 5.1	1.5 - 7.8	1.0	10.0	
	Be	2.4 ppm	1.51	1.6 - 3.7	1.1 - 5.6	N	10.0	
	Wd	too few values			N	150.0 ppm		
	Miscellaneous	Ag	too few values				N	3.0 ppm
	Economic Elements	Ri	too few values				N	70.0 ppm
	Mo	too few values			N	30.0 ppm		

* Central Range = geom.mean/geom. dev. to geom. mean x geom. dev.

**Expected Range = geom. mean/(geom.dev.)² to geom. mean x (geom. dev.)²

G = > greater than accompanying value (upper limit of detection)

L = > less than accompanying value (lower limit of detection)

N = > not detected in a sample

TABLE II

Analytic results for miscellaneous elements not shown in general element groups of TABLE I.

Element	Number of samples element was detected in	Limit of detection (lower limit except for Si)	Element	Number of samples element was detected in	Limit of detection (lower limit except for Si)
Ag	5	0.7 ppm	Hf	0	50.0 ppm
As	3	100.0 ppm	In	0	1.0 ppm
Au	0	7.0 ppm	Li	0	100.0 ppm
Bi	2	7.0 ppm	Re	0	7.0 ppm
Cd	0	7.0 ppm	Ta	0	50.0 ppm
Mo	5	2.0 ppm	Th	0	150.0 ppm
P	54	0.1 %	Tl	0	3.0 ppm
Pd	0	1.0 ppm	Pr	0	20.0 ppm
Pt	0	5.0 ppm	Nd *	3	20.0 ppm
Sb	8	20.0 ppm	Sm	0	50.0 ppm
Sn	23	2.0 ppm	Eu	0	1.5 ppm
Te	0	300.0 ppm	Gd	0	5.0 ppm
U	0	150.0 ppm	Tb	0	100.0 ppm
W	0	10.0 ppm	Dy**	0	20.0 ppm
Si***	179	10.0% upper limit	Ho	0	5.0 ppm
Ce	9	50.0 ppm	Er	0	30.0 ppm
Ga	151	0.7 ppm	Tm	0	2.0 ppm
Ge	0	7.0 ppm	Lu	0	15.0 ppm

* Looked for only when La or Ce is found

** Looked for only when Y is >50 ppm

***Si was a major component in all samples analyzed, i.e., >10.0%. However, exact values cannot be assigned above this limit.

TABLE III

A. Lists most closely related or disrelated elements according to the correlation coefficients between their log values.

B. Lists elements most close related to the first four factor loadings according to the correlations between their non-log values.

A.

<u>Ga</u>	<u>Fe</u>	<u>Mg</u>	<u>Ca</u>	<u>Ti</u>	<u>Mn</u>	<u>B</u>
La .4950	Cu .8323	Ca .5861	Mg .5861	Fe .7251	Fe .7738	K .4929
Se .4047	Ni .8101	Co .5151	Sr .5469	Sc .7180	Zn .6657	Ba .4508
Ti .3806	Zn .7868	Ni .4949		Mn .6617	Ti .6617	
	Co .7503			Ni .6153	Cu .6612	*Ni -.5464
	Ti .7251				Y .6103	
	Sc .6326					
	Mn .7738					

<u>Ba</u>	<u>Be</u>	<u>Co</u>	<u>Cr</u>	<u>Cu</u>	<u>La</u>	<u>Nb</u>
K .8040	La .3720	Ni .8263	Ni .6132	Fe .8823	Sc .5572	B .2884
Na .6847	Yb .3388	Fe .7503	Ti .5623	Zn .8023	Sn .5539	*Ca-.3232
Sr .6241	Sc .3351	Cu .6296	Sc .5274	Ni .6833	Ba .5508	
Al .6092				Mn .6612	V .5189	
				Co .6296	K .5171	

<u>Ni</u>	<u>Pb</u>	<u>Sc</u>	<u>Sr</u>	<u>V</u>	<u>Y</u>	<u>Zn</u>
Co .8263	Cu .5114	Ti .7180	K .6994	Sc .5790	Mn .6103	Cu .8023
Fe .8101	Zn .4194	Fe .6326	Na .6863	La .5189	Yb .5678	Fe .7868
Cu .6833	*Na-.4041	V. 5790	Al .6140	Cu .4801	Fe .5563	Mn .6657
Ti .6153		La .5572	Ba .6241	Yb .4589	Ti .5435	Ni .6142
Zn .6142		Mn .5571	La .5539	Zn .4584		Co .5982
Cr .6132.			Cu .5469			

<u>Zr</u>	<u>Al</u>	<u>Na</u>	<u>K</u>	<u>Yb</u>
La .4933	Na .8348	Al .8348	Ba .8040	Mn .5729
Y .4552	K .6999	K .7935	Na .7935	Zn .5713
Ti. 4059	Sr .6140	Sr .6863	Al .6999	Y. 5678
	Ba. 6092	Ba .6847	Sr .6994	
	*Pb-.4041			

B.

<u>Factor I</u>	<u>Factor II</u>	<u>Factor III</u>	<u>Factor IV</u>
B .54	Y .72	Ba .71	Nb .41
V .27	Fe .66	Na .67	
	Mn .65	Sr .65	
	Ti .63	La .61	
	Yb .57	K .59	
	Zn .54	Ga. 57	
	Co .50	Al .57	

*Extreme negative correlation.

TABLE IV

Correlation coefficients between element log values

D0101 CORRELATION ANALYSIS - USGS STATPAC (04/27/77)

DATE 4/11/79

ARRAY OF CORRELATION COEFFICIENTS -

	1	2	3	4	5	6	7	8	9	10
	GA PPM-S	FE X-S	MG X-S	CA X-S	TI X-S	MN PPM-S	B PPM-S	BA PPM-S	CO PPM-S	CR PPM-S
1 GA PPM-S	1.0000	0.3289	0.1181	0.1505	0.3806	0.1154	-0.0253	0.1866	0.2649	0.3128
2 FE X-S	0.3289	1.0000	0.3884	0.2678	0.7251	0.7738	-0.3164	-0.0398	0.7503	0.4796
3 MG X-S	0.1181	0.3884	1.0000	0.5861	0.3884	0.2669	-0.2313	-0.1395	0.5151	0.3331
4 CA X-S	0.1505	0.2678	0.5861	1.0000	0.2823	0.1458	-0.0424	0.0475	0.2837	0.2014
5 TI X-S	0.3806	0.7251	0.3884	0.2823	1.0000	0.6617	-0.1365	0.0932	0.5067	0.5623
6 MN PPM-S	0.1154	0.7738	0.2669	0.1458	0.6617	1.0000	-0.2643	-0.1461	0.5187	0.3113
7 B PPM-S	-0.0253	-0.3164	-0.2313	-0.0424	-0.1365	-0.2643	1.0000	0.4508	-0.4110	-0.2177
8 BA PPM-S	0.1866	-0.0398	-0.1395	0.0475	0.0932	-0.1461	0.4508	1.0000	-0.2254	0.2336
9 CO PPM-S	0.2649	0.7503	0.5151	0.2837	0.5067	0.5187	-0.4110	-0.2254	1.0000	0.3879
10 CR PPM-S	0.3128	0.4796	0.3331	0.2014	0.5623	0.3113	-0.2177	0.2336	0.3879	1.0000
11 CU PPM-S	0.2418	0.8323	0.2714	0.2434	0.5682	0.6612	-0.2482	0.0008	0.6296	0.3522
12 LA PPM-S	0.4950	0.3369	0.0688	0.2879	0.4473	0.2424	0.2815	0.5508	0.1032	0.3629
13 NB PPM-S	0.1875	-0.0777	-0.2974	-0.3232	0.0435	-0.0686	0.2884	0.1651	-0.1894	-0.0039
14 NI PPM-S	0.3090	0.8101	0.4949	0.2480	0.6153	0.5954	-0.5464	-0.1467	0.8263	0.6132
15 PB PPM-S	0.0227	0.3106	-0.2186	0.0812	-0.0118	0.2615	-0.0271	-0.0241	0.2152	-0.2529
16 SC PPM-S	0.4047	0.6326	0.3565	0.3371	0.7180	0.5571	0.0724	0.3589	0.3984	0.5274
17 SR PPM-S	0.3097	0.0081	0.1979	0.5469	0.1885	-0.1694	0.1981	0.6241	-0.0661	0.3323
18 V PPM-S	0.0446	0.4039	0.2333	0.1561	0.4352	0.3714	0.2196	0.3529	0.2090	0.3407
19 Y PPM-S	0.2224	0.5563	0.1480	0.2392	0.5435	0.6103	0.0590	-0.0607	0.4272	0.1015
20 ZN PPM-S	0.2140	0.7868	0.1528	0.0466	0.5717	0.6657	-0.1722	0.0552	0.5982	0.2692
21 ZR PPM-S	0.2732	0.2547	0.1485	0.2224	0.4059	0.2388	0.1497	0.3694	0.1450	0.3005
22 AL X-S	0.2245	0.0585	0.2193	0.2679	0.2162	-0.1887	0.4328	0.6092	0.0046	0.2365
23 NA X-S	0.2528	-0.0524	0.1963	0.2352	0.1629	-0.2520	0.4109	0.6847	-0.1178	0.3354
24 K X-S	0.1800	-0.1536	0.0225	0.2076	0.0296	-0.2734	0.4929	0.8040	-0.3177	0.1947
25 YB PPM-S	-0.0617	0.5294	-0.0234	0.0692	0.5181	0.5729	0.1397	0.1760	0.2138	0.1956
26 BE PPM-S	0.1098	0.2741	-0.0618	0.0194	0.3058	0.2558	0.0945	0.2710	0.0144	0.1313

Table IV cont.

00101 CORRELATION ANALYSIS - USGS STATPAC (04/27/77)

DATE 4/11/79

ARRAY OF CORRELATION COEFFICIENTS - CONT.

	11 CU PPM-S	12 LA PPM-S	13 NB PPM-S	14 NI PPM-S	15 PB PPM-S	16 SC PPM-S	17 SR PPM-S	18 V PPM-S	19 Y PPM-S	20 ZN PPM-S
1 GA PPM-S	0.2418	0.4950	0.1875	0.3090	0.0227	0.4047	0.3097	0.0446	0.2224	0.2140
2 FE X-S	0.8323	0.3369	-0.0777	0.8101	0.3106	0.6326	0.0081	0.4039	0.5563	0.7868
3 MG X-S	0.2714	0.0688	-0.2974	0.4949	-0.2186	0.3565	0.1979	0.2333	0.1480	0.1528
4 CA X-S	0.2434	0.2879	-0.3232	0.2480	0.0812	0.3371	0.5469	0.1561	0.2392	0.0466
5 TI X-S	0.5682	0.4473	0.0435	0.6153	-0.0118	0.7180	0.1885	0.4352	0.5435	0.5717
6 MN PPM-S	0.6612	0.2424	-0.0686	0.5954	0.2615	0.5571	-0.1694	0.3714	0.6103	0.6657
7 B PPM-S	-0.2482	0.2815	0.2884	-0.5464	-0.0271	0.0724	0.1981	0.2196	0.0590	-0.1722
8 BA PPM-S	0.0008	0.5508	0.1651	-0.1467	-0.0241	0.3589	0.6241	0.3529	-0.0607	0.0552
9 CO PPM-S	0.6296	0.1032	-0.1894	0.8263	0.2152	0.3984	-0.0661	0.2090	0.4272	0.5982
10 CR PPM-S	0.3522	0.3629	-0.0039	0.6132	-0.2529	0.5274	0.3323	0.3407	0.1015	0.2692
11 CU PPM-S	1.0000	0.4102	-0.1300	0.6833	0.5114	0.5470	0.0144	0.4801	0.4842	0.8023
12 LA PPM-S	0.4102	1.0000	0.1089	0.1760	0.2100	0.5572	0.5539	0.5189	0.3886	0.3333
13 NB PPM-S	-0.1300	0.1089	1.0000	-0.0983	-0.0720	-0.0297	-0.0829	0.0931	0.0139	0.0709
14 NI PPM-S	0.6833	0.1760	-0.0983	1.0000	0.1626	0.4481	0.0041	0.2766	0.3516	0.6142
15 PB PPM-S	0.5114	0.2100	-0.0720	0.1626	1.0000	-0.0439	-0.0772	0.0053	0.3701	0.4194
16 SC PPM-S	0.5470	0.5572	-0.0297	0.4481	-0.0439	1.0000	0.3238	0.5790	0.4335	0.5294
17 SR PPM-S	0.0144	0.5539	-0.0829	0.0041	-0.0772	0.3238	1.0000	0.2163	-0.0675	-0.1362
18 V PPM-S	0.4801	0.5189	0.0931	0.2766	0.0053	0.5790	0.2163	1.0000	0.2237	0.4584
19 Y PPM-S	0.4842	0.3886	0.0139	0.3516	0.3701	0.4335	-0.0675	0.2237	1.0000	0.4121
20 ZN PPM-S	0.8023	0.3333	0.0700	0.6142	0.4194	0.5294	-0.1362	0.4584	0.4121	1.0000
21 ZR PPM-S	0.1452	0.4933	0.1213	0.2615	0.0857	0.3509	0.3286	0.2401	0.4552	0.1914
22 AL X-S	-0.0534	0.3294	0.2116	-0.0162	-0.2630	0.3365	0.6140	0.3314	-0.0457	-0.0332
23 NA X-S	-0.1747	0.3754	0.2021	-0.0615	-0.4041	0.3212	0.6863	0.2713	-0.1440	-0.1644
24 K X-S	-0.1474	0.5171	0.1445	-0.1998	-0.1277	0.2040	0.6994	0.2661	-0.1034	-0.1840
25 YB PPM-S	0.5112	0.3746	0.1340	0.3027	0.2547	0.4278	-0.0703	0.4589	0.5678	0.5713
26 BE PPM-S	0.3211	0.3720	0.0378	0.0884	0.1790	0.3351	0.2056	0.2900	0.2444	0.2771

TABLE IV cont.

D0101 CORRELATION ANALYSIS - USGS STATPAC (04/27/77)

DATE 4/11/79

ARRAY OF CORRELATION COEFFICIENTS - CONT.

	21	22	23	24	25	26
	ZR PPM-S	AL X-S	NA X-S	K X-S	YB PPM-S	BE PPM-S
1 GA PPM-S	0.2732	0.2245	0.2528	0.1800	-0.0617	0.1098
2 FE X-S	0.2547	0.0585	-0.0524	-0.1536	0.5294	0.2741
3 MG X-S	0.1485	0.2193	0.1963	0.0225	-0.0234	-0.0618
4 CA X-S	0.2224	0.2679	0.2352	0.2076	0.0692	0.0194
5 TI X-S	0.4059	0.2162	0.1629	0.0296	0.5181	0.3058
6 MN PPM-S	0.2388	-0.1887	-0.2520	-0.2734	0.5729	0.2558
7 B PPM-S	0.1497	0.4328	0.4109	0.4929	0.1397	0.0945
8 BA PPM-S	0.3694	0.6092	0.6847	0.8040	0.1760	0.2710
9 CO PPM-S	0.1450	0.0046	-0.1178	-0.3177	0.2138	0.0144
10 CR PPM-S	0.3005	0.2365	0.3354	0.1947	0.1956	0.1313
11 CU PPM-S	0.1452	-0.0534	-0.1747	-0.1474	0.5112	0.3211
12 LA PPM-S	0.4933	0.3294	0.3754	0.5171	0.3746	0.3720
13 NB PPM-S	0.1213	0.2116	0.2021	0.1445	0.1340	0.0378
14 NI PPM-S	0.2615	-0.0162	-0.0615	-0.1998	0.3027	0.0884
15 PB PPM-S	0.0857	-0.2630	-0.4041	-0.1277	0.2547	0.1790
16 SC PPM-S	0.3509	0.3365	0.3212	0.2040	0.4278	0.3351
17 SR PPM-S	0.3286	0.6140	0.6863	0.6994	-0.0703	0.2056
18 V PPM-S	0.2401	0.3314	0.2713	0.2661	0.4589	0.2900
19 Y PPM-S	0.4552	-0.0457	-0.1440	-0.1034	0.5678	0.2444
20 ZN PPM-S	0.1914	-0.0332	-0.1644	-0.1840	0.5713	0.2771
21 ZR PPM-S	1.0000	0.2784	0.3000	0.3778	0.3322	0.2169
22 AL X-S	0.2784	1.0000	0.8348	0.6999	0.0953	0.1454
23 NA X-S	0.3000	0.8348	1.0000	0.7935	0.0077	0.0699
24 K X-S	0.3778	0.6999	0.7935	1.0000	0.0875	0.2228
25 YB PPM-S	0.3322	0.0953	0.0077	0.0875	1.0000	0.3388
26 BE PPM-S	0.2169	0.1454	0.0699	0.2228	0.3388	1.0000

TABLE V

Correlation coefficients between Q-mode Factor loading values and non-log element values.

D0101 CORRELATION ANALYSIS - US65 STATPAC (04/27/77)

DATE 3/23/78

ARRAY OF CORRELATION COEFFICIENTS -

	1	2	3	4	5	6	7	8	9	10
	factor1	factor2	factor3	factor4	GA PPM-S	FE X-S	MG X-S	CA X-S	TI X-S	MN PPM-S
1 factor1	1.0000	-0.3258	-0.1758	0.0181	-0.5480	-0.5093	-0.4750	-0.4209	-0.3586	-0.3352
2 factor2	-0.3258	1.0000	-0.2785	-0.4808	0.0926	0.6616	0.1630	0.1168	0.6328	0.6527
3 factor3	-0.1758	-0.2785	1.0000	-0.1591	0.5729	-0.1304	-0.0144	0.1668	0.2239	-0.2896
4 factor4	0.0181	-0.4808	-0.1591	1.0000	0.1481	-0.4933	-0.1958	-0.2655	-0.4254	-0.4867
5 GA PPM-S	-0.5480	0.0926	0.5729	0.1481	1.0000	0.2323	0.0767	0.1157	0.3407	0.0346
6 FE X-S	-0.5093	0.6616	-0.1304	-0.4933	0.2323	1.0000	0.3534	0.1270	0.6022	0.8405
7 MG X-S	-0.4750	0.1630	-0.0144	-0.1958	0.0767	0.3534	1.0000	0.4199	0.2847	0.0851
8 CA X-S	-0.4209	0.1168	0.1668	-0.2655	0.1157	0.1270	0.4199	1.0000	0.2017	0.0055
9 TI X-S	-0.3586	0.6328	0.2239	-0.4254	0.3407	0.6022	0.2847	0.2017	1.0000	0.4214
10 MN PPM-S	-0.3352	0.6527	-0.2896	-0.4867	0.0346	0.8405	0.0851	0.0055	0.4214	1.0000
11 B PPM-S	0.5397	-0.1656	-0.0089	0.1728	0.1575	-0.2368	-0.2685	-0.1292	-0.1006	-0.2229
12 BA PPM-S	0.1990	-0.3470	0.7106	-0.1613	0.4000	-0.1194	-0.2644	-0.1561	0.0600	-0.1898
13 CO PPM-S	-0.6072	0.5020	-0.1428	-0.2790	0.1962	0.7835	0.5335	0.1775	0.3948	0.6020
14 CR PPM-S	-0.3911	0.2104	0.1073	-0.2136	0.1573	0.4351	0.6329	0.1227	0.4659	0.1228
15 CU PPM-S	-0.3316	0.4444	-0.2692	-0.3765	0.0312	0.6852	0.0005	-0.0025	0.1593	0.6637
16 LA PPM-S	-0.0977	0.1546	0.6073	-0.4107	0.5193	0.1447	-0.0687	0.1215	0.3340	0.0494
17 NB PPM-S	0.1628	-0.0266	-0.1231	0.4133	0.1705	-0.1652	-0.2389	-0.3283	-0.0241	-0.1243
18 NI PPM-S	-0.4219	0.2246	-0.1548	-0.2109	0.0263	0.5145	0.6984	0.0401	0.2242	0.2827
19 PB PPM-S	-0.3033	0.3939	-0.3279	-0.3356	-0.0372	0.5928	-0.0839	0.0072	0.0383	0.6280
20 SC PPM-S	-0.2070	0.4598	0.4683	-0.5150	0.4777	0.4371	0.1420	0.1943	0.6401	0.3225
21 SR PPM-S	-0.2944	-0.2621	0.6476	-0.1438	0.3909	-0.0342	0.1171	0.5443	0.1646	-0.1729
22 V PPM-S	0.2703	0.2858	0.2886	-0.5579	0.1720	0.1910	0.0242	-0.0143	0.3205	0.1154
23 Y PPM-S	-0.2662	0.7176	-0.1753	-0.3921	0.1518	0.5309	-0.0513	0.2354	0.4335	0.6178
24 ZN PPM-S	-0.3199	0.5440	-0.2229	-0.4407	0.1069	0.7869	0.0044	-0.0616	0.2700	0.7980
25 ZR PPM-S	-0.0689	0.0418	0.0825	-0.0516	0.1167	0.0155	-0.0335	0.0277	0.1798	0.0307
26 AL X-S	0.0527	-0.2436	0.5707	0.0729	0.4666	-0.0257	0.0199	0.1024	0.2603	-0.2648
27 NA X-S	-0.0308	-0.3275	0.6674	0.0416	0.5404	-0.0169	0.0233	0.0863	0.2380	-0.2490
28 K X-S	0.0796	-0.4179	0.5948	-0.0583	0.4125	-0.1494	-0.1554	0.0003	0.0118	-0.2329
29 YB PPM-S	0.1620	0.5663	-0.1618	-0.5081	0.0283	0.4684	-0.1397	-0.0357	0.4097	0.5124

TABLE VI

A. Q-mode scaled varimax factor scores relating which elements are most correlative with each factor (in order of descending importance).

B. Elements most typical of the first 4 R-mode factor groupings.

A.

<u>Factor I</u>	<u>Factor II</u>	<u>Factor III</u>	<u>Factor IV</u>
B 2.74	Y 2.05	La -2.02	Nb -2.40
V 2.10	Yb 1.78	Na -1.98	Ga -2.35
Yb 1.62	Ti 1.75	Ga -1.70	B -1.97
Ba 1.22	Fe 1.52	Ba -1.70	Al -1.67
Al 1.05	Sc 1.49	Sr -1.67	Na -1.38
	Cu 1.28	Sc -1.46	
	V 1.08	K 1.29	
	Mn 1.04	V -.93	
		Al -.86	

B.

<u>Factor I</u>	<u>Factor II</u>	<u>Factor III</u>	<u>Factor IV</u>
Fe .92	K .90	Pb .79	Ca .78
An .85	Ba .85	Y .40	Mg .65
Cu .84	Na .84		Sr .42
Mn .83	Sr .79		
Ti .81	Al .78		
Ni .79	La .68		
Co .71			
Sc .71			
Yb .66			
Y .65			

TABLE VII

Q-mode varimax factor matrix associating samples into factor groupings.

00097 FACTOR ANALYSIS (Q-MODE) - U S G S STATPAC 06/07/77

Q factor analysis on 25 col bu

VARIMAX FACTOR MATRIX

	COMM.	1	2	3	4
1 69ANC100	0.9484	0.4232	0.3825	-0.6162	-0.4924
2 69ASC101	0.9440	0.4416	0.3271	-0.6588	-0.4562
3 69ASC105	0.9773	0.4202	0.2779	-0.5858	-0.6167
4 69ANC107	0.9481	0.4572	0.1810	-0.5552	-0.6310
5 69ANC114	0.9585	0.4006	0.2533	-0.7559	-0.4031
6 69ANC116	0.9727	0.4459	0.3677	-0.6634	-0.4455
7 69ANC121	0.9322	0.4167	0.3968	-0.6592	-0.4082
8 69ASC155	0.9613	0.5693	0.1800	-0.5227	-0.5758
9 69ANC200	0.9300	0.5229	0.3561	-0.3572	-0.6292
10 69ANC206	0.9646	0.4532	0.2277	-0.5654	-0.6222
11 69ANC208	0.9632	0.4163	0.2146	-0.7042	-0.4980
12 69ANC209	0.9499	0.4636	0.1901	-0.6528	-0.5271
13 69ANC220	0.9368	0.4127	0.1696	-0.6747	-0.5315
14 69ANC221	0.9680	0.3569	0.1194	-0.7602	-0.4984
15 69ANC224	0.9364	0.3438	0.2519	-0.7037	-0.5095
16 69ANC227	0.9097	0.3356	0.1820	-0.7413	-0.4632
17 69ANC229	0.9336	0.4469	0.0843	-0.6401	-0.5632
18 69ANC232	0.9720	0.4616	0.3126	-0.6604	-0.4745
19 69ANC235	0.9514	0.4560	-0.0240	-0.5355	-0.6753
20 69ANC247	0.9029	0.5502	0.2904	-0.5967	-0.3998
21 70ANC7B	0.9609	0.5759	0.2251	-0.6379	-0.4144
22 70ANC11B	0.8948	0.4364	0.2424	-0.5643	-0.5719
23 70ANC13B	0.9458	0.5066	0.2030	-0.5994	-0.5372
24 70ANC14B	0.9156	0.5066	0.2926	-0.6510	-0.3221
25 70ANC15S	0.9610	0.5425	0.2433	-0.6660	-0.4050
26 70ANC16S	0.9303	0.4445	0.0799	-0.7395	-0.4235
27 70ASC20S	0.9261	0.4357	0.1942	-0.6840	-0.4804
28 70ANC24S	0.9578	0.4122	0.1384	-0.6691	-0.5666
29 70ANC27B	0.9337	0.5181	0.2702	-0.6696	-0.3794
30 70ANC29S	0.9383	0.5582	0.3855	-0.6325	-0.2792
31 70ANC32B	0.9757	0.4818	0.3486	-0.6964	-0.3701
32 70ANC35S	0.9597	0.5424	0.3971	-0.5493	-0.4540
33 70ANC40B	0.9432	0.4999	0.3090	-0.6018	-0.4854
34 70ANC45S	0.9362	0.5548	0.3249	-0.5934	-0.4131
35 70ANC47B	0.9337	0.5830	0.3417	-0.5284	-0.4448
36 70ANC48B	0.9373	0.5555	0.3395	-0.6292	-0.3428
37 70ANC53S	0.8663	0.4755	0.3627	-0.6375	-0.3198
38 70ANC54S	0.9484	0.5384	0.2752	-0.5928	-0.4811
39 70ANC56B	0.9460	0.4945	0.3379	-0.6426	-0.4083
40 70ANC59T	0.9532	0.4870	0.3153	-0.6643	-0.4188
41 70ANC61T	0.9266	0.4721	0.1501	-0.5394	-0.6247
42 67ANC30	0.8690	0.5279	0.4974	-0.4106	-0.4176
43 68AWF31D	0.8950	0.4137	0.4762	-0.2763	-0.6486
44 68AWF327	0.8661	0.4049	0.5763	-0.3370	-0.5065
45 68AWF33R	0.9619	0.3472	0.4583	-0.5557	-0.5680
46 68AWF343	0.9319	0.3005	0.3751	-0.4177	-0.7256
47 68AWF344	0.9537	0.3296	0.2750	-0.3425	-0.8076
48 68AWF345	0.9547	0.3733	0.4562	-0.4144	-0.6599
49 68AWF346	0.9133	0.3573	0.3553	-0.3982	-0.7073

TABLE VII cont.

50	68AWF350	0.9629	0.4113	0.4042	-0.6142	-0.5031
51	68AWF354	0.9516	0.3236	0.3658	-0.4953	-0.6522
52	68AWF355	0.9614	0.2864	0.3079	-0.4429	-0.7671
53	68AWF357	0.9739	0.4131	0.4332	-0.5483	-0.5612
54	68AWF410	0.9652	0.4131	0.3524	-0.6053	-0.5514
55	68AWF430	0.9464	0.4607	0.4339	-0.5155	-0.5292
56	68AWF440	0.9318	0.3728	0.3901	-0.5148	-0.6128
57	68AWF505	0.8597	0.4819	0.2095	-0.4516	-0.6161
58	68ANC308	0.9547	0.4479	0.2959	-0.2083	-0.7894
59	68ANC618	0.7867	0.2441	0.4051	-0.6690	-0.3398
60	68ANC709	0.7790	0.3230	0.2936	-0.6989	-0.3161
61	68ANC958	0.9286	0.3070	0.0497	-0.6824	-0.6052
62	68ANC105	0.9189	0.2003	0.2794	-0.6621	-0.6020
63	68ANC112	0.9572	0.3260	0.1645	-0.7143	-0.5601
64	68ANC115	0.8643	0.0644	0.3589	-0.7140	-0.4706
65	68ANC118	0.9271	0.2252	0.3215	-0.7242	-0.4985
66	68ANC120	0.9278	0.3284	0.3170	-0.6561	-0.5377
67	68ANC126	0.9013	0.3785	0.1983	-0.6157	-0.5828
68	68ANC140	0.9207	0.3305	0.2739	-0.7270	-0.4561
69	68ANC154	0.9565	0.3945	0.1499	-0.5947	-0.6517
70	68ANC166	0.9550	0.5444	0.1272	-0.3336	-0.7289
71	68ANC179	0.9630	0.4315	0.4627	-0.5643	-0.4943
72	68ANC181	0.6896	0.3151	0.2304	-0.4730	-0.5599
73	68ANC182	0.7059	0.6045	0.1876	-0.3397	-0.4358
74	68ANC187	0.9552	0.7767	0.3260	-0.3369	-0.3636
75	68ANC190	0.2377	0.2429	0.0979	-0.3257	-0.2547
76	68ANC200	0.9855	0.7714	0.2255	-0.3393	-0.4738
77	68ANC212	0.9527	0.7923	0.2554	-0.2870	-0.4212
78	68ANC215	0.9290	0.6878	0.0987	-0.5117	-0.4293
79	68ANC231	0.9559	0.6885	0.2961	-0.5342	-0.3299
80	68ANC233	0.9644	0.7508	0.3190	-0.4152	-0.3557
81	68ANC234	0.9749	0.7168	0.4826	-0.4212	-0.2255
82	68ANC240	0.9616	0.6988	0.3902	-0.5404	-0.1703
83	68ANC241	0.9604	0.7254	0.3452	-0.4834	-0.2852
84	68ANC244	0.9608	0.7342	0.4107	-0.3938	-0.3132
85	68ANC248	0.9450	0.6889	0.3396	-0.5418	-0.2480
86	68ANC251	0.9441	0.7140	0.4263	-0.3571	-0.3536
87	68ANC768	0.9643	0.7788	0.1157	-0.3990	-0.4303
88	68ANC798	0.9259	0.7315	0.0777	-0.4545	-0.4221
89	68ANC839	0.8958	0.6669	0.1483	-0.5800	-0.3045
90	68ANC148	0.9128	0.6197	0.2206	-0.6148	-0.3195
91	68ANC156	0.9196	0.6771	0.0916	-0.4854	-0.4660
92	68ANC158	0.9298	0.6897	0.0385	-0.5289	-0.4158
93	68ANC160	0.9347	0.7136	0.0897	-0.4858	-0.4260
94	68ANC163	0.9380	0.7013	0.1127	-0.4868	-0.4433
95	68ANC169	0.9581	0.7503	0.2086	-0.2989	-0.5121
96	68ANC194	0.9382	0.7383	0.2261	-0.4120	-0.4151
97	68ANC214	0.9341	0.7696	0.1105	-0.2665	-0.5086
98	68ANC218	0.9431	0.7240	0.2095	-0.3586	-0.4964
99	68ANC221	0.9782	0.5222	0.2021	-0.5020	-0.6424
100	68ANC223	0.8672	0.5486	0.2991	-0.4402	-0.5320
101	68ANC225	0.9577	0.4280	0.4083	-0.6715	-0.3960
102	69ANC102	0.9520	0.5282	0.3186	-0.5835	-0.4806
103	69ANC104	0.9427	0.5190	0.2885	-0.6475	-0.4134
104	69ANC110	0.9483	0.4746	0.3688	-0.5990	-0.4778
105	69ANC111	0.9826	0.5322	0.2469	-0.7074	-0.3714
106	69ANC112	0.9611	0.4927	0.4057	-0.6827	-0.2960
107	69ANC113	0.9761	0.5112	0.2272	-0.7182	-0.3838
108	69ANC115	0.9590	0.4929	0.3073	-0.6860	-0.3888
109	69ANC117	0.9817	0.4617	0.3162	-0.5951	-0.5607

TABLE VII cont.

110	69ANC119	0.9573	0.4507	0.3894	-0.6482	-0.4270
111	69ANC205	0.9750	0.3932	0.2409	-0.6342	-0.6002
112	69ANC211	0.9485	0.4283	0.1794	-0.6123	-0.5983
113	69ANC218	0.9444	0.3355	0.0940	-0.7666	-0.4851
114	70ANC28	0.9794	0.4698	0.2444	-0.6882	-0.4737
115	70ANC381	0.9619	0.5256	0.2684	-0.4585	-0.6352
116	70ANC421	0.9727	0.5306	0.2564	-0.5538	-0.5646
117	70ANC51	0.9664	0.5337	0.3643	-0.5537	-0.4922
118	70ANC521	0.9699	0.4673	0.3150	-0.6362	-0.4975
119	70ANC571	0.9510	0.5293	0.3472	-0.5384	-0.5103
120	70ANC60	0.9771	0.4312	0.2863	-0.5677	-0.6221
121	69ANC120	0.9785	0.4103	0.3880	-0.6828	-0.4398
122	68ANC39	0.9534	0.5340	0.4619	-0.5668	-0.3655
123	68ANC89	0.9299	0.3639	0.0614	-0.6924	-0.5531
124	65ANC15	0.6726	0.4328	0.3754	-0.3558	-0.4666
125	68ANC23	0.8771	0.4001	0.1920	-0.3137	-0.7627
126	65PR23	0.7044	0.3410	0.5527	-0.4380	-0.3013
127	69ANC127	0.9288	0.5259	0.5832	-0.2720	-0.4880
128	69ANC130	0.9336	0.4827	0.6779	-0.2361	-0.4310
129	69ANC145	0.8808	0.5048	0.2053	-0.4436	-0.6221
130	69ANC147	0.9073	0.4125	0.4665	-0.3157	-0.6480
131	68AWF801	0.8641	0.2954	0.8409	-0.1481	-0.2185
132	68AWF802	0.7666	0.1953	0.8215	-0.2112	-0.0950
133	68AWF807	0.8339	0.0931	0.8944	-0.1420	-0.0717
134	68AWF827	0.5930	0.0293	0.7592	-0.1209	-0.0338
135	69ANC85	0.7732	0.0829	0.4862	-0.6355	-0.3551
136	69ANC86	0.3821	-0.1003	0.4880	-0.2841	-0.2307
137	69ANC95	0.7883	0.1965	0.4825	-0.6085	-0.3829
138	69ASC97	0.8668	0.2822	0.4972	-0.6231	-0.3891
139	69ANC307	0.7034	0.3949	0.3192	-0.4779	-0.4660
140	68ANC304	0.8314	0.4120	0.2272	-0.6094	-0.4885
141	68ANC307	0.8992	0.3947	-0.0038	-0.6653	-0.5485
142	68ANC309	0.9053	0.3274	0.0545	-0.7469	-0.4871
143	68ANC216	0.9539	0.5533	0.2698	-0.4974	-0.5723
144	68ANC235	0.9410	0.5004	0.4194	-0.5074	-0.5072
145	69ANC204	0.9306	0.5730	0.1613	-0.5032	-0.5684
146	69ANC207	0.9716	0.4669	0.2338	-0.7072	-0.4459
147	69ANC223	0.9668	0.4421	0.1071	-0.7505	-0.4434
148	69ANC230	0.9778	0.5789	0.0915	-0.4893	-0.6283
149	69ANC245	0.9505	0.5858	0.2288	-0.5193	-0.5343
150	69ANC252	0.9125	0.5596	0.3766	-0.5227	-0.4292
151	69ANC255	0.9838	0.5897	0.1446	-0.4297	-0.6561
152	70ANC58H	0.9349	0.5320	0.3934	-0.6332	-0.3100
153	M131032	0.9666	0.4302	0.4735	-0.7269	-0.1703
154	M131033	0.8264	0.5580	0.5431	-0.4786	-0.2260
155	M131034	0.9500	0.6335	0.2132	-0.3338	-0.6260
156	M131036	0.5672	0.1702	0.2717	-0.6376	-0.2405
157	M131037	0.9312	0.6037	0.3913	-0.3729	-0.5239
158	M131038	0.9499	0.4790	0.4085	-0.6896	-0.2791
159	M131039	0.9473	0.5429	0.2660	-0.5197	-0.5583
160	M131040	0.9628	0.4795	0.4457	-0.6432	-0.3469
161	M131041	0.9207	0.3196	0.4762	-0.7256	-0.2555
162	M131042	0.9703	0.4903	0.4222	-0.6961	-0.2590
163	M131043	0.9545	0.4090	0.4931	-0.6481	-0.3522
164	M131044	0.9611	0.4793	0.4695	-0.6693	-0.2510
165	M131045	0.9821	0.4390	0.4919	-0.7040	-0.2277
166	M131046	0.9843	0.4023	0.3589	-0.7529	-0.3561
167	M131047	0.9418	0.3364	0.4083	-0.7642	-0.2792
168	M131048	0.9797	0.3698	0.3793	-0.7891	-0.2766
169	M131049	0.9728	0.4587	0.3965	-0.7315	-0.2648

TABLE VII cont.

170	M131050	0.9535	0.5231	0.3978	-0.6951	-0.1961
171	M131051	0.9812	0.4966	0.4842	-0.7183	-0.2348
172	M131052	0.8930	0.4699	0.3032	-0.7200	-0.2489
173	M131053	0.9741	0.4610	0.3655	-0.7673	-0.1980
174	M131054	0.9671	0.4966	0.2958	-0.6839	-0.4065
175	M131055	0.9704	0.3806	0.2975	-0.7991	-0.3139
176	M131056	0.9670	0.5309	0.2372	-0.6532	-0.4497
177	M131057	0.9307	0.4832	0.2691	-0.6349	-0.4709
178	M131059	0.9561	0.4526	0.4419	-0.6690	-0.3292
179	M131064	0.9384	0.4293	0.3202	-0.7184	-0.3682
	VARIANCE		24.232	11.842	33.379	22.489
	CUM. VAR		24.232	36.074	69.453	91.942

TABLE VIII

R-mode varimax factor matrix associating elements into factor groupings.

D0096 FACTOR ANALYSIS - U S G S STATPAC (05/26/77)

VARIMAX FACTOR MATRIX -

		1	2	3	4
1	GA PPM-S	0.33694	0.30051	-0.20740	0.07917
2	FE %S	0.92115	-0.04429	-0.03510	0.18639
3	MG %S	0.31079	0.05100	-0.38214	0.64860
4	CA %S	0.16913	0.32331	0.07138	0.78413
5	TI %S	0.80949	0.19792	-0.21161	0.07601
6	MN PPM-S	0.83472	-0.17520	0.10975	0.03172
7	B PPM-S	-0.23109	0.60177	0.29367	-0.35888
8	BA PPM-S	0.01259	0.84640	0.02468	-0.16420
9	CO PPM-S	0.70616	-0.22846	-0.17397	0.38374
10	CR PPM-S	0.51621	0.25099	-0.56431	0.12504
11	CU PPM-S	0.84223	-0.04240	0.21000	0.18519
12	LA PPM-S	0.44852	0.68135	0.20847	0.03509
13	N3 PPM-S	0.06181	0.19076	-0.14943	-0.70709
14	NI PPM-S	0.78890	-0.17064	-0.30282	0.30366
15	PD PPM-S	0.29266	-0.11387	0.78539	0.10637
16	SC PPM-S	0.70533	0.41560	-0.15604	0.09670
17	SR PPM-S	-0.04983	0.79306	-0.09565	0.41783
18	V PPM-S	0.53451	0.41370	-0.02074	-0.11797
19	Y PPM-S	0.64945	0.05857	0.40072	0.05789
20	ZN PPM-S	0.84975	-0.06833	0.14256	-0.09389
21	ZR PPM-S	0.36511	0.48674	0.09222	0.03875
22	AL %S	0.01490	0.78280	-0.29654	0.02684
23	NA %S	-0.08165	0.83533	-0.40235	0.01955
24	K %S	-0.15134	0.90351	-0.03496	-0.00170
25	Y3 PPM-S	0.66016	0.17932	0.31016	-0.27220

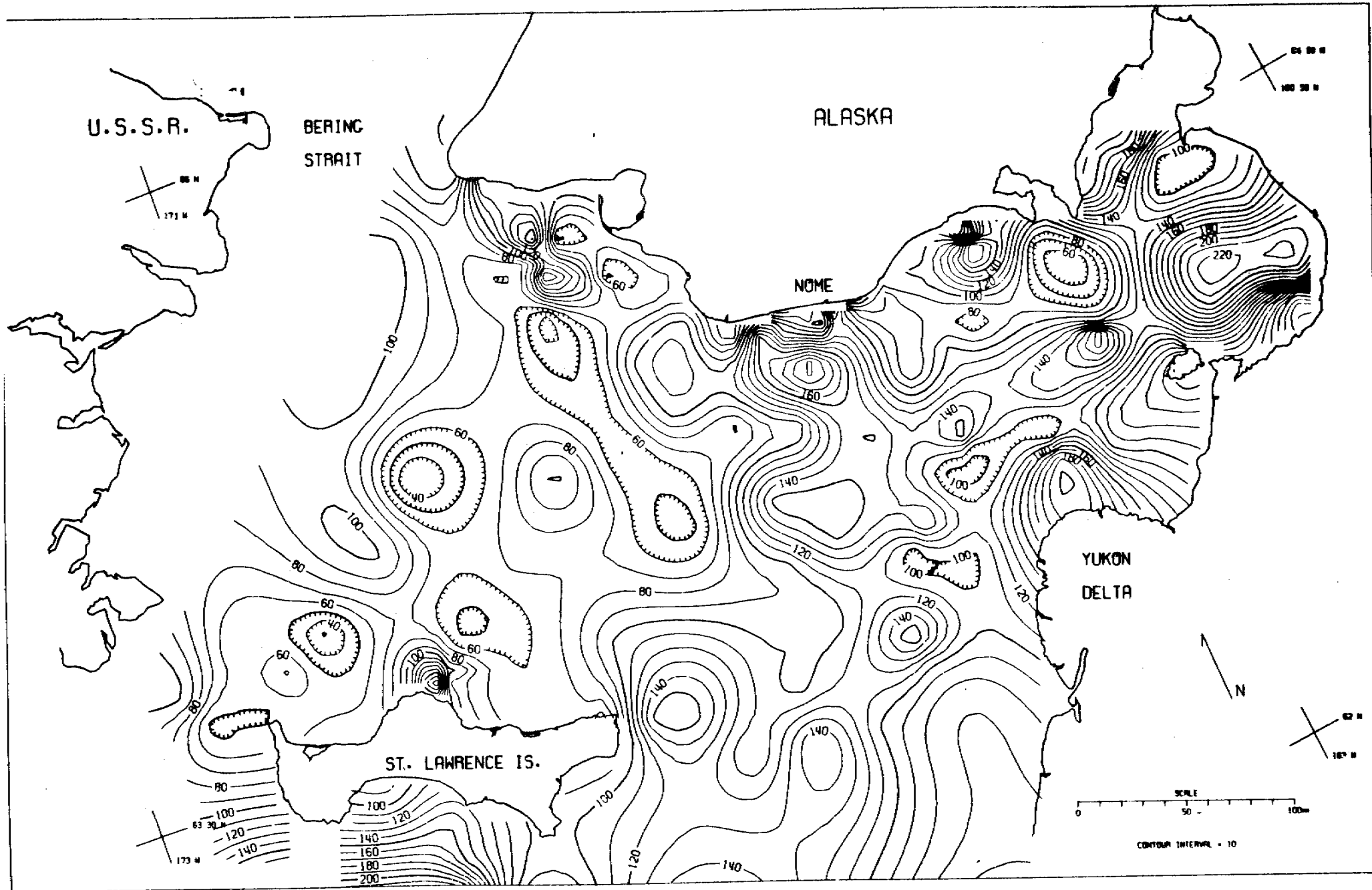
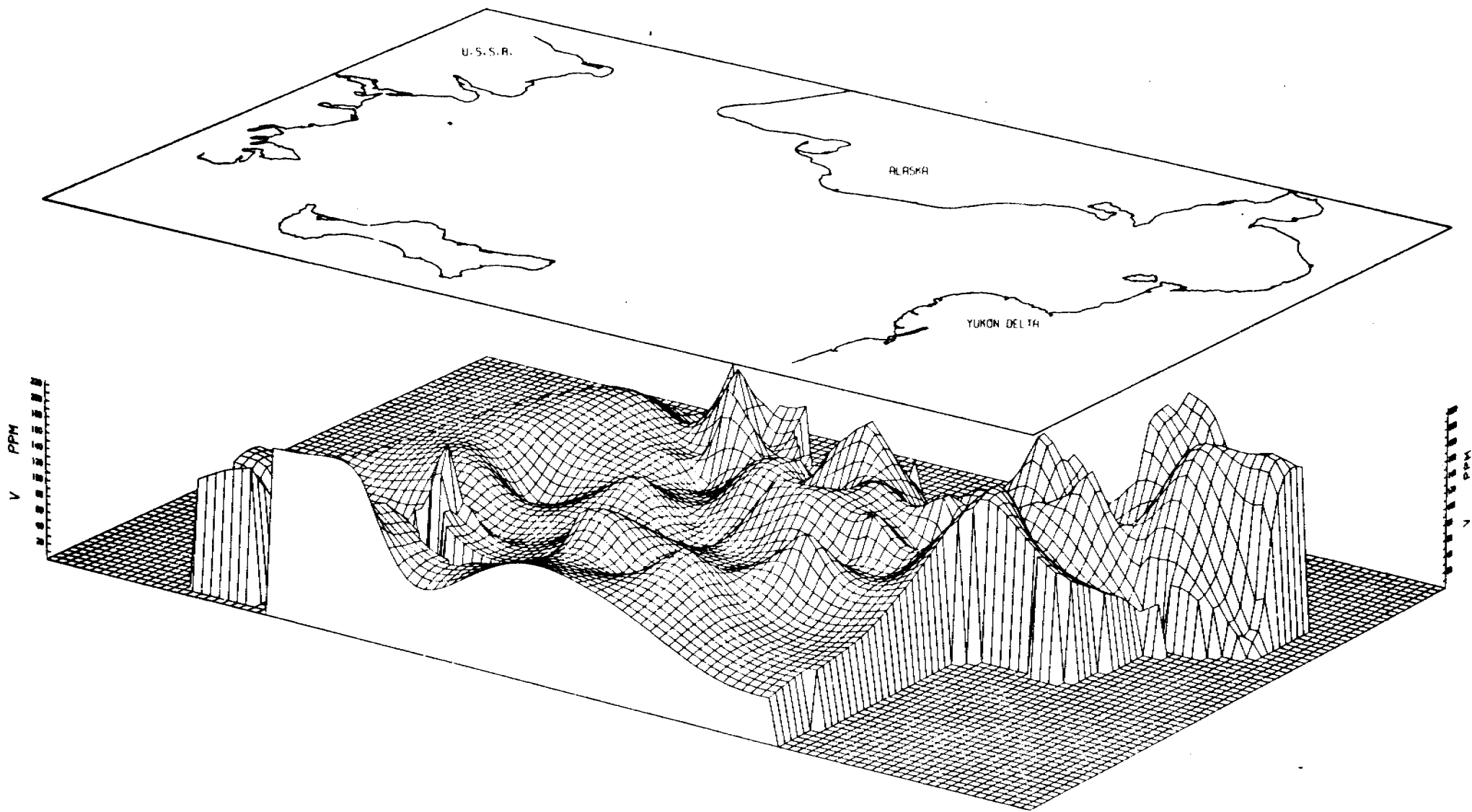


FIG 6 V PPM IN BOTTOM SURFACE SEDIMENT OF NORTON BASIN, BERING SEA



507

FIG 7 V PPM IN BOTTOM SURFACE SEDIMENT OF NORTON BASIN, BERING SEA

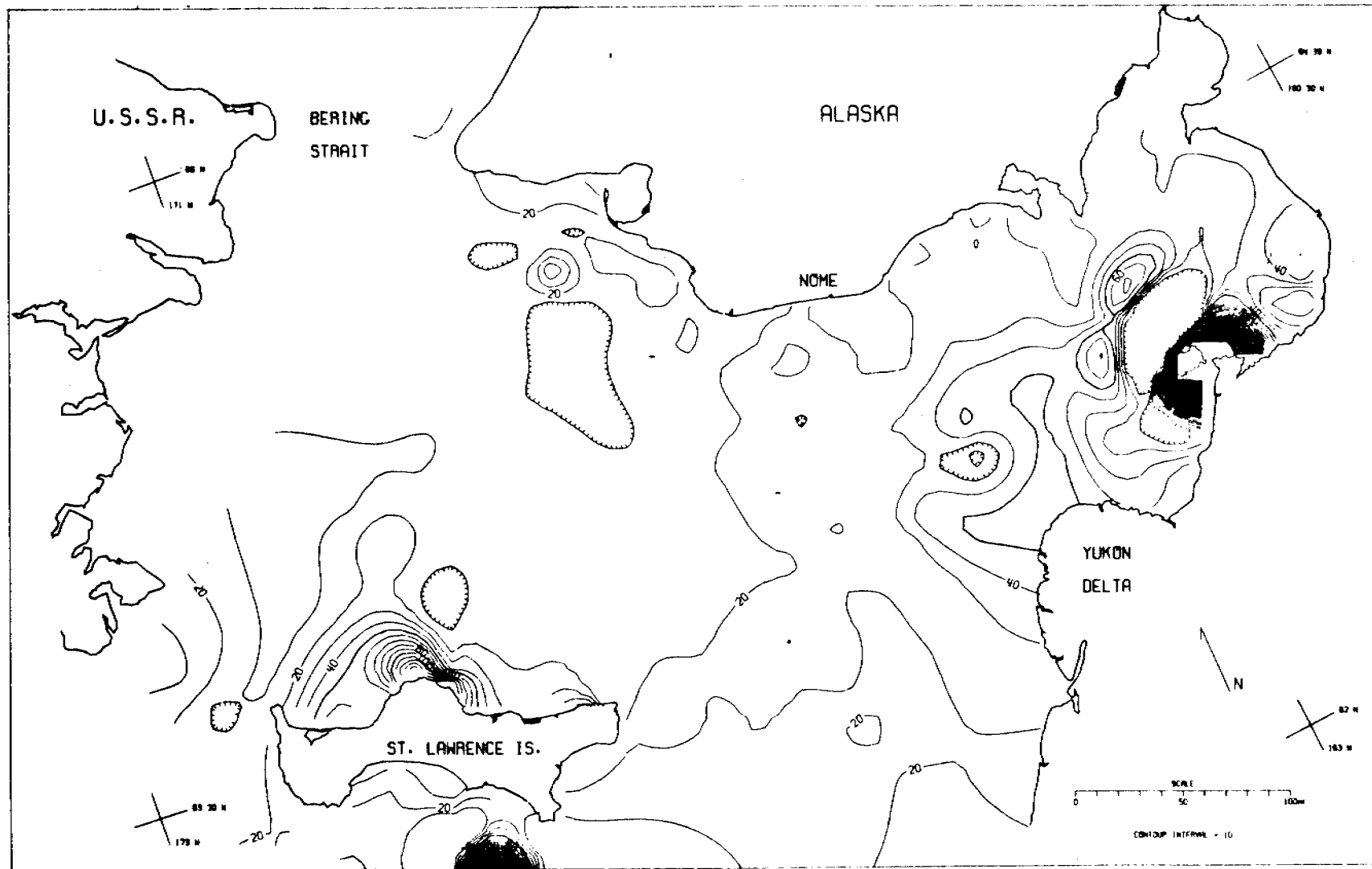


FIG 8 NI PPM IN BOTTOM SURFACE SEDIMENT OF NORTON BASIN, BERING SEA

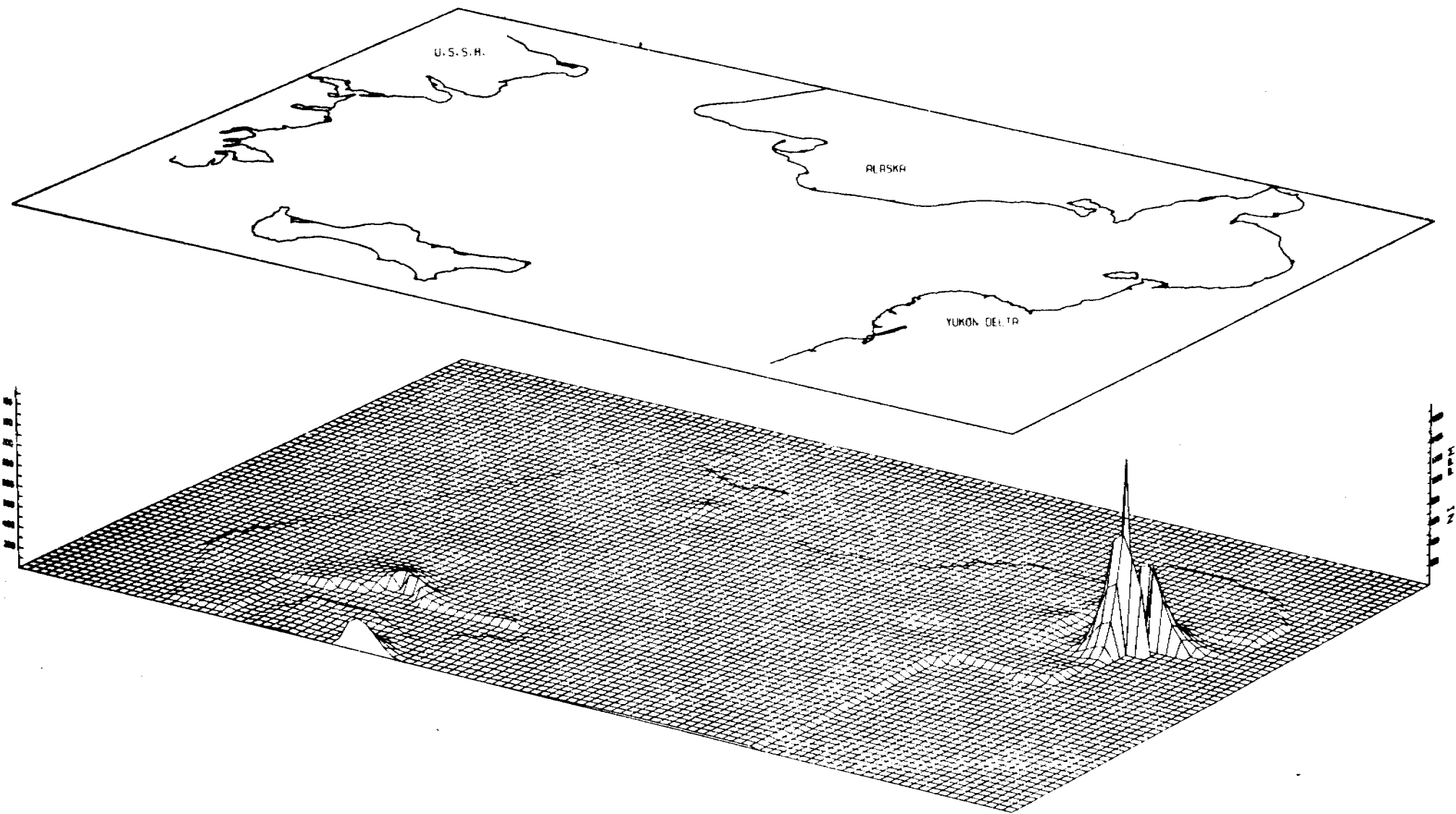


FIG 9 NI PPM IN BOTTOM SURFACE SEDIMENT OF NORTON BASIN, BERING SEA

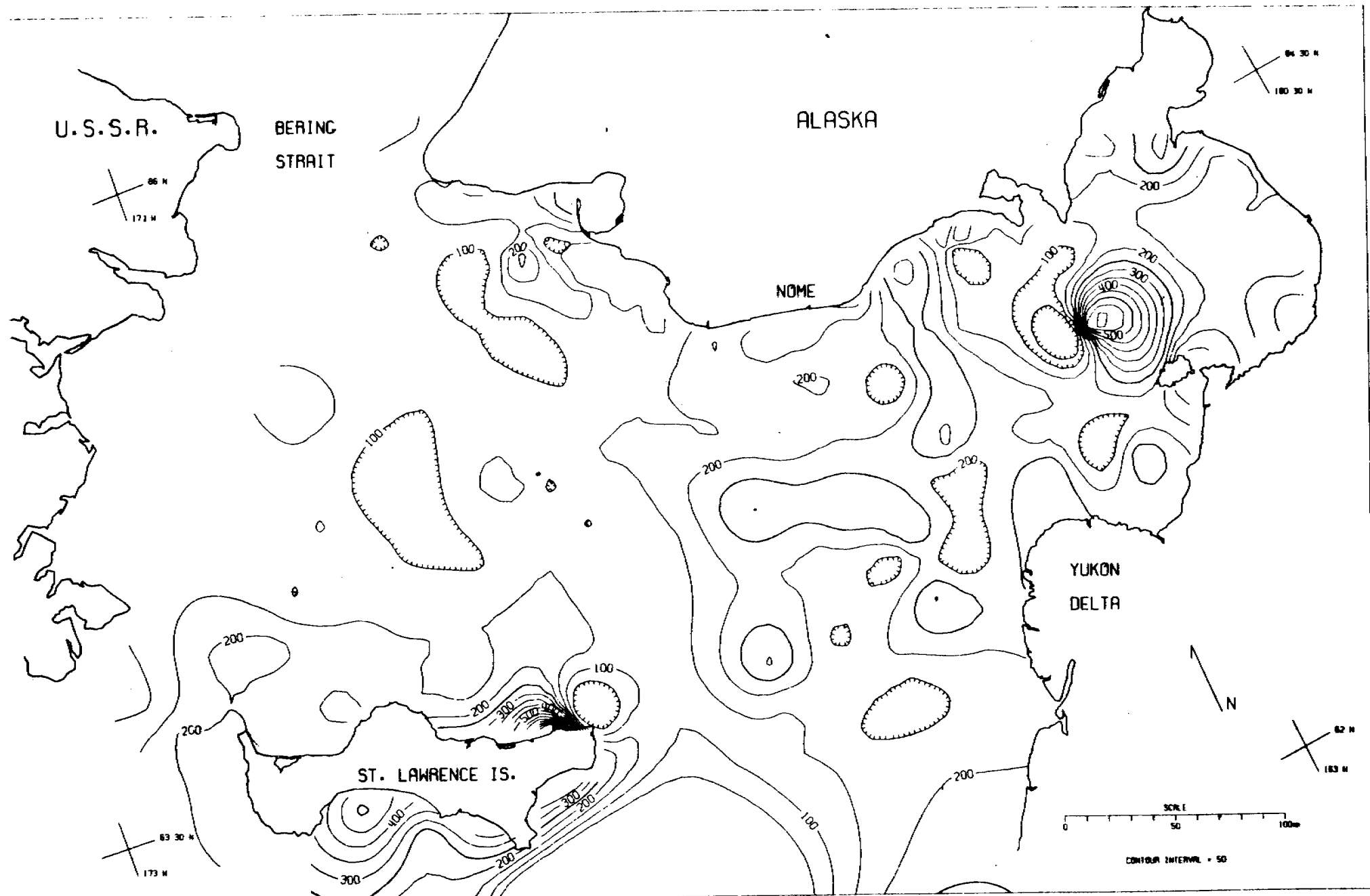


FIG 10 ZR PPM IN BOTTOM SURFACE SEDIMENT OF NORTON BASIN, BERING SEA

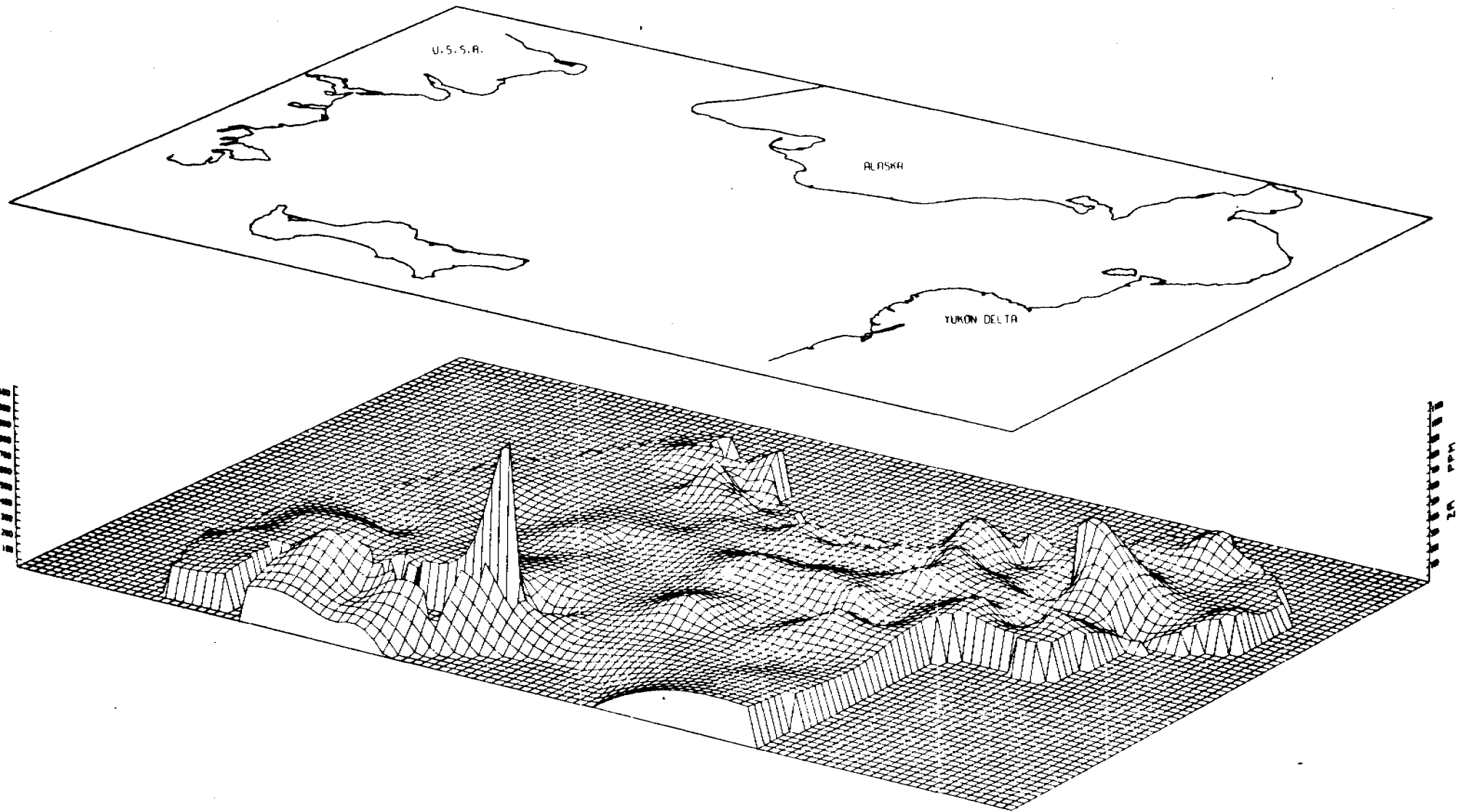


FIG 11 Zr PPM IN BOTTOM SURFACE SEDIMENT OF NORTON BASIN, BERING SEA

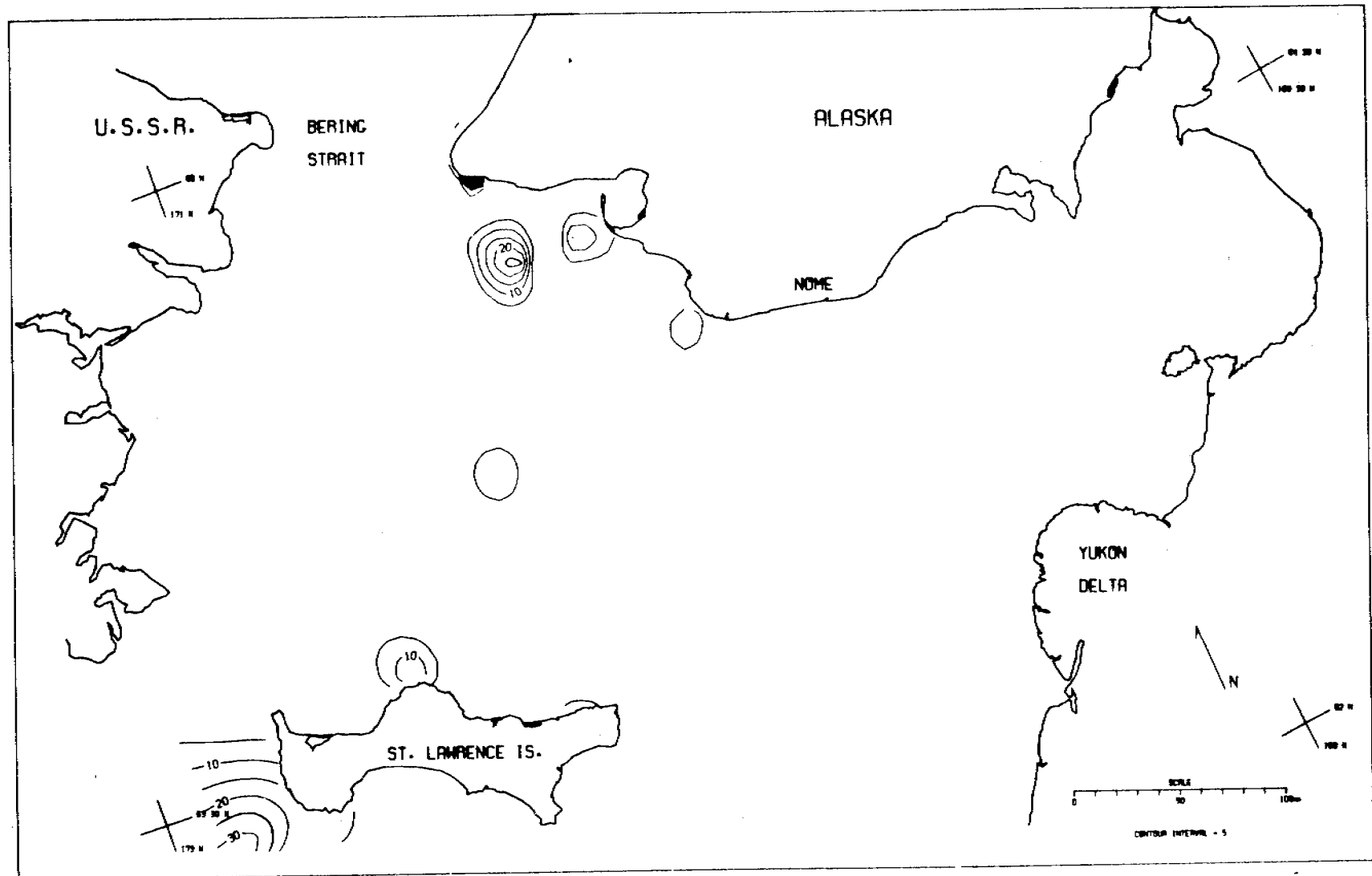


FIG 12 SN PPM IN BOTTOM SURFACE SEDIMENT OF NORTON BASIN, BERING SEA

NORTON BASIN PERSPECTIVE VIEW

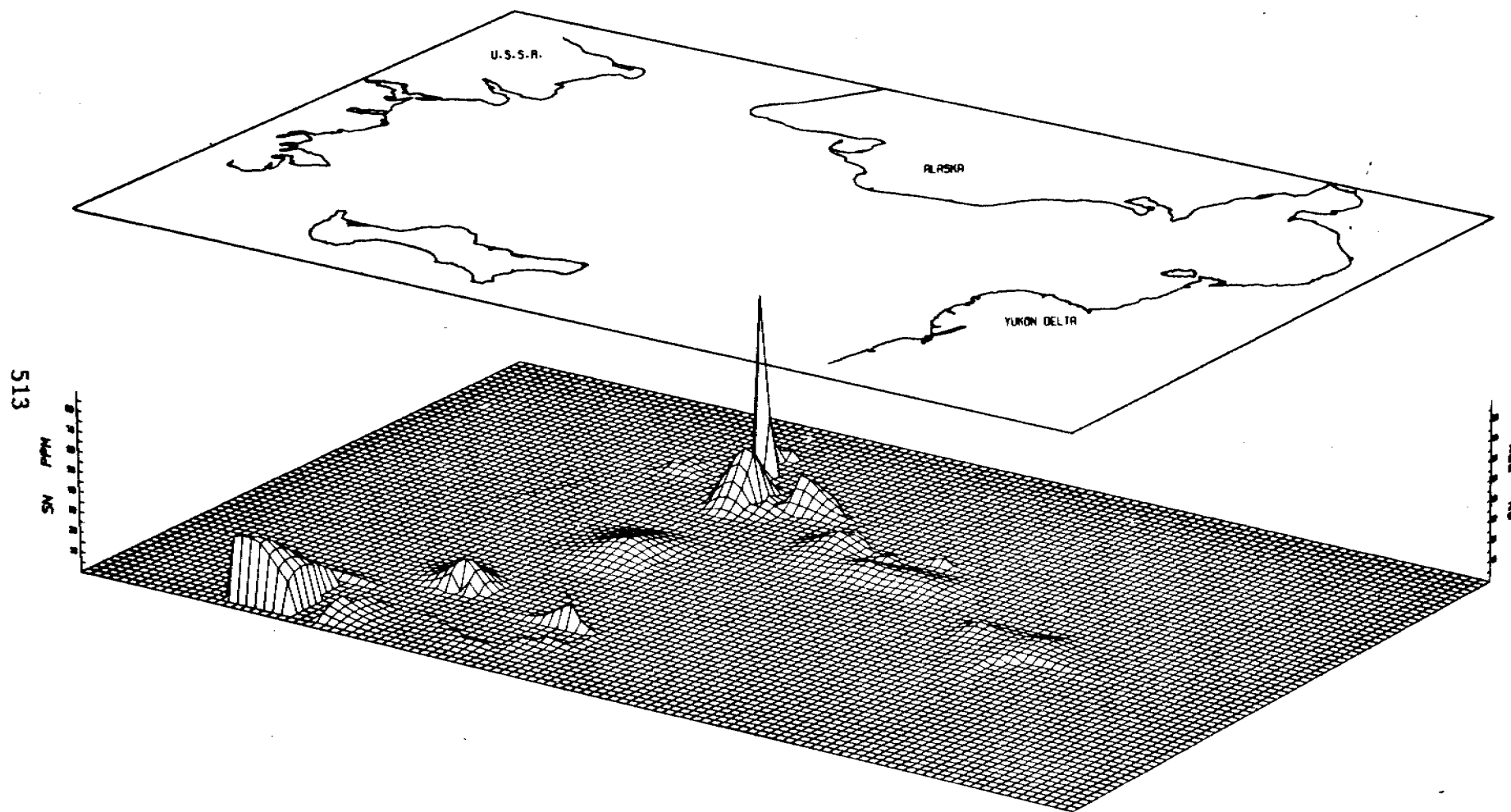


FIG 13 SN PPM IN BOTTOM SURFACE SEDIMENT OF NORTON BASIN, BERING SEA

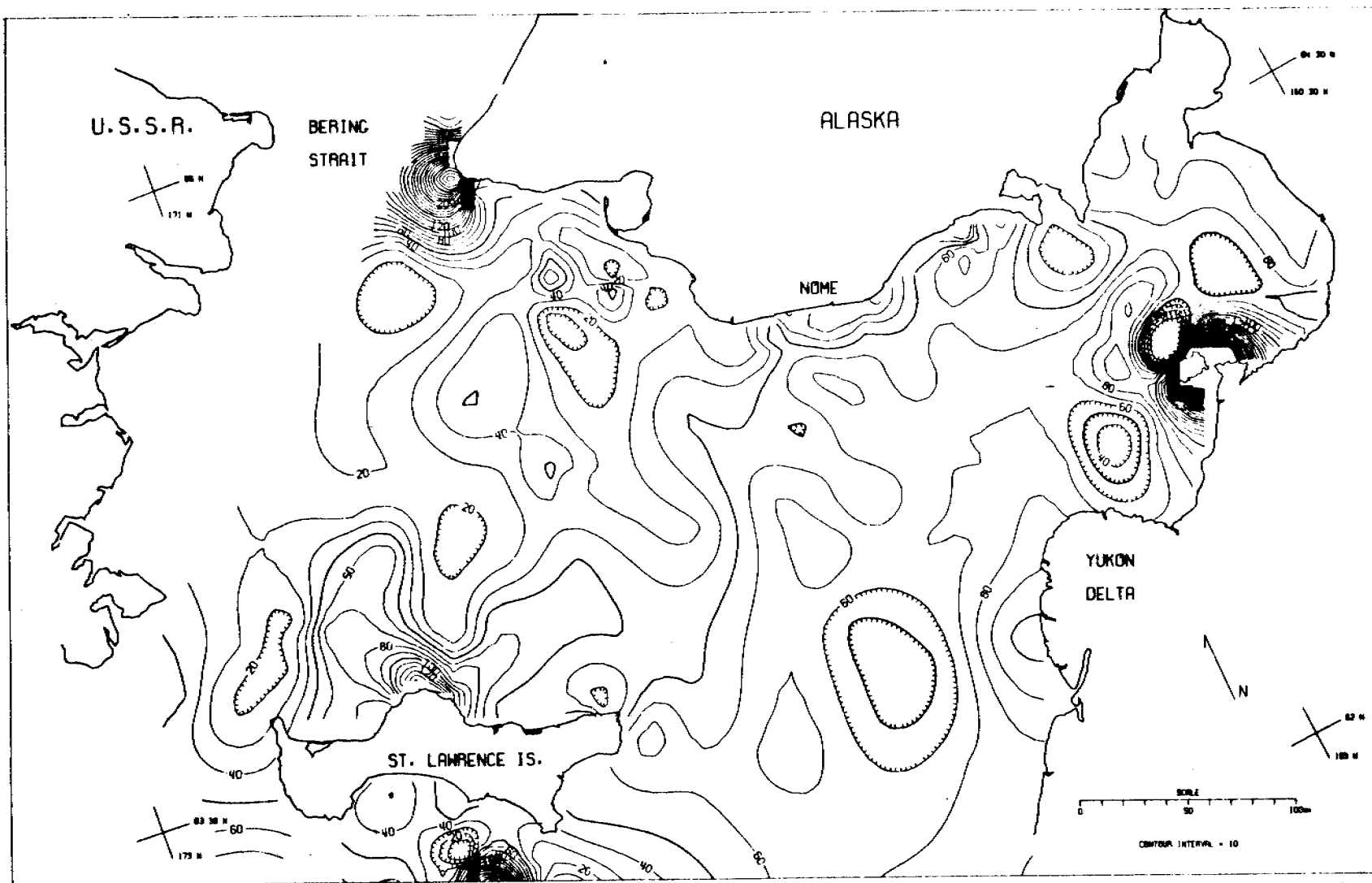


FIG 14 CR PPM IN BOTTOM SURFACE SEDIMENT OF NORTON BASIN, BERING SEA

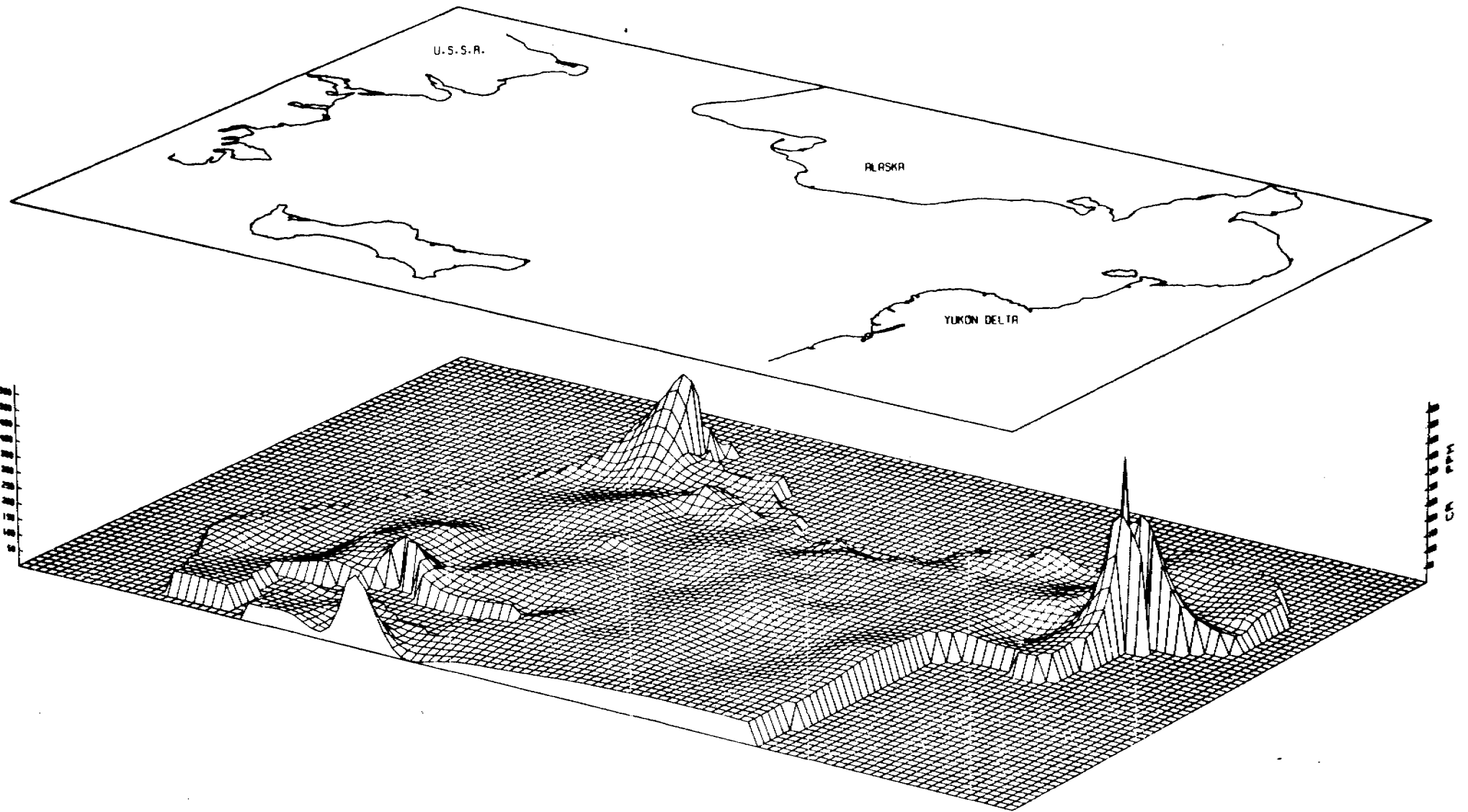


FIG 15 CR PPM IN BOTTOM SURFACE SEDIMENT OF NORTON BASIN, BERING SEA

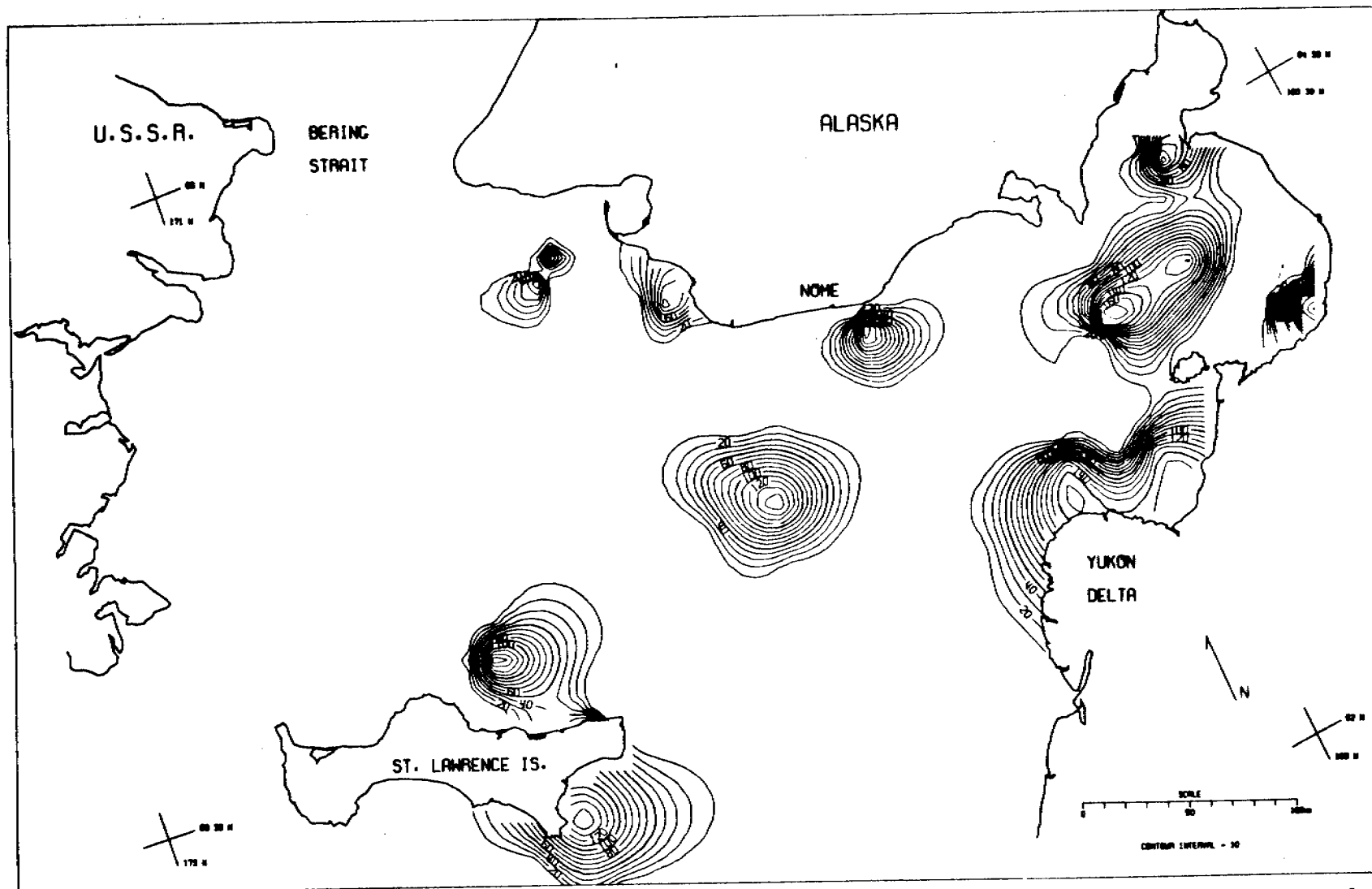


FIG 16 CE PPM IN BOTTOM SURFACE SEDIMENT OF NORTON BASIN, BERING SEA

NORTON BASIN PERSPECTIVE VIEW

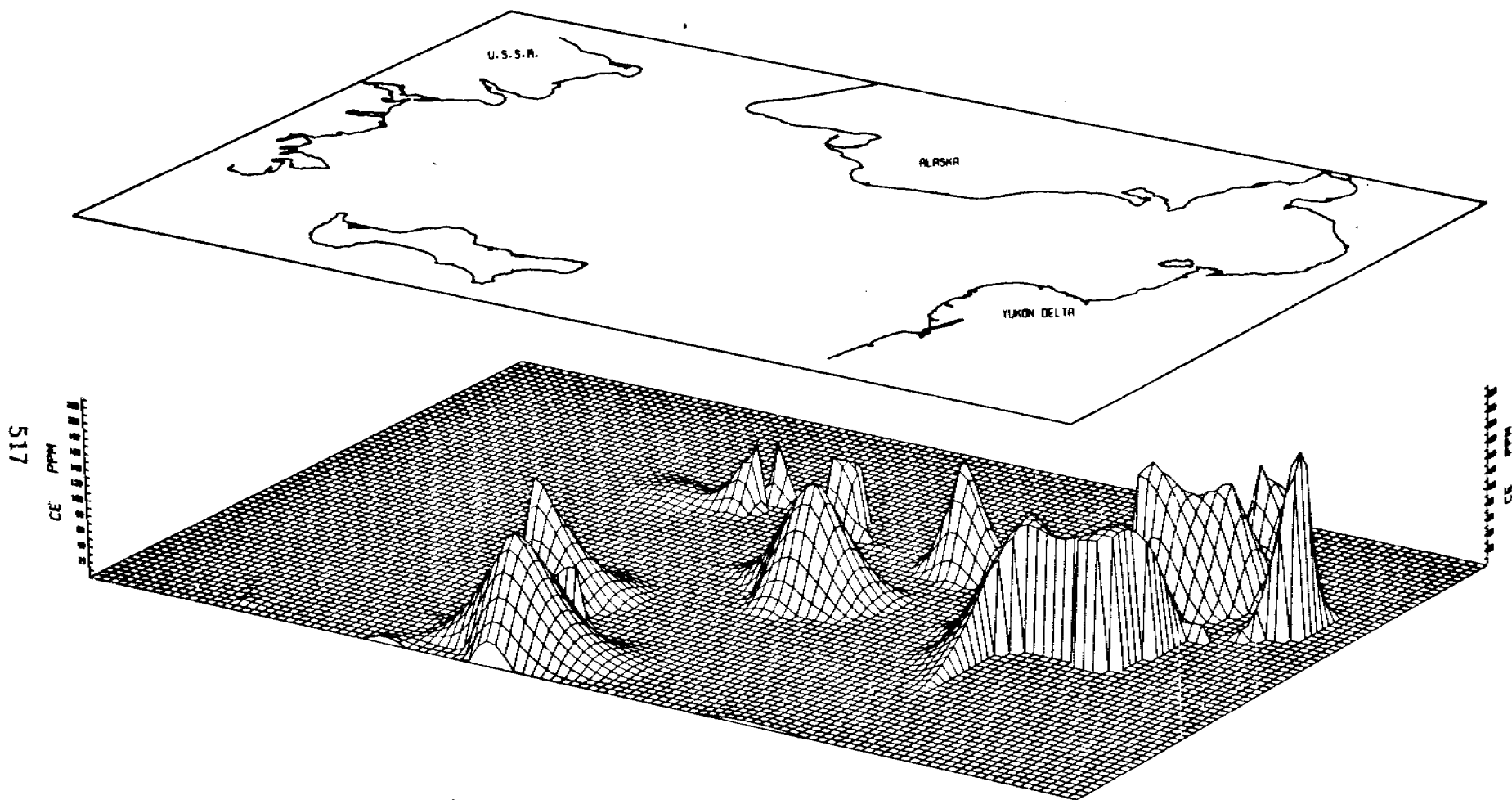


FIG 17 CE PPM IN BOTTOM SURFACE SEDIMENT OF NORTON BASIN, BERING SEA .

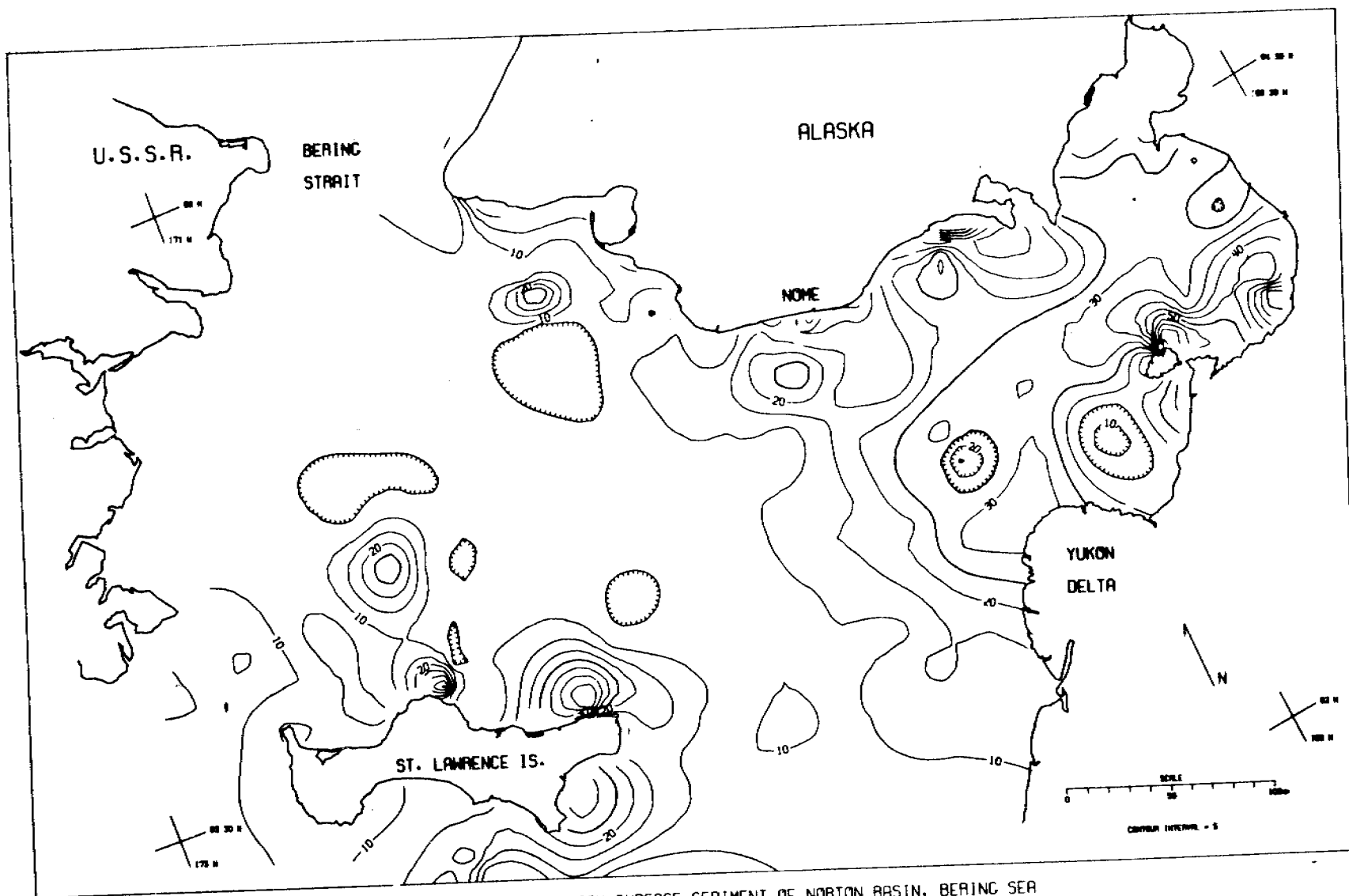


FIG 18 CU PPM IN BOTTOM SURFACE SEDIMENT OF NORTON BASIN, BERING SEA

NORTON BASIN PERSPECTIVE VIEW

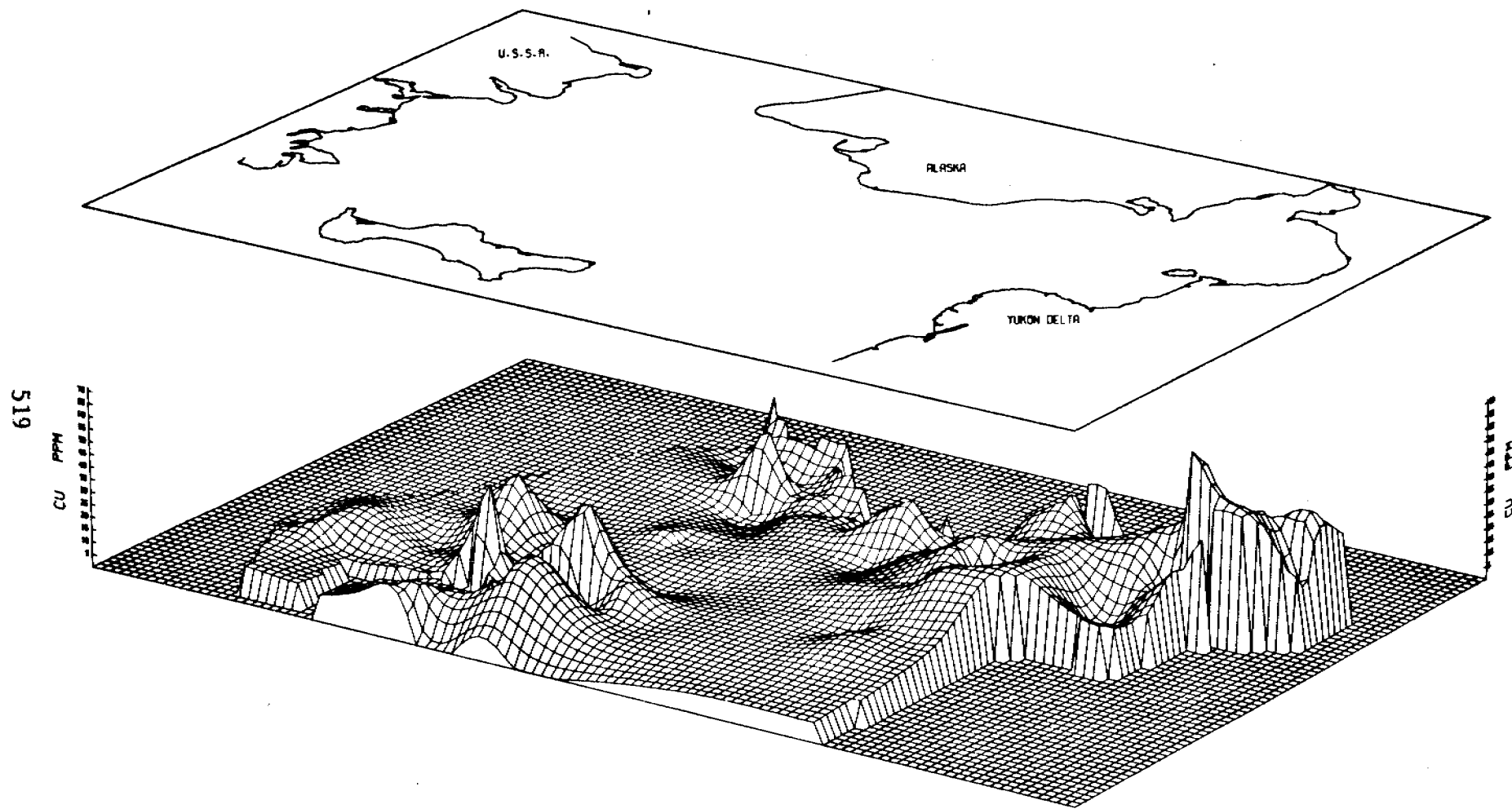


FIG 19 CU PPM IN BOTTOM SURFACE SEDIMENT OF NORTON BASIN, BERING SEA

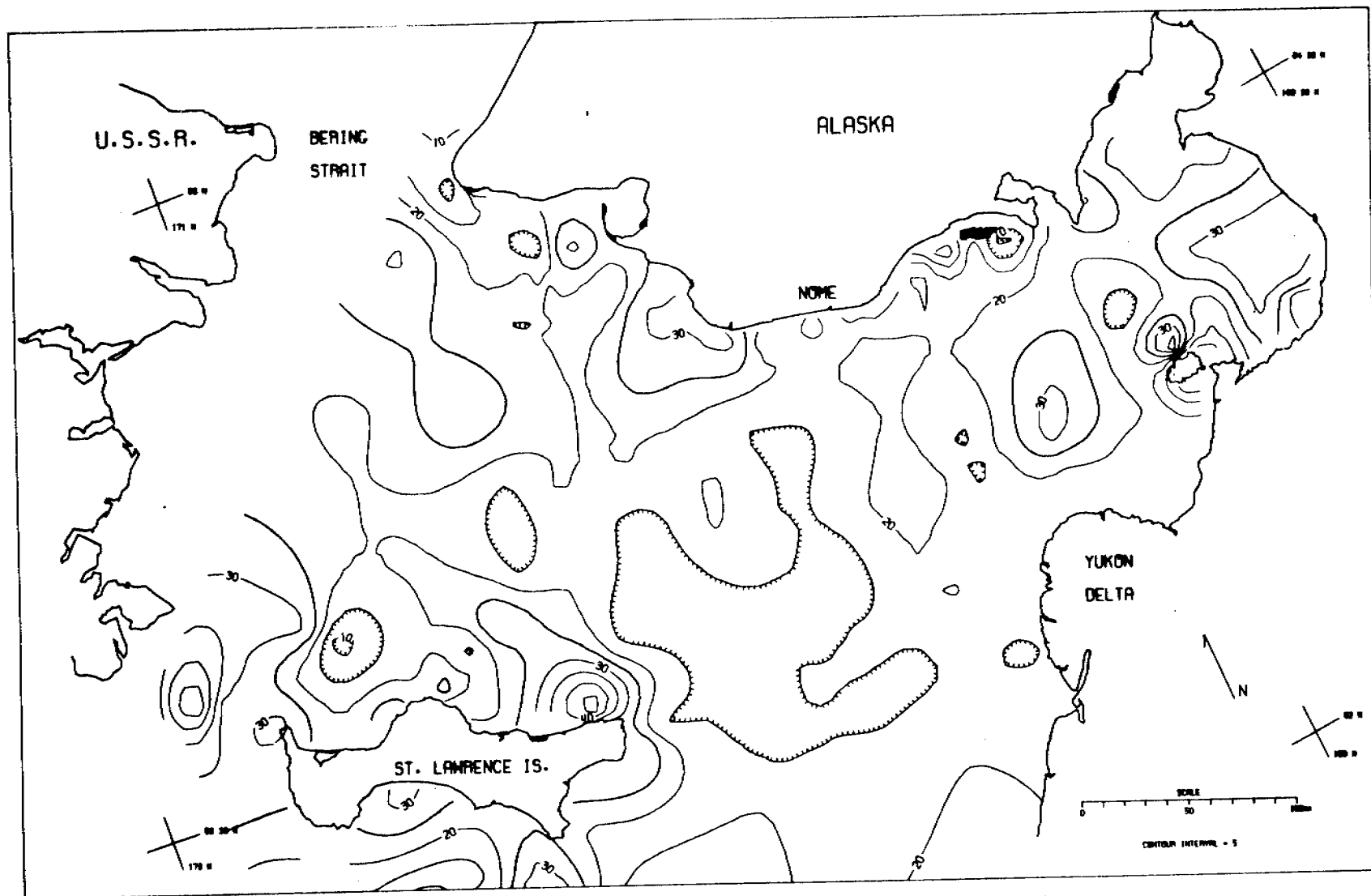


FIG 20 PB PPM IN BOTTOM SURFACE SEDIMENT OF NORTON BASIN, BERING SEA

NORTON BASIN PERSPECTIVE VIEW

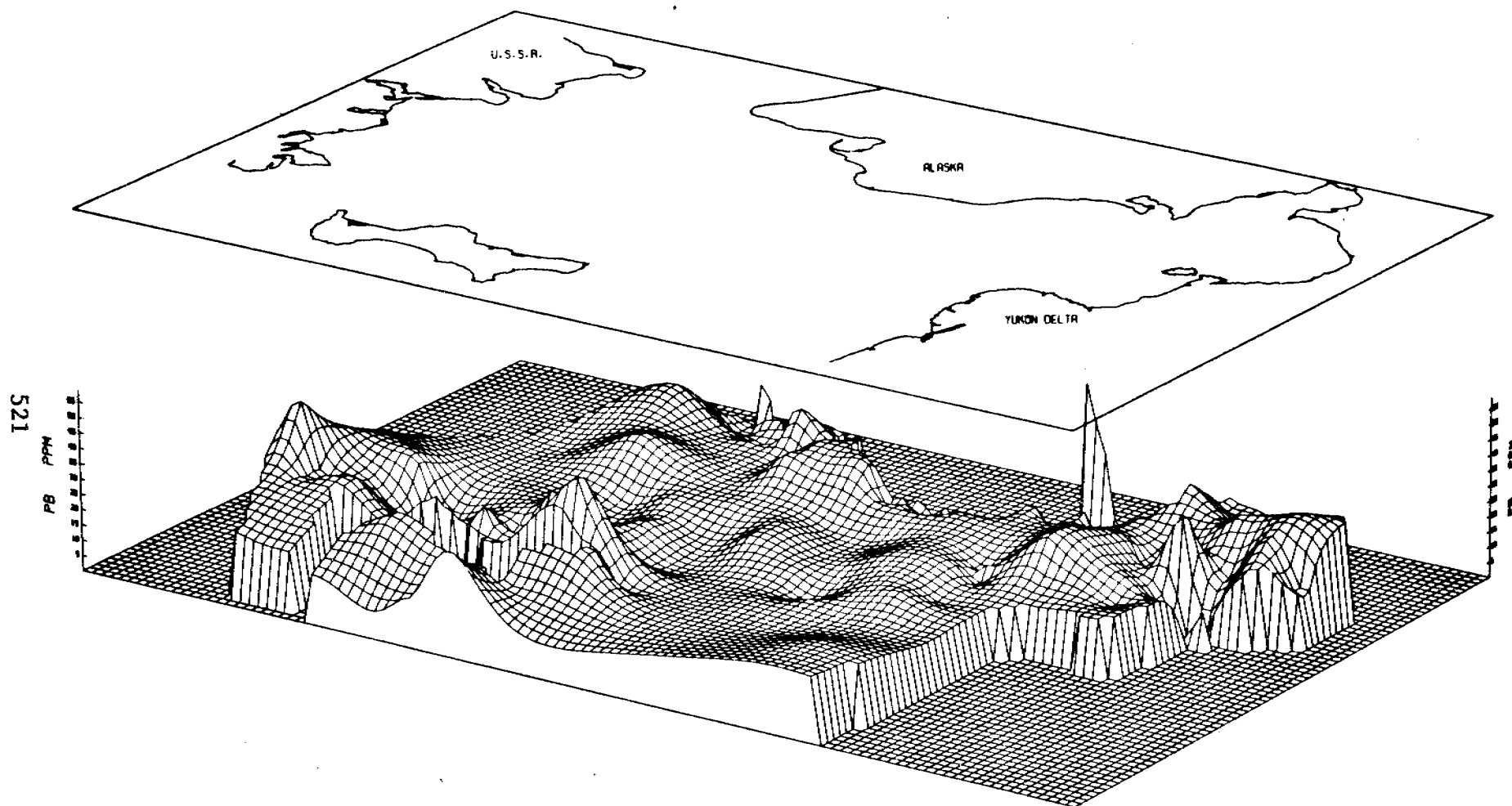


FIG 2/ PB PPM IN BOTTOM SURFACE SEDIMENT OF NORTON BASIN, BERING SEA

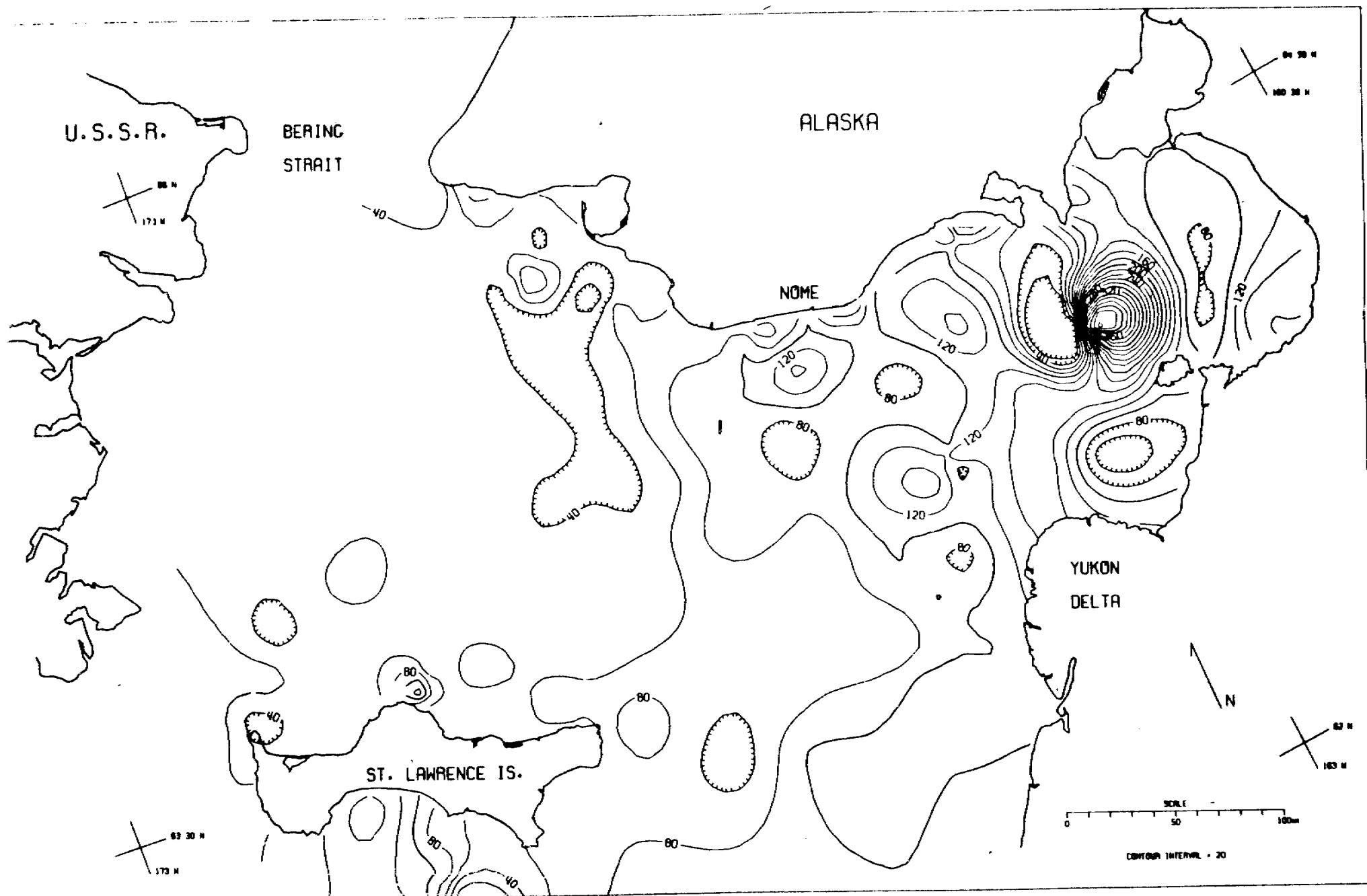


FIG 22 ZN PPM IN BOTTOM SURFACE SEDIMENT OF NORTON BASIN, BERING SEA

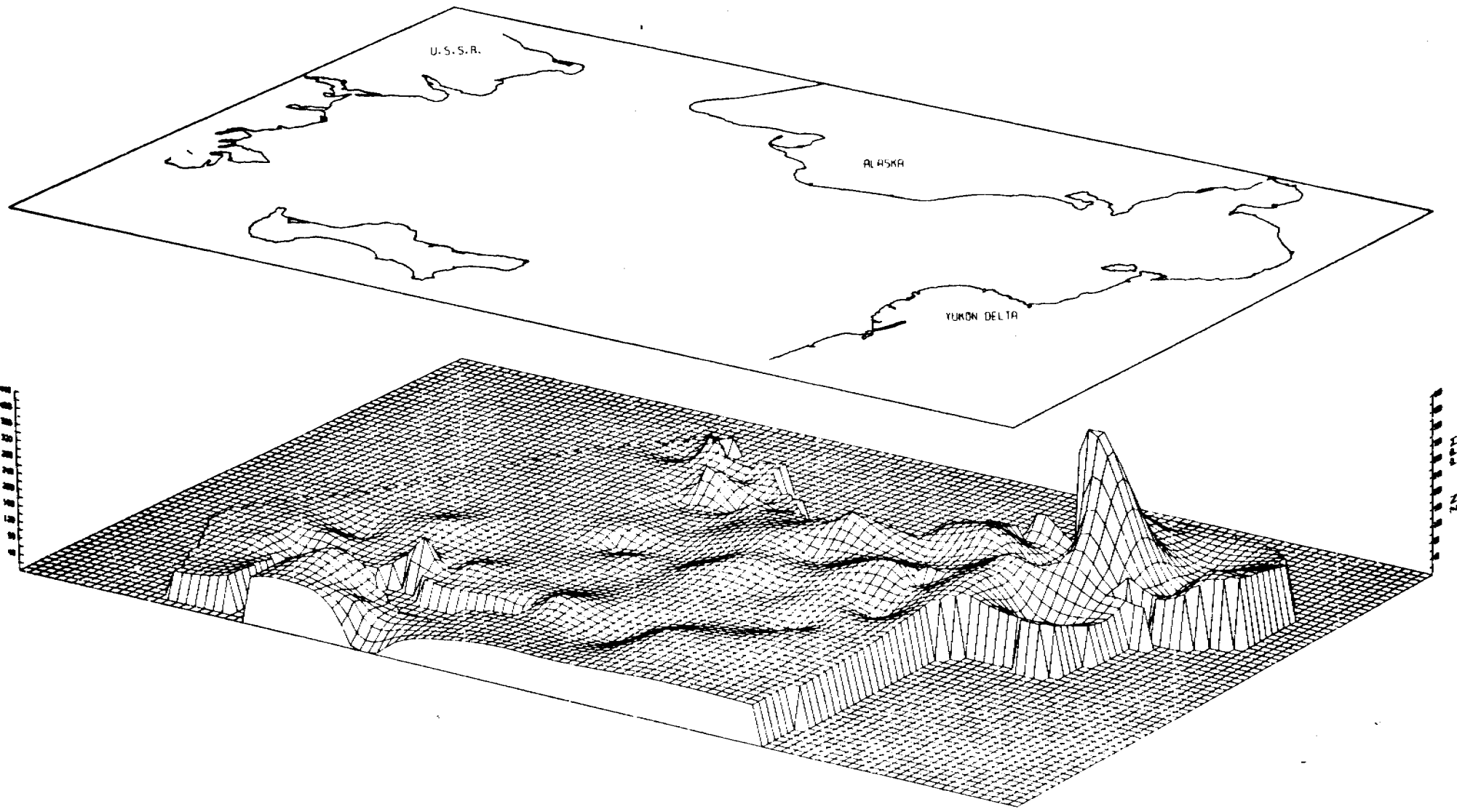


FIG. 23 ZN PPM IN BOTTOM SURFACE SEDIMENT OF NORTON BASIN, BERING SEA

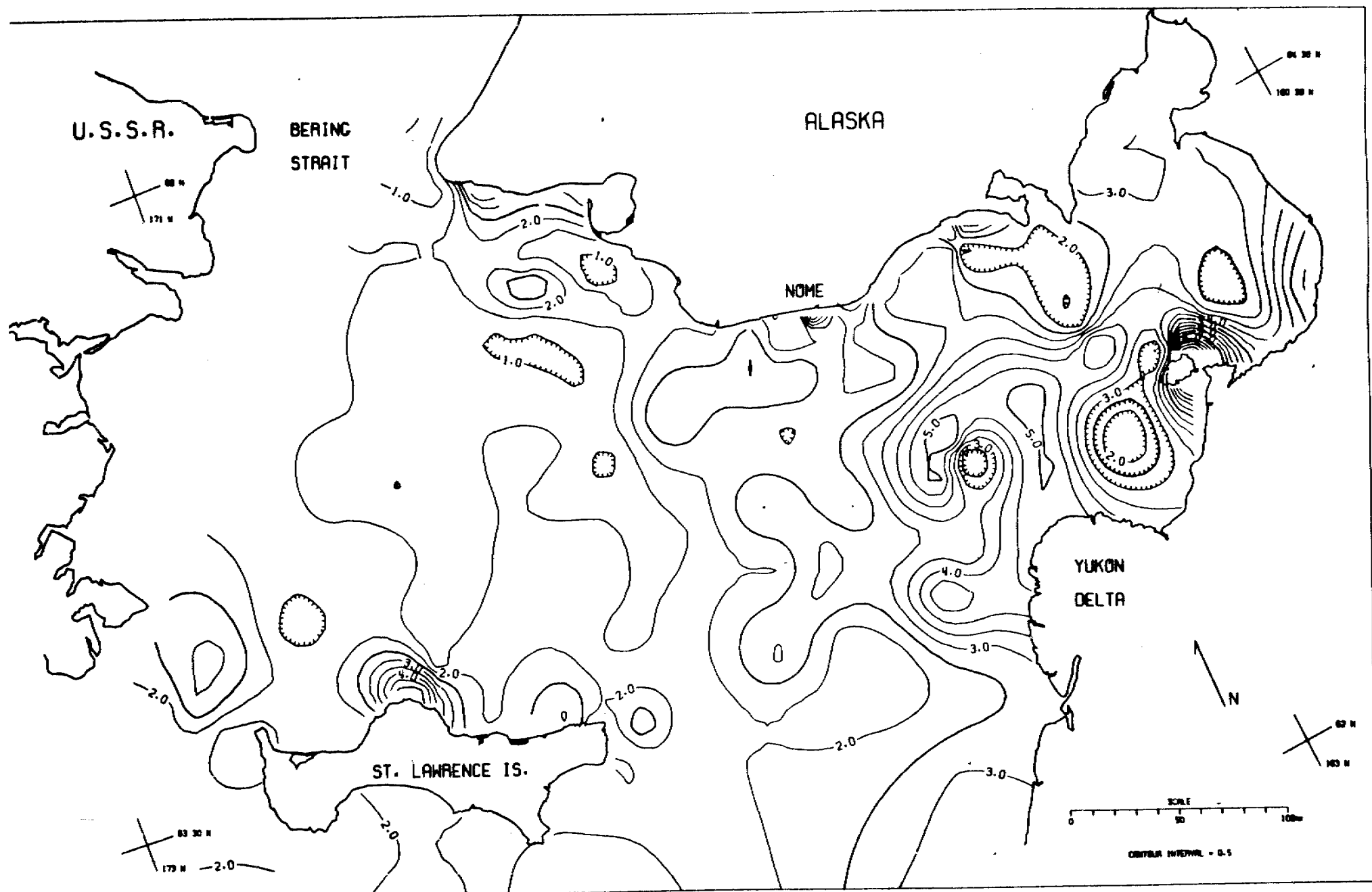


FIG 24Fe % IN BOTTOM SURFACE SEDIMENT OF NORTON BASIN, BERING SEA

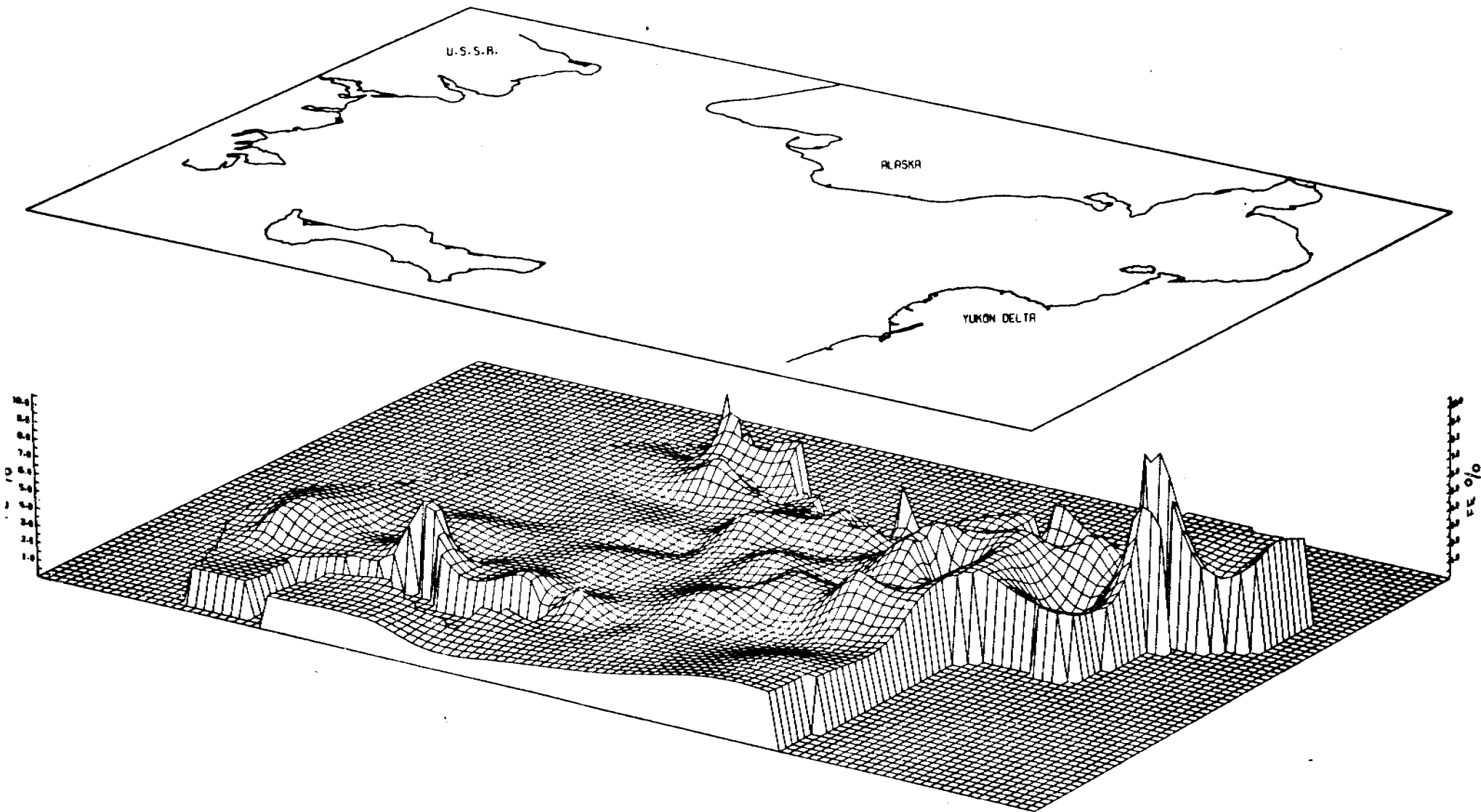


FIG 25 FE % IN BOTTOM SURFACE SEDIMENT OF NORTON BASIN, BERING SEA

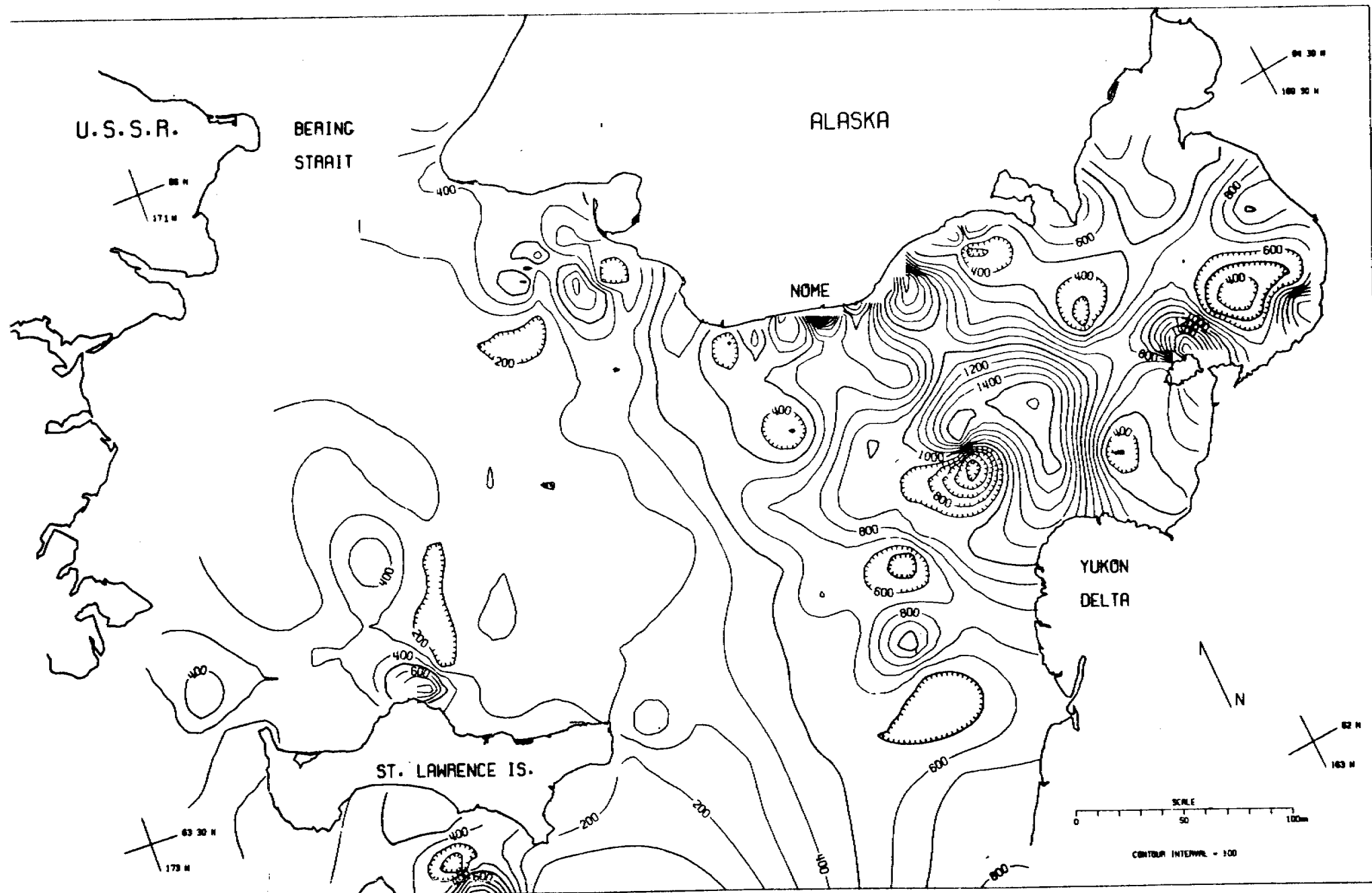


FIG 26 MN PPM IN BOTTOM SURFACE SEDIMENT OF NORTON BASIN, BERING SEA

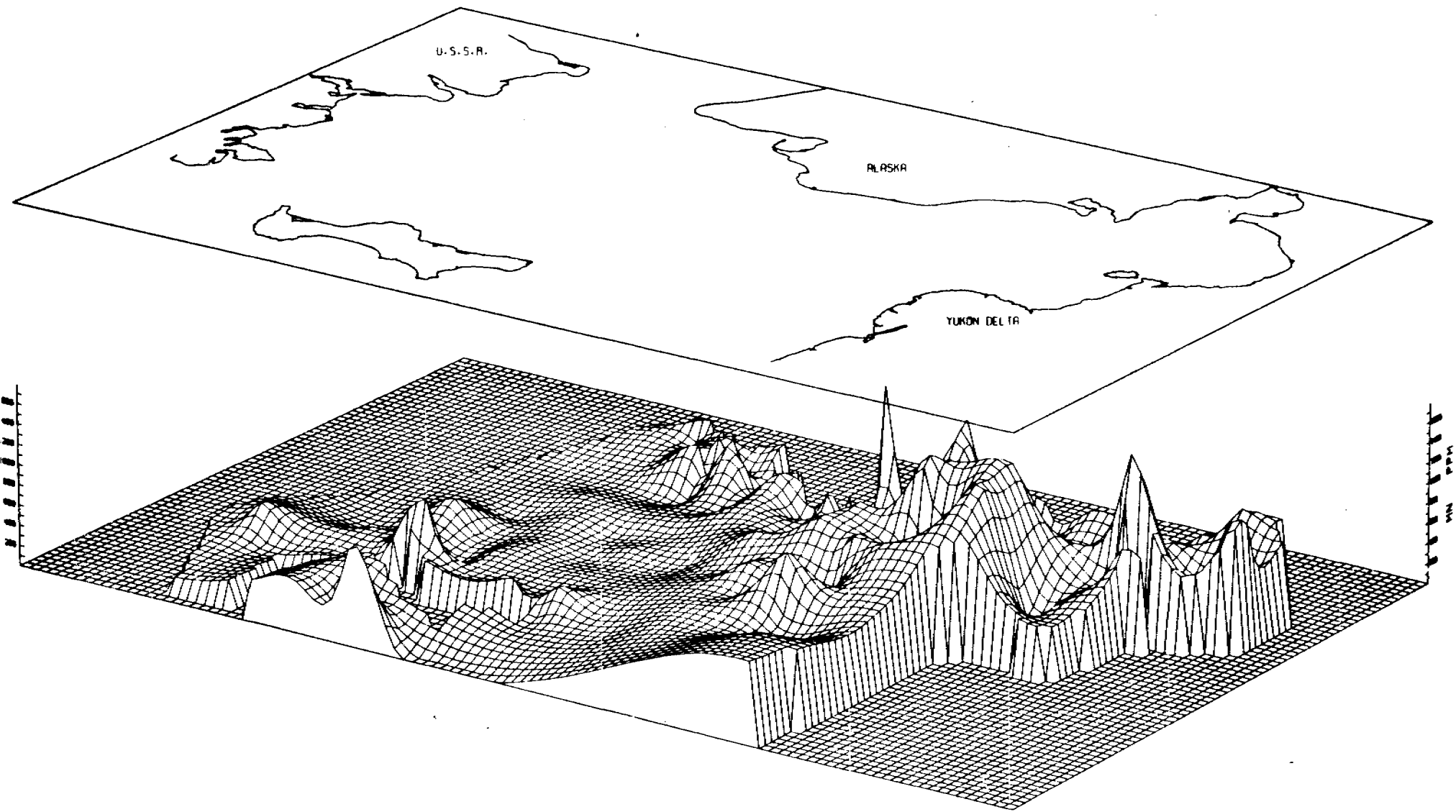


FIG 27 MN PPM IN BOTTOM SURFACE SEDIMENT OF NORTON BASIN, BERING SEA

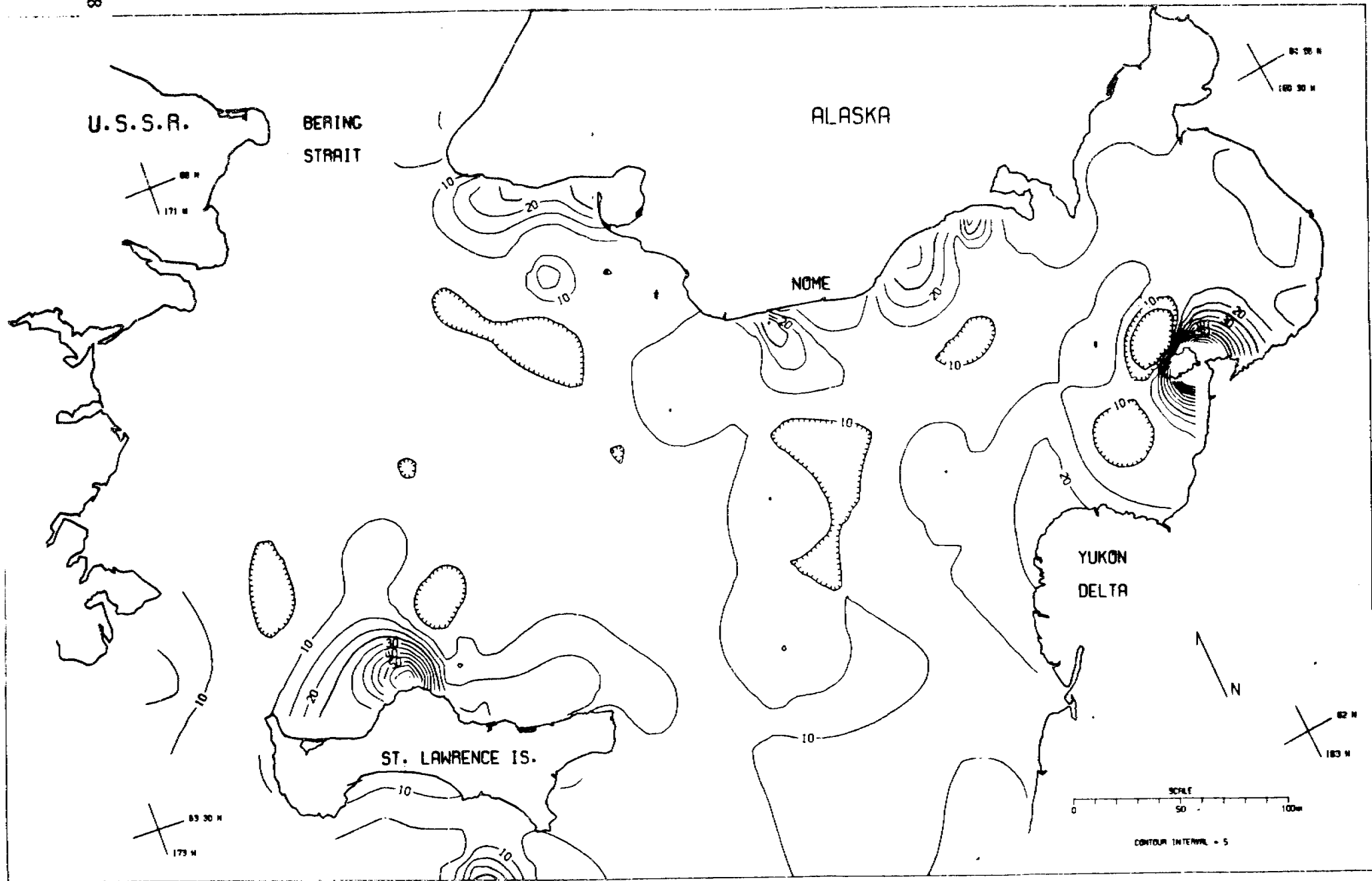


FIG 20CC PPM IN BOTTOM SURFACE SEDIMENT OF NORTON BASIN, BERING SEA

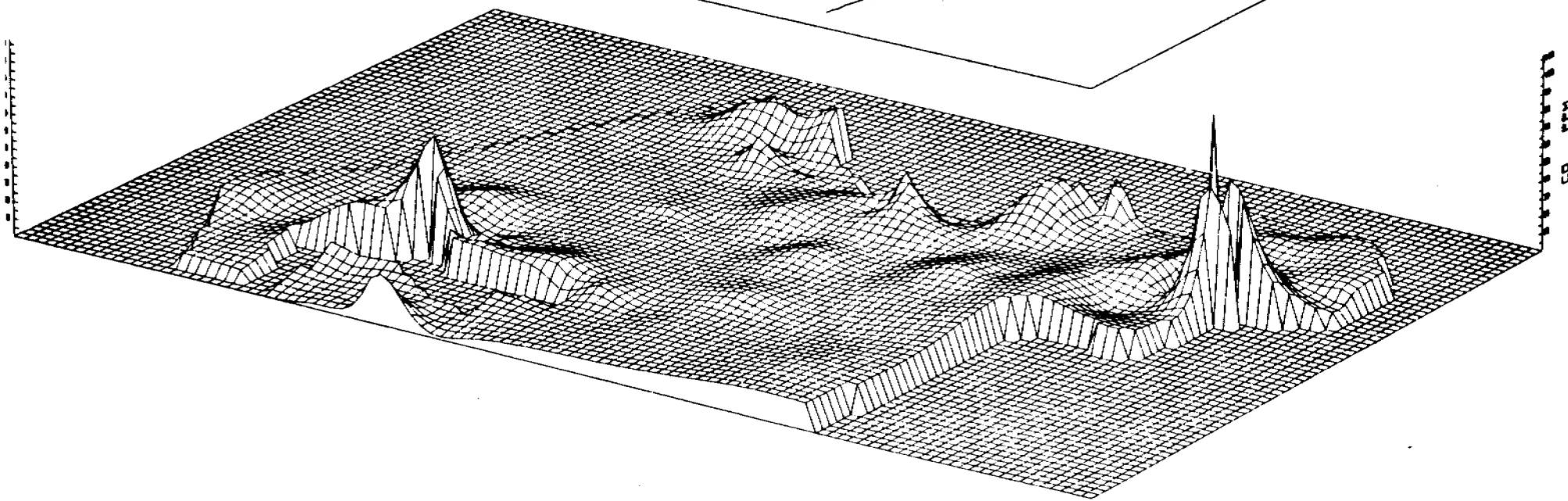
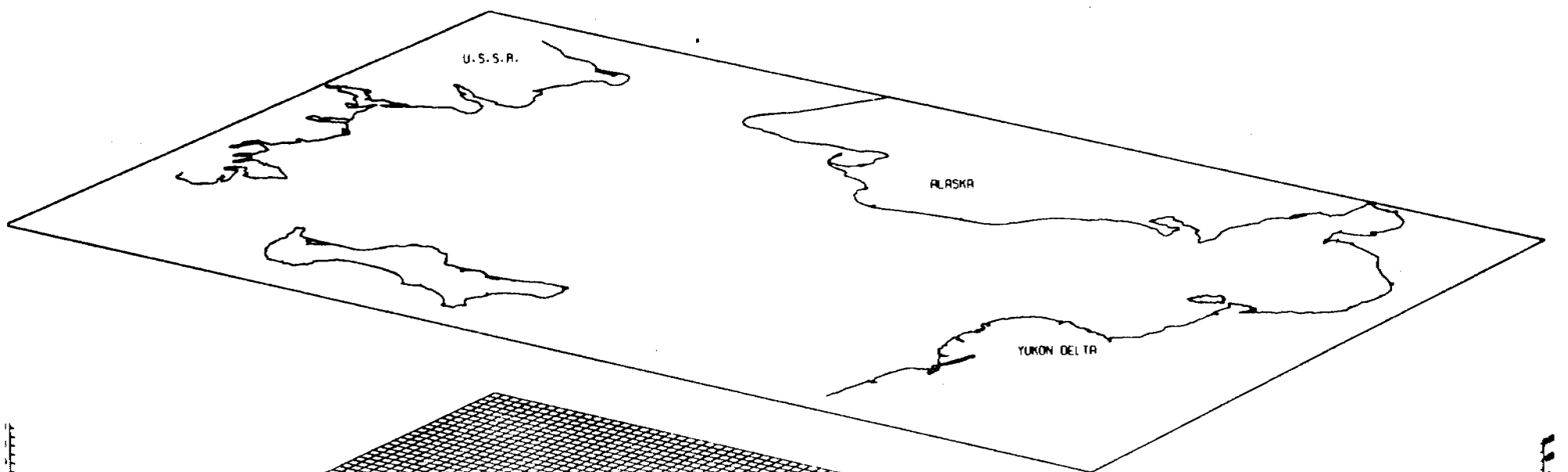


FIG 29 CO PPM IN BOTTOM SURFACE SEDIMENT OF NORTON BASIN, BERING SEA

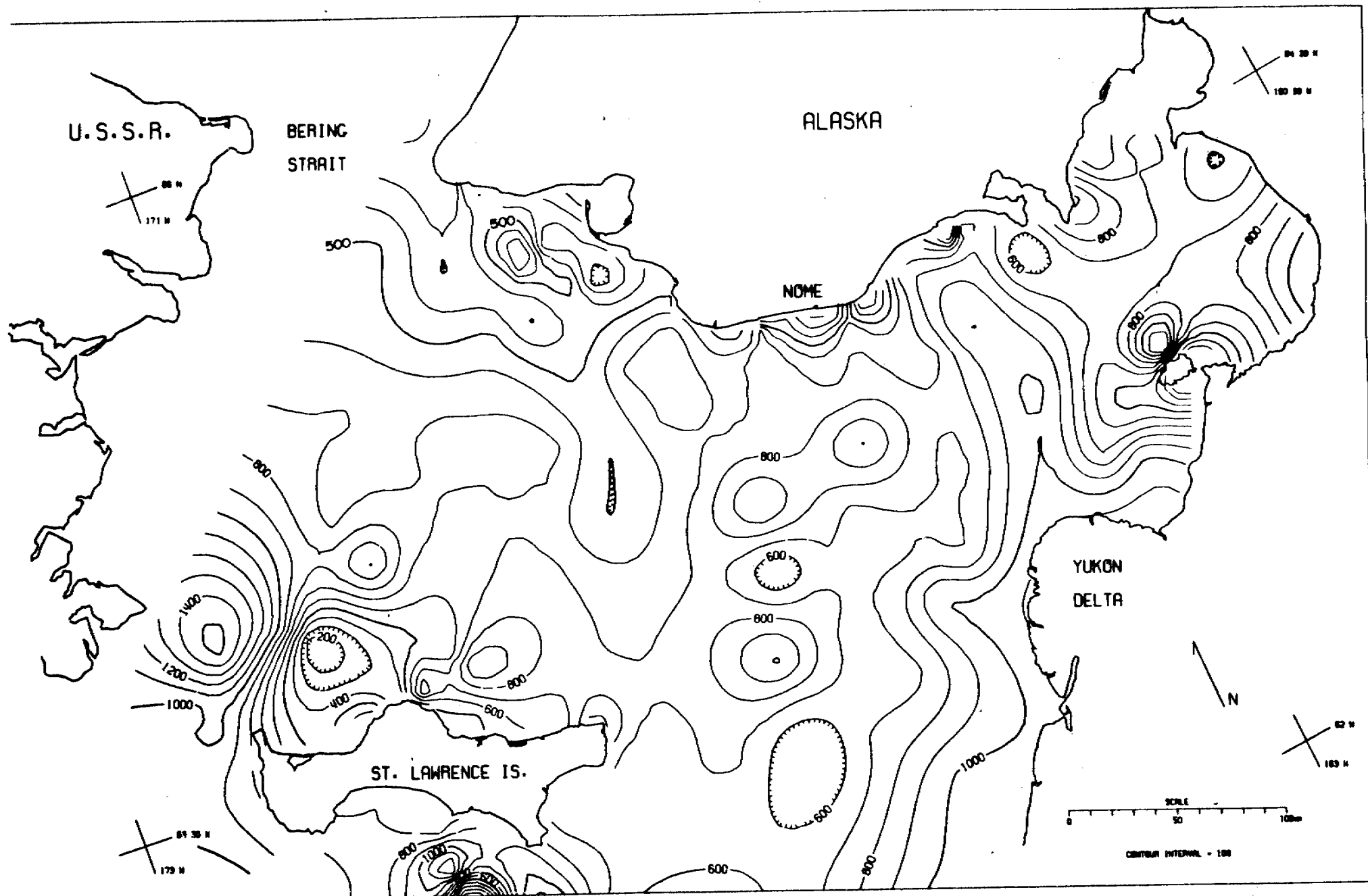
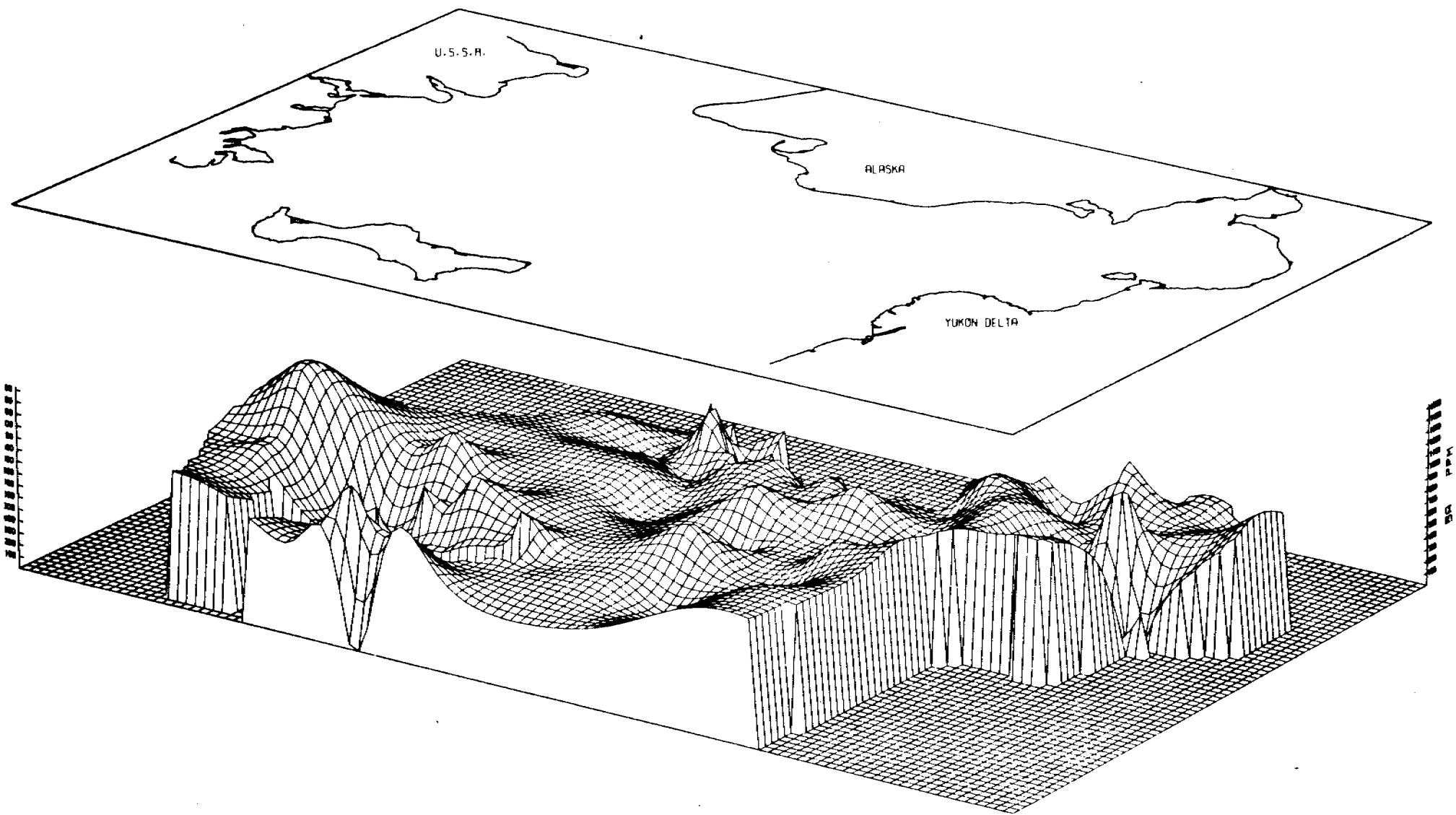


FIG 30 BA PPM IN BOTTOM SURFACE SEDIMENT OF NORTON BASIN, BERING SEA



531

FIG 31 BA PPM IN BOTTOM SURFACE SEDIMENT OF NORTON BASIN, BERING SEA

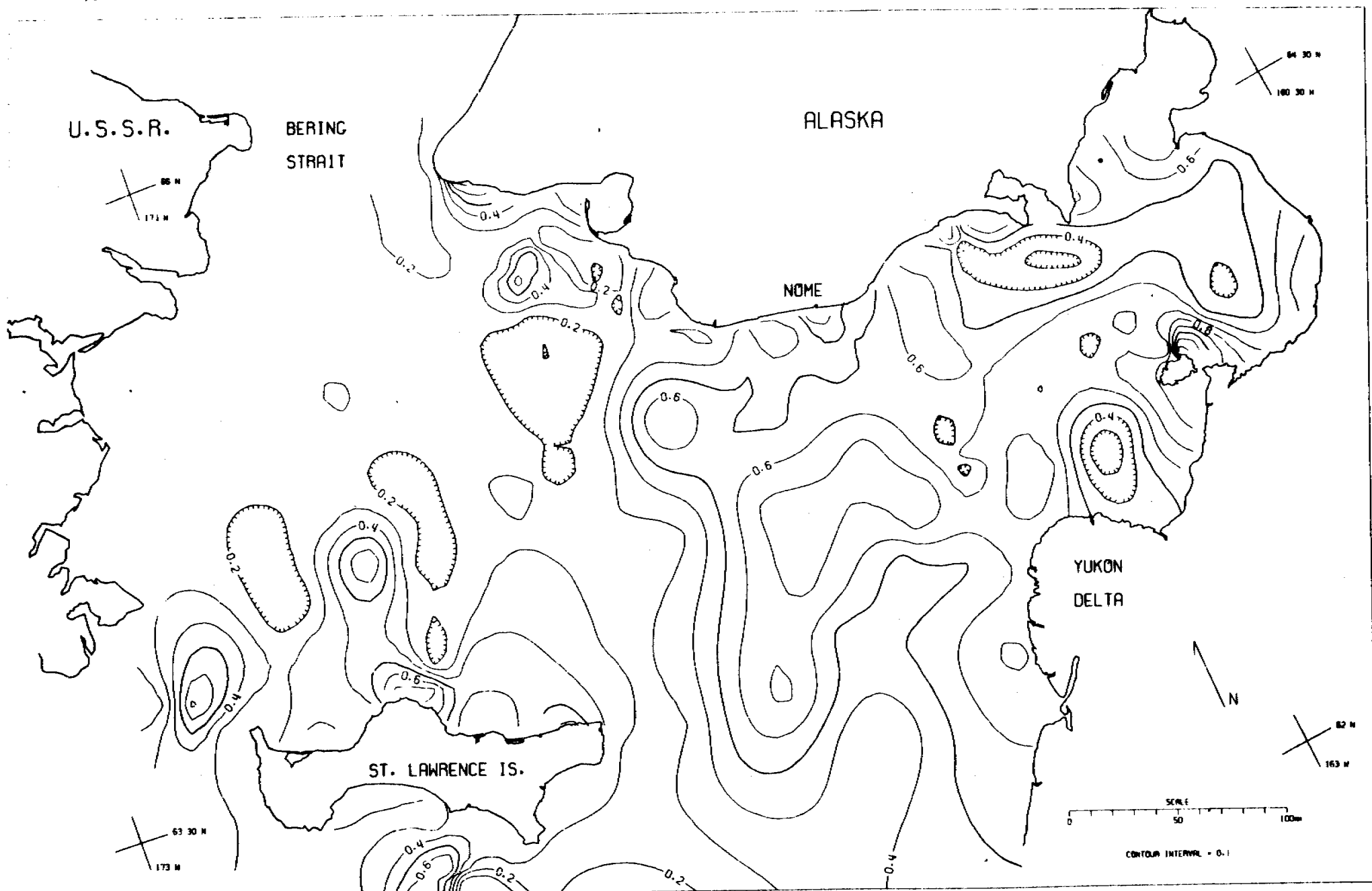


FIG 32 TI % IN BOTTOM SURFACE SEDIMENT OF NORTON BASIN, BERING SEA

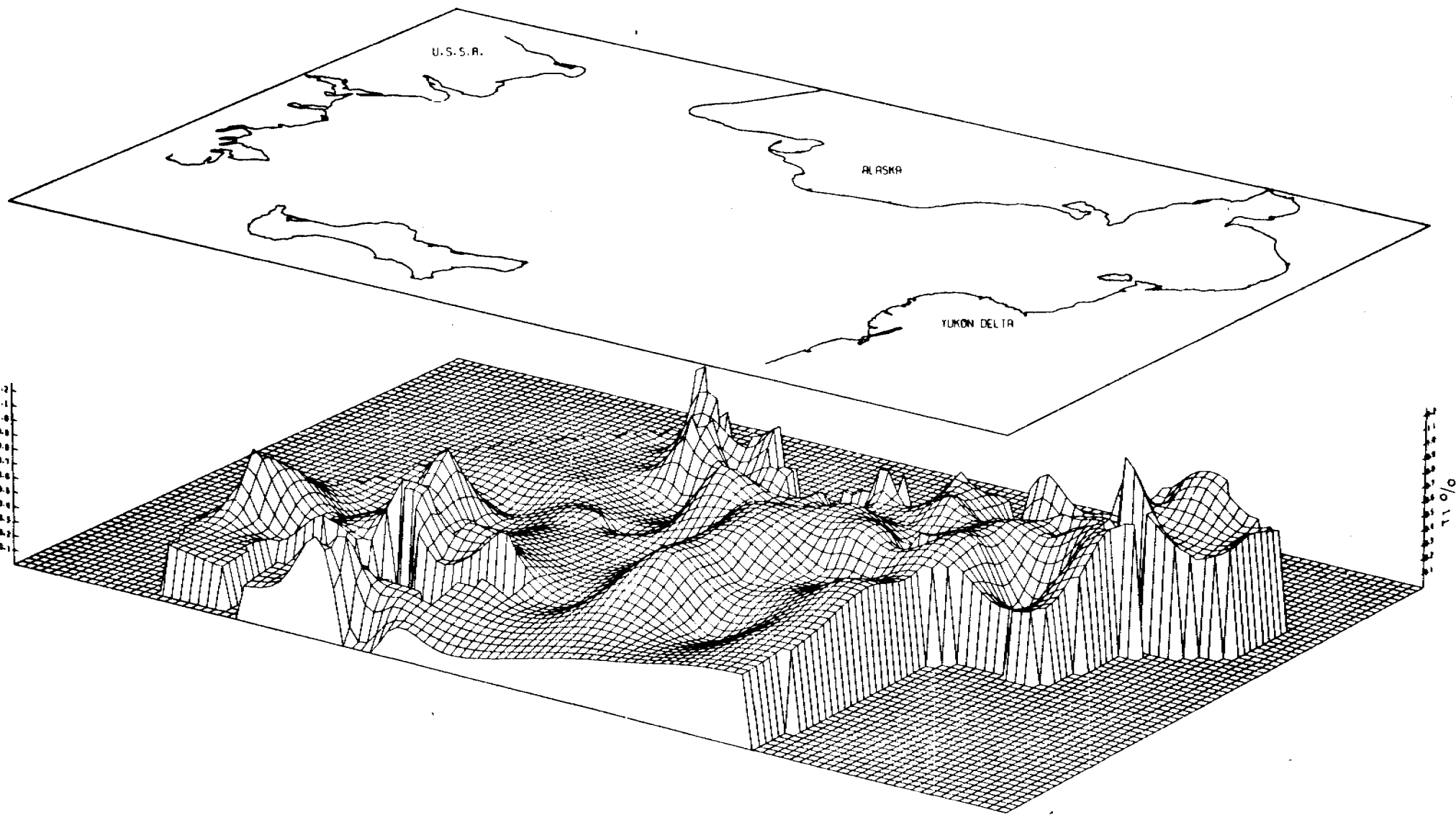


FIG 33 Ti % IN BOTTOM SURFACE SEDIMENT OF NORTON BASIN, BERING SEA

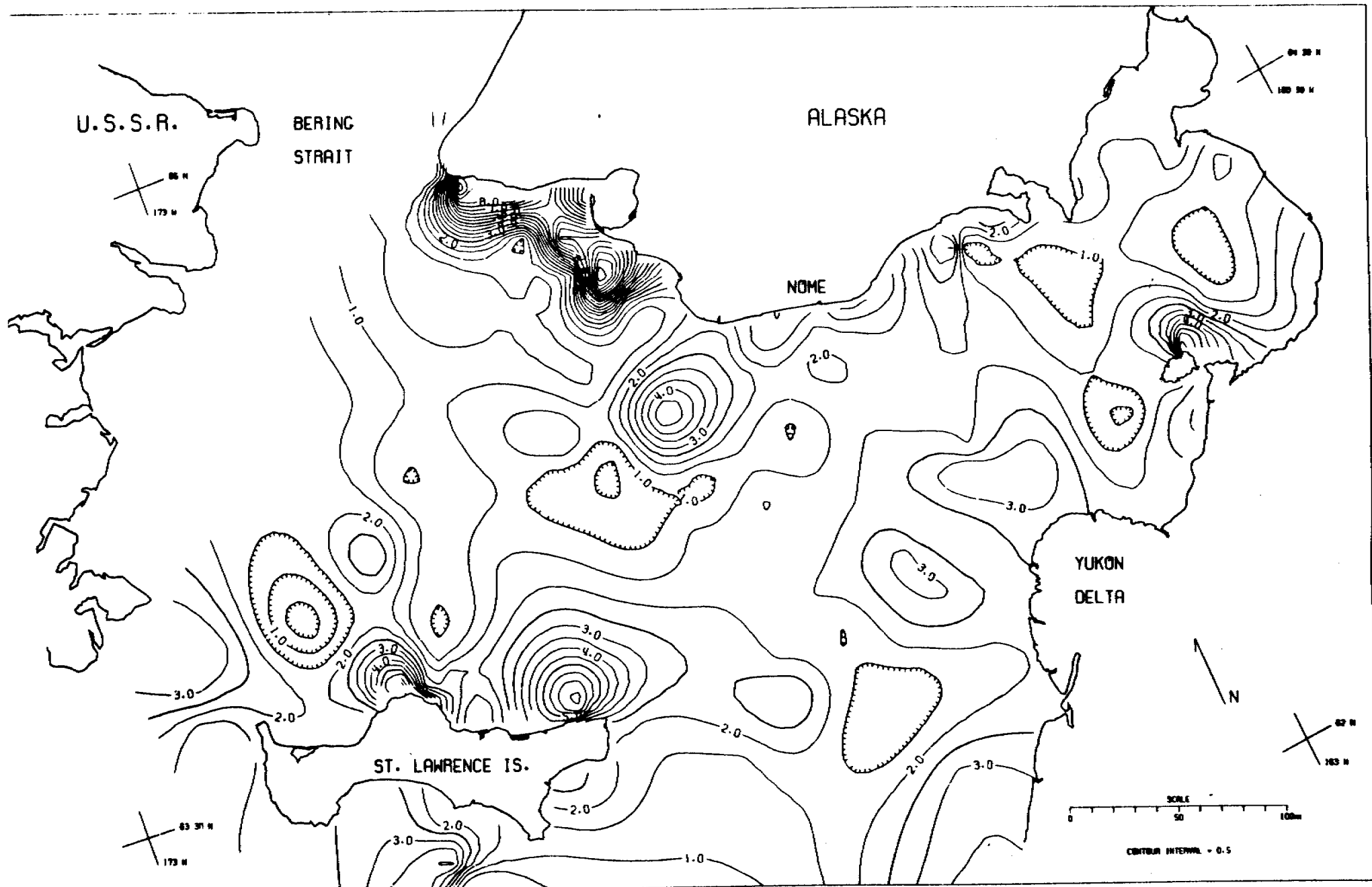


FIG 35 CA

IN BOTTOM SURFACE SEDIMENT OF NORTON BASIN, BERING SEA

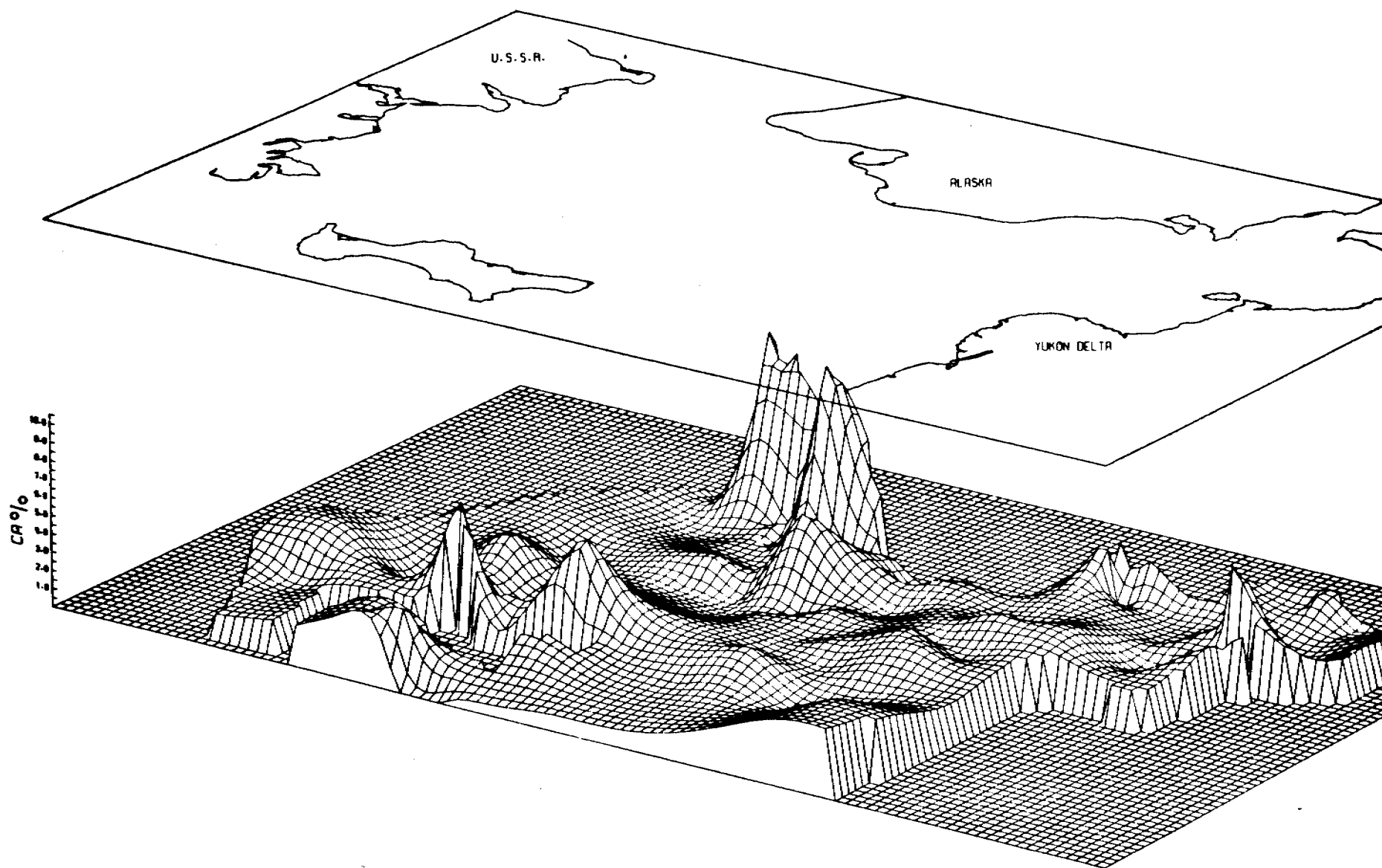


FIG 36 CA % IN BOTTOM SURFACE SEDIMENT OF NORTON BASIN, BERING SEA

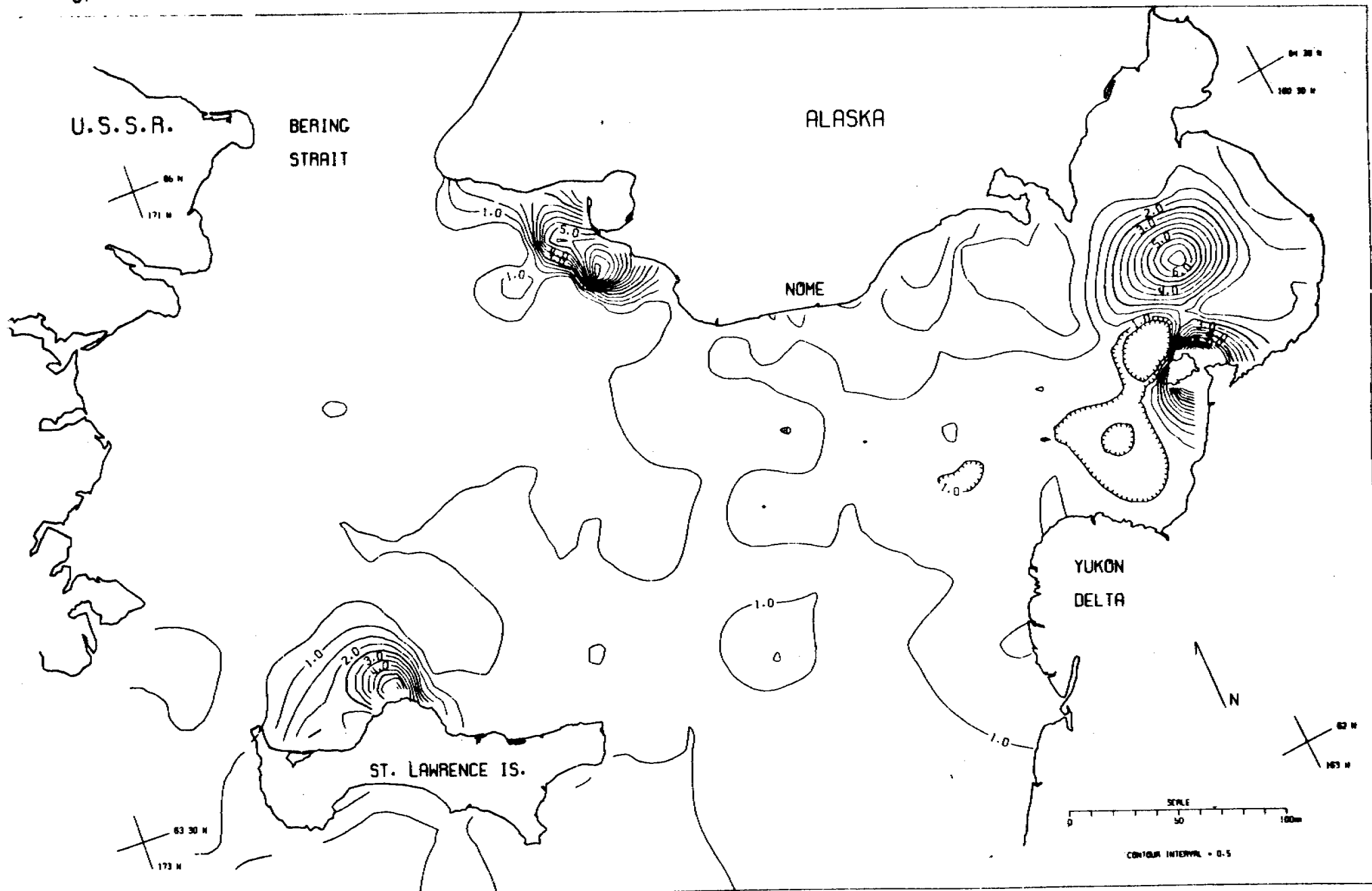
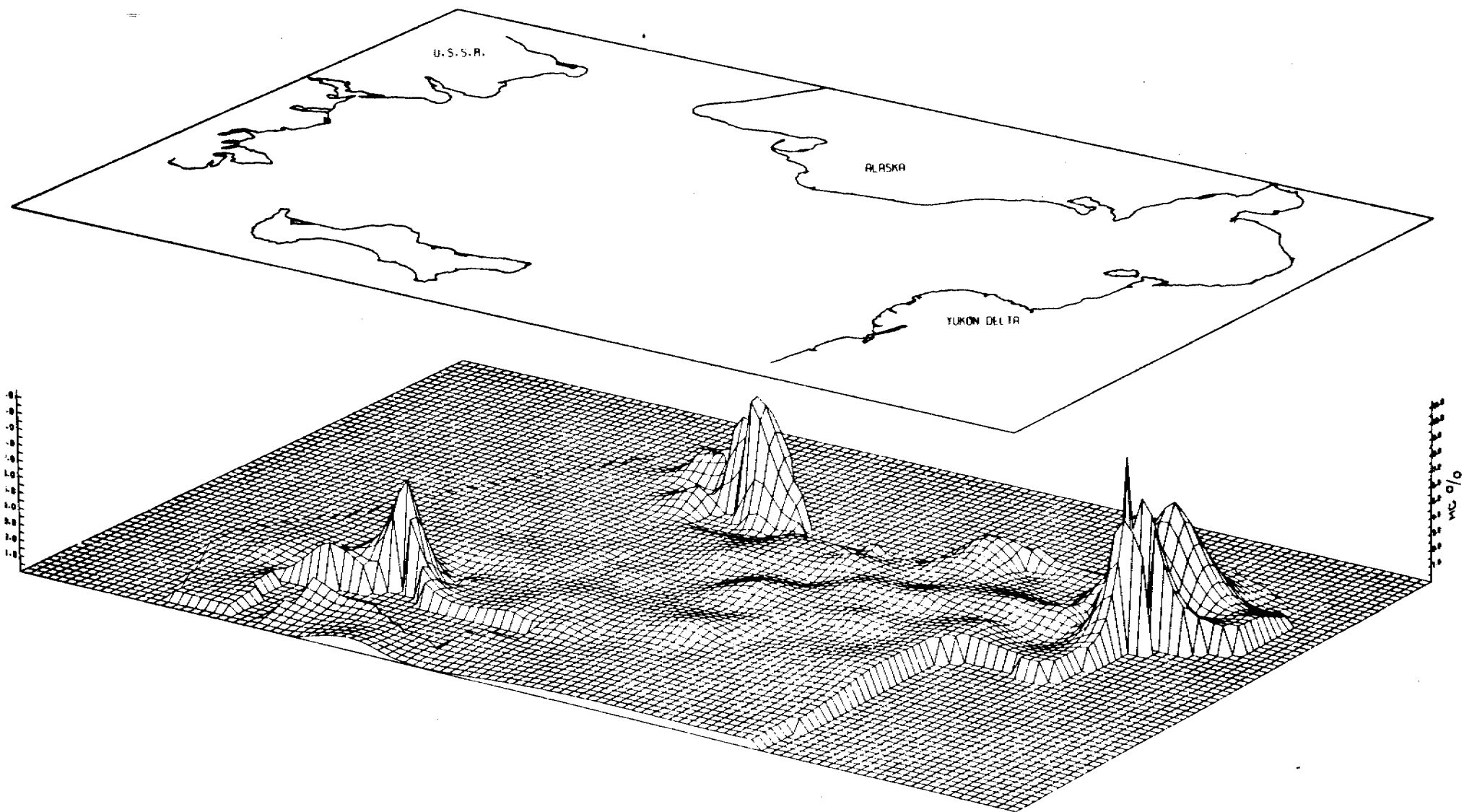


FIG 37 MG % IN BOTTOM SURFACE SEDIMENT OF NORTON BASIN, BERING SEA



537

FIG 38 MG % IN BOTTOM SURFACE SEDIMENT OF NORTON BASIN. BERING SEA

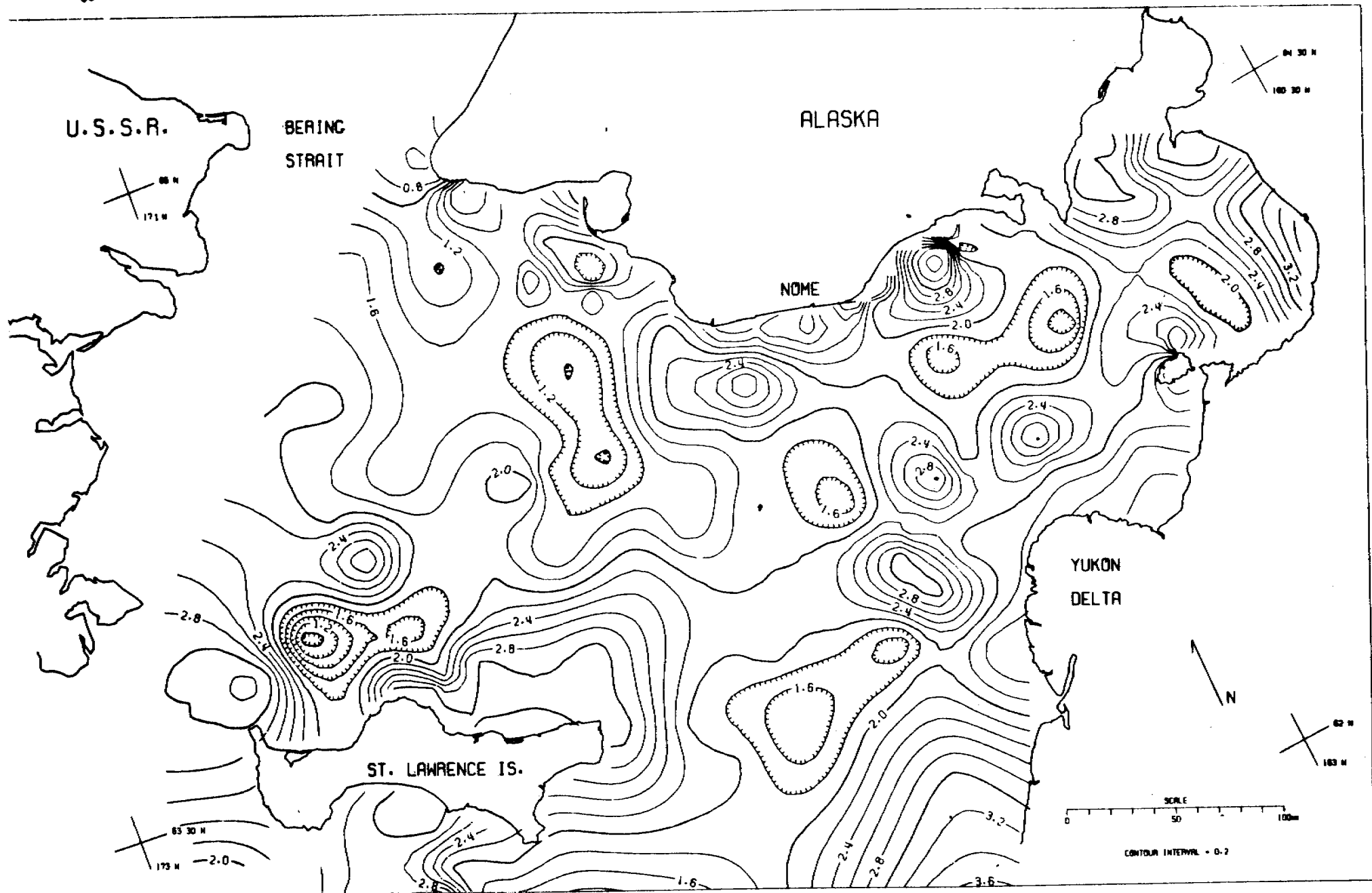


FIG 39 Na % IN BOTTOM SURFACE SEDIMENT OF NORTON BASIN, BERING SEA

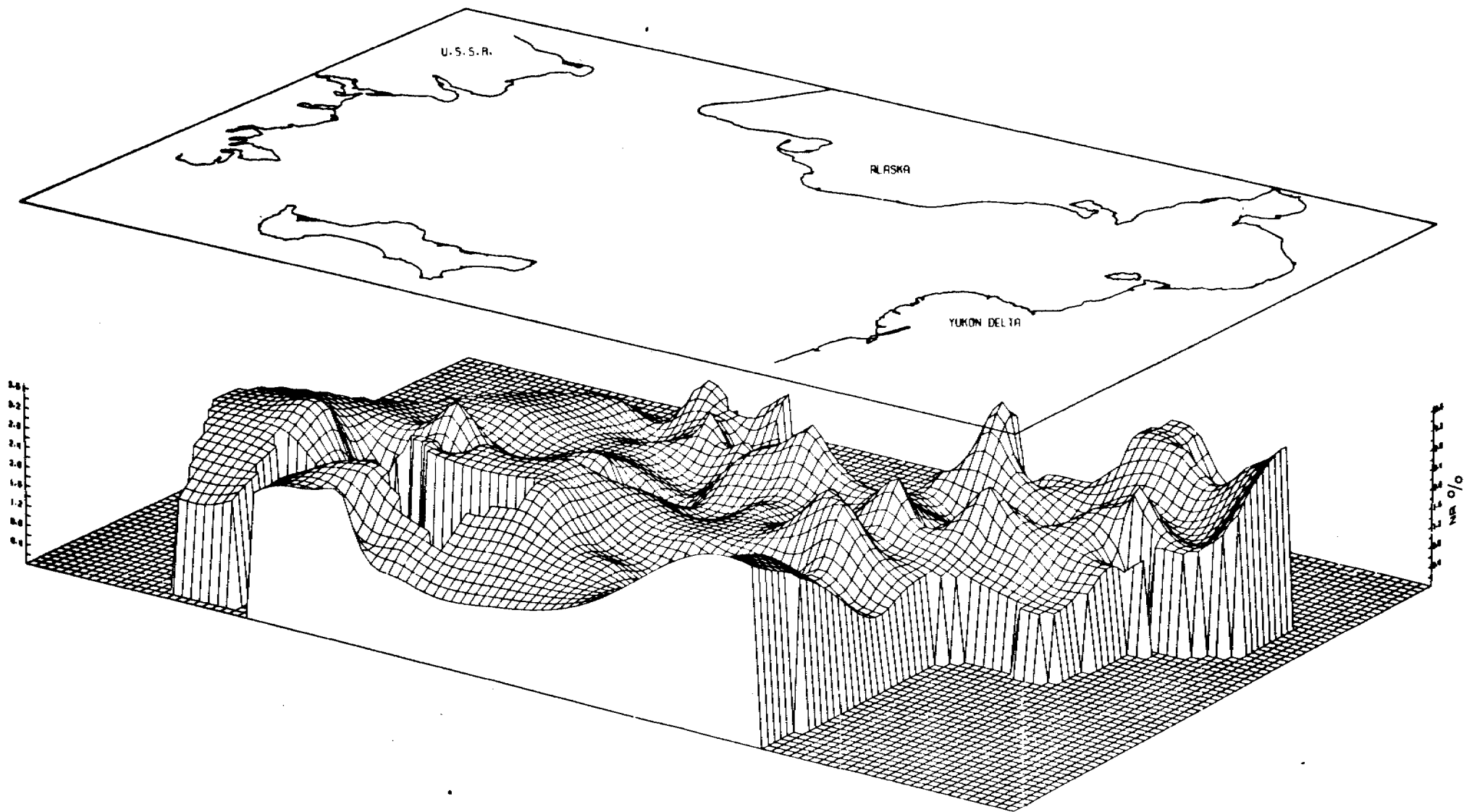


FIG 40 NA % IN BOTTOM SURFACE SEDIMENT OF NORTON BASIN, BERING SEA

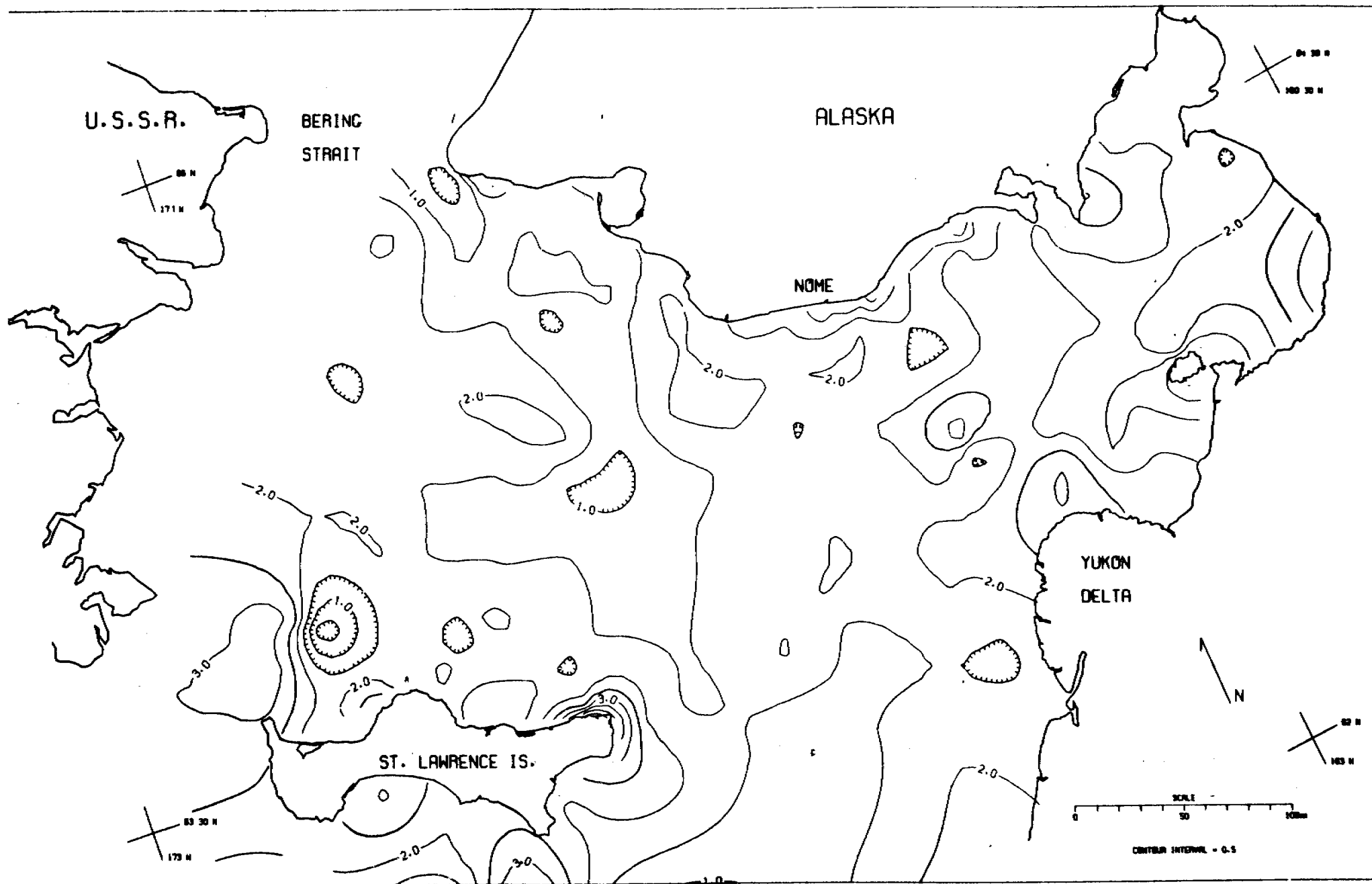


FIG 41 K % IN BOTTOM SURFACE SEDIMENT OF NORTON BASIN, BERING SEA

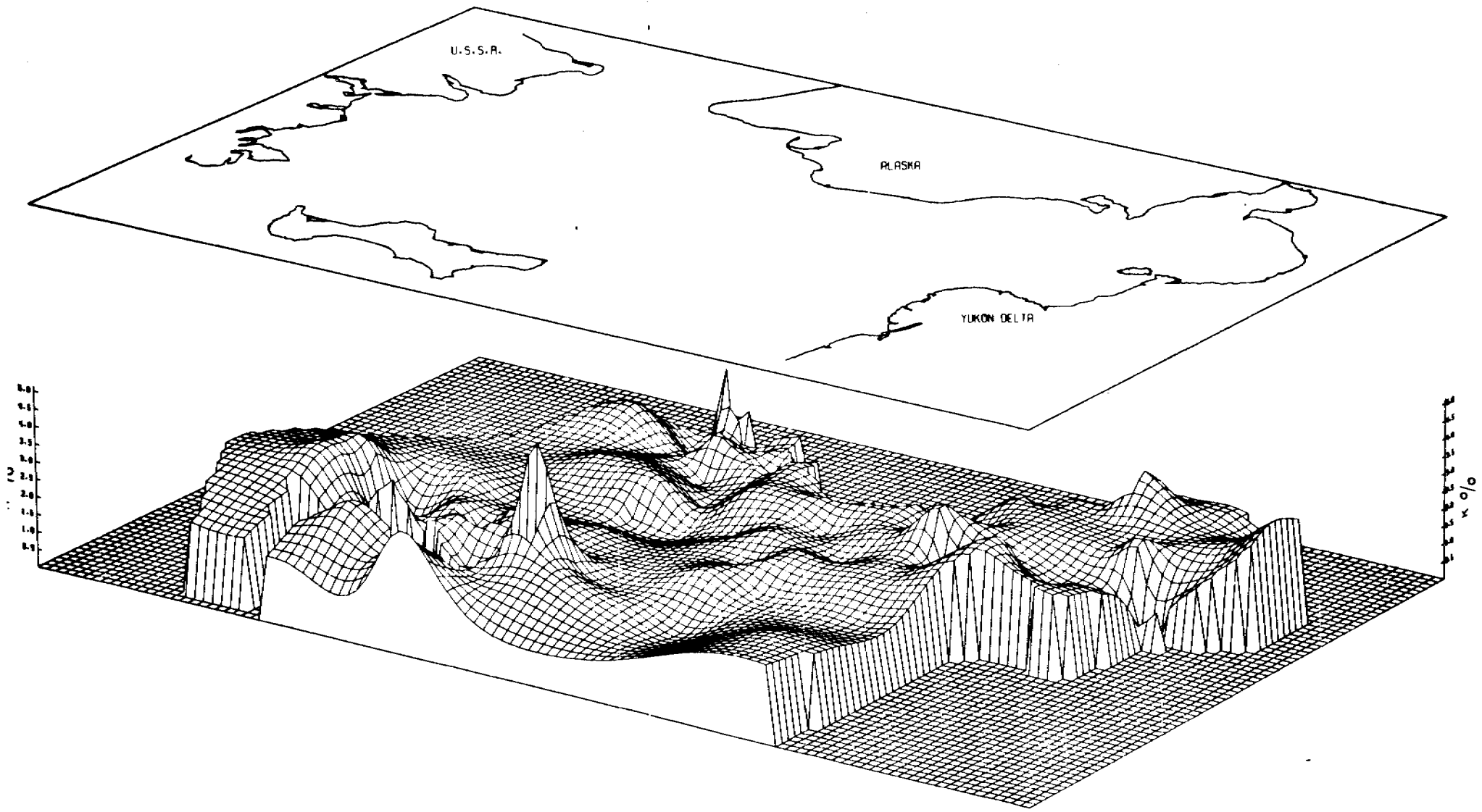


FIG 42 K % IN BOTTOM SURFACE SEDIMENT OF NORTON BASIN, BERING SEA

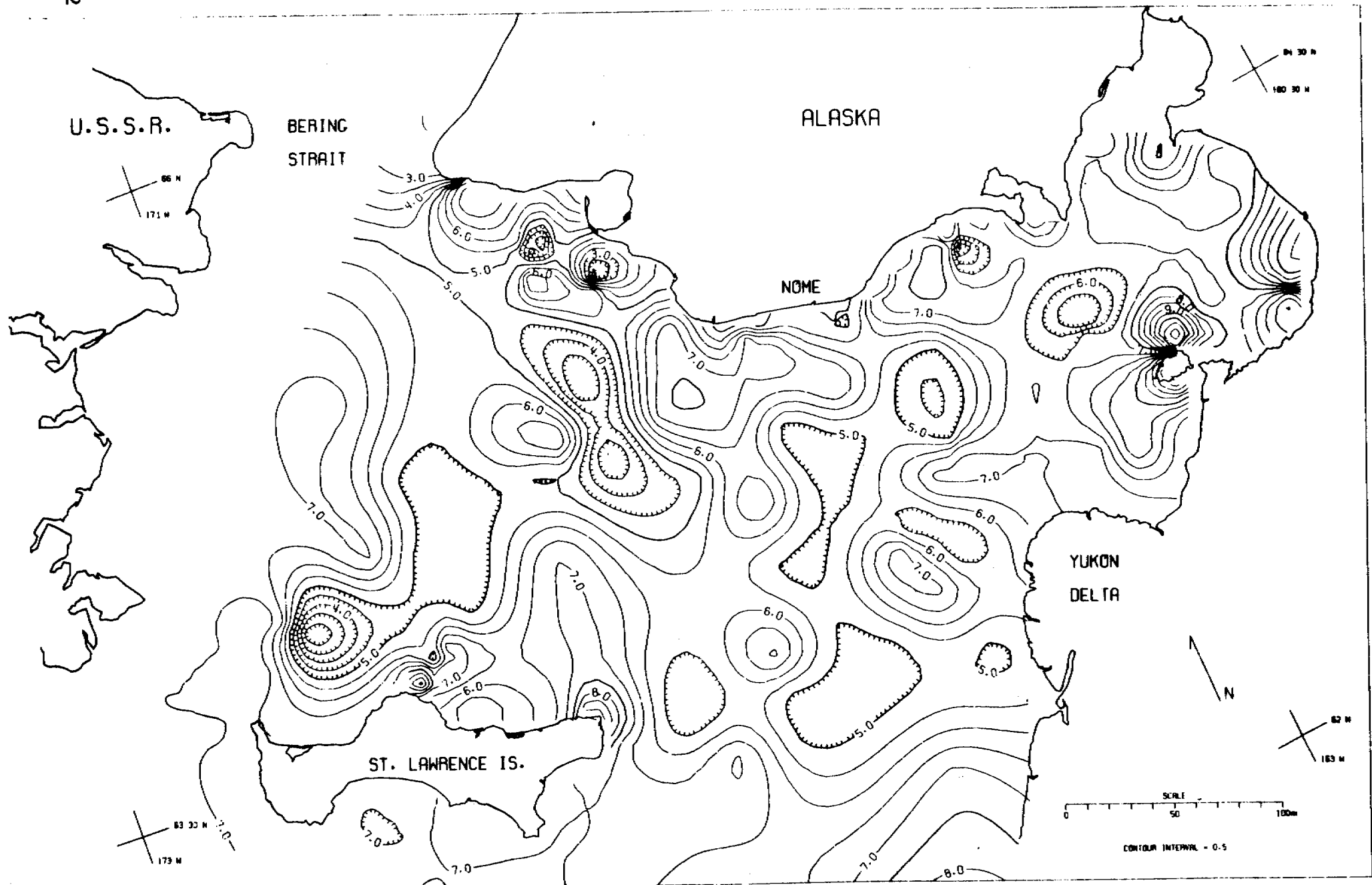
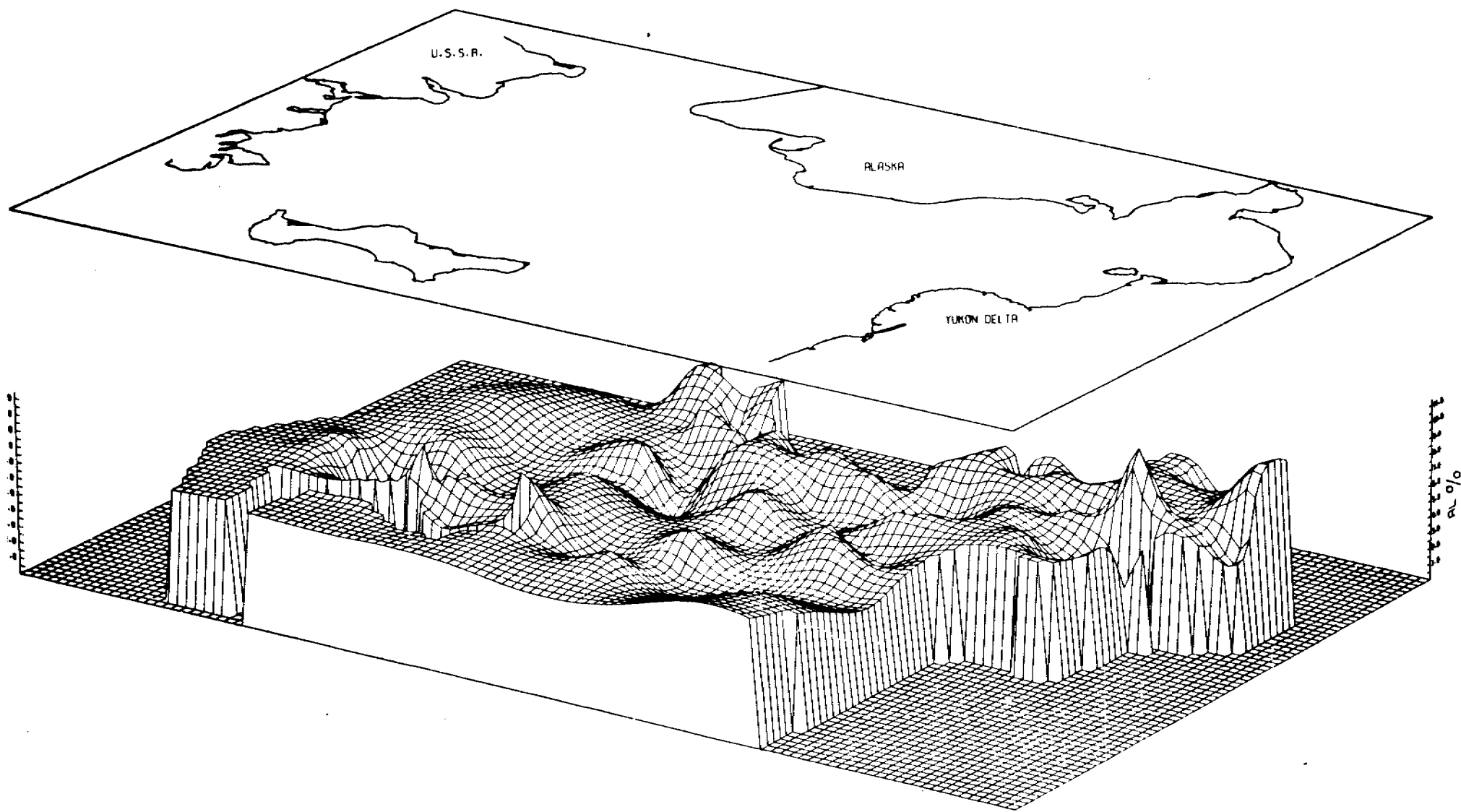


FIG 43 AL % IN BOTTOM SURFACE SEDIMENT OF NORTON BASIN, BERING SEA



543

FIG 44 AL% IN BOTTOM SURFACE SEDIMENT OF NORTON BASIN, BERING SEA

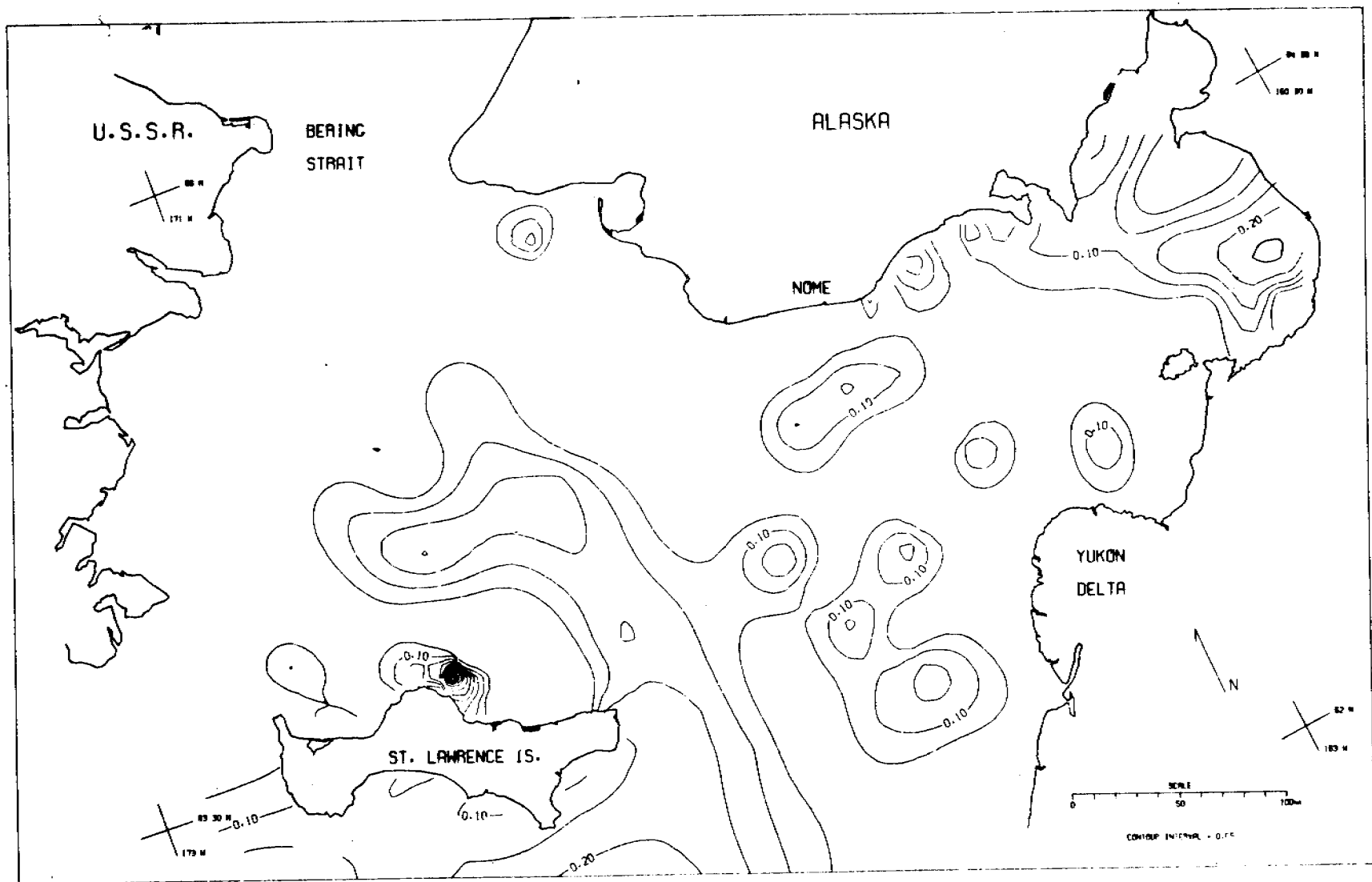


FIG 45 P PPM IN BOTTOM SURFACE SEDIMENT OF NORTON BASIN, BERING SEA

NORTON BASIN PERSPECTIVE VIEW

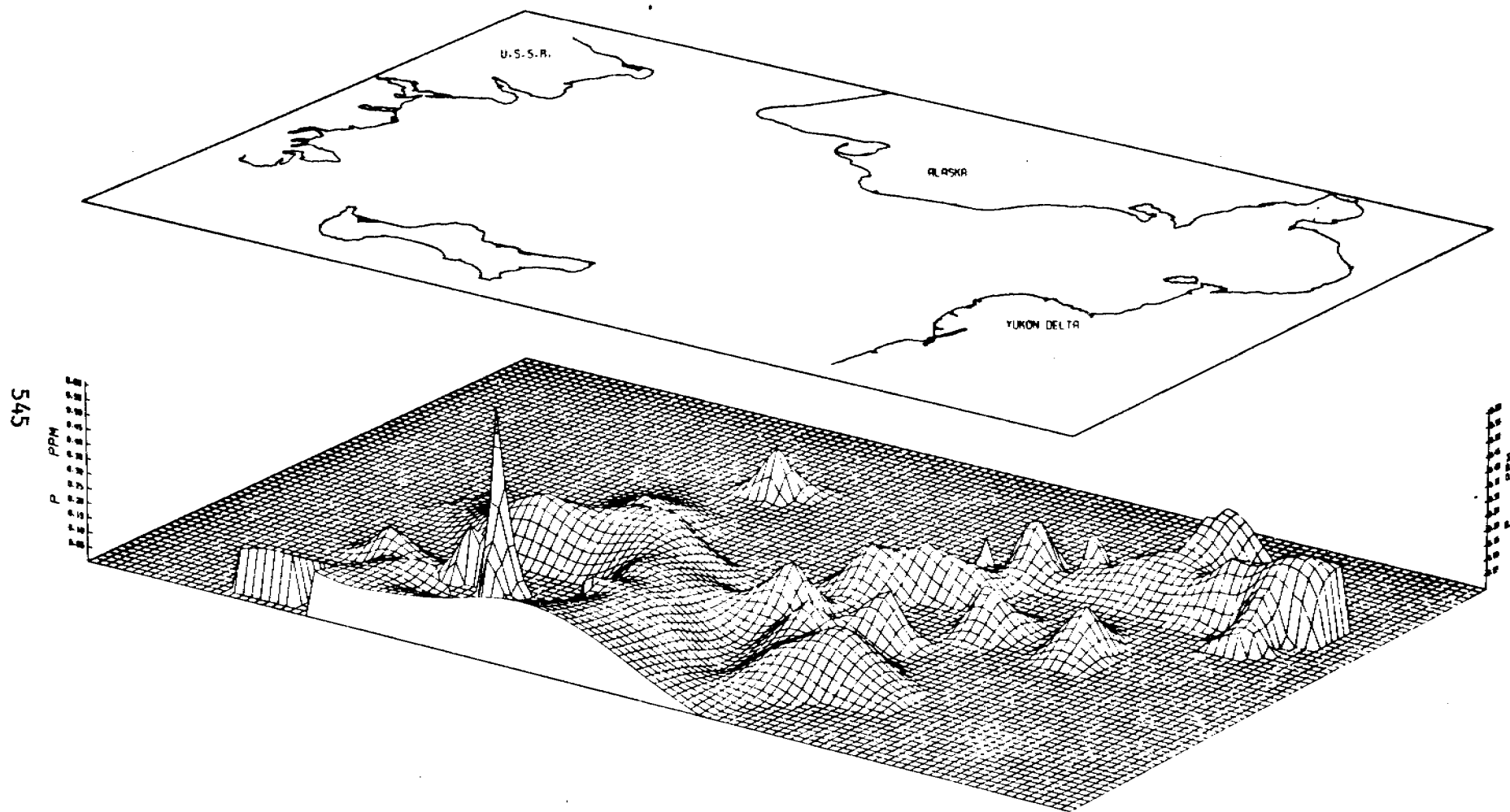


FIG 4_b P PPM IN BOTTOM SURFACE SEDIMENT OF NORTON BASIN, BERING SEA

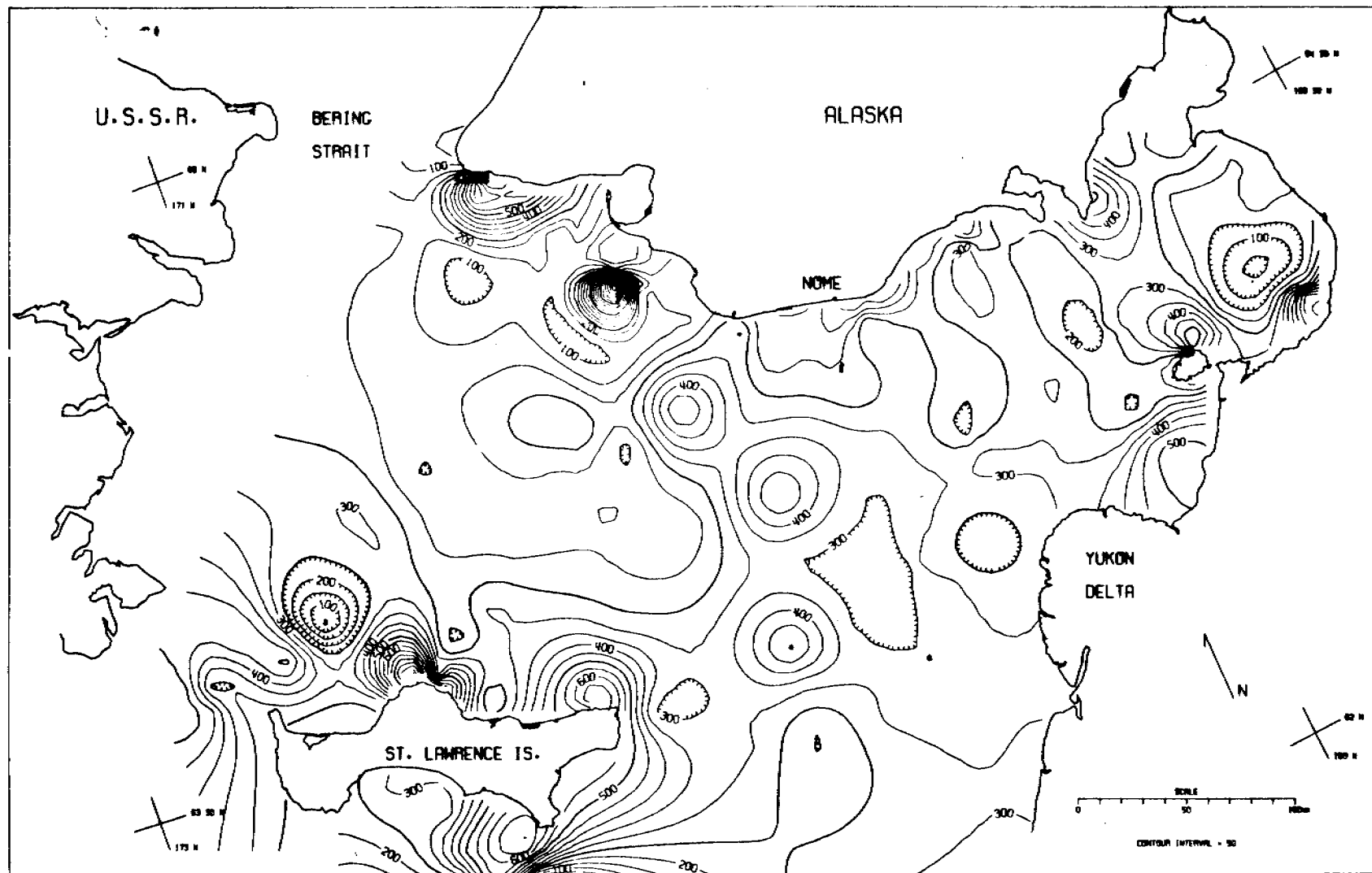


FIG 47 SR PPM IN BOTTOM SURFACE SEDIMENT OF NORTON BASIN, BERING SEA

NORTON BASIN PERSPECTIVE VIEW

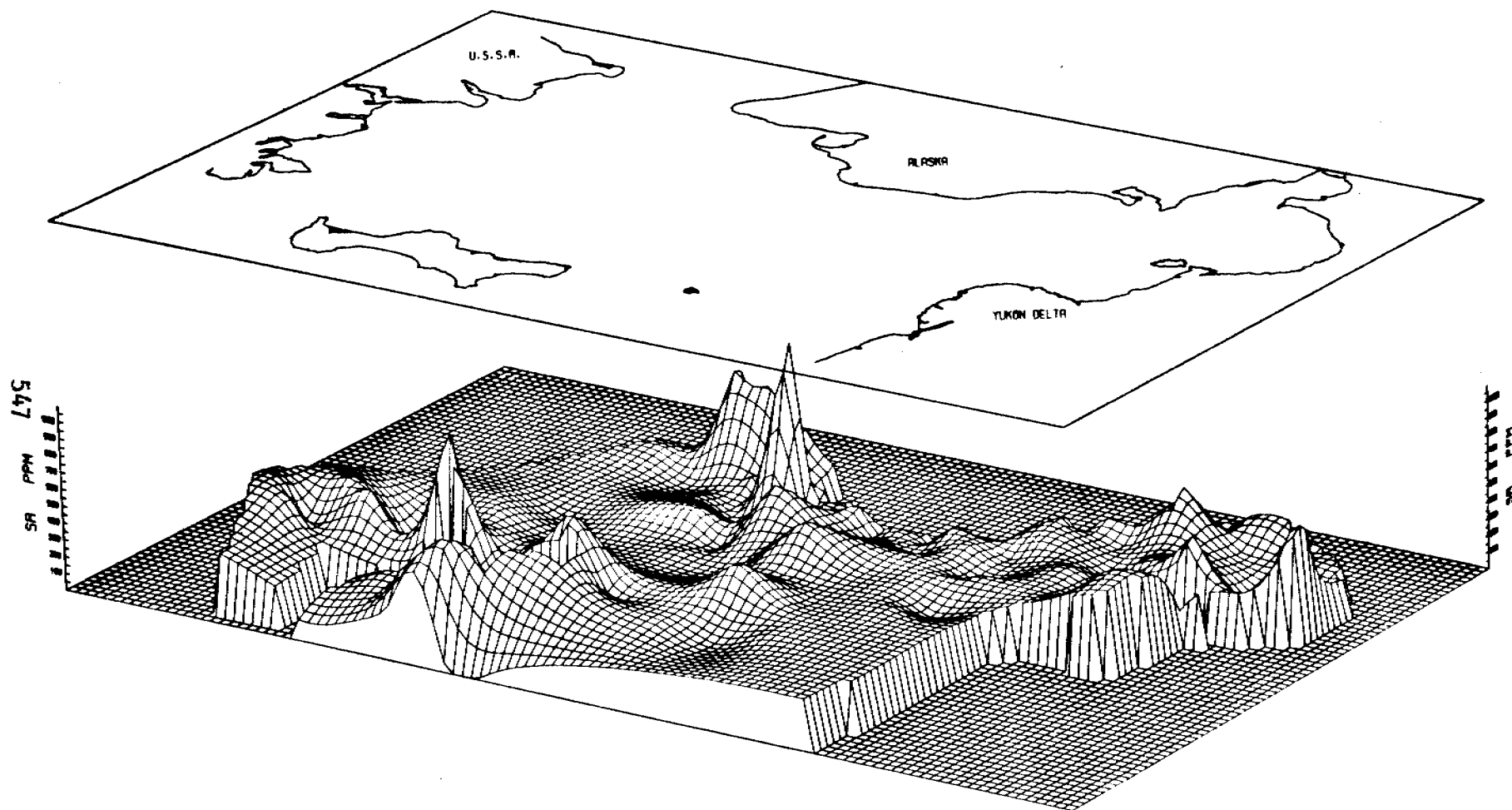


FIG 48 SR PPM IN BOTTOM SURFACE SEDIMENT OF NORTON BASIN, BERING SEA

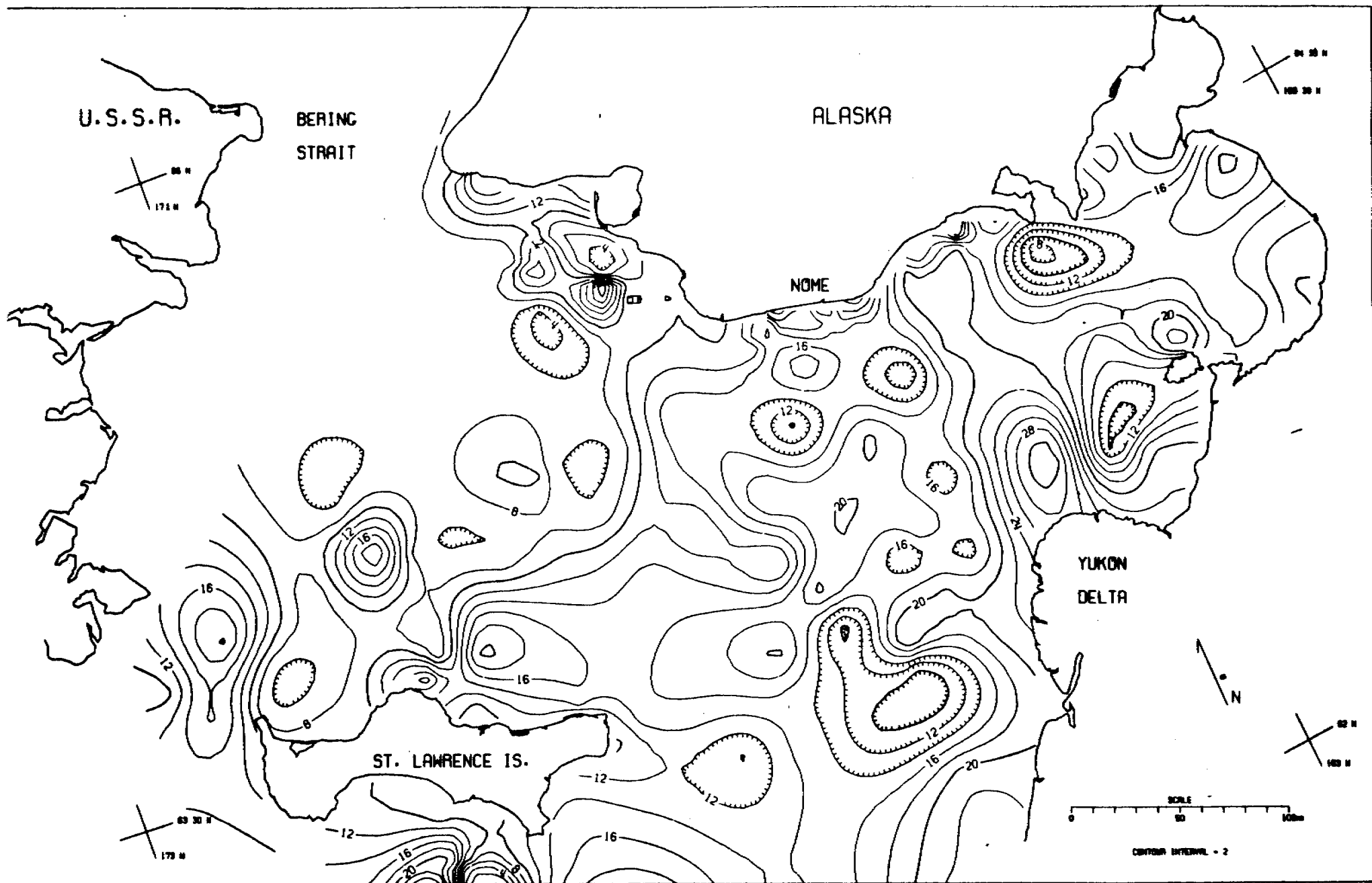


FIG 49 SC PPM IN BOTTOM SURFACE SEDIMENT OF NORTON BASIN, BERING SEA

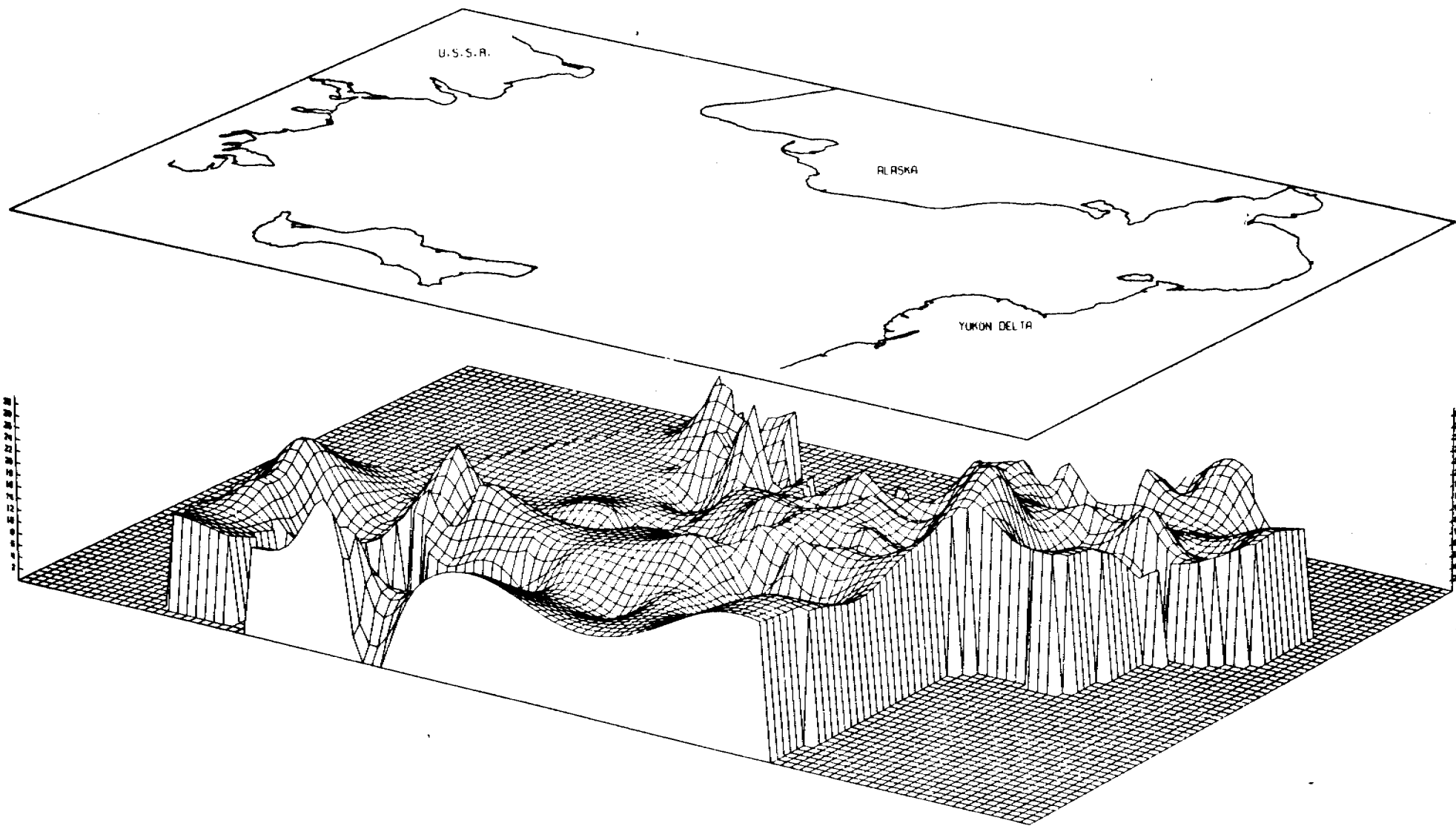


FIG 50 SC PPM IN BOTTOM SURFACE SEDIMENT OF NORTON BASIN, BERING SEA

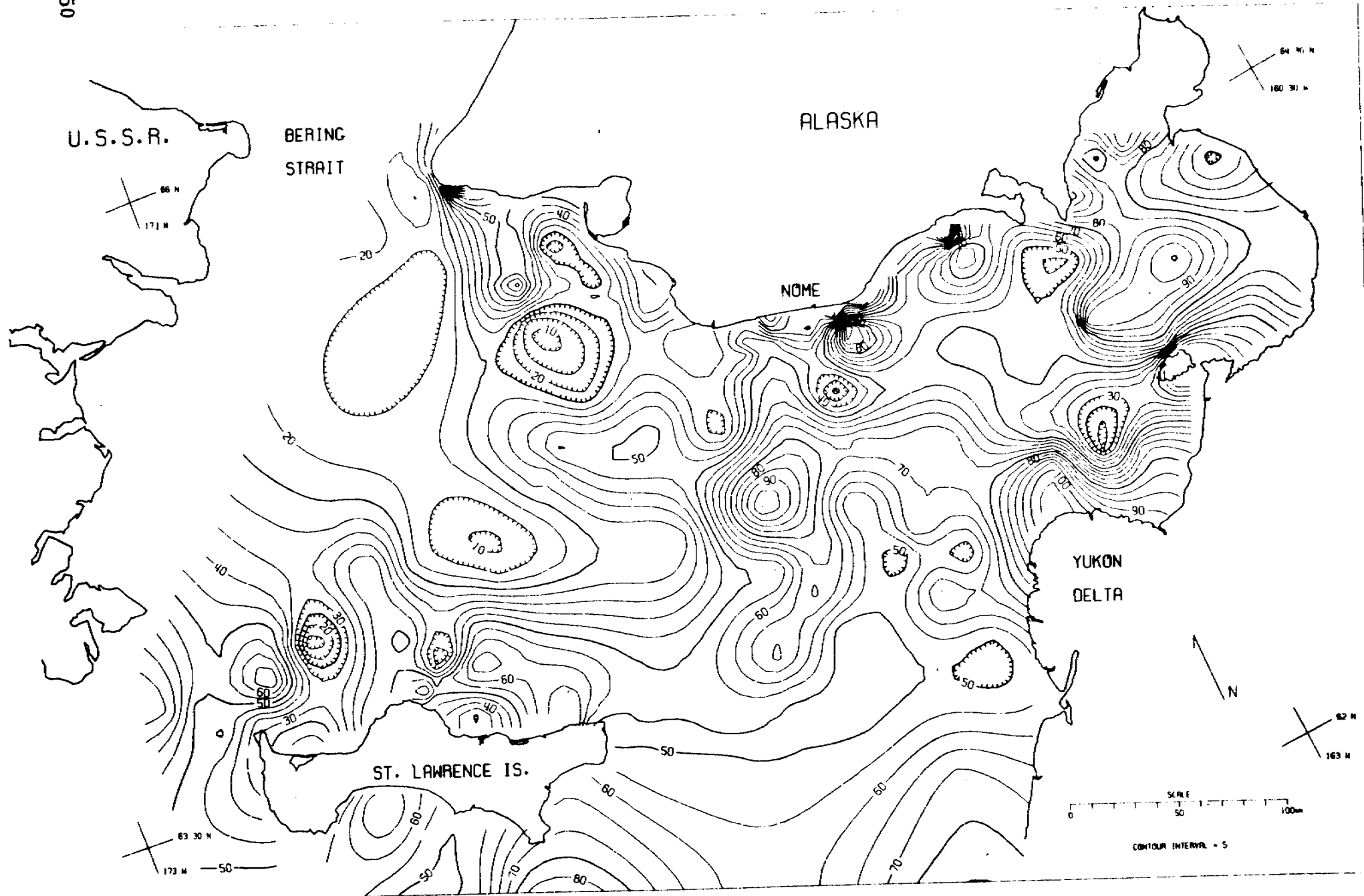
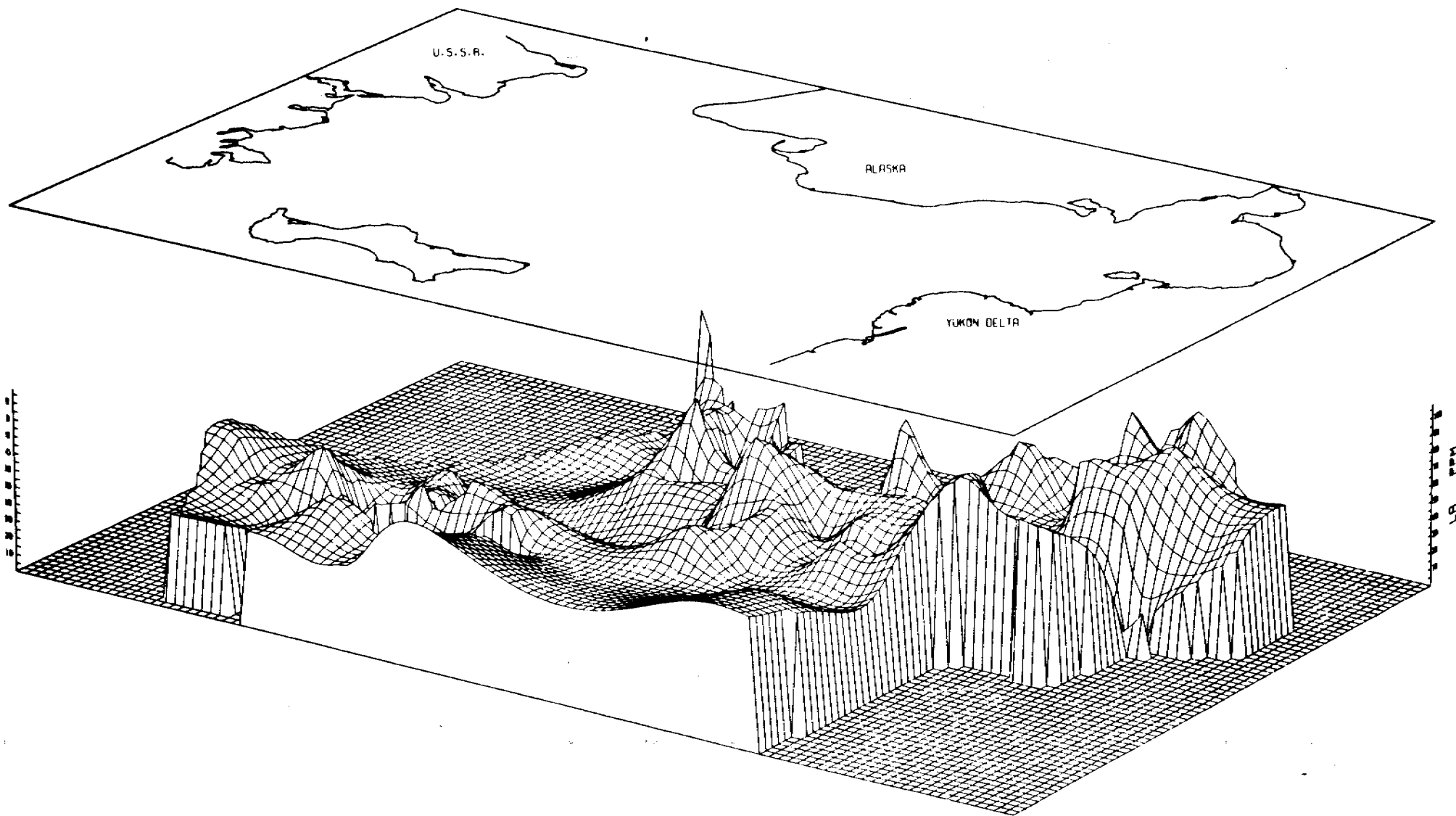


FIG. 51. LA PPM IN BOTTOM SURFACE SEDIMENT OF NORTON BASIN, BERING SEA



551

FIG 5Z LA PPM IN BOTTOM SURFACE SEDIMENT OF NORTON BASIN, BERING SEA

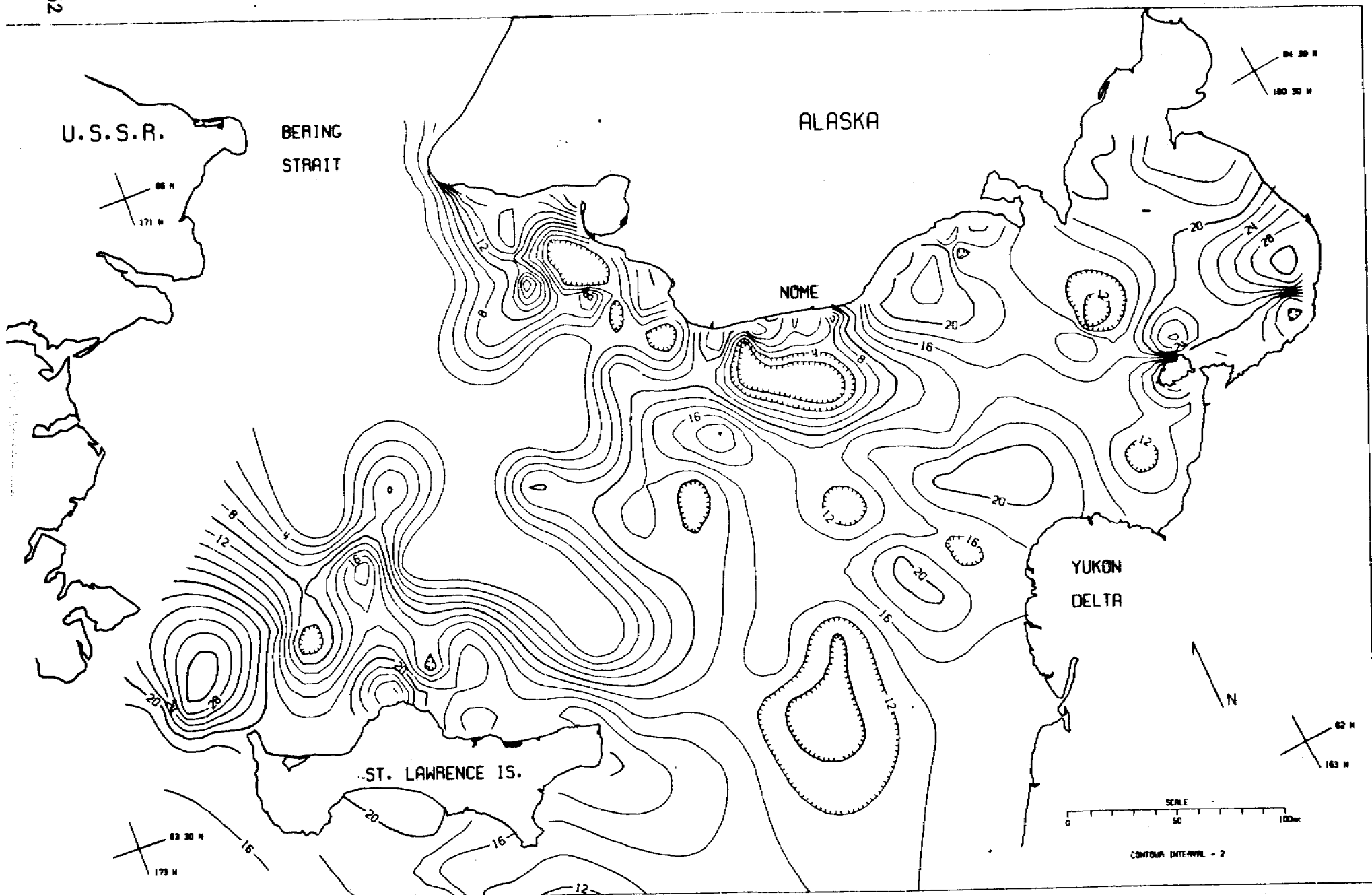


FIG 53 CA PPM IN BOTTOM SURFACE SEDIMENT OF NORTON BASIN, BERING SEA

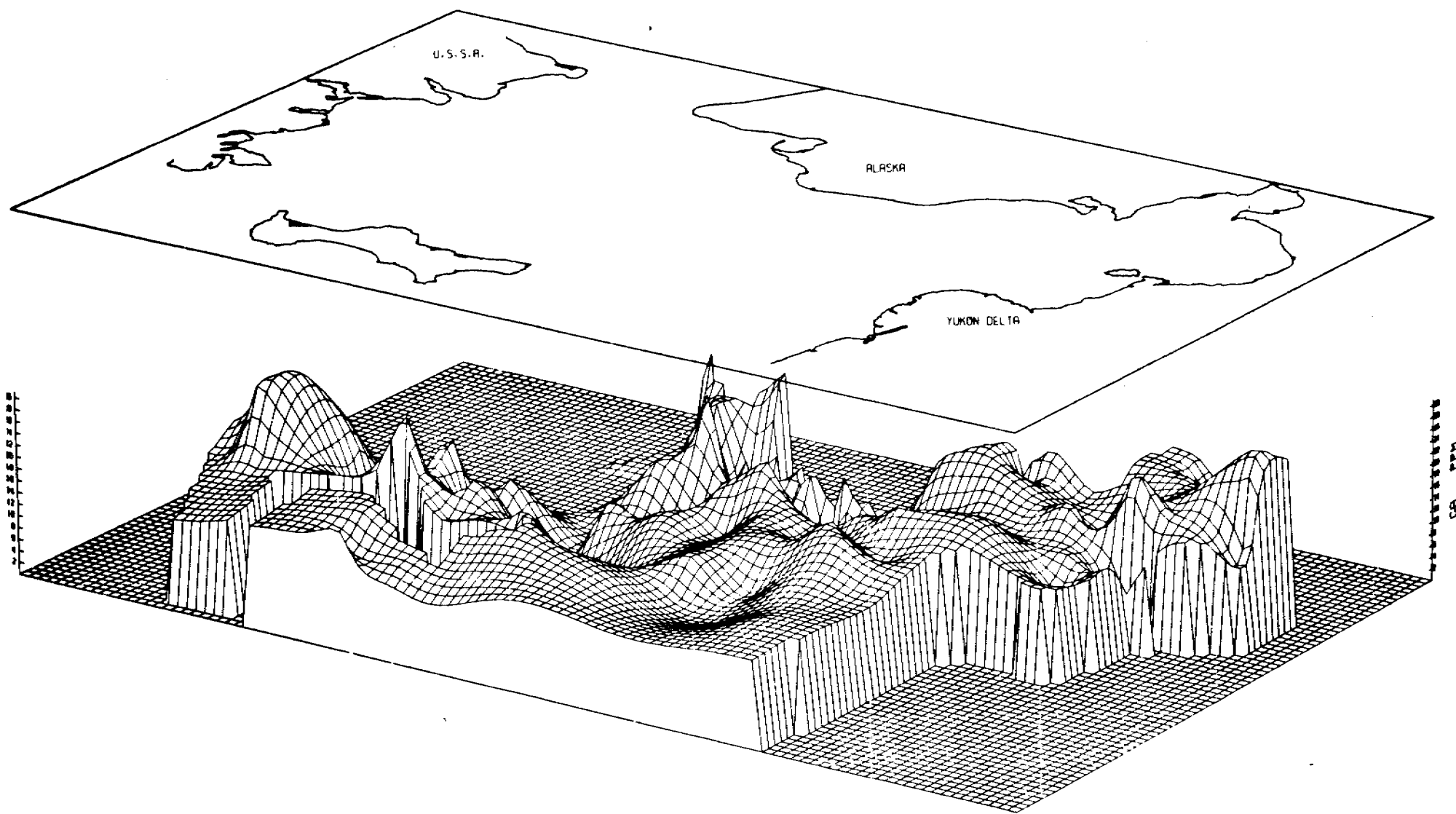


FIG 54 CA PPM IN BOTTOM SURFACE SEDIMENT OF NORTON BASIN, BERING SEA

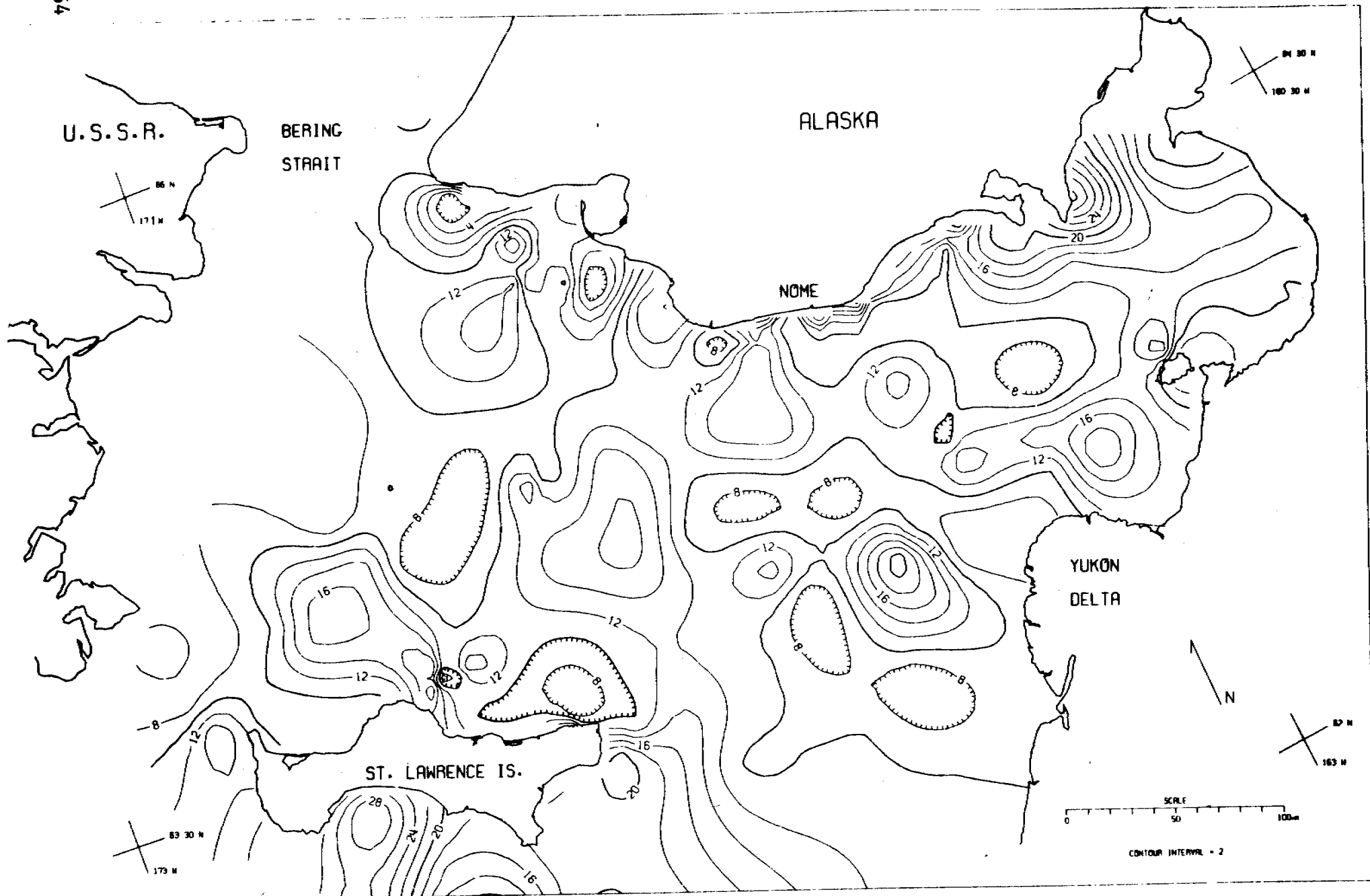
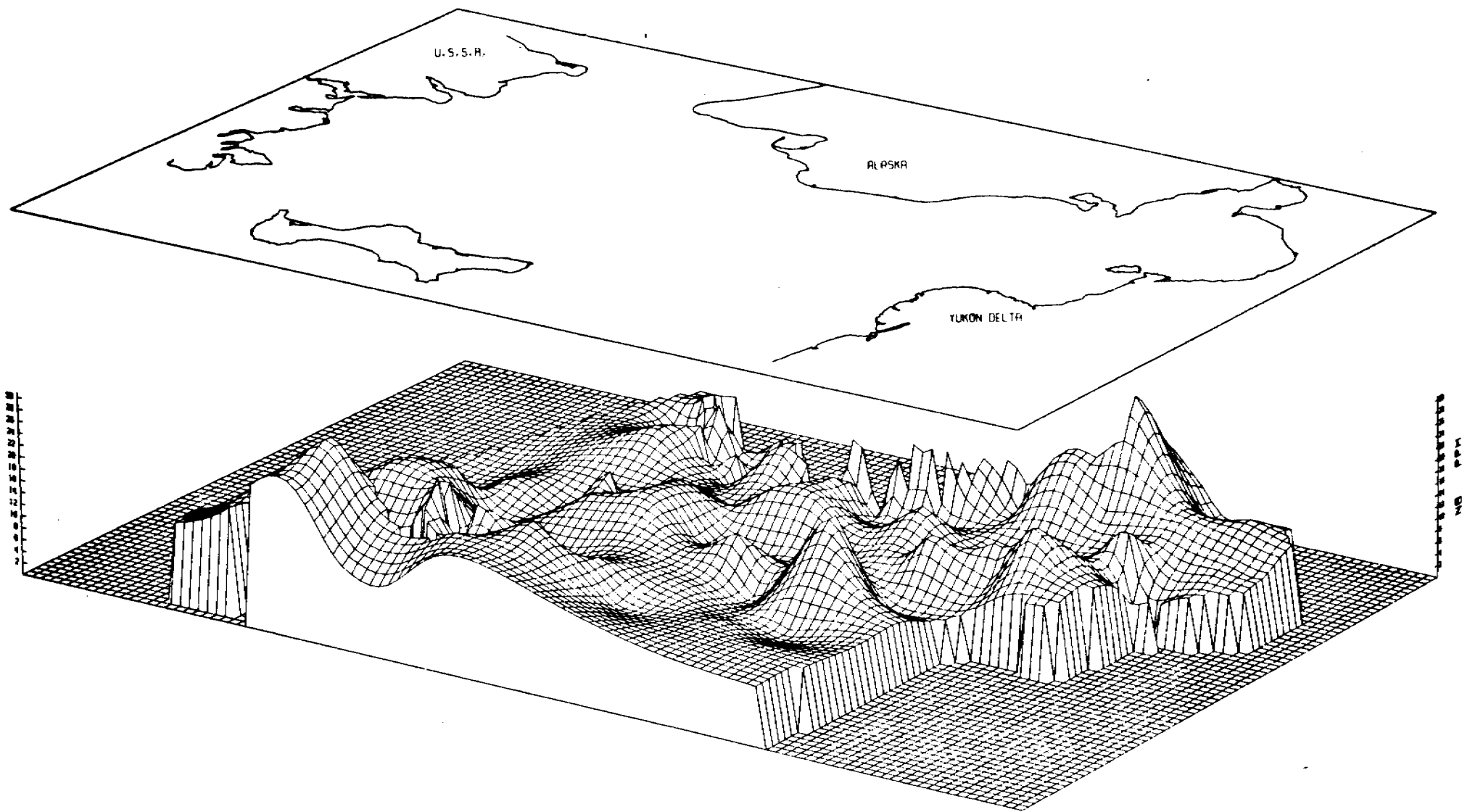


FIG 55 NB PPM IN BOTTOM SURFACE SEDIMENT OF NORTON BASIN, BERING SEA



555

FIG 56 NB PPM IN BOTTOM SURFACE SEDIMENT OF NORTON BASIN, BERING SEA

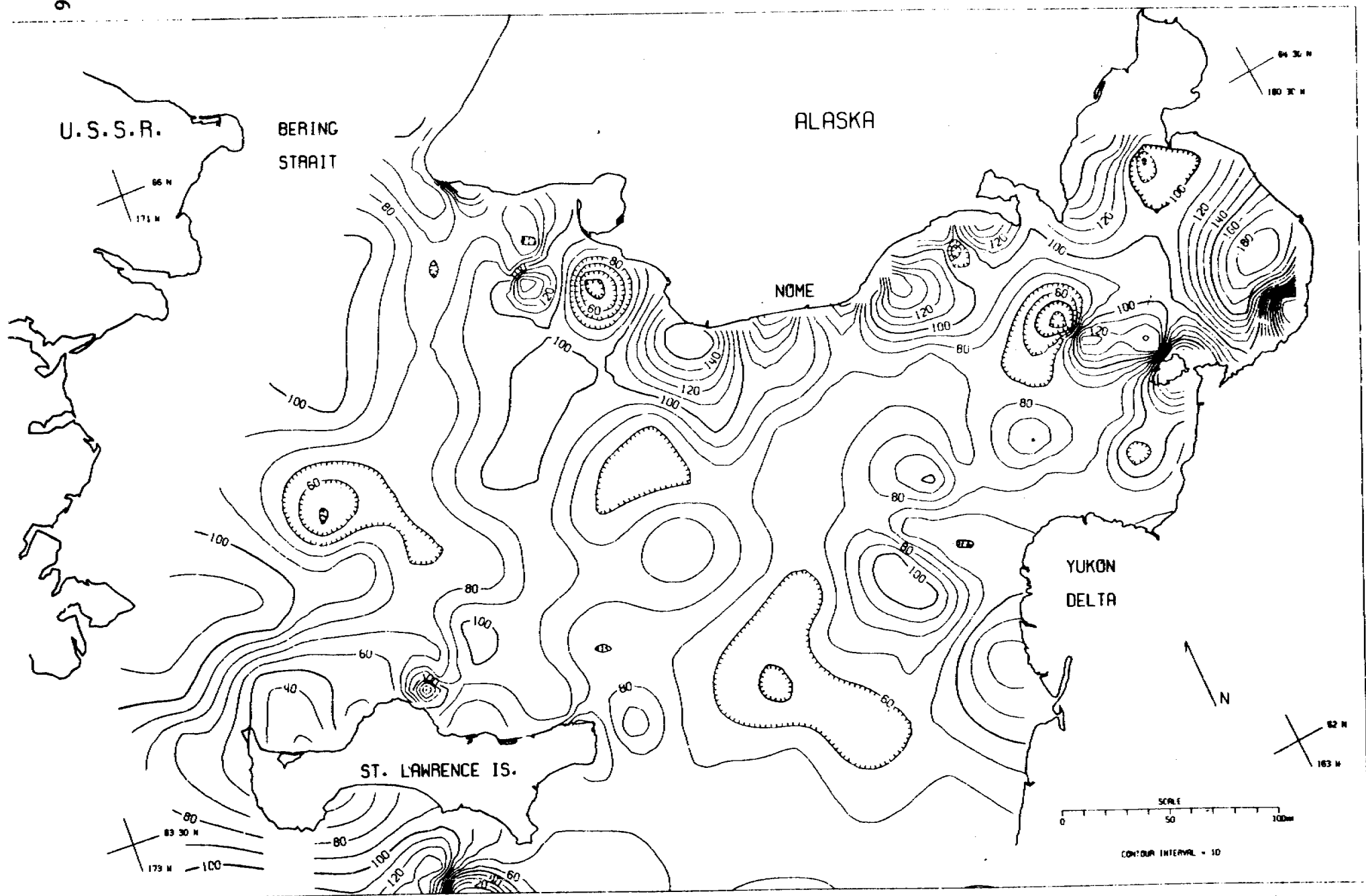
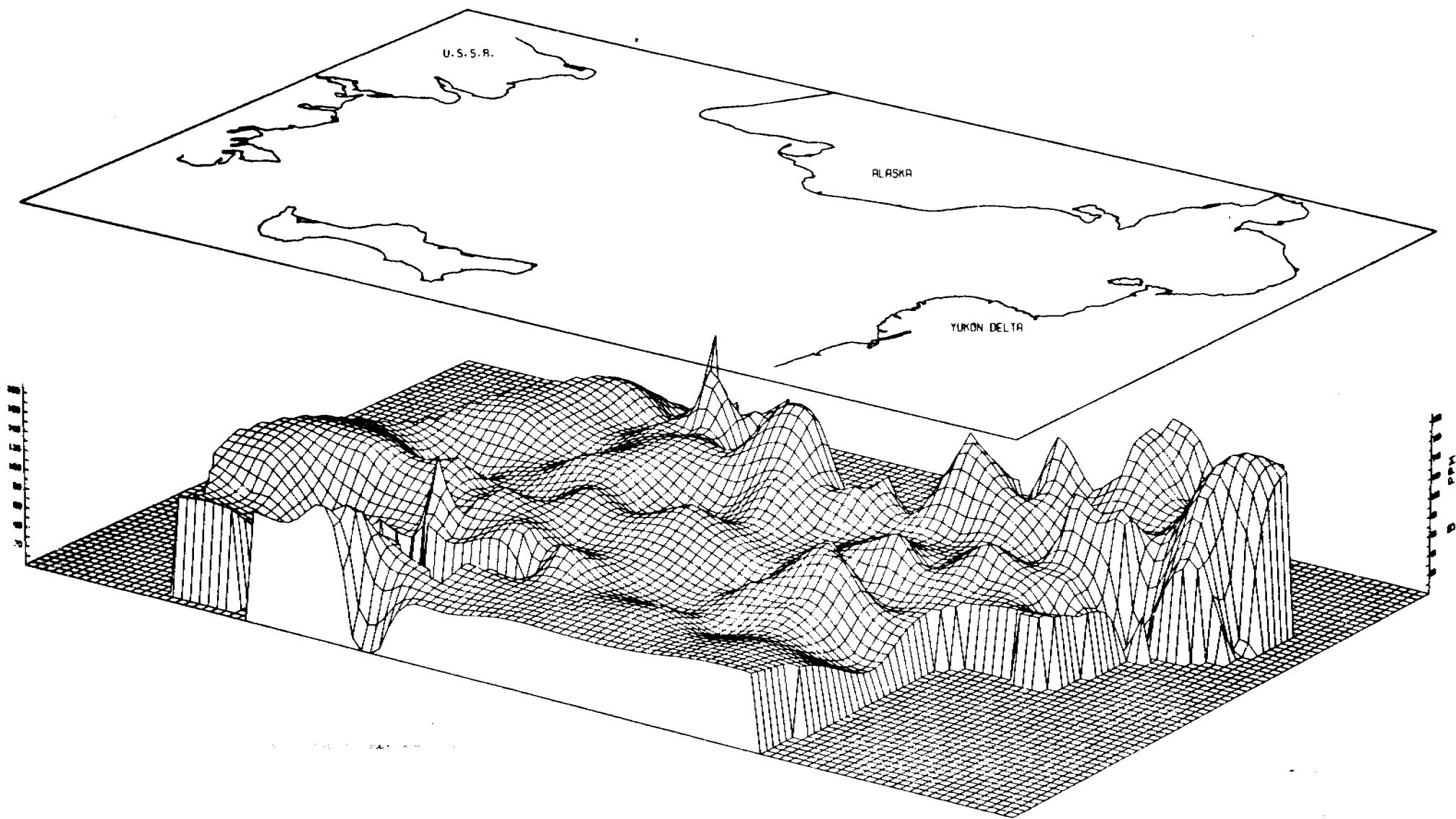


FIG 57 B PPM IN BOTTOM SURFACE SEDIMENT OF NORTON BASIN, BERING SEA



557

FIG 58 B PPM IN BOTTOM SURFACE SEDIMENT OF NORTON BASIN, BERING SEA

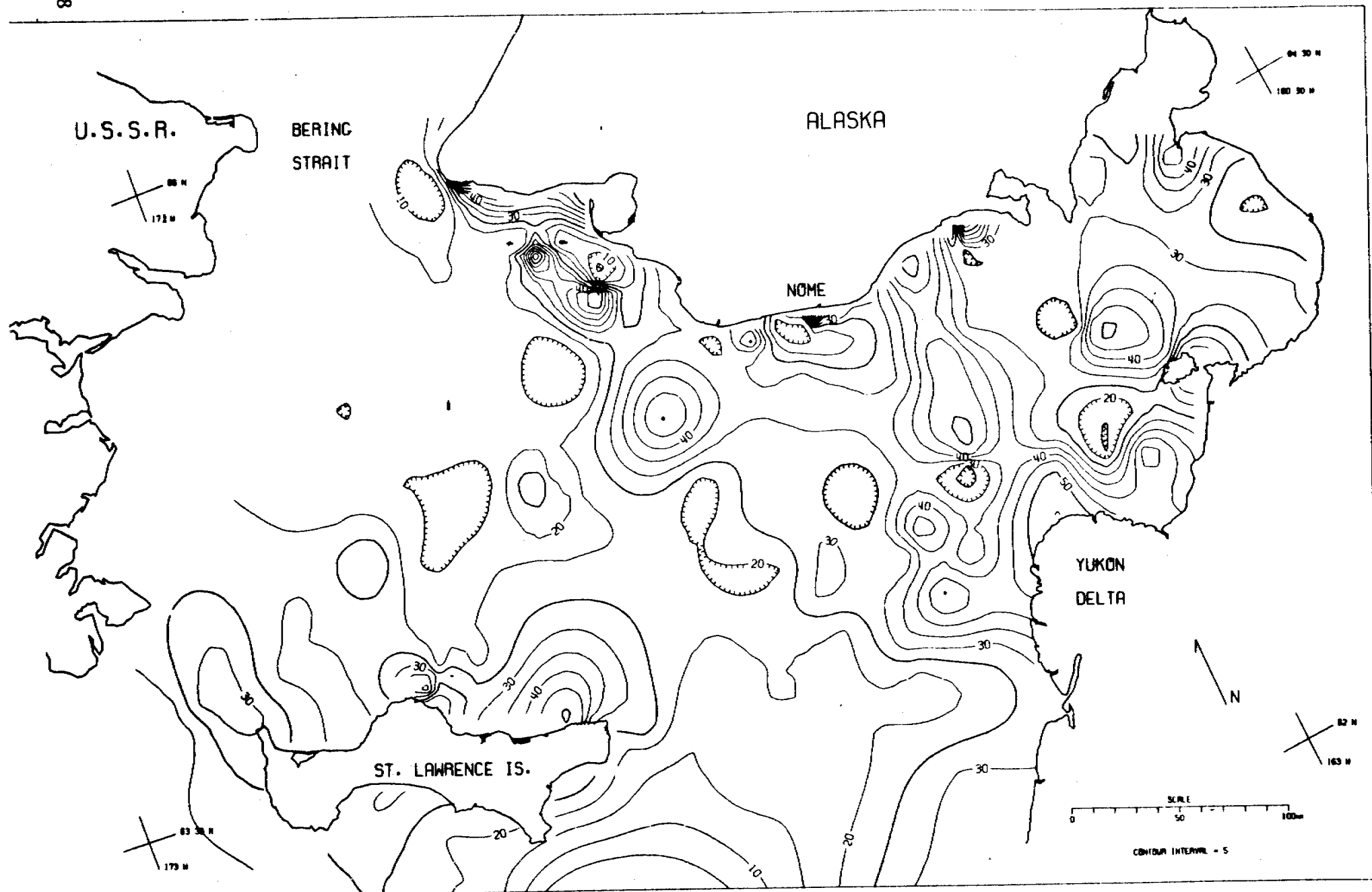
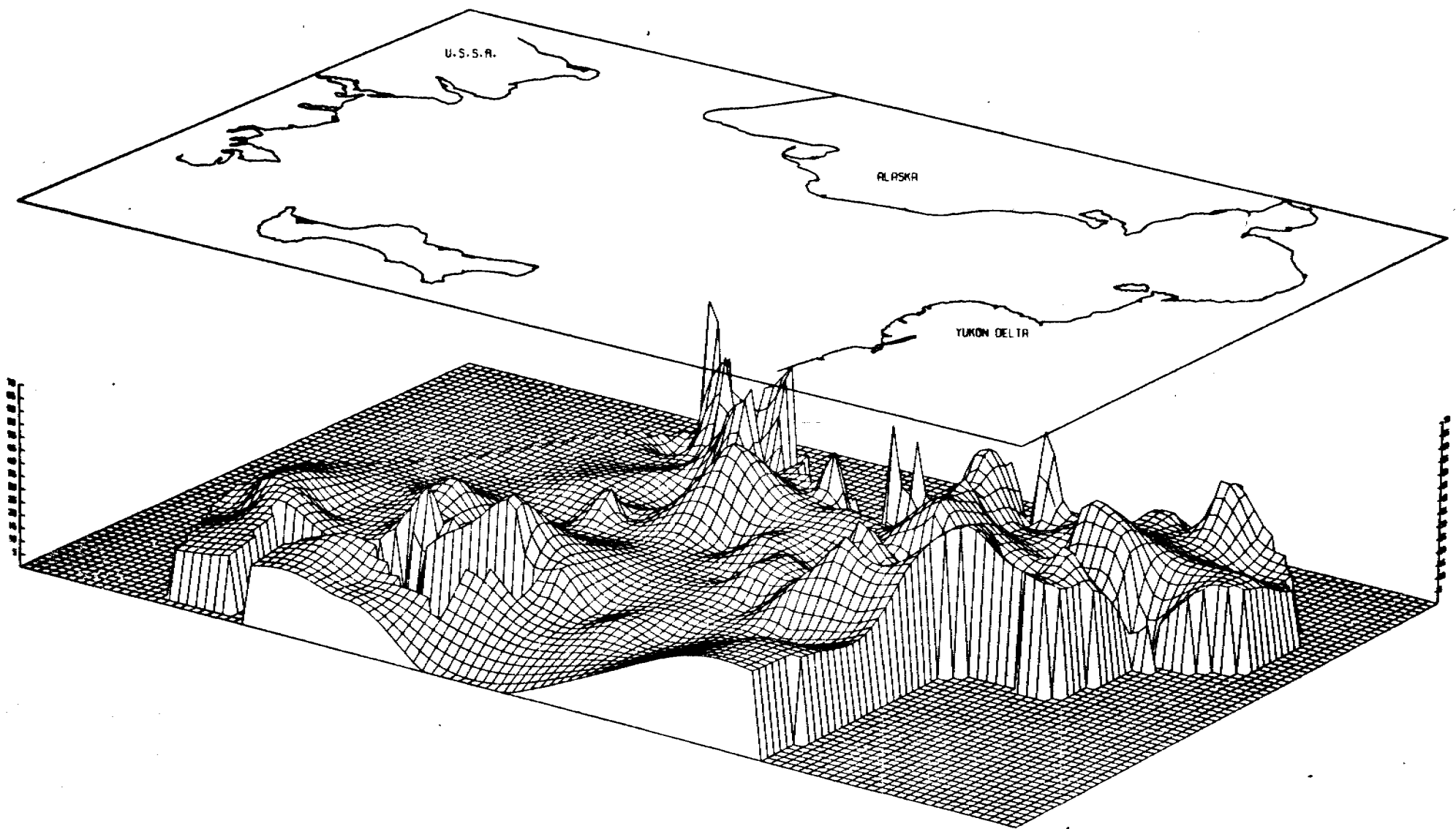


FIG 59 Y PPM IN BOTTOM SURFACE SEDIMENT OF NORTON BASIN, BERING SEA

NORTON BASIN PERSPECTIVE VIEW



559

FIG 60 Y PPM IN BOTTOM SURFACE SEDIMENT OF NORTON BASIN, BERING SEA

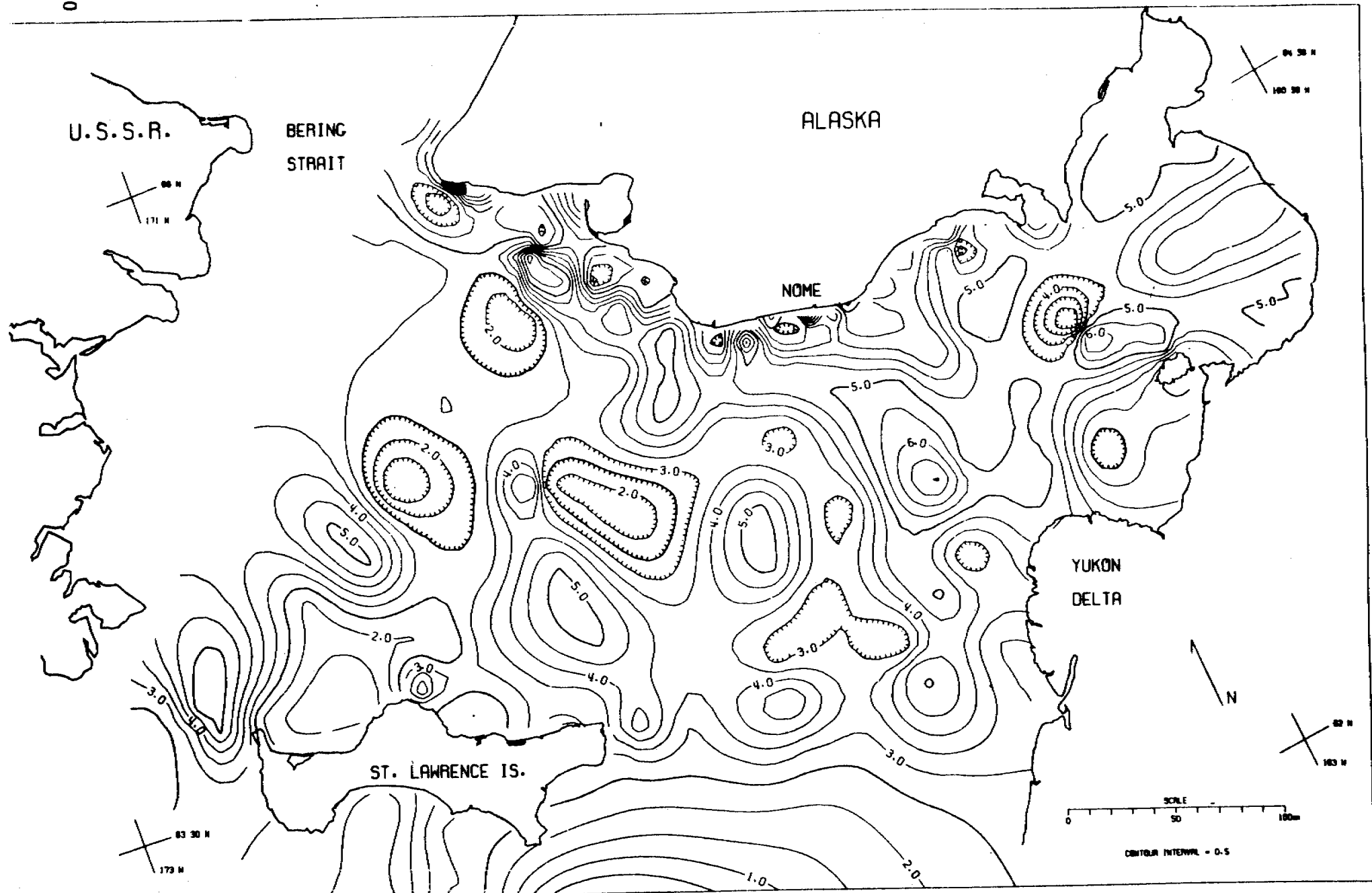
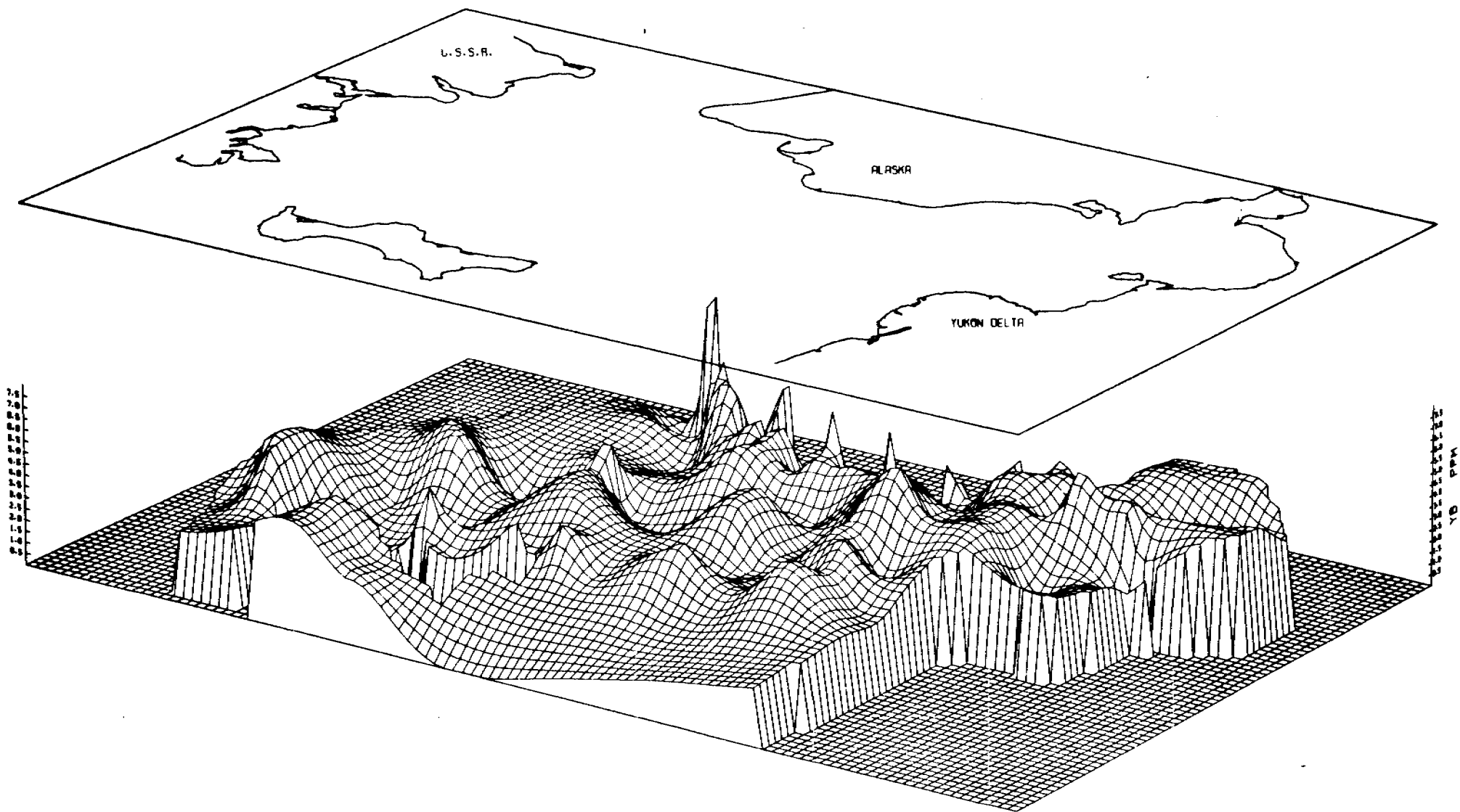


FIG 61 YB PPM IN BOTTOM SURFACE SEDIMENT OF NORTON BASIN, BERING SEA



561

FIG 62 YB PPM IN BOTTOM SURFACE SEDIMENT OF NORTON BASIN, BERING SEA

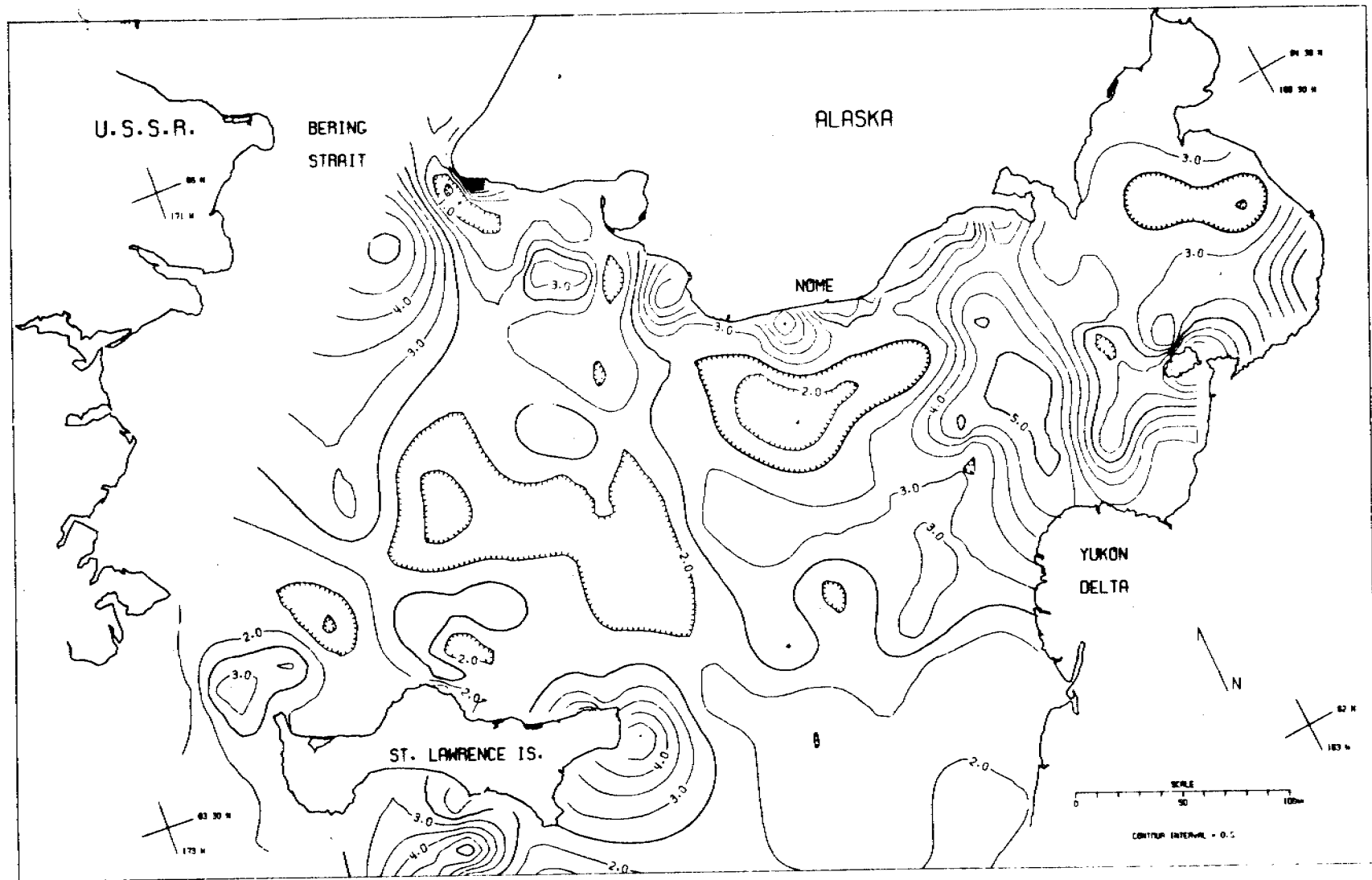


FIG 63 BE PPM IN BOTTOM SURFACE SEDIMENT OF NORTON BASIN, BERING SEA

NORTON BASIN PERSPECTIVE VIEW

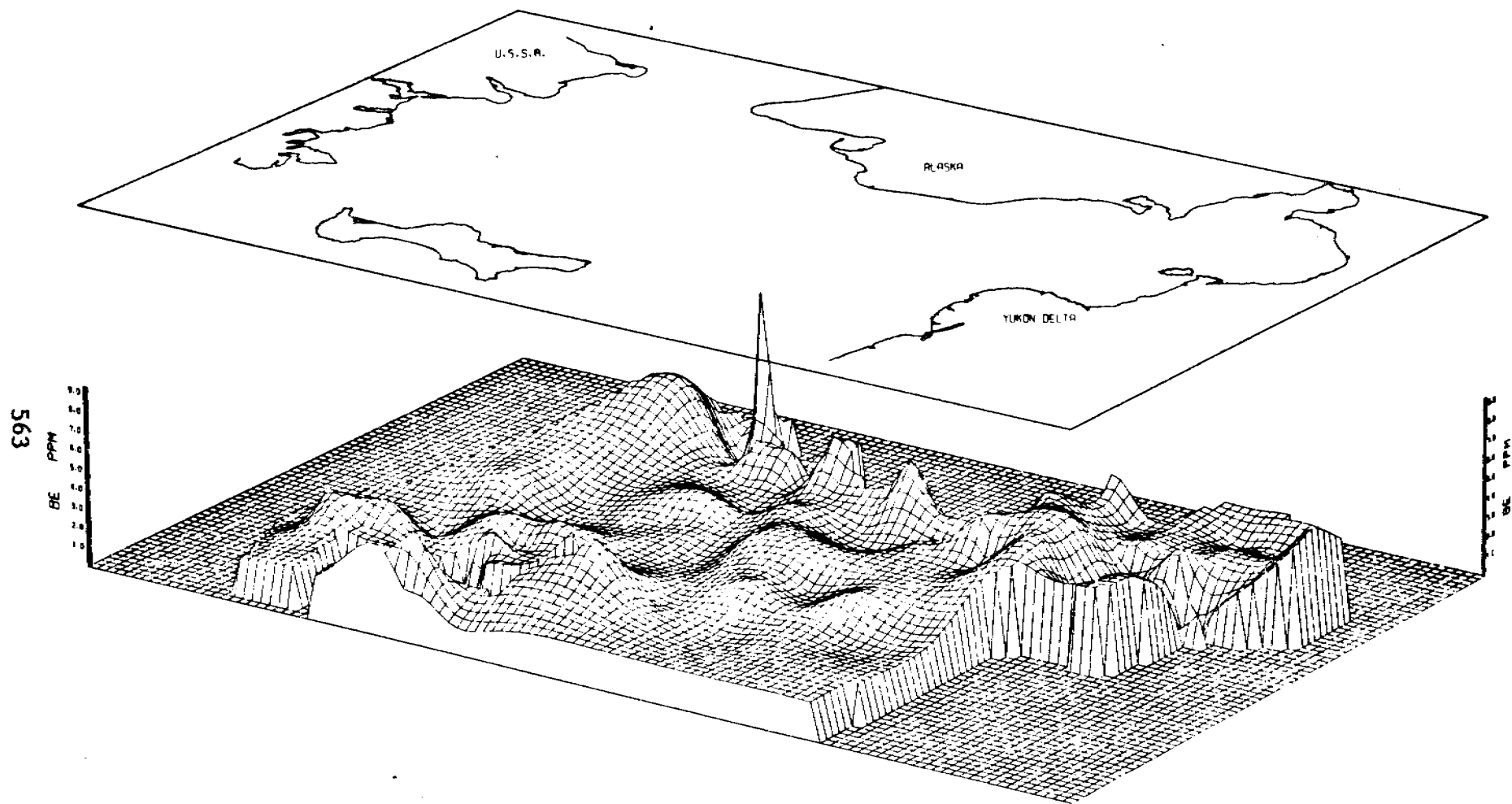


FIG. 64 BE PPM IN BOTTOM SURFACE SEDIMENT OF NORTON BASIN, BERING SEA

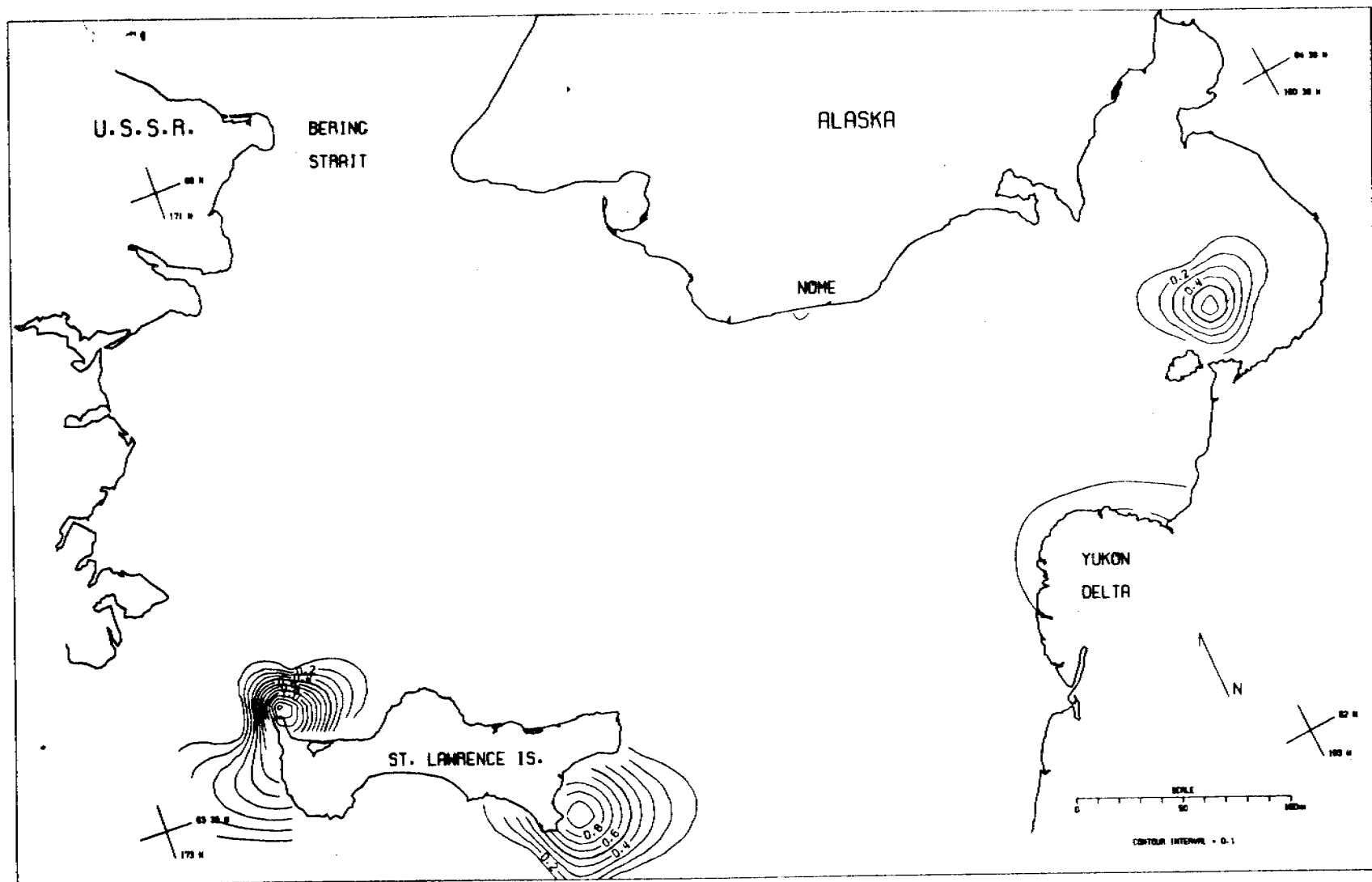


FIG 65 AC PPM IN BOTTOM SURFACE SEDIMENT OF NORTON BASIN, BERING SEA

NORTON BASIN PERSPECTIVE VIEW

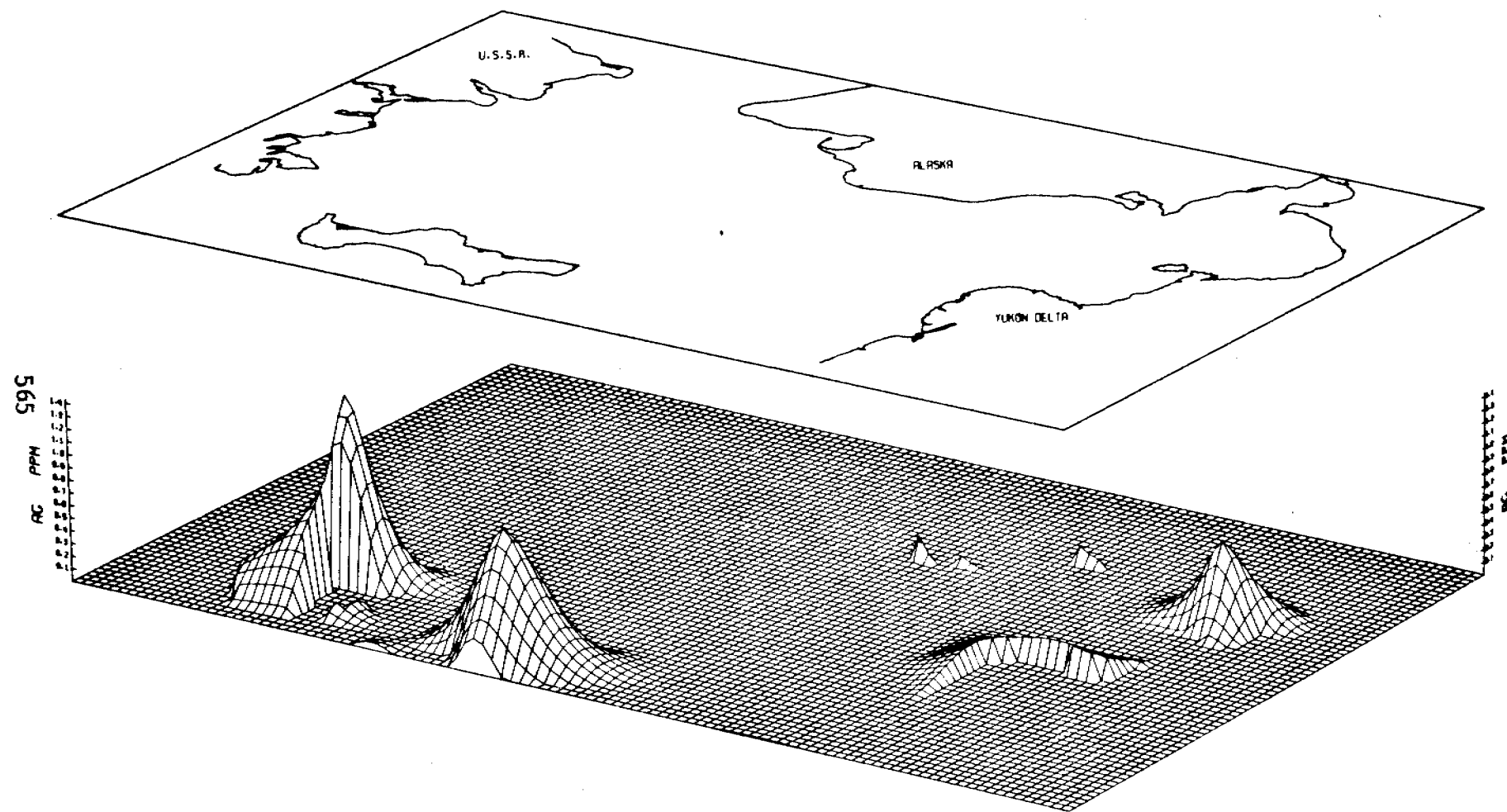


FIG 66 AG PPM IN BOTTOM SURFACE SEDIMENT OF NORTON BASIN, BERING SEA

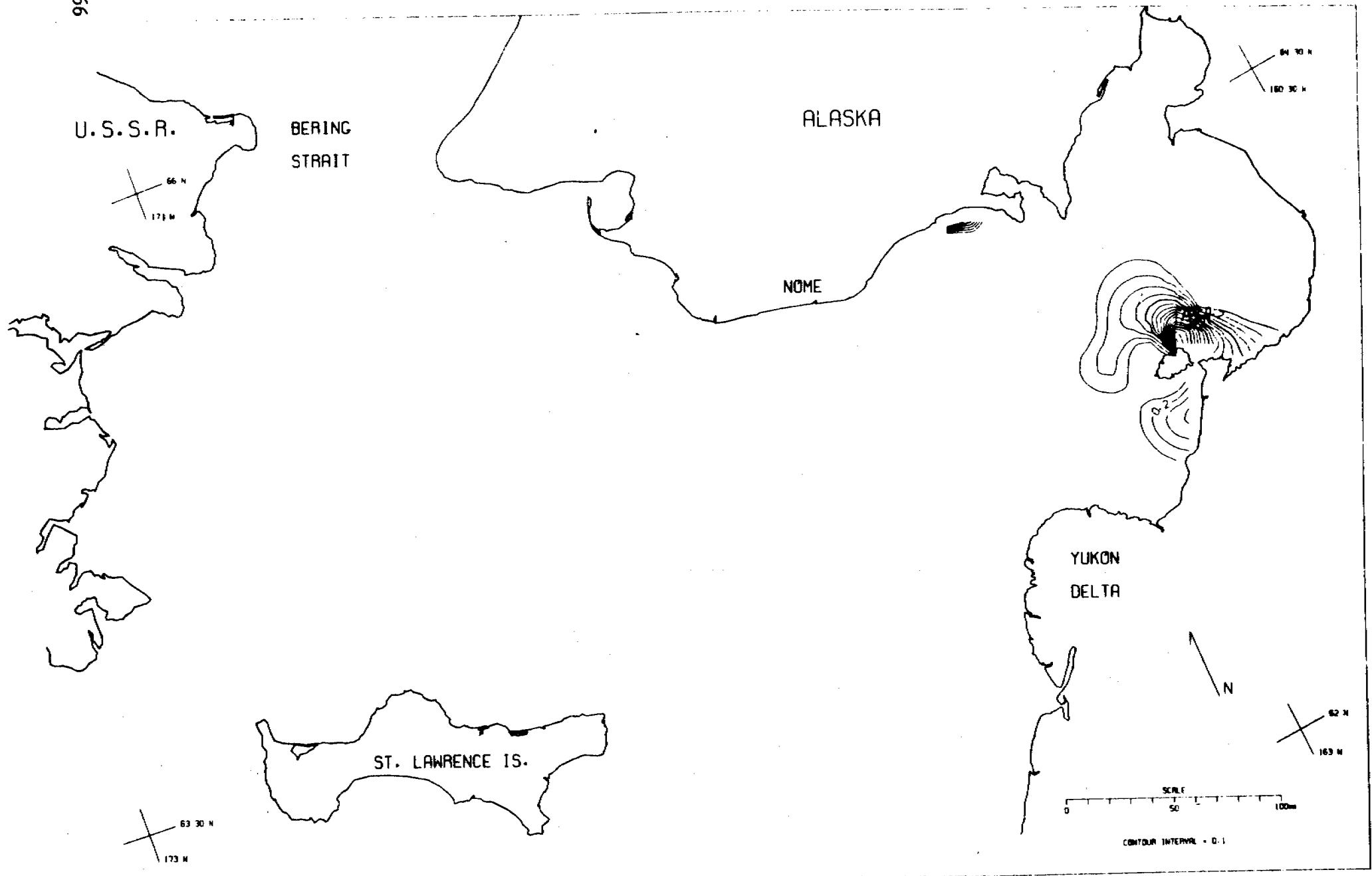


FIG 67 M0 PPM IN BOTTOM SURFACE SEDIMENT OF NORTON BASIN, BERING SEA

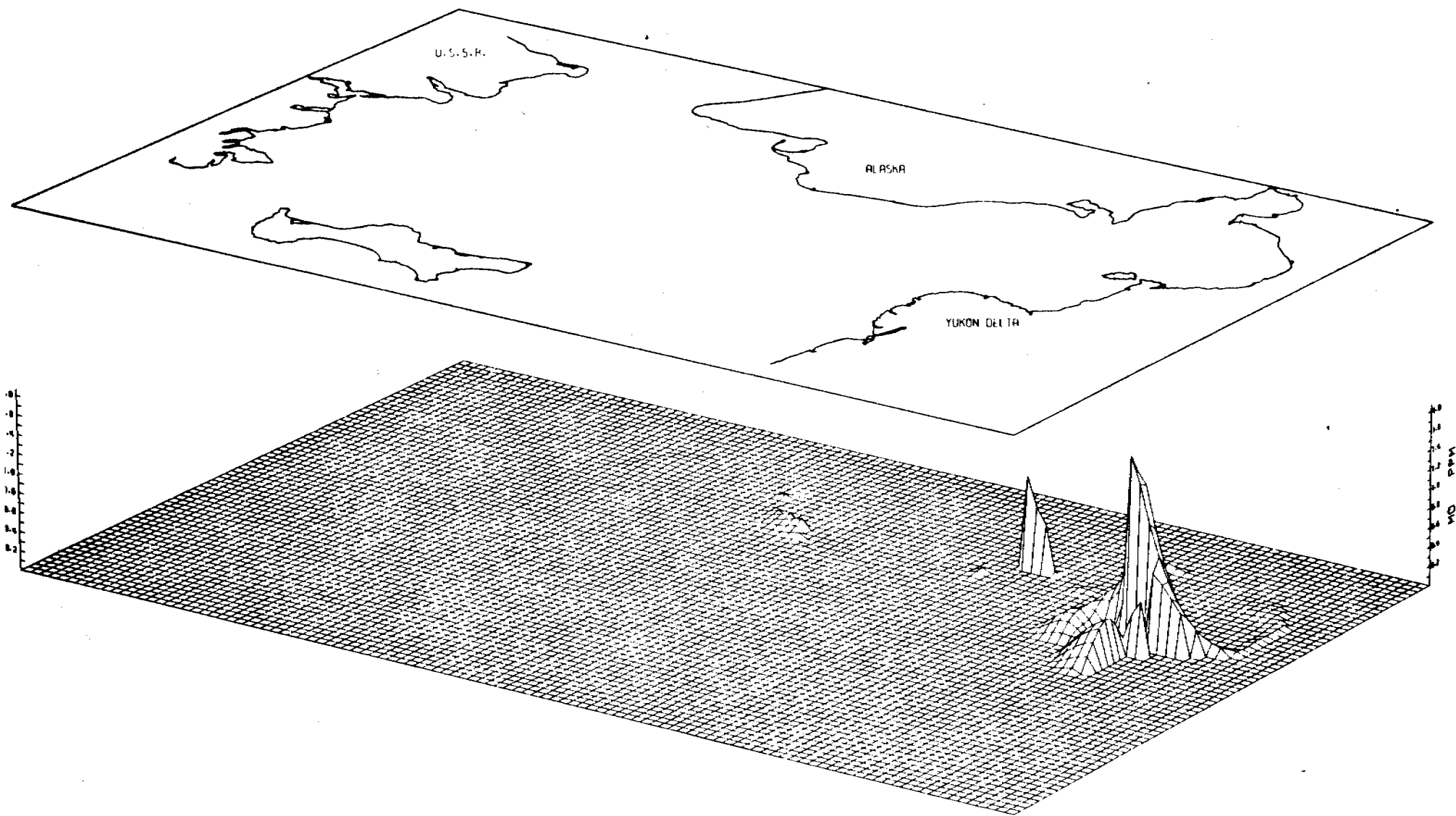


FIG 68 MO PPM IN BOTTOM SURFACE SEDIMENT OF NORTON BASIN, BERING SEA

Miscellaneous Geologic Maps

by Devin R. Thor

U.S. Geological Survey, Menlo Park, California

The four maps that make up this section are based on research being conducted in northern Bering Sea, but in themselves were not topical investigations.

Preliminary Isopach Map of Holocene Marine Sediment

Post-glacial sea-level rise started to flood northeastern Bering Sea about 12,000 BP (Nelson and Creager, 1977). Present marine limits and circulation patterns were established by 9500 BP (Nelson and Creager, 1977). For the most part, marine sedimentation is dominated by fine, sandy silt derived from the Yukon River. The modern Yukon Delta established its present position about 5000 BP and has built a wedge of prodelta sediment since that time. The asymmetry of the prodelta deposits is due to strong north-flowing currents that minimize deposition on the western portion of the delta and transport sediment northward (Nelson and Creager, 1977).

Anomalous Acoustic Response on High-Resolution Geophysical Records

High-resolution boomer records show acoustic anomalies to be ubiquitous in Norton Sound. Records with acoustic anomalies show subsurface reflectors terminating at "blank" zones. A blank zone (no reflection returned or acoustic anomaly) is caused by bubble-phase gas in nearsurface sediment (Kvenvolden and others, 1979). The gas-charged sediment acts as an acoustic sink so that little or no energy is returned to the geophones. The gas is the result of the biogenic production of methane from nearsurface, nonmarine peaty mud (Nelson and others, 1979). In conclusion, nearsurface gas-charged sediment is common in Norton Sound.

Subsurface Channels in Norton Sound

Episodes of erosion and channeling represent pre-transgressive, nonmarine history. The older channeling is filled with pre-Holocene fluvial sediment whereas Holocene channels are filled with Holocene marine sediment. Four types or areas of major drainage have been identified:

(1) West of the Yukon Delta, channel systems represent meanders and abandoned subaqueous, sub-ice channels (Dupré and Thompson, 1979) and pre-transgressive drainage of a previous Yukon distributary system.

2) A portion of a southwest-trending fluvial drainage system in central Norton Sound is as much as 25 km wide and has been traced for a length of 75 km. This system possibly represents drainage from glaciers on Seward Peninsula.

(3) A system of similar trend, magnitude, and origin as in (2) exists south of Nome/Safety Sound area.

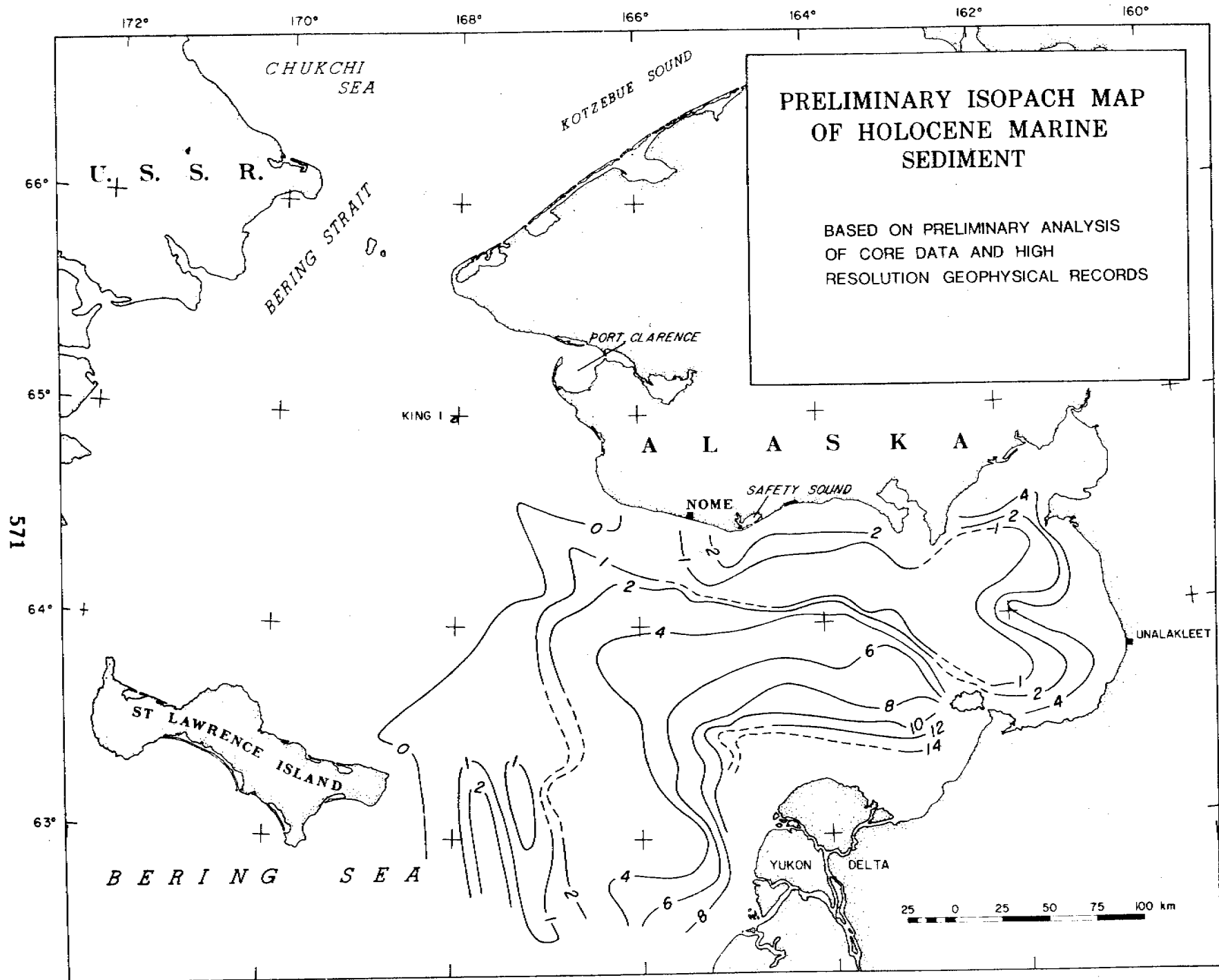
(4) Scattered throughout western Norton Sound is channeling that is not obviously interconnected. These channels possibly represent minor fluvial systems and/or tidal-channel systems developed during the marine transgression.

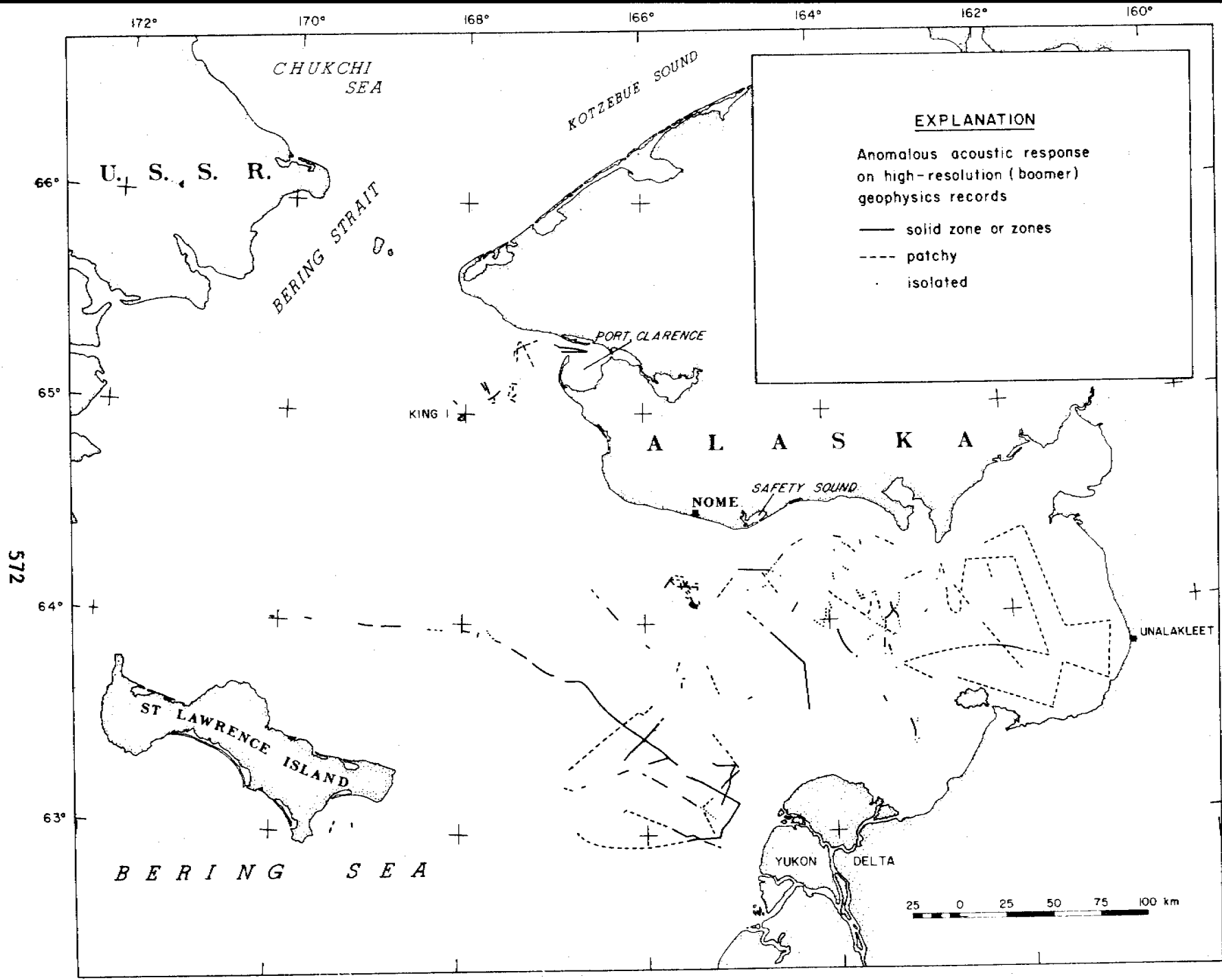
Preliminary Map of Surface and Nearsurface Bedrock

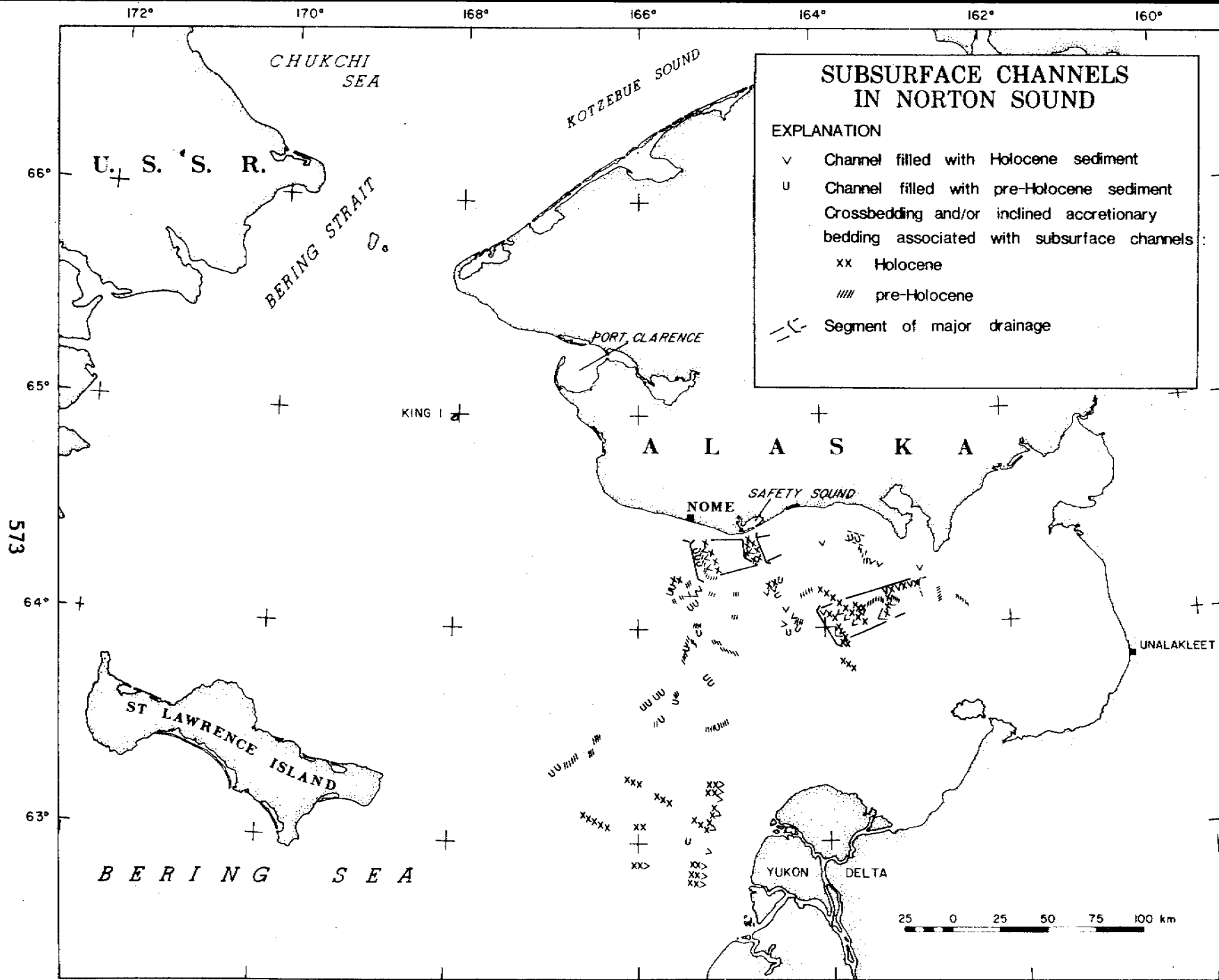
Pre-Holocene subaerial erosion, modern nondeposition, or modern submarine erosion have kept bedrock exposed locally offshore from St. Lawrence Island and western Seward Peninsula. The bedrock has not been sampled, but by inference, it is most likely that bedrock is part of the Main Layered Sequence, which consists of gently folded, late and middle Tertiary, marine and nonmarine rocks (Nelson and others, 1974).

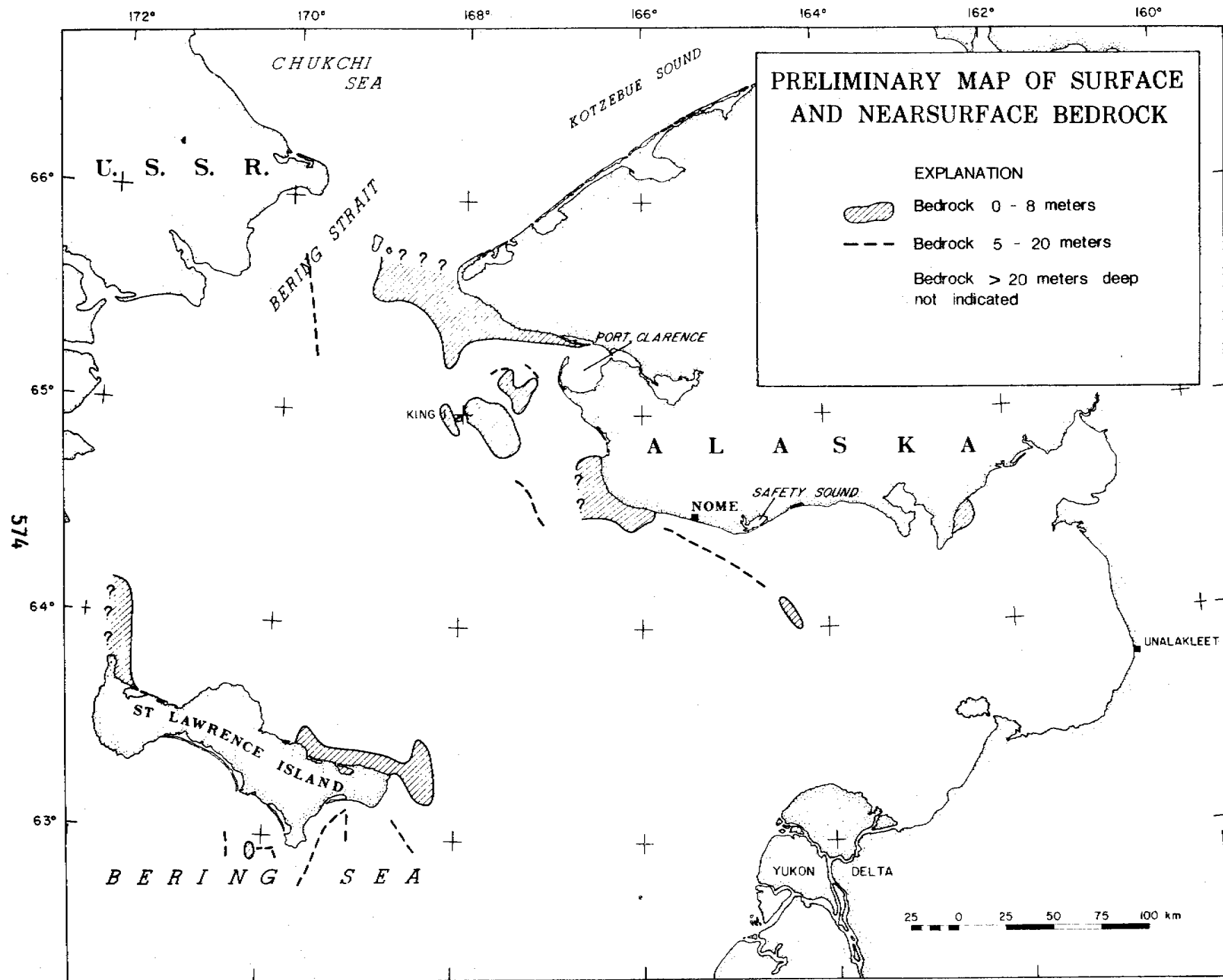
References

- Dupré, W.R., and Thompson, R., 1979, The Yukon Delta: A model for deltaic sedimentation in an ice-dominated environment; Proc. Offshore Technology Conference, Paper 3434, p. 657-664.
- Kvenvolden, K.A., Nelson, C.H., Thor, D.R., Larsen, M.C., Redden, G.D., Rapp, J.B., Des Marais, D.J., 1979, Biogenic and thermogenic gas in gas-charged sediment of Norton Sound, Alaska: Proc. Offshore Technology Conference, Paper 3412, p. 479-486.
- Nelson, C.H., Hopkins, D.M., Scholl, D.W., 1974, Cenozoic sedimentary and tectonic history of the Bering Sea, in: Hood, D.W, and Kelley, E.J. (eds.), Oceanography of the Bering Sea: Institute of Marine Science, University of Alaska Press, p. 485-516.
- Nelson, C.H., and Creager, J.S., 1977, Displacement of Yukon-derived sediment from Bering Sea to Chukchi Sea during Holocene time: Geology, v. 5, p. 141-146.
- Nelson, C.H., Thor, D.R., Sandstrom, M.W., and Kvenvolden, K.A., 1979, Modern Biogenic gas-generated craters (sea-floor "pockmarks") on the Bering Shelf, Alaska: Geological Society of America Bulletin, Part I, v. 90, p. 1144-1152.









ANNUAL REPORT

Contract #: 03-5-022-55

Research Unit #: 483

Reporting Period: 1 April 1979 -
31 March 1980

Number of Pages: 44

SEISMOTECTONIC STUDIES OF WESTERN ALASKA AND
SEA ICE STUDIES IN BEAUFORT SEA

Principal Investigators

N. N. Biswas
W. M. Sackinger
L. Gedney

Geophysical Institute
University of Alaska
Fairbanks, Alaska 99701

Prepared for the

National Oceanic and Atmospheric Administration

Under Contract No. 03-5-022-55

TABLE OF CONTENTS

	<u>Page</u>
Table of Contents.....	576
List of Figures	578
List of Tables.....	579
I. Summary: Objectives, Conclusions and Implications for Oil and Gas Developments.....	580
II. Introductions.....	580
A. General Nature and Scope of Study.....	580
B. Scientific Objective.....	582
C. Relevance to Problems of Petroleum Development.....	583
III. Current State of Knowledge.....	583
A. Seismicity of Western Alaska.....	583
B. Sea Ice Studies.....	584
IV. Study Area, Sources, Methods and Rational of Data Collection.....	585
A. Norton and Kotzebue Sounds.....	585
B. Beaufort Sea.....	587
V. Results.....	588
A. Western Alaska.....	588
B. Beaufort Sea.....	590
VI. Discussion.....	591
VII. Conclusion.....	595
VIII. Summary: Fourth Quarter Operations.....	596
A. Task Objectives.....	596
B. Field and Laboratory Activities.....	596
C. Results.....	597

D. Preliminary Interpretation.....	597
E. Problems Encountered.....	597
F. Estimate of Funds Expended.....	597
Acknowledgements.....	598
References.....	599

LIST OF FIGURES

		<u>Page</u>
Figure 1.	Outline of the study area in western Alaska shown in relationships to the locations of earthquakes in and near Alaska compiled by Meyers, 1976.	602
Figure 2.	Epicenter plot of all earthquakes located in western Alaska as listed in Meyers' (1976) catalogue. Earthquakes of $m_b \geq 4.0$ are labelled with year and magnitude.	603
Figure 3.	Number of icequakes per day shown in relationships to net wind velocity (mph), wind direction and northerly component of wind velocity (mph). Note the correlation of the occurrence of icequakes with the higher northerly component of wind velocity.	604
Figure 4.	Layout of the seismographic station in western Alaska used for this study.	605
Figure 5.	Layout of seismographic network and stress gauges shown in relationship to the zone of highest ridging occurred during 1976.	606
Figure 6.	Plot of the epicenters of earthquakes in western Alaska located exclusively by the local network during 1977-79.	607
Figure 7.	System response of stress gauges shown as a function of temperature during the laboratory test. Note the response stability in the temperature range of 20°C to -24°C.	608
Figure 8.	Seismograms of type A and B recorded for icequakes occurring in landfast ice sheets in Kotzebue Sound.	609
Figure 9.	Seismograms of type C and D recorded for icequakes occurring in landfast ice sheets in Kotzebue Sound.	610
Figure 10.	The data of Figure 6 are plotted on an overlay of mapped traces of geologic structures in western Alaska.	611
Figure 11.	Mapped traces of geologic structures as shown in Figure 10 are shown separately.	612
Figure 12.	Tectonic provinces and their lithologies in west and northwest Alaska and northeast Siberia (after Patton and Tailleir, 1977). The solid and dashed line is the suggested boundary between two tectonic provinces.	613

LIST OF TABLES

		<u>Page</u>
Table 1.	Location details of the seismographic network in western Alaska and their gain settings at a period of 0.2 sec.	614
Table 2.	P-wave velocity structure of the crust and upper mantle used to compute travel times for hypocenter locations.	615
Table 3.	Location details of earthquakes, located during 1979 on and around Seward Peninsula by the local seismographic network.	616

I. SUMMARY: OBJECTIVES, CONCLUSIONS AND IMPLICATIONS FOR OIL AND GAS DEVELOPMENTS

The objectives under the present study are to evaluate the extent of seismic hazards posed by earthquakes around Norton and Kotzebue Sounds. Additional objectives concern a feasibility study for locating the seasonal formations of pressure ridges and open leads in the sea ice in Beaufort Sea around the barrier islands. The sea ice study involves the monitoring of data in real time from short-period seismographic stations and stress gauges, which are located on and a few hundred meters off the barrier islands, respectively.

The ongoing investigation of earthquakes employing a local seismographic network around Norton and Kotzebue Sounds continue to show offshore and onshore seismic activity. The observed earthquake distribution patterns closely follow the mapped traces of geologic features, principally faults. Seismicity in the region is tentatively identified as of the intraplate type.

Due to the movement of sea ice, the propagation of seismic waves through the ice sheet gives rise to four principal types of seismograms. In order to sample the wave characteristics over a wider frequency band than permitted by the conventional seismographic system, two rosettes of ice-stress gauges have been incorporated into the seismic array installed along the barrier islands.

II. INTRODUCTION

A. General Nature and Scope of Study

(i) Seismicity Studies

In this report a preliminary attempt is made to synthesize the available earthquake data for the western Alaska area. The outline

of the study area is shown by heavy lines in Figure 1. The locations of earthquake epicenters shown in this figure were compiled by Meyers (1976) from the Alaskan earthquake catalog of the United States Geological Survey. The data represent the time period from 1867 through 1974.

As Figure 1 illustrates, the predominant seismically active areas of Alaska are distributed along the southern coastal belts and in the central interior. West of 154°W , earthquake activity is much more diffuse. The earthquakes in Meyers' (1976) catalog of magnitude 4.0 and above in the region of interest are labelled and shown at a larger scale in Figure 2. In this figure, a distinct concentration of epicenters with a northwest-southeast trend can be seen near 66°N , 156°W . This concentration reflects the magnitude 7.3 (m_b) Huslia earthquake of 1958 and its aftershock sequence. The surface effects on and around the epicenter of this earthquake have been reported by Davis (1960).

West of 156°W , and on and around the Seward Peninsula, a number of earthquakes of magnitude greater than 5.0 occurred during the past 30 years. Because the area is sparsely populated, local effects passed largely undocumented. However, despite inadequate seismographic coverage achieved so far, it could be demonstrated from this study that the areas offshore and onshore of Seward Peninsula are seismically quite active.

(ii) Sea Ice Studies

In earlier studies (Biswas et al., 1977) of icequakes located in Kotzebue Sound, it was shown that the formations of compressional and tensional fractures in landfast sea ice due to meteorological instabilities, impart seismic energies into the ice sheets. The ice sheets act as wave guides and transmit the seismic energies in the form of seismic waves.

These can be recorded by conventional seismographic system with a large signal-to-noise ratio.

The icequakes appear in swarms which show good correlation with the higher values for the northerly component of wind velocity. An example of this phenomenon is shown in Figure 3. To further investigate these findings, an array comprising three seismographic stations was installed during the first quarter of 1980 along the barrier islands which are located north of Prudhoe Bay. The array is now functional and the recording of data in real time is progressing satisfactorily.

B. Scientific Objectives

The specific objectives of the studies for the respective areas (western Alaska and Beaufort Sea) are the following:

(i) To determine the spatial and temporal characteristics of the seismicity, and its relationship to mapped tectonic features.

(ii) To determine the predominant failure mechanisms associated with the earthquakes located along or near the known geological features or trends.

(iii) To determine magnitudes, and if possible, recurrence rates of strong earthquakes in Norton Sound for use in projections as to possible activity in the future.

(iv) To determine the characteristics of velocity spectra and seismic energy attenuation as functions of epicentral distance.

(v) To synthesize results of studies under (i)-(iv) in order to integrate the seismotectonic settings of the study areas with the overall tectonic framework of Alaska.

(vi) To locate the seasonal formations of pressure ridges and tensional cracks in sea ice from telemetered data from remote sites during the period of low visibility (November - February) and to deduce the variations of the stress fields during these episodes.

C. Relevance to Problems of Petroleum Development

Large scale exploration programs for hydrocarbon concentrations, and their eventual development in the offshore areas around Seward Peninsula are anticipated to take place in the near future. Consequently, the evaluation of the level of seismicity for these areas is a logical undertaking to assist in the planning and design of future construction projects.

Similar development, planning and construction in the recently leased areas in the Beaufort Sea are expected to occur soon. However, the mitigation of hazards posed to the structures by the seasonal movements of sea ice has not yet been satisfactorily resolved. Since the present study is concerned with locating the spatial and temporal zones of maximum (pressure ridges) and minimum (open leads) stress concentrations in the ice sheets, results of the study should be pertinent to the overall sea ice hazard assessment program of the Arctic region.

III. CURRENT STATE OF KNOWLEDGE

A. Seismicity of Western Alaska

As mentioned earlier, it appears from the past data that seismic activity around Seward Peninsula in western Alaska tends to occur in both offshore and onshore areas. The largest earthquake to have been instrumentally documented in western Alaska occurred about 30 km inland

from the northern coast of Norton Sound in 1950, and was of magnitude 6.5. Since then, recording at stations remote from the area has failed to reveal any further significant seismic activity. However, the present study utilizing a localized seismographic network demonstrates clearly that a characteristic of the ongoing seismicity is an approximate north-south distribution of epicenters passing through the area of the 1950 earthquake. In addition, earthquakes located during a three-year period (1977-79) were widely distributed throughout the entire area, including Norton and Kotzebue Sounds. Most significantly, there are a number of instances where earthquake clusters tend to lie along, or parallel to, mapped faults or linear structural trends. Earthquakes recorded during 1979 ranged in magnitude from about 1 to 4.27.

B. Sea Ice Studies

Gunter et al. (1979) summarized the different aspects of sea ice movements in the Beaufort Sea. They also outlined the current state of knowledge pertaining to the factors affecting man-made structures by the seasonal movements of sea ice at various distances from the coastline of Beaufort Sea.

It can be seen in the referenced summaries that most of the unknown features involving the interaction between sea ice conditions and structures concern areas lying in the water depth range of about 20 m and greater. However, it appears from the literature that not all physical characteristics of the land fast ice (from the coast line to 20 m water depth) could be resolved satisfactorily from the available data base. An example would be a knowledge of the variations of stress levels as a function of distance and thickness of the ice sheet from pressure ridges. Other unknown factors concern the locations of ridges and open leads during

the period of low visibility, the variations of the forms and frequencies of seismic waves as they propagate to different distances from source (ridges and open leads) areas and the precision with which elastic parameters can be deduced for the ice sheets from the analyses of propagating waves. These are a few of the problems relevant to the assessment of sea ice hazards in the Arctic environment.

IV. STUDY AREA, SOURCES, METHODS AND RATIONAL OF DATA COLLECTION

A. Norton and Kotzebue Sounds

The outline of the study area is shown in Figure 1 and the locations of the seismographic stations around Norton and Kotzebue Sounds are shown in Figure 4. It may be noted in these figures that the area of interest is relatively large in relationship to the seismographic coverage which is so far inadequate. However, the planned densification of the network around Norton Sound to be carried out during the coming field season will alleviate the current deficiencies for that area.

Each station of the operational network consists of a short period vertical component seismometer (Geotech S13), set to a nominal one-second natural period with 0.7 of critical damping. However, the station located at Kotzebue (KTA) has three components (vertical, north-south and east-west) and is equipped with different model seismometers (Geotech S500) than the other stations. This model of seismometer is small enough (0.057 m diameter and 0.165 m length) to facilitate installation, and has the added benefit of being insensitive to ground tilt. This is particularly important because a layer of permafrost is encountered at shallow depth (1-2 ft) at this station site. In addition, the network

includes a vertical component (Geotech SL210) long period station at Nome (ANV). Station location details are given in Table 1.

The signals from the seismometers are preamplified by either Geotech Model 42-21 or Monitron Model 2000 amplifiers. These signals are then telemetered to the central recording site at the Northwest Community College at Nome by frequency-modulated audio subcarriers via a combination of satellite and microwave communication circuits where the data are recorded on magnetic tapes. The tapes are changed daily and shipped to the Geophysical Institute on a weekly basis for playback and analyses.

The recording setup at the Community College at Nome, though functional, needs further improvement. The available local power (110V) is unstable and reduces the signal-to-noise ratio in the recorded traces. It is anticipated that the planned installation of a voltage stabilizer, in the near future will resolve this problem.

The electronic systems of the stations, except for those at two remote sites, Candle (CDL) and Devil Mountain (DMA), are powered by locally available 110 V lines. At DMA and CDL, the power supplies consist of five Carbonaire Model ST-22 batteries delivering 1100 Amp-hr of service. The data are telemetered from DMA and CDL by VHF (transmitter: Monitron T15F; receiver: Monitron R15F) to the nearest station (KTA) where access to the satellite circuit is available.

The system response of the short period stations at a period of 0.2 sec is given in Table 1. It may be noted that the period of the first few cycles in the recorded signal usually varies from 0.1 to 0.3 sec. Because the microseismic background varies considerably from one station to the next, the operational gains were set to attain maximum signal-to-noise ratio. Consequently, all stations of the network are not operated at identical gain settings.

Data from station ANV are recorded on heat sensitive paper by Helicorder (Geotech RV-301 B), as well as on magnetic tape. This recording mode facilitates the identification of local earthquakes and approximate origin times for rapid scaling of the daily record. The following data are scaled from the records: first arrival times of the P-wave and the S-wave when possible, direction of P-wave first motion, and the maximum amplitude and period in the recorded trace.

For impulsive arrivals, the first onset times for P-waves could be scaled with a precision of ± 0.1 sec, while for emergent arrivals, the uncertainty in the arrival times might be as high as ± 0.5 sec. For S-wave arrivals, uncertainty of the measurement is even larger.

Scaled data for each earthquake are punched in appropriate format on computer cards and processed by the computer program of Lee and Lahr (1975) for location purposes. The magnitudes (M_L) of the earthquakes are computed by using the formula of Richter (1958) for local earthquakes, incorporating a correction factor for the instrumentation used.

B. Beaufort Sea

Initially it was planned to install four short-period seismographic stations, one each on Cross, Narwhal, Pole and Duck Islands, supplemented by two rosettes of stress gauges located a few hundred meters north of the coastline of Narwhal Island. The entire system has been emplaced except the seismographic station on Duck Island. This was due to high background noise encountered at this site caused by oil well drilling activities. The layout of the currently operational array is shown in Figure 5.

The data from the Cross and Pole Islands are telemetered by VHF, to the Narwhal Island where these signals are multiplexed with the local ones. The multiplexed signals are finally telemetered, also by VHF to the Sohio Communication facility at Deadhorse. Here the data are recorded in real time on magnetic tape in cooperation with Sohio. In addition to recording data on magnetic tape, the seismic signals from the Narwhal station are recorded simultaneously by Helicorder (Geotech RV-301B) on heat sensitive paper. This mode of recording is utilized to provide a visual check of any sea ice movement. The magnetic tape and the helicorder paper are changed once a day and the records are shipped to the Geophysical Institute at Fairbanks on a weekly basis.

The sensor and the associated electronics of the seismographic stations are identical to those used in the earthquake studies elsewhere in Alaska. The stress gauges of the two rosettes are uniaxial load cells, of the type originally designed by Nelson et al. (1973). They are cylindrical in shape and consist of a temperature compensated four-element Wheatstone bridge, with strain gauges as the bridge elements. The stress gauges are capable of recording stresses up to the point of ice fracture, and the amplifier response was made d.c. coupled so that the long-term ice stress buildup could be detected as well.

V. RESULTS

A. Western Alaska

The crust and upper mantle structure of western Alaska is not yet known. However, an attempt will be made to resolve this problem, particularly for the Norton Sound area, from the data of the densified network of that area in the near future. At present P-wave travel time used in

locating earthquakes are based on a plane layered P-wave velocity model for the crust obtained from central Alaskan data from earthquakes and quarry blasts. The upper mantle section is taken from Biswas and Bhattacharya (1974). The details of this model are shown in Table 2. A ratio of 1.78 between P- and S-wave velocities, corresponding to Poisson's solid, is used for the computation of S-wave travel times.

With the limitations mentioned above, a preliminary computer run on the scaled data is made and the output is examined for reading errors. If the time residuals for an earthquake (that is, the difference between the observed and computed travel times) for any station exceed 1 sec, the records are rescaled to reduce the uncertainties to a minimum. The corrected data are then used for a second computer run allowing all focal parameters to vary. The results obtained by following these steps show that focal depths range between the surface and about 20 km for 90 percent or more of the events. In subsequent computer runs, focal depths are constrained to 10 km to eliminate one degree of freedom in the location program, thereby facilitating the identification of possible areas of local clustering.

The details of the earthquakes located during 1979 are given in Table 3. All solutions are based on a weighted least squares minimization technique. The symbols NO, GAP, DMIN, RMS, ERH and ERZ of this table refer, respectively, to the number of station readings used to locate each earthquake, largest azimuthal difference between two neighboring stations with respect to the epicenter, distance of the epicenter from the nearest station, the root mean square of travel time residuals, the standard error in epicentral location and the standard error in focal depth. It may be noted in this table that despite fixing focal depths

in the location of each event, a number of event locations still display significant uncertainties. It is anticipated that this range of errors can be reduced, particularly for the Norton Sound area by the planned densification of the network in that area.

As mentioned before, the magnitude of the events located during 1979 ranged from about 1.0 to 4.27. In comparison to the number of earthquakes recorded during the past two years (1977-78), relatively fewer events could be located during 1979. This was primarily due to our efforts to start recording the data locally with the cooperation of the personnel of the Community College who could not familiarize with the recording system in time. However, the spatial pattern in the tectonic activity detected during 1979 is very similar to the earlier years. A synthesized plot of the events recorded during the three-year period (1977-79) is shown in Figure 6. The events have not been sorted according to the magnitude in this plot.

B. BEAUFORT SEA

It was planned initially to install the array in Beaufort Sea around mid-December, 1979. However, unexpected difficulties were encountered in achieving the required stability as a function of temperature for the electronic system of the stress gauges. Due to these factors, the array could not be installed until mid-March of 1980.

The performance during the laboratory tests of the total system (stress gauge) used for the array is shown in Figure 7. The tests of the system were carried out in the temperature range from +20° to -24°C. It may be noted in Figure 7 that the stress gauges and the associated electronics could be stabilized over the above temperature range with a few millivolt background noise. The pass band for the signal is set to

± 125 psi, a level which is about half of the peak value observed at points very close to the pressure ridges for Beaufort Sea as cited in the literature. The present trial setting of the operational gauges is anticipated to be sensitive enough to respond to stresses several hundred meters from pressure ridges or open lead formation activities in sea ice.

The seismic signals recorded during earlier years (1977-78) and 1979 for icequakes around Kotzebue Sound show four predominant types of seismograms, an example of which is shown in Figures 8 and 9. Type A (Figure 8a) seismograms are characterized by small amplitude first onsets after which several cycles of oscillations are followed by a large amplitude phase. The icequake on this record represent an event of magnitude (M_L) equal to 2.51.

The characteristics of seismic phases arriving earlier than the large amplitude phase for the type B and C seismograms (Figures 8b and 9a) are similar, except in the arrival of a prominent phase for type B which is labelled as S1 in Figure 9a. Also, the coda of type B (Figure 8b) is relatively well developed compared to Type A and C. The type D (Figure 9b) consists, predominantly of a dispersed wave train. Since the seismograms of Figures 8 and 9 were recorded by the same station (KTA-Z), the relative difference in amplitudes shown for the different events of these figures are real.

VI. DISCUSSION

To relate the epicenter locations to known tectonic features, all earthquakes shown in Figure 6 are plotted on an overlay of the mapped

structural traces in the study area. The result is shown in Figure 10. Because the dense clustering of epicenters, particularly inland, partially obscures the structural features, these are shown separately in Figure 11. The mapped geologic features located north of Kotzebue Sound, on Seward Peninsula and offshore in Norton Sound were taken from Eittreim et al. (1979), Grantz et al. (1979), Hudson (1977), and Johnson and Holmes (1977), respectively. The traces were enlarged photographically by a factor of about 10, digitized at close intervals, and converted to the same projection and scale as that used to plot the epicenters.

Despite the considerable scatter in the distribution of earthquakes seen in Figure 6, a number of distinct trends can be discerned. The inland trace of the Kaltag fault (Figure 11), a major tectonic element of the area, appears to traverse through the clusters labelled A (Figure 10). Offshore in Norton Sound, the earthquakes align along a trend (B-B) which appears to be offset 20-30 km northwest from the trace of the Kaltag fault. Along the trend B-B, a number of faults have been mapped by Johnson and Holmes (1977) from using marine geophysical data.

The seismic trend C-C in Norton Sound appears to follow closely a series of mapped faults and a basement ridge identified by Johnson and Holmes (1977). They also mapped a number of offshore faults (Figure 11) trending east-west from Port Clarence (Figure 4) where earthquakes tend to cluster (D-D).

In Kotzebue Sound, where published results from marine geophysical surveys are lacking, two trends in the east-west direction (E-E and G-G) and one in the north-south direction (F-F) appear in the earthquake data. The trends E-E and G-G parallel the young geologic structures of Hope basin and the mountains east of the basin (Figure 11), but it would be necessary to extend the marine surveys to this area to see if there are structural implications to the observed trends in seismicity.

Inland on the Seward Peninsula, the clustering of earthquakes and mapped fault traces is quite significant. For instance, the cluster H-H closely follows a well defined fault system along the Darby mountains, and traverses the epicentral area of the 1950 earthquake ($m_b = 6.5$). About 75-100 km to the west of this zone, a second trend in seismicity (I-I) cuts across the Bendeleben-Kigluaik mountain trend, and closely follows the en-echelon type of fault system mapped there. Similar clustering of earthquakes apparently associated with mapped faults appears immediately to the east and northeast of Port Clarence. Grantz (1979, personal communication) suggests that the seismicity on the lower third of the Seward Peninsula may represent the tectonic activity along the young fault systems of the Kigluaik, Bendeleben and Darby complexes. Inland further east, the cluster labelled J coincides with the aftershock zone of the Huslia earthquake of 1958 (A_1 - A_2 , Figure 2). There are also a number of earthquakes located inland which cannot be associated with any mapped structures.

East of the study area, in central Alaska, earthquakes are a direct consequence of lithospheric plate subduction as shown by Bhattacharya and Biswas (1979). This phenomenon results in normal and strike-slip faulting at earthquake foci in the depth interval of 0-60 km, and underthrusting at greater depth. However, it is difficult to invoke this phenomenon as being the immediate cause of earthquakes in western Alaska, an area approximately 500 km distant from the Alaskan subduction zone. Rather, the seismicity in the study area appears to be of intraplate type and to belong to a separate tectonic regime.

In the evolutionary sequence, the region around Bering Strait in northwest Alaska and northeast Siberia have been interpreted by Grantz

(1966), Churkin (1970, 1972) and Patton and TAILLEUR (1977) as having passed through compression in an east-west direction in the geologic past. This interpretation is based on the observed change in the orientation of structural grains from east-west and northwest-southeast directions in the Brooks Range and the Chukchi Sea (Figure 11), respectively, to a predominantly north-south direction on and around Seward Peninsula. The structural trend in the latter area undergoes an oroclinal bend (Patton and TAILLEUR, 1977) on and near St. Lawrence Island in the northern Bering Sea and terminates on Chukotsk Peninsula.

A number of authors have used lithologic correlation to substantiate the above interpretation and to classify the area of interest as a representative of a tectonic province separate from the adjoining section (Yukon-Koyukuk) of Alaska. These features, as summarized by Patton and TAILLEUR (1977), are shown in Figure 12.

The current orientation of the stress tensor in the study area is yet to be ascertained from the data concurrently gathered by the local seismographic installations. However, Sykes and Sbar (1974) have given the focal mechanism solution of one earthquake ($m_b = 5.8$) which occurred in 1966 near the coast of Norton Sound. The solution shows normal faulting with the tension axis oriented approximately northeast-southwest (see Figure 2). Although a single focal mechanism solution is inadequate for ascertaining the direction of regional compressional stress operative today (particularly for a large tectonic province), the direction of fault strike implied for this earthquake is in agreement with the north-south regional structural trend of the area.

Concerning the inferred intraplate nature of seismicity of western Alaska, note that the trend of seismicity H-H (Figure 10), in addition to

lying on a fault zone, tends to follow closely a plutonic belt with alkaline magnetism (Figure 12). Further, this belt is aligned transversely to the northern coast line of Norton Sound. These features are some of the typical characteristics of many other zones of intraplate seismicity as noted by Sykes (1978). However, the seismic data (Figure 6) do not show any correlation between the locations of earthquakes and similar zones of magmatism (Figure 12) occurring immediately east of Kotzebue Sound, on the southern coast of St. Lawrence Island, or at the northeastern corner of Chukotsk Peninsula.

VII. CONCLUSION

Within the last 20 years, the strongest instrumentally recorded earthquake in western Alaska was a magnitude 7.3 earthquake, located near Huslia in the Koyukuk River basin. Several earthquakes of magnitude greater than 5.0 have occurred on and around the Seward Peninsula with one event located about 400 km offshore in the Chukchi Sea. Because the areas around the epicenters of these earthquakes are thinly populated, their seismic impact passed largely undocumented.

Crustal earthquakes commonly migrate with time along a fault or fault system. This means that if a given section of an active fault yields (resulting in an earthquake), then at a later time a somewhat distant point of the same fault may yield to accumulated stresses. This points to the necessity of determining the trend of the faults both in offshore and onshore areas for an appropriate geohazard assessment for an area.

Since the installation of a local seismographic network, about 450 earthquakes, predominantly of crustal origin, and in the magnitude range

of $1.0 \leq M_L \leq 4.5$ have been located during a period of about three years (1977-79). Despite location uncertainties due to unknown crust-upper mantle velocity structure and the relatively sparse local seismographic coverage attained to date, the epicenters of these earthquakes are found in some cases to follow closely the offshore and onshore traces of mapped faults. Some of these seismic trends traverse the epicentral areas of the past strong earthquakes.

We make no attempt at this stage of our study to interpret the detailed tectonic significance of the observed trends in seismicity and the associated seismic hazards posed by these features from the available data. However, in contrast to the contiguous areas of central Alaska, the Seward Peninsula area appears to represent a separate tectonic province with associated seismicity of the intraplate type.

VIII. SUMMARY: FOURTH QUARTER OPERATIONS

A. Task Objectives

(i) To install the seismographic array and stress gauges along the barrier islands in Prudhoe Bay.

(ii) To acquire and test field equipment for the densification of the seismographic network around Norton Sound.

(iii) To continue scaling and processing of daily recorded data.

B. Field and Laboratory Activities

(i) The stress gauges and associated electronic system have been modified to attain desirable stability as a function of temperature.

(ii) After necessary laboratory tests of both the seismographic system and stress gauges, these have been emplaced in the field. The system as a whole is functioning normally.

(iii) The needed equipment for the densification of the seismographic network to be installed during the coming field season have been acquired. The assembly of the electronic packages and their laboratory tests are in progress.

(iv) The daily recordings of data for the operational seismographic network around Norton and Kotzebue Sounds at the Community College are continued. However, some improvements of the recording setup are required. The necessary steps are nearing completion to eliminate these deficiencies.

C. Results

None

D. Preliminary Interpretation

None

E. Problem Encountered

Several problems encountered in the modification of the stress gauges. However, these have been resolved and the gauges could be emplaced in the field.

F. Estimate of Funds Expended

\$160,000

ACKNOWLEDGEMENTS

We thank Drs. Arthur Grantz and David Hopkins of the U.S. Geological Survey (Menlo Park) for frequent stimulating discussions on the tectonic settings of the Alaskan Arctic and sub-Arctic regions during the reporting period. We also thank Drs. G. Weller and J. Gravitz of the Arctic Project Office (OCSEAP) for their continuous support and encouragement during the study period. We express appreciation to Mr. R. Eppley and other members of the Alaskan Tsunami Warning Center of N.O.A.A. for their cooperation in operating the seismographic network. We are also grateful to Mr. D. Brooks of OCSEAP for logistic support in time.

This research was supported by the NOAA Contract No. 03-6-022-55, Task #12, and by the State of Alaska funds appropriated to the Geophysical Institute through the University of Alaska.

REFERENCES

- Bhattacharya, B. and N. N. Biswas (1979). Implications of North Pacific plate tectonics in central Alaska: Focal mechanisms of earthquakes, *Tectonophysics*, 53, 99-130.
- Biswas, N. N. and B. Bhattacharya (1974). Travel-time relations for the upper mantle P-wave phases from central Alaskan data, *Bull. Seismol. Soc. Am.*, 64, 1953-1965.
- Biswas, N. N., L. Gedney and P. Huang, (1977). Seismicity Studies: (A) Northeast Alaska and (B) Norton and Kotzebue Sounds, Environmental Assessment of the Alaskan Continental Shelf: Hazard and data management, NOAA Report XVIII, 269-315.
- Churkin, M., Jr. (1970). Fold belts of Alaska and Siberia and drift between North America and Asia, in Proceedings of the geological seminar on the North Slope of Alaska, Los Angeles, Am. Assoc. Petroleum Geologists, Pacific Sec., eds. W. L. Adkinson and M. M. Brosge.
- Churkin, J., Jr. (1972). Western boundary of the North American continental plate in Asia, *Geol. Soc. Am. Bull.*, 83, 1027-1036.
- Davis, T. N. (1960). A field report on the Alaskan earthquakes of April 7, 1958, *Bull. Seismol. Soc. Am.*, 50, 489-490.
- Eittreim, S., A. Grantz and O. T. Whitney (1979). Cenozoic sedimentation and tectonics of Hope Basin, southern Chukchi Sea, *in* Sission, Alexander, ed., The relationship of plate tectonics to Alaskan geology and resources: Proceedings of the Sixth Alaska Geological Society Symposium, April 1977, Anchorage, Alaska: Alaska Geological Society, B-1 to B-11.
- Grantz, A. (1966). Strike-slip faults in Alaska, U. S. Geol. Survey Open-file Rept., No. 267.

- Grantz, A., S. Eittreim and D. A. Dinter (1979). Geology and tectonic development of the continental margin north of Alaska, to appear in Tectonophysics.
- Gunter, W., D. Norton and T. Johnson, (1979). Environmental stipulations relating to OCS development of the Beaufort Sea, Special Bulletin #25, NOAA.
- Hudson, T. (1977). Geologic map of Seward Peninsula, Alaska, U.S. Geol. Survey Open-file Rept. No., 77-796A.
- Johnson, J. L. and M. L. Holmes (1977). Preliminary report on surface and subsurface faulting in Norton and northeastern Chirikov Basin, Alaska, in Environmental Assessment of the Alaskan Continental Shelf: Hazards and Data Management, N.O.A.A. Report XVIII, 14-41.
- Lee, W. H. K. and J. C. Lahr (1975). A computer program for determining hypocenter, magnitude, and first motion patterns of local earthquakes, U.S. Geol. Survey Open-file Rept., No. 75-311.
- Meyers, H. (1976). A historical summary of earthquake epicenters in and near Alaska, N.O.A.A. Technical Memorandum EDS NDS DG-1.
- Nelson, R. D., M. Tauranineu and J. Borghorst, (1973). Techniques for measuring stress in sea ice, Alaska Sea Grant Report 76-18, Univ. of Alaska.
- Patton, W. W., Jr. and I. L. Tailleir (1977). Evidence in the Bering Strait region for differential movement between North America and Eurasia, Geol. Soc. Am. Bull., 88, 1298-1304.
- Richter, C. (1958). Elementary Seismology, W. H. Freeman and Co., San Francisco.

Sykes, L. R. and M. L. Sbar (1974). Focal mechanism solutions of intraplate earthquakes and stress in the lithosphere, in Geodynamics of Iceland and the North Atlantic Area, Proc. NATO Advanced Study Inst., Reykjavik, Iceland, ed. L. Kristjanssen, D. Reidel Pub. Co., U.S.A.

Sykes, L. R. (1978). Intraplate seismicity, reactivation of pre-existing zones of weakness, alkaline magnetism, and other tectonic post-dating continental fragmentation, Rev. Geophys. and Space Phys., 16, 621-688.

EARTHQUAKES IN AND NEAR ALASKA (MEYERS, 1976)

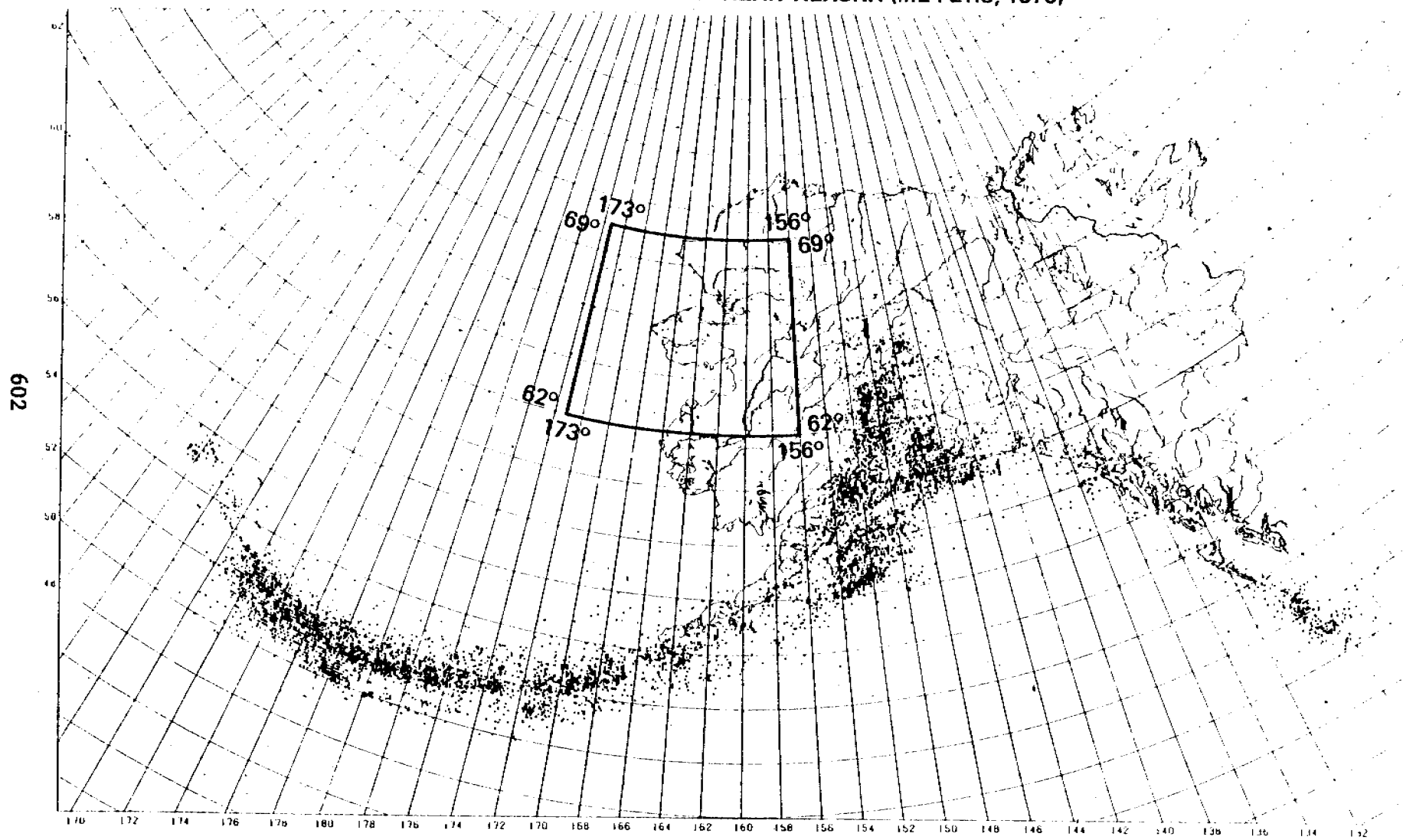


Figure 1

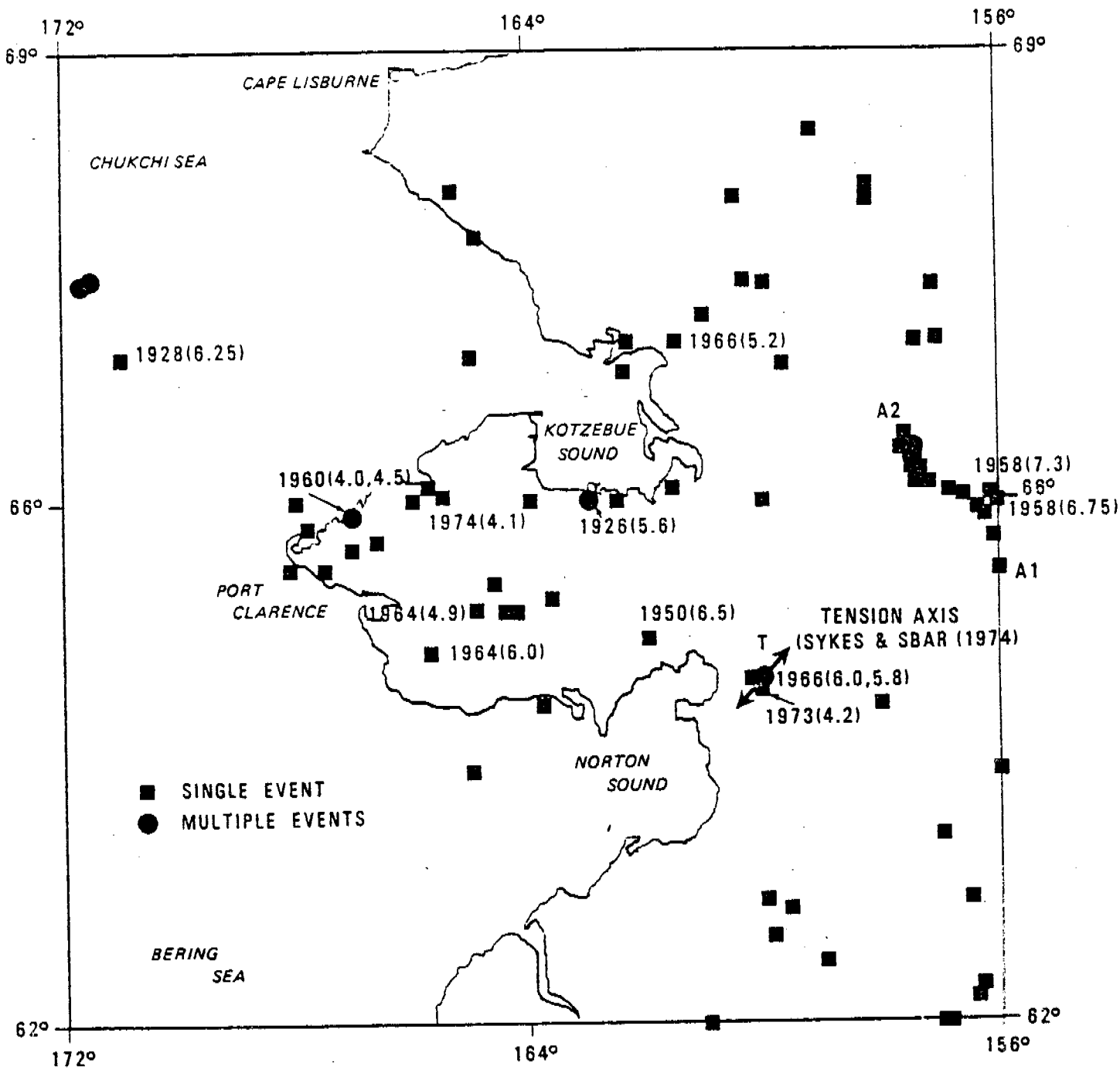


Figure 2

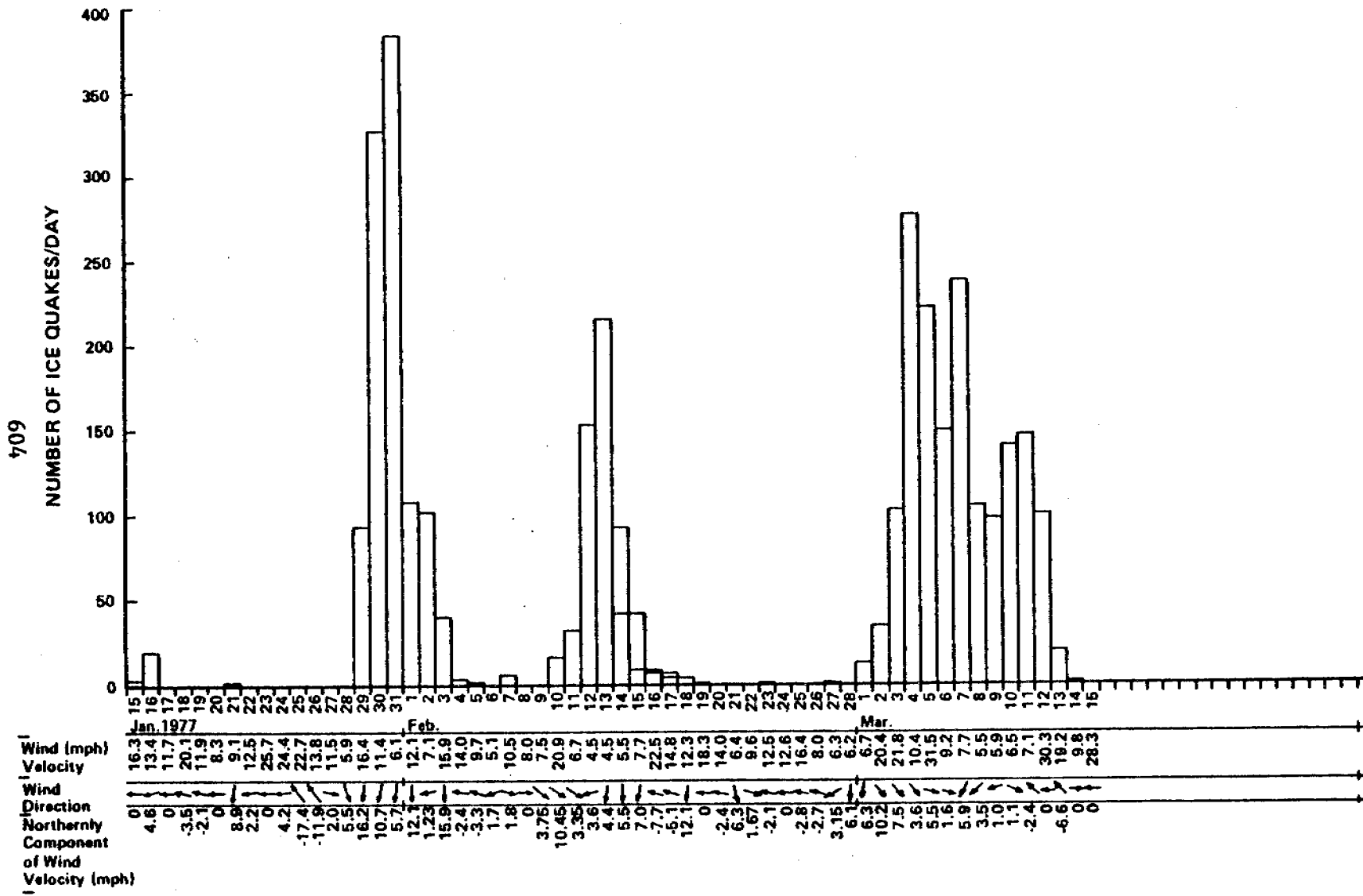


Figure 3

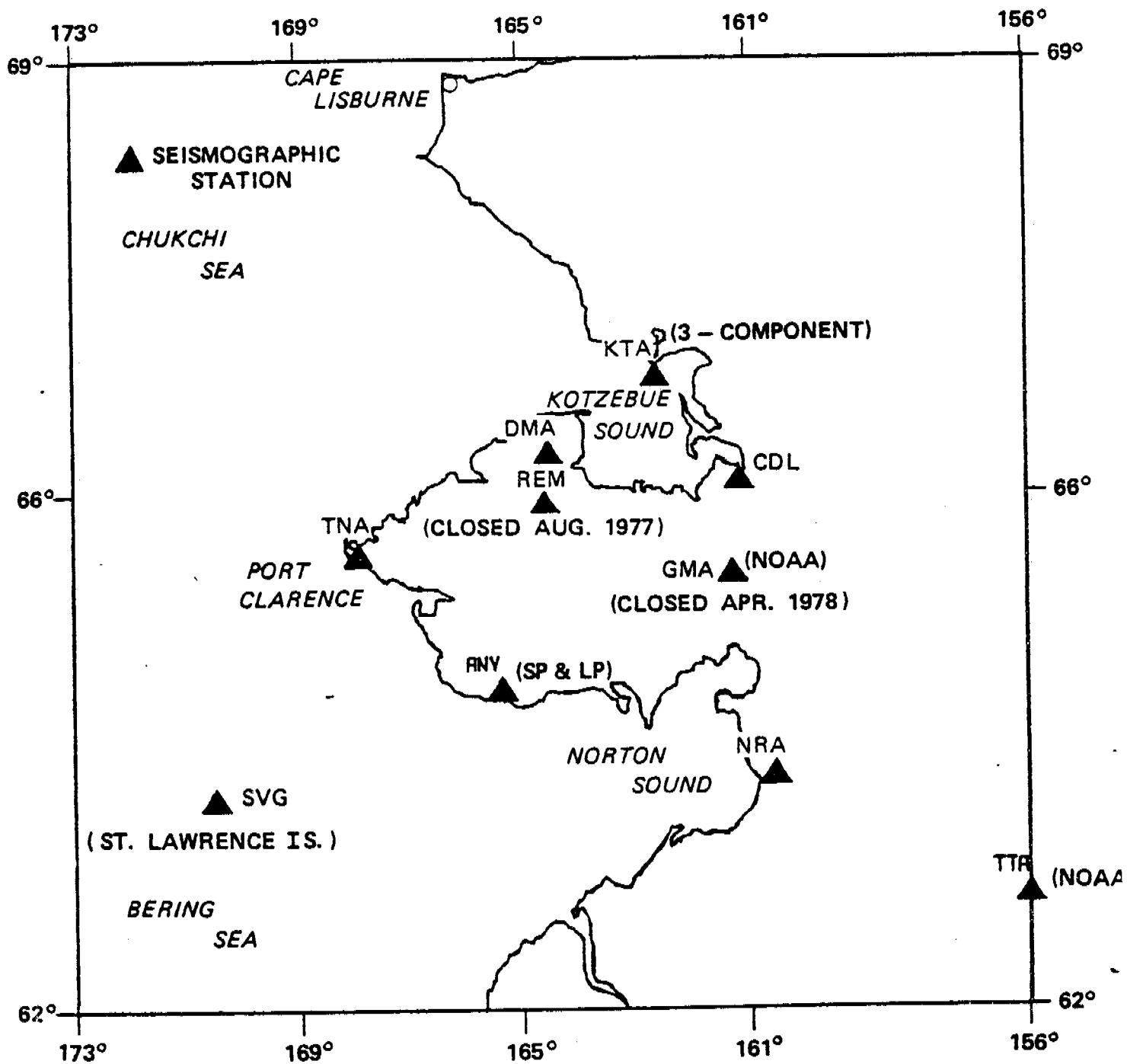


Figure 4

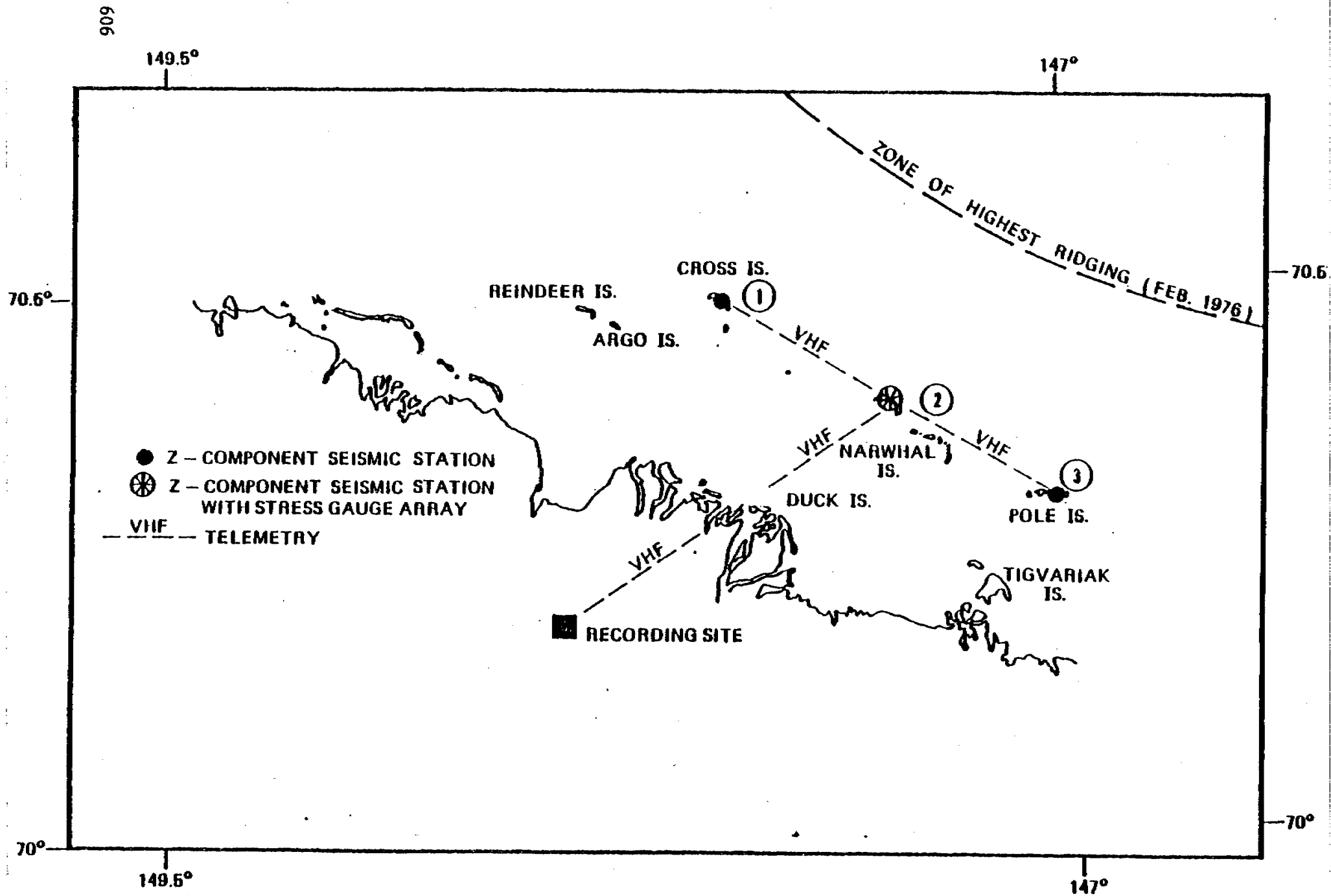


Figure 5

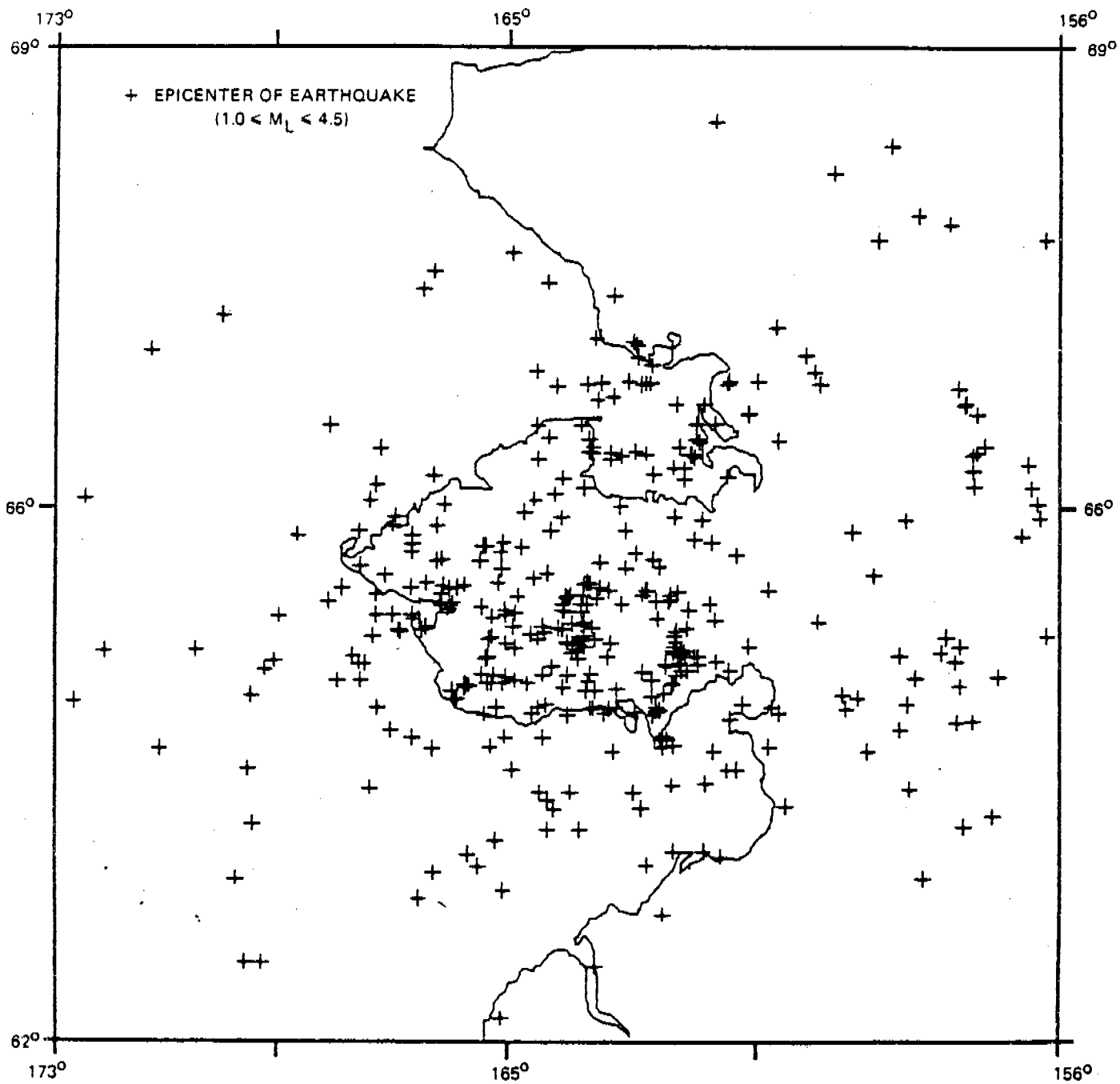


Figure 6

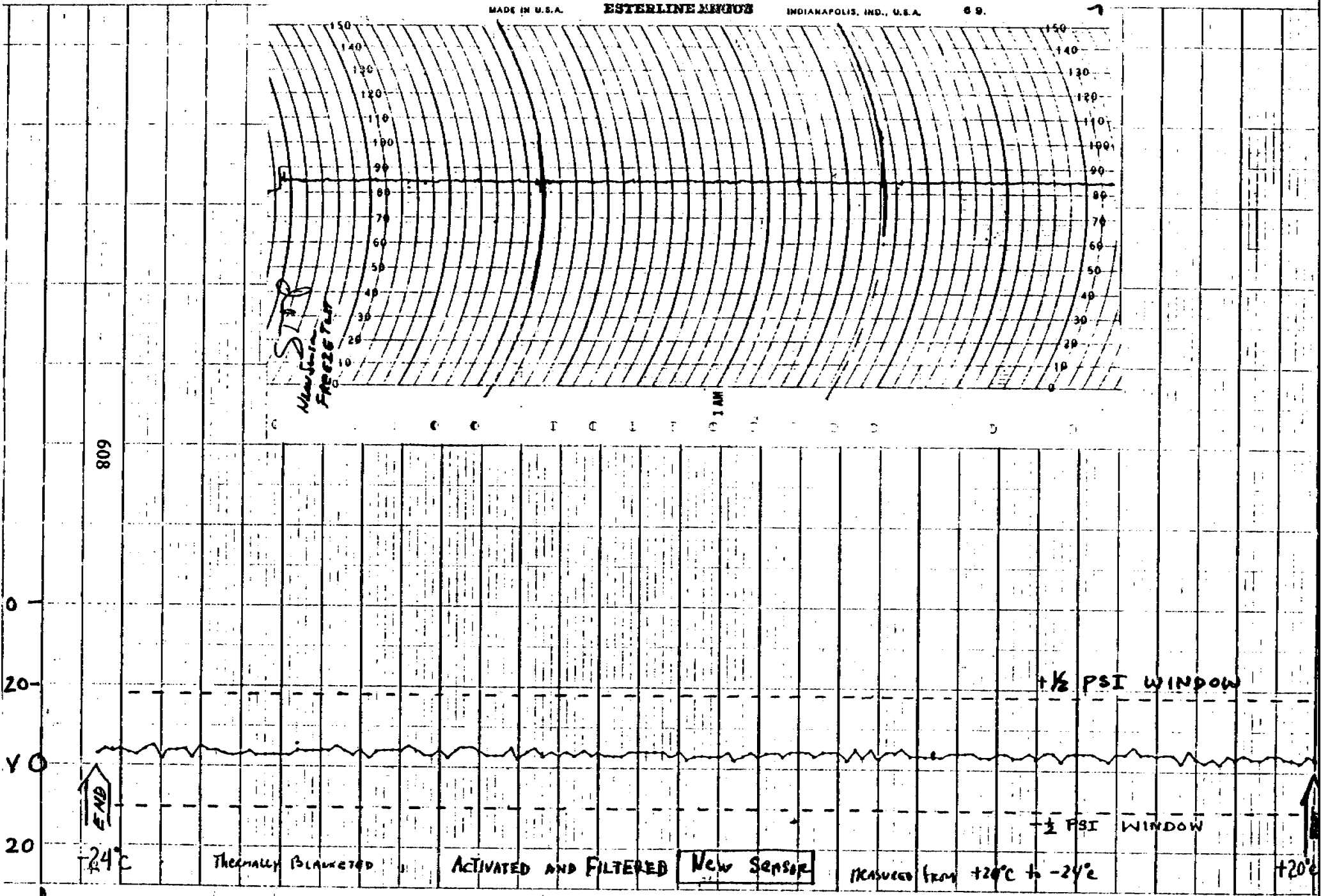


Figure 7

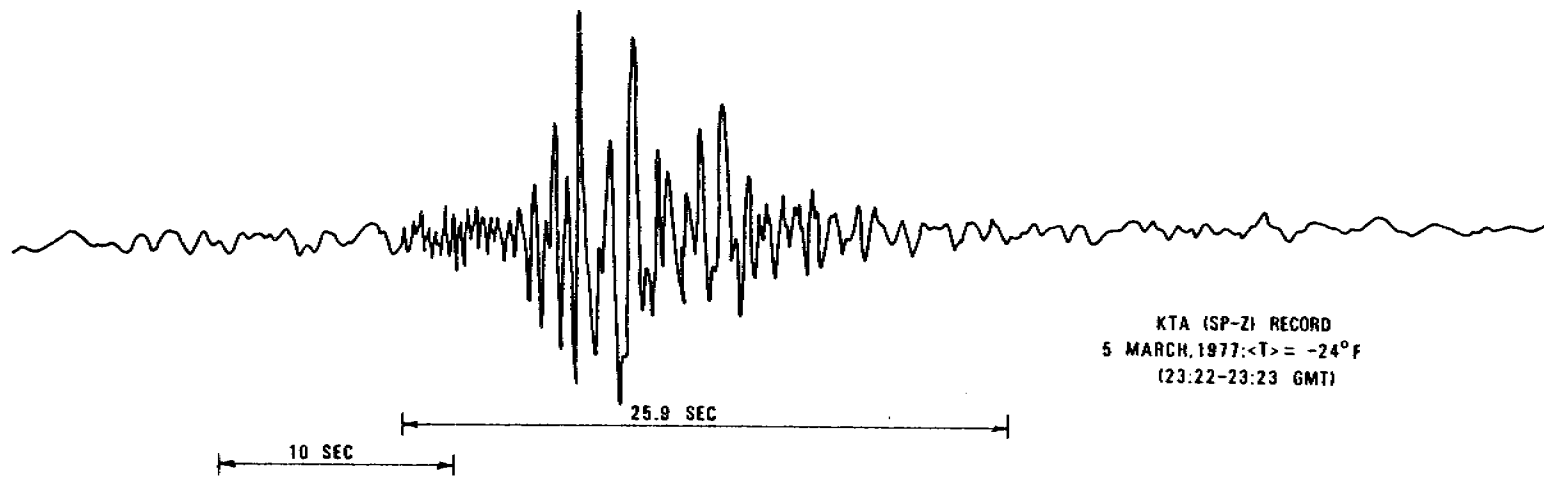


Figure 8a

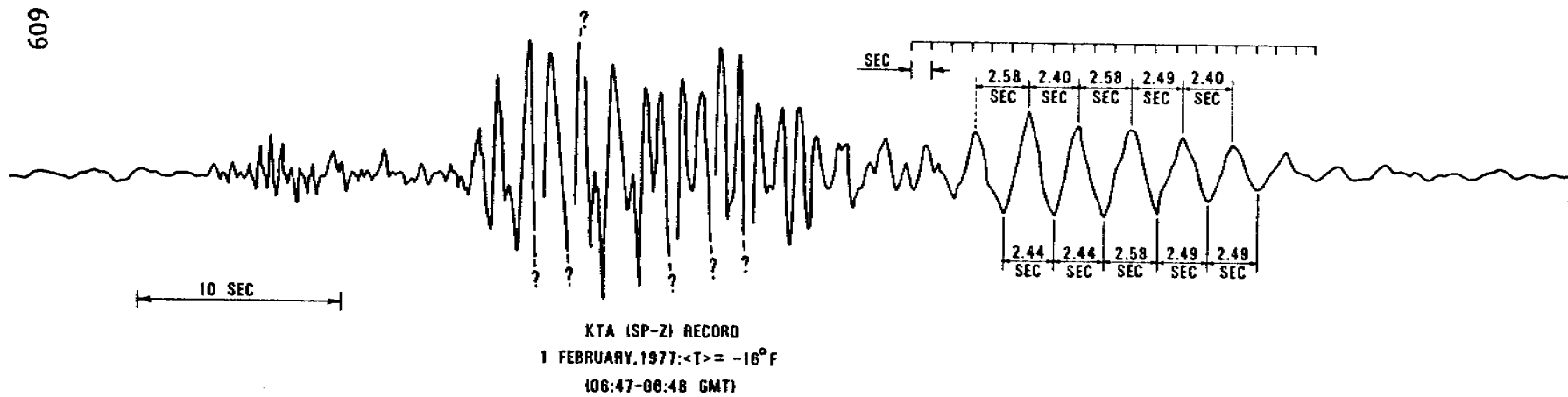


Figure 8b

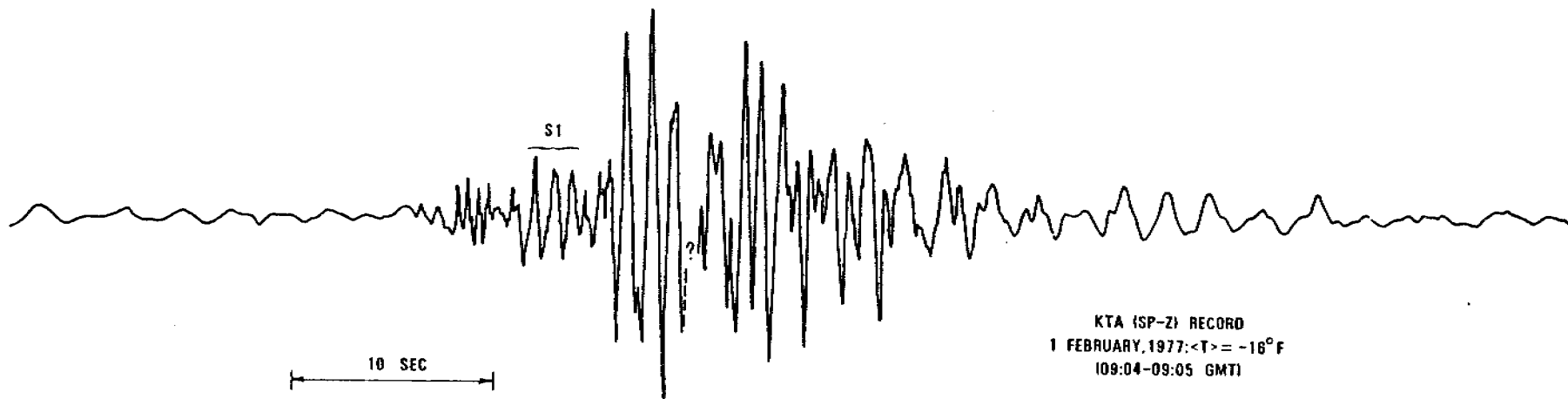


Figure 9a

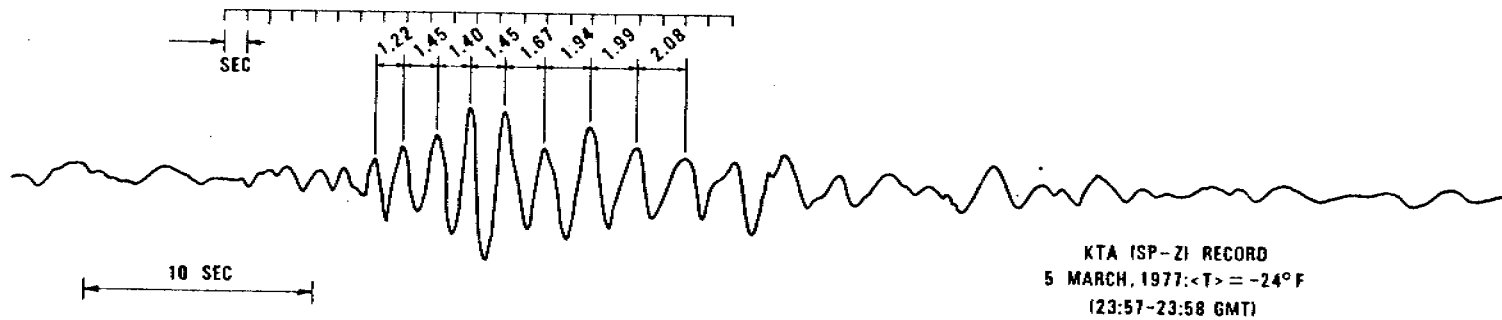


Figure 9b

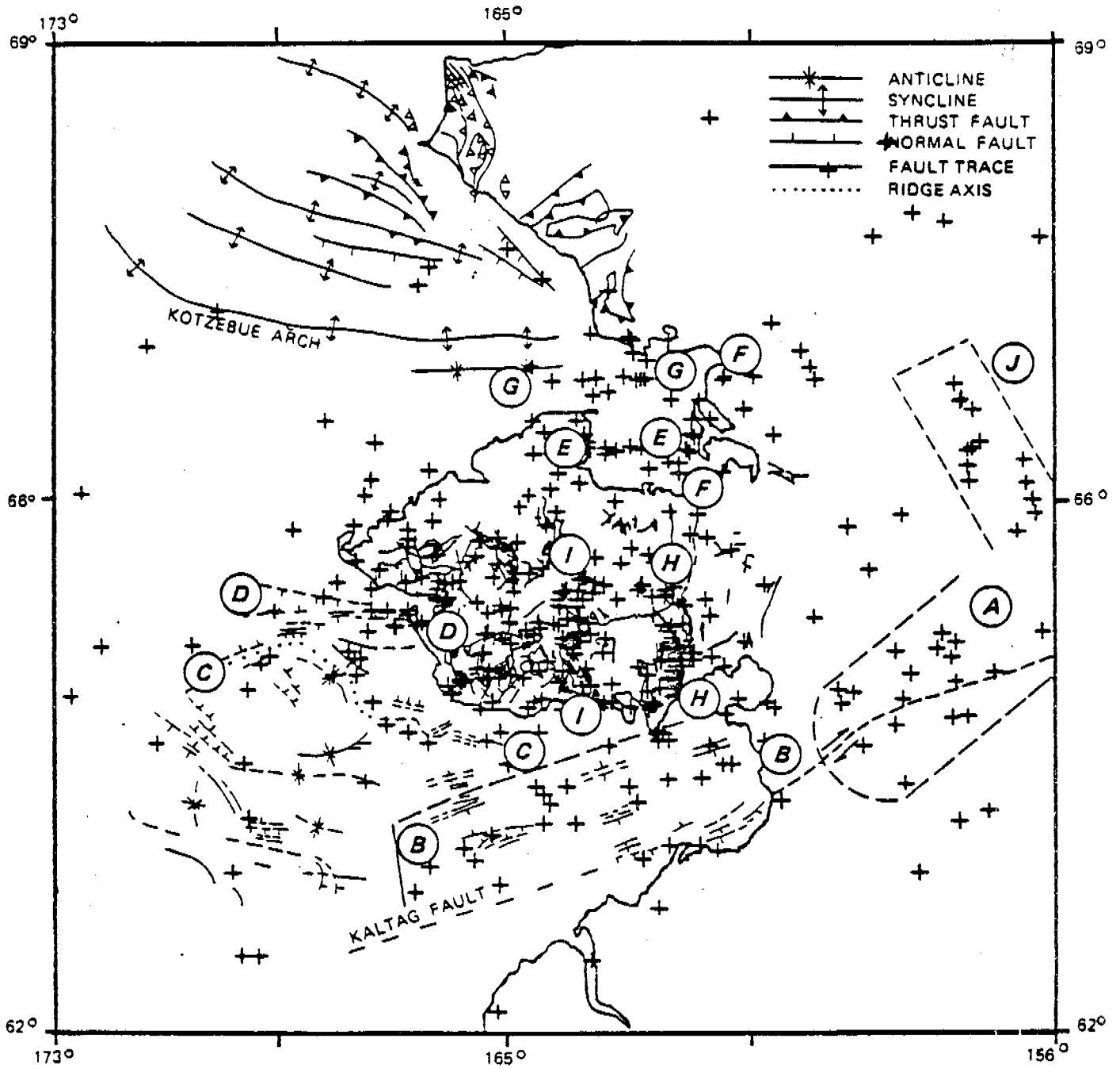
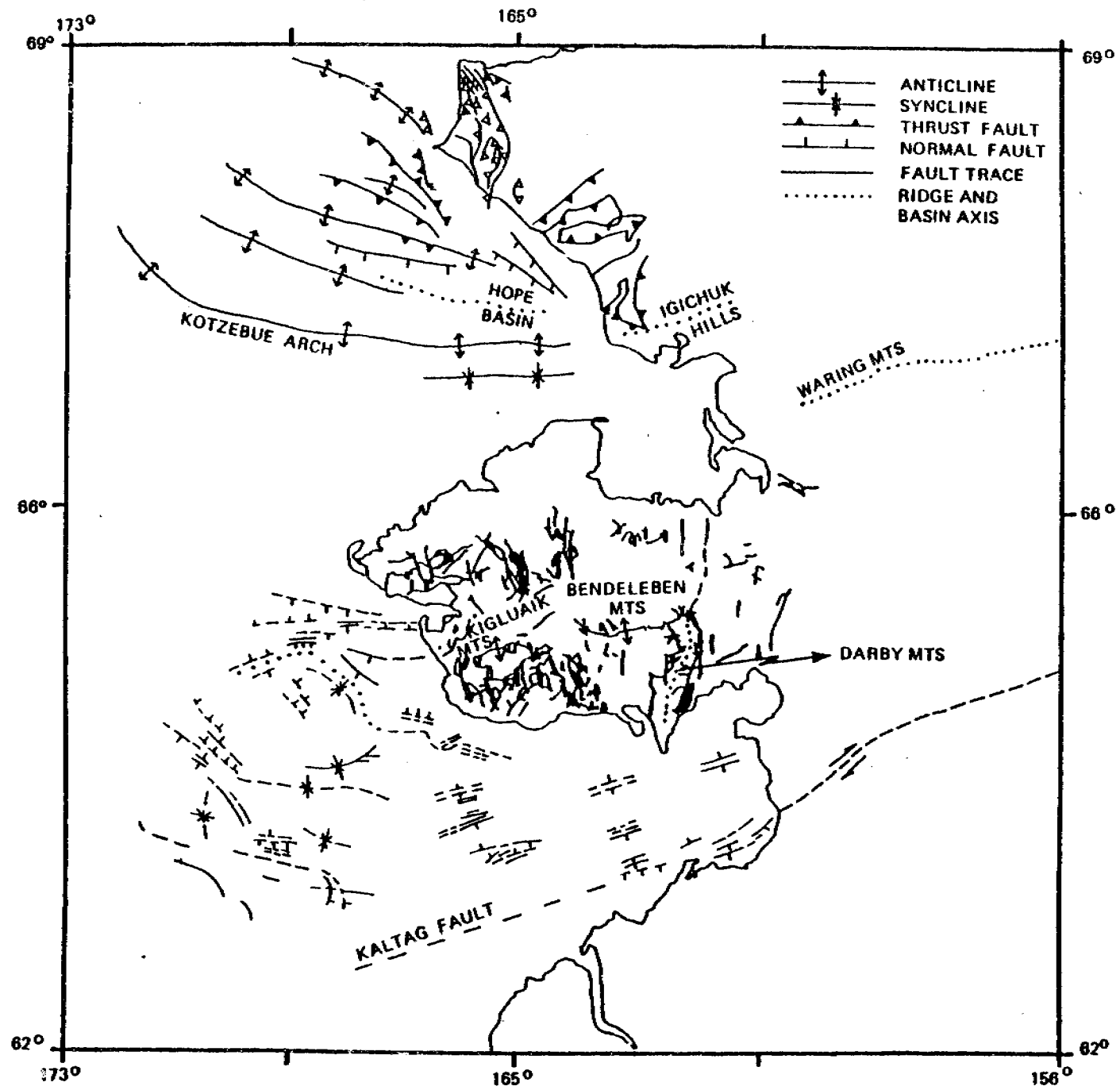


Figure 10



612

Figure 11

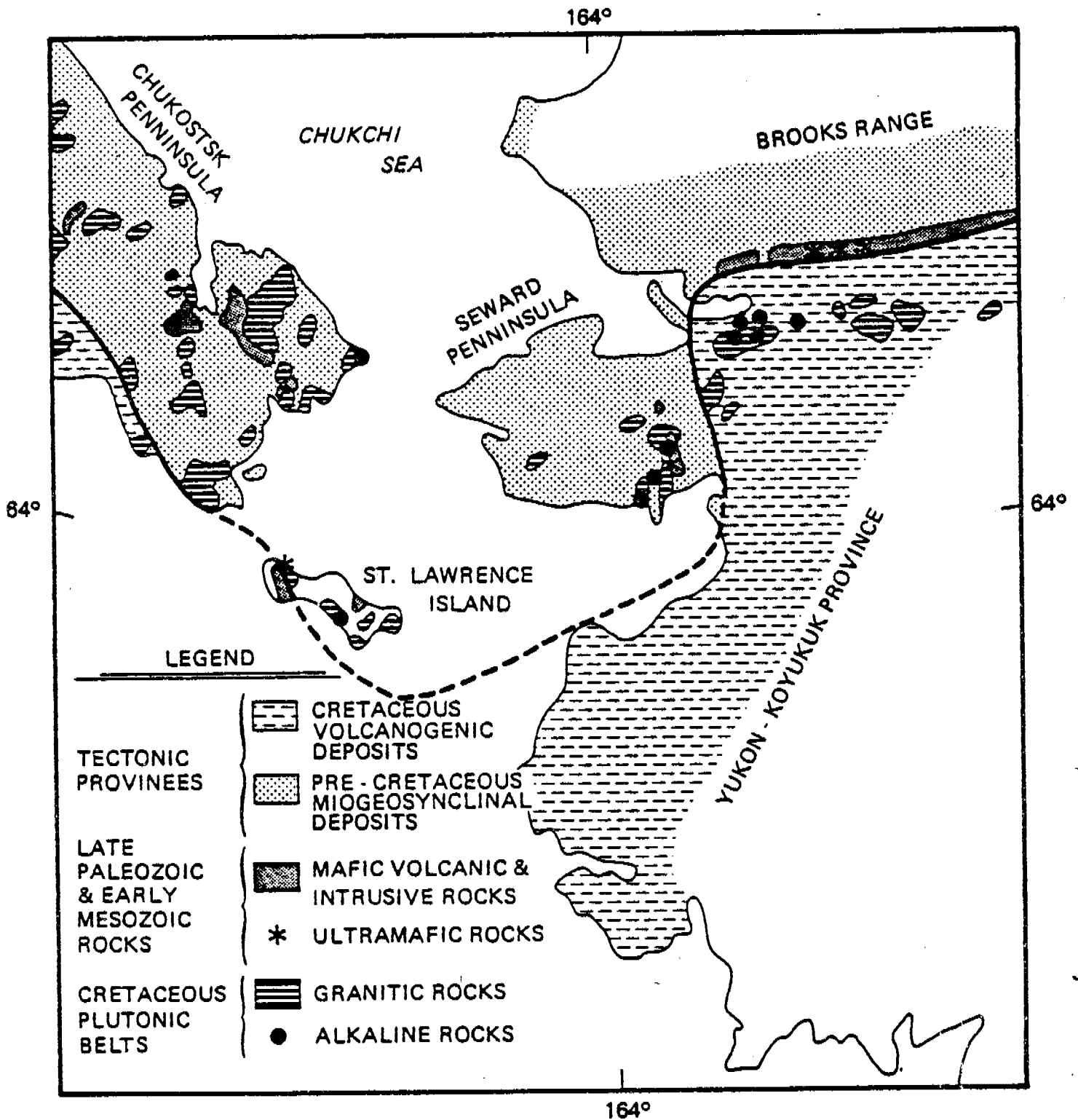


Figure 12

TABLE 1

Location Details of the Seismographic Network in Western
Alaska and Their Gain Settings at a Period of 0.2 sec.

Station Name	Code	Latitude (north)	Longitude (west)	Elevation (m)	Site (Geologic Formation)	System gain (0.2 sec)
Anvil Mountain	ANV	64.56°	165.37°	327	Granite-Gneiss	2.6×10^6
Candle Creek	CDL	66.11°	161.66°	75	Siliceous metasedimentary	3.3×10^6
Devil Mountain	DMA	66.31°	164.52°	243	Basalt	1.3×10^6
Granite Mountain	GMA	65.43°	161.23°	858	Basalt	1.0×10^5
Kotzebue	KTA	66.85°	162.61°	26	Permafrost	1.1×10^6
North River	NRA	63.89°	160.51°	107	Metamorphic	2.7×10^6
Remote	REM	65.95°	164.58°	358	Basalt	6.9×10^5
Tatalina	TTA	62.93°	156.06°	914	Sedimentary	1.0×10^5
Tin City	TNA	65.56°	167.92°	76	Beach deposits	2.4×10^5
Savoonga	SVG	63.69°	170.48°	15	Beach deposits	6.7×10^5

TABLE 2

P-wave Velocity Structure of the Crust and Upper Mantle
Used to Compute Travel Times for Hypocenter Locations

Layer Thickness (km)	P-Wave Velocity (km/sec)
24.4	5.9
15.8	7.4
35.8	7.9
225.0	8.29
244.0	10.39
∞	12.58

Table 3

Location details of earthquakes located on and around Seward Peninsula during 1979 by the local seismographic network.

Date	Origin	Time	Lat(N)	Long(W)	Depth (km)	Mag. (M_L)	No.	GAP (°)	DMIN (Km)	RMS (See)	ERH (Km)	ERZ (Km)
790101	10 2	10.41	63-52.55	164-39.66	10.00*		4	306	83.7	0.72		
790101	1624	12.18	65-33.99	165-28.13	10.00*		4	118	90.8	9.83		
790103	150	44.22	65-18.05	166-20.31	10.00*	2.70	3	149	58.8	0.00		
790103	331	40.81	65- 0.77	161-13.94	10.00*	1.64	3	265	124.3	0.25		
790107	1031	5.41	64-21.25	162-25.77	10.00*	1.32	3	158	99.7	2.34	751.8	
790108	1149	18.03	65-35.75	163-46.41	10.00*	1.36	5	210	86.9	1.01		
790106	1545	32.77	63-28.84	157-55.68	10.00*	3.09	4	146	113.9	0.63	12.6	92.9
790110	2 9	40.86	64-56.09	165-41.56	10.00*	2.94	4	151	44.5	0.64		
790110	438	15.02	64-56.30	165-41.03	10.00*	1.50	4	150	44.8	0.64		
790110	440	31.85	64-55.57	165-43.49	10.00*	1.91	4	154	44.2	0.89	46.7	54.6
790111	826	35.21	64-22.50	166-51.05	10.00*	2.47	3	274	74.1	3.01		
790111	915	22.38	64-48.45	165-34.92	10.00*	1.46	3	154	29.4	0.78	4.5	5.0
790115	2255	57.42	65-26.55	166-58.96	10.00*	2.00	5	160	24.9	1.37	126.7	176.5
790117	2332	55.40	66-50.19	163- 3.20	10.00*	3.29	6	215	19.6	0.00		
790118	16 3	14.54	65-45.36	165-25.38	10.00*		3	180	95.0	0.00		
790121	1350	40.23	65- 9.20	164-44.89	10.00*	2.17	3	151	72.4	1.04		
790124	16 4	26.51	64-11.87	161-35.03	10.00*	1.09	4	283	187.0	1.53	162.4	233.7
790126	517	24.72	65- 5.07	165-37.51	10.00*	3.09	5	134	59.7	0.91		
790126	558	44.03	65-12.29	159-59.49	10.00*	2.19	4	226	127.0	1.26		
790126	856	54.02	63-20.25	157-43.05	10.00*	2.25	4	221	159.5	0.00		
790126	12 0	14.17	65- 0.36	165-14.37	10.00*	2.39	3	174	50.1	0.00		
790126	1444	0.04	64-14.43	158-39.56	10.00*	1.93	3	152	105.7	0.69	6.9	7.9
790128	434	18.02	65-17.18	166-22.42	10.00*	3.52	9	152	58.2	0.01		
790130	736	43.47	66-55.78	170-12.95	10.00*	1.73	3	312	333.2	0.93		
790207	1510	39.94	65-20.95	167-39.75	10.00*	3.37	3	255	25.9	0.11		
790212	1038	29.23	64-27.21	162-21.39	10.00*	2.45	3	147	102.7	0.78	229.9	485.1
790212	19 1	58.74	65- 2.61	164-20.42	10.00*	2.11	5	145	72.8	4.64		
790214	1016	5.88	66-32.08	161-52.85	10.00*	3.16	4	210	48.0	2.44	50.7	29.1
790214	1946	8.83	67- 7.41	154-37.40	10.00*	1.78	6	313	331.6	0.34		
790218	1236	50.32	65-14.15	162-25.29	10.00*	3.11	4	131	104.0	0.48		
790221	22 3	36.72	64-47.71	165-14.93	10.00*	1.77	4	117	26.8	0.52	3.4	4.5
790222	037	14.14	66- 9.24	163-44.45	10.00*	2.28	6	204	39.4	0.00		
790222	21 7	6.03	65- 6.03	165-10.65	10.00*	0.92	3	107	61.0	3.38	51.9	83.9
790223	11 6	46.64	65-46.04	165-50.46	10.00*	1.89	5	152	76.8	0.73	9.6	9.8
790223	1437	17.86	64- 6.15	163-57.96	10.00*	1.64	5	209	85.0	1.06	0.8	0.6
790223	1724	33.34	65-45.70	165-57.59	10.00*	2.50	6	155	71.4	1.02	12.7	14.0
790224	1614	20.21	65-46.09	165-53.72	10.00*	2.15	5	154	74.5	0.62	6.6	6.7
790301	1631	36.31	64- 4.57	165-12.22	10.00*	1.95	7	165	54.5	0.84	10.4	11.0
790308	1815	58.01	64-58.68	164-15.44	10.00*	2.90	5	104	70.5	1.02	11.6	20.1
790310	22 1	4.34	67- 3.15	163-11.04	10.00*	1.72	3	275	33.1	0.27		
790311	513	3.18	64-57.05	161-50.25	10.00*	0.75	4	166	130.0	9.39		
790314	1619	14.69	66- 5.36	163-42.31	10.00*	1.55	4	163	44.5	0.70		
790321	1051	1.32	66-19.20	162-33.68	10.00*	1.48	3	150	46.8	0.00		
790321	1439	33.40	65- 3.75	161-32.17	10.00*	0.80	3	165	117.4	0.00		
790324	0 2	20.72	65- 0.06	162-17.19	10.00*	1.58	6	135	127.5	1.34	11.6	190.0
790403	944	12.68	65- 1.54	165- 9.64	10.00*	2.33	5	138	52.9	2.93	48.1	88.2
790403	2236	58.69	66-51.14	163-19.64	10.00*	1.33	4	217	31.4	0.34		
790407	1117	59.94	65-47.32	162-27.26	10.00*	1.99	4	180	51.3	0.32		
790409	1510	4.61	68-11.89	166-10.25	10.00*	1.99	4	304	213.3	0.53	55.4	90.3
790409	1919	38.85	64- 5.98	164- 3.98	10.00*	2.74	6	211	81.3	0.32	2.9	2.2
790411	036	18.16	65-13.25	162-53.57	10.00*	2.30	5	184	114.7	0.00		
790411	1324	51.27	66-31.94	157-32.95	10.00*	1.42	3	211	181.2	0.00		
790411					10.00*	2.84	3					

Date	Origin	Time	Lat(N)	Long(W)	Depth (km)	Mag. (M _L)	No.	GAP (°)	DMIN (Km)	RMS (See)	ERH (Km)	ERZ (Km)	
790413	820	23.50	65-	8.38	162-54.90	10.00*	1.71	4	114123.2	0.75			
790414	459	58.16	64-59.72	165-34.65	10.00*	2.02	3	150	49.5	0.01			
790414	1610	54.49	65-35.01	161-33.67	10.00*	1.66	6	172	59.3	2.43	40.9	49.9	
790414	1719	51.61	64-47.72	165-28.02	10.00*	1.67	4	143	26.6	1.08			
790414	1848	32.93	67-31.38	158-	2.13	10.00*	4.10	5	244314.5	16.46	742.9		
790414	19	1	53.36	64-46.55	165-15.55	10.00*	1.39	4	118	24.6	0.50		
790415	1316	30.06	64-48.38	165-13.77	10.00*	1.45	4	145	28.3	0.81			
790416	2042	35.16	64-55.64	163-28.74	10.00*	1.42	3	213	99.1	0.02			
790417	1325	39.67	64-30.45	165-27.66	10.00*	0.86	4	277	7.3	1.52			
790430	2124	15.31	65-26.52	168-24.08	10.00*	2.00	4	214	46.6	0.78			
90506	2351	2.72	64-11.68	170-24.63	10.00*	3.33	4	322207.5	1.44				
90513	436	12.56	65-53.37	160-23.51	10.00*	1.92	4	177146.6	9.17				
90515	1724	34.08	65-15.54	168-51.09	10.00*		5	215	73.9	0.44	3.9	3.0	
90515	1742	18.03	65-12.25	168-45.22	10.00*		5	210	73.0	0.66	6.8	4.8	
90515	1844	56.02	65-20.99	168-45.23	10.00*	2.80	3	225	65.4	0.00			
90516	1332	16.99	64-45.38	165-27.17	10.00*	1.49	3	156	22.2	0.00			
90517	239	36.97	64-24.15	162-31.81	10.00*	2.14	5	155106.7	1.34	224.2	467.0		
90517	1153	13.33	65-30.47	169-	2.80	10.00*	3.08	5	224	74.7	2.97	48.5	32.8
90521	1359	26.92	65-	2.55	168-47.39	10.00*	2.27	5	199	85.6	3.61	60.7	47.4
90526	553	53.89	66-49.79	163-42.92	10.00*		3	235	48.7	0.03			
90526	744	37.52	67-	7.33	164-18.78	10.00*	2.27	5	253	79.9	0.32	12.1	5.6
90527	140	6.19	65-14.51	170-31.55	10.00*	2.69	5	247147.9	2.31	81.4	360.1		
90529	1125	22.56	65-24.10	167-57.67	10.00*	1.87	4	201	30.1	0.64			
90529	1650	25.05	67-36.98	164-18.64	10.00*	2.82	5	288112.1	0.03	3.4	1.0		
90530	3	0	28.91	66-44.32	162-31.87	10.00*	1.05	3	254	13.7	0.34		
90530	1329	16.06	66-53.03	163-39.99	10.00*		4	225	46.3	0.08			
90601	838	47.26	64-58.37	165-13.86	10.00*		3	176	46.5	0.00			
90601	1422	7.15	65-19.93	161-47.81	10.00*		4	174165.9	0.41				
90602	834	31.17	65-22.12	163-	1.42	10.00*	4	139125.7	0.15				
90616	6	4	46.19	65-23.61	168-47.15	10.00*	2.87	3	230	65.2	0.09		
90617	1449	13.11	64-44.89	161-26.42	10.00*	2.94	4	276188.7	2.69				
90620	2235	22.56	67-25.53	165-36.91	10.00*	3.05	3	275133.0	0.11				
90621	312	53.40	65-26.75	168-11.95	10.00*	2.29	4	211	37.6	1.64			
90622	521	19.50	65-36.84	165-44.98	10.00*	1.02	3	136	78.1	0.00			
90623	1617	58.23	68-46.99	175-16.46	10.00*	4.27	4	335494.0	0.50				
90624	1159	41.11	67-10.89	169-12.34	10.00*	3.24	5	269197.1	0.24	10.2	43.4		
90626	118	8.14	66-17.56	166-17.39	10.00*	2.37	3	216	79.4	0.07			
90703	1921	5.45	65-	3.95	163-58.20	10.00*		3	240	87.2	0.00		
90708	2112	31.78	65-18.24	164-37.62	10.00*	0.78	3	175	90.1	0.20			
90712	954	52.88	65-15.75	166-49.06	10.00*	1.72	6	180	44.1	1.00	29.6	24.1	
90714	5	9	53.26	64-55.52	160-24.16	10.00*		3	241237.8	0.16			
90719	1728	49.40	66-41.70	162-48.02	10.00*	2.00	3	214	19.9	0.56			
90723	1246	14.59	66-	5.33	167-44.98	10.00*	2.61	3	274	60.5	0.48		
90724	112	56.31	64-44.80	165-15.71	10.00*	1.53	3	183	21.4	0.00			
90724	1522	54.85	65-57.42	167-31.80	10.00*	2.16	5	216	44.2	0.52	14.8	10.3	

Date	Origin	Time	Lat(N)	Long(W)	Depth (km)	Mag. (M _L)	No.	GAP (°)	DMIN (Km)	RMS (See)	ERH (Km)	ER (K)
790726	1110	4.59	66-13.13	163-42.70	10.00*	0.70	3	168	37.8	0.01		
790730	418	34.45	67-19.84	165-14.96	10.00*	1.75	3	268	117.9	0.06		
790731	6 1	54.75	65-54.28	166-18.19	10.00*	2.41	3	187	64.6	0.00		
790802	819	10.31	64-44.40	165- 4.07	10.00*	1.62	3	208	24.7	0.00		
790804	2013	19.54	65- 3.67	160-17.67	10.00*	1.99	3	285	226.2	1.11		
790808	448	44.47	66-28.93	164-18.89	10.00*		3	187	21.0	0.09		
790816	058	11.86	65-27.12	163-18.48	10.00*	1.42	3	213	110.8	0.00		
790816	1944	21.50	65-19.71	163- 2.45	10.00*	2.17	3	226	129.0	0.10		
790817	10 5	58.31	66- 3.46	165-13.56	10.00*	1.84	3	226	42.6	0.18		
790818	1644	44.26	64-53.65	162-45.41	10.00*	2.35	4	136	130.1	0.24		
790820	4 0	56.45	65-26.59	158-58.16	10.00*		15	112	191.0	12.47	54.0	687.
790901	151	42.87	64-49.97	165-21.15	10.00*	2.55	5	128	30.4	1.36	27.9	35.
790901	349	29.87	64-52.45	164-48.82	10.00*	2.33	6	98	43.9	0.96	10.7	14.
790901	411	18.13	64-40.24	166-44.89	10.00*	2.36	5	236	67.1	0.91	37.9	15.
790903	439	6.00	65- 7.31	165- 3.88	10.00*	0.95	3	182	64.3	0.00		
790903	533	37.42	65-25.88	166-38.68	10.00*	1.01	3	143	39.5	0.00		
790905	920	30.80	65-31.48	163-49.79	10.00*	2.49	3	229	129.8	0.02		
790911	925	22.04	65- 2.59	162- 7.17	10.00*	2.34	6	158	145.7	1.10	3.5	42.
790914	143	4.97	65-15.02	163-28.94	10.00*		3	230	183.5	0.01		
790922	036	47.84	64-38.42	164-20.94	10.00*	1.91	3	145	49.7	0.00		
791012	1649	40.17	65-35.46	166-40.20	10.00*		3	146	35.5	0.00		
791015	713	48.41	65-35.25	166-34.11	10.00*		3	143	40.2	0.00		
791021	411	42.93	66-44.91	162-57.40	10.00*	0.86	3	176	19.4	0.01		
791024	2219	33.66	65-14.30	164-20.77	10.00*	2.26	8	82	89.8	1.93	12.9	22.0
791025	615	8.79	65-43.87	165- 1.13	10.00*	1.74	5	119	68.7	1.37	35.9	42.0
791025	712	46.13	66- 0.52	165-15.25	10.00*	0.95	3	161	47.3	0.01		
791027	033	29.56	64- 3.97	164- 8.14	10.00*	2.28	4	216	81.2	0.45		
791028	527	16.97	65-14.74	164-51.52	10.00*	1.13	6	89	80.2	1.93	11.4	20.0
791029	1513	37.50	65-21.10	165-20.73	10.00*	1.65	6	103	88.3	2.70	50.2	83.2
791101	653	48.19	64-16.92	163-22.18	10.00*	2.73	4	198	138.2	0.09		
791103	2326	29.76	66-16.17	166-42.11	10.00*		3	244	85.7	0.47		
791104	436	58.59	64-49.21	166-54.22	10.00*		3	232	78.7	0.01		

ANNUAL REPORT

Contract: 03-5-022-56
Research Unit: 530
Reporting Period: 4/1/79 - 3/31/80
Task Order: 34
Number of Pages: 14

THE ENVIRONMENTAL GEOLOGY AND GEOMORPHOLOGY OF THE BARRIER ISLAND - LAGOON
SYSTEM ALONG THE BEAUFORT SEA COASTAL PLAIN FROM PRUDHOE BAY TO
THE COLVILLE RIVER

Principal Investigator:

Dr. P. Jan Cannon
Assistant Professor of Geology
Geology/Geophysics
University of Alaska
Fairbanks, Alaska 99701

Research Assistant:

Stuart E. Rawlinson

March 31, 1980

CONTENTS

Task Objectives.....	621
Activities.....	622
Results.....	623
Interpretation Of Results.....	626
References.....	634

LIST OF FIGURES

Figure 1. Terrain and landform map of the Beechey Point Quadrangle.....	628
Figure 2. Sand-silt-clay plot of terrain unit samples.....	629
Figure 3. Bivariant plot of lakes/10 km ² vs coarse/fine for terrain unit samples.....	629
Figure 4. Diagram showing the morphologic changes between 1955 and 1979 of Egg Island and Long Island.....	630

LIST OF TABLES

Table 1. Stratigraphic sections and textural characteristics of terrain unit sample localities.....	631
Table 2. Flaxman Formation K-Ar age dates.....	633

Project Title: The Environmental Geology and Geomorphology of the
Barrier Island - Lagoon System Along the Beaufort Sea
Coastal Plain from Prudhoe Bay to the Colville River.

I. Task Objectives

During FY 79 this investigation was part of the barrier island-lagoon studies; its purpose was to determine the geological and geomorphological environments of specifically, Simpson Lagoon and generally, the entire coast of the lease area. Remote sensing methods, supplemented with field observations, were used to determine geomorphic features of the islands and nearshore coastal plain, and to assess (1) possible hazards associated with features (e.g. instability, etc.), (2) possible impacts associated with petroleum development (e.g. construction of artificial gravel islands and causeways), and (3) resources (e.g. gravel).

During FY 80 this study will be completed by examining the morphology and stability of the Colville, Kuparuk, Sagavanirktok and Canning River deltas, and developing a comprehensive report describing the geomorphic history and probable future of the Alaskan Arctic coastal plain. The objectives are listed below.

1. Perform quantitative and qualitative analyses of the stability and morphology of the Colville, Kuparuk, Sagavanirktok and Canning River systems, emphasizing the deltas, and their influence on the coastline and offshore areas.
2. Perform an analysis of the timing and magnitude of drainage basin and alluvial valley discharges of water and sediment, and the

resulting influence on deltaic processes within the systems given above. The analysis includes identification of areas within the drainage basins and alluvial valleys that have the greatest influence on other parts of the systems.

3. Construct a comprehensive geomorphology of the Alaskan Arctic coastal plain using FY 80 results and others reported previously. This final report will contain, but not be limited to:
 - a. description and quantification, where possible, of the geomorphic processes active on the coastal plain and offshore areas;
 - b. the history of the landforms (islands, lagoon systems, lakes, river deltas, water courses, etc.);
 - c. the projected future of these landforms in the absence of external (man-made) influences; and
 - d. an estimate of the influence of petroleum development (using scenarios described in the OCS draft environmental impact statement) on the projected future of landforms as described in "c."

II. Activities

Activities this quarter were:

1. textural analyses of terrain unit samples;
2. enlargement to 1:25,000 of 1955 and 1979 aerial photographs of the Simpson Lagoon area and other selected localities along the coastal plain;
3. contact-printing of available photography of the Colville, Kuparuk, Sagavanirktok and Canning River deltas, and construction of nine photomosaics;

4. synthesis of geological literature;
5. transference of published geological maps to a 1:500,000 base map;
6. receipt of a K-Ar date of a rock from the Flaxman Formation which was submitted last quarter; and
7. writing of a second draft of a paper reviewing the origin of the Flaxman Formation.

III. Results

Textural analyses of samples collected in various terrain units are briefly mentioned in the quarterly reports for the periods ending September 30, 1979 and December 22, 1979. These analyses determine the weight percent of sand, silt, and clay in each sample according to procedures in Royse (1970).

Figure 1 shows part of the Beechey Point Quadrangle terrain map and the sample localities within each unit. At each locality the tundra mat was removed and a 0.4 m square pit dug until ground ice was encountered. At localities where ground ice was beyond a depth attainable by digging, a steel coring tube was driven into the sediment until contacting ground ice. The tundra mat was replaced after sampling and documentation.

Table 1 shows the stratigraphic section at each sample locality and lists textural characteristics of the samples, surface conditions, and remarks. The sediment nomenclature shown in Table 1 is based on Shepard (1954), a classification which utilizes the 20, 50, and 75 percentiles of sand, silt, and clay (Figure 2). Silty-sand (38%) is the dominant sediment followed by san-si-cl (29%), and then clayey-silt (19%). Sandy-silt, silt, and silty-clay each represent 5% of the total samples.

The mean number of lakes per 10 km^2 was measured within each sampled terrain unit to determine if the surface density and morphology of lakes are controlled, at least in part, by the substrate. A circle representing 10 km^2 was overlaid on the mapped terrain unit and the number of lakes within the circle counted. In units sufficiently large, several counts were made and a mean value determined. The histogram in the top right corner of Figure 3 shows the mean number of lakes in each type of terrain unit. It is assumed that within each terrain unit, except High Density Small Lakes (HDSL), the full range of lake sizes is represented. Because the HDSL unit is differentiated on the bases of lake size and number, the histogram shows a large number of small lakes. Ideally, the ratio of area of water to area of land should be used to express the surface density of lakes. Alternatively, the surface density of lakes should be weighted according to the mean lake size within each terrain unit.

These latter two methods for expressing lake surface density, however, require considerable time. It is felt that the method used provides a reasonable approximation of lake surface density, although future work will include areas of water and land measurements. Also note that the classification of terrain units is qualitative and based on visual differences. Consequently, overlap occurs in the mean numbers of lakes and is evident in the histogram. Work is proceeding to quantify the units and delineate new boundaries.

Figure 3 is a bivariant plot of lakes/ 10 km^2 versus percent coarse/percent fine. In the latter ratio, coarse is sands and pebbles, and fine is silts and clays. The distribution of sample points is confined to the area bounded by the dashed diagonal line. Open points involve the mean coarse/fine value of two samples from the indicated sample location.

Enlargements to 1:25,000 of 1955 and 1979 photographs of the study area indicate little change in some areas and considerable change in others. Figure 4 superimposes 1955 and 1979 photographs of Long Island (upper left), the Egg Island channel, and Egg Island (lower right). Relatively little change is noted on the southeast end of Long Island. Contrarily, considerable change is noted in the channel islands and Egg Island. Several channel islands show net westward movement. Egg Island is now segmented, and each segment is recurved. The western end of the island has rotated clockwise about 25 degrees and westward spit development is marked. Changes here and elsewhere in the study area are currently being documented and quantified.

Geomorphic mapping and comparative studies between 1955 and 1979 photomosaics of the deltas are not yet started. No results concerning this aspect of the study are included this quarter.

Literature syntheses this quarter produced two draft reports. These reports outline the bedrock and surficial geology within the Kuparuk River and Colville River drainage basins. Also, a 1:500,000 composite geologic map of the drainage basins under study was synthesized from published sources. These syntheses, in addition to a draft report on the bedrock and surficial geology within the Canning River and Sagavanirktok River drainage basins produced last quarter, will aid: (1) identification of heavy mineral suites, (2) the provenance of these suites, and (3) the transport history of sediments within the drainage basins.

Last quarter a sample of pink granite (F79SR01) from the Flaxman Formation was submitted to the University of Alaska geochronology laboratory. Results are given in Table 2. In addition to the sample submitted for dating by this research unit, R.U. 529 (P.I.-Naidu)

submitted a similar sample (FLX1, shown in Table 2). The first draft of a paper reviewing the origin of the Flaxman Formation has been critically read; a second draft is in progress.

IV. Interpretation Of Results

Interpretations here are concerned primarily with the terrain map and implications of the K-Ar date on the origin of the Flaxman Formation. The degree of completion of other aspects of the study precludes interpretation at this time.

The terrain map of the Beechey Point Quadrangle (Figure 1) is primarily an evaluation of the ability to determine coastal plain substrates, and thus the relative stabilities, based on talik lakes and ground wetness. The orientation, size, and ground density of talik lakes, in addition to the relative wetness of the land surface are at least in part influenced by the grain size of the coastal plain surficial deposits, and the depth to ground ice.

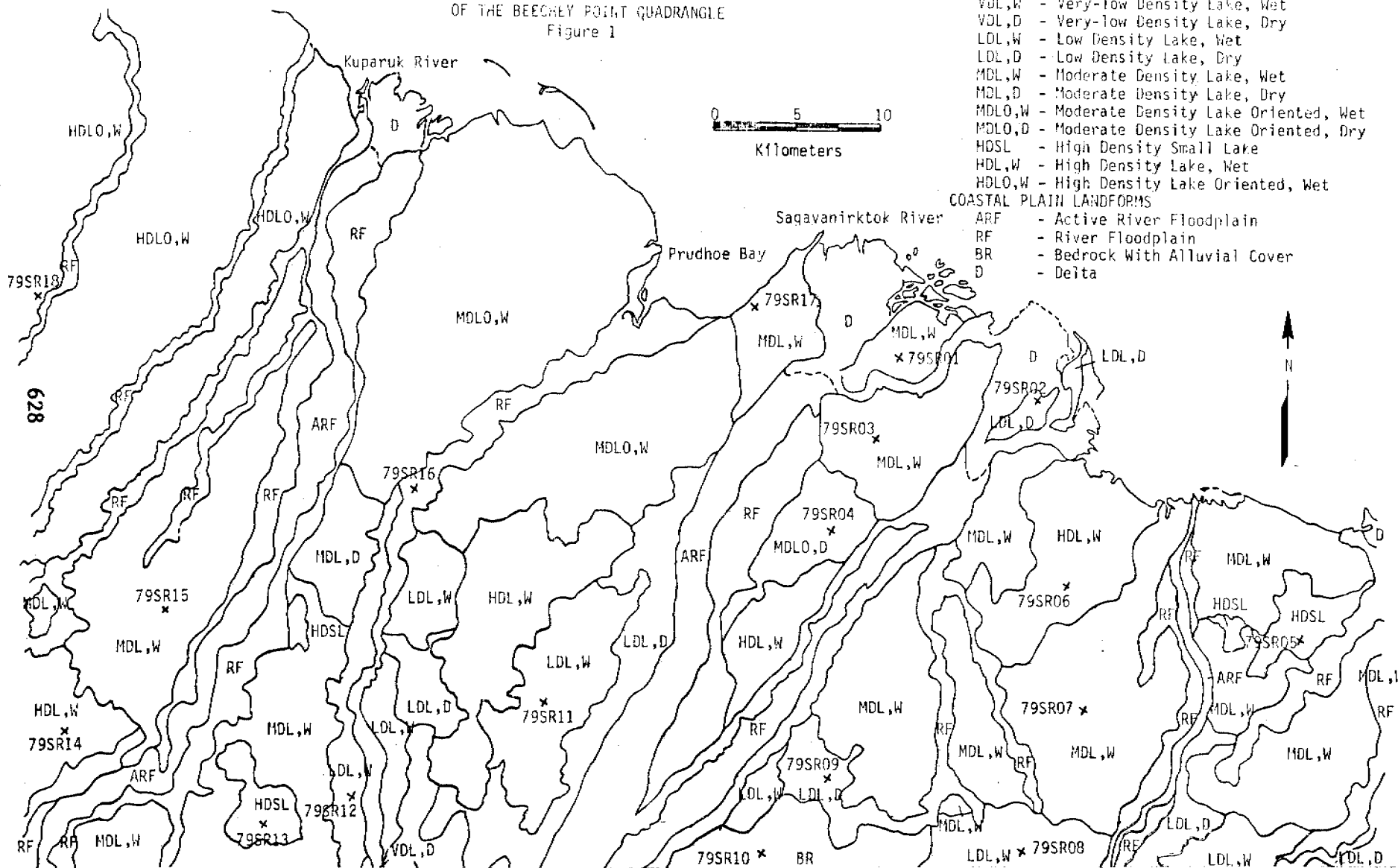
Figure 3 shows a random distribution of lake densities in substrates containing less than about 50 percent sand, with the exception of sample localities 5 and 13, which are within the HDSL terrain unit. These latter two sample localities have almost no sand and the depth to ground ice is less than 0.3 m (Table 1). Figure 3 also suggests a linear decrease in the density of surface lakes in substrates with sand contents increasing from about 50 percent. Table 1 indicates that clear ice is generally close to the surface in substrates containing small amounts of sand and relatively large amounts of silt and/or clay.

Precise substrate determination based on the density and morphology of surface lakes is not yet realized, but the concept is viable and should not be abandoned. Study is continuing, especially to determine better methods to

quantify the various parameters.

A 2.4 billion K-Ar date for the pink granite of the Flaxman Formation constrains the possible source areas. It definitely eliminates the Brooks Range and suggests an easterly source. Review of possible source areas is in progress. The Precambrian crystalline shield of interior Canada contains pink granites, as does the Canadian Archipelago. Age dates for the interior have not yet been synthesized, however, Naidu (1979, personal communication) reports published K-Ar dates similar to those reported here for granites in the Coronation Gulf area of the archipelago. Precambrian granites also crop out in northwestern Greenland from Melville Bugt north to Bache Peninsula, however, reported K-Ar dates range only from 1.6 to 1.9 b.y. (Escher and Watt, 1976). The possible sources suggest glacial or glacial-ice rafting transport mechanisms.

TERRAIN AND LANDFORM MAP
OF THE BEECHLEY POINT QUADRANGLE
Figure 1



COASTAL PLAIN TERRAIN (LAKE BASED)

- VDL,W - Very-low Density Lake, Wet
- VDL,D - Very-low Density Lake, Dry
- LDL,W - Low Density Lake, Wet
- LDL,D - Low Density Lake, Dry
- MDL,W - Moderate Density Lake, Wet
- MDL,D - Moderate Density Lake, Dry
- MDLO,W - Moderate Density Lake Oriented, Wet
- MDLO,D - Moderate Density Lake Oriented, Dry
- HDSL - High Density Small Lake
- HDL,W - High Density Lake, Wet
- HDLO,W - High Density Lake Oriented, Wet

COASTAL PLAIN LANDFORMS

- ARF - Active River Floodplain
- RF - River Floodplain
- BR - Bedrock With Alluvial Cover
- D - Deita

Figure 2

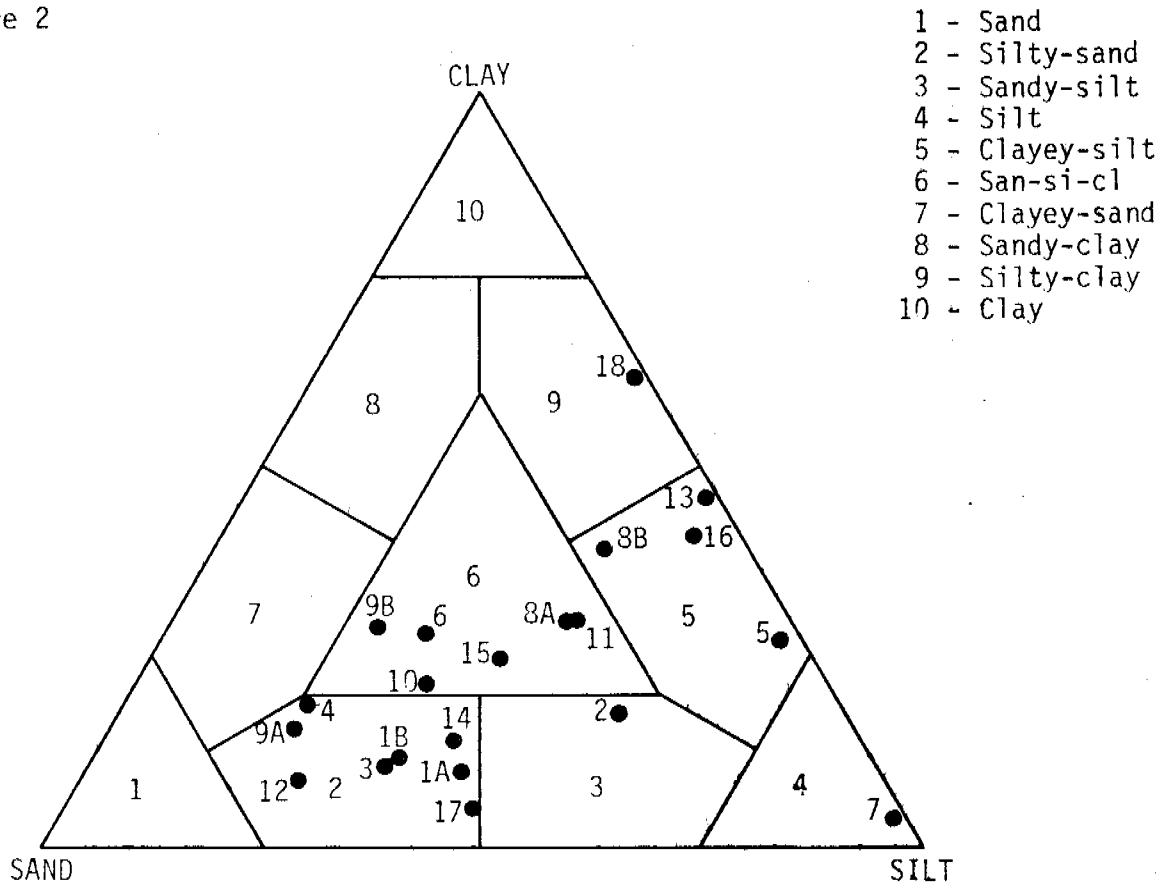
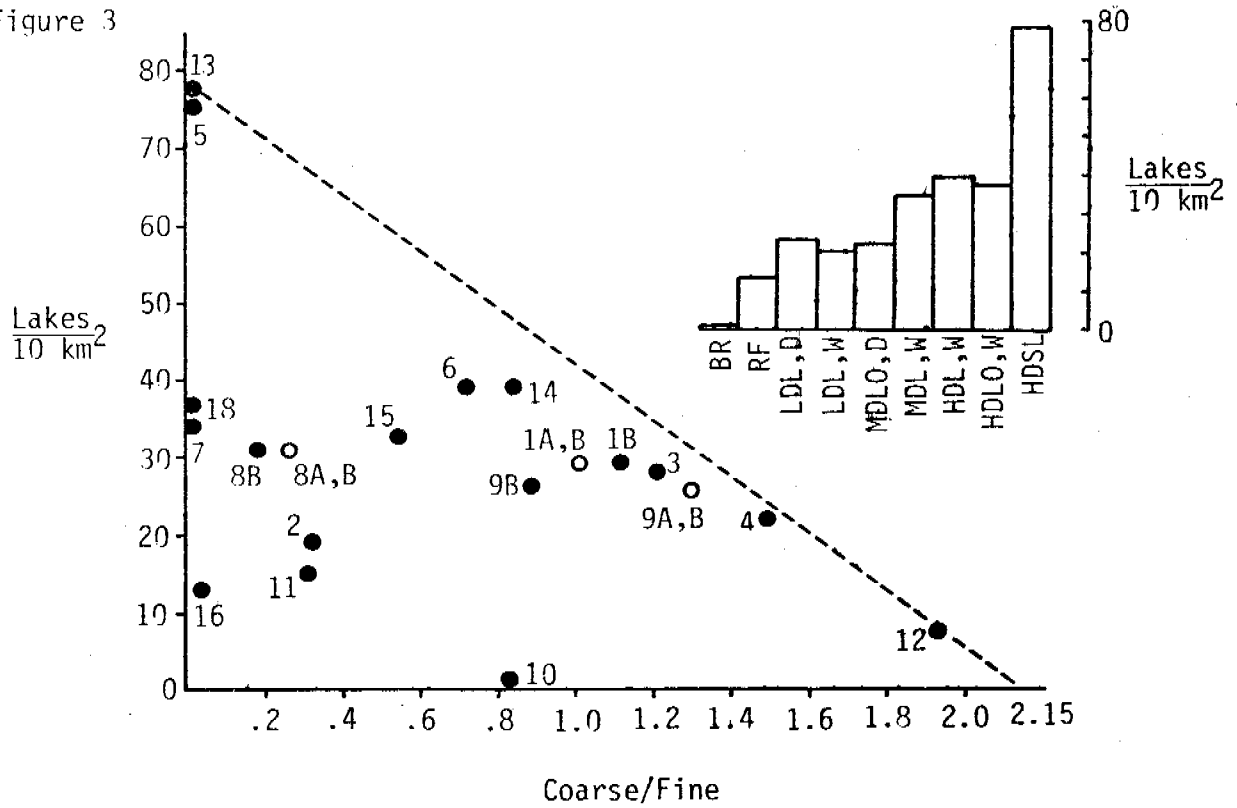
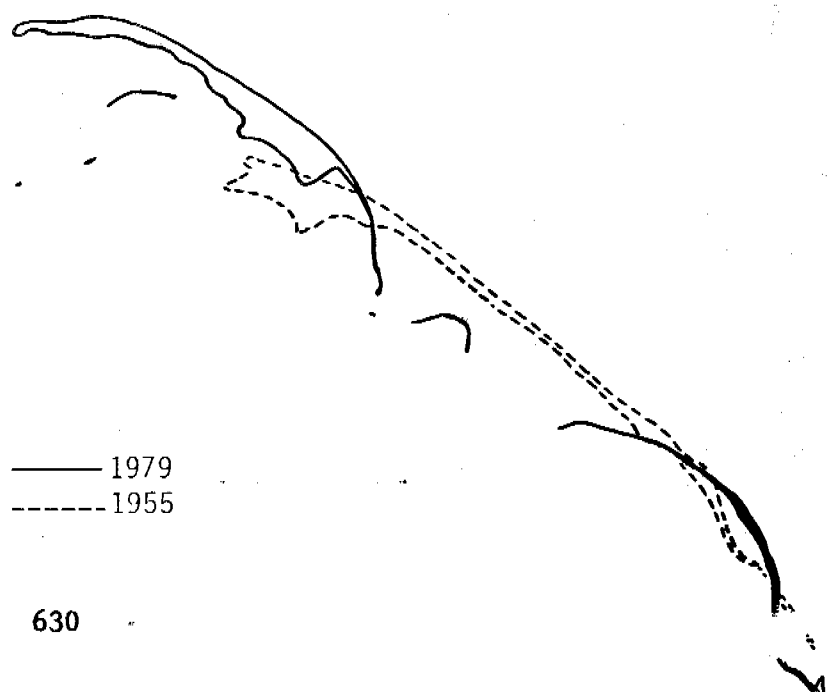
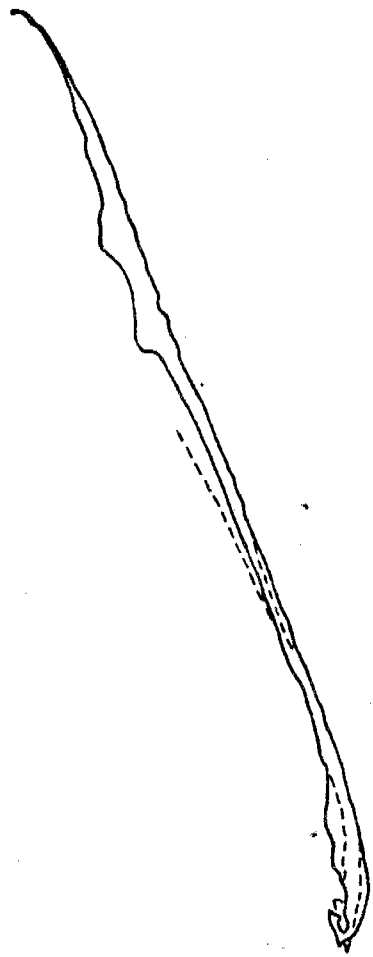


Figure 3





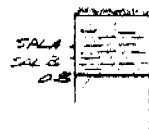
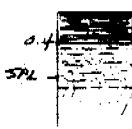
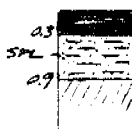


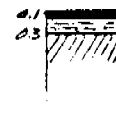

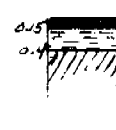
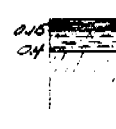
0 1
Kilometer

— 1979
- - - 1955

630

Figure 4

TABLE 1 - STRATIGRAPHIC SECTIONS AND TEXTURAL CHARACTERISTICS

LOCATION	DEPTHS IN METERS		PERCENT SAND - SILT - CLAY	COARSE/FINE	LAVES/100CM ²	SURFACE COND - REMARKS
	SPAT.	UNIT				
79SR01		A. GRASS SAND	47-43-10	0.89	29	SAND w/ GRASS
		B. SILTY-SAND SILT ICE	53-35-12	1.13		MOL, W
79SR02		A. PEAT SOIL	25-58-18	0.33	19	NET, w/ TUNDRA SILT INC. @ BASE OF TUNDRA LOL, D
		B. SILTY-SAND				
		C. ICE (?)				
79SR03		A. PEAT SOIL	55-34-11	1.22	28	DAMP, SANDY MOL, W
		B. SILTY-SAND				
		C. ICE				
79SR04		A. PEAT SOIL	60-21-19	1.50	22	TUNDRA FIBER NO TUNDRA MAT SOME FIBRILES MOL, D
		B. SILTY-SAND				
		C. ICE				
79SR05		A. PEAT SOIL (CLAY-SILT)	2-71-27	0.02	70	ICE DIRECTLY @ BASE OF TUNDRA VERY NET MOL
		B. ICE				
79SR06		A. PEAT SOIL	42-30-28	0.72	39	TUNDRA - GRAVEL MOL, W
		B. SAND-SILT-CLAY ICE				
79SR07		A. PEAT SOIL (SILT)	1-94-4	0.01	34	TUNDRA THICK 0.4m HIGH AREAS w/ TUNDRA SAMPLED ICE BELOW TUNDRA MOL, W
		B. ICE				
79SR08		A. SAND-SILT-CLAY	A. 25-45-30	0.33	31	TUNDRA MAT 0.15m LOL, W
		B. CLAY-SILT ICE				
79SR09		A. PEAT SOIL SILTY-SAND	A. 63-21-16	1.70	26	TUNDRA RELATIVELY DRY LOL, D
		B. SAND-SILT-CLAY ICE				

631

* CLOSE TO SILTY-SAND CINDER -

TABLE 1 - CONT.

LOCATION	STRAT	UNIT	SAND-SILT-CLAY	COARSE/FINE	LAKES/100M ²	SURFACE COND. REMARKS
79SR10	0.2 SPL 0.9	PEAT SOIL SAND-SILT-CLAY w/ GRAVEL ICE	45-33-22	0.84	1	BR w/ ALLUVIAL COVER
79SR11	0.1 1.0 SPL	PEAT SOIL SAND-SILT-CLAY ICE	24-47-30	0.32	15	LOL, W
79SR12	0.2 0.85 SPL	PEAT SOIL SILTY SAND w/ GRAVEL ICE	54-25-9	1.94	13	CONTAINS GRAVEL LOL, W
79SR13	0.3 SPL	TUNDRA CLAYE-SILT PEAT SOIL ICE	1-52-44	0.02	79	ICE SHALLOW LAYERED ORGANIC MSSL
79SR14	0.05 0.6 SPL	TUNDRA (GRASS) SILTY SAND ICE	46-40-14	0.85	39	TUNDRA w/ GRASS HOL, W
79SR15	0.05 0.6 SPL	TUNDRA SAND-SILT-CLAY ICE	35-39-25	0.55	33	MAL, W
79SR16	0.05 0.3 SPL	TUNDRA CLAYE-SILT ICE	5-54-41	0.05	13	RE OVERRANK SITE?
79SR17	1.0 SPL	TUNDRA (GRASS) SAND-SILT-CLAY LIMIT OF CORAL	48-47-5	0.92	34	GRASS, FOLIAGE COVER NO ICE TO 1M LAKE MESH FOR MOL, W ARETS
79SR18	0.1 SPL	PEAT SOIL SILT-CLAY ICE	1-37-62	0.01	37	SURFACE WET HOL, W

Table 2 - Flaxman Formation K-Ar age dates.

OCS - Granite Boulders From Arctic Coast

Sample No.	Rock Type	Mineral Dated	K ₂ O (weight percent)	Sample Weight (grams)	⁴⁰ Ar _{rad} (moles/gm) x 10 ⁻⁶	$\frac{^{40}\text{Ar}_{\text{rad}}}{^{40}\text{K}}$ x 10 ⁻¹	$\frac{^{40}\text{Ar}_{\text{rad}}}{^{40}\text{Ar}_{\text{total}}}$	Age ± 1 σ (b.y.)
FLX1 (80013)	Granite	Muscovite	10.753 10.760 10.760 $\bar{x} = 10.758$	0.0999	6.05	2.27	0.981	2.08 ± 0.06
*FLX1 (80035)	Granite	Muscovite	10.753 10.760 10.760 $\bar{x} = 10.758$	0.0371	6.79	2.55	0.966	2.22 ± 0.07
*79 SR01 (80032)	Granite	Muscovite	10.743 10.757 10.743 $\bar{x} = 10.748$	0.0333	7.97	2.99	0.992	2.43 ± 0.07

* Duplicate

REFERENCES

- Escher, A. and W.S. Watt (eds), 1976, Geology of Greenland: Geological Survey of Greenland, Copenhagen, 603p.
- Royse, L.F., 1970, An introduction to sediment analysis: Arizona State University, Tucson, 180p.
- Shepard, F.P., 1954, Nomenclature based on sand-silt-clay ratios: Jour. Sed. Petrology, V. 24, p. 151-158.

Technical Report Submitted to
National Oceanic and Atmospheric Administration
OCSEAP

by

The University of Texas Marine Science Institute
Galveston Geophysics Laboratory
700 The Strand
Galveston, Texas 77550

COORDINATED OCEAN BOTTOM SEISMOGRAPH MEASUREMENTS
IN THE KODIAK SHELF AREA

Contract No. NA 79 RAC 00077

1 April, 1979 - 31 March, 1980

Principal Investigator

Co-Investigators

Dr. Gary V. Latham 191-28-6294
Associate Director
Geophysics Laboratory
Marine Science Institute
The University of Texas at Austin
700 The Strand
Galveston, TX 77550

Dr. H. James Dorman 311-22-7051
Dr. Abou-Bakr K. Ibrahim 458-07-2318

Tel.: (713) 765-2173

COORDINATED OCEAN BOTTOM SEISMOGRAPH MEASUREMENTS
IN THE KODIAK SHELF AREA

Introduction

Many special working groups and panels have pointed out the need for measurements of sea floor accelerations caused by potentially damaging earthquakes in offshore zones of oil and gas potential. The Alaska continental shelf is currently the most important example of such a zone within U. S. Territory. There is also a need for recording micro-earthquakes to increase the data set available for earthquake risk assessment and to delineate active faults that may transect zones of economic interest.

A low-cost seismic station for recording earthquakes on the sea floor has been developed at the University of Texas, Marine Science Institute, and has been used extensively over the past four years.

A system for recording strong-motions of the sea floor caused by earthquakes has also been developed and field tested as part of a collaborative effort between Exxon Production Research Company (EPR), the University of Texas-Marine Science Institute (UT-MSI), and the National Oceanic and Atmospheric Administration (NOAA). Operational systems can be constructed at relatively low-cost (less than \$10,000 per station), can operate on the sea floor for one year or more with minor modification, and can be deployed and retrieved from relatively small vessels. A recoverable preload system designed to imbed a set of vertical spikes attached to the base of the frame that serves as a pier for the ocean bottom station, has also been developed. Theoretical and experimental studies show that the ocean bottom station is capable of recording

ground accelerations of up to about 1 g, in the 0.1 Hz to 10 Hz frequency band, with good fidelity (Steinmetz et al., 1979).

Field operations using a combination of microearthquake and strong-motion seismograph stations during the first year of the present program (1979-1980), and initial results, are described in the following sections of this report.

History of Program to Date

The design and testing of various types of ocean bottom seismic (OBS) stations has been a principal activity of the University of Texas-Marine Science Institute since its beginning in 1972. In 1978, the Exxon Production Research Company (EPR) awarded a contract to MSI to begin development of a 3-axis digital system capable of recording strong-motions of the sea floor. Members of the EPR research staff undertook the task of investigating techniques for obtaining adequate ground coupling in marine sediments.

Three prototype stations were installed off Kodiak, Alaska in the Fall of 1978. These were successfully recalled by acoustic command after about 1 month of operation. Five additional strong-motion stations were constructed during the Spring of 1979 with the financial support of Exxon. During the following June (1979), under the sponsorship of the NOAA/OCSEAP program, all of the 8 strong-motion OBS stations, and 11 high-gain OBS (microearthquake) OBS stations were deployed off Kodiak Island from the NOAA ship DISCOVERER at locations shown in Figure 1. Three additional strong-motion stations, modified for land use, were installed on neighboring islands in close proximity to the offshore network. The stations of the high-gain network were recovered in August of 1979. Several of the strong-

motion stations were recovered and redeployed during cruises in August and October, 1979. In the October exercise, 4 strong-motion stations were left on bottom to be recovered the following spring. These were recovered in March of 1980. Thus, 12 successful recoveries of strong-motion station have been achieved out of 15 attempts. Of the three losses, 2 were sustained at sites with hard clay sediments. Damage to the stations on impact is suspected as the cause of their failure to return to the surface. Two premature releases have occurred, and this may account for the disappearance of the third station.

Despite these losses, we now feel that enough progress has been made toward understanding and eliminating design defects, that we can enter the program planned for 1980-81 with a high level of confidence.

Brief Description of Instrumentation

The UT/Exxon strong-motion OBS is described in recent papers by Steinmetz et al. (1979 and 1980). The high-gain station used in refraction studies and normal earthquake recording has been described by Latham et al. (1978).

We wish to emphasize at this point that the primary goals of the design effort for the strong-motion OBS stations were threefold: (1) to keep system cost low enough that deployment of extensive networks of stations would be feasible; (2) to minimize power drain to the point that operational life times of one year or more could be achieved on internal battery supplies; and (3) to keep size and weight to levels that would permit the use of small vessels in the deployment and retrieval operations. The first goal is paramount. It is evident that the probability of acquiring useful strong-motion data will increase with the number of stations deployed. Also, since the radiation pattern from an earthquake

focus is not uniform, measurements over a range of distances and azimuths are needed to properly define the spatial distribution of ground accelerations related to a given earthquake.

An ocean bottom station, in sea floor configuration, is shown in Figure 2. The complete system ready for deployment, including the preload system described below, is shown in Figure 3. The primary system elements are shown schematically in Figure 4.

The circular, spiked frame is 1.2 m in diameter and the complete station without preload, weighs 81.6 kg in air. The electronic subsystems, tape recorder, battery pack, and triaxial geophone accelerometers, are contained in a single, spherical pressure vessel made of a high strength glass capable of withstanding pressures of 700 kg/cm^2 (10,000 psi). The sphere is 43 cm in diameter and has a net positive buoyancy of 6.8 kg. The bottom hemisphere of the pressure vessel fits snugly into a molded plastic cap. Two small radio beacons, used in recovery, are mounted externally on the sphere. The geophones are mounted in the bottom of the sphere. The pressure vessel, with its plastic bottom cap, recovery radios, and internal components are retrievable and redeployable and are referred to as the return capsule. When deployed, the return capsule is firmly attached to the circular steel frame footing by a spring-loaded loop of stainless steel wire, as shown schematically in Figure 4. This wire is electrolytically dissolved on acoustic command (or clock timer) releasing the return capsule which then ascends to the ocean surface from its own positive buoyancy. The new mechanical link provides enough tension between the instrument package and support frame that 1.0 g of ground acceleration in both the vertical and horizontal directions can be experienced without relative movement between the frame and package.

Up to 33 adjustable spikes are affixed to the base ring to penetrate the sea floor. A large 680 kg tripod device; used as a preload, fits over the sphere with its base locking into the base of the steel footing. This is used to increase the terminal free fall velocity and mass of the system to achieve full penetration and seating of the footing into the sea floor. The preload is decoupled and retrieved after sensor deployment to avoid the undesirable dynamic effects of the additional preload mass. Following bottom impact, a timer initiates release of gas into the air bag shown in Figures 3 and 4. High pressure air displaces water within the bag, increasing buoyancy. When sufficient lift is achieved, the preload frame is decoupled and floats to the surface. A gyrocompass, attached to the preload frame, records the azimuthal orientation of the horizontal component sensors. A more detailed discussion of this device is given by Steinmetz et al. (1980).

The electronics subsystem of the SM-OBS consists of gain-ranging sensor amplifiers, shaping filters to give geophone outputs flat to ground acceleration, analog-to-digital converter, and two microprocessors with memory to perform the functions of event detection, data transfer to magnetic tape in digital format, and tape recorder control. The recording system is "triggered" on when the signal amplitude from any of the three geophones exceeds a preset acceleration threshold (usually 10^{-3} g). First data recorded corresponds to data entered into memory 5 sec before the trigger instant. This ensures preservation of the onset of the signal that produced the trigger. Data will continue to be recorded until the acceleration threshold is not exceeded in any 5 sec time window. A crystal controlled clock provides time words incorporated into the header

of each recorded data block. Date/time groups are entered into memory and compared with clock time to initiate such functions as system turnon, activation of the transponder for possible recall by acoustic command, and release of the return capsule at the preset clock release time. A second, less accurate clock, operating on an independent battery supply, is also set to the desired release time as a backup to the master clock. The overall system dynamic range is 96 db.

Every effort has been made to minimize system power drain. At present, a station can operate on the sea floor for about 6 months using 22 D-size lithium cells mounted within the pressure vessel. By screening components for low power consumption and increasing the number of cells in the battery pack, we expect to obtain a useful lifetime of one year.

A major concern in making strong-motion measurements offshore is the dynamic behavior of the soil-instrument system. Because ocean bottom soils near the mudline can be very soft, achievement of adequate ground coupling for strong-motion measurements is a significant design problem. An extensive experimental and analytical study of this problem (see Steinmetz et al., 1979) was conducted to insure that the fidelity of the measurements were acceptable at accelerations of up to 1.0 g over the frequency range of 0.1 Hz to 10 Hz. Based on this study, it was concluded that the present system responds accurately in very soft, cohesive soils with shear strengths on the order of 490 to 975 kg/m² (100 to 200 psf). Having shown this, the accuracy of the system in stiffer soils is assured if adequate penetration of the base spikes can be achieved. The study did point out, however, that it is necessary to insure that the footing is well seated so that the base ring maintains full contact with the soil. This led to the decision to develop a means for preloading the footing

to insure adequate seating, without adding permanently to the system mass.

Brief Summary of Results to Date

The initial 6-week period of operation of the high-gain OBS network (June-August, 1979, 11 stations) was one of unusual quiescence off Kodiak. Also, faulty tape recorder operation resulted in partial loss of data from 5 of the high-gain stations. Nevertheless, sixty earthquakes were recorded by two or more OBS stations. A typical seismogram from a local earthquake recorded by one of the high-gain OBS stations is shown in Figure 5. Arrival times for all earthquake phases identified in the OBS records were transmitted to Dr. Hans Pulpan for comparison with readings from the University of Alaska land station network. Thus far, it has been possible to locate 89 earthquakes using data from the combined onshore-offshore network. The preliminary epicenter locations for these earthquakes are shown in Figure 6. The focal depths range from less than 10 km to about 200 km. Much of the activity during the period of the 1979 experiment was located beneath the Lower Cook Inlet. The hypocenters of the detected events are concentrated along the inclined (Benioff) zone associated with the subduction of the Pacific plate beneath western Alaska.

Since we plan to repeat the microearthquakes experiment off Kodiak during the summer of 1980, we defer further comment on the seismicity of the region until the much larger data set that we anticipate, can be assembled. We point out; however, that the location accuracy, particularly depth estimates, for the earthquakes that occurred between Kodiak and the trench axis during the 1979 experiment is much greater than would have been possible without the OBS network.

Concerning the strong-motion portion of the program, no earthquakes large enough to produce meaningful strong-motion data have occurred in the Kodiak zone since monitoring operations were begun under this program.

An important new research opportunity may emerge from the data set obtained from the high-gain OBS stations off Kodiak during 1979. For years we have been puzzled as to the origin of a set of distinctive seismic signals that have been recorded in every OBS experiment in widely ranging locations. These were much more numerous in the Kodiak experiment than had previously been encountered. The Kodiak experiment was the first one in which we deployed the ocean bottom stations over a large range of water depths. A plot of the daily rate of occurrence of these events, versus station depth, is shown in Figure 7. It is evident that the rate of occurrence diminishes rapidly with increasing depth until a depth of about 1500 m is reached. Also, the sources are local, i.e., a given event is never recorded at more than one station. Hence, the distribution of sources with depth is as shown in Figure 7. Finally, these same signals are recorded in zones of no known seismic activity, e.g., the Gulf of Mexico. Taken together, these facts are almost indisputable evidence that the strange events are of biological origin. If so, the important point of Figure 7, is that the activity does not diminish to zero at abyssal depths, but remains at a fairly high level (14 to 35 events per day). By adding a bottom camera capable of imaging the OBS station at the time of each trigger, we may have discovered a new method of surveying benthic sea life.

Field Operations and Construction Plans

1. Strong-motion measurements. Industry support has been obtained for the construction of 12 additional strong-motion stations over the next two years. Briefly, our present plan for field operations and construction is the following:

- (a) Deploy the four existing stations in the Kodiak shelf zone in June, 1980.
- (b) Construct six additional stations. Deploy these new stations plus the balance of the present stations, at the approximate locations shown in Figure 8, in September, 1980. Recover these stations in June, 1981.
- (c) Construct six additional stations. Deploy these new stations plus the balance of the previously constructed stations at the earlier sites, and install at least 1 station at a new site in Norton Sound, in June-July, 1981. Recover and redeploy all stations in June-July, 1982.

The selection of sites for installation of strong-motion stations proposed here is based upon a combination of factors including: (1) regional seismicity, (2) the locations of sedimentary basins of possible interest to the oil industry, and (3) the need to obtain data that will permit testing and refinement of the earthquake risk assessments derived in the Offshore Alaska Seismic Exposure Study (OASES).

Obviously, the probability of obtaining strong-motion data is highest within the belts of highest seismicity. However, site specific data, i.e., measurements obtained on the specific sediment types to be encountered in future production operations, is also required. Finally, we prefer a combination of sites that will record signals from earthquake sources

that follow raypaths that traverse the major structural elements of the offshore Alaska provinces.

As shown in Figure 9, the seismically active belt of greatest concern extends along the Aleutian Trench, past Kodiak Island, and into interior Alaska along a N-S trend. A weaker trend extends in an E-W direction into Norton Sound. Two "gaps" in seismic activity have been identified within the major seismic belt: one in the northern Gulf of Alaska and one centered on the Shumagin Islands. The term seismic gap has taken on a variety of meanings in recent scientific literature. Here, we mean the region bordered by major rupture zones (as defined by aftershocks) of earlier earthquakes. Presumably, these gaps are the most likely candidates for future large earthquakes; although, this point is not well established.

During the first year of the program, we propose to concentrate the strong-motion stations along the OCS regions of the western Gulf of Alaska and Aleutian Islands, with several stations located behind the Island Arc in the Bristol and St. George Basins of the Bering Sea. A suggested distribution is shown in Figure 8. A total of ten stations are indicated in the network. This assumes that we have 4 stations remaining after recovery in October, 1980 of the network now operating off Kodiak, and that six additional stations can be constructed during the summer of 1980. Note that we have included stations in the vicinity of the Shumagin Gap.

In the second and following years of the program, we propose to extend the network northward with at least one station operating in Norton Sound. The stations of the proposed network span a large segment of the Aleutian seismic belt. In the event of a large earthquake within this belt, the raypaths of recorded signals will traverse the major structural

elements of the region: (1) forearc shelf, (2) island ridge, and (3) backarc basin. These data will contribute importantly to the refinement of model parameters, particularly attenuation, assumed in the OASES study. In addition, they will provide the first records of the actual waveforms of sea bottom accelerations.

We wish to point out that site surveys (precision depth profile and sonobuoy refraction lines) and sediment cores will be needed to properly interpret any strong-motion data eventually obtained. We propose that such surveys be deferred until useful strong-motion data are obtained at a given site.

2. Microearthquake measurements. Owing to the limited success of the microearthquake measurements program in 1979, we plan to return to the Kodiak zone during the summer of 1980 with 8 of our high-gain OBS stations to repeat the experiment. Suggested station locations are numbered 1-8 in Figure 1. Three additional high-gain stations will be constructed during 1980 to increase the total number available to thirteen.

Improvements in station design are proposed in two areas: (1) Improve tape recorder reliability by installing new drive motors, and eliminating the optical end of tape sensor which has failed to operate properly in many cases; and (2) increase the reliability of the acoustic recall system so that it can serve as the primary recovery method.

3. Construction of six strong-motion stations for use on land. Six additional strong-motion stations for use on land will be constructed in 1980. These will be installed and operated by personnel of the University of Alaska as part of their existing network of radio-telemetering seismic stations.

Data Processing and Analysis Plans

1. Microearthquake (high gain OBS) data analysis. A series of tasks will be accomplished jointly with the University of Alaska. (a) First we will generate a list of readings of times of first arrivals for all events recorded on OBS playouts. (b) These data will be used by the University of Alaska in their standard quarterly bulletin calculations. The University of Alaska presently has the capability of producing a seismological bulletin with earthquake origin times, locations, depths, magnitudes and statistical parameters about one month after receipt of data. Their existing system will be able to absorb the additional station locations and additional arrival time readings without serious impact. A subset of well recorded earthquakes from the final bulletin list will be selected for (c) focal mechanism studies, and (d) crust-mantle structural analyses. Secondary phases and frequency content will be analyzed. It seems likely that progress can be made in identifying tectonic units characterized by particular seismic velocities, in elastic absorption, and focal mechanism patterns. These problems will be of interest to both groups, and copies of original data on these events will be exchanged. (e) the same data will also be of use in more detailed studies of wave propagation characteristics over the joint network. Surface wave data will be studied by normal mode methods, and a comprehensive effort will be made to understand the details of generation and propagation of waves in these well-recorded events. In particular, short period surface waves generated by moderate to large earthquakes in the region will provide waveforms which can be interpreted in terms of rigidity profiles for the upper sedimentary layers of the continental shelf. These results will ultimately be useful to platform design engineers.

Seismic bulletins will be distributed as at present by the University of Alaska.

2. Strong-motion data analysis. Strong-motion data will be reformatted to produce computer compatible 9-track data tapes. These, along with analog playouts and supporting documentation (locations, calibrations, available information on sub-bottom structure, and source parameters) will be distributed to NOAA and the industrial sponsors.

REFERENCES

- Latham, G., P. Donoho, K. Griffiths, A. Roberts, and A. K. Ibrahim, The Texas Ocean-Bottom Seismograph: Proceedings of the 10th Annual Offshore Technology Conference, Houston, Texas, May 8-11, 1978, pp. 1467-1476.
- Steinmetz, R., P. Donoho, J. Murff, and G. Latham, Soil Coupling of a Strong-motion, Ocean Bottom Seismometer: Proceedings of the 11th Annual offshore Technology Conference, Houston, Texas, April 30-May 3, 1979, pp. 2235-2249.
- Steinmetz, R., J. Murff, G. Latham, A. Roberts, P. Donoho, L. Babb, and T. Eichel, Seismic Instrumentation of the Kodiak Shelf: accepted for publication in Marine Geotechnology, 1980.

FIGURE CAPTIONS

- Figure 1. Map showing locations of ocean bottom seismic stations installed in June, 1979. Strong-motion and high-gain stations of the University of Alaska network on Kodiak and adjacent islands are also shown. Repeat installation of high-gain stations at sites marked 1-8 is proposed for the summer program of 1980.
- Figure 2. A strong-motion seismic station as it would appear on the sea floor.
- Figure 3. Photograph of a strong-motion seismic station, with preload system, prepared for launch.
- Figure 4. Sketch of the major elements of the strong-motion ocean bottom seismography system.
- Figure 5. Typical earthquake record from a high-gain OBS off Kodiak.
- Figure 6. Locations of epicenters of earthquakes recorded by the combined land and ocean bottom seismic network during the summer of 1979.
- Figure 7. Number of events believed to be of biological origin detected by various high-gain OBS stations versus station depth.
- Figure 8. Map showing recommended distribution of an initial 10-station network of strong-motion OBS stations. One or two additional stations would be placed in Norton Sound during the second and succeeding years of the program.
- Figure 9. Map showing the distribution of earthquakes of magnitude greater than 5 that have occurred in the Alaska zone during the past decade. Major sedimentary basins of the region are also indicated.

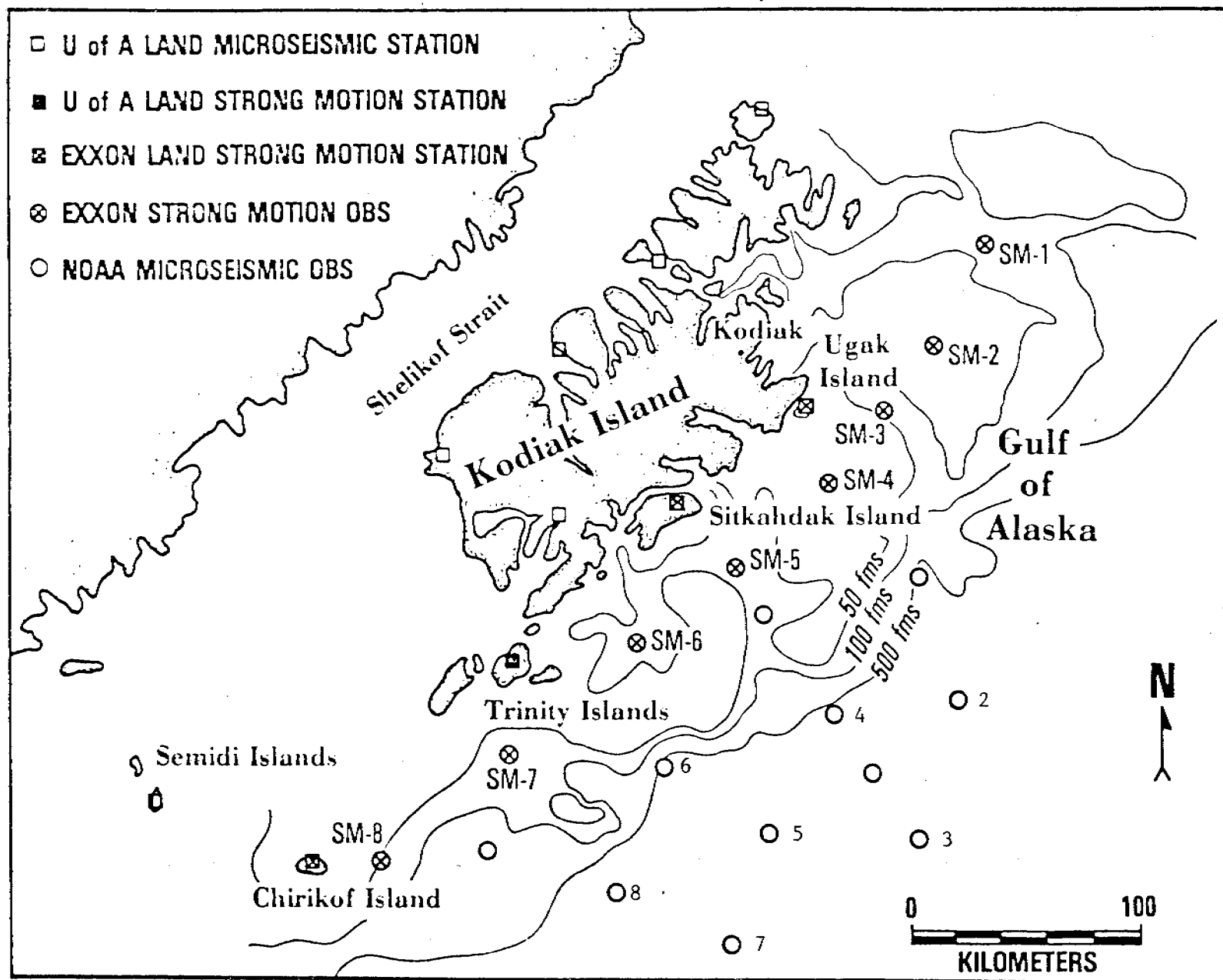
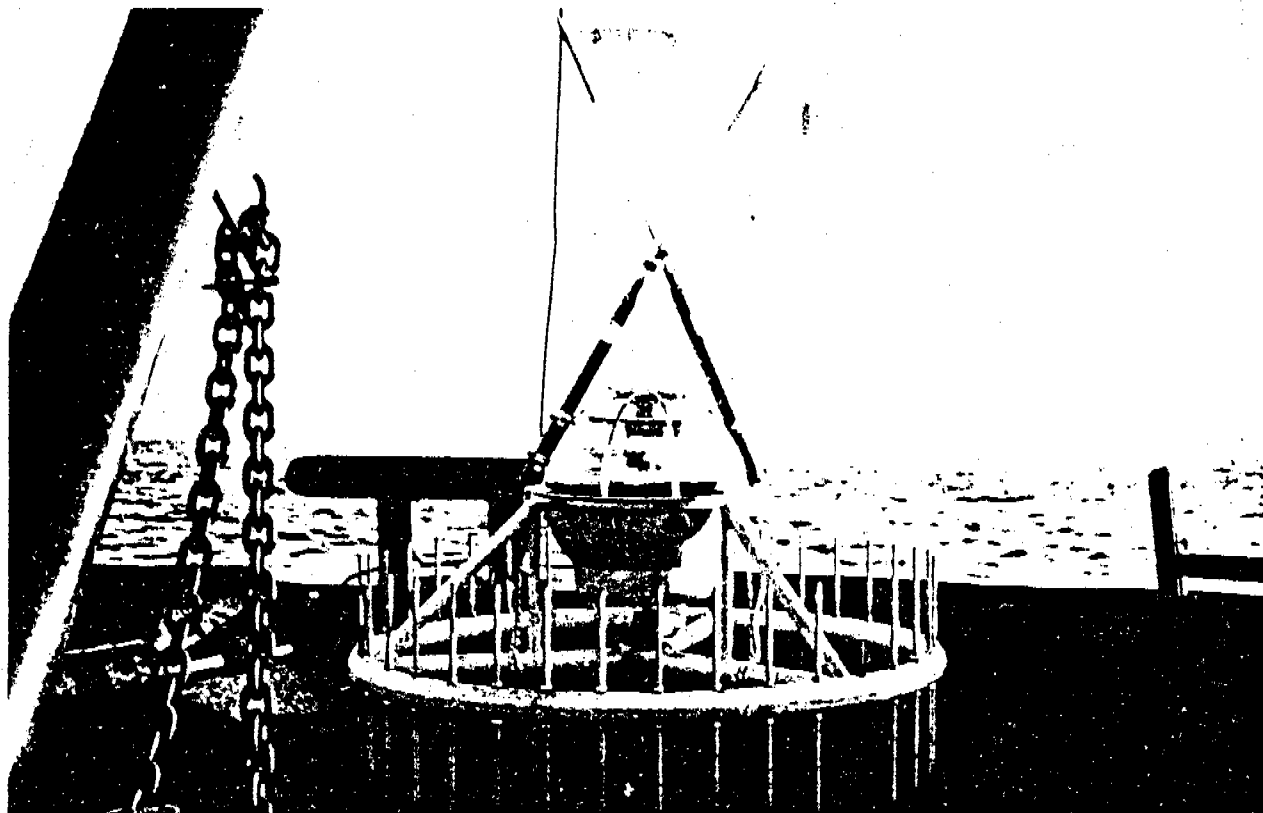
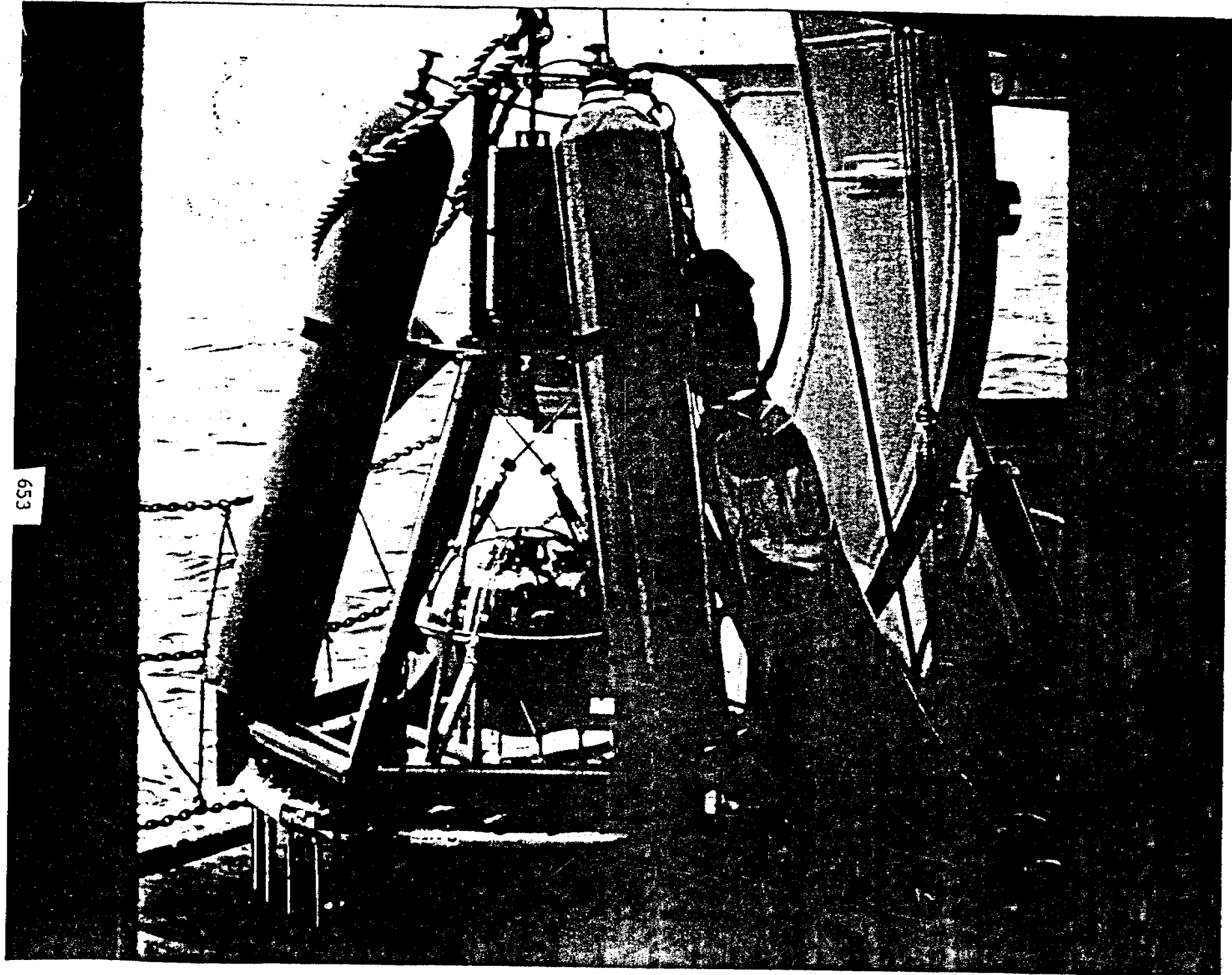


Figure 1



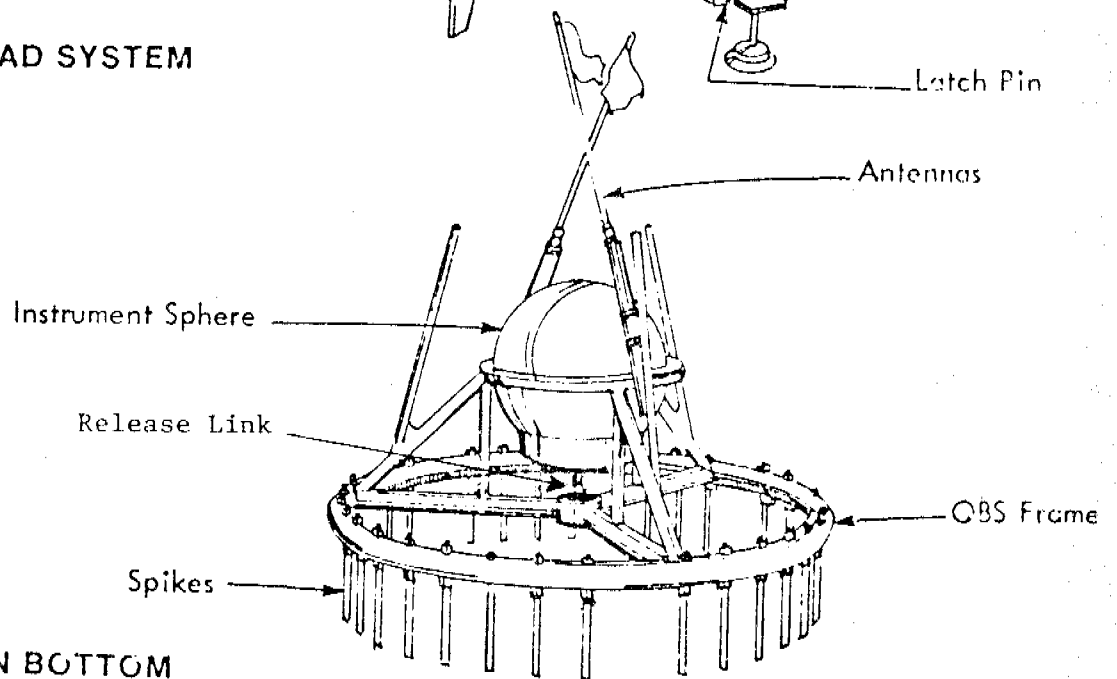
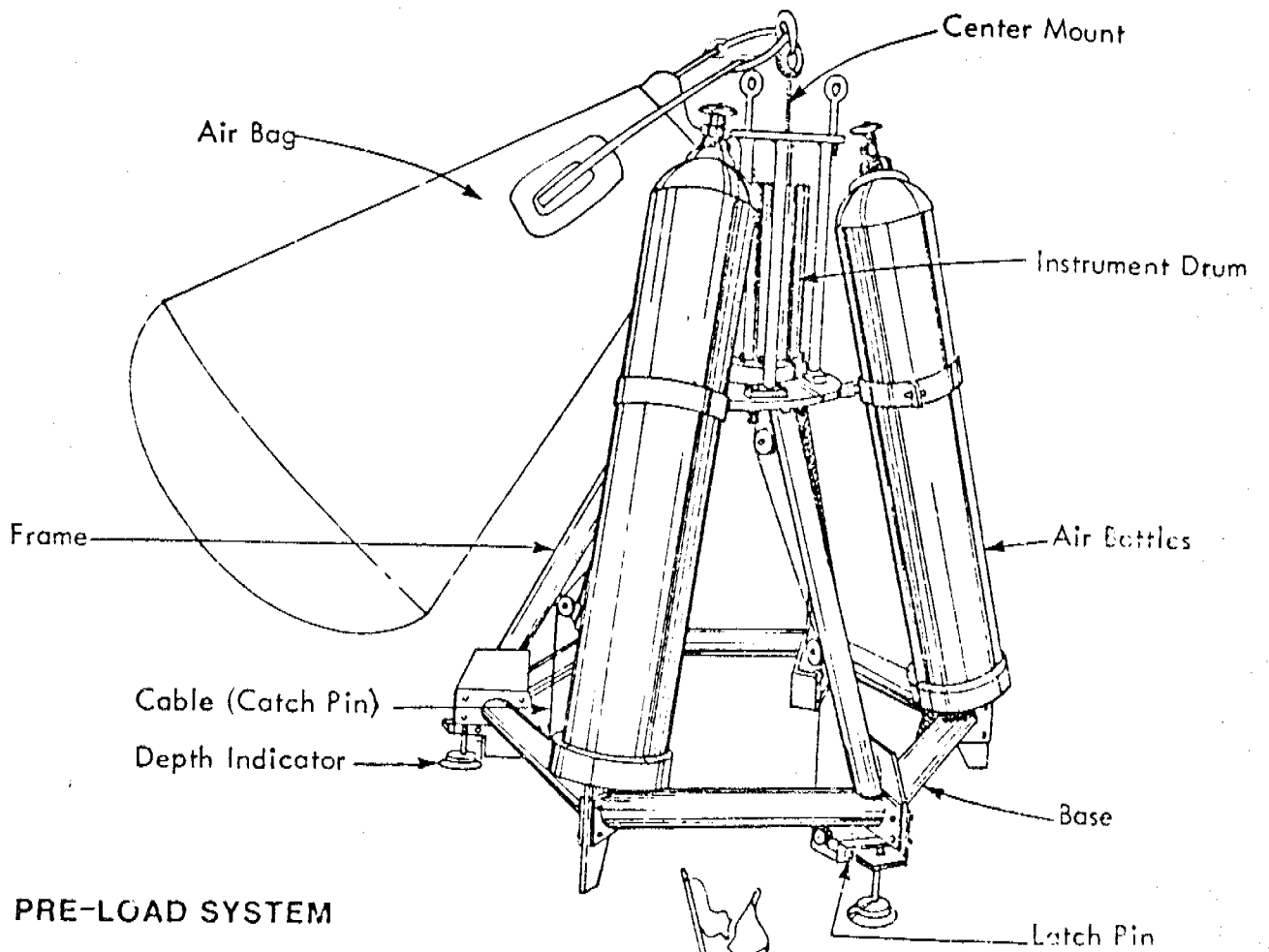
STRONG MOTION OCEAN BOTTOM SEISMOMETER

Figure 2



653

Figure 3



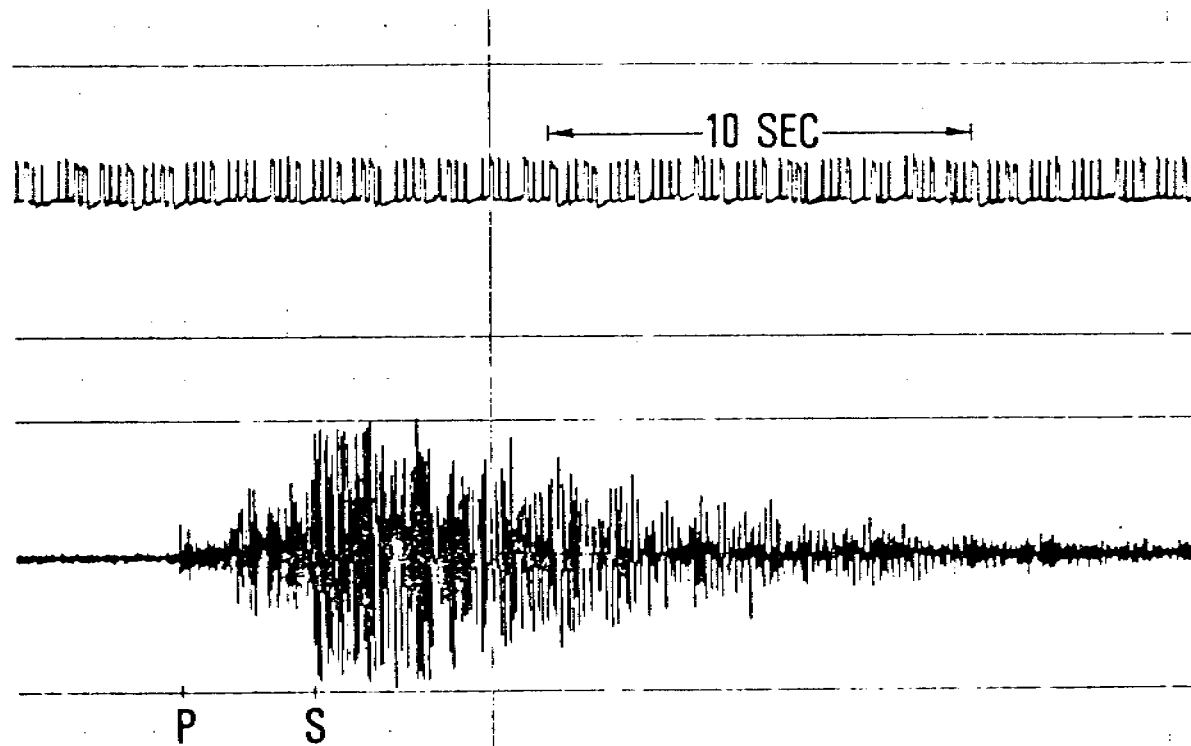


Figure 5. Record of an Earthquake as Recorded by HG-OBS #5.
Identified arrivals are the compressional wave (P) and the
shear wave (S).

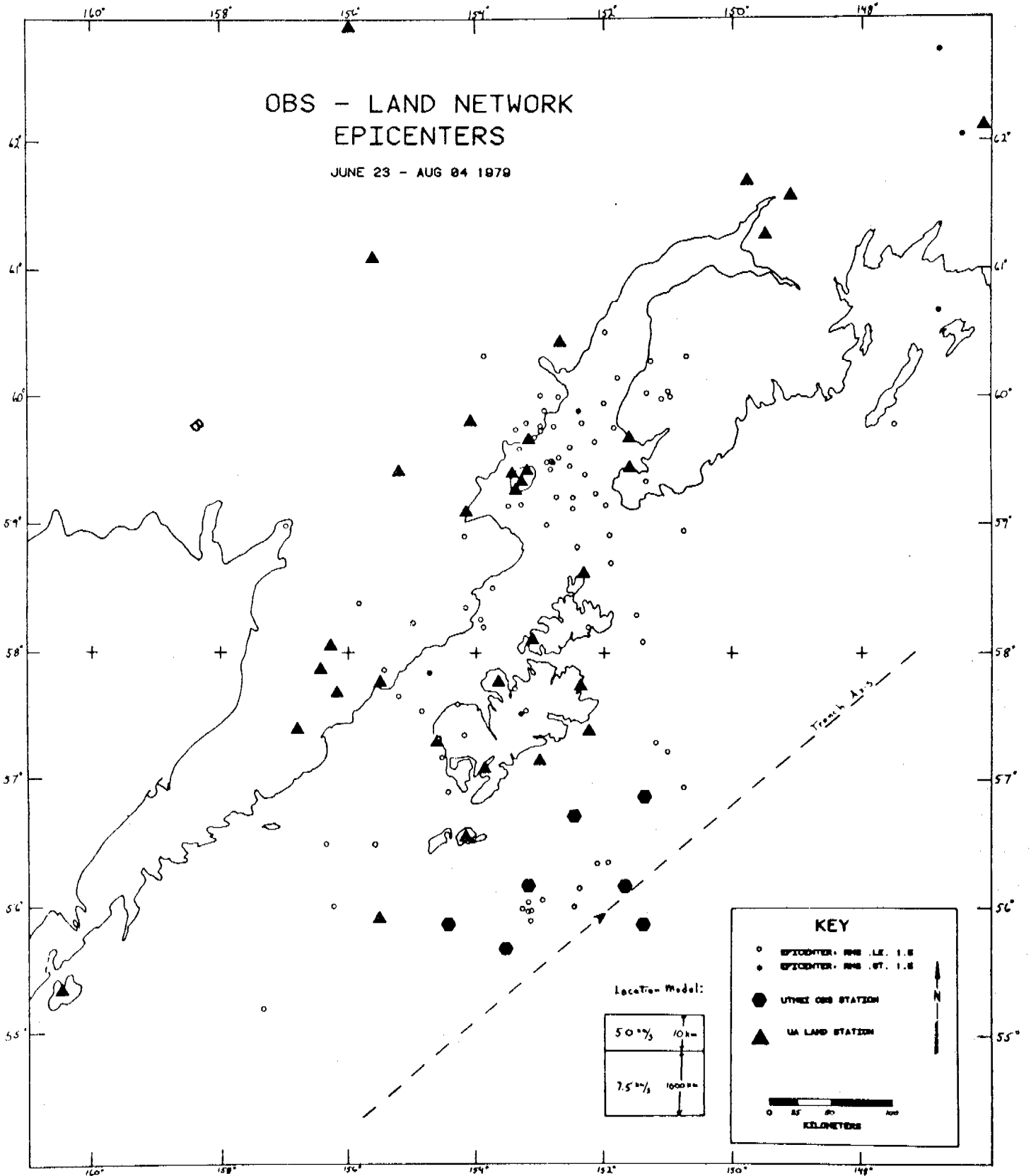


Figure 6

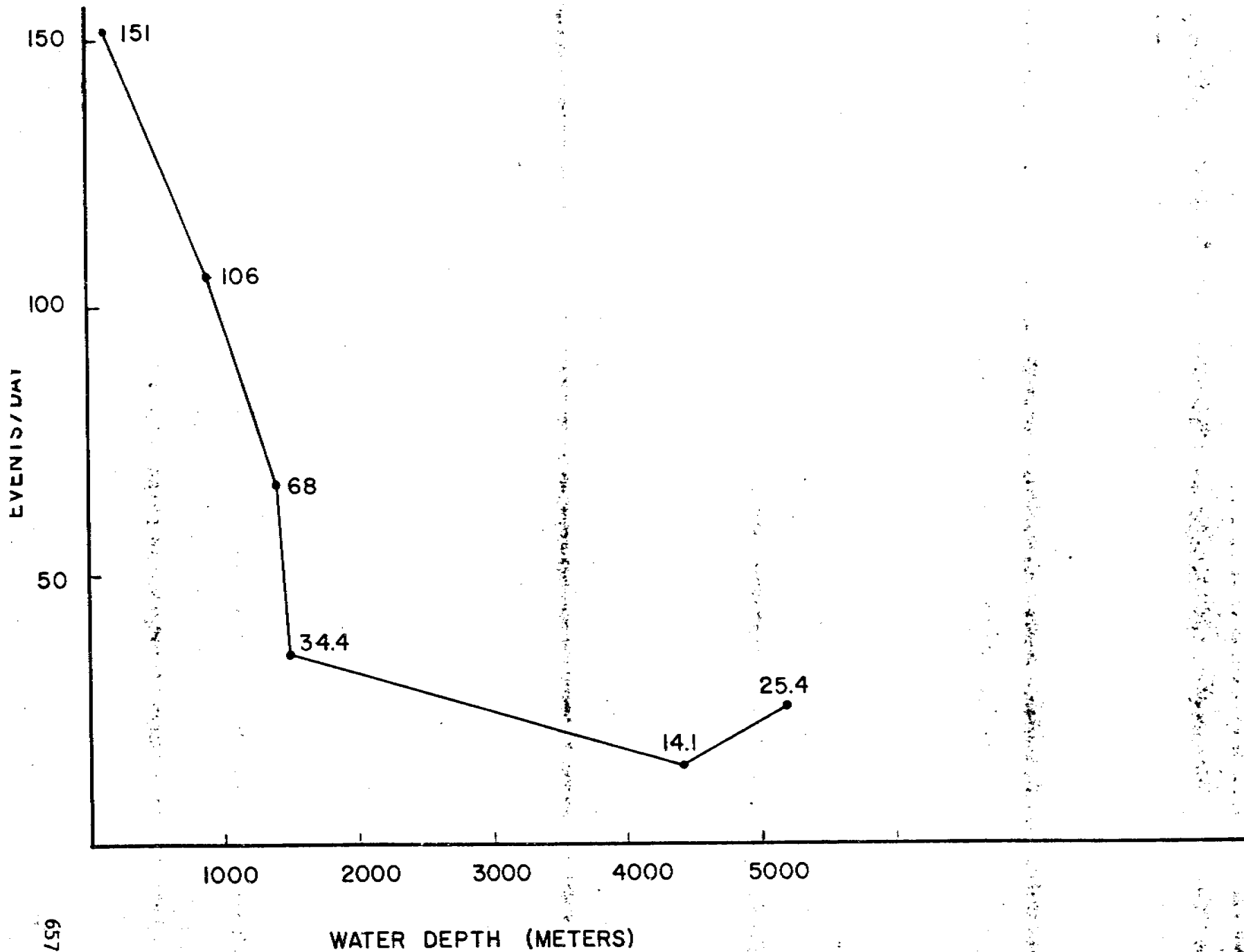


Figure 7

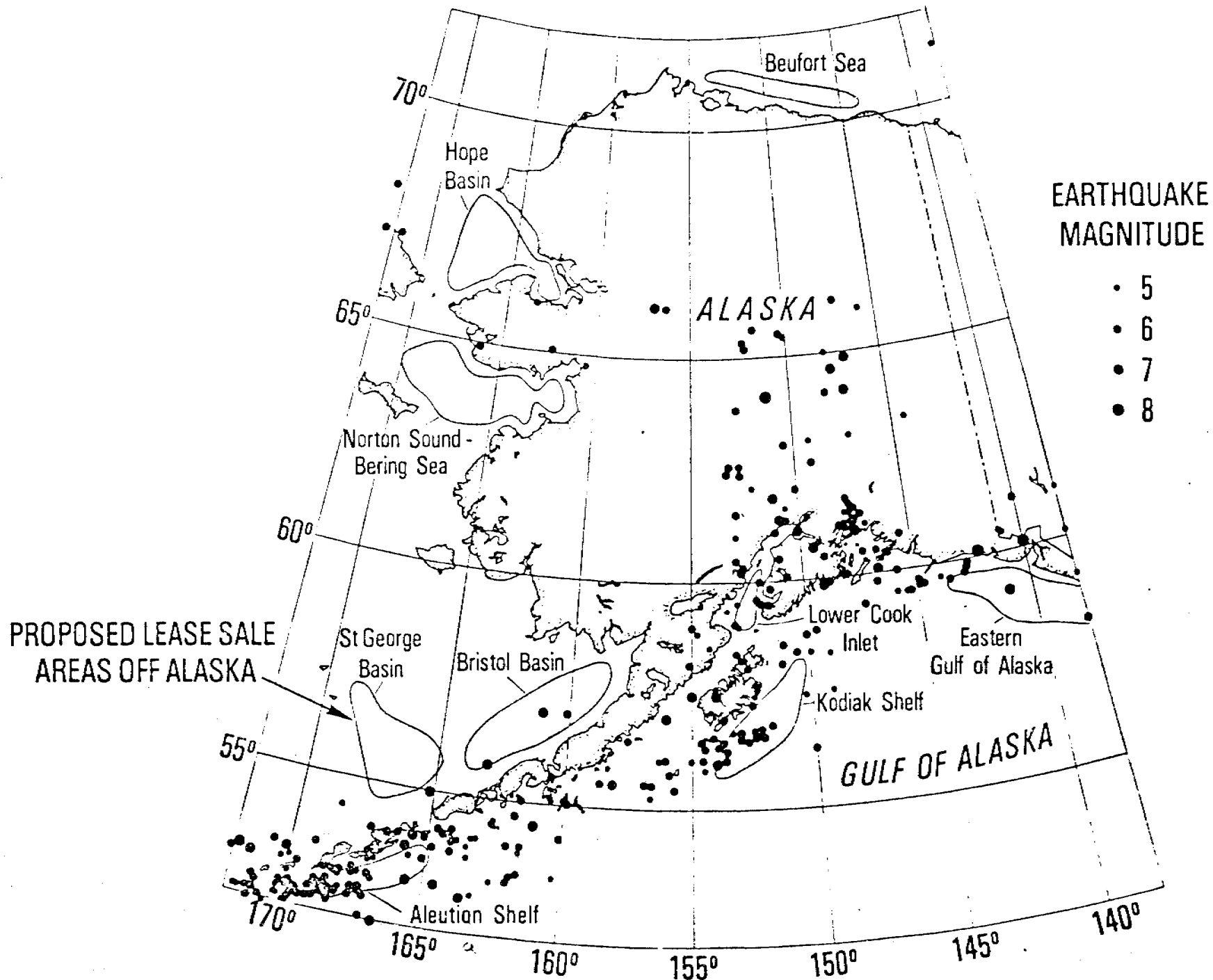


Figure 9

